Synthesis and Photophysical Properties of Silsesquioxane Based Molecules and Polymers

by

Jun Guan

A dissertation submitted in partial fulfillment
of the requirements for the degree of
Doctor of Philosophy
(Materials Science and Engineering)
in the University of Michigan
2021

Doctoral Committee:

Professor Richard M. Laine, Chair
Professor John Kieffer
Professor Jinsang Kim
Professor Brain Love

Jun Guan

junguan@umich.edu

ORCID iD: 0000-0002-0860-2204

Dedication

To My Family[a]

[a] Genetic and otherwise

Life is not worth living without them

Acknowledgements

I would like to first thank the following people for their guidance, assistance, patience, and friendship, without all of which this dissertation would not have been finished: my parents and relatives, my advisor Professor Richard M. Laine, and the entire Laine research group, past and present, including Zijing Zhang, Dr. Xinyu Zhang, Dr. Eleni Temeche, Mengjie Yu, Taylor Brandt, Philyong Kim, Mitra Khiabani Moghadam and Dr. Eongyu Yi.

I am also grateful to my committee: Professor Jinsang Kim, Professor John Kieffer and Professor Brain Love.

I also thank the following people for training me and their contributions in the experimental photophysical characterization: Mr. Long Cheng, Dr. Krishnandu Makhal, Dr. Minh Tuan Trinh and Professor Stephen C. Rand, Mr. Wenhao Shao and Professor Jinsang Kim, Mr. Ifeanyi Madu and Professor Theodore Goodson III, Professor Joseph Coy Furgal from Bowling Green State University, and Professor Aleksander Rebane from Montana State University.

I would also like to thank the following people for their support and assistance in the modeling studies: Mr. Ramin Ansari, Dr. Daniel Hashemi and Professor John Kieffer, Dr. Nuttapon Yodsin and Professor Siriporn Jungsuttiwong from Ubon Ratchathani University in Thailand.

Special thanks are in order to Dr. Yujia Liu and Professor Masafumi Unno from Gunma University in Japan for their gifts of ladder silsesquioxanes.

Gratitude is also given to the following visiting scholars and undergraduate students who have contributed to this dissertation: Dr. Jonathan Rubio Arias, Kenji Tomobe, Zejun Sun and Sakiko Watkins. I also would like to thank the LSA chemistry staff: Mr. Eugenio Alvarado, Mr. Christopher Kojiro, and Mr. James Windak.

Special gratitude is given to the VeryUs Dance Crew and all of my other great friends for their patience, stubbornness and kindness. Without them there is no way I could have handled all the stress of graduate school and I love them all dearly.

I would also like to express my appreciation once again to my dearest parents, my auntie and uncle-in-law for getting me interested in a doctoral degree in the first place, as well as conversations about school and life toward maintaining my sanity.

Finally, I would like to acknowledge the financial support from the National Science Foundation.

Table of Contents

Dedication ii
Acknowledgements iii
List of Tables ix
List of Schemes xi
List of Figures xii
List of Appendices xx
Abstract xxi
Chapter 1. Introduction 1
1.1 Project goals and objectives 1
1.2 Definitions, structures and nomenclatures of silsesquioxanes 1
1.3 Completely condensed silsesquioxanes 5
1.3.1 Octa-, deca- and dodeca- polyhedral oligomeric silsesquioxanes 5
1.3.2 Octaphenylsilsesquioxane 7
1.3.3 Iodination and bromination of phenylsilsesquioxanes 8
1.4 Incompletely Condensed Silsesquioxanes 9
1.4.1 Double decker silsesquioxanes 10
1.4.2 Silsesquioxane-based polymers 11
1.5 Ladder silsesquioxanes 12
1.6 Photophysical properties of silsesquioxanes 13
1.6.1 Electron delocalization involving the silsesquioxane core 14
1.6.2 Electron delocalization in beads-on-a-chain polymers 19

1.6.3 Theoretical studies 20
1.6.4 Photoluminescence quantum yields 21
1.7 Overview of subsequent chapters 22
References 23
Chapter 2. Experimental Methods 33
2.1 Materials 33
2.2 Syntheses 33
2.2.1 Corner missing silsesquioxanes $(PhSiO_{1.5})_7(O_{0.5}H)_3$ 33
2.2.2 Double decker silsesquioxanes $(PhSiO_{1.5})_8(O_{0.5}H)_4$ 36
2.2.3 Double decker silsesquioxanes derived copolymers 37
2.2.4 Ladder silsesquioxane derived copolymers 40
2.2.5 Double decker silsesquioxane derived terpolymers 42
2.3 Characterization 43
2.3.1 Analytical characterization 43
2.3.2 Photophysical characterization 44
References 46
Chapter 3. Partially Functionalized Phenylsilsesquioxane: $[RSiO_{1.5}]_7[Me/nPrSiO_{1.5}]$ and $[RSiO_{1.5}]_7[O_{0.5}SiMe_3]_3$ (R = 4-Me/4-CN-Stilbene) 48
Abstract 48
3.1 Introduction 48
3.2 Experimental 52
3.3 Results and discussion 52
3.3.1 Synthesis and characterization of $RStil_xT_8R'$ and $RStil_xT_7$-trisiloxy. 52
3.3.1 Photophysical properties. 53
3.3.3 Optical magnetization properties 57
3.3.4 Modeling studies 64

3.4 Conclusions 65

References 66

Chapter 4. Functionalized Double Decker Phenylsilsesquioxane Macromonomers: $[PhSiO_{1.5}]_8[OSiMe_2]_2$ and $[PhSiO_{1.5}]_8[O_{0.5}SiMe_3]_4$ 69

Abstract 69

4.1 Introduction 69

4.2 Experimental 70

4.3 Results and discussion 70

4.3.1 Synthesis and characterization of $RStil_xDDMe_4$ and $RStil_xDD(OTMS)_4$. 72

4.3.2 Photophysics of *o*-$RStil_7DDMe_4$ and *o*-$RStil_7DD(OTMS)_4$. 73

4.3.3 Photophysics of *p*-$MeStil_7DDMe_4$ and *p*-$MeStil_2Ph_6DD(OTMS)_4$. 75

4.3.4 Fluorescence and two-photon absorption (TPA) data 75

4.3.5 Optical magnetization properties 76

4.3.6 Theoretical studies 81

4.4 Conclusions 83

References 84

Chapter 5. Unconventional Conjugation via Siloxane Bridges May Imbue Semiconducting Properties in Double Decker Copolymers 88

Abstract 88

5.1 Introduction 89

5.2 Experimental 92

5.3 Results and discussion 92

5.3.1 Model silane compound synthesis and analytical characterization 93

5.3.2 Polymer synthesis and analytical characterization. 93

5.3.3 Model cage compound syntheses and analytical characterization. 94

5.3.4 Steady-state photophysical studies 95

5.3.5 Two-photon photophysical studies 101

5.3.6 Further evidence suggesting unconventional conjugation 104

5.4 Conclusions 111

References 112

Chapter 6. Unconventional Conjugation via Siloxane Bridges in Ladder Silsesquioxane Copolymers 118

Abstract 118

6.1 Introduction 119

6.2 Experimental 120

6.3 Results and discussion 120

6.4 Conclusions 127

References 127

Chapter 7. Double Decker Silsesquioxane Derived Alternating Terpolymers Give Excited-state Conjugation Averaging that of the Corresponding Co-polymers. 130

Abstract 130

7.1 Introduction 130

7.2 Experimental 132

7.3 Results and discussion 132

7.4 Conclusions 137

References 137

Chapter 8. Future Work 140

8.1 Summaries 140

8.2 Hairy polymers 141

8.2 Bromination patterns in various SQ architectures 144

8.3 Donor-acceptor system 145

References 149

Appendices 151

List of Tables

Table 1.1.Photoluminescence quantum yields and two-photon absorption properties of silsesquioxane derivatives. 18

Table 1.2. Density functional theoretical (DFT) HOMO-LUMO calculations for selected silsesquioxane molecules. 20

Table 3.1. Photophysical data for *p*-MeStil$_8$OPS, RStil$_x$T$_8$R' and RStil$_x$T$_7$-trisiloxy. 55

Table 4.1. MALDI-TOF and GPC data for DDMe$_4$ and DD(OTMS)$_4$. 72

Table 4.2. MALDI-TOF, TGA and GPC data for *o*-Br$_x$DDMe$_4$, *o*-RStil$_x$DDMe$_4$, *p*-I$_x$DDMe$_4$, *p*-RStil$_x$DDMe$_4$, *o*-Br$_x$DD(OTMS)$_4$, *o*-RStil$_x$DD(OTMS)$_4$, *p*-I$_x$DD(OTMS)$_4$ and *p*-RStil$_x$DD(OTMS)$_4$. 72

Table 4.3. Photophysical data for *p*-MeStil$_8$OPS, RStil$_x$DDMe$_4$ and RStil$_x$DD(OTMS)$_4$. 74

Table 4.4. λ_{max} in nm of DD(OTMS)$_4$ and DDMe$_4$ structures using TD-DFT calculations. 83

Table 5.1. Steady-state data for vinylMeSi(OMe)$_2$ derived model silane compounds (blue), vinylDDvinyl derived polymers (red) and model cage compounds (green). 100

Table 5.2. Optical band gaps calculated from UV-Vis absorption λ_{max}, band gaps from CV of (R'StilbenevinylT)$_{10/12}$[61] and corrected band gaps of T$_{10/12}$[29] and vinylDDvinyl derived polymers. 106

Table 6.1. GPC and steady-state photophysical data for vinylDDvinyl derived polymers[9] and vinyl-LL(Me)-vinyl derived polymers. 121

Table 6.2. MALDI-TOF and GPC data for DD-co-thiophene, short LL-co-thiophene isolated by TLC and long LL-co-thiophene. 123

Table 7.1. MALDI-TOF, GPC and TGA data for terpolymers. 134

Table 7.2. UV-vis, photoluminescent data and quantum yields for DD derived copolymers[19] and terpolymers. 136

Table 8.1. Steady-state spectra data of RStyrene and RStyryl-functionalized in DCM or ACN. 147

Table 8.2. Steady-state spectra data of Stilbene-compounds. 148

Table A.1. MALDI-TOF, GPC and ^{1}H-NMR data for Ph$_7$T$_8$R' and Ph$_7$T$_7$(TMS)$_3$. 151

Table A.2. ^{1}H-NMR peaks of *o*-Br$_x$Ph$_7$T$_8$R' and *p*-I$_x$Ph$_7$T$_8$R' 151

Table A.3. MALDI-TOF ([a] As Ag^+ adduct), TGA and GPC data for *o*-$Br_xPh_7T_8R'$, *o*-$RStil_xT_8R'$, *p*-$I_xPh_7T_8R'$, *p*-$RStil_xT_8R'$, *o*-$Br_xPh_7T_7(TMS)_3$, *o*-$RStil_xT_7(TMS)_3$, *p*-$I_xPh_7T_7(TMS)_3$ and *p*-$RStil_xT_7(TMS)_3$. 152

Table B.1. ^{1}H-NMR peaks for $DDMe_4$ and $DD(OTMS)_4$ 161

Table C.1. ^{1}H-NMR peaks of model silane compounds. 166

Table C.1. Representative FTIR data of selected compounds. 168

Table C.3. MALDI-TOF, GPC and TGA data for vinylDDvinyl and derived polymers. 172

Table C.4. MALDI-TOF, GPC and TGA data for vinylDDvinyl derived model cage compounds. 178

Table C.5. Two photon absorption (2PA) cross section values of polymers DD-co-phenyl, -thiophene, -dimethylfluorene, -BTH and -carbazole and model cage compound $(Styryl)_2DD$ at discrete excitation wavelength. 185

Table C.6. Experimental and modeling data for *trans*- vinylDDvinyl and its derived polymers DD-co-phenyl, -thiophene, -dimethylfluorene, -BTH and -carbazole. 190

Table D.1. MALDI-TOF, GPC and TGA data for vinyl-LL-vinyl and derived polymers. 198

Table D.2. Representative FTIR data of selected compounds. 200

Table D.3. ^{1}H and ^{13}NMR data of vinyl-LL(Me)-vinyl derived polymers. 203

Table D.4. Experimental and modeling data for vinyl-LL(Me/Ph)-vinyl. 214

Table E.1. ^{1}H and ^{13}C NMR peaks 219

Table E.2. Representative FTIR data of selected compounds. 220

Table F.1. GPC and TGA data for DD-co-biphenyl and derived products as in Scheme **8.2a**. 228

Table F.1. GPC and TGA data for brominated vinylDDvinyl and derived products as in Scheme **8.2b**. 231

List of Schemes

Scheme 1.1. Acid or base-catalyzed hydrolysis and condensation of trifunctional silane. 2

Scheme 1.2. The structure and synthetic route to the tetrasilanol double decker phenylsilsesquioxanes. 4

Scheme 1.3. Functionalization of octaphenylsilsesquioxane OPS: (a) iodination, (b) bromination, (c) Buchwald-Hartwig, (d and i) Sonogashira, (f and j) Suzuki, (g and h) Heck cross-coupling reaction. 7

Scheme 1.4 Synthesis of incompletely condensed silsesquioxane derivatives via the hydrolysis of completely condensed silsesquioxanes. 10

Scheme 1.5. Reaction routes to di- and tetra-functional double decker silsesquioxanes. 11

Scheme 1.6. Di- and tetra-functional double decker silsesquioxanes derived copolymers. 12

Scheme 3.1. Synthesis of stilbene-SQs. 51

Scheme 4.1. Synthetic scheme for DD stilbene-SQs. 71

Scheme 5.1. Heck catalytic cross coupling polymerization reactions of vinylDDvinyl and related model compounds. 91

Scheme 6.1. Heck cross coupling of (a) model compounds, (b) vinylDDvinyl derived copolymers and (c) vinyl-LL-vinyl derived copolymers. 120

Scheme 7.1. Syntheses of DD derived alternating terpolymers. 132

Scheme 8.1. Syntheses of hairy polymers. 141

Scheme 8.2. (a) Syntheses by bromination of DD copolymers. (b) Syntheses by bromination of DD cage. 142

Scheme 8.3. Structure of donor-acceptor DD. 146

Scheme 8.4. Synthesis of di-styryl functionalized DD (Gen 1), and di-stilbenevinyl functionalized DD (Gen 2). 146

Scheme 8.5. Synthesis of symmetrical and unsymmetrical molecular DD compounds (Gen 1.5). 149

List of Figures

Figure 1.1. Representative structures of silsesquioxanes. 3

Figure 1.2. Torsion angles of all-isopropyl ladder silsesquioxanes. 3

Figure 1.3. Silsesquioxane nomenclature. 5

Figure 1.4. Structures of $T_{8,10,12}$ condensed cage silsesquioxanes. 6

Figure 1.5. Typical sizes and volume of a T_8 silsesquioxane molecule 6

Figure 1.6. Atomic structures and electron density isocontours of $T_{8,10,12}$ silsesquioxanes. 8

Figure 1.7. a. Photoluminescence and absorption of T_8 and b. $[ClCH_2(CH_2)_2\text{-}T]_{8,10,12}$ in THF excited by laser at 325 nm. 14

Figure 1.8. Vinyl-biphenyl functionalized silsesquioxane cores and their normalized absorption (black) and photoluminescence (blue) spectra. 15

Figure 1.9. Normalized absorption (empty symbols) and photoluminescence (closed symbols) of 4'-vinylbiphenyl-3,5-dimethylalcohol functionalized silsesquioxane (blue) and 4'-vinylbiphenyl-3,5-dimethylalcohol (red). 16

Figure 1.10. Silsesquioxane molecule with electron-donating 4-carbazolephenyl group (blue). 16

Figure 1.11. Absorption and photoluminescence comparison of ortho and para (o/p)-MeStilbene functionalized silsesquioxanes to p-MeStilbene in THF. 17

Figure 1.12. (a) Me_2NStilbene-corner, (b) Me_2NStilbene-half, and (c) Me_2NStilbene-full. 18

Figure 1.13. Absorption and emission of $T_{10,12}$-based BoC oligomer and -$Si(OEt)_3$ end-capped model compounds. 19

Figure 1.14. Experimental setup for integrating sphere measurements. 22

Figure 3.1. Venus flytrap mechanism for ortho bromination. 49

Figure 3.2. Asymmetric bromination. 50

Figure 3.3. Janus bromination of octaphenylsilsesquioxanes. 50

Figure 3.4. Polyhedral germsesquioxane cage with LUMO centered within cage. 50

Figure 3.5. Normalized steady-state absorption (solid) and emission (dashed) spectra for Ph_7T_8R', *p*-$MeStil_8OPS$ and *o*-$RStil_xT_8R'$. 54

Figure 3.6. Normalized steady-state absorption (solid) and emission (dashed) spectra for *p*-$MeStil_8OPS$ and *o/p*-$RStil_xT_7$-trisiloxy. 56

Figure 3.7. Normalized steady-state one-(a) and (b) two-photon fluorescence spectra (λ_{ex}=800 nm laser light) for *o*-RStil$_7$T$_8$R' and *o*-RStil$_7$T$_7$-trisiloxy. 58

Figure 3.8. Dependence of 2-photon-induced fluorescence emission intensity on input power at λ_{ex}=800 nm in three different SQ samples: (a) Methyl, (b) Propyl, and (c) TMS. 59

Figure 3.9. (a) Raw data on co- (red) and cross-polarized (blue) scattered light intensity vs. incident polarization angle in *o*-MeStil$_7$T$_8$Me at fixed input intensity (λ_{ex}= = 800 nm). (b) Radiation pattern (polar plot) of the raw data in part (a) after subtraction of the constant background component, showing that purely dipolar electric and magnetic dipole components are induced in the scattered light at the intensity of our experiments. 60

Figure 3.10. (a) Raw data on co- (red) and cross-polarized (blue) scattered light intensity vs. incident polarization angle in *o*-MeStil$_7$T$_8$Pr at fixed input intensity (λ_{ex}= = 800 nm). (b) Radiation pattern (polar plot) of the raw data in part (a) after subtraction of the constant background component, showing that purely dipolar electric and magnetic dipole components are induced in the scattered light at the intensity of our experiments. 60

Figure 3.11. (a) Raw data on co- (red) and cross-polarized (blue) scattered light intensity vs. incident polarization angle in *o*-MeStil$_7$T$_7$-trisiloxy at fixed input intensity (λ_{ex}= = 800 nm). (b) Radiation pattern (polar plot) of the raw data in part (a) after subtraction of the constant background component, showing that purely dipolar electric and magnetic dipole components are induced in the scattered light at the intensity of our experiments. 61

Figure 3.12. Polar plots of raw light scattering data in methyl, propyl and TMS monomers after solvent subtraction. The solid curves are least squares fits to dipole radiation patterns together with a fitted constant background signal..... 62

Figure 3.13. HOMO and LUMO modeling of the Me$_8$T$_8$ silsesquioxane. 64

Figure 3.14. HOMO and LUMO models for the permethylated corner missing cage. 65

Figure 4.1. Steady-state absorption (solid) and emission (dashed) spectra for *p*-MeStil$_8$OPS and *o*-RStil$_7$DDMe$_4$ and *o*-RStil$_7$DD(OTMS)$_4$..... 74

Figure 4.2. Steady-state (solid) and emission (dashed) spectra for *p*-MeStil$_8$OPS, *p*-MeStil$_7$DDMe$_4$ and *p*-MeStil$_2$Ph$_6$DD(OTMS)$_4$. 75

Figure 4.3. Normalized steady-state one- (a) and (b), (c) two-photon fluorescence spectra of DD(OTMS)$_4$ and DDMe$_4$ (λ_{ex}=800 nm laser light). 77

Figure 4.4. Dependence of 2-photon-induced fluorescence emission intensity on input power at λ_{ex}=800 nm in double-decker compounds (a) DD(OTMS)$_4$ and (b) DDMe$_4$. 77

Figure 4.5. (a) Raw data for co- (red) and cross-polarized (blue) scattered light intensity vs. incident polarization angle in 0.1 mM DD(OTMS)$_4$ in DCM at fixed input intensity (λ_{ex}= 800 nm). (b) Radiation pattern (polar plot) of the raw data in part (a) after subtraction of the constant background component, showing purely dipolar electric and magnetic dipole components are induced in the scattered light at the intensity of our experiments..... 78

Figure 4.6. (a) Raw data from co- (red) and cross-polarized (blue) scattered light intensity vs. incident polarization angle in $DDMe_4$ at fixed input intensity (λ_{ex}= = 800 nm). (b) Radiation pattern (polar plot) of the raw data in (a) after subtracting background component, showing that purely dipolar electric and magnetic dipole components are induced in the scattered light at the intensity of our experiments. 79

Figure 4.7. Optimized $DD(OTMS)_4$ and $DDMe_4$ structures with HOMO and LUMO at B3LYP/6-31G(d,p) level of theory..... 81

Figure 4.8. Absorption spectra for $DD(OTMS)_4$ and $DDMe_4$, calculated at the TD-M06-2X/6–31G (d) level of theory..... 82

Figure 4.9. Optimized DD-open and DD-close structures with HOMO and LUMO at B3LYP/6-31G(d,p) level of theory..... 83

Figure 4.10. Comparison of absorption and emission of di- and tristyrylDD with DD-co-Phenyl (10 k Da M_w)..... 84

Figure 5.1. (a) Synthese of silane-end-capped DD; (b) normalized steady-state spectra of 1,4-$[(MeO)_2Sivinyl]_2$benzene, DD-co-phenyl and silane-end-capped DD..... 97

Figure 5.2. Absorption and emission of model compounds and BoC oligomers of $T_{10,12}$..... 98

Figure 5.3. Normalized steady-state spectra of 2,5-$[(MeO)_2Sivinyl]_2$thiophene, DD-co-thiophene and $(Thiophenevinyl)_2DD$..... 99

Figure 5.4. Normalized steady-state spectra of 3,6-$[(MeO)_2Sivinyl]_2$carbazole and DD-co-carbazole and after protonation by 1.0 M MSA. 101

Figure 5.5. 2PA cross section spectra (red empty circles) and values (red solid circles) of DD polymers DD-co-phenyl, -thiophene, -dimethylfluorene, -BTH, -carbazole and the model cage compound $(Styryl)_2DD$. Corresponding molar extinction spectra (blue line) shown for comparison. 102

Figure 5.6. (a) The characteristic region of $\nu C \equiv N$ in FTIR spectra for DD-co-thiophene, -bithiophene, -thienothiophene mixing with 10 mol% F_4TCNQ and pristine F_4TCNQ. (b) normalized steady-state absorption of DD-co-bithiophene:F_4TCNQ 10 mol%, undoped DD-co-bithiophene, $F_4TCNQ^{\bullet-}$ and F_4TCNQ in CH_2Cl_2. 109

Figure 5.7. Normalized steady-state absorption and emission spectra of 2,5-$[(MeO)_2Sivinyl]_2$thiophene, DD-co-thiophene, Ladder-co-thiophene in CH_2Cl_2.[70]..... 111

Figure 6.1. Normalized steady-state absorption and emission spectra of 1,4-$[(MeO)_2Sivinyl]_2$benzene, DD-co-phenyl and LL-co-phenyl in CH_2Cl_2. 122

Figure 6.2. Normalized progressive emission spectra of 2,5-$[(MeO)_2Sivinyl]_2$thiophene, DD-co-thiophene, short (DP~3) and long (DP~7) LL-co-thiophene in CH_2Cl_2..... 124

Figure 6.3. FTIR of νCN region for pristine F_4TCNQ and mixture of LL-co-bithiophene:F_4TCNQ 10 mol%..... 125

Figure 6.4. Absorption spectra of undoped LL-co-bithiophene and LL-co-bithiophene: F_4TCNQ 10 mol%, F_4TCNQ and $F_4TCNQ^{\bullet-}$ shown for reference. 125

Figure 6.5. (a) Bromination and debromination of LL-co-phenyl. (b) Steady-state spectra in CH_2Cl_2. 126

Figure 7.1. (a) GPC of the product mixture of DD with thiophene (3:1 molar ratio), isolated DD-thiophene-DD via column chromatography and terpolymer of DD-thiophene-DD with biphenyl. (b) TGA of DD-thiophene-DD, terpolymer DD-thiophene-biphenyl, and copolymers of DD-co-biphenyl and DD-co-thiophene. 133

Figure 7.2. (a) Normalized absorption and emission of DD-thiophene-DD, mixture of DD:thiophene 3:1 and longer DD-co-thiophene (1:1). (b) Absorption and emission of terpolymer DD-Thio-DD-Biph and corresponding copolymers, DD-co-biphenyl and DD-co-thiophene. .. 136

Figure 8.1. Cyano-region in the FTIR of cyano-stilbene DD-co-biphenyl. 143

Figure 8.2. Normalized absorption and emission of cyano-stilbene hairy polymers synthesized by brominating DD-co-biphenyl (Scheme **8.2a**) and vinylDDvinyl (Scheme **8.2b**). 144

Figure 8.3. Novel SQ structures as probes for expanding structures wherein cage centered LUMOs form. 145

Figure 8.4. Absorption and emission of 4-NH_2Styrene (blue), (4-NH_2Styryl)DDvinyl (red) and (4-NH_2Styryl)$_2$DD. 148

Figure 8.5. (a) Structure of unsymmetrical DD compounds; (b) Uv-Vis for set of model compounds with moieties of different degrees of conjugation. 149

Figure A.1. MALDI-TOF of *o*-$Br_xPh_7T_8Me$. 151

Figure A.2. MALDI-TOF of *o*-$MeStil_xT_8Me$. 152

Figure A.3. MALDI-TOF of *o*-$CNStil_xT_8Me$. 153

Figure A.4. MALDI-TOF of *o*-$Br_xPh_7T_8Pr$. 153

Figure A.5. MALDI-TOF of *o*-$MeStil_xT_8Pr$. 154

Figure A.7. MALDI-TOF of *p*-$I_xPh_7T_8Me$. 155

Figure A.8. MALDI-TOF of *p*-$MeStil_xT_8Me$. 155

Figure A.9. MALDI-TOF of *p*-$CNStil_xT_8Me$. 156

Figure A.11. MALDI-TOF of *p*-$MeStil_xT_8Pr$. 157

Figure A.12. MALDI-TOF of *p*-$CNStil_xT_8Pr$. 157

Figure A.13. TGA of $Br_6Ph_7T_8Me$ and o-$RStil_6T_8Me$. 158

Figure A.14. TGA of $Br_7Ph_7T_8Pr$ and *o*-$RStil_xT_8Pr$. 158

Figure A.15. TGA of $I_7Ph_7T_8Me$ and *p*-$RStil_7T_8Me$. 159

Figure A.16. TGA of $I_7Ph_7T_8Pr$ and *p*-$RStil_7T_8Pr$. 159

Figure B.1. MALDI-TOF of *o*-Br_7DDMe_4. 161

Figure B.2. MALDI-TOF of *o*-MeStil$_7$DDMe$_4$. 162
Figure B.3. MALDI-TOF of *o*-CNStil$_8$DDMe$_4$. 162
Figure B.4. MALDI-TOF of *o*-Br$_7$DD(TMS)$_4$..... 163
Figure B.5. MALDI-TOF of *o*-MeStil$_7$DD(OTMS)$_4$. 163
Figure B.6. MALDI-TOF of *p*-MeStil$_2$Ph$_6$DD(OTMS)$_4$. 164
Figure B.7. TGA of *o*-Br$_7$DDMe$_4$ and *o*-RStil$_7$DDMe$_4$. 164
Figure B.8. TGA of *o*-RStil$_7$DD(OTMS)$_4$. 165
Figure C.1. ^{1}H NMR of 4,4''-[(MeO)$_2$Sivinyl]$_2$terphenyl. 167
Figure C.2. GPC of 3,6-[(MeO)$_2$Sivinyl]$_2$carbazole, 3,6-dibromocarbazole and vinylMeSi(OMe)$_2$. 167
Figure C.3. FTIR of 5,5'-[(MeO)$_2$Sivinyl]$_2$bithiophene and vinylMeSi(OMe)$_2$. 168
Figure C.4. ^{1}H NMR of pure *trans*-vinylDDvinyl. 170
Figure C.5. (a) ^{29}Si NMR of pure *trans*-vinylDDvinyl; (b) zoom-in. 171
Figure C.6. (a) ^{29}Si NMR of mixed cis-, *trans*-vinylDDvinyl; (b) zoom-in. 172
Figure C.7. GPC of vinylDDvinyl. 173
Figure C.8. GPC of DD-co-benzene. 173
Figure C.9. GPC of DD-co-biphenyl. 174
Figure C.10. GPC of DD-co-terphenyl. 174
Figure C.11. GPC of DD-co-stilbene..... 175
Figure C.12. GPC of DD-co-thiophene. 175
Figure C.14. GPC of DD-co-thienothiophene. 176
Figure C.15. GPC of DD-co-dimethylfluorene. 177
Figure C.16. GPC of DD-co-BTH. 177
Figure C.17. GPC of DD-co-carbazole. 178
Figure C.19. FTIR of DD-co-phenyl and (Styryl)$_2$DD. 179
Figure C.20. FTIR of DD-co-thiophene and (Thiophenevinyl)$_2$DD. 180
Figure C.21. FTIR of DD-co-dimethylfluorene and (Dimethylfluorenevinyl)$_2$DD. 180
Figure C.22. FTIR of Silane-end-capped DD. 181
Figure C.23. TGA of vinylDDvinyl. 181
Figure C.24. TGA of DD-co-phenyl, (Styryl)$_2$DD and (Styryl)$_3$DD. 182
Figure C.27. TGA of DD-co-bithiophene and DD-co-thienothiophene. 183

Figure C.28. TGA of DD-co-dimethylfluorene, (Dimethylfluorene)$_2$DD and (Dimethylfluorene)$_4$DD. 184

Figure C.29. TGA of DD-co-BTH and DD-co-carbazole. 184

Figure C.30. Normalized steady-state spectra of 2,7-[(MeO)$_2$Sivinyl]$_2$dimethylfluorene, DD-co-dimethylfluorene and (Dimethylfluorene)$_2$DD inserted with amplification of absorption shoulders around 389 nm. 185

Figure C.31. HOMO and LUMO modeling of vinylDDvinyl. 187

Figure C.32. HOMO and LUMO modeling of *trans*-vinylDDvinyl derived polymers DD-co-phenyl, -thiophene, -dimethylfluorene, -BTH and carbazole. 189

Figure C.33. Experimental absorption and emission spectra (blue) and modeling absorption spectra (grey) for *trans*-vinylDDvinyl and its derived polymers DD-co-phenyl, -thiophene, -dimethylfluorene, -BTH and -carbazole calculated at TD-CAM-B3LYP/6-31G(d) level of theory. 190

Figure C.34. Energy diagram of the molecular orbitals of vinylDDvinyl showing cage centered LUMO+4 and LUMO+5, calculated using PBE potentials as implemented in VASP. 191

Figure C.35. Energy diagram of the molecular orbitals of methyl substituted DD with two Si(O-)$_2$ unites per opposing edge showing cage centered LUMO and LUMO+1, calculated using PBE potentials as implemented in VASP. 192

Figure D.1. (a) ^{1}H NMR, (b) ^{13}C NMR, (c) ^{29}Si NMR of vinyl-LL(Me)-vinyl..... 195

Figure D.2. (a) ^{1}H NMR, (b) ^{13}C NMR, (c) ^{29}Si NMR of vinyl-LL(Ph)-vinyl..... 196

Figure D.3. Left: (a) Raw MALDI-TOF of vinyl-LL(Me)-vinyl, (b) Modified MALDI-TOF of vinyl-LL(Me)-vinyl, (c) Modified MALDI-TOF of vinyl-LL(Ph)-vinyl. Right: (a) Raw MALDI-TOF of LL(Me)-co-phenyl, (b) Modified MALDI-TOF of LL(Me)-co-phenyl, (c) Modified MALDI-TOF of LL(Ph)-co-phenyl. 197

Figure D.4. (a) TGA of vinyl-LL(Me)-vinyl and vinyl-LL(Ph)-vinyl, (b) TGA of LL(Me)-co-terphenyl and LL(Ph)-co-phenyl..... 198

Figure D.5. FTIR of vinyl-LL(Me)-vinyl and vinyl-LL(Ph)-vinyl..... 199

Figure D.6. FTIR of LL(Me)-co-phenyl and LL(Ph)-co-phenyl. 199

Figure D.7. (a) ^{1}H NMR, (b) ^{13}C NMR of LL(Me)-co-terphenyl..... 201

Figure D.8. (a) ^{1}H NMR, (b) ^{13}C NMR of LL(Me)-co-thiophene. 202

Figure D.9. Normalized steady-state spectra of 4,4'-[(MeO)$_2$Sivinyl]$_2$biphenyl, DD-co-biphenyl and LL(Me/Ph)-co-biphenyl in CH_2Cl_2. 203

Figure D.10. Normalized steady-state spectra of 4,4''-[(MeO)$_2$Sivinyl]$_2$terphenyl, DD-co-terphenyl and LL(Me/Ph)-co-terphenyl in CH_2Cl_2. 204

Figure D.11. Normalized steady-state spectra of 4,4'-[(MeO)$_2$Sivinyl]$_2$stilbene, DD-co-stilbene and LL(Me/Ph)-co-stilbene in CH_2Cl_2..... 205

Figure D.12. Normalized steady-state spectra of 2,7-[$(MeO)_2$Sivinyl]$_2$dimethylfluorene, DD-co-dimethylfluorene and LL(Me/Ph)-co-dimethylfluorene in CH_2Cl_2. 206

Figure D.13. Normalized steady-state spectra of 5,5'-[$(MeO)_2$Sivinyl]$_2$bithiophene, DD-co-bithiophene and LL(Me/Ph)-co-bithiophene in CH_2Cl_2. 207

Figure D.14. Normalized steady-state spectra of 2,5-[$(MeO)_2$Sivinyl]$_2$thienothiophene, DD-co-thienothiophene and LL(Me/Ph)-co-thienothiophene in CH_2Cl_2. 208

Figure D.15. GPC of vinyl-LL-vinyl, short oligomers of LL-co-thiophene separate from TLC and long oligomers of LL-co-thiophene. 208

Figure D.16. GPC of vinyl-LL-vinyl, short oligomers of LL-co-biphenyl separate from TLC and long oligomers of LL-co-biphenyl. 209

Figure D.17. Normalized progressive emission spectra of 4,4'-[$(MeO)_2$Sivinyl]$_2$biphenyl, DD-co-biphenyl, short (DP~3) and long (DP~8) LL-co-biphenyl in CH_2Cl_2. 209

Figure D.18. ^{13}C NMR of LL-co-phenyl (zoom-in). 210

Figure D.19. ^{13}C NMR of brominated LL-co-phenyl (zoom-in). 210

Figure D.20. Bromination and debromination of DD-co-phenyl. 211

Figure D.21. ^{29}Si NMR of DD-co-phenyl. 211

Figure D.22. ^{29}Si NMR of brominated DD-co-phenyl. 212

Figure D.23. ^{13}C NMR of DD-co-phenyl (zoom-in). 212

Figure D.24. ^{13}C NMR of brominated DD-co-phenyl (zoom-in). 213

Figure D.25. Steady-state spectra of DD-co-phenyl, brominated and debrominated DD-co-phenyl in CH_2Cl_2. 213

Figure D.26. (a) boat conformation of *trans*-vinyl-LL(Me)-vinyl, (b) chair conformation, calculated at B3LYP/6-31G(d,p) level. 215

Figure D.27. Energy diagram of the molecular orbitals of methyl substituted vinyl-LL(Me)-vinyl. 215

Figure D.28. Energy diagram of the molecular orbitals of vinyl-LL(Me)-vinyl. 216

Figure E.1. MALDI of DD-thiophene-DD/Ag^+. 217

Figure E.2. MALDI of DD-bithiophene-DD/H^+ (2574 m/z) and DD-bithiophene-DD/Ag^+(2682 m/z). 218

Figure E.3. MALDI of DD-thienothiophene-DD/Ag^+. 218

Figure E.4. MALDI of terpolymer DD-thiophene-terphenyl/Ag^+. 219

Figure E.5. (a)^{1}H NMR of DD-thiophene-DD. (b) ^{13}C NMR in $CDCl_3$. 221

Figure E.6. (a) ^{1}H NMR of DD-Thio-DD-Biph. (b) ^{13}C NMR in $CDCl_3$. 222

Figure E.7. FTIR of DD-thiophene-DD/H^+ (red) and terpolymer DD-Thio-DD-Biph (green). 223

Figure E.8. Emission of terpolymer DD-Thio-DD-Biph exited at 315 nm (Abs. λmax. of DD-co-biphenyl) and 345 nm (Abs. λmax. of DD-co-thiophene). 223

Figure E.9. (a) Normalized absorption and emission of terpolymer DD-Thio-DD-Terph. (b) Emission excited at 325 and 340 nm. 224

Figure E.10. (a) Normalized absorption and emission of terpolymer DD-Thio-DD-Stil. (b) Emission excited at 340 and 360 nm. 225

Figure E.11. Normalized absorption and emission of DD-bithiophene-DD, mixture of DD:bithiophene 3:1 and longer DD-co-bithiophene..... 226

Figure E.12. Normalized absorption and emission of DD-thienothiophene-DD, mixture of DD:thienothiophene 3:1 and longer DD-co-thienothiophene (DP~5). 226

Figure E.13. (a) Normalized absorption and emission of terpolymer DD-Ththio-DD-Biph. (b) Emission excited at 315 and 360 nm. 227

Figure F.1. GPC of the starting DD-co-biphenyl..... 228

Figure F.2. GPC of the self-bromination of DD-co-biphenyl after 2 h. 229

Figure F.3. GPC of the brominated DD-co-biphenyl (Br_9DD-co-biphenyl). 229

Figure F.4. GPC of the zinc debrominated DD-co-biphenyl (Br_5DD-co-biphenyl)..... 229

Figure F.5. GPC of CN$Stil_5$DD-co-biphenyl. 230

Figure F.6. TGA of the starting DD-co-biphenyl, Br_9DD-co-biphenyl, Br_5DD-co-biphenyl and CN$Stil_5$DD-co-biphenyl. 230

Figure F.7. Normalized steady-state spectra of the starting DD-co-biphenyl, Br_9DD-co-biphenyl, Br_5DD-co-biphenyl and CN$Stil_5$DD-co-biphenyl..... 231

Figure F.8. GPC of the starting vinylDDvinyl..... 232

Figure F.9. GPC of the brominated DD (Br_{12}DD)..... 232

Figure F.10. GPC of the Heck cross-coupled DD (CN$Stil_8Br_4$DD). 232

Figure F.11. GPC of the debrominated DD (CN$Stil_8$vinylDDvinyl)..... 233

Figure F.12. GPC of CN$Stil_8$DD-co-biphenyl (Heck polymerization)..... 233

Figure F.13. TGA of Br_{12}DD (brominated vinylDDvinyl), CN$Stil_8Br_4$DD, CN$Stil_8$vinylDDvinyl and CN$Stil_8$DD-co-biphenyl. 234

Figure F.14. Normalized steady-state spectra of CN$Stil_8Br_4$DD, CN$Stil_8$vinylDDvinyl and CN$Stil_8$DDMe_4 in CH_2Cl_2. 234

List of Appendices

Appendix A. Characterization of Partially Functionalized Phenylsilsesquioxane: $[RSiO_{1.5}]_7[Me/nPrSiO_{1.5}]$ and $[RSiO_{1.5}]_7[O_{0.5}SiMe_3]_3$ (R = 4-Me/4-CN-Stilbene) 151

Appendix B. Characterization of Partially Functionalized Double Decker Phenylsilsesquioxane Macromonomers: $[PhSiO_{1.5}]_8[O0.5SiMe_2]_2$ and $[PhSiO_{1.5}]_8[O_{0.5}SiMe_3]_4$..... 161

Appendix C. Unconventional Conjugation via Siloxane Bridges May Imbue Semiconducting Properties in Double Decker Copolymers 166

Appendix D. Unconventional Conjugation Siloxane Bridges in Ladder Silsesquioxane Copolymers 194

Appendix E. Double Decker Derived Alternating Terpolymers Give Excited-state Conjugation Averaging that of the Corresponding Co-polymers. 217

Appendix F. Double Decker Silsesquioxane Derived Hairy Polymers 228

Abstract

Completely condensed polyhedral silsesquioxanes (SQs), $[RSiO_{1.5}]_{8,10,12}$, appended with organic conjugated chromophores can offer high symmetry, high thermal stability, highly red-shifted emissions and charge separation compared with the free chromophores, indicating unconventional conjugation in the excited state and involving the SQ cages. This dissertation presents the synthesis and characterization of unsymmetrical and incomplete SQ cages with organic chromophores as well as the SQ-based organic-inorganic hybrid polymers/oligomers with emphasis on the mapping structure-property relationships and understanding their unique photophysical properties for potential uses in optoelectrical devices.

First, this dissertation describes the synthesis of corner-modified, corner-missing, double decker closed and open SQs via silylation of the respective silanol phenyl-SQ precursors. Subsequent iodination/bromination of the phenyl groups on the cages and then Heck coupling of the halogenated derivatives provides stilbene-functionalized SQs where stilbene is a model for conjugated chromophore.

Open SQ cages with ~7 stilbene groups display essentially the same fluoresce behavior as found for symmetric closed octa-stilbene functionalized SQs, with absorption ~300 nm and emission ~410 nm. The red-shifts of ~60 nm in emission relative to the free chromophores demonstrate excited-state electronic communication between the π^* orbitals of the stilbenes and through the cages, which indicates removing a corner or breaking two opposing bridges has little effect on LUMO formation. Interestingly, when the cages have only 2 stilbenes attached, they show similar absorption and emission to stilbene itself; however, with quite high luminescence quantum yields ($\geq$0.7 vs. $\approx$ 0.07) proving that there is a threshold for the excited state conjugation to occur but also demonstrating that the cage does affect photophysical properties nonetheless.

Organic-inorganic hybrid polymers with SQs in the main chain are prepared via Heck cross coupling of di-vinyl functionalized double decker vinylMeSiO$[PhSiO_{1.5}]_8$OSiMevinyl and ladder vinylMeSiO$[PhSiO_{1.5}]_4$OSiMevinyl SQs with dibromo-aromatic tethers. Double decker SQ-based polymers/oligomers show red-shifted emission from model bis-dimethoxysilyldivinyl-aryl

analogs in the range of 50-120 nm, again supporting the electronic communication along the polymer chain through the SQ cage in the excited state, even with two -$(O)_2$Si siloxane bridges.

Coincidentally, the non-cage ladder SQs derived polymers/oligomers exhibit even further red-shifted emission beyond analogous double decker polymers in the range of 20-50 nm, even with shorter chain lengths, suggesting more efficient electronic interaction in ladders. In both systems, copolymers with biphenyl, terphenyl and stilbene display high photoluminescent quantum yields up to 0.8, suggesting potential emitting components in optoelectronic devices.

Double decker derived terpolymers are synthesized with alternating biphenyl and thiophene linkers via stepwise Heck cross-coupling with the goal of shifting emission wavelengths to towards the visible coincident with high quantum yields. The resulting terpolymers display emissions at 430 nm, intermediate between those of the respective copolymers rather than emission from both units as would be expected from physical mixtures. This again provides further evidence for excited-state conjugation along polymer chains and through cages via disiloxane conjugated linkers.

In addition, the quantum yields of the terpolymers DD-thiophene-DD terphenyl and DD-thiophene-DD-stilbene improve from 0.09 for the DD-co-thiophene copolymer to 0.20 and 0.24 respectively, providing successful examples of novel combination of improved quantum yields as well as longer-wavelength emission around 480 nm and new opportunities to tailor photophysical properties by modifying structures. Lastly, ‘hairy polymers’ are prepared via further functionalization of halogenated phenyl groups to stilbenes on the SQ cages in the main chain of hybrid polymers to explore possible 3-dimentional conjugation.

Chapter 1. Introduction

1.1 Project goals and objectives

Polyhedral oligosilsesquioxanes offer multiple unique properties and have gained increasing attention over the past 30 years.[1–10] These compounds can be viewed as the hybrid organic-inorganic materials with silicon and oxygen atoms as inorganic cage-like frameworks decorated with organic substituents in three dimensional arrangements. These hybrid materials display novel properties arising from the combination of these two components, including a robust nature from the inorganic frameworks and multiply and selective functionalization of the organic groups at 1-3 nm length scales.

Recently, it was found that completely condensed silsesquioxanes decorated with chromophores can interact electronically with conjugated organic substituents in the excited state as evidenced by red-shifted emissions with respect to the individual chromophores. Detailed experimental and computational studies of the mechanisms behind such unconventional conjugation suggest cage-centered LUMOs. The objectives of the work described in this dissertation are to explore the formation of possible LUMOs in various cage architectures to map structure-property relationships and develop facile and effective routes to tailor their properties by simple modifications for different applications.

1.2 Definitions, structures and nomenclatures of silsesquioxanes

The term "silsesquioxane (SQ)" refers to a class of Si-O based material with the empirical chemical formula, $[(RSiO_{1.5})_n]$, where R can be hydrogen, halogens, or various organic groups such as alkyl, alkylene, aryl, arylene, or siloxy groups.[7] The term can be broken up into four parts: sil- (silicon), -sesqui- (one and a half), -ox- (oxygen), and -ane (hydrocarbon R group), which self-indicates the 1.5 ratio of the silicon to oxygen atoms. As a result of their unique structures, silsesquioxanes have been found to offer novel properties, including high thermal stabilities, oxidation resistance, non-flammability and hydrophobicity, etc.

Silsesquioxane based materials have been used in various applications such as components in polymer nanocomposites, catalysts, models for silica surfaces and heterogeneous catalysts, low-k

dielectrics, antimicrobial agents, emissive layers in organic light-emitting diodes (OLEDs) and coatings.[1,8–24]

In general, silsesquioxanes can be prepared via acid or base-catalyzed hydrolysis and condensation of trifunctional organosilanes, where the functional group X = -Cl, -OH, -OCH_3 or -OCH_2CH_3 as shown in Scheme **1.1**. The synthetic process is easily influenced by multiple experimental factors, such as the nature of R group, X group, the pH, solvent, concentration of starting organosilanes, addition rate and quantity of H_2O, reaction time, solubility of the product, etc.[25] So far, a suitable kinetic mechanism has yet to be developed for the complex synthetic process, hence no universal protocols have been established. However, the reaction conditions can be tailored to favor the formation of specific silsesquioxanes, which results in many published papers and patents in recent years.[1,3,4,7,26,27]

It is generally found that formation of discrete molecular species is favored at lower concentrations, due to lower rates of hydrolysis and hence higher possibilities for intramolecular reactions, while polymeric structures form more readily at higher concentrations. Most of the commercial activity concerning silsesquioxanes, based on the number of patents, has occurred in three countries, Japan, United States and Russia. The structures of the final products are interdependent on the abovementioned reaction conditions and Figure **1.1** below, which shows the structures of silsesquioxanes known in literature.[7,25]

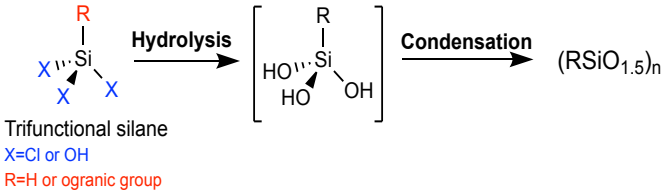

Scheme 1.1. Acid or base-catalyzed hydrolysis and condensation of trifunctional silane.

Random structured silsesquioxanes are polymeric and without long-range order[28] and are primarily used as coatings or encapsulants in many applications. In contrast, ladder structures, an oligomeric form of silsesquioxanes, display regular and recurring structural fragments.[7]

The name ladder is self-explanatory, indicating the construction of double-stranded polymers, where the two lateral Si-O-Si chains were connected by the O 'rung'.[29] The synthesis of the first tricyclic ladder silsesquioxanes was reported by Brown in 1965[30] and the synthesis of the first bicyclic ladder was reported by Shklover in 1980.[31] Since then, many groups have attempted to

develop synthetic routes as well as the characterization methods for pentacyclic, heptacyclic and even nonacyclic ladder silsesquioxanes.[32] Due to steric repulsion of the substituents and the flexible nature of Si-O-Si framework, ladder silsesquioxanes all display intriguing helical structures.[32]

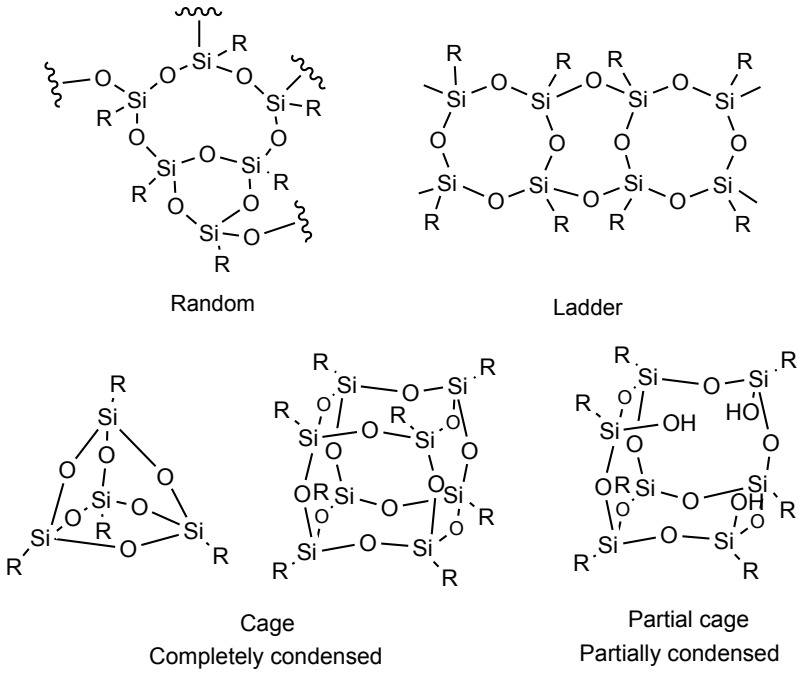

Figure 1.1. Representative structures of silsesquioxanes.

Figure **1.2** illustrates the torsion angles of all-isopropyl ladders SQs.[33] In general, larger angles suggest tighter helical structures and angles of 0° indicate the absence of helicity. The torsion angles of anti-ladder SQs depicted in Figure **1.2** increase up to tricyclic structures while no helicity is shown in the pentacyclic ladder SQs due to the center of symmetry. In the case of all-anti ladder polysiloxanes, helical structures were also observed in the crystal structures.[32,33]

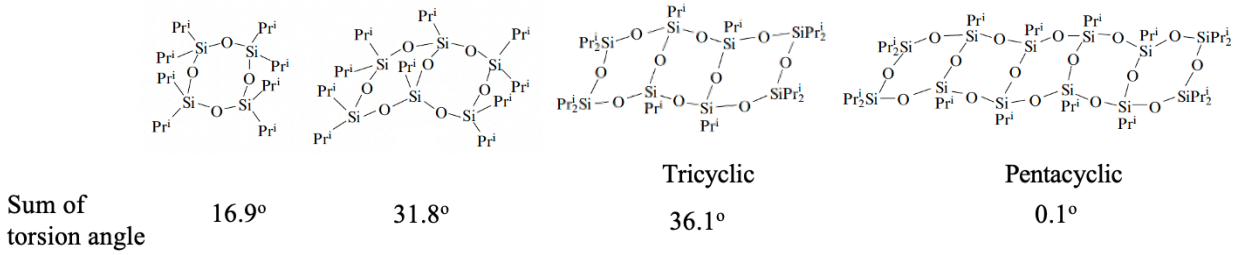

Figure 1.2. Torsion angles of all-isopropyl ladder silsesquioxanes.

Cage silsesquioxanes are completely condensed, closed molecules with an even number n in the empirical chemical formula [$(RSiO_{1.5})_n$]. The smallest existing frame of a cage silsesquioxane

is when n = 4 in Figure **1.1**, while an example of one of the largest cages with n = 18, was obtained by the Calzaferri group in 1990.[34]

These compounds are often called polyhedral oligomeric silsesquioxanes or "POSS" trademarked by Hybrid Plastics, Inc. They possess well-defined, 3-dimensional nano-structures with high degrees of symmetry, robust natures as well as many other interesting properties, as discussed further in this chapter.[7]

Partial cage structures are defined as incompletely condensed cages containing one or more free Si-OH silanol groups. They can serve as important precursors for preparing more complicated silsesquioxane systems via condensation reactions. One interesting group of partial cage silsesquioxanes is the double-decker silsesquioxane, a new efficient synthesis of which was discovered by the Yoshida group just over a decade ago as shown in Scheme **1.2**.[35] Other synthetic methods, current chemistries and applications of this structure are discussed further just below.

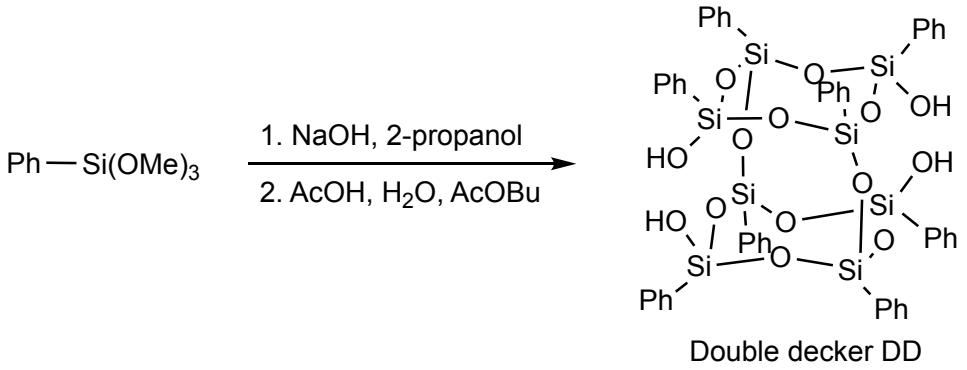

Scheme 1.2. The structure and synthetic route to the tetrasilanol double decker phenylsilsesquioxanes.

Nomenclature conventions for silsesquioxanes are as follows. The IPUAC naming rules are complicated and thus not commonly used. Sometimes silsesquioxanes are called spherosiloxanes since these cage structures can be considered to be topologically equivalent to spheres.[2] Silsesquioxanes are more commonly named using a systematic nomenclature similar to polymer repeat units, indicating the substituents on the silicon atoms and the number of silsesquioxane units ($SiO_{1.5}$) in the molecule. As an example, $[PhSiO_{1.5}]_8$ or octaphenylsilsesquioxane, suggests phenyl groups attached to the silicon atoms sitting at the corners of an octameric cage.

Shorthand notations have also been developed and are used commonly in siloxane chemistry,[7] see Figure **1.3**. Letters are used to demote the types of silicon and numerical subscripts are used to denote the number of these silicon. Optional subscripts can be used to the type of functional groups

attached. An "M" unit is referred to a silicon bonded to one oxygen atom, a "D" unit consists of a silicon atom bound to two oxygens, a "T" unit silicon is bonded to three oxygen atoms and a 'Q' unit has a silicon atom bound to four oxygens. Thus, the example earlier, octaphenylsislsesquioxane would be denoted as Ph_8T_8, with the substituent R group before the description letter.

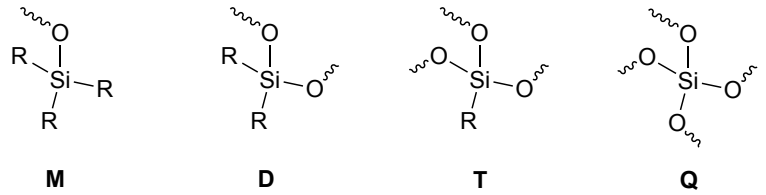

Figure 1.3. Silsesquioxane nomenclature.

1.3 Completely condensed silsesquioxanes

1.3.1 Octa-, deca- and dodeca- polyhedral oligomeric silsesquioxanes

Among all cage silsesquioxanes, the cubic T_8 structure has been studied extensively due to its ease of synthesis, cubic symmetry (O_h), a well-defined 3-dimensonal nanostructure to which functional groups can be attached such that they occupy each octant in Cartesian space. Synthetic routes providing high yields at reasonable quantities have been described.[36–38] Efficient synthetic strategies for T_{10} and T_{12} have been discovered recently, such as the fluoride ion catalyzed rearrangement of T_8 cages, "T"-resins, or directly from $RSi(OEt)_3$ in THF (tetrahydrofuran), which can provide essentially quantitative conversion to mixtures of T_{10} and T_{12} with a statistically controlled distribution of functionalities.[39-41] This synthetic method is attractive because the random-structured precursors can be used for fluoride-mediated rearrangement reactions, which can be significant byproducts of syntheses of the related T_8 octamers.[39-41]

The T_{10} is comprised of two distorted-pentagonal cyclosiloxane rings stacked on top of one another and connected by oxygen atoms, offering D_{5h} symmetry. The T_{12} contains four distorted-pentagonal faces and four distorted square-triangular faces and can have multiple possible symmetries, D_{2d} and D_{6h}, with D_{2d} being the most common as indicated by crystallographic analysis.[39–41] These two cage structures allow larger numbers of functional groups than T_8 in the same nanometer scale. In addition, T_{10} and T_{12} may offer improved solubility and processability.[39–41] All complete cage structures are shown in Figure **1.4**.

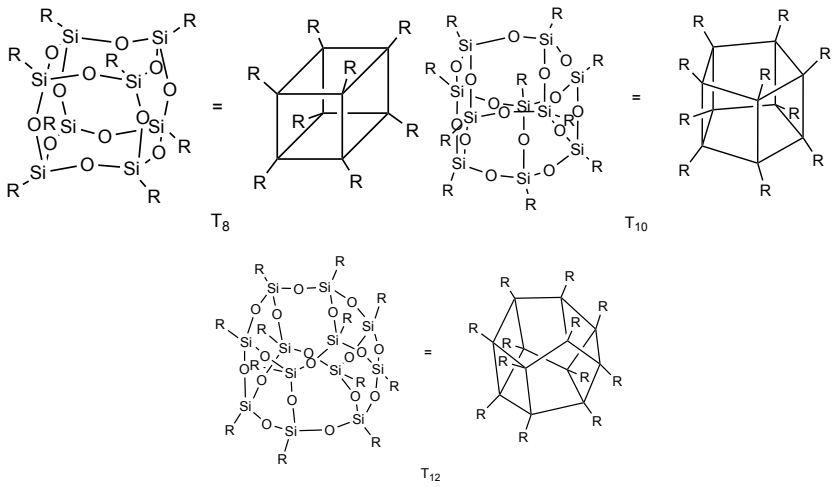

Figure 1.4. Structures of $T_{8,10,12}$ condensed cage silsesquioxanes.

The properties required for candidates for nanobuilding blocks are as follows: nanometer dimensions, high degrees of symmetry and the potential to add multiple functionalities. Nanosized building blocks can be expected to allow assembly of materials at the finest length scales. The high degree of symmetry can help decrease the introduction of defects during assembly since lower energy will be required for realignment of misaligned components with high symmetry.

It is also important to be able to append multiple functionalities since it these can be essential in bonding with adjacent components to anchor them permanently providing easy access to assembling new materials nm by nm. In addition, the functionalities should also be tunable and easily tailored for different purposes. Due to the abovementioned properties, completely condensed silsesquioxanes, $T_{8,10,12}$ can be outstanding candidates as nanobuilding blocks especially T_8 cages offering cubic symmetry and consisting of orthogonal functional groups localized in separate octants in Cartesian space as shown in Figure **1.5**. Furthermore, the rigid core can be considered as a single silica crystal. Consequently, inorganic-organic hybrid cage silsesquioxanes have a much more robust nature compared to organic-only materials, with high thermal stabilities, oxidation resistance and low flammability.[3–5,42,43]

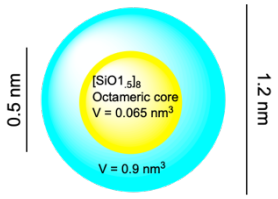

Figure 1.5. Typical sizes and volume of a T_8 silsesquioxane molecule.

1.3.2 Octaphenylsilsesquioxane

Octaphenylsilsesquioxane (OPS) was first synthesized by Olsson in 1958, by hydrolysis of phenylchlorosilane ($PhSiCl_3$) in refluxing methanol catalyzed by aqueous HCl. However, the yield was only 9%. A number of groups have spent considerable time optimizing OPS reaction synthesis conditions ever since.[27,44,45] Our group was able to improve yields to > 90%[46] by modifying Brown's synthetic method.[47] The two-step synthesis involves first ethanolysis of commercially available $PhSiCl_3$, followed by hydrolysis and condensation in toluene [either $PhSi(OEt)_3$ or oligomers based on the reaction conditions], using catalytic amounts of KOH using H_2O starved conditions.

OPS is obtained as a microcrystalline, white powder with very high thermal stability (up 500 ^oC in air).[6] However, its utility in the synthesis of nanocomposites is limited due to the fact that it decomposes before melting and is poorly soluble in common organic solvents. The solubility and reactivity can be improved thereby improving the utility of OPS by functionalizing the phenyl rings.

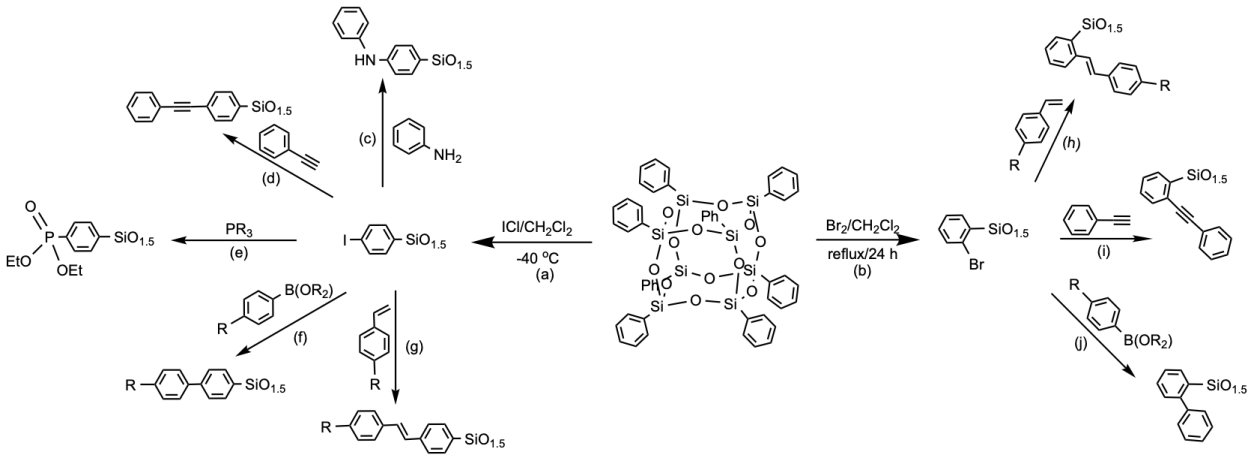

Scheme 1.3. Functionalization of octaphenylsilsesquioxane OPS: (a) iodination, (b) bromination, (c) Buchwald-Hartwig, (d and i) Sonogashira, (f and j) Suzuki, (g and h) Heck cross-coupling reaction.

Multiple publications have reported examples of reactions functionalize phenyl groups, especially electrophilic aromatic substitution.[37,48–51] Halogenation followed by catalytic cross-coupling using Suzuki, Sonagashira and Heck methods,[3,52–55] has become a primary route, see Scheme **1.3**. For instance, iodination of OPS is easily affected using iodine monochloride (ICl) in

dichloromethane at -40 °C in dry-ice bath.[36] The para-substituted iodinated OPS preserves the cubic symmetry of the parent OPS material and is highly soluble in common solvents.[36,50]

1.3.3 Iodination and bromination of phenylsilsesquioxanes

A paper by Feher and Budzichowski reports finding silsesquioxane cages offer strong electron-withdrawing characteristics equivalent to a trifluoromethyl (-CF_3) group according to the ^{13}C NMR chemical shift data,[26] which should lead to electrophilic substitution at the meta position of the phenyl rings attached at the cage corners.

Surprisingly, our group found that iodination and bromination of phenyl silsesquioxanes without catalyst favor para and ortho substituted products respectively.[36,56] Even though we have yet to identify the mechanism behind para-iodination, the modeling of ortho-bromination done by the Kieffer group using first-principles calculations identified the formation of cage centered LUMOs that extend out of the cage faces as shown in Figure **1.6**,[56] and can interact with the incoming Br_2 via hydrogen bonding to the phenyl ortho-hydrogen.

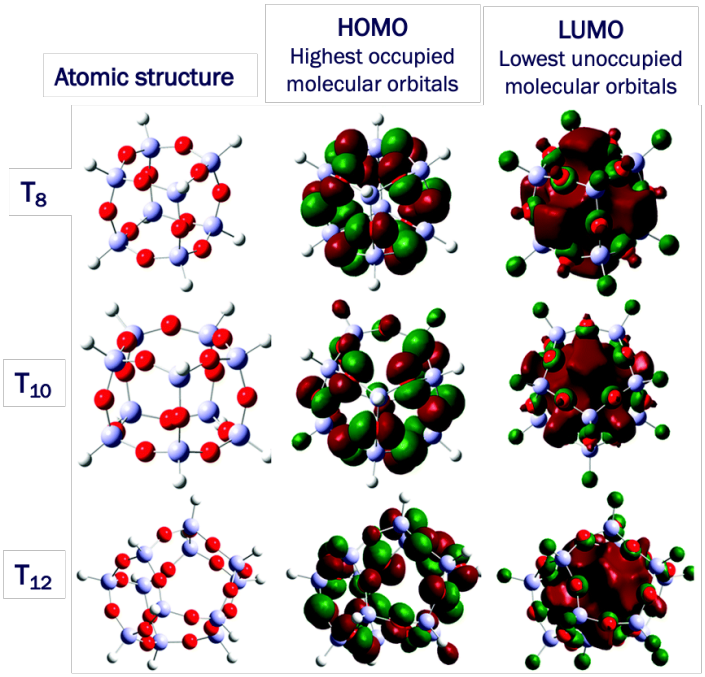

Figure 1.6. Atomic structures and electron density isocontours of $T_{8,10,12}$ silsesquioxanes.

Since our original work in this area, it appears that the cage-centered LUMOs seem to form often in SQ cages, they have also been found in germasesquioxane cages.[57] The generality of cage-localized LUMOs is a focus of this dissertation.

The iodination of phenyl $T_{8,10,12}$ cages is exclusively > 90% para.[36] However, without a catalyst, they brominate selectively at the ortho position. The ortho selectivity of phenyl $T_{8,10,12}$ is 85%, 70% and 60% due to the fact that the angle/separation between adjacent phenyls on the cage decreases from 90°, 72° and 60° as the cage size increases; thus, reducing Br_2 access to the cage face and coincidentally the ortho hydrogens.[56] Furthermore, the fact that the bromination of OPS occurs in dilute dichloromethane without catalyst was also surprising since uncatalyzed bromination of phenyl groups has only been reported to occur with active aromatic systems such as anisoles and phenols.[58] Finally, if an iron catalyst is used, bromination occurs para.[48]

One of the special properties arising from functionalization of halogenated cages via catalytic crosscoupling reactions and the presence of cage centered LUMOs is the apparent 3-D conjugation with the appended conjugated organics.

On adding conjugated chromophores to silsesquioxane cages, we find unexpected photophysical properties, Our initial studies used stilbene derivatives as model compounds for these studies.[52,53] Red-shifted emissions of 60-100 nm were observed in various stilbene-functionalized T_8 cages with respect to free stilbene, which can be considered as an indication of semiconducting behavior. Modeling also supports electronic communication between stilbene π^* orbitals and cage-centered LUMOs in the exited state.[52,53] Since rigid silsesquioxanes can be decorated with organic chromophores in all dimensions and exhibit the rare observation of 3-D conjugation and semiconducting properties, they point to new opportunities as tunable highly absorbing/emitting, light harvesting materials.

The synthetic methods outline above can also be used to prepare stilbene functionalized silsesquioxanes with partial and open cage structures as discussed in Chapter **3** and **4**.

1.4 Incompletely Condensed Silsesquioxanes

Incompletely condensed silsesquioxanes possess one or more free Si-OH groups and are very useful as building blocks for silsesquioxane-based network solids,[59,60] precursors to silsesquioxane-containing polymers,[61,62] and silica-supported catalyst,[59] etc. In 1997, Feher and co-workers developed practical procedures for preparing incomplete condensed frameworks via the controlled cleavage of completely condensed polyhedral silsesquioxane frameworks under both acidic and basic conditions.[59] Motived by this result, various groups have devised facile syntheses of different incompletely condensed silsesquioxanes from completely condensed structures. Examples are shown in Scheme **1.4**.

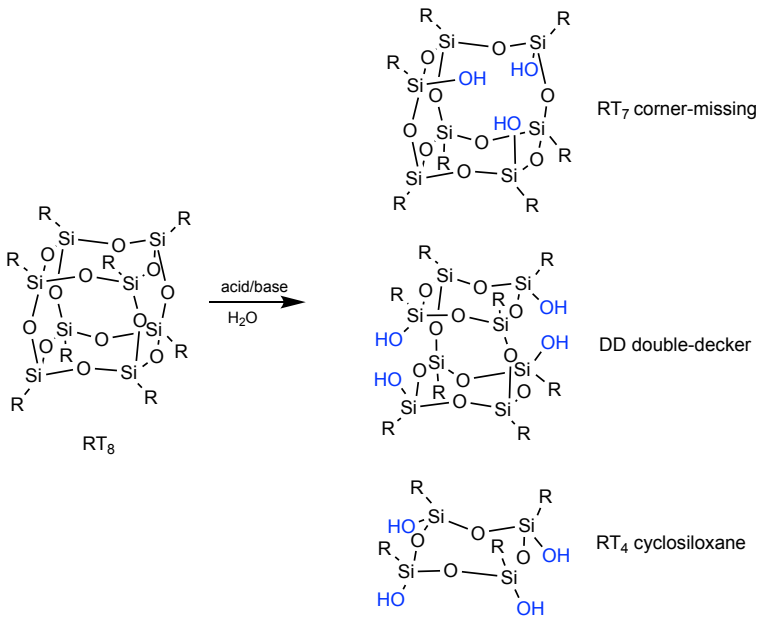

Scheme 1.4 Synthesis of incompletely condensed silsesquioxane derivatives via the hydrolysis of completely condensed silsesquioxanes.

1.4.1 Double decker silsesquioxanes

The facile synthetic method and the common name for this double deckers (DDs) structure was reported by Yoshida's group.[63] The double decker structure is different from T_8 with cubic symmetry. This open cage consists of two stacked phenylcyclosiloxane ring "decks". These rings are joined by two oxygen bridges. The intermediate tetrasilanol double decker silsesquioxanes can be modified easily by reaction with mono- or dichlorosilanes, giving access to di- or tetra-functional DDs as illustrated in Scheme **1.5**.[62,64] The di- and tetra-functional double decker SQs can be obtained in high yield and can serve as precursors for further modification.[28]

Before the advent of DD silsesquioxanes, the majority of cage silsesquioxanes did not offer cis- and trans-isomeric structures.[5,65,66] However, a few earlier studies characterized unexpected formation of geometrical cis- and trans-isomers resulting from different orientations of R and R' groups with respect to the Si-O cage core in Scheme **1.5**.

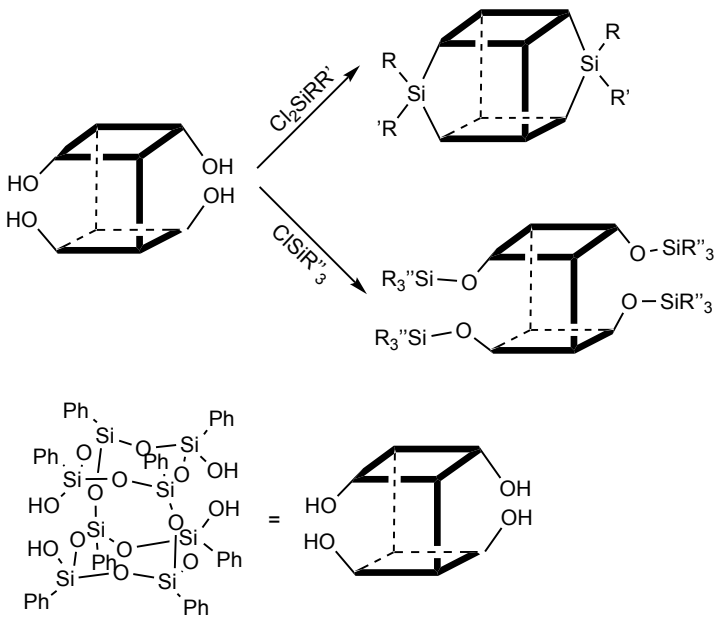

Scheme 1.5. Reaction routes to di- and tetra-functional double decker silsesquioxanes.

The two DD isomers are very similar in many respects best distinguished by ^{29}Si NMR spectra.[67,68] Lee's group has reported several examples of successful separation of cis- and trans-isomers derived from DD silsesquioxanes via skillful selection of solvents depending on solubility differences between these isomers and fractional crystallization.[69,70]

1.4.2 Silsesquioxane-based polymers

A number of groups have investigated the synthesis and characterization of silsesquioxane-based polymers as a method of modifying existing polymeric materials.[71–80] Silsesquioxanes are found to improve the properties of polymers in many useful ways, such as improved thermal stability, lower dielectric constants and low flammability.[2,4,28] General ways to incorporate silsesquioxanes into polymers to form hybrid materials and nanocomposites are as follows:

1. Copolymerization of silsesquioxanes and organic monomers with the same or similar functional groups. Silsesquioxanes can be incorporated as pendant groups, terminal groups or cross-linkers based on the number of reactive functional groups.
2. Polymerization of organic monomers in the presence of inert silsesquioxanes, such as alkyl decorated silsesquioxanes. In this way silsesquioxanes can be blended in the polymeric matrix providing they show some degree of miscibility.
3. Direct cross-linking between silsesquioxane functional groups without co-polymerization to form a 3-dimensional network structure.[28]

Depending on the reaction conditions, silsesquioxanes can form either well-dispersed or aggregated phases in the hybrid polymers and nanocomposites, which in turn affects many physicochemical properties of the final materials. Di-functional DD silsesquioxanes give easy access to copolymers with silsesquioxanes embedded in the main chain and tetra-functionalized DD silsesquioxanes will form cross-linked networks as shown in Scheme **1.6**.

In either case, DD silsesquioxanes are dispersed at a molecular level and can be considered as building blocks of hybrid polymers, which predominantly affect the physicochemical characteristics of the resulting materials.[28]

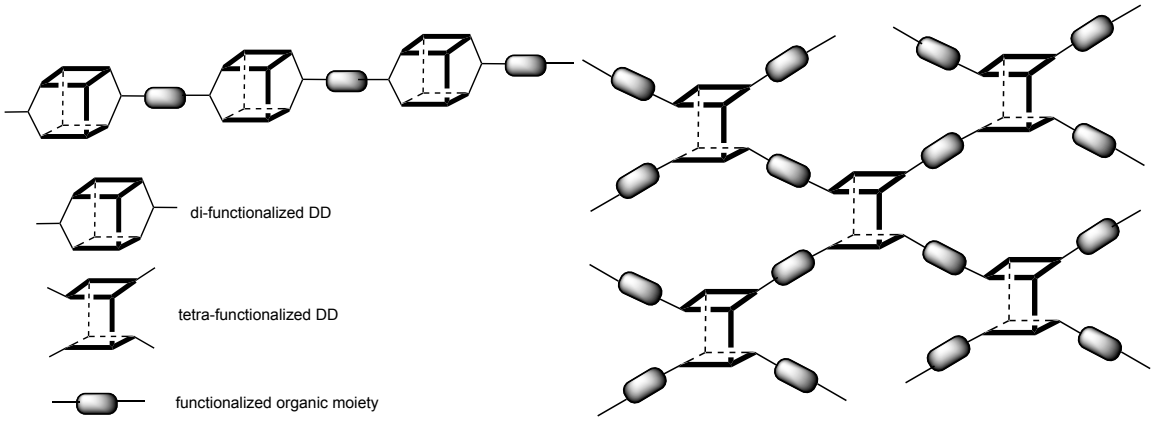

Scheme 1.6. Di- and tetra-functional double decker silsesquioxanes derived copolymers.

1.5 Ladder silsesquioxanes

Ladder silsesquioxanes, also called ladder siloxanes, are comprised of highly ordered, double-chain structures and can be considered as intermediate between polyhedral silsesquioxanes and single-chain linear siloxanes. They have attracted increasing research attention due to their excellent physiochemical properties such as high thermal stability, low dielectric constant, hydrophobicity,[81] and good film-forming properties.[81,82,83]

The regularity of the backbone of ladder-type silsesquioxanes depends greatly on the reaction conditions as well as the nature of the substituent at the Si atom.[84] Generally the number of structural defects increases with increasing molecular weight until random structures form.[85] A few synthetic protocols have been developed recently to ensure the backbone consists of double strands of Si and O atoms.[86,87] Thus, precursors with weak supramolecular interactions (H-bonding, $\pi - \pi$ stacking, etc.) between silanol and/or template molecules favor the synthesis of well-defined ladder silsesquioxanes via stepwise coupling and polycondesation.[86]

In this way, soluble ladder phenyl-silsesquioxanes with triple and even quadruple rings have been successfully prepared. [86,88–90] Another method of synthesizing linear ladder silsesquioxanes is via condensation of di-siloxanes $[RSiX_2]_2O$ and cyclotetrasiloxanes $[RXSiO]_4$, where R = Me, Ph and X = H, OEt, NCO.[91] Condensation polymerization of cis-trans-cis or all-cis of cyclic isocyanates with disilanols[92] or polymerization of tetrasilanols[93] can yield linear polymers with defined tacticity and high regularity. A series of ladder silsesquioxanes was reported by the Unno group using stepwise stereo-controlled condensation of cyclosilanols with chlorosilanes, including bi-, tri-, tetra- and pentacyclic ladder silsesquioxanes with an all-anti conformation, nonacyclic and heptacyclic ladder silsesquixoane.[33,94]

Silsesquioxanes prepared from $[RSi(OH)O]_4$ bear only simple Me or Ph side groups, which can be used as pure materials, but offer more utility if functionalized or incorporated with other components or polymers via various chemical reactions. Reactive groups such as vinyl, chloropropyl or Si-H can be introduced to ladder silsesquioxanes.[87,93] The di-vinyl functionalized ladder silsesquioxane used to prepare hybrid polymers was further discussed in the Chapter **6**, displaying novel semiconducting properties.

1.6 Photophysical properties of silsesquioxanes

In general, steady-state Uv-vis and photoluminescence measurements can be applied to characterize the electronic structures and transitions, HOMO-LUMO gaps between ground and excited states, intermolecular interactions and dynamic properties of silsesquioxanes on the molecular scale.[95] Non-linear optical characterization techniques such as two photo absorption and fluorescence up-conversion can give additional information about polarizability, transition dipole moments, energy transfer in the excited state, and fluorescence lifetimes as discussed in more detail below. The abovementioned characterization techniques have been used extensively to analyze functionalized silsesquioxanes for applications in the field of electronic devices such as photovoltaics, photonics and light-emitting diodes.[96]

The Ossadnik[97] and Azinovic[95] groups reported the absorption and emission behavior of several silsesquioxane cores $(RT)_{8,10,12}$ $[(RSiO_{1.5})_{8,10,12}]$ where R=H or alkyl in Figure **1.7a**,[97] finding that the HOMO-LUMO gap of H_8T_8 is 4.4 eV. This result is unexpected since the hexagonal boron nitride, which is considered as a wide bandgap semiconductor, exhibits a bandgap of ~6.0 eV.[128] In addition, absorption and emission in the blue spectral region was observed for all R groups and the intensity of fluorescence depends on the ligand electronegativity and cage size, with more

electron-rich ligands and larger cage sizes displaying higher fluorescence efficiencies. Figure **1.7b**[97] compares the absorption and emission of $[ClCH_2(CH_2)_2\text{-}SiO_{1.5}]_{8,10,12}$ at ~260 nm (4.8 eV) and ~387 nm (3.2 eV) respectively. This does not capture the most important discovery of low lying LUMO.

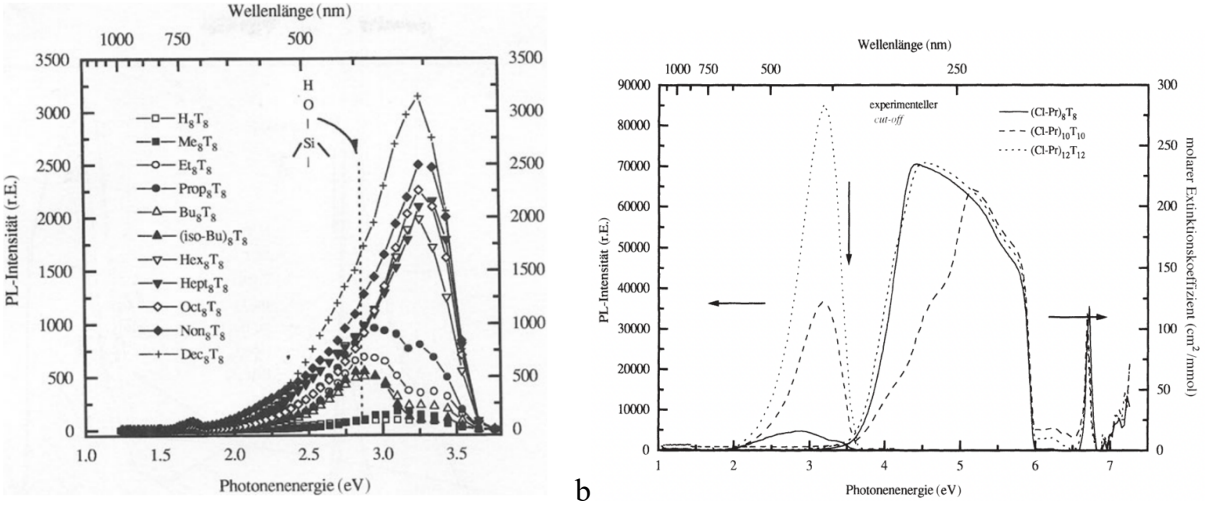

Figure 1.7. a. Photoluminescence and absorption of T_8 and b. $[ClCH_2(CH_2)_2\text{-}T]_{8,10,12}$ in THF excited by laser at 325 nm.

1.6.1 Electron delocalization involving the silsesquioxane core

Silsesquioxanes with conjugated organic moieties attached might be expected to have smaller HOMO-LUMO gaps since their conjugation lengths will be extended allowing their electronic interaction with the silsesquioxane core. While an alternate theory is that the silsesquioxane core simply acts as an anchor for the organic groups, suggesting that all electronic transitions would be localized on the organic groups.

If this were the case, the photophysical behavior of these materials should be expected to be nearly identical to the free chromophores unbound to the core. Considering silsesquioxane cores offer electron-withdrawing characteristics comparable to a $-CF_3$ group,[26] blue-shifted absorption and emission spectra should be observed for conjugated organics attached to the core due to the decreased electron density. Indeed, a large number of studies have targeted organic substituents conjugated and anchored to the silsesquioxane core with respect to their utility in applications such as OLEDs,[98] in that the silsesquioxane cores distribute the chromophores in 3D and thus prevent $\pi - \pi$ stacking that causes quenching of the luminescence to improve the quantum yields.[99,100]

However, numerous papers published recently by several groups show that silsesquioxane cores can act as more than just insulating anchors for organic chromophores, especially smaller conjugated organic moieties, such as stilbene and biphenyl.[52, 101-103] The absorption spectra of these molecules are similar to the free unbound molecules due to the absence of the HOMO interactions in the ground state, while the emission spectra show significant red-shifts relative to the small molecules resembling spectra from more conjugated molecules.[52, 101-103]

André et al. reported the photophysical behavior of a series of 4-vinylbiphenyl octa-functionalized T_8 silsesquioxanes in Figure **1.8**.[101] These molecules exhibit only slightly red-shifted absorption and emission compared to small model analogs in CH_2Cl_2, ~10 and ~15 nm respectively. Theoretical studies suggest that these slight red-shifts in the photophysical spectra are caused by formation of partial electron delocalization from the organic tethers to the silsesquioxane core possibly via intramolecular charge-transfer.

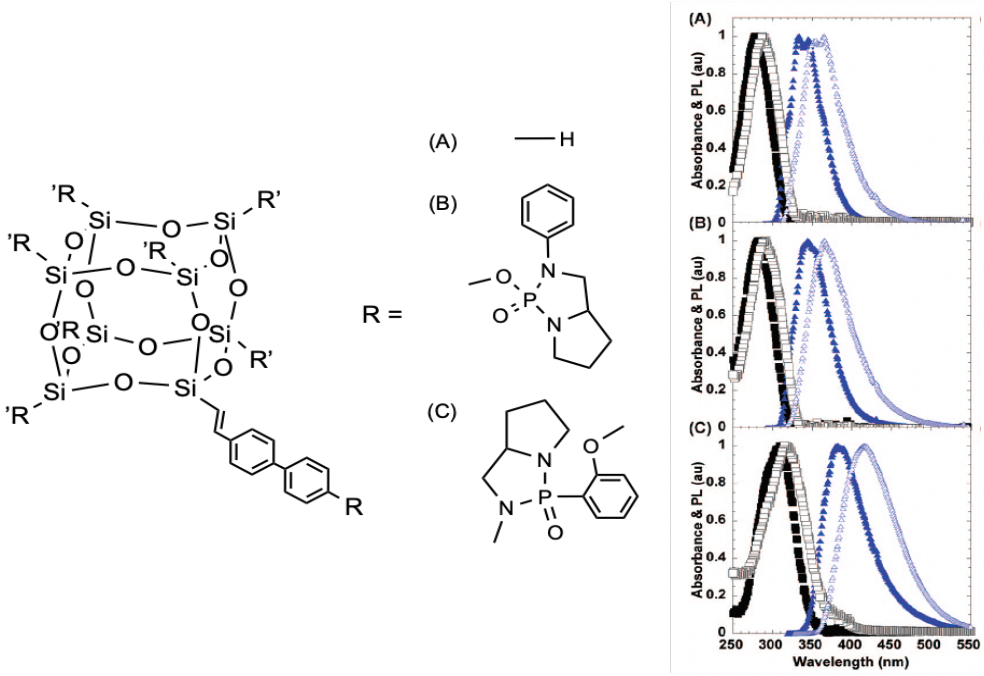

Figure 1.8. Vinyl-biphenyl functionalized silsesquioxane cores and their normalized absorption (black) and photoluminescence (blue) spectra.

Another study from the same group on 4'-vinylbiphenyl-3,5-dimethylalcohol substituted T_8, observes a red-shifted emission of 60 nm from the free model analog in Figure **1.9**,[102] while only a ~7 nm red-shift was observed in absorption.[102] The red-shift of 60 nm in the photoluminescence of diol compound compared to the small model molecule suggests chromophores on the cage offer "longer" conjugation lengths than free individual chromophores. Indeed, Andre et al. attributed

this large red-shift to electron-delocalization involving the silsesquioxane core based on their theoretical studies.

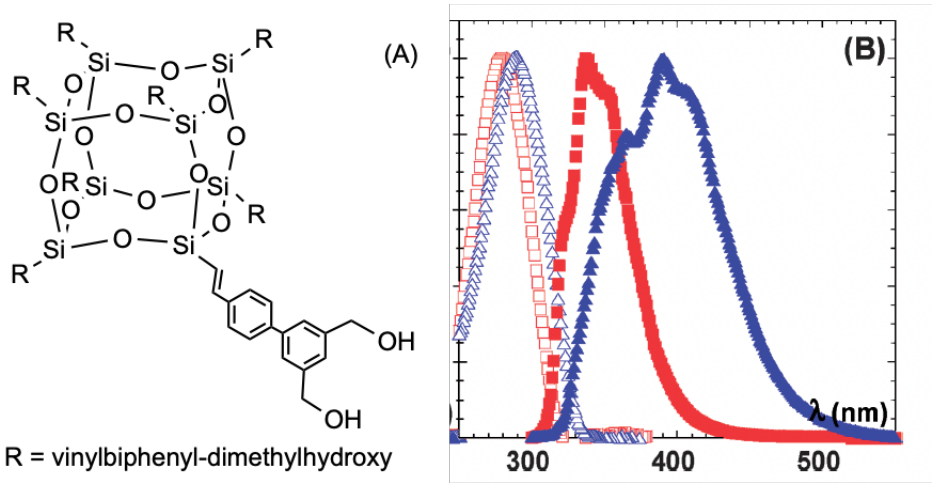

Figure 1.9. Normalized absorption (empty symbols) and photoluminescence (closed symbols) of 4'-vinylbiphenyl-3,5-dimethylalcohol functionalized silsesquioxane (blue) and 4'-vinylbiphenyl-3,5-dimethylalcohol (red).

Zhen and coworkers used frontier orbital theory to characterize a series of cubic silsesquioxanes functionalized with one electron-donating (4-carbazolephenyl) and/or one electron-withdrawing (4-cyanophenyl) group as shown in Figure **1.10**.[103] Their calculations found that the HOMO-LUMO gap is reduced to 3.70 eV, close to Ossadnik's result of 4.4 eV and corresponding to the energy of near violet light, with both electron-donating and electron-withdrawing groups attached to the silsesquioxane core.

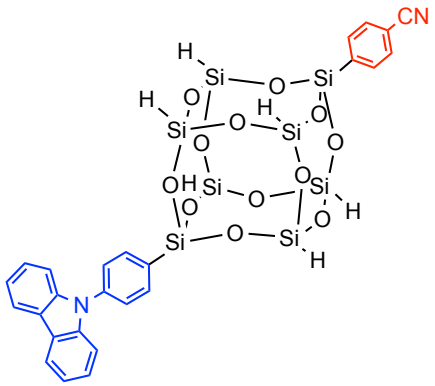

Figure 1.10. Silsesquioxane molecule with electron-donating 4-carbazolephenyl group (blue) and electron-withdrawing 4-cyanophenyl group (red).[103]

The authors offer a similar conclusion, that the silsesquioxane core cannot be considered simply as a non-conjugated moiety. They suggest electron delocalization occurs involving the

organic groups and the silsesquioxane core with the silsesquioxane core acting as an electron acceptor. This concept was also explored by our group using a new set of stilbene-substituted silsesquioxanes derivatives and is discussed further below.

The first studies done by our group on the photophysical behavior of silsesquioxanes explored stilbene derivatives synthesized both from $[o\text{-Br}_x\text{PhSiO}_{1.5}]_8$ and $[p\text{-IPhSiO}_{1.5}]_8$.[52] Compared to the molecular stilbenes, both *ortho* and *para* octa-stilbene substituted T_8 exhibit slight red-shifts of ~5 nm in absorption despite the CF_3-characteristic electronic-withdrawing nature of the SQ cage while emission was red-shifted by ~60 nm, indicating electron delocalization between stilbene tethers and the cage core, similar to what was observed by other groups as discussed above.

Particularly, stilbene-functionalized silsesquioxanes are of great interest due to their robust nature, ease of synthesis, but especially because they serve as models of phenylene-vinylene polymers known to be excellent blue emitters, but suffering from very poor solubility.[5] By creating 3-D analogs, we hoped to make soluble analogs.

Figure **1.11**[52] compares the absorption and photoluminescence spectra of the $[o\text{-Br}_x\text{PhSiO}_{1.5}]_8$ and $[p\text{-IPhSiO}_{1.5}]_8$ derived *o*- and *p*-methylstilbene silsesquioxanes to that of *p*-methylstilbene.

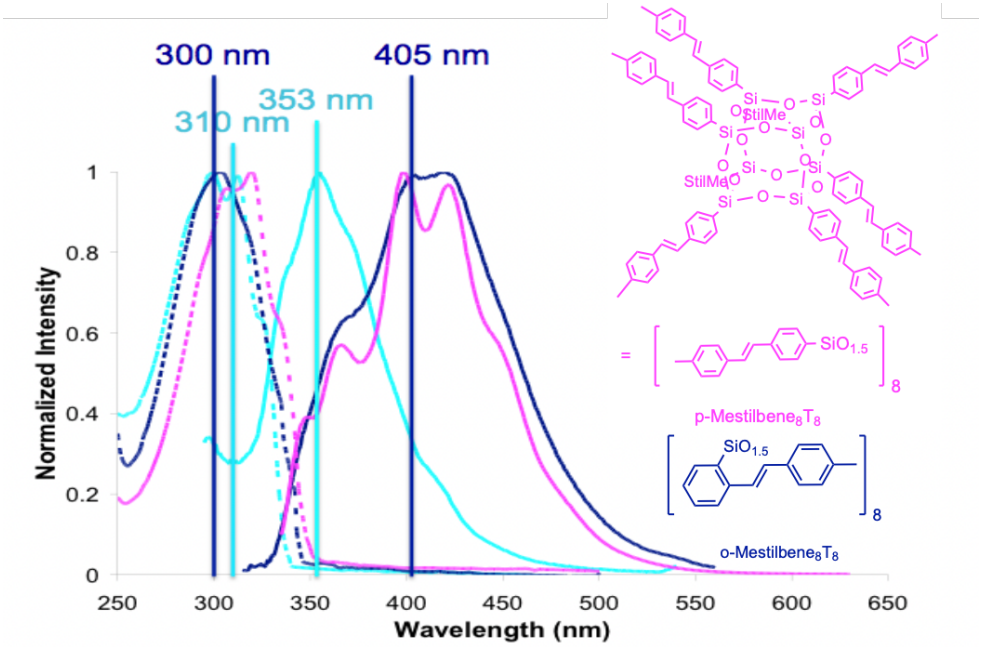

Figure 1.11. Absorption and photoluminescence comparison of ortho and para (o/p)-MeStilbene functionalized silsesquioxanes to p-MeStilbene in THF.

Collaboration with the Ugo group provided access to a set of model compounds including dimethylaminostilbene-functionalized siloxane and cyclosiloxane molecules that are equivalent to

corner units and halves of the cubic silsesquioxane molecules as shown in Figure **1.12**,[52] respectively.[52] By comparing the photophysical behavior of these molecules along with the octa- substituted silsesquioxane analog allowed us to assess the degree of conjugation between the organic moieties and different numbers of silsesquioxane units.

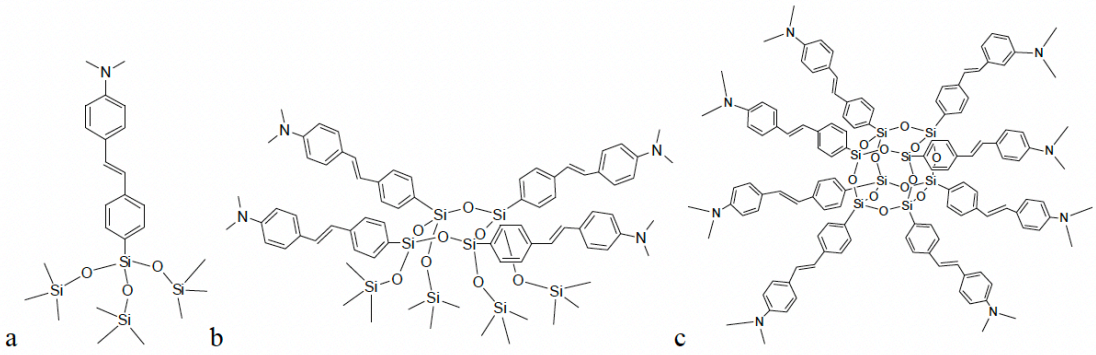

Figure 1.12. (a) Me_2NStilbene-corner, (b) Me_2NStilbene-half, and (c) Me_2NStilbene-full.

The absorption and emission spectra of the "corner" and "half' molecules in THF and CH_2Cl_2 are basically the same, while those of the full cage molecules are slightly red-shifted by ~5 and 10 nm for absorption and emission respectively. These molecules all show low photoluminescence quantum yields and structureless emission spectra, indicating charge-transfer (CT) processes. This conclusion was supported by solvent studies showing 15-25 nm red-shifted absorption and emissions in the more polar solvent mixture of 20% THF/80% CH_3CN which stabilizes the CT excited state.

Table 1.1.Photoluminescence quantum yields and two-photon absorption properties of silsesquioxane derivatives.

	TPA-δ (GM)	δ/moiety (GM)	Φ_F(-)
$MeStil_8T_8$	11	1.2	0.06
Me_2NStil-corner	12	12	0.08
Me_2NStil-half	30	7.5	0.09
$Me_2NStil_8T_8$	211	26	0.03
$Stilvinyl_8T_8$	25	3	0.36
$MeOStilvinyl_8T_8$	110	14	0.12
$NH2Stilvinyl_8T_8$	810	101	0.05

The photoluminescence quantum yields (Φ_F) are 6% for the "corner" molecule, 8% for the "half', and 3% for the "full cage". Two-photon absorption (TPA) studies found that the TPA cross-sections with the "corner" molecule ≈ 12 GM/moiety, the "half" ≈ 8 GM/moiety, while the "full cage" ≈ 26 GM/moiety, as shown in Table **1.1**.[52] If these molecules were to display identical CT characteristics, they should also exhibit identical TPA cross-sections/moiety. Considering that the

"full cage" has the lowest photoluminescence quantum yield and the highest TPA cross-section/moiety can be explained by the fact that the "full cage" has the greatest CT characteristics among the three. The influence of the silsesquioxane cage core as a whole on the photophysical behavior of the molecule is more than the sum of the eight $SiO_{1.5}$ fragments.

1.6.2 Electron delocalization in beads-on-a-chain polymers

Our group has also developed synthetic routes to silsesquioxane-based "beads on a chain" (BoC) polymers/oligomers with 1,4-divinylbenzene linkers between deca- and dodecameric silsesquioxane cages as shown in Figure **1.13**.[104] A model compound was also prepared with -$Si(OEt)_3$ end-caps to simulate the cage corners of the BoC oligomers. Figure **1.13** compares absorption and photoluminescence of BoC and the model compound. Both show similar absorption maxima at ~260 nm while the emission maximum for the BoC oligomers is red-shifted to 386 nm from that of the model compound at 326 nm. These results imply that the extension of conjugation length in BoC by connecting the silsesquioxane cages with conjugated bridges and electron delocalization in the silsesquioxane cages in the excited state. This also indicates $T_{10,12}$ offer similar semi-conducting behavior equivalent to T_8.

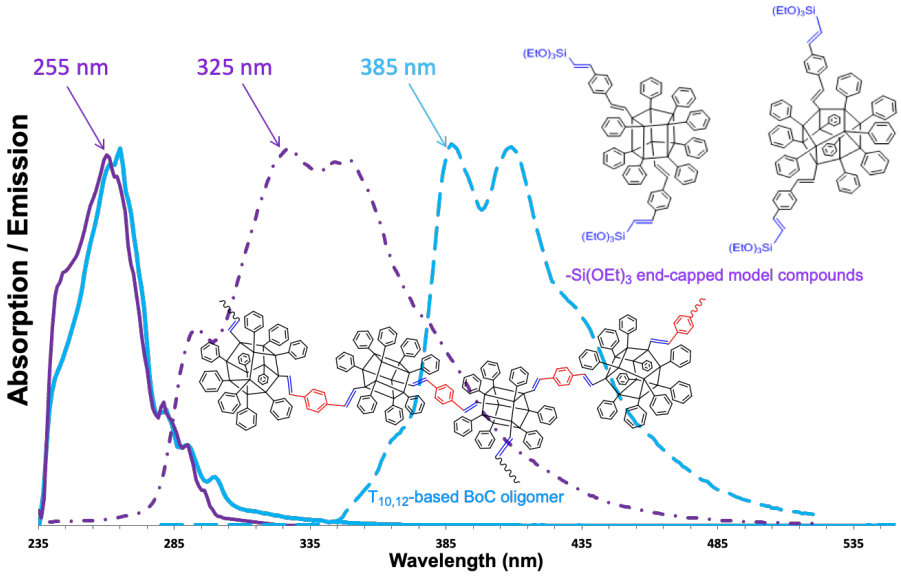

Figure 1.13. Absorption and emission of $T_{10,12}$-based BoC oligomer and -$Si(OEt)_3$ end-capped model compounds.

Coughlin et al. coincidentally have reported similar effects for ortho-linked carborane-polyfluorene copolymers with significantly red-shifted photoluminescence from a fluorene dimer, however these shifts are not observed in para-carborane copolymers,[105–107] which implies that potential

CT interactions occur on the carborane cage face as discussed above for SQs. This unique photophysical behavior of silsesquioxanes has opened up a whole new class of materials, discussed further in this dissertation.

1.6.3 Theoretical studies

The modeling work in Chapter **3** and **4** was done by Jungsuttiwong group and the modeling in Chapter **5** and **6** were done in both Jungsuttiwong and the Kieffer's groups in aid to the work presented. Previous modeling studies of stilbene-functionalized silsesquioxanes reveal that the HOMO of *p*-stilbene$_8$T$_8$ lies on the π-state of stilbene moieties and the LUMO is comprised of interactions between Si atoms and the π*-state of the stilbene moieties. The HOMO-LUMO energy gap of *p*-stilbene$_8$T$_8$ is 2.6 eV, while the gap between the HOMO and the molecular orbital inside the silsesquioxane core ("core MO") is 4.2 eV. However, if we consider the 1.6 eV difference found for H$_8$T$_8$ silsesquioxane between calculation and experiment (4.4 eV and 6.0 eV respectively),[95,97,108–110] the energy gap between HOMO and core MO could be reduced to 2.6 eV, approximately the same as the stilbene-based bandgap and thus allowing for the possibility of stilbene-cage interactions. This offers further evidence for electron delocalization involving the silsesquioxane core to the extent that there is a possibility of 3-D conjugation through the core.

Table 1.2. Density functional theoretical (DFT) HOMO-LUMO calculations for selected silsesquioxane molecules.

(eV)	H8T8	Ph8T8	StilSi(OSiMe3)3a	Stil1T8b	Stil8T8
HOMO	-7.519	-5.529	-5.165	-5.466	-4.519
Core-MO	-0.541	-0.035	-0.213	-0.406	-0.293
Organic-MO		-0.865	-2.461	-2.767	-1.906
Core-gap	6.978	5.564	4.95	5.056	4.227
Organic-gap		4.664	2.70	2.695	2.613

[a] Stilbene-functionalized "corner" molecule. [b] Silsesquioxane T$_8$ cage with 1 stilbene group and 7 H atoms.

Calzaferri's group also reported similar interactions in theoretical studies of octavinylsilsesquioxanes (vinyl$_8$T$_8$) with naphthyl and biphenyl groups attached, displaying behavior ranging from insulating to conducting.[110–112] This result implied that the conjugation could be "3-D" along the edges of the cage rather than through the cage, offering an argument for charge delocalization throughout the cage system and a possible explanation for the red-shifts observed in emission.

1.6.4 Photoluminescence quantum yields

The photoluminescence quantum yields (Φ) are simply the total number of emitted photons which escape a bulk sample divided by the total number of absorbed photons.[113] It is an essential parameter that allows assessment of the sensitivity of a proposed fluorimetric determination of materials.[114] Maximizing the external quantum efficiency is usually the motivation driving research in electro-luminescent devices, such as organic,[115] perovskite,[116] or quantum dot LEDs.[117] Quantum yields up to 2 are theoretically possible in this specific case.[118] Compounds with the highest quantum yields, such as rhodamines (Φ of rhodamine 6 G in ethanol = 0.94),[119] exhibit the brightest emissions. However, substances with quantum yields of 0.10 can still be considered to be quite fluorescent.[120] Several of our silsesquioxane-based compounds exhibit quantum yields in the range of 0.40 to 0.85, as further discussed in Chapters **5** and **6**.

Various ways have been used to determine the quantum yield. One method that is frequently used for solutions is by comparing the luminescence of the molecule of investigation to the one of a known standard.[121,122] However, there are many experimental limitations to the method, including the small number of standards available, the accuracy of the standard yield value, differences in refractive index, polarization effects, differences in wavelength response of monochromators and detectors and inner-filter effects.[119]

An alternate method directly measures the number of absorbed photons and the number of emitted photons without comparing to a second material. This method was introduced by de Mello et al. in 1997,[123] with the basic principle published two years earlier from the same group.[124] This technique is widely used currently and also tested for solutions.[125] In contrast to the comparative method, the direct determination of the quantum yield is fast and does not rely on a known standard. In this approach, the quantum is given by

$$\Phi = \frac{E_{in}(\lambda) - (1-\alpha)E_{out}(\lambda)}{X_{empty}(\lambda)\alpha} \quad \textbf{Equation 1.1}$$

with

$$\alpha = \frac{X_{out}(\lambda) - X_{in}(\lambda)}{X_{out}(\lambda)} \quad \textbf{Equation 1.2}$$

$X_{empty}(\lambda)$ is the integrated excitation profile with an empty integrating sphere. α is the absorptance, the fraction of light absorbed, equal to one minus the transmittance by IUPAC definition. α is measured by the integrated excitation bands, i.e. the emission signal measured across the excitation wavelength (±5 nm), for two positions of the sample as follows: $X_{in}(\lambda)$ is the integrated

excitation when the sample lies directly in the excitation path and $X_{out}(\lambda)$ is the integrated excitation when the excitation light first hits the sphere wall.[125] $E_{in}(\lambda)$ and $E_{out}(\lambda)$ are the integrated emission(s) as a result of direct excitation of the sample (sample IN) and secondary excitation (sample OUT) respectively. The secondary emission comes from the sample excited by the excitation light reflected from the integrating sphere walls.

The experimental setup is shown in Figure **1.14**,[125] consisting of an excitation source, which can be a LED or laser.[125] The light hits the luminescent sample located within an integrating sphere. The integrating sphere is a hollow sphere coated with a diffusely reflecting material on the inside. The flux received at the exit port or an aperture in the sphere is proportional to the total number of light produced within the sphere, independent of its angular distribution.[126] All the reflected, transmitted, or emitted light will be collected and then detected within the sphere.[127]

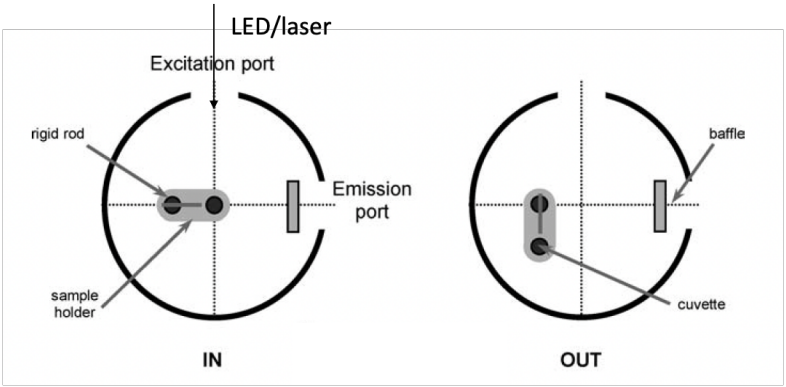

Figure 1.14. Experimental setup for integrating sphere measurements.

1.7 Overview of subsequent chapters

The following chapters are organized as follows.

Chapter **2** describes synthetic and experimental techniques used in this dissertation. Synthesis procedures include chlorosilane-capping, halogenation and Heck cross-coupling; various characterization tools including: ^{1}H, ^{13}C and ^{29}Si NMR (nuclear magnetic resonance spectroscopy), MALDI-TOF (matrix assisted laser desorption ionization time of flight mass spectrometry), TGA (thermal gravimetric analysis), GPC (gel permeation chromatography), FTIR (Fourier-transform infrared spectroscopy) etc. In addition, photophysical property analysis techniques are described using steady-state UV-Vis and photoluminescence spectroscopy, and integrating sphere quantum yield measurements.

Chapter **3** describes the functionalization and characterization of incompletely condensed trisilanol phenylsilsesquioxanes after capping with trichlorosilanes and chlorotrimethylsilane. Di- and

hepta-halogenated T_7 are prepared, followed by their conversion to stilbene functionalization. Their photophysical properties are studied to explore the effect of cage geometry and number of functional groups on the cage-centered LUMOs. Besides, the comparative sphericity of LUMOs is characterized using magnetic scattering for the first time along with computational analyses.

Chapter **4** describes the synthesis, and photophysical properties of another incompletely condensed phenylsilsesquioxanes, tetrasilanol double decker silsesquioxanes DD. The capping reaction of tetrasilanol DD with dichlorodimethylsilane and chlorotrimethylsilane is followed by halogenation and then Heck cross-coupling. Finally the photophysical behavior stilbene-functionalized DD is also discussed as to map out the structure-photophysical property relationships of single SQ cages.

Chapter **5** describes the synthesis of DD SQ derived copolymers via Heck cross-coupling of di-vinyl functionalized DD SQs with a series of dibromo aromatic compounds. This is followed by a discussion of the characterization and finally photophysical properties of these systems to explore possible through-chain conjugation even with the siloxane units in the SQ cages. Doping with electron acceptor F_4TCNQ gives insight into the integer charge transfer process involved in hybrid SQ polymers and p-type dopant.

Chapter **6** describes the preparation of similar SQ derived copolymers but with ladder SQs in the main chain that can be considered as half of the DD SQ cage and also detailed photophysical properties analysis. Conjugation breaking and restoring via bromination and debromination of the vinyl groups in the polymer chains gives another evidence of the unconventional conjugation in the excited state involving SQs and organic tethers.

Chapter **7** describes the preparation of DD derived alternating terpolymers via stepwise Heck reaction, with the goal of incorporation of long-wavelength emission and high quantum yields, which are important for displaying components in applications such as OLEDs.

Chapter **8** gives the overall summary and conclusions of this work followed by a discussion of future work.

References

(1) Feher, F. J.; Budzichowski, T. A.; Blanski, R. L.; Weller, K. J.; Ziller, J. W. Facile Syntheses of New Incompletely Condensed Polyhedral Oligosilsesquioxanes: $[(C\text{-}C_5H_9)_7Si_7O_9(OH)_3]$, $[(c\text{-}C_7H_{13})_7Si_7O_9(OH)_3]$, and $[(c\text{-}C_7H_{13})_6Si_6O_7(OH)_4]$. *Organometallics* **1991**, *10* (7), 2526–2528. https://doi.org/10.1021/om00053a070.

(2) Cordes, D.B. and Lickiss, P.D., 2011. Preparation and characterization of polyhedral oligosilsesquioxanes. In *Applications of polyhedral oligomeric silsesquioxanes*. Springer, Dordrecht, **2011**; Vol. 3. (pp. 47-133).
(3) Laine, R. M.; Roll, M. F. Polyhedral Phenylsilsesquioxanes. *Macromolecules* **2011**, *44* (5), 1073–1109. https://doi.org/10.1021/ma102360t.
(4) Cordes, D. B.; Lickiss, P. D.; Rataboul, F. Recent Developments in the Chemistry of Cubic Polyhedral Oligosilsesquioxanes. *Chem. Rev.* **2010**, *110* (4), 2081–2173. https://doi.org/10.1021/cr900201r.
(5) Li, G.; Wang, L.; Ni, H.; Jr, C. U. P. Polyhedral Oligomeric Silsesquioxane (POSS) Polymers and Copolymers: A Review. *Journal of Inorganic and Organometallic Polymers*, **2001**, *11*(3), pp.123-154
(6) Fina, A.; Tabuani, D.; Carniato, F.; Frache, A.; Boccaleri, E.; Camino, G. Polyhedral Oligomeric Silsesquioxanes (POSS) Thermal Degradation. *Thermochimica Acta* **2006**, *440* (1), 36–42. https://doi.org/10.1016/j.tca.2005.10.006.
(7) Baney, R. H.; Itoh, M.; Sakakibara, A.; Suzuki, T. Silsesquioxanes. 22.
(8) Asuncion, M. Z.; Laine, R. M. Silsesquioxane Barrier Materials. *Macromolecules* **2007**, *40* (3), 555–562. https://doi.org/10.1021/ma062305p.
(9) Sellinger, A.; Laine, R. M. Silsesquioxanes as Synthetic Platforms. 3. Photocurable, Liquid Epoxides as Inorganic/Organic Hybrid Precursors. *Chem. Mater.* **1996**, *8* (8), 1592–1593. https://doi.org/10.1021/cm9601493.
(10) Feher, F. J.; Newman, D. A.; Walzer, J. F. Silsesquioxanes as Models for Silica Surfaces. *J. Am. Chem. Soc.* **1989**, *111* (5), 1741–1748. https://doi.org/10.1021/ja00187a028.
(11) Ropartz, L.; Morris, R. E.; Schwarz, G. P.; Foster, D. F.; Cole-Hamilton, D. J. Dendrimer-Bound Tertiary Phosphines for Alkene Hydroformylation. *Inorganic Chemistry Communications* **2000**, *3* (12), 714–717. https://doi.org/10.1016/S1387-7003(00)00167-2.
(12) Riollet, V.; Quadrelli, E. A.; Copéret, C.; Basset, J.-M.; Andersen, R. A.; Köhler, K.; Böttcher, R.-M.; Herdtweck, E. Grafting of [Mn(CH2tBu)2(Tmeda)] on Silica and Comparison with Its Reaction with a Silsesquioxane. *Chem. Eur. J.* **2005**, *11* (24), 7358–7365. https://doi.org/10.1002/chem.200500401.
(13) Duchateau, R.; Abbenhuis, H. C. L.; van Santen, R. A.; Thiele, S. K.-H.; van Tol, M. F. H. Half-Sandwich Titanium Complexes Stabilized by a Novel Silsesquioxane Ligand: Soluble Model Systems for Silica-Grafted Olefin Polymerization Catalysts. *Organometallics* **1998**, *17* (24), 5222–5224. https://doi.org/10.1021/om980572g.
(14) Contreras-Torres, F. F.; Basiuk, V. A. Imidazo[1,2- *a*]Pyrazine-3,6-Diones Derived from α-Amino Acids: A Theoretical Mechanistic Study of Their Formation via Pyrolysis and Silica-Catalyzed Process. *J. Phys. Chem. A* **2006**, *110* (23), 7431–7440. https://doi.org/10.1021/jp061331m.
(15) Gromilov, S. A.; Basova, T. V.; Emel'yanov, D. Yu.; Kuzmin, A. V.; Prokhorova, S. A. Layer Arrangement in the Structure of Octakis-(Trimethylsiloxy)Octasilsesquioxane and Dodecakis-(Trimethylsiloxy)Cyclohexasiloxane. *J Struct Chem* **2004**, *45* (3), 471–475. https://doi.org/10.1007/s10947-005-0015-8.
(16) Feher, F.J. and Budzichowski, T.A. Silasesquioxanes as ligands in inorganic and organometallic chemistry. *Polyhedron*, **1995**, *14*(22), pp.3239-3253.
(17) Maschmeyer, T.; C. Klunduk, M.; M. Martin, C.; S. Shephard, D.; F. G. Johnson, B.; Maschmeyer, T.; Meurig Thomas, J. Modelling the Active Sites of Heterogeneous Titanium-

Centred Epoxidation Catalysts with Soluble Silsesquioxane Analogues. *Chem. Commun.* **1997**, No. 19, 1847. https://doi.org/10.1039/a703642f.
(18) Choi, J.; Kim, S. G.; Laine, R. M. Organic/Inorganic Hybrid Epoxy Nanocomposites from Aminophenylsilsesquioxanes. *Macromolecules* **2004**, *37* (1), 99–109. https://doi.org/10.1021/ma030309d.
(19) Chojnowski, J.; Fortuniak, W.; Rościszewski, P.; Werel, W.; Łukasiak, J.; Kamysz, W.; Hałasa, R. Polysilsesquioxanes and Oligosilsesquioxanes Substituted by Alkylammonium Salts as Antibacterial Biocides. *J Inorg Organomet Polym* **2006**, *16* (3), 219–230. https://doi.org/10.1007/s10904-006-9048-5.
(20) Gromilov, S. A.; Emel'yanov, D. Yu.; Kuzmin, A. V.; Prokhorova, S. A. Structural Organization of Layers in Octakis-(Trimethylsiloxy)Octasilsesquioxane. *Journal of Structural Chemistry* **2003**, *44* (4), 704–706. https://doi.org/10.1023/B:JORY.0000017949.97279.e6.
(21) Solans-Monfort, X.; Eisenstein, O. Structure, Spectroscopic and Electronic Properties of a Well Defined Silica Supported Olefin Metathesis Catalyst, [(RSiO)Re(RCR)(QCHR)(CH2R)], through DFT Periodic Calculations: Silica Is Just a Large Siloxy Ligandw. **2006**, 9.
(22) Majumdar, P.; Lee, E.; Gubbins, N.; Stafslien, S. J.; Daniels, J.; Thorson, C. J.; Chisholm, B. J. Synthesis and Antimicrobial Activity of Quaternary Ammonium-Functionalized POSS (Q-POSS) and Polysiloxane Coatings Containing Q-POSS. *Polymer* **2009**, *50* (5), 1124–1133. https://doi.org/10.1016/j.polymer.2009.01.009.
(23) Leu, C.-M.; Reddy, G. M.; Wei, K.-H.; Shu, C.-F. Synthesis and Dielectric Properties of Polyimide-Chain-End Tethered Polyhedral Oligomeric Silsesquioxane Nanocomposites. *Chem. Mater.* **2003**, *15* (11), 2261–2265. https://doi.org/10.1021/cm0208408.
(24) Lahann, J. Vapor-Based Polymer Coatings for Potential Biomedical Applications. *Polym. Int.* **2006**, *55* (12), 1361–1370. https://doi.org/10.1002/pi.2098.
(25) Pescarmona, P. P.; Maschmeyer, T. SQ Review 2002. *Aust. J. Chem.* **2001**, *54* (10), 583. https://doi.org/10.1071/CH02003.
(26) Feher, F. J.; Budzichowski, T. A. Syntheses of Highly-Functionalized Polyhedral Oligosilsesquioxanes. *Journal of Organometallic Chemistry* **1989**, *379* (1–2), 33–40. https://doi.org/10.1016/0022-328X(89)80022-1.
(27) Dare, E. O.; Liu, L.-K.; Peng, J. Modified Procedure for Improved Synthesis of Some Octameric Silsesquioxanes via Hydrolytic Polycondenzation in the Presence of Amberlite Ion-Exchange Resins. *Dalton Trans.* **2006**, No. 30, 3668. https://doi.org/10.1039/b603325c.
(28) Dudziec, B.; Marciniec, B. Double-Decker Silsesquioxanes: Current Chemistry and Applications. *COC* **2018**, *21* (28). https://doi.org/10.2174/1385272820666151228193728.
(29) Brown, J. F.; Vogt, L. H.; Katchman, A.; Eustance, J. W.; Kiser, K. M.; Krantz, K. W. DOUBLE CHAIN POLYMERS OF PHENYLSILSESQUIOXANE. *J. Am. Chem. Soc.* **1960**, *82* (23), 6194–6195. https://doi.org/10.1021/ja01508a054.
(30) Brown, J. F.; Vogt, L. H. The Polycondensation of Cyclohexylsilanetriol. *J. Am. Chem. Soc.* **1965**, *87* (19), 4313–4317. https://doi.org/10.1021/ja00947a016.
(31) . Dubchak, I.L., Shklover, V.E., Struchkov, Y.T., Khynku, E.S. and Zhdanov, A.A. Crystal structure of organosilicon compounds. *Journal of Structural Chemistry*, **1982**, *22*(5), pp.770-775.
(32) Unno, M.; Suto, A.; Matsumoto, T. Laddersiloxanes — Silsesquioxanes with Defined Ladder Structure. *Russ. Chem. Rev.* **2013**, *82* (4), 289–302. https://doi.org/10.1070/RC2013v082n04ABEH004360.

(33) Unno, M.; Tanaka, R.; Tanaka, S.; Takeuchi, T.; Kyushin, S.; Matsumoto, H. Oligocyclic Ladder Polysiloxanes: Alternative Synthesis by Oxidation. *Organometallics* **2005**, *24* (4), 765–768. https://doi.org/10.1021/om049324c.
(34) Bürgy, H.; Calzaferri, G. Separation of the Oligomeric Silsesquioxanes (HSiO3/2)8–18 by Size-Exclusion Chromatography. *Journal of Chromatography A* **1990**, *507*, 481–486. https://doi.org/10.1016/S0021-9673(01)84227-8.
(35) Ganachaud, F., Boileau, S., Boury, B., *Silicon Based Polymers: Advances in Synthesis and Supramolecular Organization*; Springer: Berlin, **2008**.
(36) Roll, M. F.; Asuncion, M. Z.; Kampf, J.; Laine, R. M. *Para* -Octaiodophenylsilsesquioxane, [*p* -IC $_6$ H $_4$ SiO $_{1.5}$] $_8$, a Nearly Perfect Nano-Building Block. *ACS Nano* **2008**, *2* (2), 320–326. https://doi.org/10.1021/nn700196d.
(37) Tamaki, R.; Tanaka, Y.; Asuncion, M. Z.; Choi, J.; Laine, R. M. Octa(Aminophenyl)Silsesquioxane as a Nanoconstruction Site. *J. Am. Chem. Soc.* **2001**, *123* (49), 12416–12417. https://doi.org/10.1021/ja011781m.
(38) Brick, C. M.; Ouchi, Y.; Chujo, Y.; Laine, R. M. Robust Polyaromatic Octasilsesquioxanes from Polybromophenylsilsesquioxanes, Br $_x$ OPS, via Suzuki Coupling. *Macromolecules* **2005**, *38* (11), 4661–4665. https://doi.org/10.1021/ma0501141.
(39) Furgal, J. C.; Jung, J. H.; Goodson, T.; Laine, R. M. Analyzing Structure–Photophysical Property Relationships for Isolated T $_8$, T $_{10}$, and T $_{12}$ Stilbenevinylsilsesquioxanes. *J. Am. Chem. Soc.* **2013**, *135* (33), 12259–12269. https://doi.org/10.1021/ja4043092.
(40) Hwan Jung, J.; Furgal, J. C.; Goodson, T.; Mizumo, T.; Schwartz, M.; Chou, K.; Vonet, J.-F.; Laine, R. M. 3-D Molecular Mixtures of Catalytically Functionalized [VinylSiO $_{1.5}$] $_{10}$ /[VinylSiO $_{1.5}$] $_{12}$. Photophysical Characterization of Second Generation Derivatives. *Chem. Mater.* **2012**, *24* (10), 1883–1895. https://doi.org/10.1021/cm300587s.
(41) Miyazato, A.; Pakjamsai, C.; Kawakami, Y. Octa, Deca, and Dodeca(4-Nitrophenyl) Cage Silsesquioxanes via 4-Trimethylsilylphenyl Derivatives. *Dalton Trans.* **2010**, *39* (13), 3239. https://doi.org/10.1039/b923122f.
(42) Laine, R. M. Nanobuilding Blocks Based on the [OSiO1.5]x (X= 6, 8, 10) Octasilsesquioxanes. *J. Mater. Chem.* **2005**, *15* (35–36), 3725. https://doi.org/10.1039/b506815k.
(43) Chan, K. L.; Sonar, P.; Sellinger, A. Cubic Silsesquioxanes for Use in Solution Processable Organic Light Emitting Diodes (OLED). *J. Mater. Chem.* **2009**, *19* (48), 9103. https://doi.org/10.1039/b909234j.
(44) Brown, J. F.; Vogt, L. H.; Prescott, P. I. Preparation and Characterization of the Lower Equilibrated Phenylsilsesquioxanes. *J. Am. Chem. Soc.* **1964**, *86* (6), 1120–1125. https://doi.org/10.1021/ja01060a033.
(45) Bassindale, A. R.; Liu, Z.; MacKinnon, I. A.; Taylor, P. G.; Yang, Y.; Light, M. E.; Horton, P. N.; Hursthouse, M. B. A Higher Yielding Route for T8 Silsesquioxane Cages and X-Ray Crystal Structures of Some Novel Spherosilicates. *Dalton Trans.* **2003**, No. 14, 2945. https://doi.org/10.1039/b302950f.
(46) Schubert, U., Hüsing, N., Laine, R. M. *Materials Syntheses: A Practical Guide*; Springer: Wien ; New York, **2008**.
(47) Brown, J. F. The Polycondensation of Phenylsilanetriol. *J. Am. Chem. Soc.* **1965**, *87* (19), 4317–4324. https://doi.org/10.1021/ja00947a017.
(48) Brick, C. M.; Tamaki, R.; Kim, S.-G.; Asuncion, M. Z.; Roll, M.; Nemoto, T.; Ouchi, Y.; Chujo, Y.; Laine, R. M. Spherical, Polyfunctional Molecules Using

Poly(Bromophenylsilsesquioxane)s as Nanoconstruction Sites. *Macromolecules* **2005**, *38* (11), 4655–4660. https://doi.org/10.1021/ma0473014.

(49) Li, Z.; Yang, R. Synthesis, Characterization, and Properties of a Polyhedral Oligomeric Octadiphenylsulfonylsilsesquioxane. *J. Appl. Polym. Sci.* **2014**, *131* (20), n/a-n/a. https://doi.org/10.1002/app.40892.

(50) Roll, M. F.; Kampf, J. W.; Kim, Y.; Yi, E.; Laine, R. M. Nano Building Blocks via Iodination of $[PhSiO_{1.5}]_n$, Forming $[p\text{-}I\text{-}C_6H_4SiO_{1.5}]_n$ (n = 8, 10, 12), and a New Route to High-Surface-Area, Thermally Stable, Microporous Materials via Thermal Elimination of I_2. *J. Am. Chem. Soc.* **2010**, *132* (29), 10171–10183. https://doi.org/10.1021/ja102453s.

(51) Chimjarn, S.; Kunthom, R.; Chancharone, P.; Sodkhomkhum, R.; Sangtrirutnugul, P.; Ervithayasuporn, V. Synthesis of Aromatic Functionalized Cage-Rearranged Silsesquioxanes (T_8, T_{10}, and T_{12}) via Nucleophilic Substitution Reactions. *Dalton Trans.* **2015**, *44* (3), 916–919. https://doi.org/10.1039/C4DT02941K.

(52) Laine, R. M.; Sulaiman, S.; Brick, C.; Roll, M.; Tamaki, R.; Asuncion, M. Z.; Neurock, M.; Filhol, J.-S.; Lee, C.-Y.; Zhang, J.; Goodson, T.; Ronchi, M.; Pizzotti, M.; Rand, S. C.; Li, Y. Synthesis and Photophysical Properties of Stilbeneoctasilsesquioxanes. Emission Behavior Coupled with Theoretical Modeling Studies Suggest a 3-D Excited State Involving the Silica Core. *J. Am. Chem. Soc.* **2010**, *132* (11), 3708–3722. https://doi.org/10.1021/ja9087709.

(53) Sulaiman, S.; Zhang, J.; Goodson, III, T.; Laine, R. M. Synthesis, Characterization and Photophysical Properties of Polyfunctional Phenylsilsesquioxanes: [O-RPhSiO1.5]8, [2,5-R2PhSiO1.5]8, and [R3PhSiO1.5]8. Compounds with the Highest Number of Functional Units/Unit Volume. *J. Mater. Chem.* **2011**, *21* (30), 11177. https://doi.org/10.1039/c1jm11701g.

(54) Asuncion, M. Z.; Roll, M. F.; Laine, R. M. Octaalkynylsilsesquioxanes, Nano Sea Urchin Molecular Building Blocks for 3-D-Nanostructures. *Macromolecules* **2008**, *41* (21), 8047–8052. https://doi.org/10.1021/ma801480p.

(55) Pérez-Ojeda, M. E.; Trastoy, B.; Rol, Á.; Chiara, M. D.; García-Moreno, I.; Chiara, J. L. Controlled Click-Assembly of Well-Defined Hetero-Bifunctional Cubic Silsesquioxanes and Their Application in Targeted Bioimaging. *Chem. Eur. J.* **2013**, *19* (21), 6630–6640. https://doi.org/10.1002/chem.201300339.

(56) Bahrami, M.; Hashemi, H.; Ma, X.; Kieffer, J.; Laine, R. M. Why Do the $[PhSiO_{1.5}]_{8,10,12}$ Cages Self-Brominate Primarily in the Ortho Position? Modeling Reveals a Strong Cage Influence on the Mechanism. *Phys. Chem. Chem. Phys.* **2014**, *16* (47), 25760–25764. https://doi.org/10.1039/C4CP03997A.

(57) Ohshita, J.; Tsuchida, T.; Komaguchi, K.; Yamamoto, K.; Adachi, Y.; Ooyama, Y.; Harima, Y.; Tanaka, K. Studies on Spherically Distributed LUMO and Electron-Accepting Properties of Caged Hexakis(Germasesquioxanes). *Organometallics* **2017**, *36* (14), 2536–2540. https://doi.org/10.1021/acs.organomet.6b00950.

(58) Sulaiman, S. *Synthesis and characterization of polyfunctional Polyhedral Silsesquioxane Cages* (Doctoral dissertation, University of Michigan), **2011**.

(59) Feher, F. J.; Soulivong, D.; Lewis, G. T. Facile Framework Cleavage Reactions of a Completely Condensed Silsesquioxane Framework. *J. Am. Chem. Soc.* **1997**, *119* (46), 11323–11324. https://doi.org/10.1021/ja972436t.

(60) Lichtenhan, J. D.; Otonari, Y. A.; Carr, M. J. Linear Hybrid Polymer Building Blocks: Methacrylate-Functionalized Polyhedral Oligomeric Silsesquioxane Monomers and Polymers. *Macromolecules* **1995**, *28* (24), 8435–8437. https://doi.org/10.1021/ma00128a067.
(61) Wu, S.; Hayakawa, T.; Kikuchi, R.; Grunzinger, S. J.; Kakimoto, M.; Oikawa, H. Synthesis and Characterization of Semiaromatic Polyimides Containing POSS in Main Chain Derived from Double-Decker-Shaped Silsesquioxane. *Macromolecules* **2007**, *40* (16), 5698–5705. https://doi.org/10.1021/ma070547z.
(62) Seino, M.; Hayakawa, T.; Ishida, Y.; Kakimoto, M.; Watanabe, K.; Oikawa, H. Hydrosilylation Polymerization of Double-Decker-Shaped Silsesquioxane Having Hydrosilane with Diynes. *Macromolecules* **2006**, *39* (10), 3473–3475. https://doi.org/10.1021/ma052631p.
(63) Ootake, N.; Yoshida, K. Organic Silicon Compound and Method for Producing Same, and Polysiloxane and Method for Producing Same. *20060155091 A* **2006**, *1*.
(64) Yoshida, K.; Hattori, T.; Ootake, N.; Tanaka, R.; Matsumoto, H. Silsesquioxane-Based Polymers: Synthesis of Phenylsilsesquioxanes with Double-Decker Structure and Their Polymers. In *Silicon Based Polymers*; Ganachaud, F., Boileau, S., Boury, B., Eds.; Springer Netherlands: Dordrecht, **2008**; pp 205–211. https://doi.org/10.1007/978-1-4020-8528-4_14.
(65) Joshi, M.; Butola, B. S. Polymeric Nanocomposites—Polyhedral Oligomeric Silsesquioxanes (POSS) as Hybrid Nanofiller. *Journal of Macromolecular Science, Part C: Polymer Reviews* **2004**, *44* (4), 389–410. https://doi.org/10.1081/MC-200033687.
(66) Kannan, R. Y.; Salacinski, H. J.; Butler, P. E.; Seifalian, A. M. Polyhedral Oligomeric Silsesquioxane Nanocomposites: The Next Generation Material for Biomedical Applications. *Acc. Chem. Res.* **2005**, *38* (11), 879–884. https://doi.org/10.1021/ar050055b.
(67) Ervithayasuporn, V.; Wang, X.; Kawakami, Y. Synthesis and Characterization of Highly Pure Azido-Functionalized Polyhedral Oligomeric Silsesquioxanes (POSS). *Chem. Commun.* **2009**, No. 34, 5130. https://doi.org/10.1039/b909802j.
(68) Ervithayasuporn, V.; Sodkhomkhum, R.; Teerawatananond, T.; Phurat, C.; Phinyocheep, P.; Somsook, E.; Osotchan, T. Unprecedented Formation of Cis- and Trans-Di[(3-Chloropropyl)Isopropoxysilyl]-Bridged Double-Decker Octaphenylsilsesquioxanes. *European Journal of Inorganic Chemistry* **2013**, *2013* (19), 3292–3296. https://doi.org/10.1002/ejic.201300283.
(69) Schoen, B. W.; Lira, C. T.; Lee, A. Separation and Solubility of Cis and Trans Isomers in Nanostructured Double-Decker Silsequioxanes. *J. Chem. Eng. Data* **2014**, *59* (5), 1483–1493. https://doi.org/10.1021/je4010245.
(70) Vogelsang, D. F.; Dannatt, J. E.; Schoen, B. W.; Maleczka, R. E.; Lee, A. Phase Behavior of *Cis – Trans* Mixtures of Double-Decker Shaped Silsesquioxanes for Processability Enhancement. *ACS Appl. Nano Mater.* **2019**, *2* (3), 1223–1231. https://doi.org/10.1021/acsanm.8b02114.
(71) Lee, D. W.; Kawakami, Y. Incompletely Condensed Silsesquioxanes: Formation and Reactivity. *Polym J* **2007**, *39* (3), 230–238. https://doi.org/10.1295/polymj.PJ2006169.
(72) Schoen, B. W.; Holmes, D.; Lee, A. Identification and Quantification of *Cis* and *Trans* Isomers in Aminophenyl Double-Decker Silsesquioxanes Using ^{1}H- ^{29}Si GHMBC NMR: Quantification of *Cis* and *Trans* Isomers in Double-Decker Silsesquioxanes. *Magn. Reson. Chem.* **2013**, *51* (8), 490–496. https://doi.org/10.1002/mrc.3962.
(73) Żak, P.; Dudziec, B.; Kubicki, M.; Marciniec, B. Silylative Coupling versus Metathesis-Efficient Methods for the Synthesis of Difunctionalized Double-Decker Silsesquioxane Derivatives. *Chem. Eur. J.* **2014**, *20* (30), 9387–9393. https://doi.org/10.1002/chem.201402862.

(74) Gayanthi Kumari Attanayake. STUDY OF DIFFERENT ROUTES TO DEVELOP ASYMMETRIC DOUBLE DECKER SILSESQUIOXANE (DDSQ). **2015**. https://doi.org/10.13140/RG.2.2.36605.36322.
(75) Żak, P.; Majchrzak, M.; Wilkowski, G.; Dudziec, B.; Dutkiewicz, M.; Marciniec, B. Synthesis and Characterization of Functionalized Molecular and Macromolecular Double-Decker Silsesquioxane Systems. *RSC Adv.* **2016**, *6* (12), 10054–10063. https://doi.org/10.1039/C5RA20848C.
(76) Żak, P.; Dudziec, B.; Dutkiewicz, M.; Ludwiczak, M.; Marciniec, B.; Nowicki, M. A New Class of Stereoregular Vinylene-Arylene Copolymers with Double-Decker Silsesquioxane in the Main Chain. *J. Polym. Sci. Part A: Polym. Chem.* **2016**, *54* (8), 1044–1055. https://doi.org/10.1002/pola.27957.
(77) Mituła, K.; Duszczak, J.; Brząkalski, D.; Dudziec, B.; Kubicki, M.; Marciniec, B. Tetra-Functional Double-Decker Silsesquioxanes as Anchors for Reactive Functional Groups and Potential Synthons for Hybrid Materials. *Chem. Commun.* **2017**, *53* (75), 10370–10373. https://doi.org/10.1039/C7CC03958A.
(78) Mituła, K.; Dudziec, B.; Marciniec, B. Synthesis of Dialkenyl-Substituted Double-Decker Silsesquioxanes as Precursors for Linear Copolymeric Systems. *J Inorg Organomet Polym* **2018**, *28* (2), 500–507. https://doi.org/10.1007/s10904-017-0746-y.
(79) Żak, P.; Delaude, L.; Dudziec, B.; Marciniec, B. N-Heterocyclic Carbene-Based Ruthenium-Hydride Catalysts for the Synthesis of Unsymmetrically Functionalized Double-Decker Silsesquioxanes. *Chem. Commun.* **2018**, *54* (34), 4306–4309. https://doi.org/10.1039/C8CC01316K.
(80) Tanaka, T.; Hasegawa, Y.; Kawamori, T.; Kunthom, R.; Takeda, N.; Unno, M. Synthesis of Double-Decker Silsesquioxanes from Substituted Difluorosilane. *Organometallics* **2019**, *38* (4), 743–747. https://doi.org/10.1021/acs.organomet.8b00896.
(81) Kowalewska, A.; Nowacka, M. Synthesis of Ladder Silsesquioxanes by in Situ Polycondensation of Cyclic Tetravinylsiloxanetetraols. *Silicon* **2015**, *7* (2), 133–146. https://doi.org/10.1007/s12633-014-9209-z.
(82) Choi, S.-S.; Lee, A. S.; Lee, H. S.; Jeon, H. Y.; Baek, K.-Y.; Choi, D. H.; Hwang, S. S. Synthesis and Characterization of UV-Curable Ladder-like Polysilsesquioxane. *Journal of Polymer Science Part A: Polymer Chemistry* **2011**, *49* (23), 5012–5018. https://doi.org/10.1002/pola.24942.
(83) Kamino, B. A.; Bender, T. P. The Use of Siloxanes, Silsesquioxanes, and Silicones in Organic Semiconducting Materials. *Chem. Soc. Rev.* **2013**, *42* (12), 5119. https://doi.org/10.1039/c3cs35519e.
(84) Pielichowski, K.; Njuguna, J.; Janowski, B.; Pielichowski, J. Polyhedral Oligomeric Silsesquioxanes (POSS)-Containing Nanohybrid Polymers. In *Supramolecular Polymers Polymeric Betains Oligomers*; Advances in Polymer Science; Springer: Berlin, Heidelberg, **2006**; pp 225–296. https://doi.org/10.1007/12_077.
(85) Brook, M. A. Silicon in Organic, Organometallic, and Polymer Chemistry /; Michael A. Brook. **2000**.
(86) Zhang, Z.-X.; Hao, J.; Xie, P.; Zhang, X.; Han, C. C.; Zhang, R. A Well-Defined Ladder Polyphenylsilsesquioxane (Ph-LPSQ) Synthesized via a New Three-Step Approach: Monomer Self-Organization−Lyophilization—Surface-Confined Polycondensation. *Chem. Mater.* **2008**, *20* (4), 1322–1330. https://doi.org/10.1021/cm071602l.

(87) Unno, M.; Suto, A.; Matsumoto, T. Laddersiloxanes — Silsesquioxanes with Defined Ladder Structure. *Russ. Chem. Rev.* **2013**, *82* (4), 289–302. https://doi.org/10.1070/RC2013v082n04ABEH004360.
(88) Ren, Z.; Xie, P.; Jiang, S.; Yan, S.; Zhang, R. Study of the Supramolecular Architecture-Directed Synthesis of a Well-Defined Triple-Chain Ladder Polyphenylsiloxane. *Macromolecules* **2010**, *43* (5), 2130–2136. https://doi.org/10.1021/ma100145j.
(89) Chen, Z.; Li, Z.; Guo, H.; Zhang, J.; Ren, Z.; Yan, S.; Xie, P.; Zhang, R. Supramolecular Template-Directed Synthesis of Soluble Quadruple-Chain Ladder Polyphenylsiloxane (Ph-QCLP) with High Molecular Weight. *Chem. Mater.* **2012**, *24* (10), 1968–1973. https://doi.org/10.1021/cm300951x.
(90) Jia, X. W.; Rong, M. Z.; Zhang, M. Q.; Ye, X. J. A Facile Approach for Preparing Polymethylphenylsilsesquioxane with Well-Defined Ladder Structure via Nonhydrolytic Condensation. *Chem. Lett.* **2010**, *39* (9), 1010–1012. https://doi.org/10.1246/cl.2010.1010.
(91) Seki, H.; Kajiwara, T.; Abe, Y.; Gunji, T. Synthesis and Structure of Ladder Polymethylsilsesquioxanes from Sila-Functionalized Cyclotetrasiloxanes. *Journal of Organometallic Chemistry* **2010**, *695* (9), 1363–1369. https://doi.org/10.1016/j.jorganchem.2010.02.008.
(92) Seki, H.; Abe, N.; Abe, Y.; Gunji, T. Synthesis and Structure of *Syn* , *Anti* , *Syn* -Pentacyclic Ladder Oligomethylsilsesquioxane. *Chem. Lett.* **2011**, *40* (7), 722–723. https://doi.org/10.1246/cl.2011.722.
(93) Lee, H. S.; Choi, S.-S.; Baek, K.-Y.; Hong, S. M.; Lee, E. C.; Lee, J.-C.; Hwang, S. S. Synthesis and Structure Characterization of Ladder-like Polymethylsilsesquioxane (PMSQ) by Isolation of Stereoisomer. *European Polymer Journal* **2012**, *48* (6), 1073–1081. https://doi.org/10.1016/j.eurpolymj.2012.03.008.
(94) Unno, M.; Matsumoto, T.; Matsumoto, H. Nonacyclic Ladder Silsesquioxanes and Spectral Features of Ladder Polysilsesquioxanes. *International Journal of Polymer Science* **2012**, *2012*, 1–4. https://doi.org/10.1155/2012/723892.
(95) Azinovic, D.; Cai, J.; Eggs, C.; Ko, H. Photoluminescence from Silsesquioxanes R8ðSiO1:5Þ8. *Journal of Luminescence* **2002**, 11.
(96) Furgal, J.C. *Synthesis and structure-photophysical property relationships of T 8, T 10, T 12 and oligomeric organic functionalized silsesquioxanes* (Doctoral dissertation, University of Michigan), **2015**.
(97) Schubert, U., *Silicon Chemistry*; Springer Vienna: Vienna, **1999**. https://doi.org/10.1007/978-3-7091-6357-3.
(98) Chan, K. L.; Sonar, P.; Sellinger, A. Cubic Silsesquioxanes for Use in Solution Processable Organic Light Emitting Diodes (OLED). *J. Mater. Chem.* **2009**, *19* (48), 9103. https://doi.org/10.1039/b909234j.
(99) Xiao, S.; Nguyen, M.; Gong, X.; Cao, Y.; Wu, H.; Moses, D.; Heeger, A. J. Stabilization of Semiconducting Polymers with Silsesquioxane. *Advanced Functional Materials* **2003**, *13* (1), 25–29. https://doi.org/10.1002/adfm.200390000.
(100) Lee, J.; Cho, H.-J.; Cho, N. S.; Hwang, D.-H.; Shim, H.-K. Synthesis of Polyhedral Oligomeric Silsesquioxane-Functionalized Polyfluorenes: Hybrid Organic–Inorganic π-Conjugated Polymers. *Synthetic Metals* **2006**, *156* (7–8), 590–596. https://doi.org/10.1016/j.synthmet.2006.02.011.
(101) André, P.; Cheng, G.; Ruseckas, A.; van Mourik, T.; Früchtl, H.; Crayston, J. A.; Morris, R. E.; Cole-Hamilton, D.; Samuel, I. D. W. Hybrid Dendritic Molecules with Confined

Chromophore Architecture to Tune Fluorescence Efficiency. *J. Phys. Chem. B* **2008**, *112* (51), 16382–16392. https://doi.org/10.1021/jp806031q.
(102) Vautravers, N. R.; André, P.; Cole-Hamilton, D. J. Fluorescence Activation of a Polyhedral Oligomeric Silsesquioxane in the Presence of Reducing Agents. *J. Mater. Chem.* **2009**, *19* (26), 4545. https://doi.org/10.1039/b818060a.
(103) Zhen, C.-G.; Becker, U.; Kieffer, J. Tuning Electronic Properties of Functionalized Polyhedral Oligomeric Silsesquioxanes: A DFT and TDDFT Study. *J. Phys. Chem. A* **2009**, *113* (35), 9707–9714. https://doi.org/10.1021/jp903796m.
(104) Asuncion, M. Z.; Laine, R. M. Fluoride Rearrangement Reactions of Polyphenyl- and Polyvinylsilsesquioxanes as a Facile Route to Mixed Functional Phenyl, Vinyl T_{10} and T_{12} Silsesquioxanes. *J. Am. Chem. Soc.* **2010**, *132* (11), 3723–3736. https://doi.org/10.1021/ja9087743.
(105) Peterson, J. J.; Simon, Y. C.; Coughlin, E. B.; Carter, K. R. Polyfluorene with P-Carborane in the Backbone. *Chem. Commun.* **2009**, No. 33, 4950. https://doi.org/10.1039/b908131c.
(106) Peterson, J. J.; Werre, M.; Simon, Y. C.; Coughlin, E. B.; Carter, K. R. Carborane-Containing Polyfluorene: *O*- Carborane in the Main Chain. *Macromolecules* **2009**, *42* (22), 8594–8598. https://doi.org/10.1021/ma901703r.
(107) Peterson, J. J.; Davis, A. R.; Werre, M.; Coughlin, E. B.; Carter, K. R. Carborane-Containing Poly(Fluorene): Response to Solvent Vapors and Amines. *ACS Appl. Mater. Interfaces* **2011**, *3* (6), 1796–1799. https://doi.org/10.1021/am2000856.
(108) Xiang, K.-H.; Pandey, R.; Pernisz, U. C.; Freeman, C. Theoretical Study of Structural and Electronic Properties of H-Silsesquioxanes. *J. Phys. Chem. B* **1998**, *102* (44), 8704–8711. https://doi.org/10.1021/jp981840r.
(109) Lin; He; Xiao, Y. Theoretical Studies of Monosubstituted and Higher Phenyl-Substituted Octahydrosilsesquioxanes. *J. Phys. Chem. B* **2003**, *107* (50), 13788–13792. https://doi.org/10.1021/jp036044m.
(110) Laine, R. M.; Sulaiman, S.; Brick, C.; Roll, M.; Tamaki, R.; Asuncion, M. Z.; Neurock, M.; Filhol, J.-S.; Lee, C.-Y.; Zhang, J.; Goodson, T.; Ronchi, M.; Pizzotti, M.; Rand, S. C.; Li, Y. Synthesis and Photophysical Properties of Stilbeneoctasilsesquioxanes. Emission Behavior Coupled with Theoretical Modeling Studies Suggest a 3-D Excited State Involving the Silica Core. *J. Am. Chem. Soc.* **2010**, *132* (11), 3708–3722. https://doi.org/10.1021/ja9087709.
(111) Sulaiman, S.; Bhaskar, A.; Zhang, J.; Guda, R.; Goodson, T.; Laine, R. M. Molecules with Perfect Cubic Symmetry as Nanobuilding Blocks for 3-D Assemblies. Elaboration of Octavinylsilsesquioxane. Unusual Luminescence Shifts May Indicate Extended Conjugation Involving the Silsesquioxane Core. *Chem. Mater.* **2008**, *20* (17), 5563–5573. https://doi.org/10.1021/cm801017e.
(112) Calzaferri, G.; Hoffrnann, R. The SymmetricaI Octasilasesquioxanes &s I80 2: Electronic Structure and Reactivityt. *J. CHEM. SOC. DALTON TRANS.* **1991**, 12.
(113) Crosby, G. A.; Demas, J. N. Measurement of Photoluminescence Quantum Yields. Review. *J. Phys. Chem.* **1971**, *75* (8), 991–1024. https://doi.org/10.1021/j100678a001.
(114) Stephen, W. I. *CA Parker, Photoluminescence of Solutions: Elsevier Publishing Company, Amsterdam, 1968, Xvi+ 544 Pp., Price Dfl. 85,—*; Elsevier**, 1969**.
(115) Song, J.; Kim, K.-H.; Kim, E.; Moon, C.-K.; Kim, Y.-H.; Kim, J.-J.; Yoo, S. Lensfree OLEDs with over 50% External Quantum Efficiency via External Scattering and

Horizontally Oriented Emitters. *Nat Commun* **2018**, *9* (1), 3207. https://doi.org/10.1038/s41467-018-05671-x.
(116) Zhao, B.; Bai, S.; Kim, V.; Lamboll, R.; Shivanna, R.; Auras, F.; Richter, J. M.; Yang, L.; Dai, L.; Alsari, M.; She, X.-J.; Liang, L.; Zhang, J.; Lilliu, S.; Gao, P.; Snaith, H. J.; Wang, J.; Greenham, N. C.; Friend, R. H.; Di, D. High-Efficiency Perovskite–Polymer Bulk Heterostructure Light-Emitting Diodes. *Nature Photon* **2018**, *12* (12), 783–789. https://doi.org/10.1038/s41566-018-0283-4.
(117) Caruge, J. M.; Halpert, J. E.; Wood, V.; Bulović, V.; Bawendi, M. G. Colloidal Quantum-Dot Light-Emitting Diodes with Metal-Oxide Charge Transport Layers. *Nature Photon* **2008**, *2* (4), 247–250. https://doi.org/10.1038/nphoton.2008.34.
(118) Smith, M. B.; Michl, J. Singlet Fission. *Chem. Rev.* **2010**, *110* (11), 6891–6936. https://doi.org/10.1021/cr1002613.
(119) Fischer, M.; Georges, J. Fluorescence Quantum Yield of Rhodamine 6G in Ethanol as a Function of Concentration Using Thermal Lens Spectrometry. *Chemical Physics Letters* **1996**, *260* (1), 115–118. https://doi.org/10.1016/0009-2614(96)00838-X.
(120) Braslavsky, S. E. Glossary of Terms Used in Photochemistry, 3rd Edition (IUPAC Recommendations 2006). *Pure and Applied Chemistry* **2007**, *79* (3), 293–465. https://doi.org/10.1351/pac200779030293.
(121) Weber, G.; Teale, F. W. J. Determination of the Absolute Quantum Yield of Fluorescent Solutions. *Trans. Faraday Soc.* **1957**, *53*, 646. https://doi.org/10.1039/tf9575300646.
(122) Montalti, M.; Credi, A.; Prodi, L.; Gandolfi, M. T. *Handbook of Photochemistry*; CRC Press, **2006**.
(123) Mello, J. C. de; Wittmann, H. F.; Friend, R. H. An Improved Experimental Determination of External Photoluminescence Quantum Efficiency. *Advanced Materials* **1997**, *9* (3), 230–232. https://doi.org/10.1002/adma.19970090308.
(124) Greenham, N. C.; Samuel, I. D. W.; Hayes, G. R.; Phillips, R. T.; Kessener, Y. A. R. R.; Moratti, S. C.; Holmes, A. B.; Friend, R. H. Measurement of Absolute Photoluminescence Quantum Efficiencies in Conjugated Polymers. *Chemical Physics Letters* **1995**, *241* (1), 89–96. https://doi.org/10.1016/0009-2614(95)00584-Q.
(125) Porrès, L.; Holland, A.; Pålsson, L.-O.; Monkman, A. P.; Kemp, C.; Beeby, A. Absolute Measurements of Photoluminescence Quantum Yields of Solutions Using an Integrating Sphere. *J Fluoresc* **2006**, *16* (2), 267–273. https://doi.org/10.1007/s10895-005-0054-8.
(126) Walsh, J. W. T. Photometry". Constable, London. **1953**.
(127) Fries, F.; Reineke, S. Statistical Treatment of Photoluminescence Quantum Yield Measurements. *Sci Rep* **2019**, *9* (1), 15638. https://doi.org/10.1038/s41598-019-51718-4.
(128) Cassabois, G., Valvin, P. and Gil, B., 2016. Hexagonal boron nitride is an indirect bandgap semiconductor. *Nature photonics*, *10*(4), pp.262-266.

Chapter 2. Experimental Methods

2.1 Materials

Tetrahydrofuran (THF), hexane, and toluene were purchased from Fisher and distilled from Na/benzophenone prior to use. Dichloromethane (CH_2Cl_2) and acetonitrile (CH_3CN) were purchased from Fisher and distilled from CaH_2 under N_2 prior to use. Methanol (CH_3OH) and anhydrous diethyl ether was purchased from Fisher and used as received. Tris(dibenzylideneacetone)dipalladium(0) ($Pd_2(dba)_3$), bis-(tri-tert-butylphosphine)palladium(0) ($Pd(t\text{-}Bu_3P)_2$), Grubbs 1st [$RuCl_2(=CHPh)(PCy_3)_2$] and 2nd generation catalyst [$RuCl_2(=CHPh)(NHC)(PCy_3)$] were purchased from Sigma-Aldrich and used as received.

Trisilanol phenylsilsesquioxane $(PhSiO_{1.5})_7(O_{0.5}H)_3$ and tetrasilanol phenylsilsesquioxane $(PhSiO_{1.5})_8(O_{0.5}H)_4$ were purchased from Hybrid Plastics Inc. Ladder phenylsilsesquixoanes vinyl(Me/Ph)$Si(O_{0.5})_2(PhSiO_{1.5})_4(O_{0.5})_2$Si(Me/Ph)vinyl were a gift from Professor Masafumi Unno's group from Gunma University in Japan.

Methyltrichlorosilane (CH_3SiCl_3), n-propyltrichlorosilane ($nC_3H_7SiCl_3$), trimethylchlorosilane [$(CH_3)_3SiCl$] and dimethyldichlorosilane [$(CH_3)_2SiCl_2$] were purchased from Sigma-Aldrich and used as received. 4-methylstyrene, 4-cyanostyrene, 1,4-dibromobenzene, 1,4-diiodobenzene, 4,4′-dibromo-1,1′-biphenyl, 4,4″-dibromo-p-terphenyl, 4,4′-dibromo-trans-stilbene, 2,5-dibromothiophene, 5,5′-dibromo-2,2′-bithiophene, 2,5-dibromothieno[3,2-b]thiophene, 2,7-dibromo-9,9-dimethylfluorene, 4,7-dibromobenzothiadiazole, 3,6-dibromocarbazole, bromobenzene, 2-bromothiophene, 2-bromo-9,9-dimethylfluorene, 4-bromo-1,2,3-benzothiaidaozle, and 3-bromocarbazole., 2,3,5,6-Tetrafluoro-7,7,8,8-tetracyanoquinodimethane F_4TCNQ and all other chemicals were purchased from Fisher or Sigma-Aldrich and used as received.

2.2 Syntheses

2.2.1 Corner missing silsesquioxanes $(PhSiO_{1.5})_7(O_{0.5}H)_3$

Synthesis of close cage Ph_7T_8R (R=Me or nPr).[1] To a dry 250 mL Schlenk flask under N_2 were added $(PhSiO_{1.5})_7(O_{0.5}H)_3$ (10.0 g, 10.75 mmol), 75 mL of THF, and $RSiCl_3$ (11.83 mmol). Following the addition, a 25 mL of THF solution of Et_3N (4.4 g, 43.0 mmol) was added over a 10 min

period. The reaction was stirred magnetically under N_2 for 24 h and then transferred to a separatory funnel. It was washed with brine (50 mL), 1 M HCl (10 mL), and brine (50 mL), and diethyl ether was added to extract the organic layer. Thereafter, the organic layer was dried over $MgSO_4$, and most solvent was removed by rotary evaporation. The resulting thick slurry was slowly poured into cold, well-stirred methanol (100 mL) to fully precipitate the product, which was recovered by filtration and dried under vacuum to give a 75% yield of white product. Ph_7T_8Me: MALDI-TOF (Ag^+) m/z=1079, Calculated=1078; GPC M_n=715, M_w=725, PDI=1.01; ^1H NMR (400 MHz, $CDCl_3$) 7.74 (m, 14H, Ph); 7.36 (m, 21H, Ph); 0.31 ppm (s, 3H, Me). Ph_7T_8Pr: MALDI-TOF (Ag^+) m/z=1107, Calculated=1106; GPC M_n=757, M_w=770, PDI=1.02; ^1H NMR (400 MHz, $CDCl_3$) 7.73 (m, 14H, Ph); 7.36 (m, 21H, Ph); 1.53 (m, 2H, nPr); 0.98 (t, 3H, nPr); 0.85 ppm (t, 2H, nPr)

Synthesis of corner-missing cage $Ph_7T_7(O_{0.5}SiMe_3)_3$. To a dry 250 mL Schlenk flask under N_2 were added $(PhSiO_{1.5})_7(O_{0.5}H)_3$ (10.0 g, 10.75 mmol), 100 mL of THF, Et_3N (6.5 g, 64.5 mmol), and Me_3SiCl (7.0 g, 64.5 mmol). The reaction was stirred magnetically under N_2 for 24 h and then transferred to a separatory funnel. It was washed with brine (50 mL), 1 M HCl (10 mL), and brine (50 mL), and diethyl ether was added to extract the organic layer. Thereafter, the organic layer was dried over $MgSO_4$, and most solvent was removed by rotary evaporation. The resulting thick slurry was slowly poured into cold, well-stirred methanol (100 mL) to fully precipitate the product, which was recovered by filtration and dried under vacuum to give a 70% yield of white product. $Ph_7T_7(O_{0.5}SiMe_3)_3$: MALDI-TOF (Ag^+) m/z=1255, Calculated=1254; GPC M_n=766, M_w=779, PDI=1.02; ^1H NMR (400 MHz, $CDCl_3$) 7.43 (m, 7H, Ph); 7.31 (m, 14H, Ph); 7.12 (m, 14H, Ph); 0.25 ppm (s, 27H, Me).

General bromination of Ph_7T_8R and $Ph_7T_7(O_{0.5}SiMe_3)_3$.[2] To a dry 100 mL Schlenk flask under N_2 were added Ph_7T_8R and $Ph_7T_7(O_{0.5}SiMe_3)_3$ (5.0 mmol, phenyl: 35.0 mmol) and 25 mL of CH_2Cl_2. A condenser was then attached, and the flask was heated to 45 °C in an oil bath. Thereafter, Br_2 (3.0 mL, 57.8 mmol) was added dropwise to the solution, and an additional 3 mL of CH_2Cl_2 was added to wash the condenser. After that, a vent to a bubbler containing aqueous base was added, and the solution was stirred magnetically under reflux at 45 °C for 5.5 h. At this point, 20 g of $Na_2S_2O_5$ and 10 g of Na_2CO_3 were dissolved in 40 mL of water and then added to the solution with vigorous stirring until the Br_2 color disappeared. The mixture was then transferred to a separatory funnel, and the organic layer was extracted and washed sequentially with brine (20 mL). Thereafter, the organic layer was dried over $MgSO_4$. Then charcoal and Celite were added and

stirred for 10 min. The black mixture was filtered to give a clear, colorless liquid. Most solvent was removed by rotary evaporation, and the resulting solid was redissolved in a minimal amount of THF and slowly poured into cold, well-stirred methanol (100 mL) to fully precipitate the product, which was recovered from filtration and dried under vacuum to give a 60% yield of white product. *o*-$Br_6Ph_7T_8Me$: MALDI-TOF (Ag^+) m/z=1546; GPC M_n=531, M_w=540, PDI=1.02; ^1H NMR (400 MHz, $CDCl_3$) 7.73 (m, 7H, Ph); 7.54 (m, 7H, Ph); 7.37 (m, 7H, Ph); 7.26 (d, 7H, Ph); 0.42 (s, 3H, Me); TGA (air, 10 °C/min 1000 °C): found 30%, calc 32%, $T_{d5\%}$: 436 °C. *o*-$Br_7Ph_7T_8Pr$: MALDI-TOF m/z=1540; GPC M_n=546, M_w=556, PDI=1.02; ^1H NMR (400 MHz, $CDCl_3$) 7.74 (m, 7H, Ph); 7.54 (m, 7H, Ph); 7.37 (m, 7H, Ph); 7.26 (d, 7H, Ph); 1.53 (m, 2H, nPr); 0.96 (t, 3H, nPr); 0.85 (t, 2H, nPr); TGA (air, 10 °C/min 1000 °C): found 31%, calc 31%, $T_{d5\%}$: 435 °C.

General iodination of Ph_7T_8R and $Ph_7T_7(O_{0.5}SiMe_3)_3$.[3] To a dry 250 mL Schlenk flask under N_2 was added 70 mL of a 1 M solution ICl in CH_2Cl_2. The flask was then cooled to −40 °C with a cold bath (50% v/v of ethylene glycol in ethanol). Ph_7T_8R and $Ph_7T_7(O_{0.5}SiMe_3)_3$ (5.0 mmol) was added slowly to the reaction mixture. After that, a vent to a bubbler containing aqueous base was added, and the solution was stirred magnetically at −40 °C for 6.0 h. At this point, 20 g of $Na_2S_2O_5$ and 10 g of Na_2CO_3 were dissolved in 40 mL of water and then added to the solution with vigorous stirring until the ICl color disappeared. The mixture was then transferred to a separatory funnel, and the organic layer was extracted and washed sequentially with brine (20 mL). Thereafter, the organic layer was dried over $MgSO_4$, and charcoal and Celite were added and stirred for 10 min. The black mixture was filtered to give a clear, colorless liquid. Most solvent was removed by rotary evaporation. The resulting was solid redissolved in minimal THF and slowly poured into cold, well-stirred methanol (100 mL) to fully precipitate the product. The product was recovered by filtration and dried under vacuum to give a 80% yield of white product. *p*-$I_7Ph_7T_8Me$: MALDI-TOF (Ag^+) m/z=1962; GPC M_n=428, M_w=496, PDI=1.16; ^1H NMR (400 MHz, $CDCl_3$) 7.72 (d, 14H, Ph); 7.37 (d, 14H, Ph); 0.34 (s, 3H, Me); TGA (air, 10 °C/min 1000 °C): found 26%, calc 26%, $T_{d5\%}$: 406 °C. *p*-$I_7Ph_7T_8Pr$: MALDI-TOF (Ag^+) m/z=1990; GPC M_n=412, M_w=498, PDI=1.20; ^1H NMR (400 MHz, $CDCl_3$) 7.72 (d, 14H, Ph); 7.37 (d, 14H, Ph); 1.52 (m, 2H, nPr); 0.93 (t, 3H, nPr); 0.81 (t, 2H, nPr); TGA (air, 10 °C/min 1000 °C): found 26%, calc 26%, $T_{d5\%}$: 396 °C.

General Heck reaction of brominated and iodinated Ph_7T_8R and $Ph_7T_7(O_{0.5}SiMe_3)_3$.[2] To a dry 100 mL Schlenk flask under N_2 were added brominated or iodinated Ph_7T_8R and

$Ph_7T_7(O_{0.5}SiMe_3)_3$ (1.0 mmol), $Pd[P(t\text{-}Bu_3)]_2$ (38.7 mg, 0.08 mmol), and $Pd_2(dba)_3$ (34.6 mg, 0.04 mmol), followed by 30 mL of THF, NCy_2Me (2.8 g, 14.0 mmol), and 4-methyl/cyano-styrene (14.0 mmol). The mixture was stirred magnetically at 70 °C for 24 h and then quenched by filtering through 1 cm Celite, which was washed with THF (5 mL). The solution was then concentrated and precipitated into cold, well-stirred methanol (100 mL) and filtered, and the yellowish solid was redissolved in THF (10 mL). The solution was then filtered again through a 1 cm Celite column to remove remaining Pd particles, concentrated, and reprecipitated into cold methanol (50 mL) to give a crude yellow product. *o*-$MeStil_6T_8Me$: MALDI-TOF m/z=1659; GPC M_n=846, M_w=877, PDI=1.04; TGA (air, 10 °C/min 1000 °C): found 30%, calc 29%, $T_{d5\%}$: 444 °C. *o*-$CNStil_6T_8Me$: MALDI-TOF (Ag^+) m/z=1843; GPC M_n=1286, M_w=1386, PDI=1.09; TGA (air, 10 °C/min 1000 °C): found 28%, calc 28%, $T_{d5\%}$: 439 °C. *p*-$MeStil_7T_8Me$: MALDI-TOF (Ag^+) m/z=1894; GPC M_n=897, M_w=1196, PDI=1.33; TGA (air, 10 °C/min 1000 °C): found 28%, calc 27%, $T_{d5\%}$: 448 °C. *p*-$CNStil_7T_8Me$: MALDI-TOF (Ag^+) m/z=1971; GPC M_n=1007, M_w=1151, PDI=1.14; TGA (air, 10 °C/min 1000 °C): found 26%, calc 26%, $T_{d5\%}$: 443 °C. *o*-$MeStil_7T_7(TMS)_3$: MALDI-TOF (Ag^+) m/z=2080; GPC M_n=1322, M_w=1434, PDI=1.08; TGA (air, 10 °C/min 1000 °C): found 30%, calc 31%, $T_{d5\%}$: 4415 °C. *o*-$CNStil_7T_7(TMS)_3$: MALDI-TOF (Ag^+) m/z=2137; GPC M_n=2193, M_w=2519, PDI=1.15; TGA (air, 10 °C/min 1000 °C): found 28%, calc 28%, $T_{d5\%}$: 402 °C. *p*-$MeStil_2Ph_5T_7(TMS)_3$: MALDI-TOF (Ag^+) m/z=1415; GPC M_n=1700, M_w=1987, PDI=1.17.

Removal of Pd catalyst.[4] To a dry 50 mL Schlenk flask under N_2 were added the above product dissolved in toluene (10 mL) and N-acetyl-L-cysteine (0.1 g) dissolved in THF (1 mL). The solution was stirred magnetically overnight at room temperature and then filtered through 1 cm Celite to remove the insoluble Pd−cysteine complex. Most solvent was removed by rotary evaporation, and the resulting solid was redissolved in a minimal amount of THF and slowly poured into cold, well-stirred methanol (50 mL) to fully precipitate the product. The product was then recovered by filtration and dried under vacuum to give a 70% yield of yellowish product.

2.2.2 Double decker silsesquioxanes $(PhSiO_{1.5})_8(O_{0.5}H)_4$

Synthesis of close cage $DDMe_4$. To a dry 500 mL Schlenk flask under N_2 were added $(PhSiO_{1.5})_8(O_{0.5}H)_4$ (10.0 g, 9.4 mmol), 200 mL of THF, and Me_2SiCl_2 (2.8 g, 21.5 mmol). Following the addition, a 10 mL THF solution of Et_3N (5.0 g, 49.5 mmol) was added over a 10 min period. The reaction was stirred magnetically under N_2 for 24 h and then transferred to a separatory

funnel. It was washed with brine (50 mL), 1 M HCl (10 mL) and brine (50 mL) and diethyl ether was added to extract the organic layer. Thereafter, the organic layer was dried over $MgSO_4$, and most of the solvent was removed by rotary evaporation. The resulting thick slurry was slowly poured into cold, well-stirred methanol (100 mL) to fully precipitate the product, which was recovered by filtration and dried under vacuum to give a 72% yield of a white product. $DDMe_4$: MALDI-TOF (Ag^+) m/z=1290, Calculated=1289; GPC M_n=756, M_w=807, PDI=1.07; ^1H NMR (400 MHz, $CDCl_3$) 7.53 (t, 8H, Ph); 7.39 (m, 16H, Ph); 7.17 (d, 16H, Ph); 0.31 (s, 12H, Me).

Synthesis of doubly-open cage $DD(O_{0.5}SiMe_3)_4$. To a dry 500 mL Schlenk flask under N_2 were added $(PhSiO_{1.5})_8(O_{0.5}H)_4$ (16.0 g, 15.0 mmol), 300 mL of THF, Et_3N (12.1 g, 120.0 mmol), and Me_3SiCl (13.0 g 120.0 mmol). The reaction was stirred magnetically under N_2 for 24 h and then transferred to a separatory funnel. It was washed with brine (50 mL), 1 M HCl (10 mL) and brine (50 mL) and diethyl ether was added to extract the organic layer. Thereafter, the organic layer was dried over $MgSO_4$ and most of the solvent was removed by rotary evaporation. The resulting thick slurry was slowly poured into cold, well-stirred methanol (100 mL) to fully precipitate the product, which was recovered by filtration and dried under vacuum to give a 74% yield of a white product. $DD(OTMS)_4$: MALDI-TOF (Ag^+) m/z=1466, Calculated=1465; GPC M_n=1026, M_w=1100, PDI=1.07; ^1H NMR (400 MHz, $CDCl_3$) 7.52 (m, 8H, Ph); 7.36 (m, 16H, Ph); 7.27 (m, 8H, Ph); 7.16 (t, 8H, Ph); 0.10 (s, 36H, Me).

General methods of halogenation, Heck coupling, purification, and photophysical analyses are identical to methods used in Chapter **2.2.1** above.

2.2.3 Double decker silsesquioxanes derived copolymers

Synthesis of vinyl(Me)DD(Me)vinyl or vinylDDvinyl. To an oven-dried 500 mL Schlenk flask under N_2 were added $(PhSiO_{1.5})_8(O_{0.5}H)_4$ (10.0 g, 9.4 mmol), 200 mL of THF, and vinyl-$MeSiCl_2$ (3.0 g, 21.5 mmol). Thereafter, 10 mL of THF solution of Et_3N (5.0 g, 49.5 mmol) was added dropwise via a pipet over a 10 min period. The reaction mixture was stirred magnetically under N_2 for 24 h at room temperature and then transferred to a 1000 mL separatory funnel. The organic layer was separated out by adding brine (50 mL) and then washed with 1 M HCl (10 mL) and brine (50 mL) sequentially to neutral. Diethyl ether can be added to help extract the organic layer from water solution. After that, the organic layer was separated out and dried over $MgSO_4$. The clear solution was then concentrated by rotary evaporation. The resulting thick slurry was

slowly added dropwise into cold, well-stirred methanol (200 mL) to fully precipitate the product, which was collected by filtration and dried in a vacuum oven overnight to give a 80% yield of white product. VinylDDvinyl: MALDI-TOF (Ag^+) m/z=1315, Calculated=1314; GPC M_n=1010, M_w=1080, PDI=1.07; ^{29}Si NMR (700 MHz, $CDCl_3$) -31.4, -78.4, -78.8, -79.5 ppm; TGA (air, 10 °C/min 1000 °C): found 49%, calc 50%, $T_{d5\%}$: 540 °C.

Fractional crystallization of vinylDDvinyl.[5] To an Erlenmeyer flask was added mixed isomers of vinylDDvinyl (1.20 g, 1.0 mmol). Minimal warm THF (8 mL) was added until the solid completely dissolved. Warm hexane (25 mL) was added dropwise until a white suspension persisted. The mixture was slowly cooled to room temperature and allowed to sit over 2 day. The precipitate was collected by filtration and dried in a vacuum oven overnight to give 69% yield of pure trans. ^{1}H NMR (400 MHz, $CDCl_3$) 7.62-7.33 (40H, Ph); 6.22 (d, 2H, -CH=CH2); 6.05 (m, 4H, -CH=CH2); 0.44 (s, 6H, Me); ^{29}Si NMR (700 MHz, $CDCl_3$) -31.4, -78.3, -79.5 ppm.

General Heck polymerization of vinylDDvinyl with X-Ar-X (X=Br, I, Ar=aromatic, benzene/phenyl, biphenyl, terphenyl, stilbene, 9,9-dimethylfluorene, thiophene, bithiophene, theinothiophene).[6] Previous work on synthesis of a series of functionalized SQs indicates efficient Heck cross-coupling catalyzed by $Pd[P(t\text{-}Bu)_3]_2$ and $Pd_2(dba)_3$ with molar ratio of 2:1. Such conditions were used to prepare model compounds in general Heck reaction of $vinylMeSi(OMe)_2$ with X-Ar-X and reaction of vinylDDvinyl with Br-Ar, as shown below. In Heck polymerization of vinylDDvinyl with X-Ar-X, different reaction conditions were tested and optimized to achieve polymers of high M_n. It was found that $Pd[P(t\text{-}Bu)_3]_2$ alone with a Pd:P of 1:2 better promotes polymerization and providing higher degrees of polymerization.

To an oven-dried 100 mL Schlenk flask under N_2 were added vinylDDvinyl (1.20 g, 1.0 mmol), NCy_2Me (0.81 g, 4.0 mmol), X-Ar-X (1.0 mmol), followed by 30 mL of THF and $Pd[P(t\text{-}Bu)_3]_2$ (38.7 mg, 0.08 mmol). The mixture was stirred magnetically at 100 °C and tracked by GPC. The reaction was filtered through 1 cm Celite which was washed with THF (5 mL). The resulting filtrate was concentrated by rotary evaporation, and the resulting concentrated solution was then precipitated into cold, well-stirred methanol (150 mL), filtered, and the colored solid redissolved in THF (10 mL). The solution was then filtered again through a 1 cm Celite column to further remove residual Pd particles, and concentrated, reprecipitated into cold, stirred methanol (100 mL) to give crude colored product. DD-co-phenyl: MALDI-TOF (monomer) m/z=1280, Calculated=1280; GPC M_n=19550, M_w=49410, PDI=2.53; ^{13}C NMR (700 MHz, $CDCl_3$) 146.2, 137.7,

134.0, 132.0, 131.1, 130.8, 130.4, 127.9, 127.7, 127.6, 127.0, 124.3, -0.7; ^{29}Si NMR (700 MHz, $CDCl_3$) -30.2, -78.2, -79.2, -79.4, -79.7; TGA (air, 10 °C/min 1000 °C): found 46%, calc 47%, $T_{d5\%}$: 460 °C. DD-co-biphenyl: MALDI-TOF (monomer) m/z=12355, Calculated=1356; GPC M_n=11690, M_w=24480, PDI=2.09; TGA (air, 10 °C/min 1000 °C): found 43%, calc 44%, $T_{d5\%}$: 400 °C. DD-co-thiophene: MALDI-TOF (monomer) m/z=1290, Calculated=1286; GPC M_n=22540, M_w=43250, PDI=1.92; TGA (air, 10 °C/min 1000 °C): found 47%, calc 47%, $T_{d5\%}$: 540 °C. DD-co-bithiophene: MALDI-TOF (monomer) m/z=1370, Calculated=1368; GPC M_n=3580, M_w=7200, PDI=2.01; TGA (air, 10 °C/min 1000 °C): found 42%, calc 44%, $T_{d5\%}$: 520 °C.

General Heck reaction of vinylMeSi(OMe)$_2$ with X-Ar-X. To an oven-dried 100 mL Schlenk flask under N_2 were added vinylMeSi(OMe)$_2$ (0.69 g, 5 mmol), NCy_2Me (0.41 g, 2.0 mmol), X-Ar-X (1.0 mmol). Following the addition 10 mL of THF, Pd[P(t-Bu)$_3$]$_2$ (19.4 mg, 0.04 mmol), and $Pd_2(dba)_3$ (17.3 mg, 0.02 mmol) were added. The mixture was stirred magnetically under N_2 at 70 °C and tracked by GPC. The reaction mixture was filtered through Celite to remove Pd catalyst, and the excess vinylMeSi(OMe)$_2$ was further removed by fractional distillation of the filtrate. 1,4-[(MeO)$_2$Sivinyl]$_2$benzene: ^{1}H NMR (400 MHz, $CDCl_3$) 7.39 (d, 4H, Ph); 7.17 (d, 2H, vinyl); 6.31 (d, 2H, vinyl); 3.62 (s, 12H, MeO); 0.30 (s, 6H, Me); 4,4'-[(MeO)$_2$Sivinyl]$_2$biphenyl: ^{1}H NMR (400 MHz, $CDCl_3$) 7.64 (d, 4H, Ph); 7.41 (d, 4H, Ph); 7.09 (d, 2H, vinyl); 6.22 (d, 2H, vinyl); 3.60 (s, 12H, MeO); 0.27 (s, 6H, Me); 2,5-[(MeO)$_2$Sivinyl]$_2$thiophene: ^{1}H NMR (400 MHz, $CDCl_3$) 7.22 (d, 2H, thiophene); 7.21 (d, 2H, vinyl); 6.40 (d, 2H, vinyl); 3.70 (s, 12H, MeO); 0.30 (s, 6H, Me); 5,5'-[(MeO)$_2$Sivinyl]$_2$bithiophene: ^{1}H NMR (400 MHz, $CDCl_3$) 7.61 (m, 2H, thiophene); 7.22 (m, 2H, thiophene); 7.11 (d, 2H, vinyl); 6.23 (d, 2H, vinyl); 3.61 (s, 12H, MeO); 0.29 (s, 6H, Me).

General Heck Reaction of vinylDDvinyl with Br-Ar. To an oven-dried 100 mL Schlenk flask under N_2 were added vinylDDvinyl (1.20 g, 1.0 mmol), Pd[P(t-Bu)$_3$]$_2$ (38.7 mg, 0.08 mmol), and $Pd_2(dba)_3$ (34.6 mg, 0.04 mmol). Following the addition 30 mL of THF, NCy_2Me (0.81 g, 4.0 mmol), and Br-Ar (2.2 mmol) were added. The mixture was stirred magnetically at 70 °C for 24 h and then filtered through 1 cm Celite which was washed with THF (5 mL). The resulting filtrate was concentrated by rotary evaporation and precipitated into cold, well-stirred methanol (150 mL), filtered, and the lightly colored solid redissolved in THF (10 mL). The solution was then filtered again through a 1 cm Celite column to further remove residual Pd particles and concentrated and

reprecipitated into cold, stirred methanol (100 mL) to give crude product. $(Styryl)_2$DD: MALDI-TOF (Ag^+) m/z=1467, Calculated=1466; GPC M_n=1121, M_w=1129, PDI=1.01; TGA (air, 10 °C/min 1000 °C): found 43%, calc 44%, $T_{d5\%}$: 431 °C. $(Styryl)_3$DD: MALDI-TOF (Ag^+) m/z=1543, Calculated=1542; GPC M_n=1126, M_w=1149, PDI=1.02; TGA (air, 10 °C/min 1000 °C): found 42%, calc 42%, $T_{d5\%}$: 435 °C. $(Thiophenevinyl)_2$DD: MALDI-TOF (Ag^+) m/z=1480, Calculated=1478; GPC M_n=1149, M_w=1161, PDI=1.01; TGA (air, 10 °C/min 1000 °C): found 43%, calc 44%, $T_{d5\%}$: 445 °C. $(Dimethylfluorenevinyl)_2$DD: MALDI-TOF ($Ag^+$) m/z=1697, Calculated=1698; GPC M_n=1545, M_w=1663, PDI=1.07; TGA (air, 10 °C/min 1000 °C): found 36%, calc 38%, $T_{d5\%}$: 358 °C. $(Dimethylfluorenevinyl)_4$DD: MALDI-TOF m/z=1977, Calculated=1976; GPC M_n=1715, M_w=1828, PDI=1.07; TGA (air, 10 °C/min 1000 °C): found 30%, calc 30%, $T_{d5\%}$: 400 °C.

2.2.4 Ladder silsesquioxane derived copolymers

General Heck polymerization of vinyl-LL(Me/Ph)-vinyl [vinyl(Me/Ph)$Si(O_{0.5})_2(PhSiO_{1.5})_4(O_{0.5})_2$Si(Me/Ph)vinyl] with Br-Ar-Br.[7] To a dry 50 ml Schlenk flask under N_2 were added vinyl-LL-vinyl (0.8 mmol), NCy_2Me (0.4 g, 2.0 mmol), Br-Ar-Br (0.8 mmol), followed by 30 mL of distilled THF and $Pd[P(t\text{-}Bu_3)]_2$ (38.7 mg, 0.08 mmol). The mixture was stirred magnetically at 70 °C and tracked by GPC. The reaction was quenched by filtering through 1 cm celite which was washed with THF (5 mL). The solution was then concentrated and precipitated into 100 ml cold, well-stirred methanol (yield: 70%). The precipitated product was further purified by column chromatography (silica, 1:1 CH_2Cl_2:hexane). LL(Me)-co-phenyl: MALDI-TOF (Monomer) m/z=764, Calculated=765; GPC M_n=5420, M_w=15190, PDI=2.80; ^{1}H NMR (400 MHz, $CDCl_3$) 7.7-7.2 (m, 20H, cage-Ph); 7.2-7.0 (m, 4H, co-Ph); 6.9 (d, 2H, vinyl); 6.5 (d, 2H, vinyl); 0.5 (m, 6H, Me); ^{13}C NMR(700 MHz, $CDCl_3$) 146.1; 137.8; 134.0; 132.0; 131.1; 127.7; 127.0; 124.2; -0.6; TGA (air, 10 °C/min 1000 °C): found 46%, calc 46%, $T_{d5\%}$: 430 °C. LL(Me)-co-biphenyl: MALDI-TOF (Monomer) m/z=839, Calculated=841; GPC M_n=11700, M_w=44000, PDI=3.78; ^{1}H NMR (400 MHz, $CDCl_3$) 7.6-7.2 (m, 20H, Ph); 7.2-7.0 (m, 8H, Ph); 6.9 (d, 2H, vinyl); 6.5 (d, 2H, vinyl); 0.4 (m, 6H, Me); ^{13}C NMR(700 MHz, $CDCl_3$) 146.1; 140.6; 136.7; 134.2; 132.0; 130.8 127.8; 126.9; 124.3; -0.7; TGA (air, 10 °C/min 1000 °C): found 42%, calc 42%, $T_{d5\%}$: 410 °C. LL(Me)-co-thiophene: MALDI-TOF (Monomer) m/z=772, Calculated=771; GPC M_n=3170, M_w=6190, PDI=1.95; ^{1}H NMR (400 MHz, $CDCl_3$) 7.6-7.1 (m, 22H);

6.9 (d, 2H, vinyl); 6.4 (d, 2H, vinyl); 6.2 (t, 2H, vinyl); 6.0 (q, 1H, vinyl); 0.5 (m, 6H, Me); ^{13}C NMR(700 MHz, $CDCl_3$) 144.2; 139.1; 134.4; 134.0; 131.9; 130.4; 127.8; 127.5; 124.0; -0.7; TGA (air, 10 °C/min 1000 °C): found 42%, calc 42%, $T_{d5\%}$: 410 °C. LL(Me)-co-bithiophene: MALDI-TOF (Monomer) m/z=853, Calculated=853; GPC M_n=5540, M_w=11330, PDI=2.05; ^{1}H NMR (400 MHz, $CDCl_3$) 7.7-7.2 (m, 24H); 6.9 (d, 2H, vinyl); 6.5 (d, 2H, vinyl); 6.2 (t, 2H, vinyl); 5.9 (q, 1H, vinyl); 0.5 (m, 6H, Me); ^{13}C NMR(700 MHz, $CDCl_3$) 144.2; 139.1; 138.1; 134.1; 134.0; 132.5; 131.8; 130.4; 127.7; 127.5; 124.0; -0.7; TGA (air, 10 °C/min 1000 °C): found 40%, calc 42%, $T_{d5\%}$: 440 °C.

General bromination of DD-co-phenyl and LL(Me)-co-phenyl. To a dry 100 mL Schlenk flask under N_2 were added DD-co-phenyl or LL-co-phenyl (DD/LL SQ: 1.0 mmol), 20 mL of CH_2Cl_2 and NCy_2Me (4.0 mmol). After completely dissolving, Br_2 (4.0 mmol) was added drop-wise, and an additional 5 ml of CH_2Cl_2 was added to wash. Thereafter, a vent to a bubbler containing aqueous base was added, and the solution was stirred magnetically at room temperature for 1 d. At this point, 10 g of $Na_2S_2O_5$ and 5 g of Na_2CO_3 were dissolved in 40 ml of water and then added to the solution with vigorous stirring until the Br_2 color disappeared. The mixture was then transferred to a separatory funnel, and the organic layer was extracted and washed sequentially with 20 ml brine. Thereafter, the organic layer was dried over $MgSO_4$. Then celite was added and stirred for 10 min. The mixture was filtered to give a clear, colorless liquid. Most solvent was removed by rotary evaporation, and the resulting solid was redissolved in a minimal amount of THF and slowly poured into 150 ml cold, well-stirred methanol to fully precipitate the white product (yield: 80%). Brominated DD-co-phenyl: ^{13}C NMR (700 MHz, $CDCl_3$) 139.8, 134.0, 130.9, 130.7, 130.4, 127.9, 127.8, -0.7; ^{29}Si NMR (700 MHz, $CDCl_3$) -32.6, -78.2, -79.0, -79.2.

General zinc debromination of brominated DD-co-phenyl and LL(Me)-co-phenyl.[8] To a dry 100 mL Schlenk flask under N_2 were added above brominated DD-co-phenyl or LL-co-phenyl (DD/LL SQ: 0.8 mmol), 20 mL of diethyl ether, followed by 3 drops of glacial acetic acid and Zn dust (2.0 mmol). The mixture was stirred vigorously under N_2 at room temperature. After the grey Zn dust turned into white $ZnBr_2$ powder, the reaction mixture was then filtered. The resulting filtrate was concentrated and precipitated into 100 ml cold, well-stirred methanol to give the yellowish product (yield 65%).

2.2.5 Double decker silsesquioxane derived terpolymers

General Heck cross-coupling of vinylDDvinyl with Br-Ar1-Br (3:1 molar ratio, Ar1=thiophene, bithiophene, thienothiophene). To a dry 200 ml Schlenk flask under N_2 were added 3.62 g (3.0 mmol) vinylDDvinyl, 38.7 mg (0.08 mmol) $Pd[P(t\text{-}Bu)_3]_2$, followed by 45 ml distilled THF, 0.80 g (4.0 mmol) NCy_2Me and Br-Ar1-Br (1.0 mmol). The mixture was stirred magnetically 70 ^oC and tracked by GPC. The reaction was quenched after 2 d by filtering through 1 cm celite which was washed with THF (5 mL). The resulting filtrate was concentrated by rotary evaporation and the resulting concentrated solution was then precipitated into 150 ml cold, well-stirred methanol, filtered, and the colored solid re-dissolved in 10 ml THF. The solution was then filtered again through a 1 cm celite column to further remove residual Pd particles, and concentrated, re-precipitated into 100 ml cold, stirred methanol to give a ~85% yield of crude colored product for most reactions studied. The two-cage product (vinylDD-Ar1-DDvinyl) was then isolated using column chromatography (CH_2Cl_2:hexane 1:2 volume ratio, silica gel). DD-thiophene-DD: MALDI-TOF (Ag^+) m/z=2600, Calculated=2600; GPC M_n=1690, M_w=1770, PDI=1.05; ^1H NMR (400 MHz, $CDCl_3$) 7.80 (d, 2H, -C4H2S-); 7.77-7.06 (m, 80H, -C6H5); 6.94 (d, 2H, -CH=CH-); 6.45 (d, 2H, -CH=CH-); 6.20-6.14 (m, 2H, -CH=CH2); 6.05-5.99 (m, 4H,-CH=CH2); 0.42 (s, 6H, -CH3); 0.37 (s, 6H, -CH3); ^{13}C NMR(700 MHz, $CDCl_3$) 144.3, 139.1,137.4, 135.2, 134.5, 134.2, 134.1, 134.0, 132.0, 131.9, 131.1, 131.0, 130.7, 130.6, 130.4, 130.3, 127.9, 127.8, 127.7, 127.6, 124.1, -0.66, -1.13; TGA (air, 10 ^oC/min 1000 ^oC): found 48%, calc 48%, $T_{d5\%}$: 545 ^oC. DD-bithiophene-DD: MALDI-TOF (Ag^+) m/z=2682, Calculated=2682; GPC M_n=1780, M_w=1890, PDI=1.06; ^1H NMR (400 MHz, $CDCl_3$) 7.77 (d, 2H, -C8H4S2-); 7.73 (d, 2H,-C8H4S2-); 7.64-7.06 (m, 80H, -C6H5); 6.89 (d, 2H, -CH=CH-); 6.53 (d, 2H, -CH=CH-); 6.20-6.12 (m, 2H, -CH=CH2); 6.06-5.96 (m, 4H,-CH=CH2); 0.43 (s, 6H, -CH3); 0.38 (s, 6H, -CH3); ^{13}C NMR(700 MHz, $CDCl_3$) 144.2, 138.8, 137.4, 135.2, 134.4, 134.1, 134.0, 131.9, 130.4, 127.8, 127.8, 127.6, 127.5, 124.5, 124.2, 123.8, -0.70, -1.17; TGA (air, 10 ^oC/min 1000 ^oC): found 46%, calc 47%, $T_{d5\%}$: 530 ^oC. DD-thienothiophene-DD: MALDI-TOF (Ag^+) m/z=2655, Calculated=2655; GPC M_n=1720, M_w=1790, PDI=1.04; ^1H NMR (400 MHz, $CDCl_3$) 7.81 (d, 2H, -C6H2S2-); 7.77-7.07 (m, 80H, -C6H5); 6.98 (d, 2H, -CH=CH-); 6.46 (d, 2H, -CH=CH-); 6.22-6.14 (m, 2H, -CH=CH2); 6.06-5.96 (m, 4H,-CH=CH2); 0.46 (s, 6H, -CH3); 0.42 (s, 6H, -CH3); ^{13}C NMR(700 MHz, $CDCl_3$) 146.9, 139.7, 138.8, 135.2, 134.5, 134.2, 134.1, 134.0, 132.0, 131.9, 131.1, 131.0, 130.8, 130.5, 130.4, 130.3,

127.9, 127.8, 127.7, 127.6, 123.7, 112.0, -0.53, -1.13; TGA (air, 10 °C/min 1000 °C): found 46%, calc 47%, $T_{d5\%}$: 530 °C.

General Heck polymerization of vinylDD-Ar1-DDvinyl with Br-Ar2-Br (Ar2=biphenyl, ter-phenyl, stilbene). To a dry 50 ml Schlenk flask under N_2 were added above vinylDD-Ar1-DDvinyl (0.04 mmol), 4.0 mg (0.008 mmol) $Pd[P(t\text{-}Bu)_3]_2$, followed by 20 ml distilled THF, 64 mg (0.32 mmol) NCy_2Me and Br-Ar2-Br (0.04 mmol). The mixture was stirred magnetically 70 °C and tracked by GPC. The reaction was quenched after 14 d by filtering through 1 cm celite which was washed with THF (5 mL). The resulting filtrate was concentrated by rotary evaporation and the resulting concentrated solution was then precipitated into 100 ml cold, well-stirred methanol to give a yield of 75% colored product. DD-thiophene-DD-biphenyl: MALDI-TOF (monomer) m/z=2752, Calculated=2752; GPC M_n=7000, M_w=11900, PDI=1.70; ^{1}H NMR (400 MHz, $CDCl_3$) 7.77-7.07 (m, 90H, -C6H5, -C4H2S-); 7.00-6.95 (m, 4H, -CH=CH-); 6.53-6.49 (m, 4H, -CH=CH-); 6.13-6.11 (m, -CH=CH2); 0.49 (s, 6H, -CH3); 0.44 (s, 6H, -CH3); ^{13}C NMR(700 MHz, $CDCl_3$) 146.1, 140.6, 136.8, 134.2, 134.1, 134.0, 132.0, 131.9, 130.8, 130.4, 127.9, 127.8, 127.7, 127.6, 127.3, 126.9, 124.1, 1.05, -0.72; TGA (air, 10 °C/min 1000 °C): found 44%, calc 45%, $T_{d5\%}$: 500 °C. DD-thiophene-DD-terphenyl: MALDI-TOF (Ag^+) m/z=2823, Calculated=2823; GPC M_n=4500, M_w=7400, PDI=165; ^{1}H NMR (400 MHz, $CDCl_3$) 7.90-7.04 (m, -C6H5, -C4H2S-); 6.99-6.90 (m, 4H, -CH=CH-); 6.53-6.46 (m, 2H, -CH=CH-); 0.47 (s, 6H, -CH3); 0.41 (s, 6H, -CH3); ^{13}C NMR(700 MHz, $CDCl_3$) 146.1, 140.5, 139.7, 139.0, 136.8, 134.5, 134.2, 134.1, 134.0, 134.0, 131.9, 130.6, 130.4, 127.9, 127.8, 127.7, 127.6, 127.4, 127.0, 124.1, 1.05, -0.71; TGA (air, 10 °C/min 1000 °C): found 45%, calc 44%, $T_{d5\%}$: 520 °C.

2.3 Characterization

2.3.1 Analytical characterization

Matrix-assisted laser desorption/ionization time-of-flight spectrometry. MALDI-TOF was done on a Micromass TOF Spec-2E equipped with a 337 nm nitrogen laser in positive-ion reflec-tron mode using poly(ethylene glycol) as calibration standard, dithranol as matrix, and $AgNO_3$ as ion source. Samples were prepared by mixing solutions of 5 parts matrix (10 mg/mL in THF), 5 parts sample (1 mg/mL in THF), and 1 part $AgNO_3$ (2.5 mg/mL in THF) and blotting the mixture on target plate.

Nuclear magnetic resonance. All ^{1}H NMR spectra were collected from samples dissolved in $CDCl_3$ and recorded on a Varian INOVA 400 MHz spectrometer. All ^{13}C and ^{29}Si spectra were collected from samples dissolved in $CDCl_3$ and recorded on an Ytterbium 700 MHz spectrometer. ^{1}H NMR spectra were collected at 400 MHz using a spectral width of 6000 Hz, a relaxation delay of 0.5 s, 30k data points, a pulse width of 38°, and $CHCl_3$ (7.24 ppm) as the internal reference. ^{13}C NMR spectra were collected at 100 MHz using a 25000 Hz spectral width, a relaxation delay of 1.5 s, 75k data points, a pulse width of 40°. ^{29}Si NMR spectra were collected at 100 MHz using a 14000 Hz spectral width, a relaxation delay of 20 s, 65k data points, a pulse width of 7°.

Gel permeation chromatography. GPC analyses were done on a Waters 440 system equipped with Waters Styragel columns (7.8300, HT 0.5, 2, 3, 4) with RI detection using Waters refractometer and THF as solvent. The system was calibrated using polystyrene.

Thermogravimetric analyses. TGAs were run on a SDT Q600 Simultaneous Differential DTA-TGA Instrument (TA Instruments, Inc., New Castle, DE). Samples (15-20 mg) were loaded in alumina pans and ramped at 10 °C/min to 1000 °C under dry air with a flow rate of 60 mL/min.

Fourier-transform infrared spectroscopy. Diffuse reflectance Fourier transform (DRIFT) spectra were recorded on a Nicolet 6700 Series FTIR spectrometer (Thermo Fisher Scientific, Inc., Madison, WI). Optical grade, random cuttings of KBr (International Crystal Laboratories, Garfield, NJ) were ground by hand in an alumina mortar pestle, with 1.0 wt % of the sample to be analyzed. For DRIFT analyses, samples were packed firmly and leveled off at the upper edge to provide a smooth surface. The FTIR sample chamber was flushed continuously with N_2 prior to data acquisition in the range 4000−400 cm^{-1} with a precision of ±4 cm^{-1}.

2.3.2 Photophysical characterization

UV−Vis spectrometry. UV−vis measurements were recorded on a Shimadzu UV-1601 UV−vis transmission spectrometer. Samples were dissolved in CH_2Cl_2 and diluted to a concentration (10^{-3}−10^{-4} M) where the absorption maximum was <10% for a 1 cm path length.

Photoluminescence spectrometry. Photoluminescent spectra were recorded on a Fluoromax-2 fluorometer in the required solvent using 300 nm excitation. Samples from UV-vis spectroscopy were diluted (10^{-5}-10^{-6} M) to avoid excimer formation and fluorometer detector saturation.

Quantum yield measurements. All compounds were dissolved in CH_2Cl_2 (Sigma-Aldrich, spectrophotometric grade) for carrying out the optical measurements. The absorption spectra of

the molecules were measured using an Agilent (Model No. 8341) spectrophotometer. To measure the molar extinction coefficients, the original stock solutions were diluted to 10^{-6} M. The fluorescence spectra were acquired using a Spexfluorolog spectrofluorometer. The quantum yields of the molecules were measured using a known procedure.[9] Bis-MSB [p-bis(omethylstyryl)benzene] has been used as the standard. The absorbance was limited to less than 0.03. The solutions were purged with argon for 3 min prior to measuring their emission spectra. Then, the following relation was used to measure the quantum yield:

$$\phi_F = (\phi_F)_S \frac{\int J(\bar{\nu})\, d\bar{\nu}}{\int J_S(\bar{\nu})\, d\bar{\nu}} \frac{(J_a)_S}{J_a} \frac{n^2}{n_S^2}$$

where $(\phi_F)_S$ is the quantum yield of the standard, $\int J(\bar{\nu})\, d\bar{\nu}$ the area under the fluorescence emission curve for the sample, $\int J_S(\bar{\nu})\, d\bar{\nu}$ the area under the fluorescence emission curve for the standard $(J_a)_S$ the absorbance of the standard, J_a the absorbance of the sample, n^2 the refractive index of the solvent used for the sample, and n_S^2 the refractive index of the solvent used for the standard.

Two-Photon excited fluorescence measurements. To measure the two-photon absorption cross sections, we followed the two-photon excited fluorescence (TPEF) method.[10] A 10^{-4} M Coumarin 307 (7-ethylamino-6-methyl-4-trifluoromethylcoumarin) solution in methanol was used as the reference for measuring TPA cross sections at different wavelengths. The laser used for the study was a Mai Tai Diode-pumped mode-locked Ti:sapphire laser, which is tunable from 700 to 1000 nm. The beam was directed on to the sample cell (quartz cuvette, 0.5 cm path length), and the resultant fluorescence was collected in a direction perpendicular to the incident beam. A 1 in. focal length plano-convex lens was used to direct the collected fluorescence into a monochromator. The output from the monochromator was coupled to a PMT. The photons were converted into counts by a photon counting unit. A logarithmic plot between collected fluorescence photons and input intensity gave a slope of 2, ensuring a quadratic dependence. The intercept enabled us to calculate the two-photon absorption cross sections at different wavelengths.

Magnetic scattering studies.[11–13] Polarization-selective light scattering was investigated in samples excited with 100 fs pulses from an amplified Ti:sapphire laser system operating at 10 kHz repetition rate (amplitude/continuum). Samples were prepared as 0.1 mM solutions in CH_2Cl_2 and placed in standard quartz cuvettes to measure light scattering caused by the (nonlinear) magneto-electric interaction that occurs at the molecular level for intensities in the range 108−1010 W/cm^2.

Complete radiation patterns were recorded for induced electric and magnetic dipole moment strengths in this intensity range by analyzing scattered light to distinguish co-polarized and cross-polarized signal components. By fitting each radiation pattern with a combination of unpolarized and dipolar components versus polar angle, it was possible to compare the librational response determined by the azimuthal potential surface in different samples.

References

(1) Li, Z.; Kawakami, Y. Formation of Incompletely Condensed Oligosilsesquioxanes by Hydrolysis of Completely Condensed POSS via Reshuffling. *Chem. Lett.* **2008**, *37* (7), 804–805. https://doi.org/10.1246/cl.2008.804.

(2) Roll, M. F.; Mathur, P.; Takahashi, K.; Kampf, J. W.; Laine, R. M. [PhSiO1.5]8 Promotes Self-Bromination to Produce [o-BrPhSiO1.5]8: Further Bromination Gives Crystalline [2,5-Br2PhSiO1.5]8 with a Density of 2.32 g Cm−3 and a Calculated Refractive Index of 1.7 or the Tetraicosa Bromo Compound [Br3PhSiO1.5]8. *J. Mater. Chem.* **2011**, *21* (30), 11167. https://doi.org/10.1039/c1jm11536g.

(3) Roll, M. F.; Asuncion, M. Z.; Kampf, J.; Laine, R. M. *Para* -Octaiodophenylsilsesquioxane, [*p* -IC $_6$ H $_4$ SiO $_{1.5}$] $_8$, a Nearly Perfect Nano-Building Block. *ACS Nano* **2008**, *2* (2), 320–326. https://doi.org/10.1021/nn700196d.

(4) Bahrami, M.; Furgal, J. C.; Hashemi, H.; Ehsani, M.; Jahani, Y.; Goodson, T.; Kieffer, J.; Laine, R. M. Synthesis and Characterization of Nanobuilding Blocks [*o*- RStyrPhSiO $_{1.5}$] $_{10,12}$ (R = Me, MeO, NBoc, and CN). Unexpected Photophysical Properties Arising from Apparent Asymmetric Cage Functionalization as Supported by Modeling Studies. *J. Phys. Chem. C* **2015**, *119* (28), 15846–15858. https://doi.org/10.1021/acs.jpcc.5b02678.

(5) Vogelsang, D. F.; Dannatt, J. E.; Schoen, B. W.; Maleczka, R. E.; Lee, A. Phase Behavior of *Cis – Trans* Mixtures of Double-Decker Shaped Silsesquioxanes for Processability Enhancement. *ACS Appl. Nano Mater.* **2019**, *2* (3), 1223–1231. https://doi.org/10.1021/acsanm.8b02114.

(6) Asuncion, M. Z.; Laine, R. M. Fluoride Rearrangement Reactions of Polyphenyl- and Polyvinylsilsesquioxanes as a Facile Route to Mixed Functional Phenyl, Vinyl T $_{10}$ and T $_{12}$ Silsesquioxanes. *J. Am. Chem. Soc.* **2010**, *132* (11), 3723–3736. https://doi.org/10.1021/ja9087743.

(7) Guan, J.; Arias, J. J. R.; Tomobe, K.; Ansari, R.; Marques, M. de F. V.; Rebane, A.; Mahbub, S.; Furgal, J. C.; Yodsin, N.; Jungsuttiwong, S.; Hashemi, D.; Kieffer, J.; Laine, R. M. Unconventional Conjugation via VinylMeSi(O−) $_2$ Siloxane Bridges May Imbue Semiconducting Properties in [Vinyl(Me)SiO(PhSiO $_{1.5}$) $_8$ OSi(Me)Vinyl-Ar] Double-Decker Copolymers. *ACS Appl. Polym. Mater.* **2020**, *2* (9), 3894–3907. https://doi.org/10.1021/acsapm.0c00591.

(8) Brook, A. G.; Duff, J. M.; Reynolds, W. F. The Bromination, Debromination and Debromosilylation of Silylstyrenes and Other Vinylsilanes. *Journal of Organometallic Chemistry* **1976**, *121* (3), 293–306. https://doi.org/10.1016/S0022-328X(00)85083-4.

(9) Sulaiman, S.; Zhang, J.; Goodson, III, T.; Laine, R. M. Synthesis, Characterization and Photophysical Properties of Polyfunctional Phenylsilsesquioxanes: [O-RPhSiO1.5]8, [2,5-R2PhSiO1.5]8, and [R3PhSiO1.5]8. Compounds with the Highest Number of Functional

Units/Unit Volume. *J. Mater. Chem.* **2011**, *21* (30), 11177. https://doi.org/10.1039/c1jm11701g.
(10) Xu, C.; Webb, W. W. Measurement of Two-Photon Excitation Cross Sections of Molecular Fluorophores with Data from 690 to 1050 Nm. *J. Opt. Soc. Am. B* **1996**, *13* (3), 481. https://doi.org/10.1364/JOSAB.13.000481.
(11) Rand, S. C.; Fisher, W. M.; Oliveira, S. L. Optically Induced Magnetization in Homogeneous, Undoped Dielectric Media. *J. Opt. Soc. Am. B* **2008**, *25* (7), 1106. https://doi.org/10.1364/JOSAB.25.001106.
(12) Fisher, A. A.; Dreyer, E. F. C.; Chakrabarty, A.; Rand, S. C. Optical Magnetization, Part I: Experiments on Radiant Optical Magnetization in Solids. *Opt. Express* **2016**, *24* (23), 26055. https://doi.org/10.1364/OE.24.026055.
(13) Dreyer, E. F. C.; Fisher, A. A.; Smail, G.; Anisimov, P.; Rand, S. C. Optical Magnetization, Part III: Theory of Molecular Magneto-Electric Rectification. *Opt. Express* **2018**, *26* (14), 17755. https://doi.org/10.1364/OE.26.017755.

Chapter 3. Partially Functionalized Phenylsilsesquioxane: $[RSiO_{1.5}]_7[Me/nPrSiO_{1.5}]$ and $[RSiO_{1.5}]_7[O_{0.5}SiMe_3]_3$ (R = 4-Me/4-CN-Stilbene)

Published: Guan, J., Tomobe, K., Madu, I., Goodson III, T., Makhal, K., Trinh, M.T., Rand, S.C., Yodsin, N., Jungsuttiwong, S. and Laine, R.M. 2019. *Macromolecules*, *52*(11), 4008-4019.

With contributions from Professors Theodore Goodson III, Stephen C. Rand and Siriporn Jungsuttiwong.

Abstract

Macromonomers $[RPhSiO_{1.5}]_{8,10,12}$ and $[RCH{=}CHSiO_{1.5}]_{8,10,12}$, where R = conjugated group have previously been shown to offer photophysical properties wherein excitation promotes an electron from the HOMO to an excited state LUMO that sits in the center of the cage and allows communication between all conjugated groups suggesting 3-D delocalization. In the current work, we explore replacing one conjugated group in $[RPhSiO_{1.5}]_8$ either with Me or nPr or simply removing one corner from the cage, $[RPhSiO_{1.5}]_7(O_{0.5}SiMe_3)_3$ and examine its effect on any potential LUMO that might form. We report here that such changes seem to have no effect on the existence of a 3-D LUMO derived delocalization as witnessed by emission red-shifts from the R = 4-Me-/4-CN-stilbene moieties essentially identical to those for the original $[RPhSiO_{1.5}]_8$ macromonomers. Of particular importance is the fact that removing one corner from the cage also has little effect on the photophysics, indeed significantly improving fluorescence emission quantum efficiencies. However, removing most of the conjugated groups on the corner missing cage (from 7 to 2), e. g $[MeStilSiO_{1.5}]_2[PhSiO_{1.5}]_5(O_{0.5}SiMe_3)_3$ eliminates the red shift implying the absence of a LUMO inside the cage. This suggests a minimum number of groups are needed to form such a LUMO. Also, for the first time, the radiation patterns for nonlinear, optically-induced magnetic scattering at elevated light intensities are reported for these compounds and shown to support the same conclusion, a spherical LUMO exists inside the cage.

3.1 Introduction

Research on silsesquioxane macromonomers has grown over the past 30 years such that the field has become a major area of chemical exploration with approximately 17 reviews and one book written in this period.[1-18] As part of our exploration of the chemistries of T_8, T_{10} and T_{12} cage

macromonomers, we have been particularly interested in the chemistries and photophysical properties of the vinyl and phenyl derivatives. This comes from our discovery that they offer properties quite different from what was anticipated to be organic decorated silica. In a series of papers, we determined that these 3-D macromonomers exhibit behavior that reflects the existence of a LUMO within the center of the cage that greatly affects both cage chemistries and photophysical properties.[19-21] They also exhibit unexpected two photon absorption (TPA) behavior that suggests considerable polarization in the excited state.

In particular, although the cages are recognized to offer electron withdrawing properties similar to CF_3,[22] the phenyl cages exhibit very different reactivities during electrophilic substitution. For example, traditional Friedel Crafts acylation, sulfonylation and nitration do indeed favor formation of meta substituted products[17] as might be expected. However, bromination and iodination selectivities are quite disparate. For example, the $PhT_{8,10,12}$ cages all iodinate almost exclusively (> 90 % selectivity) in the para position. In contrast, bromination occurs selectively in the ortho position (85 % PhT_8, 70 % PhT_{10}, and 60 % PhT_{12}). This selectivity is likely defined by the separation between phenyl groups on neighboring positions on the cages. The phenyl groups are 90 °, 72 ° and 60 ° apart as the cage size increases limiting access of Br_2 to ortho hydrogens.

Although we have yet to identify a mechanistic pathway whereby iodination occurs selectively in the *para* position, we have carefully modeled the bromination process. We find that the cage centered LUMO engages an incoming Br_2 and together with hydrogen bonding to ortho hydrogens leads to formation of an energetically favored transition state akin to a Venus flytrap that selectively drives ortho bromination, Figure **3.1**.[23]

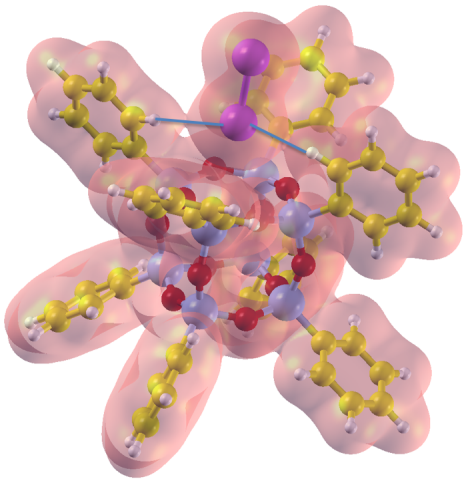

Figure 3.1. Venus flytrap mechanism for ortho bromination.

More recently, we reported that the first bromine on the cage promotes bromination on the same face of the cage as illustrated in Figures **3.2** and **3.3**.[24] The crystal structure in Figure **3.3** shows that careful bromination allows the synthesis and isolation of a Janus brominated cage.[25]

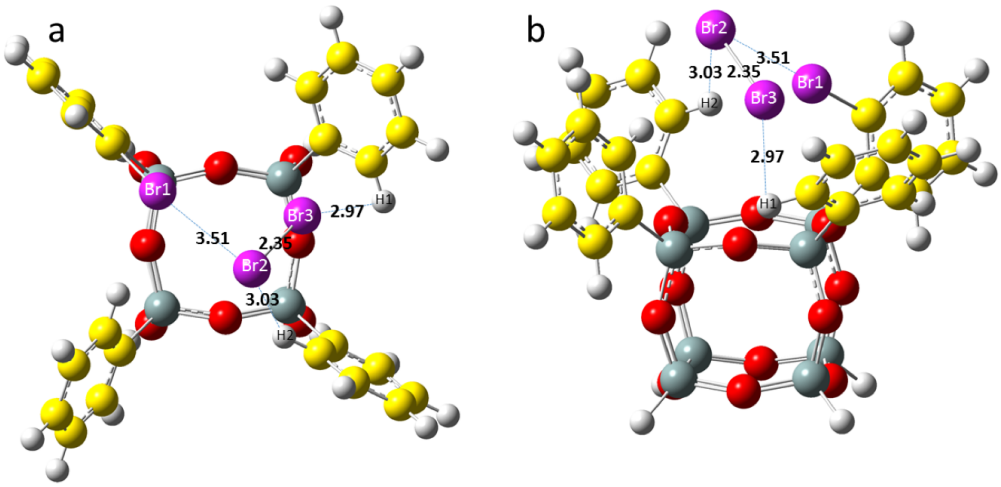

Figure 3.2. Asymmetric bromination.

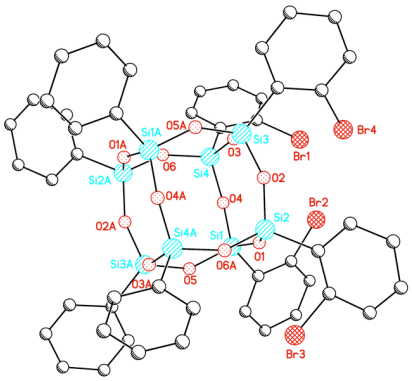

Figure 3.3. Janus bromination of octaphenylsilsesquioxanes.

Several other research groups have now isolated related cage macromonomers with cage centered LUMOs that also lead to unusual properties including a germanium analog as shown in Figure **3.4**.[26]

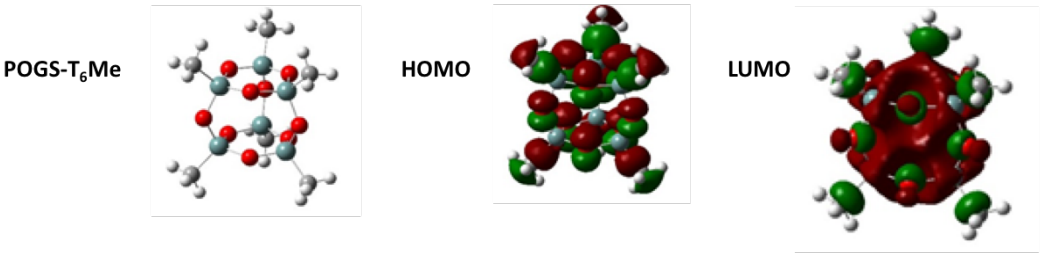

Figure 3.4. Polyhedral germsesquioxane cage with LUMO centered within cage.

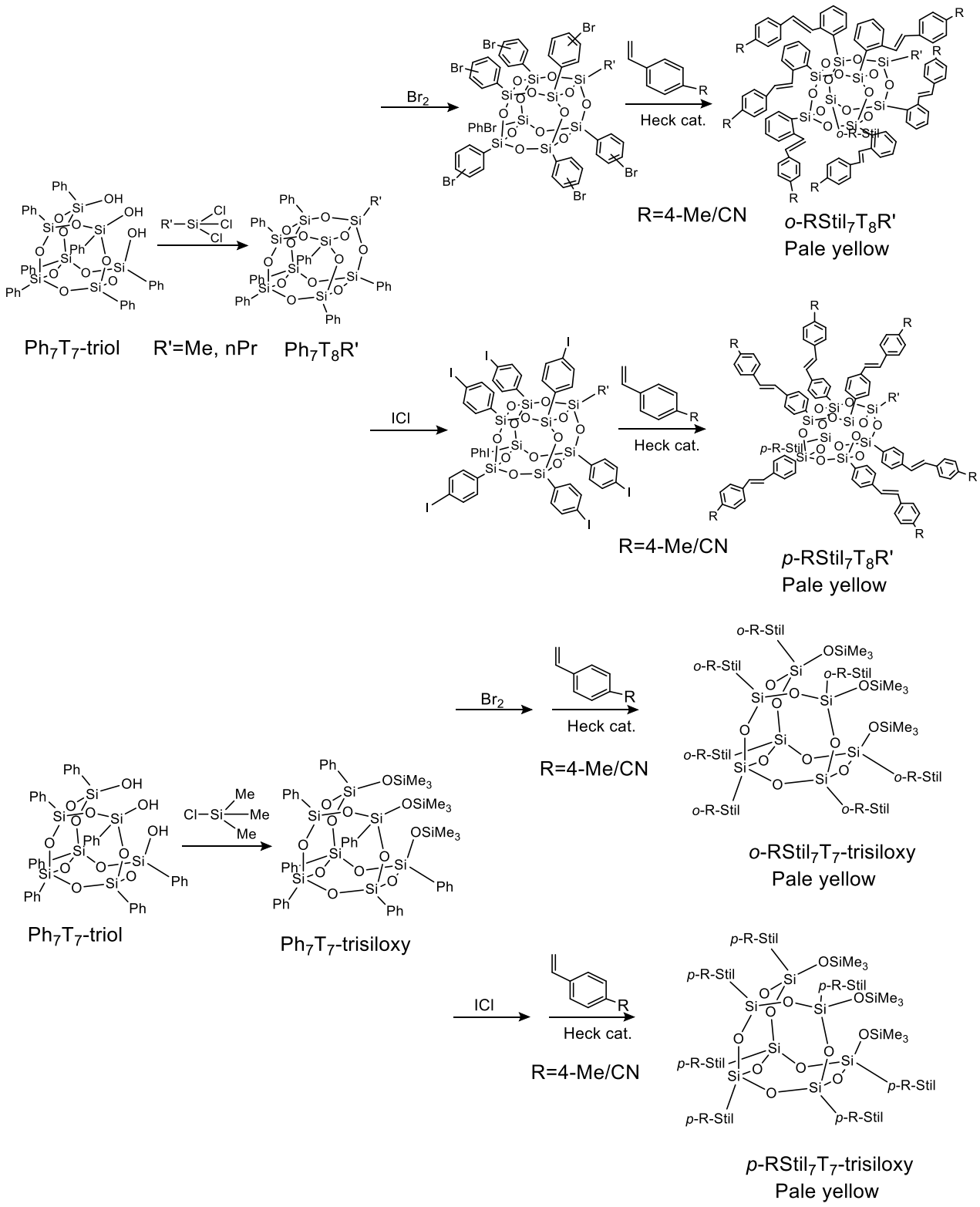

Scheme 3.1. Synthesis of stilbene-SQs.

These recent results suggest that the presence of LUMOs inside such cage macromonomers might be more common than our early results suggested. To this end, we decided to systematically study the effects of replacing one phenyl on the cage with a simple alkyl; methyl or n-propyl or simply making a cage missing a corner and exploring the synthesis of model stilbene compounds to test the potential for LUMO formation in the unsymmetrical cages: $MePh_7[SiO_{1.5}]_8$, $PrPh_7[SiO_{1.5}]_8$, $[PhSiO_{1.5}]_7(O_{0.5}SiMe_3)_3$. We report here the bromination and iodination of these model cages, their conversion to 4-methylstilbene and 4-cyanostilbene derivatives, spectroscopic characterization of the formed products and their photophysical properties. We find that indeed even with a missing corner, a LUMO forms in the cages and yields a form of excited state delocalization results as reported for the octaphenylsilsesquioxane analogs, *except in the case of* $[MeStilSiO_{1.5}]_2[PhSiO_{1.5}]_5(O_{0.5}SiMe_3)_3$.[19-21] We also report for the first time, magneto-optic properties which support the existence of spherical LUMOs inside these cages.

3.2 Experimental

The synthetic methods and characterization techniques are described in Chapter **2**.

3.3 Results and discussion

In previous studies, a set of stilbene-functionalized T_8 compounds was synthesized from $[p\text{-}IPhSiO_{1.5}]_8$ was well as $[o\text{-}BrPhSiO_{1.5}]_8$ using Heck coupling.[19-21] These fully-functionalized cages all show UV-vis absorption spectra identical to the spectrum of trans-stilbene, while the emission spectra of the full cages show red-shifts of 60-100 nm.[19-21] These large red-shifts are proposed to result from interactions of the stilbene π^* orbitals with a LUMO centered within the cage that has 3-D orbital symmetry, indicating all stilbene moieties interact in the excited state.[19] Such photophysical behavior has been reported before as indicative of semiconducting-like behavior.[19-21]

Here we demonstrate similar behavior where only monoalkylheptaphenyl or corner missing partial cages are used. In the following section, we first characterize the individual macromonomers synthesized per the experimental section, thereafter we present the photophysical data and then the theoretical modeling results as a prelude to discussions about the interpretation of this photophysical data.

3.3.1 Synthesis and characterization of $RStil_xT_8R'$ and $RStil_xT_7$-trisiloxy.

In previous studies, we discovered a synthetic route to *o*-Br_8OPS with ≥ 85% *ortho*-substitution[27] and *p*-I_8OPS with > 99% mono-iodination and > 95% *para*-substitution[29] and a series of *o*-

Br_xOPS and *p*-I_xOPS were synthesized, which were used as the starting material for the synthesis, via Heck coupling, of a series of stilbene derivatives.[19-21]

Here, we extend our efforts synthesizing a series of alkylphenyl and corner missing stilbene derivatives from the corresponding brominated and iodinated cages. The first step was to cap the trisilanol corner-missing phenylsilsesquioxane Ph_7T_7-triol with methyl/propyl-trichlorosilane and trimethylchlorosilane, which give the title closed and corner-missing open cage macromonomers respectively as characterized by MALDI-TOF, GPC and ^{1}H NMR as listed in Table **A.1** (Appendix). These derivatives were characterized by MALDI-TOF (**A.1-A.12**), TGA (**A.13-A.16**), GPC and ^{1}H NMR as listed in Tables **A.2-A.3**.

^{1}H NMR of $Br_xPh_7T_8R$ in Table **A.2** show four signals in the aromatic region. Those of $I_xPh_7T_8R$ show only two signals, indicating ortho bromination and para iodination a seen previously.

The MALDI-TOF of brominated cages presented in Figures **A.1** and **A.4** reveal only traces of dibrominated phenyls. Their TGA ceramic yields (to SiO_2) are close to theory, while MALDI-TOF of iodinated cages presented in Figures **A.7** and **A.10** do not show any peaks for diiodophenyl products. The MALDI-TOF data in Table **A.3** indicate that the substitution patterns of the Heck products are identical to those found for both the brominated and iodinated starting cages without cage breakdown during Heck coupling. Likewise, the TGA ceramic yields of the stilbene derivatives in Table **A.3** are also close to theory, strongly suggesting quantitative conversion. Decomposition onset temperatures ($T_{d5\%}$/TGA/air) for most Heck products are > 400 °C, suggesting high thermal stability arising from the silica-like core. GPC suggests cage sizes grow slightly with Heck coupling by comparing the retention times of the Heck products with starting brominated or iodinated cages. The molecular masses indicated by GPC are not accurate due to the spherical structure of cages and the retention times for all cage compounds are around 32 min.

We also purposely synthesized the 4-methylstilbene derivative from *p*-I_8OPS for comparison for reasons discussed in the section on photophysical properties.

3.3.1 Photophysical properties.

UV-Vis studies for *o*-$RStil_xT_8R'$. Figure **3.5** provides steady-state spectra (CH_2Cl_2) for *p*-$Mestil_8OPS$ synthesized from I_8OPS and *o*-$RStil_xT_8R'$. The spectra for *o*-$Mestil_xT_8R'$ are very similar to those for *p*-$Mestil_8OPS$. As indicated by previous studies as well as results shown here, their

UV-vis spectra are all red-shifted 5-10 nm from those of *p*-methylstilbene and the model compound MeStilSi(OEt)$_3$. Normally, it would be reasonable to argue that the effect of the cage on the UV-vis spectra of the attached stilbenes is small. However, it has been suggested in the literature that the -Si(O)$_3$ unit exhibits the inductive characteristics of a -CF$_3$ group.[22] Thus, a blue-shift would be a more reasonable expectation. In contrast to the mundane UV-vis absorption behavior, the emissive behavior is quite striking. As seen in Figure **3.5**, the emission spectra (normalized) show a red-shift of 50-70 nm for all compounds relative to those of *p*-methylstilbene itself, indicating 3-D conjugation in the excited state.[21]

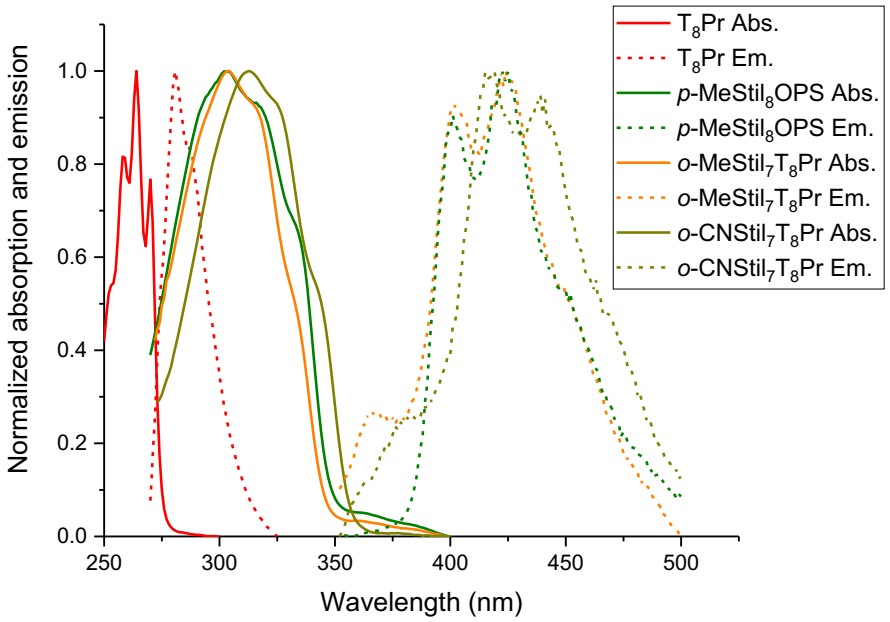

Figure 3.5. Normalized steady-state absorption (solid) and emission (dashed) spectra for Ph$_7$T$_8$R', *p*-MeStil$_8$OPS and *o*-RStil$_x$T$_8$R'.

The pair of compounds having structural differences only as a result of a methyl/propyl group show the same spectra suggesting their optical properties are independent of the non-conjugated side group. The *o*-CNStil$_x$T$_8$R' compounds display spectra similar to *o*-MeStil$_x$T$_8$R' but slightly red-shifted ascribed to increased conjugation to the cyano group. The high-degree of similarity for the *p*-MeStil$_8$OPS and *o*-MeStil$_x$T$_8$R' spectra suggest formation of 3-D conjugation even with functionalized heptaphenyl cages.

The TPA data (Table **3.1**) indicate that despite the introduction of an unfunctionalized corner, there are no gross changes in the values recorded indicating only modest polarization of the

individual stilbene groups as expected since the model stilbenes are not capable of charge transfer like behavior as seen previously.[19-21]

Table 3.1. Photophysical data for *p*-MeStil$_8$OPS, RStil$_x$T$_8$R' and RStil$_x$T$_7$-trisiloxy.

	Abs. λ_{max} (nm)	Em. λ_{max} (nm)	$E_{stoke's}$ (cm^{-1})	Φ_F(-)	TPA-δ (GM)
p-MeStilbene[9]	298, 311	355			
MeStilSi(OEt)$_3$[6]	298	352			
[*p*-NH$_2$StilvinylSiO$_{1.5}$]$_8$[19]	361	481	6911	0.06	110
[*p*-NH$_2$StilSiO$_{1.5}$]$_8$[20]	356	459	6303	0.07	26
p-MeStil$_8$OPS[10]	305, 320	400, 422	9142	0.57	0.17
o-MeStil$_6$T$_8$Me	304, 320	402, 426	9530	0.16	1.2
o-MeStil$_7$T$_8$Pr	306, 320	402, 426	9420	0.13	0.9
o-CNStil$_6$T$_8$Me	315, 325	419, 441	8185	0.15	2.0
o-CNStil$_7$T$_8$Pr	315, 325	419, 441	8185	0.19	1.4
p-MeStil$_7$T$_8$Me	305, 317	398, 420	7661	0.17	0.1
p-MeStil$_7$T$_8$Pr	305, 317	398, 421	7661	0.20	0.1
p-CNStil$_7$T$_8$Me	317, 326	415, 442	6578	0.09	2.3
p-CNStil$_7$T$_8$Pr	314, 326	412, 440	6403	0.06	2.8
o-MeStil$_7$T$_7$-trisiloxy	304, 317	406, 418	7793	0.66	0.88
o-CNStil$_7$T$_7$-trisiloxy	314, 326	422, 438	8101	0.42	5.54
p-MeStil$_2$Ph$_5$T$_7$-trisiloxy	299, 311	354	5196	0.73	0.05

[a] $\lambda_{max} \pm 1$ nm

We have included the TPA data for the highest reported values for cage macromonomers or SQs in our previous studies. These compounds have a strong charge transfer component such that in the excited state a large charge transfer (CT) transition is observed reflecting extensive molecular polarization leading to the very large TPA values per group. Coincidentally the Φ_F for these compounds are quite low (0.06/0.07) as expected for CT states.

UV-Vis data for *o/p*-RStil$_x$T$_7$-trisiloxy . Figure **3.6** provides UV-vis absorption and emission spectra for *p*-MeStil$_8$OPS and *o*-RStil$_x$T$_7$-trisiloxy . Ignoring for the moment, the data from *p*-MeStil$_2$Ph$_5$T$_7$-trisiloxy , Their spectra are very similar and all are 5-10 nm red-shifted in absorption and 50-70 nm in emission from *p*-methylstilbene and the model compound MeStilSi(OEt)$_3$, also indicating the existence of 3-D conjugation *even when a corner is missing*. *O*-RStil$_x$T$_7$-trisiloxy shows longer wavelength absorption up to 400 nm, which may arise from the presence of small amounts of dibromophenyl functionality, leading to small amounts of distyrenylbenzene in these SQs. Such longer wavelength absorption was absent in spectra of *p*-MeStil$_8$OPS due to absence of diiodophenyl functionality and *p*-MeStil$_2$Ph$_5$T$_7$-trisiloxy.

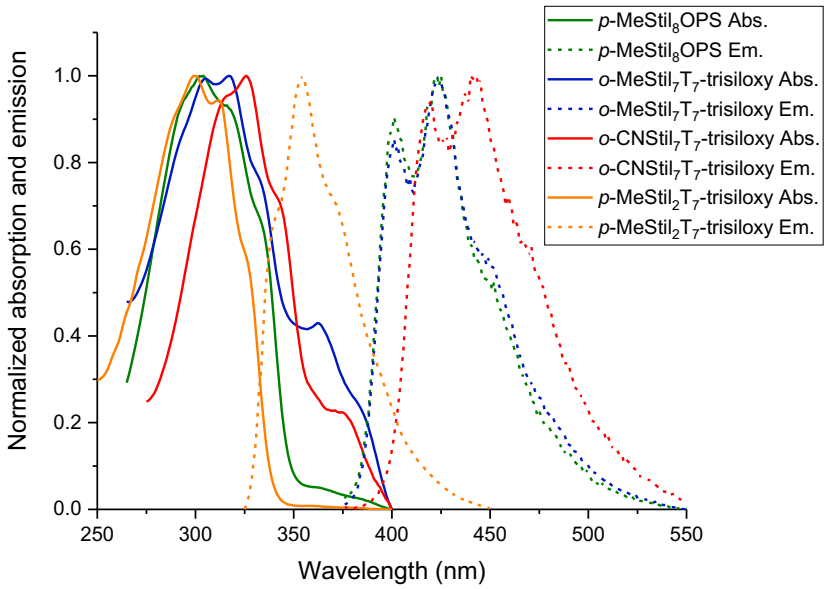

Figure 3.6. Normalized steady-state absorption (solid) and emission (dashed) spectra for *p*-MeStil$_8$OPS and *o/p*-RStil$_x$T$_7$-trisiloxy.

TPA-δ of *o*-MeStil$_7$T$_7$-trisiloxy is only slightly different from other functionalized cage compounds while the TPA-δ of *o*-CNStil$_7$T$_7$-trisiloxy is larger due to the presence of a small amount of dibromophenyl functionality as well as increased conjugation of the cyano group compared to the methyl group.

These values contrast greatly with the surprising Φ_F values for the corner missing cage which are higher to much higher than for complete cages. The reason for this is not clear but perhaps the bulky trimethylsiloxy (TMS) groups prevent radiationless decay by shielding the cage centered excited state from solvent collisions that might serve to promote thermal emission from the excited state-hence radiationless decay.

Most telling of all the Table **3.1** photophysics data reported, is that for *p*-MeStil$_2$Ph$_5$T$_7$ -trisiloxy. For the first time, we find a stilbene cage that does not show a red shift in emission. Instead, the absorption and emission are identical to *p*-methylstilbene. Indeed, there is not even a blue shift in absorption as might be anticipated based on arguments presented above. This molecule does not have a cage centered LUMO. This is extremely important because it means that these LUMOs can only form at certain degrees of conjugation. That is, there is a point where sufficient

numbers of conjugated groups must be attached for the LUMO to form inside the cage otherwise it is likely phenyl or stilbene centered.

The interpretation is that there are clearly structure-property relationships that must be satisfied for 3-D delocalization to occur. This is a valuable discovery because it suggests that there are opportunities to both probe, tailor and optimize properties for applications ranging from high efficiency luminescent components for OLED and white light applications and/or for hybrid photovoltaics, especially if the HOMO LUMO gap can be manipulated. We will in fact demonstrate some ability to do this in a later paper.

3.3.3 Optical magnetization properties

Recently, high frequency magnetization has been induced by intense laser light in a wide variety of materials including simple chemical compounds.[39-42] Nonlinear scattering experiments can characterize 3-D silsesquioxane structures in a novel way that exploits their susceptibility to the joint forces of magnetic and electric optical fields. Magneto-electric scattering at the molecular level is sensitive to the potential energy surface V within each molecule.

This follows from the fact that the slope of the potential determines the azimuthal restoring force of electrons set in motion by the 2-photon interaction32. This restoring force determines the natural frequency $\omega_{\emptyset}$ of oscillations in a torsion pendulum model of the motion33, as well as the intensity of nonlinear scattering by components of various polarizations. Using a linearized approximation to the slope in a direction perpendicular to the radius of the molecule near the equilibrium point, the natural frequency is expressible as

$$\omega_{\emptyset} \cong \frac{b}{\sqrt{I}}(dV/(d\emptyset))_{ave}$$

Here b is a constant that depends on incident light intensity and detuning. I is the molecular moment of inertia. Small values of $\omega_{\emptyset}$ correspond to a nearly flat potential. Large values indicate a steep local potential. It is important to note that $\omega_{\emptyset}$ also equals the 2-photon detuning denominator for the nonlinear scattering process observed in our experiments. It is for this reason that $\omega_{\emptyset}$ is the chief factor determining the relative intensities of polarized or unpolarized scattering channels in the optical interaction[32].

By analyzing ratios of polarized to unpolarized magneto-electric scattering in different molecules under constant experimental conditions, the libration frequencies and relative sphericity of

their orbitals can therefore be compared. To this end, co- and cross-polarized scattered light intensities were recorded and analyzed to distinguish signals of electric and magnetic origin. Then, the comparative sphericity of the excited electron orbitals was determined from the ratio of unpolarized to polarized magnetic signal intensity.

For this portion of the characterization, a separate set of absorption and emission spectra were obtained, as shown in Figure **3.7**. The laser wavelength was fixed at 800 nm, so multiphoton absorption was required to cause excitation of fluorescence. Both two-photon and three-photon ab sorption processes overlap the electronic transition centered on 320 nm in Figure **3.7a** (at 400 nm and 267 nm respectively). Two-photon absorption dominated the excitation however, in view of the close fit of quadratic intensity dependence to the observed fluorescence intensity in all three SQ samples (Figure **3.8**).

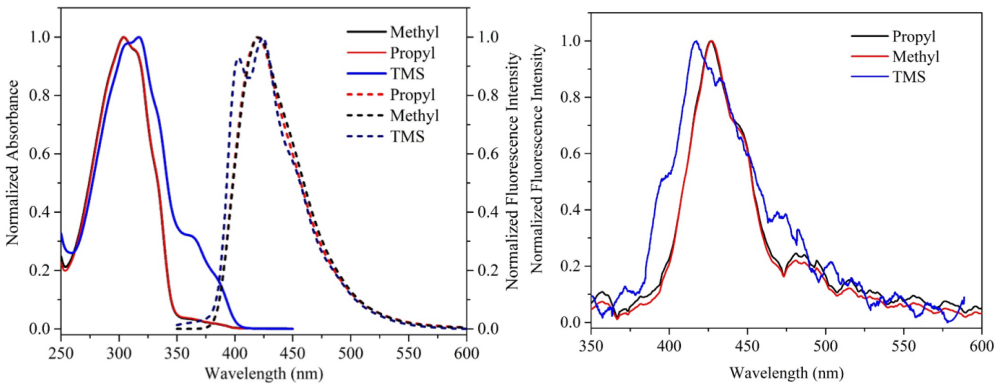

(a) (b)

Figure 3.7. Normalized steady-state one-(a) and (b) two-photon fluorescence spectra (λ_{ex}=800 nm laser light) for *o*-RStil$_7$T$_8$R' and *o*-RStil$_7$T$_7$-trisiloxy.

Impurities can also participate in 2-photon absorption at 400 nm, since this wavelength is relatively far off resonance with the transition to the excited state of the SQ. This was presumed to account for the spectral features of the emission spectrum in the range 475-600 nm that are absent from the one-photon-excited spectrum (Figures **3.7a**,**b**).

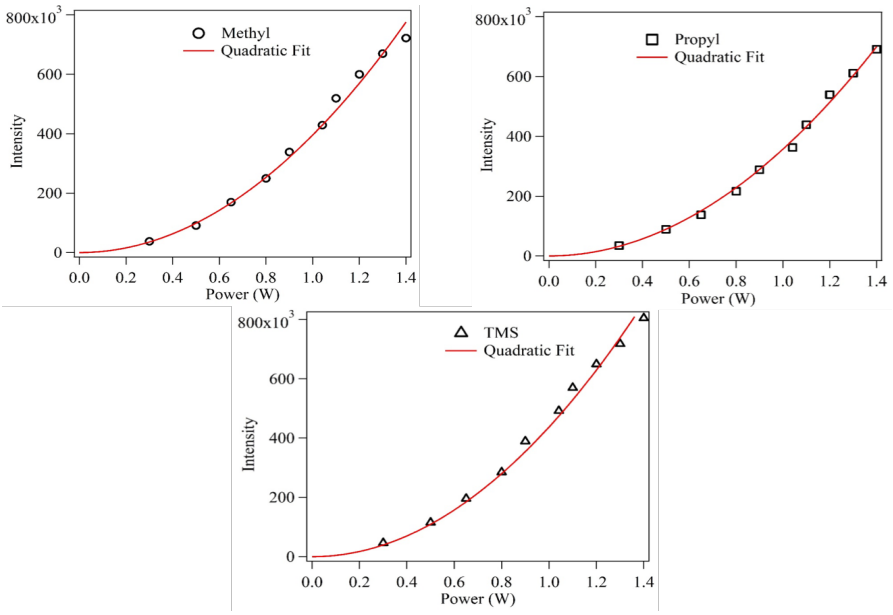

Figure 3.8. Dependence of 2-photon-induced fluorescence emission intensity on input power at λ_{ex}=800 nm in three different SQ samples: (a) Methyl, (b) Propyl, and (c) TMS.

To perform magnetic characterization of SQ samples, we measured the co- and cross-polarized scattered light intensity at 90 degrees to an input beam consisting of 100 fs pulses of various intensities at a wavelength of 800 nm. This type of experiment reveals the relative strength of induced magnetic dipole (MD) scattering in our samples, which is sensitive to azimuthal variations of the electron potential rather than radial variations.

To identify and interpret the theoretical contributions to measured light scattering, we mapped out complete radiation patterns for all samples at fixed input intensity (Figures **3.9-3.11)**. To accomplish this, the analyzer in the detection arm was held in a fixed orientation that either transmitted (red curve) or blocked (blue curve) Rayleigh scattering while the input polarization was rotated through 360 degrees. In Figures **3.9-3.12**, the component in red is therefore linear electric dipole scattering. The component in blue is nonlinear, cross-polarized scattering of magneto-electric origin. Note that the (red) electric dipole scattering and the (blue) magnetic dipole scattering share a common unpolarized background, circular in the polar plot, which is also due to magneto-electric scattering.[32] When analyzed in detail, two separate components are found to be present in each and every recorded polar radiation patterns. One has a purely dipolar ($cos^2\theta$) variation with angle and is therefore polarized. The other has no dependence on angle, and yields an unpolarized, constant background. In the case of cross-polarized scattered light, both components are of

magnetic origin.[32] The polarized component in MD scattering is a little bigger in TMS than in the methyl or propyl variants (Figures **3.11-3.12**). An increase of polarized MD intensity in TMS over that observed in the other samples, measured by the ratio of the angular excursion of scattering intensity over the constant background level in the data, can be interpreted as the result of a deformation in the potential well of the caged electron density. This is discussed next.

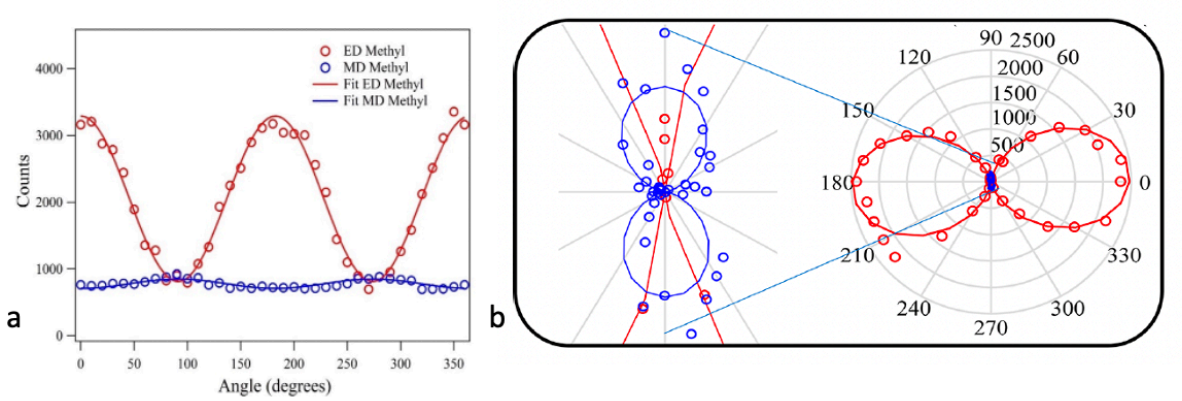

Figure 3.9. (a) Raw data on co- (red) and cross-polarized (blue) scattered light intensity vs. incident polarization angle in *o*-MeStil$_7$T$_8$Me at fixed input intensity (λ_{ex}= = 800 nm). (b) Radiation pattern (polar plot) of the raw data in part (a) after subtraction of the constant background component, showing that purely dipolar electric and magnetic dipole components are induced in the scattered light at the intensity of our experiments.

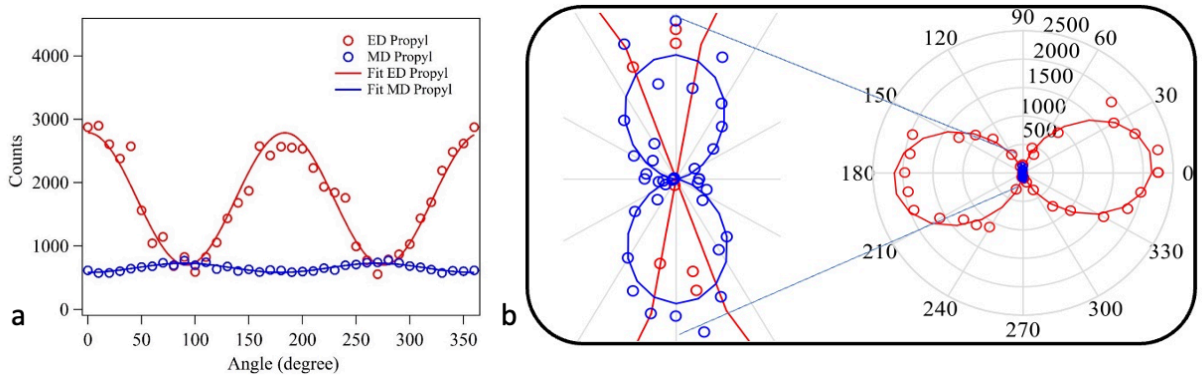

Figure 3.10. (a) Raw data on co- (red) and cross-polarized (blue) scattered light intensity vs. incident polarization angle in *o*-MeStil$_7$T$_8$Pr at fixed input intensity (λ_{ex}= = 800 nm). (b) Radiation pattern (polar plot) of the raw data in part (a) after subtraction of the constant background component, showing that purely dipolar electric and magnetic dipole components are induced in the scattered light at the intensity of our experiments.

In Figures **3.9-3.12** the observed scattered light intensities in part (a) of each figure indicate that the magnetic scattering component (blue) has a magnitude that is only 3-5 times smaller than the Rayleigh component (red). Such an intense magnetic component is not observed in linear scattering but arises here due to nonlinear scattering of magneto-electric origin at the molecular level. What is most significant is the observation that the magnetic component is almost completely unpolarized. For the relatively long duration and small bandwidth of the pulses used in the present experiments, this can only take place if the natural frequency of librations initiated by the magnetic field is extremely low.

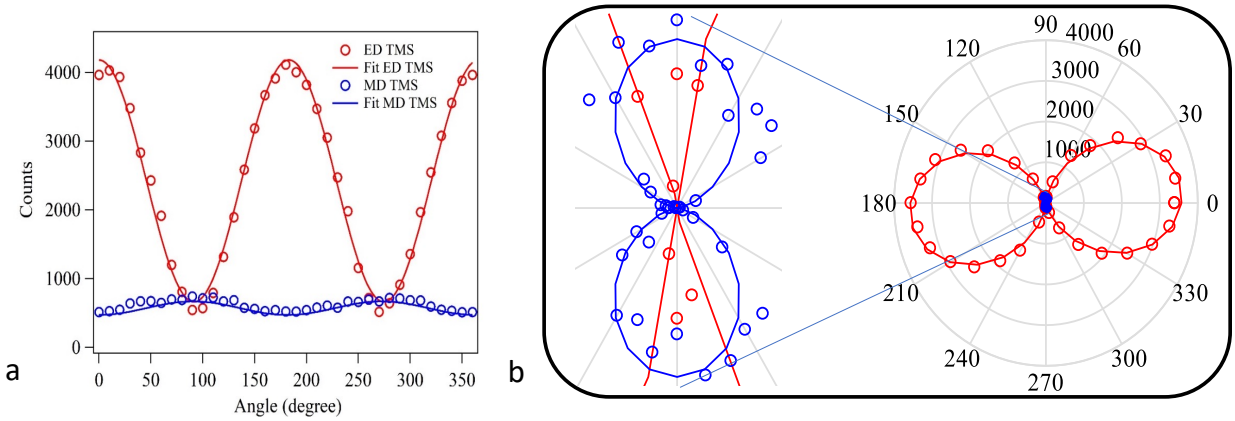

Figure 3.11. (a) Raw data on co- (red) and cross-polarized (blue) scattered light intensity vs. incident polarization angle in *o*-MeStil$_7$T$_7$-trisiloxy at fixed input intensity (λ_{ex}= = 800 nm). (b) Radiation pattern (polar plot) of the raw data in part (a) after subtraction of the constant background component, showing that purely dipolar electric and magnetic dipole components are induced in the scattered light at the intensity of our experiments.

The theoretical importance of libration frequency in MD scattering has been discussed previously[32,33]. Unpolarized (blue) MD scattering arises from electrons that are excited by the magnetic force of incident light to undergo azimuthal librations in the local potential well. Their response is governed by the detuning of the optical interaction, which has been shown to equal the resonant libration frequency. If electrons occupy a spherically-symmetric orbital whose azimuthal slope is near zero, there is little restoring force. The corresponding libration frequency is therefore low, leading to enhancement of magnetic scattering generally, and of unpolarized scattering in particular. On the other hand, if the orbital becomes less spherical through deformation, the libration frequency increases and the unpolarized magnetic scattering intensity is predicted to drop for a fixed pulse duration.

Hence the comparative sphericity of the excited state orbital can be assessed from the ratio of polarized to unpolarized MD scattering intensities. The lowest ratio corresponds to the most spherically-symmetric orbital. If MD scattering is almost completely unpolarized, one can conclude that the excited orbital occupied by the electrons is *spherically symmetric with a near-zero azimuthal slope*. Increasing ratios are indicative of a progressive loss of spherical symmetry. In order to draw conclusions from experimental data however it is important that the electric and magnetic scattering components can be accurately distinguished and that no unexpected components are present from processes that are not magneto-electric in origin. The accuracy of the separation of components was therefore checked in parts (b) of Figures **3.9-3.12**. These figures plot the measured radiation patterns for co-polarized ED scattering after subtraction of the unpolarized magnetic background. It is readily apparent that the resultant patterns are purely dipolar in character. Because the residuals are low, one may conclude that only Rayleigh scattering and magneto-electric scattering contribute significantly to the observed radiation patterns.

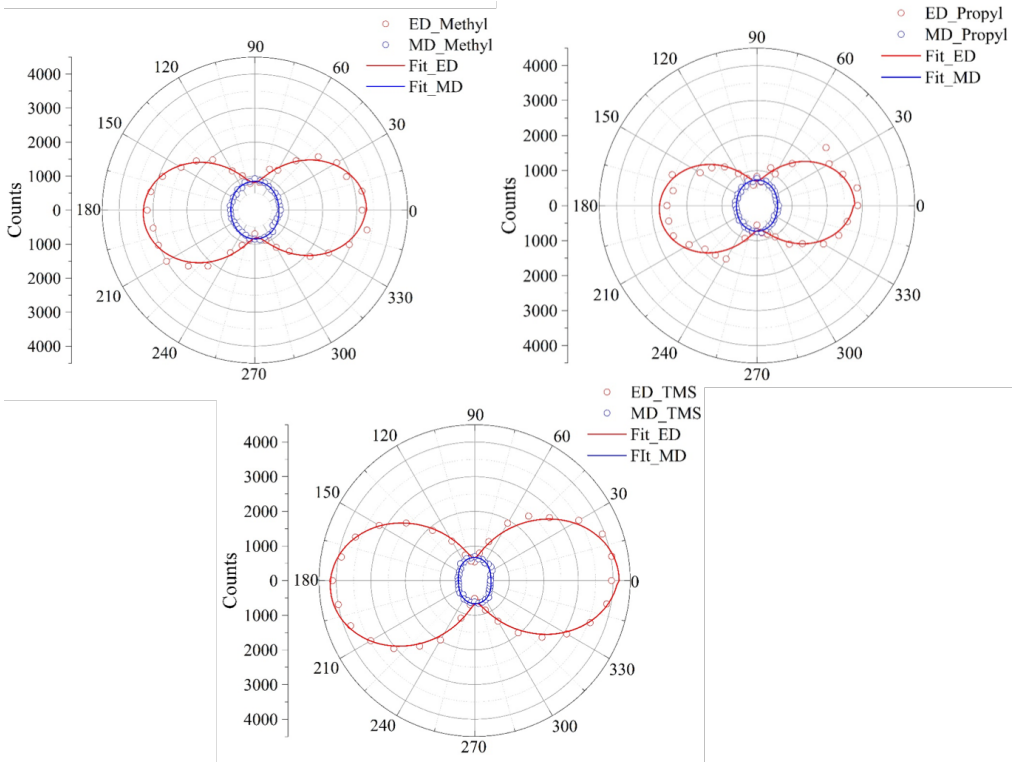

Figure 3.12. Polar plots of raw light scattering data in methyl, propyl and TMS monomers after solvent subtraction. The solid curves are least squares fits to dipole radiation patterns together with a fitted constant background signal.

Some basic trends from these studies can be identified. For example, the two-photon fluorescence intensity (two-photon fluorescence quantum yield) is maximum for TMS and minimum for Propyl at the same concentrations and conditions in DCM solvent, with Methyl being in between the two limits.

The MD unpolarized component decreases in the order:

$Methyl_{unpol,MD} > Propyl_{unpol,MD} > TMS_{unpol,MD}$.

The MD polarized component decreases in the order:

$TMS_{pol,MD} > Propyl_{pol,MD} > Methyl_{pol,MD}$

The ED polarized component follows the trend as:

$TMS_{pol,ED} > Methyl_{pol,ED} > Propyl_{pol,ED}$

These trends may be interpreted with the help of quantum theory of magneto-electric interactions on the atomic scale.[32] First, it may be noted that the progression of unpolarized MD intensity is opposite that of the polarized intensities. Theoretically the proportion of these two components is determined by the magnitude of the librational resonance frequency ω_ϕ of electrons responding to incident light. This is due to the fact that the two-photon detuning of the optical excitation equals ω_ϕ when the bandwidth $\Delta\nu$ of the incident light is small ($\Delta\nu<\omega_\phi$). Presuming the active electron density occupies the orbital centered in the cage, the trend is consistent with resonance frequencies in the order

ω_ϕ(TMS)> ω_ϕ(Propyl)> ω_ϕ(Methyl)

This ordering is justified by the conclusion that the unpolarized scattering channel experiences resonant enhancement as the librational resonance frequency ω_ϕ decreases. The intensity of magnetic scattering should also be proportional to the polarized Rayleigh or ED component, provided the character of the orbital does not change appreciably from one compound to another. This trend is upheld in a comparison of the data for Methyl and Propyl which differ only in the substituent outside the cage. However, the MD component in the TMS data is reduced in intensity despite a sizeable increase in its Rayleigh component, as compared to the other two compounds. This is most obvious in Figure **3.12** where TMS clearly exhibits the largest polarized ED and the smallest unpolarized MD signal components.

As discussed earlier, it is the slope of the orbital potential function that determines the librational resonance frequency. A spherical or nearly spherical potential has a slope close to zero, and consequently a low libration frequency which promotes unpolarized MD scattering. Hence one

interpretation of the trends in the data is that they are consistent with the idea *that removing a corner of the cage in the TMS compound distorts the sphericity of the electron orbital in the cage*. It is quite reasonable to expect that the electron potential develops an axis passing through the corner from the cage center. The introduction of this axis could be argued to lead to an increase in the ED transition moment accompanied by an anisotropy of the potential which raises the librational frequency and diminishes the magnetic scattering intensity, consistent with the data. Thus the magnetic scattering suggests there is a reduction in the sphericity of the LUMO in the cage when a corner is opened, but that the effect is relatively subtle.

3.3.4 Modeling studies

Many recent theoretical studies describe HOMO–LUMO interactions in a wide variety of SQ macromonomers.[43-52] As a prelude to understanding the behavior of the corner missing cage, we first did calculations for the permethyl cage as shown in Figure **3.13**. The presence of a spherical LUMO that matches very closely those we have reported before supports the existence of a similar LUMO in the Ph_7T_8R' cages described above.

To understand the electronic properties of the $Stil_xT_7$-trisiloxy compounds, we calculated the HOMO-LUMO structures of the simplified Me_7T_7-trisiloxy analog per Figure **3.14**. From our results for Me_7T_7-trisiloxy molecule, the HOMO and LUMO energies are -7.37 eV and 0.91 eV, respectively; a gap of 8.34 eV similar to the theoretical model obtained by Shen *et al.*[51]

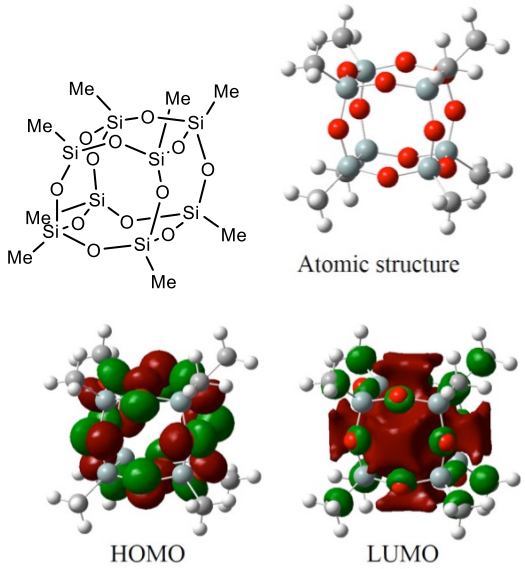

Figure 3.13. HOMO and LUMO modeling of the Me_8T_8 silsesquioxane.

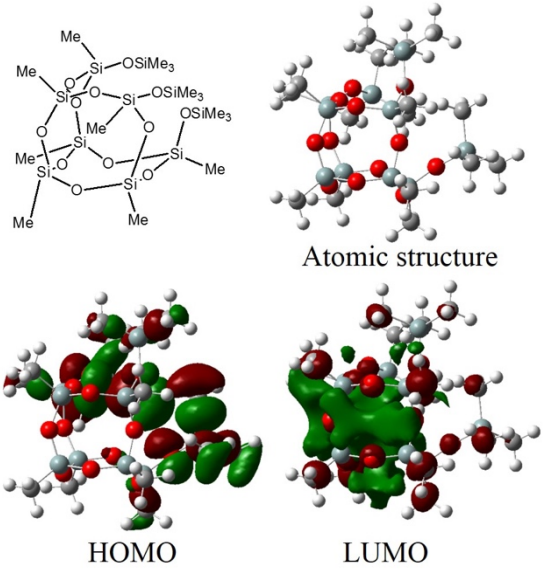

Figure 3.14. HOMO and LUMO models for the permethylated corner missing cage.

The LUMOs are again localized predominantly in the cage center. However, the LUMO appears to be asymmetric within the cage in keeping with the photomagnetic studies described above.

3.4 Conclusions

The above results offer a new perspective on the ease of formation of LUMOs in non-symmetrical and even incomplete phenyl SQs. They point to the idea that their formation may be of a more general nature than originally suspected. However, the absence of a red shift for the disubstituted corner missing SQ with only two methylstilbene moieties indicates there is a threshold for formation of a LUMO inside the cage. This means there are some mitigating electronic effects that control energy levels in and on the cage pointing to the potential for systems where this effect may be tuned through some outside stimulus. These results also set the stage for our efforts to look at double decker cages wherein for example two edges are open yet we still see LUMOs form inside the cage as further discussed in the next chapter.

Furthermore, we also find that probing magneto-electric properties using intense laser light provides a new method of confirming not only HOMO-LUMO gap energies but also LUMO structures and symmetries. We expect to develop this approach to characterization in future papers.

The continuing important point to make is that the existence of 3-D conjugation in the excited state points to electronic communication in three dimensions between conjugated moieties that potentially offers access to a wide variety of semiconducting compounds.

References

1. Voronkov, M.G.; Lavrent'yev, V.I.; "Polyhedral Oligosilsesquioxanes and Their Homo Derivatives," *Top. Curr. Chem*. **1982**, *102*, 199-236
2. Baney, R.H.; Itoh, M.; Sakakibara, A.; Suzuki, T.; "Silsesquioxanes*," Chem. Rev*., **1995**, *95,* 1409-30.
3. Loy, D.A.; Shea, K.J.; "Bridged Polysilsesquioxanes. Highly Porous Hybrid Organic-Inorganic Materials," *Chem. Rev*., **1995**, *95*, 1431-42.
4. Calzaferri, G.; "Silsesquioxanes," in Tailor-made Silicon-Oxygen Compounds, from molecules to materials, R. Corriu and P. Jutzi eds. Publ. Friedr. Vieweg&SohnmbH, Braunshweig/Weisbaden, Germany **1996**, 149-169.
5. Lichtenhan, J.; "Silsesquioxane-based Polymers," in Polymeric Materials Encyc., J.C. Salmone Ed. Vol. 10, CRC Press, N.Y., **1996**, 7768-77.
6. Provatas, A.; Matisons, J.G.; "Synthesis and Applications of Silsesquioxanes," *Trends Polym. Sci*. **1997**, *5*, 327-33.
7. G. Li, L. Wang, H. Ni, C. U. Pittman, "Polyhedral Oligomeric Silsesquioxane (POSS) Polymers and Copolymers: A Review," *J. Inorg. and Organomet. Polymers,* **2001**, *11,* 123-151.
8. Duchateau, R.; "Incompletely Condensed Silsesquioxanes: Versatile Tools in Developing Silica-Supported Olefin Polymerization Catalysts," *Chem. Rev.* **2002,** *102,* 3525-3542.
9. Abe, Y.; Gunji,T.; "Oligo- and polysiloxanes," *Prog. Poly. Sci.* **2004**, *29*, 149-182.
10. Phillips, S.H.; Haddad, T.S.; Tomczak, S.J. "Developments in Nanoscience: Polyhedral oligomericsilsesquioxane (POSS)-polymers," *Current Opinion in Solid State and Mater. Sci.* 2004, 8, 21-29.
11. Kannan, R. Y.; Salacinski, H. J.; Butler, P. E.; Seifalian, A. M.; "Polyhedral Oligomeric Silsesquioxane Nanocomposites: The Next Generation Material for Biomedical Applications," Acc. Chem. Res. 2005, 38, 879-884.
12. Laine, R.M. "Nano-building Blocks Based on the [OSiO1.5]8 Silsesquioxanes," J. Mater. Chem., 2005, 15, 3725 – 44.
13. Lickiss, P.D.; Rataboul, F., "Fully Condensed Polyhedral Silsesquioxanes: From Synthesis to Application," Adv. Organomet. Chem., 2008, 57, 1-116.
14. Chan, K. L.; Sonar, P.; Sellinger, A. "Cubic Silsesquioxanes for use in Solution Processableorganic Light Emitting Diodes (OLED)," J. Mater. Chem. 2009, 19 1-19.
15. Wu, J.; Mather, P. T.; "POSS Polymers: Physical Properties and Biomaterials Applications," Polymer Reviews, 2009, 25–63.
16. Cordes, D. B.; Lickiss, P. D.; Franck, R.; "Recent Developments in the Chemistry of Cubic Polyhedral Oligosilsesquioxanes," Chem. Rev. 2010, 10, 2081–2173 (2010).
17. Laine, R. M.; Roll, M. F.; "Polyhedral Phenylsilsesquioxanes," Macromolecules, 2011, 44, 1073-1220.
18. Hartmann-Thomson, C. Applications of Polyhedral Oligomeric Silsesquoixanes, Adv. Silicon Sci. Springer Science + Business, New York, N.Y. 2011.
19. Sulaiman, S.; Bhaskar, A.; Zhang, J.; Guda, R.; Goodson III, T.; Laine, R. M. "Molecules with perfect cubic symmetry as nanobuilding blocks for 3-D assemblies. Elaboration of octavinylsilsesquioxane. Unusual luminescence shifts may indicate extended conjugation involving the silsesquioxane core." Chem Mater. 2008, 20 5563 – 5573.
20. Laine, R. M.; Sulaiman, S.; Brick, C.; Roll, M.; Tamaki, R.; Asuncion, M. Z.; Neurock, M.; Filhol, J-S.; Lee, C-Y.; Zhang, J.; Goodson III, T.; Ronchi M.; Pizzotti, M.; Rand, S. C.; Li, Y.; "Synthesis and photophysical properties of stilbeneoctasilsesquioxanes. Emission behavior

coupled with theoretical modeling studies suggest a 3-D excited state involving the silica core," J. Am. Chem. Soc. 2010, 132 3708–3722.
21. Sulaiman, S.; Zhang, J.; Goodson III, T.; Laine, R. M.; "Synthesis, Characterization and Photophysical Properties of Polyfunctional Phenylsilsesquioxanes: [o-RPhSiO1.5]8, [2,5-R2PhSiO1.5]8, and [R3PhSiO1.5]8," J. Chem. Mater. 2011, 21, 11177-11187.
22. Feher, F.; Budzichowski, T. A. "Syntheses of highly-functionalized polyhedral oligosilsesquioxanes," J. Organomet. Chem. 1989, 379, 33-40.
23. Bahrami, M.; Hashemi, H.; Ma, X.; Kieffer, J.; Laine, R. M.; "Why do the [PhSiO1.5]8,10,12 cages self-brominate primarily in the ortho position? Modeling reveals a strong cage influence on the mechanism," Physical Chemistry Chemical Physics 2014, 16, 25760-25764.
24. Bahrami, M.; Furgal, J. C.; Hashemi, H.; Ehsani, M.; Jahani, Y.; Goodson III, T.; Kieffer, J.; Laine, R. M.; "Synthesis and Characterization of Nano-building Blocks [o-RStyrPhSiO1.5]10,12 (R = Me-, MeO-, NBoc- and CN. Unexpected Photophysical Properties Arising from Apparent Asymmetric Cage Functionalization as Supported by Modelling Studies," J. Chem. Phys. C. 2015, 119, 15846−15858.
25. Moghadam, M.; Kampf, J.; Laine, R. M.; unpublished results.
26. Ohshita, J.; Tsuchida, T.; Komaguchi, K.; Yamamoto, K.; Adachi, Y.; Ooyama, Y.; Harima, Y.; Tanaka, K.; "Studies on Spherically Distributed LUMO and Electron-Accepting Properties of Caged Hexakis(germasesquioxanes)," Organometallics 2017, 36, 2536
27. Li, Z.; Kawakami, Y.; "Formation of incompletely condensed oligosilsesquioxanes by hydrolysis of completely condensed POSS via reshuffling," Chemistry letters 2008, 37, 804-805.
28. Roll, M. F.; Mathur, P.; Takahashi, K.; Kampf, J. W.; Laine, R. M.; "[PhSiO1.5]8 promotes self-bromination to produce [o-BrPhSiO1.5]8: further bromination gives crystalline [2,5-Br2PhSiO1.5]8 with a density of 2.32 g cm−3 and a calculated refractive index of 1.7 or the tetraicosa bromo compound [Br3PhSiO1.5]8." J. Mater. Chem. 2011, 21, 11167-11176.
29. Roll, M.; Asuncion, M. Z.; Kampf, J.; Laine, R. M.; "para-Octaiodophenylsilsesquioxane, [p-IC6H4SiO1.5]8, a nearly perfect nanobuilding block," ACS Nano 2008, 2, 320-6.
30. Rand, S. C.; Fisher, W. M.; Oliveira, S. L.; "Optically-induced magnetization in Homogeneous Dielectric Media", J. Optical Soc. Am. B, 2008 25, 1106-1117.
31. Fisher, A. A.; Dreyer, E. F. C.; Chakrabarty, A.; Rand, S. C.; Optical Magnetization Part I: Experiments on Radiant Optical Magnetization in Solids, Optics Express 2016 24, 26064-20679.
32. Fisher, A. A.; Dreyer, E. F. C.; Chakrabarty, A.; Rand, S. C.; Optical Magnetization Part II: Theory of induced optical magnetism, 2016 24, 26055-20663.
33. Dreyer, E. F. C.; Fisher, A. A.; Smail, G.; Anisimov, P.; Rand, S. C.; "Optical Magnetization Part III: Theory of Molecular Magneto-electric Rectification", Optics Express 2016 24, 26064-20679.
34. Vosko, S. H.; Wilk, L.; Nusair, M., "Accurate spin-dependent electron liquid correlation energies for local spin density calculations: a critical analysis," Can. J. Physics 1980, 58, 1200-1211.
35. Lee, C.; Yang, W.; Parr, R. G., " Development of the Colle-Salvetti correlation-energy formula into a functional of the electron density," Phys. Rev. B 1988, 37, 785-789.
36. Becke, A. D.; "Density-functional exchange-energy approximation with correct asymptotic behavior," Phys. Rev. A 1988, 38, 3098-3100.

37. Grimme, S.; Antony, J.; Ehrlich, S.; Krieg, H.; “A consistent and accurate ab initio parametrization of density functional dispersion correction (DFT-D) for the 94 elements H-Pu,” J. Chem. Phys,s 2010, 132, 154104.
38. Grimme, S.; Ehrlich, S.; Goerigk, L.; “Effect of the damping function in dispersion corrected density functional theory,” J. Comp. Chem. 2011, 32, 1456-1465.
39. Anderson, S. E.; Bodzin, D. J.; Haddad, T. S.; Boatz, J. A.; Mabry, J. M.; Mitchell, C.; Bowers, M. T.; “ Structural Investigation of Encapsulated Fluoride in Polyhedral Oligomeric Silsesquioxane Cages Using Ion Mobility Mass Spectrometry and Molecular Mechanics,” Chem. Mater.s 2008, 20, 4299-4309.
40. Azinović, D.; Cai, J.; Eggs, C.; König, H.; Marsmann, H. C.; Vepřek, S.; “Photoluminescence from silsesquioxanes R8(SiO1.5)8,” J. Lumin. 2002, 97, 40-50.
41. Chen, Y.; Schneider, K. S.; Banaszak Holl, M. M.; Orr, B. G.; “Simulated scanning tunneling microscopy images of three-dimensional clusters: H8Si8O12 on Si(100)−2×1,” Phys. Rev. B 2003, 70, 085402-.
42. Li, H.-C.; Lee, C.-Y.; McCabe, C.; Striolo, A.; Neurock, M.; “Ab Initio Analysis of the Structural Properties of Alkyl-Substituted Polyhedral Oligomeric Silsesquioxanes,” J. Phys. Chem. A 2007, 111, 3577-3584.
43. Marcolli, C.; Calzaferri, G.; “Monosubstituted octasilasesquioxanes,” Appl. Organomet. Chem. 1999, 13, 213-218.
44. McCabe, C.; Glotzer, S. C.; Kieffer, J.; Neurock, M.; Cummings, P. T.; “Multiscale Simulation of the Synthesis, Assembly and Properties of Nanostructured Organic/Inorganic Hybrid Materials,” J. Comp. Theor. Nanosci. 2004, 1, 265-279.
45. Ossadnik, Christoph, et al. "Photolumineszenzeigenschaften von substituierten Silsesquioxanen der Zusammensetzung R n (SiO 1.5) n." Silicon Chemistry. Springer, Vienna, 1999. 55-68.
46. Park, S. S.; Xiao, C.; Hagelberg, F.; Hossain, D.; Pittman, C. U.; Saebo, S.; “Endohedral and Exohedral Complexes of Polyhedral Double Four-Membered-Ring (D4R) Units with Atomic and Ionic Impurities,” J. Phys. Chemistry A 2004, 108, 11260-11272.
47. Shen, J.; Cheng, W.-D.; Wu, D.-S.; Li, X.-D.; Lan, Y.-Z.; Zhang, H.; Gong, Y.-J.; Li, F.-F.; Huang, S.-P.’ “ Modeling of configurations and third-order nonlinear optical properties of methyl silsesquioxanes,” J. Chem. Phys. 2005, 122, 204709.
48. Striolo, A.; McCabe, C.; Cummings, P. T.; “Thermodynamic and Transport Properties of Polyhedral Oligomeric Silsesquioxanes in Poly(dimethylsiloxane),” J. Phys. Chem. B 2005, 109, 14300-14307.

Chapter 4. Functionalized Double Decker Phenylsilsesquioxane Macromonomers: $[PhSiO_{1.5}]_8[OSiMe_2]_2$ and $[PhSiO_{1.5}]_8[O_{0.5}SiMe_3]_4$

Published: Guan, J., Tomobe, K., Madu, I., Goodson III, T., Makhal, K., Trinh, M.T., Rand, S.C., Yodsin, N., Jungsuttiwong, S. and Laine, R.M. 2019. *Macromolecules*, *52*(19), 7413-7422.

With contributions from Professors Theodore Goodson III, Stephen C. Rand and Siriporn Jungsuttiwong.

Abstract

Bromination and iodination of title double decker (DD) phenylsilsesquioxane macromonomers occurs at ortho and para positions respectively as in $PhT_{8,10,12}$ cages. Heck cross-coupling with 4-Me/CNstyrene gives the corresponding 4-Me/CNstilbene substituted cages. All compounds were characterized by FTIR, MALDI-TOF, TGA, NMR, and GPC. These compounds show UV-vis absorptions very similar to individual stilbene analogs. However, emission for all macromonomers, except p-$MeStil_2Ph_6DD(OTMS)_4$ is red shifted 50-70 nm as seen before in full and partial cages indicating formation of cage centered LUMOs conjugated to all the stilbene moieties indicative of suggesting semiconducting behavior. Cage centered LUMO formation even occurs in a cage where two of four Si-O-Si bridges are broken suggesting that LUMO formation is an extremely common phenomenon. These results are supported by both modeling studies and the use of high intensity laser light to generate magnetic fields that form in the cage centers. The exception behaves like p-methylstilbene in both absorption and emission indicating onset of semiconducting behavior requires a minimum number of substituents and points to the potential to tailor HOMO-LUMO gaps and therefore multiple photophysical properties.

4.1 Introduction

Over the last decade, we have explored the photophysics of elaborated phenyl [$(RphenylSiO_{1.5})_{8,10,12}$] and vinyl [$(RvinylSiO_{1.5})_{8,10,12}$], silsesquioxane (SQ) macromonomers.[1-10] We find that appended moieties conjugated through phenyl or vinyl exhibit UV-vis absorption spectra unchanged from the free moieties but with exceptional red-shifts (40-100 nm) in emission. These red-shifts reflect the formation of a cage centered LUMO that allows excited state communication between all the appended moieties leading to 3-D conjugation suggesting semiconducting behavior.

We recently reported that such LUMOs also form in SQs where one phenyl is replaced with Me/nPr *or is completely removed* (corner missing SQ).[40] These results suggest that 3-D LUMOs may form inside multiple types of SQ cage macromonomers, as recently also seen in germanium analogs.[11]

There is now extensive literature on the chemistries and properties of SQs.[12-29] Most recently, multiple reports have appeared on double decker (DD) SQ macromonmers wherein $OSiR^1R^2$ groups (R^1, R^2 = same or different, cis and trans) are inserted into opposing cage edges.[30-39]

Here, we extend the concept of SQ centered LUMOs further by exploring phenyl based DD SQs, wherein opposing oxygen edge bridges are replaced either by $MeRSi(O\text{-})_2$ (R = Me or vinyl) edge bridges, $[PhSiO_{1.5}]_8[Me_2SiO]_2$ or $[PhSiO_{1.5}]_8[MevinylSiO]_2$ or without any bridges $[PhSiO_{1.5}]_8[O_{0.5}SiMe_3]_4$ again finding LUMOs and delocalization in excited states of 4-Me/CNStilbene analogs *even when the cage is doubly open* with the exception of *p*-MeS-$til_2Ph_6DD(OTMS)_4$ which behaves like simple *p*-methylstilbene.

4.2 Experimental

The synthetic methods and characterization techniques are described in Chapter **2**.

4.3 Results and discussion

In the preceding paper, we followed the identical synthetic protocol as in our previous papers synthesizing stilbene-functionalized PhT_8 and corner missing $T_7(OTMS)_3$ SQ macromonomers from [*o*-bromophenyl$SiO_{1.5}]_8$, [*p*-iodophenyl$SiO_{1.5}]_8$, [*o*-bromophenyl$SiO_{1.5}]_7[O_{0.5}SiMe_3]_3$ and [*p*-iodophenyl$SiO_{1.5}]_7[O_{0.5}SiMe_3]_3$ using traditional Heck coupling procedures.[1-5,40] This series all present UV-vis absorption spectra identical to trans-stilbene. In contrast, emission spectra show red-shifts of 60-100 nm.[1-10,40] Such red-shifts arise from stilbene π^* orbital interactions with a spherical SQ centered LUMO. The most important finding was that such a LUMO also forms and interacts in the excited state with stilbene moieties even when one $PhSiO_{1.5}$ corner is missing.[40] Such photophysical phenomena suggest semiconducting behavior.[1-10] The current effort describes the syntheses of stilbene functionalized DD open and closed SQ macromonomers per Scheme **4.1**, see experimental section below and in Appendix **B**.

As in our previous paper,[40] our approach is to carefully characterize the synthesized macromonomers followed by an assessment of their photophysical behavior, theoretical modeling of the macromonomers leading to a discussion of this photophysical data.

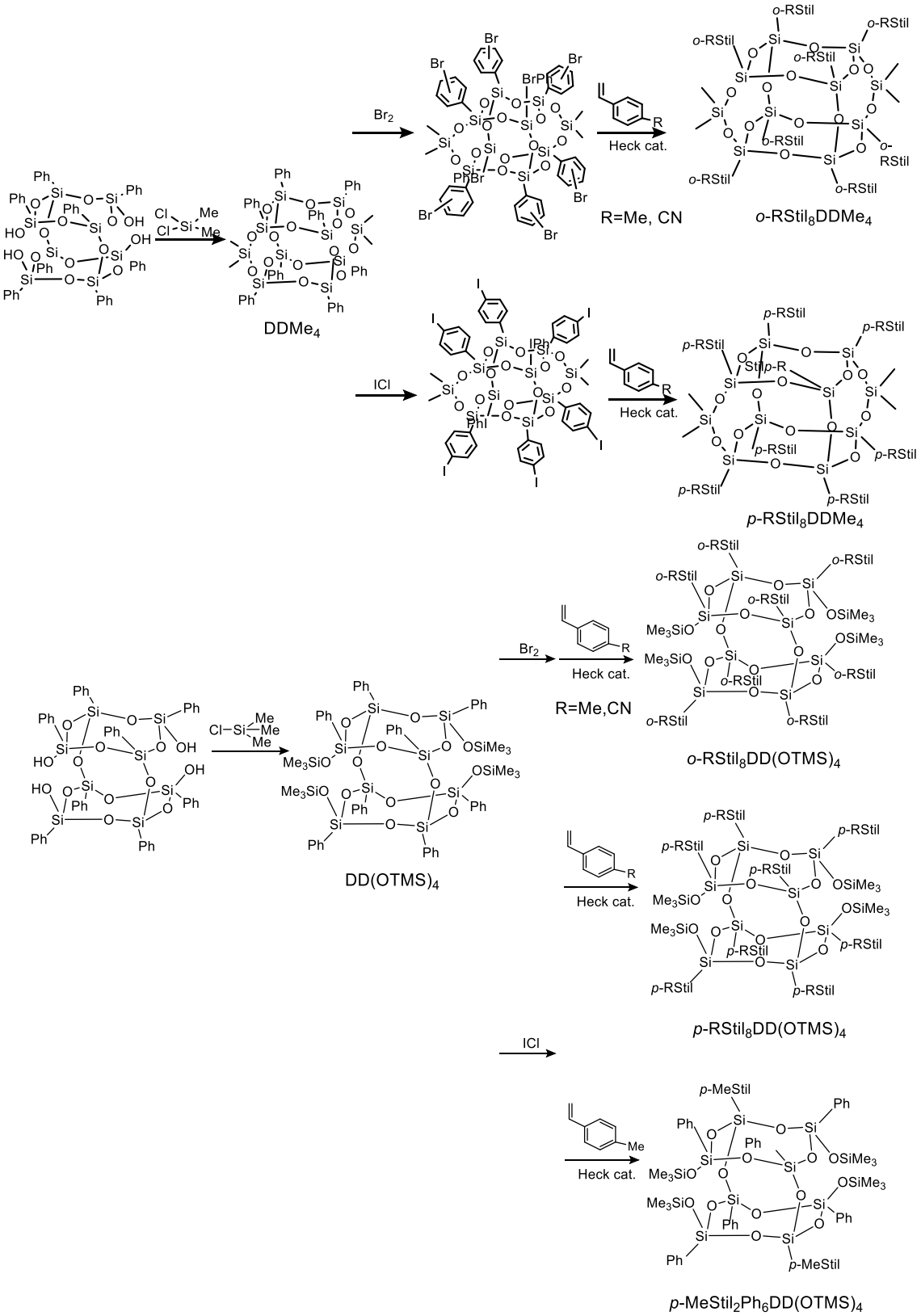

Scheme 4.1. Synthetic scheme for DD stilbene-SQs.

Table 4.1. MALDI-TOF and GPC data for $DDMe_4$ and $DD(OTMS)_4$.

	MALDI-TOFa (m/z)		GPC		
	massb	calcd	Mn	Mw	PDI
$DDMe_4$	1290	1289	756	807	1.07
$DD(OTMS)_4$	1466	1465	1026	1100	1.07

[a]As Ag^+ adduct. [b]As H^+ adduct.

Table 4.2. MALDI-TOF, TGA and GPC data for *o*-Br_xDDMe_4, *o*-$RStil_xDDMe_4$, *p*-I_xDDMe_4, *p*-$RStil_xDDMe_4$, *o*-$Br_xDD(OTMS)_4$, *o*-$RStil_xDD(OTMS)_4$, *p*-$I_xDD(OTMS)_4$ and *p*-$RStil_xDD(OTMS)_4$.

	MALDI-TOF (m/z)	Ceramic yield in TGA (%)			GPC		
	mass	actual	calc.	$T_{d5\%}$ (°C)	M_n	M_w	PDI
o-Br_7DDMe_4	1844[a]	34	34	436	470	485	1.03
o-$MeStil_7DDMe_4$	2112[a]	31	30	435	683	799	1.17
o-$CNStil_7DDMe_4$	2309[a]	27	27	427	1164	1367	1.17
p-$MeStil_7DDMe_4$	2112[a]	31	29	355	1910	1918	1.00
o-$Br_7DD(OTMS)_4$	1902				957	996	1.04
o-$MeStil_7DD(OTMS)_4$	2129	33	33	408	1300	1514	1.16
o-$CNStil_7DD(OTMS)_4$	2364[a]	29	30	382	1514	1857	1.23
p-$MeStil_2Ph_6DD(OTMS)_4$	1636[a]	45	45	359	1360	1372	1.01

[a]As Ag^+ adduct.

4.3.1 Synthesis and characterization of $RStil_xDDMe_4$ and $RStil_xDD(OTMS)_4$.

In previous papers, we carefully delineated a synthesis route to *o*-Br_8OPS (≥ 85% *ortho*[4]) and *p*-I_8OPS (>95% *para*[1-5]). From them, we synthesized and characterized a series of stilbene derivatives.[1-8] We also made analogs with $PhT_{10,12}$ cages.[41]

In the current work, we use the same synthesis methods to prepare open and closed stilbene DD SQs from the halogenated DD SQs, per Scheme **4.1**. The starting DD SQs were prepared by silylation of tetrasilanol $DD(OH)_4$, forming open and closed SQs $DD(OTMS)_4$ and $DDMe_4$ respectively. These were characterized by MALDI-TOF, GPC, NMR and FTIR, Table **4.1** and Table **B.1**. Br/I_7DDMe_4 and Br/$I_7DD(OTMS)_4$ are synthesized with less than stoichiometric amounts of halogen to purposely avoid Br_2Ph and I_2Ph moieties eliminating the chance to accidentally produce distyrenylbenzene moieties. An occasional unfunctionalized phenyl is possible and likely the one closest to the large Me_3Si- groups in open DD SQs due to steric hindrance for addition of Br or I atoms. The iodination to $I_2DD(OTMS)_4$ was tracked by MALDI-TOF and then quenched such that the primary product was the doubly iodinated. We believe that iodination likely occurs on the

phenyls most distant from the Me_3Si- groups. The halogenated and Heck functionalized DD SQs were characterized by MALDI-TOF, TGA, GPC and FTIR, see Table **4.2** and Figures **B.1**-**B.8**.

MALDI-TOF data found in Table **4.2** present Heck substitution patterns identical to those for the brominated and iodinated starting DD SQs. TGA ceramic yields are nearly identical to theory, suggesting quantitative conversion.

$T_{d5\%}$/TGA/air for all Heck products are > 350 °C arising as noted previously because of the advantageous heat capacity of the silica-like cages. GPC chromatographs show slightly larger cage sizes with Heck functionalization as revealed by comparing retention times with starting brominated or iodinated DDs. We use [*p*-$MeStilSiO_{1.5}$]$_8$ (*p*-$Mestil_8OPS$) as a standard for comparison.

4.3.2 Photophysics of *o*-$RStil_7DDMe_4$ and *o*-$RStil_7DD(OTMS)_4$.

UV-Vis studies. Figure **4.1** presents spectra (CH_2Cl_2) for *p*-$Mestil_8OPS$, *o*-$RStil_7DDMe_4$ and *o*-$RStil_7DD(OTMS)_4$. The spectra are essential the same as found for *p*-$Mestil_8OPS$. As earlier, coupled with the results shown here, UV-vis absorption spectra red-shift 5-10 nm from *p*-methylstilbene and the model $MeStilSi(OEt)_3$, which represents a corner of the methylstilbene substituted DD SQ cages.

Corner -$Si(O)_3$ species are reported to behave like a -CF_3 group[42] suggesting a blue-shift might be anticipated. However, Figure **4.1** presents 50-70 nm red-shifted emission spectra for all DD SQs vs *p*-methylstilbene, indicating 3-D conjugation in the excited state.[1-10,40] The similarity between *p*-$MeStil_8OPS$ and *o*-$MeStil_7DDMe_4$ is anticipated given the small differences in their structures. The extra two $SiMe_2$ groups in the DD structure are inserted in a regular cage structure and might not be expected to cause significant changes in the LUMO, compared to OPS. However, for the open *o*-$MeStil_7DD(OTMS)_4$, the found spectra also show 3-D conjugation. *This result is surprising since we have two SQ cyclomers joined by just two bridging oxygens.* We believe this is an extremely unexpected result.

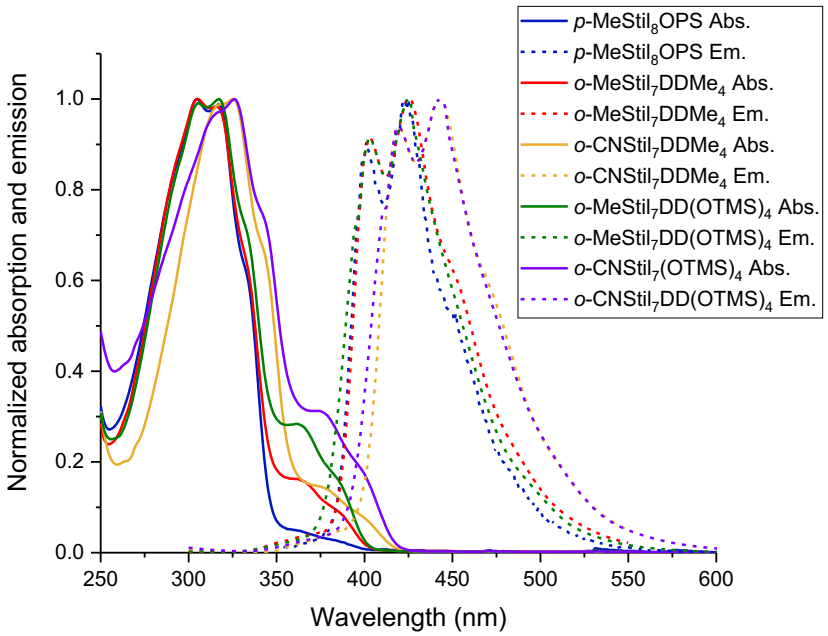

Figure 4.1. Steady-state absorption (solid) and emission (dashed) spectra for *p*-MeStil$_8$OPS and *o*-RStil$_7$DDMe$_4$ and *o*-RStil$_7$DD(OTMS)$_4$.

O-CNStil$_7$DDMe$_4$ and *o*-CNStil$_7$DD(OTMS)$_4$ compounds present spectra similar to *o*-MeStil$_7$DDMe$_4$ and *o*-MeStil$_7$DD(OTMS)$_4$ but slightly red-shifted likely due to increased conjugation from the -CN group.

Table **4.3** data permit several interesting observations. The fluorescence quantum yields (Φ_F) for the methylstilbene analogs, o- MeStil$_7$DDMe$_4$ and o-MeStil$_7$DD(OTMS)$_4$, are greater than found for the octa-substituted compound, p-MeStil$_8$OPS reported previously[10] but in keeping with the higher Φ_F for the corner missing SQ analog also presented in Table **4.3**. One explanation is that the large TMS groups sterically limit solvent aided radiationless decay.

Table 4.3. Photophysical data for *p*-MeStil$_8$OPS, RStil$_x$DDMe$_4$ and RStil$_x$DD(OTMS)$_4$.

	Abs. λ_{max} (nm)	Em. λ_{max} (nm)	$E_{stoke's}$ (cm^{-1})	Φ_F(-)	TPA-δ (GM)
p-MeStilbene[9]	298, 311	355			
MeStilSi(OEt)$_3$[6]	298	352			
p-MeStil$_8$OPS[10]	305, 320	400, 422	9090	0.57	1.4
o-MeStil$_7$T$_7$(OTMS)$_3$	304, 317	406, 418	7622	0.81	0.7
o-MeStil$_7$DDMe$_4$	305, 316	403, 426	8171	0.69	2.9
o-CNStil$_7$DDMe$_4$	317, 325	420, 442	8145	0.36	17
p-MeStil$_7$DDMe$_4$	321	427	7733	0.28	6.3
o-MeStil$_7$DD(OTMS)$_4$	305, 317	401, 421	7793	0.75	2.5
o-CNStil$_7$DD(OTMS)$_4$	314, 326	420, 442	8050	0.48	37
p-MeStil$_2$Ph$_6$DD(OTMS)$_4$	301, 312	355	5054	0.10	2.7

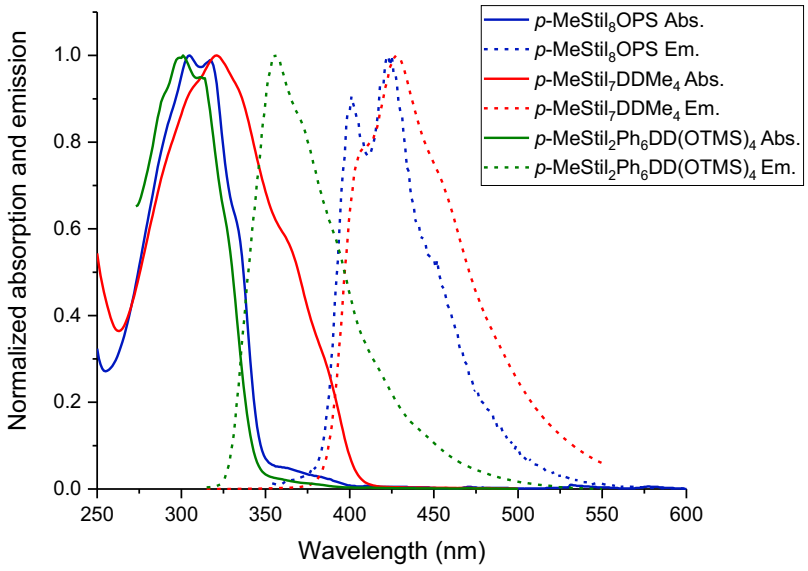

Figure 4.2. Steady-state (solid) and emission (dashed) spectra for *p*-MeStil$_8$OPS, *p*-MeStil$_7$DDMe$_4$ and *p*-MeStil$_2$Ph$_6$DD(OTMS)$_4$.

4.3.3 Photophysics of *p*-MeStil$_7$DDMe$_4$ and *p*-MeStil$_2$Ph$_6$DD(OTMS)$_4$.

In our previous paper,[40] we reported for the first time a stilbene substituted cage *p*-MeStil$_2$Ph$_5$T$_7$(OTMS)$_3$ that does not show an emission red shift. Its photophysical behavior is identical to *p*-methylstilbene indicating the absence of a cage centered LUMO. This implies that LUMOs form only above certain degrees of conjugation. Here we report another example, *p*-MeStil$_2$Ph$_6$DD(OTMS)$_4$ revealing similar structure-property relationships and further demonstrating that a threshold exists for formation of a LUMO inside cage.

4.3.4 Fluorescence and two-photon absorption (TPA) data

The fluorescence quantum yields (Φ_F) and two-photon absorption (TPA-δ) for all macromonomers are given in Table **4.3**. The methylstilbene SQs gave a higher Φ_F compared to the cyanostilbene SQs indicating lower efficiencies likely associated with charge transfer component (see below) in the excited state. The TMS open SQs also show slightly higher Φ_F relative to the closed cages. The relatively high TPA/moiety data for *o*-CNStil$_7$DDMe$_4$ and especially for *o*-CNStil$_7$DD(OTMS)$_4$ can be ascribed to relatively high polarization in the excited state perhaps associated with some CT component in the excited state; however, it is important to note that

changing solvents from CH_2Cl_2 to CH_3CN did not result in any shift in emission λ_{max}, which would signify a large CT contribution to the excited state as seen in aminated stilbene and stilbene vinyl SQs.[1,5]

4.3.5 Optical magnetization properties

As discussed in our previous paper,[40] intense laser light can induce high frequency magnetization in multiple materials and chemical compounds.[44,48] Such methods provide a separate mechanism to probe the 3-D behavior of SQ excited states, relying on nonlinear scattering to explois their susceptibility combined magnetic and electric optical fields. Non-linear magneto-electric scattering strongly reflects the molecular level potential energy surface V, which is a consequence of the slope potential determining the azimuthal restoring force of electron motion caused by 2-photon, magneto-electric interactions. The restoring force defines the frequency $\omega_{\emptyset}$ of oscillations in a torsion pendulum model,[40,47,48] coincident with intensity of nonlinear scattering by components of various polarizations. The natural frequency can be expressed using a linear approximation to the slope perpendicular to the molecular radius near equilibrium:

$$\omega_{\emptyset} \cong \frac{b}{\sqrt{I}}(dV/(d\emptyset))_{ave}$$

The incident light intensity and detuning can be used to define the constant *b*. *I* is then defined as the molecular moment of inertia. Small values of the libration frequency $\omega_{\emptyset}$ correspond to an approximately flat potential whereas large values point to a steep local potential. $\omega_{\emptyset}$ equates to the 2-photon detuning denominator for the nonlinear scattering observed in magneto-electric scattering experiments. Thus, $\omega_{\emptyset}$ is the primary factor determining relative intensities of polarized or unpolarized scattering channels in optical interactions.[46,48] Thus, from the ratios of molecular polarized to unpolarized magneto-electric scattering under constant conditions, the libration frequencies and relative orbital sphericity can be compared. Our efforts were therefore directed to measuring and analyzing co- and cross-polarized scattered light intensities to distinguish the individual electric and magnetic signals. From this data it becomes possible to characterize the sphericity of the excited electron orbitals by determining the ratio of unpolarized to polarized magnetic signal intensity.

Consequently, we obtained the Figure **4.3** absorption and emission spectra using a laser wavelength of 800 nm as done previously.[40] At 800 nm, multiphoton absorption must occur to observe

fluorescence excitation. The double-decker exhibit fluorescence intensities with a quadratic dependence on input intensity (Figure **4.4**).

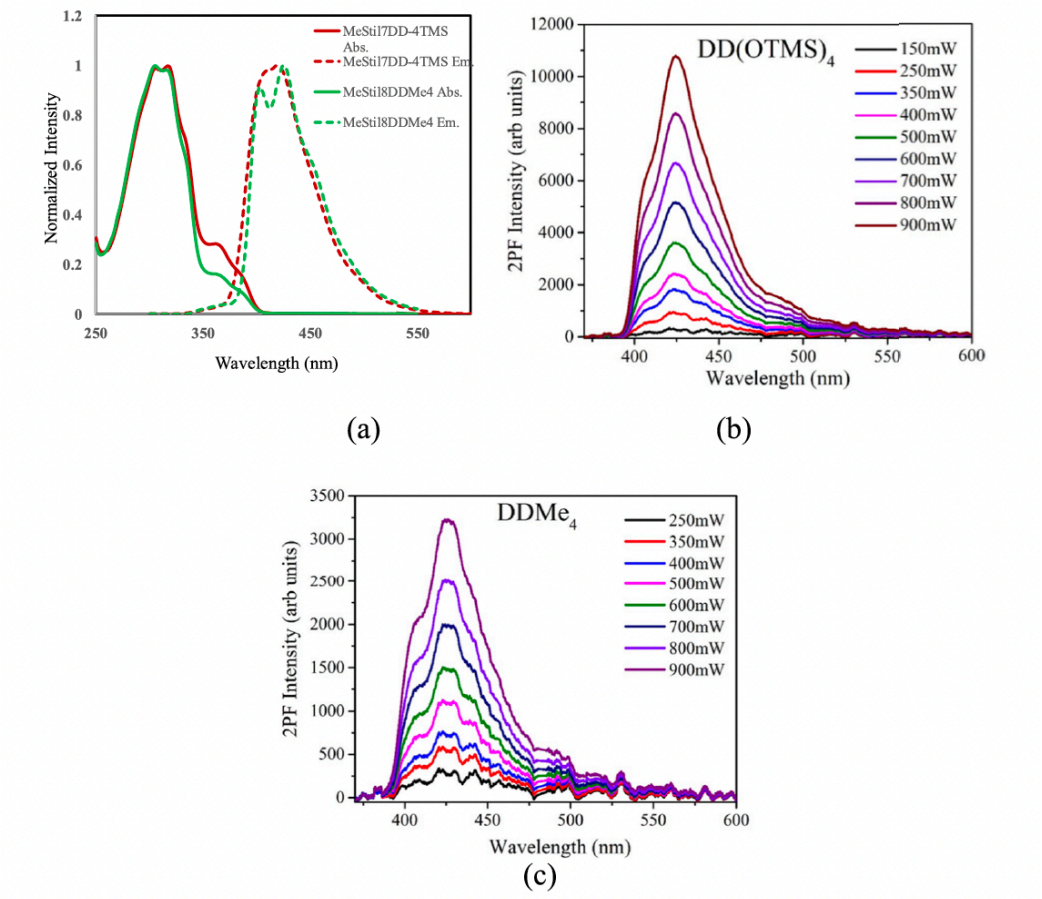

Figure 4.3. Normalized steady-state one- (a) and (b), (c) two-photon fluorescence spectra of $DD(OTMS)_4$ and $DDMe_4$ (λ_{ex}=800 nm laser light).

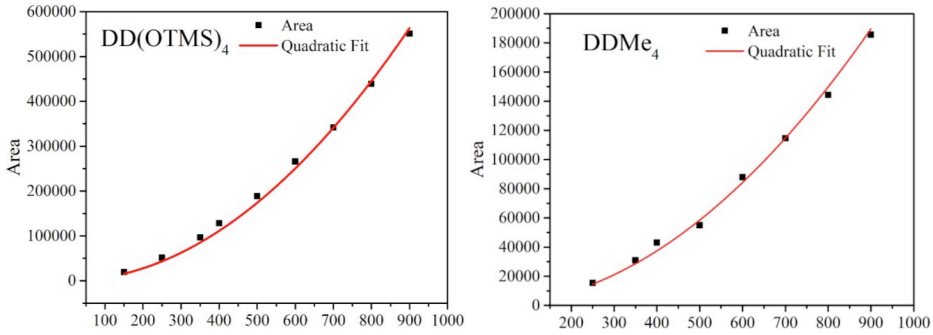

Figure 4.4. Dependence of 2-photon-induced fluorescence emission intensity on input power at λ_{ex}=800 nm in double-decker compounds (a) $DD(OTMS)_4$ and (b) $DDMe_4$.

Magnetic characterization entailed measuring the co- and cross-polarized scattered light intensities at 90 degrees vs. a 800 nm, 100 fs pulse input beam. This type of probe allows quantifying the relative strength of induced magnetic dipole (MD) scattering, which are sensitive to azimuthal rather than radial variations of the electron potential.

Thereafter, we constructed complete radiation patterns for all samples at fixed input intensity to identify and interpret the theoretical contributions to measured light scattering, (Figures **4.5** and **4.6**). Our approach was to position the analyzer in the detection arm in a fixed orientation that either transmits (red curve) or blocks (blue curve) Rayleigh scattering while the input polarization was rotated through 360 degrees.

Figures **4.5** and **4.6**, red is the linear electric dipole (ED) scattering and blue is nonlinear, and magneto-electric in origin. The polarized component of cross-polarized scattering is orthogonal to the ED component and therefore has magnetic dipole (MD) character. ED (red) and MD (blue) scattering share a common unpolarized background; also due to magneto-electric scattering.[46] In analysis, two separate components are seen in each recorded polar radiation pattern. One, with a purely dipolar ($cos^2\theta$) variation with angle, is polarized. The other has no angular dependence giving an unpolarized, constant background.

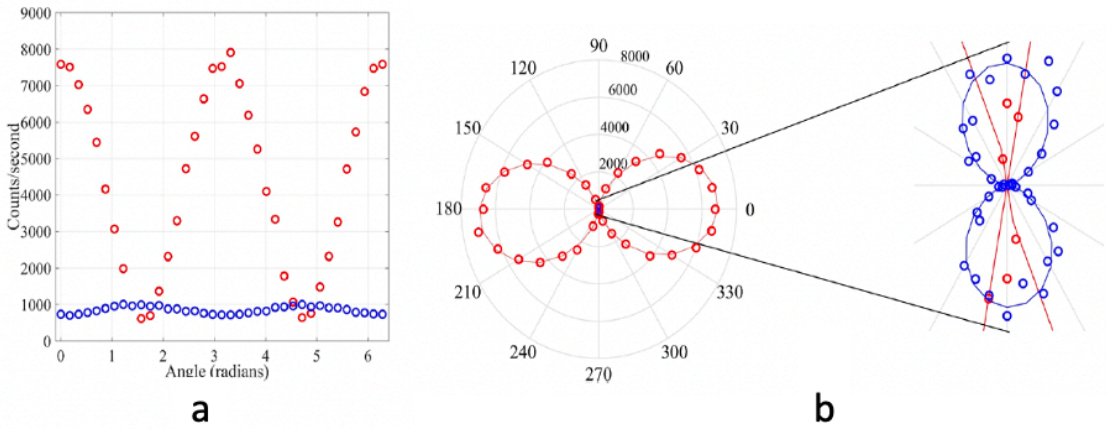

Figure 4.5. (a) Raw data for co- (red) and cross-polarized (blue) scattered light intensity vs. incident polarization angle in 0.1 mM $DD(OTMS)_4$ in DCM at fixed input intensity (λ_{ex}= 800 nm). (b) Radiation pattern (polar plot) of the raw data in part (a) after subtraction of the constant background component, showing purely dipolar electric and magnetic dipole components are induced in the scattered light at the intensity of our experiments.

For cross-polarized scattered light, both components are magnetic.[46] The polarized

component in MD scattering is slightly bigger in $DD(OTMS)_4$ than $DDMe_4$ (Figures **4.5** and **4.6**). The increase in polarized MD intensity in $DD(OTMS)_4$ vs. $DDMe_4$ as measured by the ratio of the angle-dependent variations of scattering intensity over the constant background level, can be interpreted as the result of a deformation in the potential well of the caged electron density. This is discussed next.

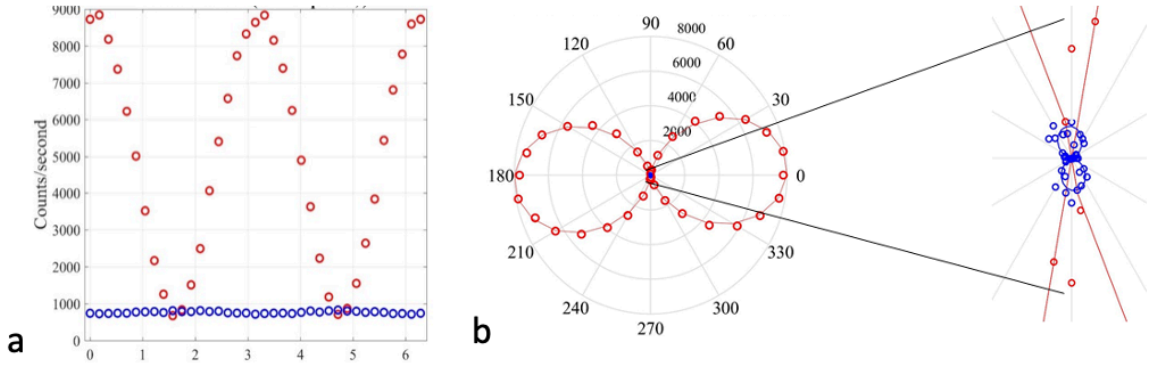

Figure 4.6. (a) Raw data from co- (red) and cross-polarized (blue) scattered light intensity vs. incident polarization angle in $DDMe_4$ at fixed input intensity (λ_{ex}= = 800 nm). (b) Radiation pattern (polar plot) of the raw data in (a) after subtracting background component, showing that purely dipolar electric and magnetic dipole components are induced in the scattered light at the intensity of our experiments.

In Figures **4.5** and **4.6,** the magnetic component (blue) is mostly independent of rotation angle, which can be interpreted to be nearly completely unpolarized. The relatively long duration and small bandwidth of the pulses used here reflects an extremely low natural frequency of libration driven by the optical magnetic field.[46] The role of libration frequency in MD scattering is discussed elsewhere.[45-47] Recent direct evidence supports this.[48]

Unpolarized (blue) MD scattering arises from electrons driven by the magnetic force of incident light to undergo azimuthal librations in the local (intramolecular) potential well. Their response is governed by the detuning of the optical interaction, which is equal the resonant libration frequency. If electrons occupy a spherically-symmetric orbital whose azimuthal slope is near zero, there is little restoring force. The corresponding libration frequency is therefore low, enhancing magnetic scattering, and unpolarized scattering in particular. In contrast, less spherical orbitals, e.g. as a result of deformation, increases libration frequency and unpolarized magnetic scattering intensity should drop for a fixed pulse duration.

The sphericity of a given excited state orbital can be determined from the ratio of polarized to unpolarized MD scattering intensities. The lower the ratio the more spherically-symmetric the orbital. If MD scattering is mostly unpolarized, the implication is that the excited orbital occupied by the electrons is spherically symmetric with a near-zero azimuthal slope. Increasing ratios indicate progressive loss of spheric symmetry.

Basic trends can be summed as follows. The two-photon fluorescence quantum yield is much greater in $DD(OTMS)_4$ than in $DDMe_4$ at identical concentrations in DCM. Relative intensities are ordered:

The MD unpolarized component decreases as:

$DD(OTMS)_{4,unpol,MD} > DDMe_{4,unpol,MD}$

The MD polarized component decreases in the order:

$DD(OTMS)_{4,pol,MD} > DDMe_{4,pol,MD}$

The ED polarized component trends:

$DDMe_{4pol,ED} > DD\ (OTMS)_{4pol,ED}$

The ED unpolarized components are similar in magnitude due to limited signal-to-noise ratios in the experiment:

$DD(OTMS)_{4unpol,ED} \sim DDMe_{4unpol,ED}$

Quantum theory for magneto-electric interactions on the atomic scale can be used to establish relationships between various scattering components.[46] Theoretically, the ratio of unpolarized to polarized components is determined by the magnitude of the librational resonance frequency ω_ϕ of electrons responding to incident light. The two-photon detuning of the optical excitation equals ω_ϕ when the bandwidth $\Delta\nu$ of the incident light is small (i.e. $\Delta\nu<\omega_\phi$). Presuming the active electron density occupies the orbital centered in the cage, the qualitative results $DD(OTMS)_{4,unpol,MD} > DDMe_{4,unpol,MD}$ together with $DD(OTMS)_{4,pol,MD} > DDMe_{4,pol,MD}$ indicate that the libration frequencies of the two compounds are both small but are ordered according to

$\omega_\phi(DD(OTMS)_4) > \omega_\phi(DDMe_4)$

This ordering reflects strengthening of unpolarized scattering as the librational resonance frequency ω_ϕ decreases, the direct result of quantum mechanical detuning dependence of M-E scattering intensity.[46] As discussed previously, the librational resonance frequency is proportional to the average azimuthal slope of the orbital potential. A spherical or nearly spherical potential has a slope close to zero, and consequently a low libration frequency which promotes unpolarized MD

scattering. The data are consistent with the idea *that opening the cage in the* $DD(OTMS)_4$ *compound distorts the sphericity of the electron orbital in the cage*. It is quite reasonable to expect that the electron potential develops *an axis or plane passing* through the cage center. Such an axis or plane of symmetry renders the intramolecular potential anisotropic, raising the librational frequency and diminishing magnetic scattering intensity, consistent with the data. Thus the magnetic scattering data suggest that there is a reduction in the spherical symmetry of the LUMO in the cage when both sides are opened, but that the effect is small.

4.3.6 Theoretical studies

Previous modeling studies of cage compounds focused on the addition of simple substituents to the cage including H, OH, F. The first studies with H substitution found cage centered LUMOs.[2] In modeling studies in the previous paper,[40] we introduced methyl groups again finding cage centered LUMOs. Multiple previous attempts to model stilbene functionalized cages were unsuccessful finding stilbene localized HOMOs and LUMOs.[2,10,43] In the current studies, modeling of stilbene substituted $DD(OTMS)_4$ and $DDMe_4$ compounds using B3LYP/6–31G(d,p) optimized geometries also resulted in stilbene localized HOMOs and LUMOs as illustrated in Figure **4.3**. To date, no one has solved this modeling problem including us; although we continue to try.

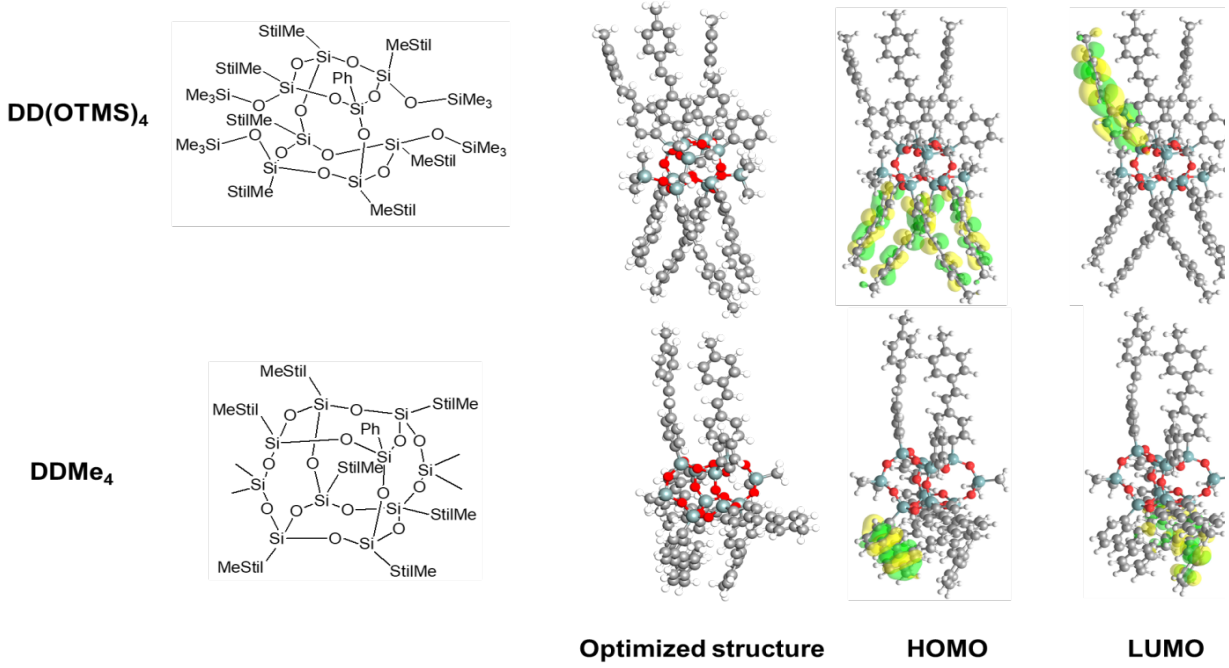

Figure 4.7. Optimized $DD(OTMS)_4$ and $DDMe_4$ structures with HOMO and LUMO at B3LYP/6-31G(d,p) level of theory.

The Figure **4.7** results are in keeping with previous calculations done on these systems, which find that the HOMO and LUMO are associated with external stilbenes rather with a cage centered LUMO. These results lead to a calculated band gap of 3.7 eV which is associated solely with these external stilbenes. Clearly the UV-Vis/Emission results indicate that the LUMO is in the center of the cage. There is a need for a further refinement of the modeling approach.

The excitation energies of the $DD(OTMS)_4$ and $DDMe_4$ molecules were calculated by using TDDFT at the B3LYP, CAM-B3LYP and M06-2X/6-31G(d,p) level. The calculated λ_{max} UV–Vis absorption wavelengths indicate that CAM-B3LYP and M06-2X are suitable for predicting $DD(OTMS)_4$ and $DDMe_4$ spectra. Table **4.4** lists found and calculated λ_{max} values. The simulated adsorption spectra and an illustration of the main electronic transition of the $DD(OTMS)_4$ and $DDMe_4$ molecules at the M06-2X/6-31G(d,p) level are shown in Figure **4.8** which corresponding to stilbene π-π* transitions. Our results provide both experimental and calculated absorption spectra for Stilbene substituted $DD(OTMS)_4$ and $DDMe_4$. The calculated results correlate well with experimental data suggesting the suitability of this method for determining selected electronic properties.

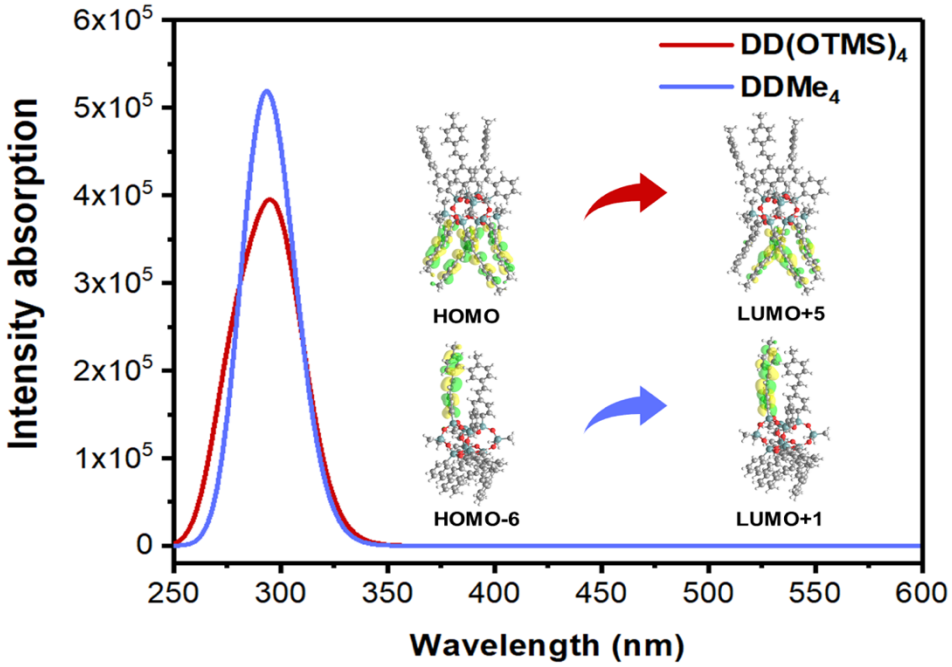

Figure 4.8. Absorption spectra for $DD(OTMS)_4$ and $DDMe_4$, calculated at the TD-M06-2X/6–31G (d) level of theory.

Table 4.4. λ_{max} in nm of $DD(OTMS)_4$ and $DDMe_4$ structures using TD-DFT calculations.

Functional	B3LYP	CAM-B3LYP	M06-2X	Expt.
DD(OTMS)4	361.29	295.05	295.53	~ 300
DDMe4	362.66	291.89	290.86	~ 300

As done in the previous paper,[40] we simplified using methyl substituents (-Me) at the same level of theory, Figure **4.9**, the HOMO and LUMO energy levels of DD-open molecule are -7.39 eV and 0.96 eV, respectively.[49-53] For the DD-close molecule, the HOMO and LUMO energy levels are -7.50 eV and 0.93 eV, respectively. In this instance, a cage centered LUMO presents whereas in the open cage it is not evident despite the red shifted emissions noted just above. This again points to the need for refinements to our modeling approach. The energy gap between HOMO and LUMO of DD-open and DD-close molecules are 8.35 eV and 8.43 eV, respectively. From these results, the large HOMO-LUMO gaps of methyl substituent differ significantly from the methylstilbene substituted compounds as evidenced by the emission red shifted emissions.

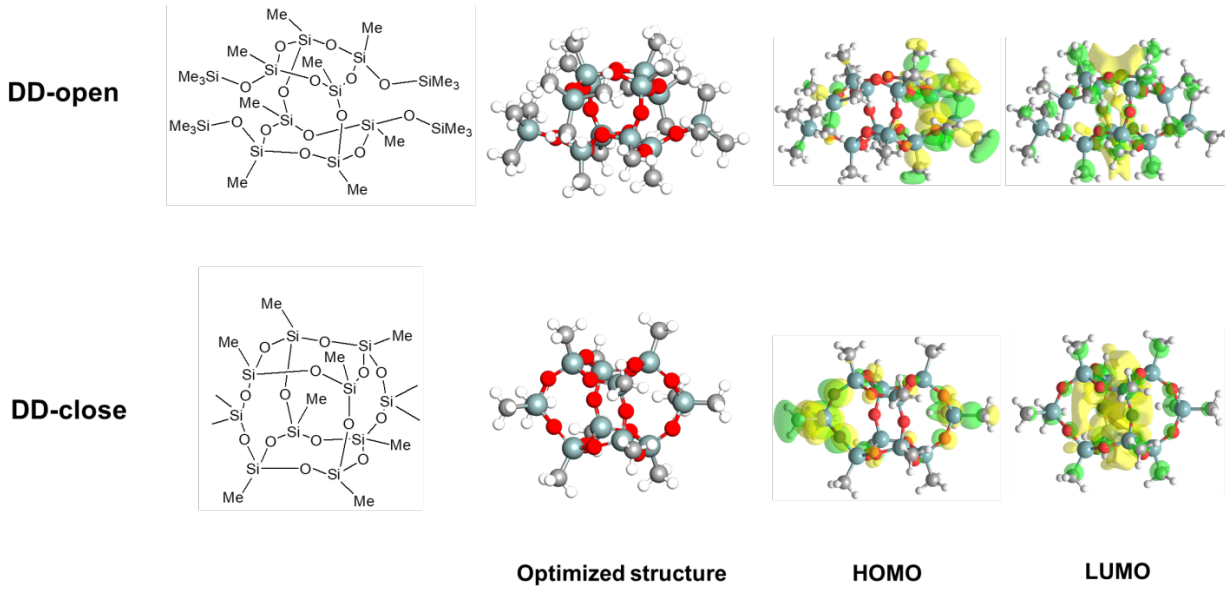

Figure 4.9. Optimized DD-open and DD-close structures with HOMO and LUMO at B3LYP/6-31G(d,p) level of theory.

4.4 Conclusions

The work reported here provides continuing evidence supporting the formation of SQ cage centered LUMOs in a wide variety of cages but most importantly, in the double edge opened cage where two silsesquioxane rings are joined by just two siloxane bridges. We believe this face to face structure is likely the minimum structure possible that leads to a cage centered LUMO. Given that the compound *p*-$MeStil_2Ph_6DD(OTMS)_4$ does not show evidence of a cage centered

LUMO,[2,40] there are clearly some electronic and/or structural features that are mandatory for a cage centered LUMO to appear.

In the next chapter we will describe polymers made from the vinylMeDDMevinyl. Figure **4.10** presents one example where introduction of two or three phenyl groups to vinylMeDDMevinyl shows no obvious conjugation but copolymerization with phenyl red shifts emission >80 nm. It also appears that the absorption is red shifted 40 nm as will be discussed at a later date.[54] Taken *in toto* an original concept of these cages being simply organic decorated silica is put to rest, they offer photophysical properties completely at odds with this idea.

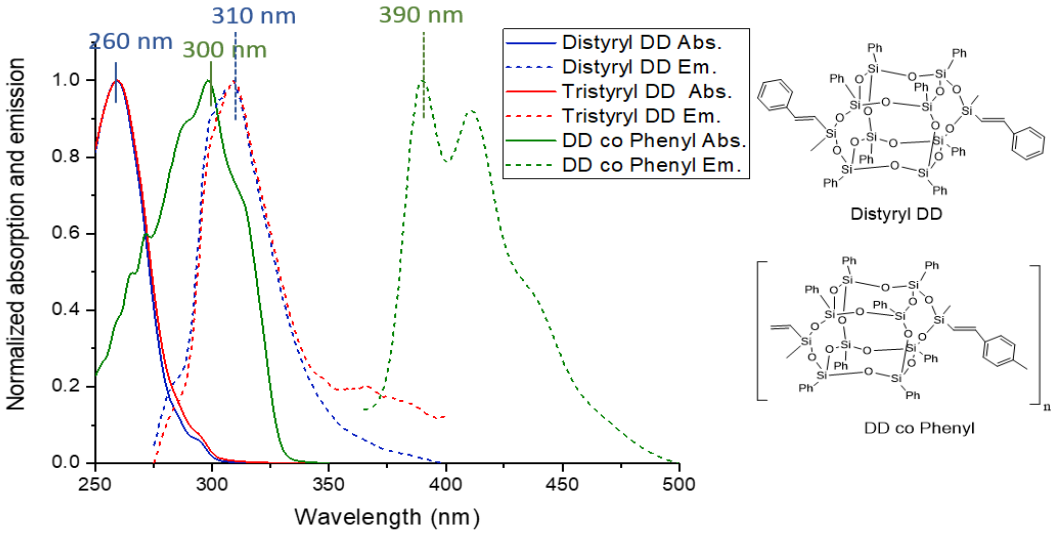

Figure 4.10. Comparison of absorption and emission of di- and tristyrylDD with DD-co-Phenyl (10 k Da M_w).

References

1. Sulaiman, S.; Bhaskar, A.; Zhang, J.; Guda, R.; Goodson III, T.; Laine, R. M., "Molecules with perfect cubic symmetry as nanobuilding blocks for 3-D assemblies. Elaboration of octavinylsilsesquioxane. Unusual luminescence shifts may indicate extended conjugation involving the silsesquioxane core." *Chem Mater*. **2008**, *20* 5563 – 5573.
2. Laine, R. M.; Sulaiman, S.; Brick, C.; Roll, M.; Tamaki, R.; Asuncion, M. Z.; Neurock, M.; Filhol, J.-S.; Lee, C.-Y.; Zhang, J.; Goodson, T., III; Ronchi, M.; Pizzotti, M.; Rand, S. C.; Li, Y. Synthesis and photophysical properties of stilbeneoctasilsesquioxanes. Emission behavior coupled with theoretical modeling studies suggest a 3-D excited state involving the silica core. *J. Am. Chem. Soc*. **2010**, *132*, 3708−3722.
3. Asuncion, M. Z., and Laine, R. M., "Fluoride rearrangement reactions of polyphenyl-and polyvinylsilsesquioxanes as a facile route to mixed functional phenyl, vinyl T_{10} and T_{12} silsesquioxanes." *J. Am. Chem. Soc*. **2010**, *132* 3723–3736.
4. Laine, R. M.; Roll, M. F., "Polyhedral phenylsilsesquioxanes." *Macromol.*, **2011**, *44*, 1073-1220.

5. Sulaiman, S.; Zhang, J.; Goodson, T., III; Laine, R. M. Synthesis, Characterization and Photophysical Properties of Polyfunctional Phenylsilsesquioxanes: [o-RPhSiO$_{1.5}$]$_8$, [2,5-R$_2$PhSiO$_{1.5}$]$_8$, and [R$_3$PhSiO$_{1.5}$]$_8$," *J. Mater. Chem*. **2011**, *21*, 11177−11187.
6. Jung, J. H.; Furgal, J.; Goodson III, T. G.; Mizumo, T.; Schwartz, M.; Chou, K.; Vonet, J.-F.; Laine, R. M.; "3-D Molecular Mixtures of Catalytically Functionalized [vinylSiO$_{1.5}$]$_{10}$/[vinylSiO$_{1.5}$]$_{12}$. Photophysical Characterization of Second Generation Derivatives." *Chem. Mater*. **2012**, *24* 1883–1895.
7. Jung, J. H., Laine, R. M.; "Beads on a Chain (BoC) Polymers with Model Dendronized Beads. Copolymerization of [(4-NH$_2$C$_6$H$_4$SiO$_{1.5}$)$_6$(IPhSiO$_{1.5}$)$_2$] and [(4-CH$_3$OC$_6$H$_4$SiO$_{1.5}$)$_6$(IPhSiO$_{1.5}$)$_2$] with 1, 4-Diethynylbenzene (DEB) Gives Through-Chain, Extended 3-D Conjugation in the Excited State That Is an Average of the Corresponding Homopolymers." *Macromol.*, **2013**, *46* 7580–7590.
8. Furgal, J. C.; Jung, J. H.; Clark, S.; Goodson III, T.; Laine, R. M.; "Beads on a chain (BoC) phenylsilsesquioxane (SQ) polymers via F–catalyzed rearrangements and ADMET or reverse Heck cross-coupling reactions: Through chain, extended conjugation in 3-D with potential for dendronization." *Macromol.*, **2013**, *46* 7591–7604.
9. Furgal, J. C.; Jung, J. H.; Goodson III, T.; Laine, R. M.; "Analyzing structure–photophysical property relationships for isolated T$_8$, T$_{10}$, and T$_{12}$ stilbenevinylsilsesquioxanes." *J. Am. Chem. Soc.*, **2013** *135* 12259–12269.
10. Bahrami, M.; Furgal, J. C.; Hashemi, H.; Ehsani, M.; Jahani, Y.; Goodson III, T.; Kieffer, J.; Laine, R. M.; "Synthesis and Characterization of Nanobuilding Blocks [o-RStyrPhSiO$_{1.5}$]$_{10,12}$ (R= Me, MeO, NBoc, and CN). Unexpected Photophysical Properties Arising from Apparent Asymmetric Cage Functionalization as Supported by Modeling Studies." *J. Chem. Phys. C*. **2015**, *119*, 15846−15858.
11. Ohshita, J., Tsuchida, T.; Komaguchi, K.; Yamamoto, K.; Adachi, Y.; Ooyama, Y.; Harima, Y.; Tanaka, K.; "Studies on Spherically Distributed LUMO and Electron-Accepting Properties of Caged Hexakis (germasesquioxanes)." *Organometallics* **2017**, *36,* 2536
12. Voronkov, M. G., and Lavrent'yev, V. I. ; "Polyhedral oligosilsesquioxanes and their homo derivatives." *Curr. Chem*. **1982**, *102*, 199-236
13. Baney, R. H.; Itoh, M.; Sakakibara, A.; Suzuki, T.; "Silsesquioxanes." *Chem. Rev*., **1995**, *95,* 1409-1430.
14. Loy, D. A., Shea. K. J.; "Bridged polysilsesquioxanes. Highly porous hybrid organic-inorganic materials." *Chem. Rev*., **1995**, *95*, 1431-1442.
15. Calzaferri, G.; "Silsesquioxanes," in Tailor-made Silicon-Oxygen Compounds, from molecules to materials, R. Corriu and P. Jutzi eds. Publ. Friedr. Vieweg & SohnmbH, Braunshweig/Weisbaden, Germany **1996**, 149-169.
16. Lichtenhan, J.; "Silsesquioxane-based Polymers," in Polymeric Materials Encyc., J.C. Salmone Ed. Vol. 10, CRC Press, N.Y., **1996**, 7768-7777.
17. Provatas, A., Matisons, J. G.; "Silsesquioxanes: synthesis and applications." *Trends Polym. Sci*. **1997**, *5*, 327-332.
18. Li, G.; Wang, L.; Ni, H.; Pittman, C. U.; "Polyhedral oligomeric silsesquioxane (POSS) polymers and copolymers: a review." *J. Inorg. and Organomet. Polymers,* **2001**, *11,* 123-151.
19. Duchateau, R. "Incompletely condensed silsesquioxanes: versatile tools in developing silica-supported olefin polymerization catalysts." *Chem. Rev.* **2002,** *102,* 3525-3542.
20. Abe, Y.; Gunji, T.; "Oligo-and polysiloxanes." *Prog. Poly. Sci.* **2004**, *29*, 149-182.

21. Phillips, S. H.; Haddad, T. S.; Tomczak, S. J.; "Developments in nanoscience: polyhedral oligomeric silsesquioxane (POSS)-polymers." *Current Opinion in Solid State and Mater. Sci.* **2004**, *8*, 21-29.
22. Kannan, R. Y.; Salacinski, H. J.; Butler, P. E.; Seifalian, A. M. "Polyhedral oligomeric silsesquioxane nanocomposites: the next generation material for biomedical applications." *Acc. Chem. Res.* **2005,** 38, 879-884.
23. Laine, R. M.; "Nanobuilding blocks based on the $[OSiO_{1.5}]_x$ (x= 6, 8, 10) octasilsesquioxanes." *J. Mater. Chem*., **2005**, *15*, 3725 – 3744.
24. Lickiss, P. D.; Rataboul, F.; "Fully condensed polyhedral oligosilsesquioxanes (POSS): From synthesis to application." *Adv. Organomet. Chem.,* **2008**, *57*, 1-116.
25. Chan, K. L., Sonar, P.; Sellinger, A.; "Cubic silsesquioxanes for use in solution processable organic light emitting diodes (OLED)." *J. Mater. Chem*. **2009**, *19* 1-19.
26. Wu, J.; Mather, P. T.; "POSS polymers: physical properties and biomaterials applications.". *Polymer Reviews,* **2009**, *49*, 25–63.
27. Cordes, D. B., Lickiss, P. D.; Rataboul, F.; "Recent developments in the chemistry of cubic polyhedral oligosilsesquioxanes." *Chem. Rev*. **2010**, *10*, 2081–2173.
28. Laine, R. M., Roll, M. F.; "Polyhedral phenylsilsesquioxanes." *Macromol.*, **2011**, *44*, 1073-1220.
29. Hartmann-Thomson, C.; Applications of Polyhedral Oligomeric Silsesquoixanes, Adv. Silicon Sci. Springer Science + Business, New York, N.Y. **2011**.
30. Seino, M.; Hayakawa, T.; Ishida, Y.; Kakimoto, M.; Watanabe, K.; Oikawa, H. "Hydrosilylation polymerization of double-decker-shaped silsesquioxane having hydrosilane with diynes." *Macromol.* **2006**, *39*, 3473–3475.
31. Wu, S; Hayakawa, T.; Kikuchi, R.; Grunzinger, S. J.; Kakimoto, M.; Oikawa, H.; "Synthesis and characterization of semiaromatic polyimides containing POSS in main chain derived from double-decker-shaped silsesquioxane." *Macromol.,* **2007,** *40,* 5698-5705.
32. Yoshida, K.; Hattori, T.; Ootake, N.; Tanaka, R.; Matsumoto, H.; "Silsesquioxane-based polymers: Synthesis of Phenylsilsesquioxanes with double-decker structure and their polymers." *Silicon Based Polymers*. Springer, Dordrecht, **2008,** 205-211.
33. Hoque, Md.; Kakihana, Y.; Shinke, S.; Kawakami, Y.;"Polysiloxanes with periodically distributed isomeric double-decker silsesquioxane in the main chain." *Macromol.,* **2009**, *42*, 3309-3315.
34. Yoshimatsu, M.; Komori, K.; Ohnagamitsu, Y.; Sueyoshi, N.; Kawashima, N.; Chinen, S.; Murakami, Y.; Izumi, J.; Inoki, D.; Sakai, K.; Matsuo, T.; Watanabe, K.; Kunitake, M.; "Necklace-shaped dimethylsiloxane polymers bearing a polyhedral oligomeric silsesquioxane cage prepared by polycondensation and ring-opening polymerization." *Chem. Lett*. **2012**, *41*, 622-624.
35. Katsuta, N.; Yoshimatsu, M.; Komori, K.; Natsuaki, T.; Suwa, K.; Sakai, K.; Matsuo, T.; Ohba, T.; Uemura, S.; Watanabe, S.; Kunitake, M.; "Necklace-shaped dimethylsiloxane polymers bearing polyhedral oligomeric silsesquioxane cages with alternating length chains." *Polymer* **2017**, *127*, 8-14.
36. Li, Z.; Kawakami, Y.; "Formation of incompletely condensed oligosilsesquioxanes by hydrolysis of completely condensed POSS via reshuffling." *Chem. Lett*. **2008**, *37*, 804–805.
37. Morimoto, Y.; Watanabe, K.; Ootake, N.; Inagaki, J.; Yoshida, K.; Ohguma, K.; U.S. Patent Application 20040249103A1, Sept **2002**.

38. Żak, P.; Delaude, L.; Dudziec, B.; Marciniec, B.; "N-Heterocyclic carbene-based ruthenium-hydride catalysts for the synthesis of unsymmetrically functionalized double-decker silsesquioxanes." *Chem. Comm.* **2018**, *54*, 4306-4309.
39. Groch, P.; Czaja, K.; Dziubek, K.; Bialek, M.; Adamczyk-Tomiak, K.; Rabiej, S.; Dudziec, *B.; J. Polymer Sci. Part A* **2017**, *55*, 3918-3934.
40. Guan, J.; Tomobe, K.; Madu, I.; Goodson III, T. G.; Makhal, K.; Trinh, T. M.; Rand, S. C.; Yodsin, N.; Jungsuttiwong, S.; Laine, R. M.; *Macromolecules,* **2019**, *52*, 4008-4019.
41. Furgal, J. C., Goodson III, T. G.; Laine, R. M.; "D5h $[PhSiO_{1.5}]_{10}$ synthesis via F− catalyzed rearrangement of $[PhSiO_{1.5}]$n. An experimental/computational analysis of likely reaction pathways." *Dalton Trans*., **2016**, 45, 1025.
42. Feher, F. J.; Budzichowski, T. A.; "Syntheses of highly-functionalized polyhedral oligosilsesquioxanes." *J. Organomet. Chem.* **1989**, *379,* 33-40.
43. Zheng, Shaohui, et al. "Ab initio study of the emissive charge-transfer states of solvated chromophore-functionalized silsesquioxanes." *J. Am. Chem. Soc.*, **2012**, *134* (16), 6944–6947
44. Homogeneous Dielectric Media", *J. Optical Soc. Am. B*, **2008** *25*, 1106-1117.
45. Fisher, A. A.; Dreyer, E. F. C.; Chakrabarty, A.; Rand, S. C.; Optical Magnetization Part I: Experiments on Radiant Optical Magnetization in Solids, *Optics Express* **2016** *24*, 26064-20679.
46. Fisher, A. A.; Dreyer, E. F. C.; Chakrabarty, A.; Rand, S. C.; Optical Magnetization Part II: Theory of induced optical magnetism, **2016** *24*, 26055-20663.
47. Dreyer, E. F. C.; Fisher, A. A.; Smail, G.; Anisimov, P.; Rand, S. C.; "Optical Magnetization Part III: Theory of Molecular Magneto-electric Rectification", *Optics Express* **2016** *24*, 26064-20679.
48. M.T. Trinh, K. Makhal, E.F.C. Dreyer, A. Shanker, S.-J. Yoon, J. Kim, and S.C. Rand, "Optical Torque induces magnetism at the molecular level", Opt. Express (accepted).
49. Vosko, S. H.; Wilk, L.; Nusair, M.; "Accurate spin-dependent electron liquid correlation energies for local spin density calculations: a critical analysis." *Can. J. Physics* **1980**, *58*, 1200-1211.
50. Lee, C., Yang, W.; Parr, R. G.; "Development of the Colle-Salvetti correlation-energy formula into a functional of the electron density." *Phys. Rev. B* **1988**, *37*, 785-789.
51. Becke, A. D.; "Density-functional exchange-energy approximation with correct asymptotic behavior," *Phys. Rev. A* **1988**, *38*, 3098-3100.
52. Grimme, S.; Antony, J.; Ehrlich, S.; Krieg, H.; "A consistent and accurate *ab initio* parametrization of density functional dispersion correction (DFT-D) for the 94 elements H-Pu," *J. Chem. Phys,s* **2010**, *132*, 154104.
53. Grimme, S.; Ehrlich, S.; Goerigk, L.; "Effect of the damping function in dispersion corrected density functional theory," *J. Comp. Chem.* **2011**, *32*, 1456-1465.

Chapter 5. Unconventional Conjugation via Siloxane Bridges May Imbue Semiconducting Properties in Double Decker Copolymers

Published: Guan, J., Arias, J.J.R., Tomobe, K., Ansari, R., Marques, M.D.F., Rebane, A., Mahbub, S., Furgal, J.C., Yodsin, N., Jungsuttiwong, S. and Hashemi, D. 2020. *ACS Applied Polymer Materials*, *2*(9), 3894-3907.

With contributions from the groups of Professors Aleksander Rebane, Joseph Furgal, Siriporn Jungsuttiwong and John Kieffer.

Abstract

A number of groups have invested considerable time synthesizing double-decker silsesquioxane (DD SQ) copolymers, however, to our knowledge, no one has sought to explore through-chain electronic communication between DD SQs via "conjugated" co-monomers. We recently demonstrated that stilbene derivatives of simple DD cages exhibit properties commensurate with formation of cage centered lowest unoccupied molecular orbitals (LUMOs), equivalent to LUMOs found in complete/incomplete SQ cages, $[RStilbeneSiO_{1.5}]_{8,10,12}$, $[RStilbeneSiO_{1.5}]_7[O_{1.5}SiMe/nPr]$, $[RStilbeneSiO_{1.5}]_7[O_{0.5}SiMe_3]_3$, $[RStilbeneSiO_{1.5}]_8[O_{0.5}\text{-}SiMe_3]_4$ and $[RStilbeneSiO_{1.5}]_8[OSiMe_2]_2$. Such LUMOs support the existence of 3-D excited state conjugation in these cages. We describe here Heck catalyzed co-polymerization of vinyl(Me)SiO$(PhSiO_{1.5})_8$OSi(Me)vinyl (vinylDDvinyl) with X-Ar-X where X = Br or I and X-Ar-X = 1,4-dihalobenzene, 4,4'-dibromo-1,1'-biphenyl, 4,4''-dibromo-*p*-terphenyl, 4,4'-dibromo-*trans*-stilbene, 2,5-dibromothiophene, 5,5'-dibromo-2,2'-bi-thiophene, 2,5-dibromothieno[3,2-*b*]thiophene and 2,7-dibromo-9,9-dimethylfluorene. Coincidentally model analogs were synthesized from vinylMeSi$(OMe)_2$. All compounds were characterized in detail by gel permeation chromatography (GPC), matrix-assisted laser desorption/ionization-time of flight (MALDI-TOF), thermogravimetric analysis (TGA), nuclear magnetic resonance (NMR), Fourier transfer infrared

spectroscopy (FTIR), ultraviolet-visible (UV-Vis) spectroscopy, photoluminescence spectrometry and two photon absorption (2PA) spectroscopy. Modeling of HOMO LUMO energy levels of related compounds with R = Me rather than Ph was also explored. In the current systems, we again see apparent conjugation in excited states, as previously observed, as indicated by *50-120 nm* red-shifts in emission from the corresponding model silane compounds. These results suggest unexpected semiconducting behavior via vinylMeSi(O-)$_2$ (siloxane) bridges between DD cages in polymers. The thiophene, bithiophene and thienothiophene copolymers display integer charge transfer (ICT) behavior on doping with 10 mol% F_4TCNQ supporting excited-state conjugation; suggesting potential as p-type, doped organic/inorganic semiconductors.

5.1 Introduction

Polysilsesquioxanes, $[RSiO_{1.5}]_n$, have received extensive attention because of their high thermal stability coupled with facile chemical modification that offers potential utility in multiple applications ranging from low-k interlayer dielectrics, to nanoimprint lithography, to mechanically hard, thermally stable, scratch resistant transparent coatings.[1-24] The majority of these applications rely on 3-D networks often generated by hydrolysis of mixtures of $RSi(OEt)_3$/R'$Si(OEt)_3$, for example, wherein the intermediates are coated or cast onto substrates and then heated to promote crosslinking through condensation coincident with elimination of water.[1-3] Alternately, one can functionalize $[RSiO_{1.5}]_{8,10,12}$ cages with reactive groups and copolymerize them by reaction with di-, tri-, etc. functional organic groups to produce 3D structures that often offer gel-like properties.[3,8,11]

We recently reported that it is also possible to cast $[RSiO_{1.5}]_n$/$[R'SiO_{1.5}]_m$ composites using nBu_4NF, an F^- catalyst source, that promotes formation of individual SQ cages n,m = 8,10,12 in THF solution but also drives polymerization when coated on a substrate and heated.[25,26] These systems can also be recycled using the same catalyst.[27]

Linear format polysilsesquioxanes can also be synthesized. The most common forms consist of traditional polymer backbones wherein the SQ is a pendant group.[1,6,11] A much rarer form begins with SQ's functionalized ≥ 2 times such that the functional

groups can be copolymerized with difunctional organic monomers.[19, 25-29] Recently, the discovery of a way to make difunctional phenylsilsesquioxanes, often called double decker (DD) cages, has led to a significant number of papers wherein the SQ cage is part of the polymer backbone and to materials with many of the above-mentioned properties but that are now relatively easily processed, see Scheme **5.1**.[22, 30-43]

We recently reported that the parent phenyl DD cages can be functionalized using standard electrophilic substitution reactions.[44,45] As with simple $[PhSiO_{1.5}]_{8,10,12}$ SQs, the octaphenyl DD compounds including $Ph_8DD(OSiMe_2)_2$ and the open cage analog $Ph_8DD(OSiMe_3)_4$ self-brominate primarily ortho and iodinate para.[46-51] The fact that they self-brominate ortho suggests that like the simple $PhenylT_{8,10,12}$ analogs, a low lying LUMO exists "directing" bromination ortho as supported by modeling studies.[51]

This behavior is also supported by 50-60 nm emission red-shifts observed in the 4-Me- and 4-CN-Stilbene functionalized cages even for the doubly open cages: $4\text{-RStilbene}_8DD(OSiMe_3)_4$ (R = Me, CN) as found for the closed cage T_8 analogs.[44,45] Additional support comes from studies wherein exposure to intense laser light generates magnetic fields with spherical character expected from cage centered LUMOs. [44,45]
The facile synthesis of vinylDDvinyl compounds (Scheme **5.1**) coupled with the apparent existence of a low lying LUMO and because previous SQ systems linked by conjugated tethers show through cage conjugation in polymeric analogs,[25,28,29] prompted us to synthesize DD equivalents per Scheme **5.1**. We anticipated that the existence of two $vinylMeSi(O\text{-})_2$ linkages, siloxane units, would result in polysiloxane-like polymers *without conjugation* given that there are no examples, to our knowledge, of conjugation through such linkages.

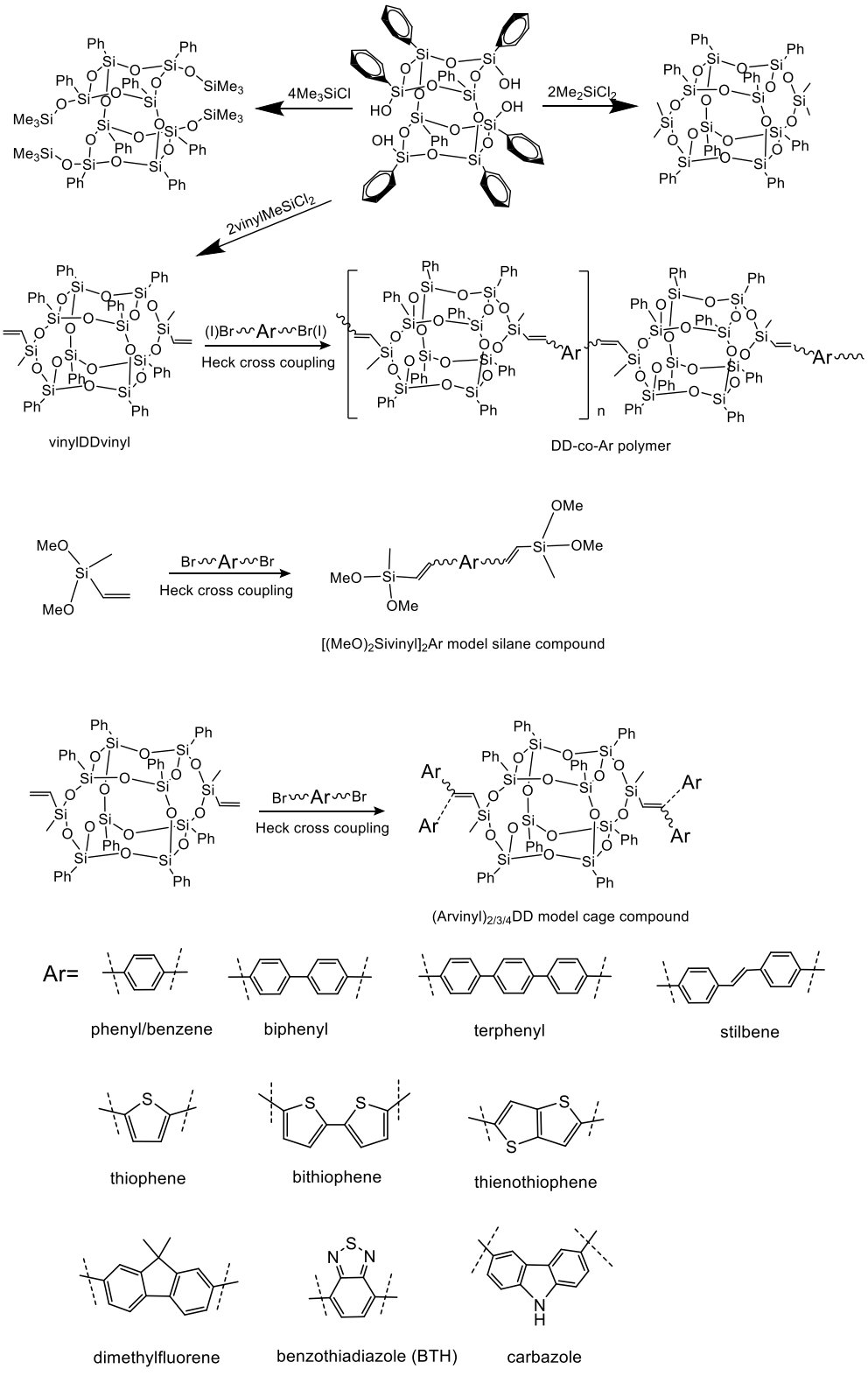

Scheme 5.1. Heck catalytic cross coupling polymerization reactions of vinylDDvinyl and related model compounds.

As a first step, a series of reference model compounds was synthesized for comparison with the corresponding copolymers. Note that as synthesized vinylDDvinyl consists of mixtures with *cis* and *trans* vinyl groups. Pure *trans* isomer can be separated via fractional crystallization using a published method.[52]

We report here the Heck catalytic cross-coupling syntheses of a series of polymers from both mixed and pure *trans* vinylDDvinyl isomers and a detailed evaluation of their photophysical properties. Much to our surprise, the photophysical properties of the oligomers/polymers synthesized here differ very little from previous cage systems found to exhibit cage centered LUMOs and emission redshifts. These results seem to suggest conjugation and semiconducting behavior, as seen previously,[25,28,29] *despite the presence of two vinylMeSi(O-)$_2$ per cage*.

5.2 Experimental

The synthetic methods and characterization techniques are described in Chapter **2**.

5.3 Results and discussion

A number of groups have invested considerable time in the synthesis of DD copolymers;[22,30-43] however, to our knowledge, as noted above, no one has sought to introduce organic co-monomers offering potential as conjugated links.

In the following sections, we first detail the syntheses of a set of model silane compounds via Heck catalytic cross coupling followed by characterization of their respective photophysics. Thereafter, we provide details of studies on conjugated oligomers/polymers derived from mixed isomers of vinylDDvinyl as well as pure trans. It turns out, mixed isomers or pure trans derived polymers share essentially identical photophysical behavior suggesting "semiconducting" properties. We also synthesized and characterized doubly substituted vinyl model cage compounds to explore effects on photophysical properties, to ensure "conjugation" was not simply a consequence of double addition to the vinyl groups.

5.3.1 Model silane compound synthesis and analytical characterization

Model silane compounds were synthesized using the same conjugated monomers as used to generate the corresponding polymers, see Scheme **5.1**.

All disubstituted model silanes were carefully characterized by ^{1}H NMR, GPC and FTIR and as recorded in Tables **C.1-C.2** (Appendix **C**) and Figures **C.1-C.3**. ^{1}H NMR of all model silanes are recorded in Table **C.1** and all display quite similar chemical shifts for methyl, methoxy and vinyl groups from vinylMeSi(OMe)$_2$ around 0.3, 3.6 and 7.0 ppm respectively, as well as corresponding aromatic groups around 7.5 ppm, as illustrated by Figure **C.1**.

GPC traces in Figure **C.2** show di-substitution of vinylMeSi(OMe)$_2$ on aromatic groups by comparison to GPCs of the corresponding starting dibromo-aromatic compounds. Model silanes M_ws appear earlier in GPC traces than respective dibromo-aromatics due to increased size. FTIR spectra in Figure **C.3** consist of the expected peaks. FTIR spectra of the model silanes present peaks for νC-H around 3000 cm^{-1} and νC=C around 1600 cm^{-1} arising from addition of aromatic moieties to vinylMeSi(OMe)$_2$ with the strongest peak for νSi-O ≈ 1100 cm^{-1}. Assignments for the FTIR peaks are given in Table **C.2**. Due to the similar structures of model silane compounds, analytical characterization finds quite similar behavior, as expected, thus not all are presented.

5.3.2 Polymer synthesis and analytical characterization.

The general synthetic scheme for DD derived polymers is presented in Scheme **5.1** above. VinylDDvinyl and derived copolymers were characterized in detail using MALDI-TOF, GPC, TGA and FTIR as presented in Table **C.3** and Figures **C.4-C.29**. *Trans*-isomers of vinylDDvinyl were separated by fractional crystallization using published method[52] but to date, it is still difficult to isolate pure *cis*-isomers.[52] ^{1}H NMR of *trans*-vinylDDvinyl displays chemical shifts for methyl groups around 0.4 ppm, vinyl groups around 6.3 and 6.0 ppm and phenyl groups around 7.4 ppm as illustrated by Figure **C.4**. ^{29}Si NMR was used to characterize pure *trans*-vinylDDvinyl and mixed isomers as shown in Figures **C.5** and **C.6** respectively. In Figure **C.5**, the chemical shift

at -31.4 ppm is assignable to the Si nucleus at the bridge of DD SQs [vinylMeSi(O-)$_2$ unit], whereas those at -78.4 and -79.5 ppm are assignable to Si nuclei at the corners of the SQ cages [PhSi(O-)$_3$ units]. The peak at -78.4 ppm in the ^{29}Si NMR of pure *trans*-vinylDDvinyl shifts to -78.9 ppm for *cis*-isomers due to different environments resulting from *cis*-configuration as shown in Figure **C.6**. MALDI-TOF analysis of each polymer always shows peaks separated by m/z of the co-monomer unit: vinylDDvinyl-Ar, indicating successful copolymerization and without di-substitution on the vinyl groups.

The GPC determined chain lengths and dispersities of all the polymers reveal formation of oligomers of 3 to 18 co-monomer units. As presented in Table **C.3** and Figures **C.7-C.17**, DD-co-bithiophene and -thienothiophene syntheses generate short oligomers with degrees of polymerization (DP) ~3. DD-co-stilbene and BTH products consist of oligomers with DP ~8 while others are polymers offer DP of 10-18. The dispersity (Đ) for all oligomers/polymers is ~2, as expected for step-growth polymerization. Figures **C.18-C.22** display representative FTIR spectra. The strongest peak in all FTIRs appears at 1100 cm^{-1} for νSi-O from the SQ cores, per Table **C.2**. All TGA results are recorded in Figures **C.23-C.29**. Theoretical TGA ceramic yields were calculated from formula weights for each co-monomer unit. The found ceramic yields are slightly smaller due to end group halogens but still do not indicate di-substituted vinyls. $T_{d5\%}$/air for DD-co-phenyl, -biphenyl, -terphenyl and -stilbene are >400 °C, while other polymers all exhibit higher $T_{d5\%}$ >500 °C, indicating high thermal stability arising from the silica particle-like backbones.

5.3.3 Model cage compound syntheses and analytical characterization.

Model cage compounds with di-, tri- and tetra-substitution were synthesized as illustrated in Scheme **5.1**. The vinylDDvinyl derived model cage compounds were synthesized to confirm that the co-polymer systems were also red-shifted from corresponding model compounds. Although MALDI-TOF and TGA of the polymers confirm the absence of double addition of aromatic moieties to one vinyl group, it is still important

to study the effects of di-substituted vinyls on photophysical properties. Thus, such model cage compounds were also synthesized.

All model DD compounds were characterized via MALDI-TOF, GPC and TGA as recorded in Table **C.4** and Figures **C.24, C.26, C.28** and FTIR in Figures **C.19-C.22**. MALDI-TOF reveals the number of substituted groups on each cage. GPC does not give the actual molecular masses of DD compounds because they are roughly spherical in nature but suggests single cages are formed for each model compound without decomposition or polymerization as Đs ~1.0 and retention times were typically 31 min, which are a bit earlier than found for vinylDDvinyl, 32 min, arising from slightly increased cage size.

FTIR spectra of the DD polymers and respective model cage compounds in Table **C.4** and Figures **C.19-C.22** are essentially identical as expected due to their similarity in monomer units and structures. The number of substituents was further verified using TGA ceramic yields as presented in Table **C.4** and Figures **C.24, C.26** and **C.28**. The $T_{d5\%}$/air for all model compounds runs ~400 °C, suggesting high thermal stability, again as consequent of the "silica"-cage cores.

5.3.4 Steady-state photophysical studies

All polymers studied were synthesized at least three times and purified by crystallization and purities determined by GPC, MALDI-TOF and thin layer chromatography to ensure that no impurities were present that might contribute to the photophysical phenomena observed. Furthermore, DD-co-phenyl was synthesized via Heck coupling vinylDDvinyl with either 1,4-diiodobenzene or 1,4-dibromobenzene and their spectra are essentially the same as expected, since the final structures are the same except different terminal halogens. UV-Vis and photoluminescence were recorded for all compounds in Table **5.1**.

As shown in Table **5.1**, the $(Styryl)_2$DD model cage compound absorbs at 260 nm and emits at 310 nm in CH_2Cl_2, typical photophysical behavior for phenyl groups. $(Styryl)_{2,3}$DD share nearly identical spectra even though $(Styryl)_3$DD has one di-

substituted vinyl per cage, which suggests that vinyl di-substitution has only mundane or even no effect on the photophysical properties of these compounds. This was further confirmed from the nearly identical spectra of (9.9-dimethylfluorenevinyl)$_{2,4}$DDwhere both cage vinyl groups were disubstituted with 9.9-dimethylfluorene moieties. Thus, spectra for (9,9-dimethyfluorenevinyl)$_4$DD are not presented in Figure **C.30**.

Figure **5.1a** presents the synthesis of a model silane-end-capped DD with a longer conjugation length than (Styryl)$_2$DD and 1,4-[(MeO)$_2$Sivinyl]$_2$benzene. Figure **5.1b** records its steady-state spectra along with 1,4-[(MeO)$_2$Sivinyl]$_2$benzene and DD-co-phenyl. All three compounds absorb with $\lambda_{max} \approx 298$ nm. Their emission spectra (298 nm excitation, CH_2Cl_2) differ considerably. Thus, 1,4-[(MeO)$_2$Sivinyl]$_2$benzene alone, emits primarily at $\lambda_{max} \approx 332$ nm with two much smaller peaks around 390 and 412 nm. The corresponding silane-end-capped DD cage emits primarily at $\lambda_{max} \approx 342$ nm along with peaks at 390 and 412 nm, which are now qualitatively somewhat larger suggesting partial extended conjugation.

On linking *two or more cages* via divinylbenzene, the emission λ_{max} are 50 nm red-shifted to ≈ *390 nm* from the silane-end-capped DD monomer, suggesting conjugation through the divinylbenzene linkers in the polymer. It also strongly suggests conjugation through two vinylMeSi(O-)$_2$ siloxane units on either side of each cage, *which is highly contrary to what is currently known about siloxane links*.

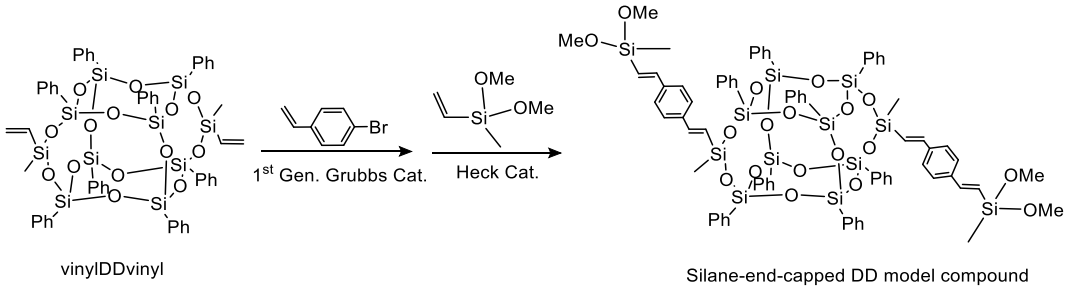

a

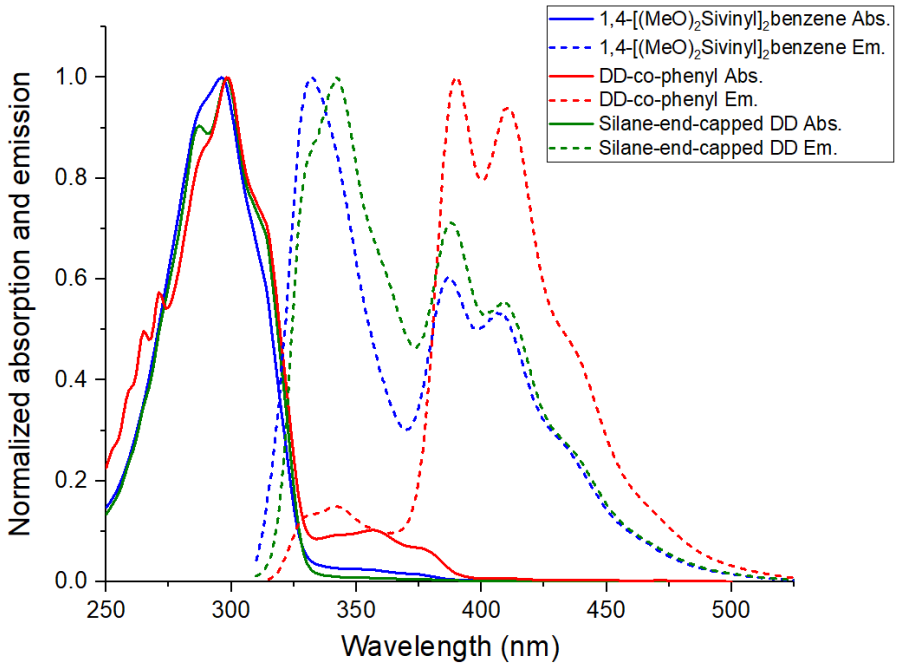

b

Figure 5.1. (a) Synthese of silane-end-capped DD; (b) normalized steady-state spectra of 1,4-[$(MeO)_2$Sivinyl]$_2$benzene, DD-co-phenyl and silane-end-capped DD.

The Figure **5.2** data comes from a previous publication[25] wherein it was found that divinylbenzene linked SQ cages (beads-on-a-chain, BoC) offered semiconducting behavior arising from a cage centered LUMO that affords delocalization by coupling with divinylbenzene linkers.

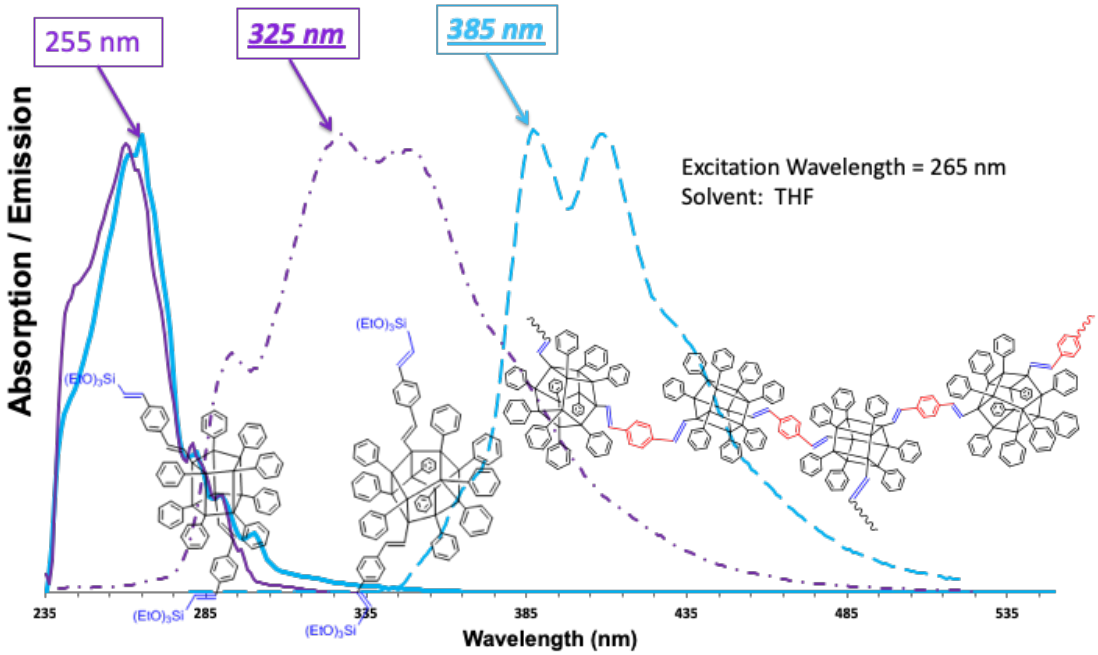

Figure 5.2. Absorption and emission of model compounds and BoC oligomers of $T_{10,12}$.

Figure **5.2** [25] compares the normalized UV-Vis spectra of the triethoxysilane-end-capped model compounds of the $PhT_{10,12}$ cages with divinylbenzene linked (tethered) T_{10} and T_{12} oligomers. Absorption and emission spectra of the model compounds give λ_{max} = 255 and 325 nm respectively, whereas the corresponding oligomer offers absorption and emission λ_{max} = 255 and 385 nm respectively. This original work was followed by a series of papers that explored "beads-on-a-chain (BoC)" SQ cage polymers,[28,29] wherein multiple examples of $PhT_{8,10,12}$ cages linked via aromatic tethers exhibited red-shifted emissions leading to the conclusion that these compounds exhibit LUMOs delocalized along the polymer chain, or *semiconducting properties*.

Here we find similar photophysical behavior for DD-co-biphenyl, -terphenyl and -stilbene where the emission peaks or shoulders at longer wavelength become more significant compared to their corresponding model silanes. Most significant of the copolymers studies are those with thiophenes and 9,9-dimethylfluorene, which exhibit exceptional redshifted visible light emissions compared to the phenyl systems per Table **5.1** and Figure **5.3**. The λ_{max} shifts in emission compared to model silanes range from

50 to *120 nm* despite DD-co-bithiophene and-thienothiophene being short oligomers with DP ~3.

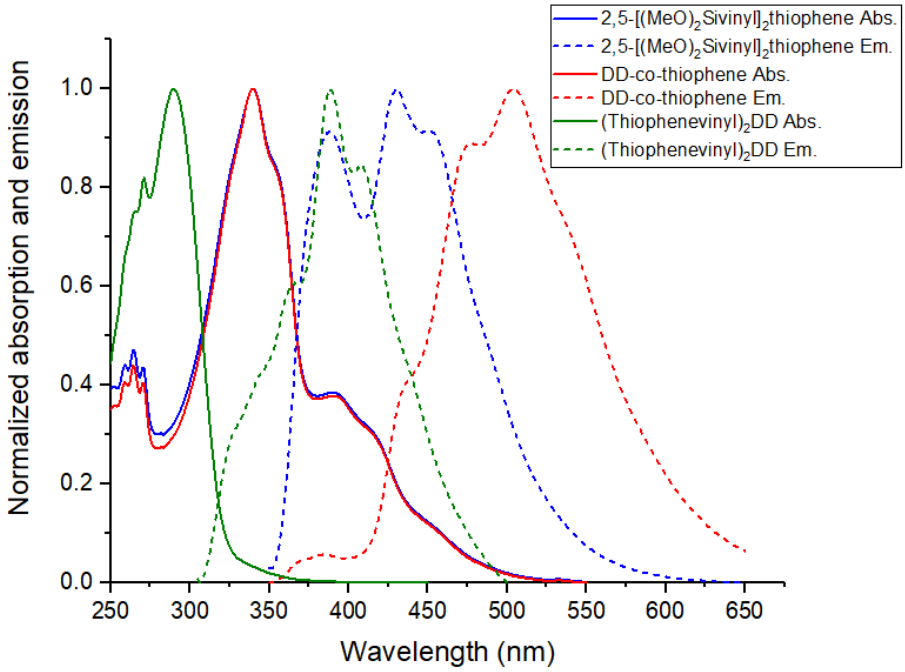

Figure 5.3. Normalized steady-state spectra of 2,5-[$(MeO)_2$Sivinyl]$_2$thiophene, DD-co-thiophene and $(Thiophenevinyl)_2$DD.

Although we present eight examples of conjugated DD polymers, benzothiadiazole (BTH) and carbazole exhibit basically the same absorption and emission spectra as their model silanes. One possible reason is that the bandgap energy of phenyl, thiophene and 9,9-dimethylfluorene systems are close to those of the DD cage with absorption λ_{max} around 250 nm thus giving better conjugation, while BTH and carbazole have smaller HOMO-LUMO gaps with absorption λ_{max} around 300 nm. Another explanation is that their emissions arise from n to π^* transitions localized on the nitrogen containing units that do not have the correct symmetry to conjugate with chain tethers. More studies need to be done to refine our understanding of this behavior, but see below.

Polymers DD-co-biphenyl, -terphenyl and -stilbene exhibit quite high Φ_F values up to 0.6-0.9 and DD-co-dimethylfluorene and -carbazole with Φ_F around 0.4. Both DD-co-stilbene and -dimethylfluoreneare potential blue emitters exhibiting *blue*

luminescence under room light in solution due to their relatively long emission wavelengths around 440 nm among DD polymers combined with high Φ_F.

Table 5.1. Steady-state data for vinylMeSi(OMe)$_2$ derived model silane compounds (blue), vinylDDvinyl derived polymers (red) and model cage compounds (green).

Model silanes	Abs. λ_{max} (nm)	Em. λ_{max} (nm)	$E_{stoke's}$ (cm^{-1})	Φ_F
Benzene	297	332, 387, 409	3550	0.01±0.001
Biphenyl	313	355, 370	4922	0.38±0.03
Terphenyl	319	373, 388	4538	0.48±0.03
Stilbene	355	391, 409	3719	0.36±0.02
Thiophene	340	430, 452	6156	0.01±0.001
Bithiophene	388	433, 457	3891	0.02±0.005
Thienothiophene	354	406, 454, 479	3618	0.02±0.001
Dimethylfluorene	336	382	3584	0.30±0.01
BTH	381	483	5543	0.02±0.005
Carbazole	298	384	7515	0.10±0.01
Polymers				
VinylDDvinyl	264	281, 315	2292	
Co-phenyl	298	390, 412	7916	0.08±0.001
Co-biphenyl	314	357, 373	5037	0.66±0.05
Co-terphenyl	321	374, 392	5642	0.87±0.04
Co-stilbene	357	393, 412, 436	3739	0.61±0.04
Co-thiophene	340	478, 505	9610	0.09±0.001
Co-bithiophene	391	505, 538	6988	0.17±0.02
Co-thienothiophene	358	496, 526	8922	0.13±0.01
Co-dimethylfluorene	339, 353	424, 448	7177	0.34±0.003
Co-BTH	392	481	4720	0.22±0.003
Co-carbazole	301	373, 392	7712	0.41±0.02
Model cage compounds				
(Styryl)$_{2,3}$DD	259	309	6248	Too small[a]
Silane-end-capped DD	298	342, 388, 409	4317	0.01±0.002
(Thiophenevinyl)$_2$DD	290	388	5697	Too small[a]
(Dimethylfluorene-vinyl)$_{2,4}$DD	317	397,419	6357	0.10±0.001[a]

[a] Measured for di-substituted DD, [b] $\lambda_{max} \pm 1$ nm

The protonation of DD-co-carbazole was carried out using methane sulfonic acid (MSA) as shown in Figure **5.4**. At 1.0 M concentration, the absorption peak at 301 nm decreases to a shoulder and no emission is detected in from 270 to 500 nm. Protonation of the nitrogen centers should result in a blue shift due to elimination of the donor-component. *This provides support for the argument just above of n to π* transitions dominating photophysical behavior.*

To study the potential for charge transfer (CT) behavior in DD-co-BTH and -carbazole, as observed in simple aminostilbenevinyl SQ compounds,[28,46,47,61] solvent polarity effects on emission of DD-co-BTH and -carbazole were explored. Since both polymers are insoluble in polar acetonitrile, a mixture of CH_2Cl_2:acetonitrile (1:1

volume ratio) was used. However, no red-shifted emissions indicative of CT behavior were observed in the more polar solvent possibly due to the poor electron-donating nature of BTH and carbazole, or limited changes in polarity for this solvent system.

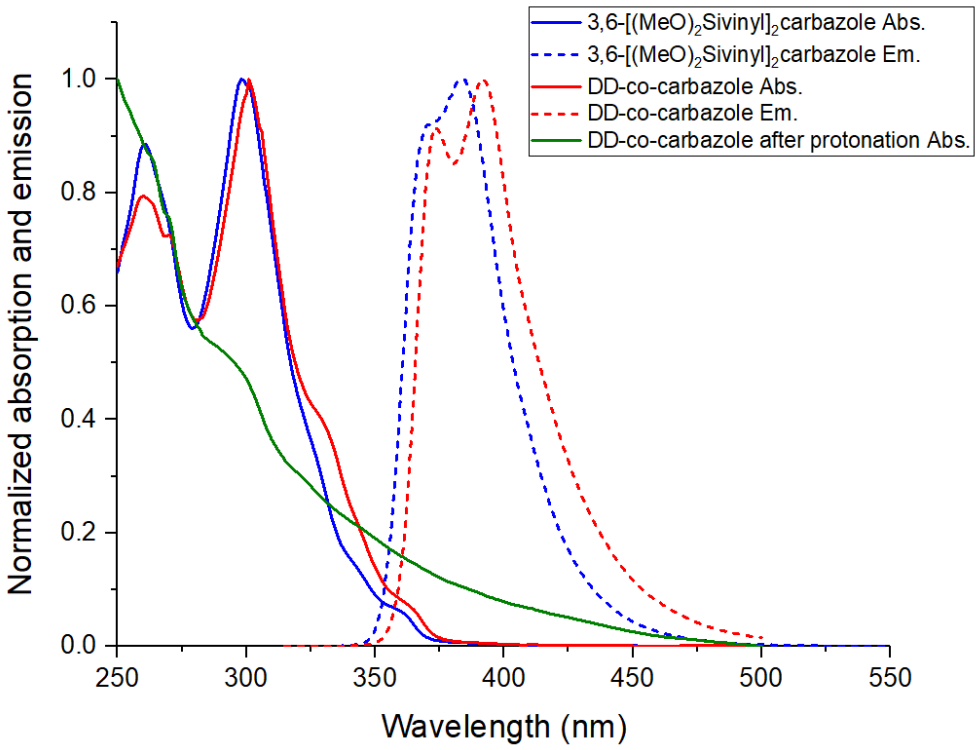

Figure 5.4. Normalized steady-state spectra of 3,6-[$(MeO)_2$Sivinyl]$_2$carbazole and DD-co-carbazole and after protonation by 1.0 M MSA.

5.3.5 Two-photon photophysical studies

For comparison with our previous studies, we also assessed two photon absorption behavior (2PA). The 2PA cross section data in Table **C.5** were measured for five polymers, DD-co-phenyl, -thiophene, -dimethylfluorene, -BTH and -carbazole, along with one model cage compound (Styryl)$_2$DD.

For comparison with our previous studies, we also assessed two photon absorption behavior (2PA). The 2PA cross section data in Table **C.5** were measured for five polymers, DD-co-phenyl, -thiophene, -dimethylfluorene, -BTH and -carbazole, along with one model cage compound (Styryl)$_2$DD, as shown below

All polymers and the model cage compounds show similar general behavior, where the 2PA cross section values increase rapidly towards the higher transition energies (shorter wavelengths), reaching maximum values at ~550 nm of 4-5 GM for DD-co-phenyl and $(Styryl)_2DD$, 20-40 GM for DD-co-thiophene, -BTH and -carbazole, and *as high as 300 GM for DD-co-dimethyfluorene*. At the same time, in the lower energy range (longer wavelengths), the cross sections decrease by two or more orders of magnitude compared to the maximum values, and drop below the detection limit when the transition energy reaches the red edge of corresponding linear absorption.

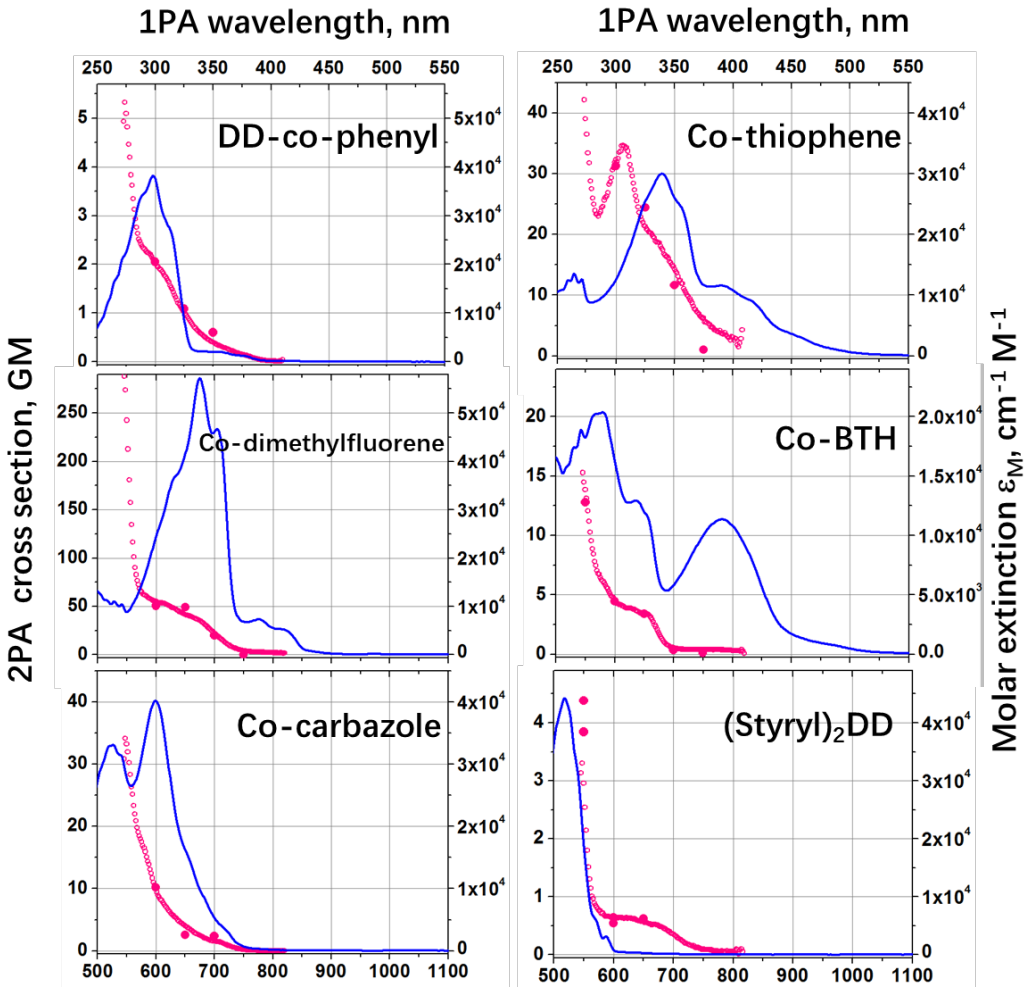

Figure 5.5. 2PA cross section spectra (red empty circles) and values (red solid circles) of DD polymers DD-co-phenyl, -thiophene, -dimethylfluorene, -BTH, -carbazole and the model cage compound $(Styryl)_2DD$. Corresponding molar extinction spectra (blue line) shown for comparison.

In case of the polymers, the 2PA spectra display a distinct shoulder at intermediate wavelengths that appears to follow the varying transition energy of a prominent absorption band in the linear spectrum. In addition, DD-co-thiophene shows a discrete band with a peak value of $\sigma_{2PA} \sim 35$ GM at 610 nm, which does not seem to immediately match any distinct transitions in the 1PA spectrum.

Perhaps the first thing to notice is that both the 1PA and 2PA polymer spectra are most likely caused by interaction between the DD core structure and the linker chromophores, rather than due to the eight peripheral phenyls. One way to observe this would be by comparing the linear absorption features observed in the short-wavelength portion 240-270 nm of the 1PA shown in Figure **5.5**, to known as linear absorption spectra of phenyl-related structures. For example, both toluene and benzene show a characteristic vibronic progression in the 240-270 nm range, which correlates (even though not identical) to the features displayed in DD-co-thiophene and -BTH.

It is notable that the average extinction coefficient values of benzene and toluene (S_0-S_1 transition is symmetry-forbidden in benzene), if multiplied by eight, roughly match those of the progressions observed in DD-co-thiophene and -BTH. In other polymers, where the overlap with main absorption is larger, a similar progression-like feature may still be observed, even though with less contrast. From this, we may conclude that, at least in the current polymers, the cage phenyls are most likely contributing only in an additive manner, especially since their corresponding 1PA and 2PA are blue-shifted and rather weak. This, together with the fact that the measured 2PA cross sections are significantly and systematically larger that the combined values of all constitutents taken separately (so-called cooperative enhancement effect), *indicates that active conjugation most likely exists between the linker and the DD core*, and perhaps even reaching the linked chromophores at the opposing capped ends all way through the core.

5.3.6 Further evidence suggesting unconventional conjugation

Based on previous studies and data presented above, the evidence for conjugation comes from exceptional red-shifts in emission and 2PA behavior that can only be explained if the systems are conjugated. Given that the above evidence points to unconventional conjugation through vinylMeSi(O-)$_2$ links, it is absolutely necessary to bring as many analytical tools to bear on this new phenomenon as possible. To this end, we sought additional evidence in support of our contentions. These include modeling, cyclic voltammetry, determining optical HOMO-LUMO gaps and comparing with gaps measured previously by CV, and doping with electron deficient molecules searching for charge transfer properties. The results of these efforts are as follows beginning with a brief summary of all that is presented above.

Photophysics (photoluminecent red-shifts). The most substantial proof to date comes from UV-Vis absorption and emission studies. In particular, we have now reported multiple cases of large red-shifts associated with emission λ_{max} in SQ cage conjugated moieties.[25,28,29] Homopolymeric versions of T_8, T_{10} and T_{12} joined by conjugated tethers all show red-shifts in emission λ_{max} not found in respective model compounds, with one example shown in Figure **5.2** above.[25,28] Additionally, by copolymerizing two different functionalized cages: (4-NH_2Stilbene)$_6$(IPh)$_2T_8$ and (4-MeOStilbene)$_6$(IPh)$_2T_8$ with 1,4-diethynylbenzene, we find redshifted emission λ_{max} between the λ_{max} of the individual respective homopolymers, rather than physical mixtures of independent emissions from both units, *indicating through cage and through tether conjugation*.[28]

Photophysics (optical magnetic field generation). Our first two papers on corner missing T_8 SQs, and open and closed DD monomer systems find that magnetic fields generated during high fluence irradiation of cages leads to formation of spherical fields that are best explained by formation of cage centered LUMOs.[44,45]

Modeling efforts. In previous papers, we and others modeled the HOMO LUMO structures of both alkyl and aryl substituted T_8 cages finding that cage centered LUMO

formation is quite common.[50] We have recently extended this family to include both corner missing cages and double decker compounds[44,45] What has been uniformly infeasible, as pointed out previously, is that modeling of $(RPh)_8T_8$ cages with conjugated moieties, R (appended either para or ortho) does not indicate formation of cage centered LUMOs.[44,45] In essentially all efforts, modeling finds HOMO LUMO orbitals on the conjugated moieties. That is because the conjugated moieties have low energy unoccupied molecular orbitals and high energy occupied ones. Both modeling teams also attempted to model the DD polymers,[46] again finding HOMO LUMO structures on conjugated moieties with RPh systems including the co-monomers or finding cage centered LUMOs if Ph is replaced by Me. Examples of our colleagues' extensive efforts are presented in Figures **C.31-3.33** and Table **C.6** in Appendix **C**.

In another effort to model the DD polymers, we replaced Ph on cage corners by Me in vinylDDvinyl and plotted the HOMO-2 to LUMO+5, see Figure **C.34**. The conjugated vinyl groups have low energy LUMOs and of course high energy HOMOs, thus in modeling of vinylDDvinyl, LUMO, +1, +2 are mainly the π* orbitals of vinyls. However, LUMO+4 and LUMO+5 are from SQ core *and cage centered*. Furthermore more, the energy difference is only ~0.6 eV between the cage centered LUMOs and vinyl π*, which suggests interactions between cage centered LUMOs and vinyl π* are possible. Modeling of a similar structure where two $Si(O-)_2$ units are inserted into the each opposing edge is presented in Figure **C.35**. With all methyl substituents, the structure again exhibits cage centered LUMO and LUMO+1.

One might choose to argue that current modeling methods are unable to successfully address the interaction of SQ cage centered LUMOs with conjugated moieties. Hence efforts to model the unique structures developed with the DD polymers wherein cage centered LUMOs must interact with co-monomer LUMOs through vinylMe$Si(O-)_2$ bridges (assuming our arguments are valid) must search for new modeling approaches.

Cyclic voltammetry. We have previously demonstrated that cyclic voltammetry (CV) can be used to measure HOMO LUMO energies in $(RvinylT)_{10/12}$ cages with conjugated moieties.[61] In these previous studies, we learned to manipulate HOMO LUMO

energies by designing $(RvinylT)_{10/12}$ cages with different strongly electron donating/accepting moieties (R). The results of this study again support the existence of cage centered LUMOs and 3-D conjugation; otherwise, one would not anticipate the found energy levels based on those of the individual moieties. Table **5.2** below compares the optical gaps calculated from absorption λ_{max} for $(R'StilbenevinylT)_{10/12}$ and those from HOMO-LUMO levels determined by CV.

As shown in the Table **5.2**, the gaps obtained from HOMO-LUMO energies are always ~0.6 eV smaller than those calculated from absorption peaks. One can interpret this to mean that the optical gap is always somewhat larger than measured as might be expected. It is known that typically the HOMO energies of organic polymers can be affected greatly by π-π interactions in the ground state. While no ground-state conjugation is observed here for either the oligomers or polymers, these compounds shouldn't be compared with typical organic polymers. The discrepancy among these systems suggests that the optical gaps recorded for DD polymers in Table **5.2** are also likely somewhat larger than actual gaps. Thus, a corrected gap based on the CV data was added.

Table 5.2. Optical band gaps calculated from UV-Vis absorption λ_{max}, band gaps from CV of $(R'StilbenevinylT)_{10/12}$[61] and corrected band gaps of $T_{10/12}$[29] and vinylDDvinyl derived polymers.

Compound	Abs. λ_{max} (nm)	Em. λ_{max} (nm)	Optical band gap (eV)[a]	Band gap (eV)
$(HStilbenevinylT)_{10/12}$[61]	333	387	3.7	3.1[b]
$(MeStilbenevinylT)_{10/12}$[61]	333	393	3.7	3.0[b]
$(MeOStilbenevinylT)_{10/12}$[61]	343	418	3.6	3.0[b]
$(NH_2StilbenevinylT)_{10/12}$[61]	363	483	3.4	2.7[b]
$(C_6F_5StilbenevinylT)_{10/12}$[61]	316	445	3.9	3.6[b]
$T_{10/12}$-co-9,9-dimethylfluorene[29]	371, 389, 410	422, 448	3.19	3.2
DD-co-phenyl	298	390, 412	4.16	3.6[c]
DD-co-biphenyl	314	357, 373	3.95	3.4[c]
DD-co-terphenyl	321	374, 392	3.86	3.3[c]
DD-co-stilbene	357	393, 412, 436	3.47	2.9[c]
DD-co-thiophene	340	478, 505	3.65	3.1[c]
DD-co-bithiophene	391	505, 538	3.17	2.6[c]
DD-co-thienothiophene	358	496, 526	3.46	2.9[c]
DD-co-9,9-dimethylfluroene	339, 353	424, 448	3.66	3.1[c]

[a] Calculated from UV-Vis absorption λ_{max}. [b] Calculated from CV. [c] Corrected band gap ~0.6 eV smaller than optical band gap.

In the current studies, we were unable to identify (easily accessible) redox behavior either in solution CV or in the solid state for the thiophene copolymers which we believe would be most likely to be easily accessible as they show the greatest red-shifts. More work needs to be done here. However, the Table **5.2** optical band gap values support the idea that through cage and through co-monomer conjugation obtains.

Note that in Table **5.2**, $(NH_2StilbenevinylT)_{10/12}$ has emission λ_{max} very similar to DD-co-thiophene and a very similar optical band gap. The data may suggest even smaller HOMO-LUMO gaps for the systems presented here. Table **5.2** also incorporates spectral data for $T_{10/12}$-co-9,9-dimethylfluorene analogues. This polymer has an absorption λ_{max} near 389 nm[29] where DD-co-9,9-dimethylfluorene also shows absorption shoulders in Figure **C.30** (only absorption λ_{max} values presented in Table **5.2**). Such long wavelength absorptions give an optical band gap of 3.19 eV, very close to the corrected band gap of 3.1 eV of DD-co-9,9-dimethylfluorene, which again supports the validity of these corrections.

In the above Figures **5.1**, **5.3** and **C.30**, we observe long-wavelength absorption edges which are found reproducibly after purification and multiple syntheses. It is possible that optical band gaps should be calculated from these results, which would reduce the observed optical band gaps. We find that many of these polymers show multiple emissions with different lifetimes that suggest their photophysics is more complicated and plan to present such studies at a later date.

One conundrum of our continuing work with SQ systems of all types is that while there are often exceptional emission λ_{max} red shifts compared to model compounds, the corresponding absorption λ_{max} do not exhibit red-shifts almost ever.[29] In traditional conjugated organic systems, both absorption and emission λ_{max} witness red-shifts associated with the degree of conjugation. One possible explanation is that these systems have indirect bandgaps and as such, the absorptions do not reflect conjugation in the excited state.

Fortunately, we have evidence from charge transfer (CT) between F_4TCNQ and several of the DD co-polymers that provides a more direct measure of the HOMO-LUMO gap and seems to be a better method of determining acceptable band gaps.

Charge-transfer studies. The advent of flat panel displays and semiconducting, molecularly doped organic semiconductors (OSCs); that is, conjugated molecules and conjugated polymers, has prompted extensive efforts to explore charge transfer in these materials.[62-65] Two different electronic interaction mechanisms have been observed in doped (p- or n-type) organic semiconductors: (1) integer charge transfer (ICT) that occurs with complete transfer of electrons from the OSC to dopant forming ion pairs; and (2) fractional charge transfer to form low-energy charge transfer complexes (CTC) via hybridization of the frontier orbitals of the two molecules.[65,66]

Early studies assumed all OSC:dopant systems displayed either integer or fractional charge transfer.[66,67,68] However, prediction of which mechanism dominates is difficult and structurally similar OSCs sometimes dope by different mechanisms. For example, poly(3-hexyl)thiophene (P3HT) blended with 2,3,5,6-tetrafluorene-7,7,8,8-tetracyanoquinodimethane (F_4TCNQ) results in ICT while shorter thiophene oligomers such as quarterthiophene (4T) and sexithiophene (6T) doped with F_4TCNQ form CTCs.[68] CTCs have also been observed in TCNQ doped 4T. TCNQ has no fluorine and hence a higher energy LUMO. Mechanistic understanding of doped OSCs is still poor but FTIR and UV-Vis are often used to measure the degree of charge transfer (δ) to F_4TCNQ.[65]

To better understand the "conjugation" occurring in vinylDDvinyl derived polymers, a series of mixtures of DD copolymers and model cage compounds with F_4TCNQ were prepared using the mixed-solution method.[65,66] A yellow-orange CH_2Cl_2 solution of F_4TCNQ was added to solutions of DD-co-thiophene, -bithiophene or -thienothiophene with bright orange to red colors, whereupon the solution colors change *to dark green, or black*, depending on the mole percent acceptor added. FTIR νC≡N band shifts reflecting these CT induced color-changes are presented in Figure **5.6a**.

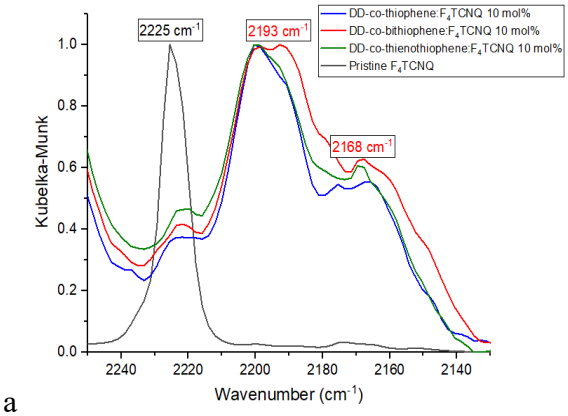

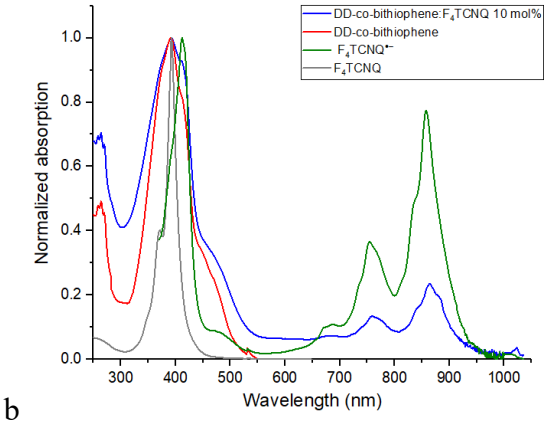

Figure 5.6. (a) The characteristic region of νC≡N in FTIR spectra for DD-co-thiophene, -bithiophene, -thienothiophene mixing with 10 mol% F_4TCNQ and pristine F_4TCNQ. (b) normalized steady-state absorption of DD-co-bithiophene:F_4TCNQ 10 mol%, undoped DD-co-bithiophene, $F_4TCNQ^{\bullet-}$ and F_4TCNQ in CH_2Cl_2.

The frequencies of the strongest νC≡N bands of the neutral and anionic forms of F_4TCNQ are known to be 2227 and 2194 cm^{-1}, respectively.[65] Shifts of characteristic νC≡N bands from 2225 to 2193 cm^{-1} are observed in the FTIR for DD-co-thiophene, -bithiophene and -thienothiophene solution mixtures with 10 mol% F_4CTNQ as shown in Figure **5.6a**. The observed shifts in νC≡N are reported to be an indicator of integer charge transfer (ICT) for P3HT:F_4TCNQ.[65,66] As the mole percent of acceptor F_4TCNQ increases to 50 mol%, FTIR results are essentially consistent, showing peaks for anionic F_4TCNQ as well as excess, therefore charge-neutral, F_4TCNQ for DD-co-thiophene, -bithiophene and -thienothiophene.

UV-Vis absorption spectra are presented in Figure **5.6b** to further characterize the ICT between DD-co-bithiophene and F_4TCNQ. Figure **5.6b** presents UV-Vis absorption spectra for: undoped DD-co-bithiophene, neutral F_4TCNQ and anionic $F_4TCNQ^{\bullet-}$ for reference. Absorption maxima for neutral F_4TCNQ is centered at 393 nm which correspond to the $S_0 \rightarrow S_1$ transition. The electronic structure of F_4TCNQ anion contains doublet states because of the presence of an unpaired single electron.[69] The UV-Vis spectrum of $F_4TCNQ^{\bullet-}$ contains two main absorption peaks around 400 and 800 nm. $D_0 \rightarrow D_1$ transition corresponds to the absorption band around 600-900 nm with local maxima at 754 and 856 nm while $D_0 \rightarrow D_2$ transition gives absorption band at 410 nm.[69] The absorption spectrum of DD-co-bithiophene:F_4TCNQ clearly shows spectral signatures from $F_4TCNQ^{\bullet-}$ at 600-900 nm and DD-co-bithiophene at 250-500 nm, strongly suggesting ICT, which is consistent with the FTIRs.

From previous studies, we can use the above CT data to estimate the band gap for the polymers that do interact with F_4TCNQ. When the HOMO of OSC is higher in energy than the dopant's LUMO, formation of CTCs by hybridization of frontier orbital also can occur. Additionally, ICT is also reported in complexes in which the OSC HOMO is only close to but still lower in energy than the dopant LUMO.[66,67,68] Specifically, numeric simulations were employed to reveal the (Gaussian) HOMO- and LUMO-level distributions of the pristine OSC and a "strong" as well as a "weak", p-dopant for the ICT case.[62] Numerical modeling defines a generic ''strong'' p-dopant with an electron affinity (EA, high energy onset of LUMO level) 0.2 eV higher than the ionization energy (IE, low energy onset of HOMO level) of OSC. In the case of the "weak" dopant, it shows an EA lower than the IE of the OSC by 0.2 eV.[68]

Since all DD-co-thiophene, -bithiophene and thienothiophene polymers exhibit ICT behavior with F_4TCNQ, with a reported LUMO of -5.2 eV, it is reasonable to say that the upper energy limit for these polymers' HOMOs should be around -5.0 eV. Since all three DD polymers appear yellow to orange, one can predict the light absorbed should range 400-600 nm, which gives a HOMO-LUMO gap no larger than 3.1 eV.

Finally, as we will describe in greater detail in the next chapter, we have now synthesized selected ladder silsesquioxane[70] copolymers analogous to the DD copolymers as suggested in Figure **5.7**. These compounds were chosen because while they are silsesquioxanes, they do not have cage structures. It was anticipated that they would not exhibit the kinds of conjugation seen here. Much to our great surprise, they not only show conjugation but *often give red-shifts greater* than those found for the DD copolymers as seen in Figure **5.7** again suggesting conjugation through vinylMeSi(O-)$_2$ mediating moieties.

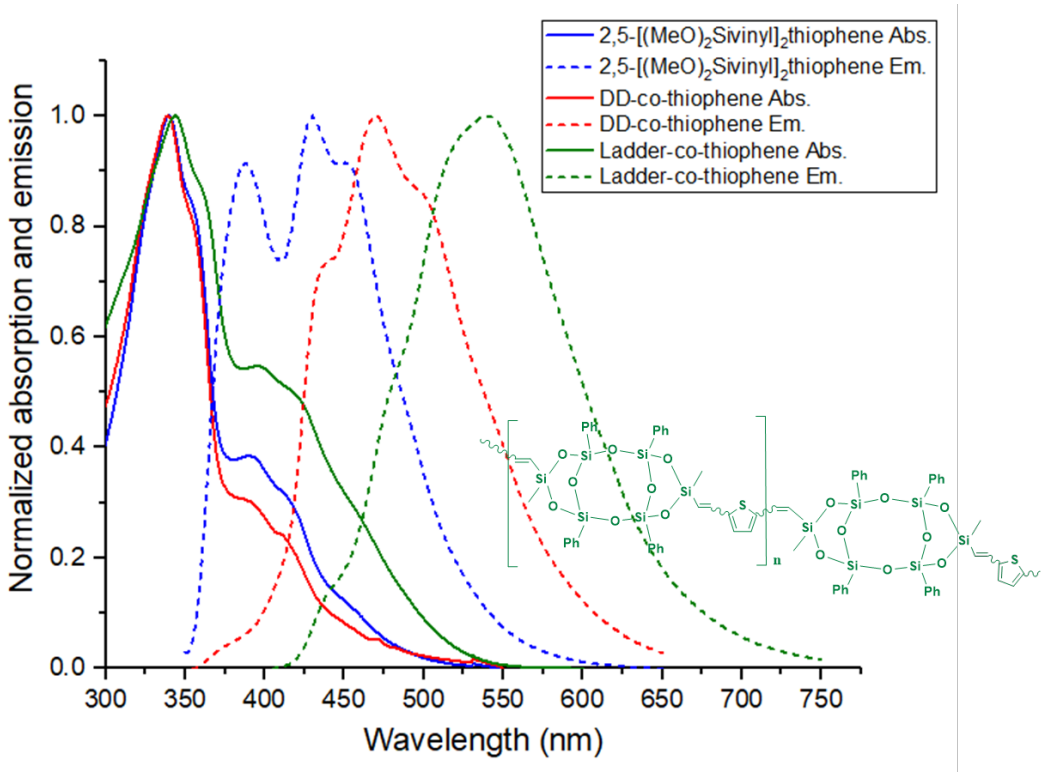

Figure 5.7. Normalized steady-state absorption and emission spectra of 2,5-[(MeO)$_2$Sivinyl]$_2$thiophene, DD-co-thiophene, Ladder-co-thiophene in CH_2Cl_2.[70]

5.4 Conclusions

This work reports the detailed synthesis and characterization of sets of copolymers of vinylDDvinyl SQs with phenyl, biphenyl, terphenyl, stilbene, thiophene, bithiophene, thienothiophene, 9,9-dimethylfluorene, benzothiadiazole and carbazole as components in the polymer backbones. Model compounds were also synthesized to explore the photophysical properties of corresponding DD copolymers. The DD-co-BTH and DD-co-

carbazole show no or very little conjugation likely because of n to π* transitions localized on the nitrogen or HOMO-LUMO gap energy of the aromatics far off from DD. The other eight polymers exhibit significantly redshifted emissions of 50-120 nm from respective model compounds, suggesting electron delocalization in the excited state through the conjugated DD cages via vinylMeSi(O-)$_2$ siloxane bridges. Such unexpected and unconventional conjugation was extensively assessed using a variety of analytical methods including cooperative enhanced 2PA cross sections of polymers and integer charge transfer with the electron acceptor F_4TCNQ. The unique photophysical properties found for DD polymers wherein there is apparent conjugation between double siloxane bridge positions offer potential access to new families of organic/inorganic hybrid semiconducting polymers. Given the importance of semiconducting materials in today's displays may provide significant impetus to expand exploration of these systems as well as the apparent existence of conjugation in complementary ladder silsesquioxane copolymers analogs.

References

1. Voronkov, M.G. and Lavrent'yev, V.I. Polyhedral Oligosilsesquioxanes and Their Homo Derivatives. *Top. Curr. Chem*. **1982**, *102*, 199-236.
2. Baney, R.H.; Itoh, M.; Sakakibara, A.; Suzuki, T. Silsesquioxanes. *Chem. Rev*. **1995**, *95,* 1409-30.
3. Loy, D.A. and Shea, K.J. Bridged Polysilsesquioxanes, Highly Porous Hybrid Organic-Inorganic Materials. *Chem. Rev*. **1995**, *95*, 1431-42.
4. Hartmann-Thomson, C. Applications of Polyhedral Oligomeric Silsesquoixanes, Adv. Silicon Sci. Springer Science + Business, New York, N.Y. **2011**.
5. Calzaferri, G. Silsesquioxanes. In *Tailor-made Silicon-Oxygen Compounds, from molecules to materials*; Corriu, R., and Jutzi, P. eds. Publ. Friedr. Vieweg & Sohn mbH: Weisbaden, Germany, **1996**, 149-169.
6. Lichtenhan, J. Silsesquioxane-based Polymers. in *Polymeric Materials Encyc.*, Salmone J.C. ed. CRC Press, N.Y., **1996**, Vol. 10, 7768-77.
7. Provatas, A. and Matisons, J.G. Synthesis and Applications of Silsesquioxanes. *Trends Polym. Sci*. **1997**, *5*, 327-33.
8. Li, G.; Wang, L.; Ni, H.; Pittman, C. U. Polyhedral Oligomeric Silsesquioxane (POSS) Polymers and Copolymers: A Review. *J. Inorg. Organomet. Polym.* **2001**, *11*, 123−151.
9. Duchateau, R. Incompletely Condensed Silsesquioxanes: Versatile Tools in Developing Silica-Supported Olefin Polymerization Catalysts. *Chem. Rev.* **2002,** *102,* 3525-42.

10. Abe, Y.;Gunji,T. Oligo- and polysiloxanes. *Prog. Poly. Sci.* **2004**, *29*, 149-182.
11. Phillips, S.H.; Haddad, T.S.; Tomczak, S.J. Developments in Nanoscience: Polyhedral oligomericsilsesquioxane (POSS)-polymers, *Current Opinion in Solid State and Mater. Sci.* **2004**, *8*, 21-29.
12. Kannan, R. Y.; Salacinski, H. J.; Butler, P. E.; Seifalian, A. M. Polyhedral Oligomeric Silsesquioxane Nanocomposites: The Next Generation Material for Biomedical Applications. *Acc. Chem. Res.* **2005,** 38, 879-884.
13. Laine, R.M. Nano-building Blocks Based on the $[OSiO_{1.5}]_8$ Silsesquioxanes. *J. Mater. Chem*. **2005**, *15*, 3725–44.
14. Lickiss, P.D. and Rataboul, F. Fully Condensed Polyhedral Silsesquioxanes: From Synthesis to Application. *Adv. Organomet. Chem.* **2008**, *57*, 1-116.
15. Wu, J. and Mather, P. T. POSS Polymers: Physical Properties and Biomaterials Applications. *Polymer Reviews.* **2009**, 25–63.
16. Chan, K. L.; Sonar, P.; Sellinger, A. Cubic Silsesquioxanes for Use in Solution Processableorganic Light Emitting Diodes (OLED). *J. Mater. Chem*. **2009**, *19,* 1-19.
17. Cordes, D. B.; Lickiss, P. D.; Franck, R. Recent Developments in the Chemistry of Cubic Polyhedral Oligosilsesquioxanes. *Chem. Rev*. **2010**, *10*, 2081–2173.
18. Laine, R. M. and Roll, M. F. Polyhedral Phenylsilsesquioxanes. *Macromolecules*, **2011**, *44*, 1073-1220.
19. Wang, M.; Chi, H.; KS, J. and Wang, F. Progress in the Synthesis of Bifunctionalized Polyhedral Oligomeric Silsesquioxane. *Polymers*. **2019**, *11(12)*, 2098.
20. Blanco, I. The Rediscovery of POSS: A molecule rather than a filler. *Polymers*, **2018**, *10*(8), 904.
21. Wang, J.; Liu, Y.; Yu, J.; Sun, Y. and Xie, W. Study of POSS on the Properties of Novel Inorganic Dental Composite Resin. *Polymers*. **2020**, *12(2)*, 478.
22. Chen, W.C.; Tsao, Y.H.; Wang, C.F.; Huang, C.F.; Dai, L.; Chen, T. and Kuo, S.W. Main Chain–Type Block Copolymers through Atom Transfer Radical Polymerization from Double-Decker–Shaped Polyhedral Oligomeric Silsesquioxane Hybrids. *Polymers*. **2020**, *12(2)*, 465.
23. Kalia, S. and Pielichowski, K. eds. Polymer/POSS Nanocomposites and Hybrid Materials: Preparation, Properties, Applications. *Springer*. **2018**.
24. Lichtenhan, J.D., Pielichowski, K. and Blanco, I. POSS-based Polymers. **2019**.
25. Asuncion, M. Z. and Laine, R. M. Fluoride Rearrangement Reactions of Polyphenyl- and Polyvinylsilsesquioxanes as a Facile Route to Mixed Functional Phenyl, Vinyl T_{10} and T_{12} Silsesquioxanes. J. Am. Chem. Soc. **2010**, *132,* 3723–36.
26. Krug, D. J. and Laine, R. M. Durable and Hydrophobic Organic–Inorganic Hybrid Coatings via Fluoride Rearrangement of Phenyl T_{12} Silsesquioxane and Siloxanes. *ACS Appl. Mater. Interfaces*, **2017**, *9*, 8378–83.
27. Krug, D. J.; Asuncion, M. Z.; Laine, R. M. Recycling Silicone Resins. *ACS Omega*, **2019**, *4*, 3782–3789.
28. Jung, J. H.; Furgal, J. C.; Clark, S.; Schwartz, M.; Chou, K.; Laine, R.M. Copolymerization of [*p*-$IPhSiO_{1.5})_8$, I_8OPS] with Divinyl (DVB)- and Diethynylbenzene

(DEB) Gives Beads on a Chain (A) Polymers with Functionalized Beads. The DEB Systems Exhibit through Chain, Extended 3-D Conjugation in the Excited State. *Macromolecules*. **2013**, *46* 7580–90.
29. Furgal, J. C.; Jung, J. H.; Clark, S.; Goodson III, T.; Laine, R. M. Beads on a Chain (BoC), Phenylsilsesquioxane (SQ), Polymers Via F^- Catalyzed Rearrangements and ADMET or Reverse Heck Cross-coupling Reactions; through Chain, Extended Conjugation in 3-D with Potential for Dendronization. *Macromolecules*, **2013**, *46,* 7591–7604.
30. Seino, M.; Hayakawa, T.; Ishida, Y.; Kakimoto, M.-a.; Watanabe, K.; Oikawa, H. Hydrosilylation Polymerization of Double-decker-shaped Silsesquioxane Having Hydrosilane with Diynes. *Macromolecules*. **2006**, *39*, 3473−75.
31. Wu, S.; Hayakawa, T.; Kikuchi, R.; Grunzinger, S. J.; Kakimoto, M.-a.; Oikawa, H. Synthesis and Characterization of Semiaromatic Polyimides Containing POSS in Main Chain Derived from Doubledecker- Shaped Silsesquioxane. *Macromolecules*. **2007**, *40,* 5698−5705.
32. Yoshida, K.; Hattori, T.; Ootake, N.; Tanaka, R.; Matsumoto, H. Silsesquioxane-Based Polymers: Synthesis of Phenylsilsesquioxanes with Double-Decker Structure and Their Polymers. Silicon Based Polymers. *Springer: Dordrecht.* **2008**; 205−211.
33. Hoque, Md. A.; Kakihana, Y.; Shinke, S.; Kawakami, Y. Polysiloxanes with Periodically Distributed Isomeric Double-decker Silsesquioxane in the Main Chain. *Macromolecules.* **2009**, *42,* 3309−15.
34. Yoshimatsu, M.; Komori, K.; Ohnagamitsu, Y.; Sueyoshi, N.; Kawashima, N.; Chinen, S.; Murakami, Y.; Izumi, J.; Inoki, D.; Sakai, K.; Matsuo, T.; Watanabe, K.; Kunitake, M. Necklace-shaped Dimethylsiloxane Polymers Bearing a Polyhedral Oligomeric Silsesquioxane Cage Prepared by Polycondensation and Ring-opening Polymerization. *Chem. Lett.* **2012**, *41,* 622−624.
35. Dudziec, B. and Marciniec, B. Double-decker Silsesquioxanes: Current Chemistry and Applications.*Current Organic Chemistry*. **2017**, *21*(28), 2794-2813.
36. Żak, P.; Majchrzak, M.; Wilkowski, G.; Dudziec, B.; Dutkiewicz, M. and Marciniec, B. Synthesis and Characterization of Functionalized Molecular and Macromolecular Double-decker Silsesquioxane Systems. *RSC advances*. **2016**, *6*(12), 10054-63.
37. Walczak, M.; Januszewski, R.; Majchrzak, M.; Kubicki, M.; Dudziec, B. and Marciniec, B. Unusual cis and trans Architecture of Dihydrofunctional Double-decker Shaped Silsesquioxane and Synthesis of its Ethyl Bridged π-conjugated Arene Derivatives. *New Journal of Chemistry*. **2017**, *41*(9), 3290-96.
38. Mituła, K.; Duszczak, J.; Brząkalski, D.; Dudziec, B.; Kubicki, M. and Marciniec, B. Tetra-functional Double-decker Silsesquioxanes as Anchors for Reactive Functional Groups and Potential Synthons for Hybrid Materials. *Chemical Communications*. **2017**, *53*(75), 10370-73.
39. Mituła, K.; Dudziec, B. and Marciniec, B. Synthesis of Dialkenyl-substituted Double-decker Silsesquioxanes as Precursors for Linear Copolymeric Systems. *Journal of Inorganic and Organometallic Polymers and Materials*. **2018**, *28*(2), 500-507.

40. Groch, P.; Dziubek, K.; Czaja, K.; Białek, M.; Mituła, K.; Dudziec, B. and Marciniec, B. Synthesis and Structural Characterization of Ethylene Copolymers Containing Double-decker Silsesquioxane as Pendant Groups and Cross-linkage Sites by Coordinative Copolymerization. *European Polymer Journal*. **2018**, *100*, 187-199.
41. Liu, N.; Wei, K.; Wang, L. and Zheng, S. Organic–inorganic Polyimides with Double Decker Silsesquioxane in the Main Chains. *Polymer Chemistry*. **2016**, *7*(5), 1158-67.
42. Zhao, B.; Wei, K.; Wang, L. and Zheng, S. Poly (hydroxyl urethane)s with Double Decker Silsesquioxanes in the Main Chains: Synthesis, Shape Recovery, and Reprocessing Properties. *Macromolecules*. **2019**.
43. Cao, J.; Fan, H.; Li, B.G. and Zhu, S. Synthesis and Evaluation of Double-Decker Silsesquioxanes as Modifying Agent for Epoxy Resin. *Polymer*, **2017**, *124*, 157-167.
44. Guan, J.; Tomobe, K.; Madu, I.; Goodson III, T.; Makhal, K.; Trinh, M.T.; Rand, S.C.; Yodsin, N.; Jungsuttiwong, S. and Laine, R.M. Photophysical Properties of Functionalized Double Decker Phenylsilsesquioxane Macromonomers: $[PhSiO_{1.5}]_8[OSiMe_2]_2$ and $[PhSiO_{1.5}]_8[O_{0.5}SiMe_3]_4$. Cage-Centered Lowest Unoccupied Molecular Orbitals Form Even When Two Cage Edge Bridges Are Removed, Verified by Modeling and Ultrafast Magnetic Light Scattering Experiments. *Macromolecules*. **2019**, *52*(19), 7413-22.
45. Guan, J.; Tomobe, K.; Madu, I.; Goodson III, T.; Makhal, K.; Trinh, M. T.; Laine, R. M. Photophysical Properties of Partially Functionalized Phenylsilsesquioxane:$[RSiO_{1.5}]_7[Me/nPrSiO_{1.5}]$ and $[RSiO_{1.5}]_7[O_{0.5}SiMe_3]_3$ (R= 4-Me/4-CN-Stilbene). Cage-Centered Magnetic Fields Form under Intense Laser Light. *Macromolecules*. **2019**, *52*(11), 4008-19.
46. Sulaiman, S.; Bhaskar, A.; Zhang, J.; Guda, R.; Goodson III, T.; Laine, R. M. Molecules with Perfect Cubic Symmetry as Nanobuilding Blocks for 3-D Assemblies. Elaboration of Octavinylsilsesquioxane. Unusual Luminescence Shifts May Indicate Extended Conjugation Involving the Silsesquioxane Core. *Chem. Mater.* **2008**, 20, 5563−73.
47. Laine, R. M.; Sulaiman, S.; Brick, C.; Roll, M.; Tamaki, R.; Asuncion, M. Z.; Neurock, M.; Filhol, J.-S.; Lee, C.-Y.; Zhang, J.; Goodson, T., III; Ronchi, M.; Pizzotti, M.; Rand, S. C.; Li, Y. Synthesis and Photophysical Properties of Stilbene-octasilsesquioxanes. Emission Behavior Coupled with Theoretical Modeling Studies Suggest a 3-D Excited State Involving the Silica Core. *J. Am. Chem. Soc.* **2010**, 132, 3708−22.
48. Sulaiman, S.; Zhang, J.; Goodson, T., III; Laine, R. M. Synthesis, Characterization and Photophysical Properties of Polyfunctional Phenylsilsesquioxanes: $[o\text{-}RPhSiO_{1.5}]_8$, $[2,5\text{-}R_2PhSiO_{1.5}]_8$, and $[R_3PhSiO_{1.5}]_8$. *J. Mater. Chem.* **2011**, 21, 11177−87.
49. Feher, F.; Budzichowski, T. A. Syntheses of Highly-functionalized Polyhedral Oligosilsesquioxanes. *J. Organomet. Chem.* **1989**, *379*, 33−40.

50. Bahrami, M.; Hashemi, H.; Ma, X.; Kieffer, J.; Laine, R. M. Why Do the $[PhSiO_{1.5}]_{8,10,12}$ Cages Self-brominate Primarily in the ortho Position? Modeling Reveals a Strong Cage Influence on the Mechanism. *Phys. Chem. Chem. Phys.* **2014**, *16*, 25760−64.
51. Bahrami, M.; Furgal, J. C.; Hashemi, H.; Ehsani, M.; Jahani, Y.; Goodson, T., III; Kieffer, J.; Laine, R. M. Synthesis and Characterization of Nano-building Blocks $[o\text{-}RStyrPhSiO_{1.5}]_{10,12}$ (R = Me-, MeO-, NBoc- and CN). Unexpected Photophysical Properties Arising from Apparent Asymmetric Cage Functionalization as Supported by Modelling Studies. *J. Phys. Chem. C*. **2015**, *119*, 15846−58.
52. Vogelsang, D.F.; Dannatt, J.E.; Schoen, B.W.; Maleczka Jr, R.E. and Lee, A. Phase Behavior of cis–trans Mixtures of Double-Decker Shaped Silsesquioxanes for Processability Enhancement. *ACS Applied Nano Materials*. **2019**, *2(3)*, 1223-31.
53. Makarov, N.S.; Drobizhev, M. and Rebane, A. Two-photon Absorption Standards in the 550–1600 nm Excitation Wavelength Range. *Optics Express*. **2008**, *16*(6), 4029-47.
54. Kresse, G. and Hafner, J. Ab Initio Molecular-dynamics Simulation of the Liquid-metal–amorphous-semiconductor Transition in Germanium. *Physical Review B*. 1**994**, *49*(20), 14251.
55. Kresse, G. and Furthmüller, J. Efficiency of ab-initio Total Energy Calculations for Metals and Semiconductors Using a Plane-wave Basis Set. *Computational Materials Science*. **1996**, *6*(1), 15-50.
56. Perdew, J. P.; Burke, K.; Ernzerhof, M. Generalized Gradient Approximation Made Simple. *Physical Review Letters.* **1996**, *77*, 3865.
57. Blöchl, P.E. Projector Augmented-wave Method. *Physical Review B*. **1994**, *50*(24), 17953.
58. Kresse, G. and Joubert, D. From Ultrasoft Pseudopotentials to the Projector Augmented-wave Method. *Physical Review B*. **1999**, *59*(3), 1758.
59. Tkatchenko, A.; DiStasio Jr, R.A.; Car, R. and Scheffler, M. Accurate and Efficient Method for Many-body Van Der Waals Interactions. *Physical Review Letters*. **2012**, *108*(23), 236402.
60. Momma, K. and Izumi, F. VESTA 3 for Three-dimensional Visualization of Crystal, Volumetric and Morphology Data. *Journal of Applied Crystallography*. **2011**, *44*(6), 1272-76.
61. Hwan Jung, J.; Furgal, J.C.; Goodson III, T.; Mizumo, T.; Schwartz, M.; Chou, K.; Vonet, J.F. and Laine, R.M. 3-D Molecular Mixtures of Catalytically Functionalized $[vinylSiO_{1.5}]_{10}/[vinylSiO_{1.5}]_{12}$. Photophysical Characterization of Second Generation Derivatives. *Chemistry of Materials*. **2012**;*24*(10), 1883-95.
62. Sirringhaus, H.; Tessler, N. and Friend, R.H. Integrated Optoelectronic Devices Based on Conjugated Polymers. *Science*. **1998**, *280*(5370), 1741-44.
63. Reineke, S.; Lindner, F.; Schwartz, G.; Seidler, N.; Walzer, K.; Lüssem, B. and Leo, K. White Organic Light-emitting Diodes with Fluorescent Tube Efficiency. *Nature*. **2009**, *459*(7244), 234-238.

64. Service, R.F. Solar Energy. Outlook Brightens for Plastic Solar Cells. *Science (New York, NY)*. **2011**, *332*(6027), 293.
65. Méndez, H.; Heimel, G.; Winkler, S.; Frisch, J.; Opitz, A.; Sauer, K.; Wegner, B.; Oehzelt, M.; Röthel, C.; Duhm, S. and Többens, D. Charge-transfer Crystallites as Molecular Electrical Dopants. *Nature Communications*. **2015**, *6*(1), 1-11.
66. Jacobs, I.E. and Moulé, A.J. Controlling Molecular Doping in Organic Semiconductors. *Advanced Materials*. **2017**, *29*(42), 1703063.
67. Salzmann, I.; Heimel, G. Toward a Comprehensive Understanding of Molecular Doping Organic Semiconductors (Review). *J. Electron Spectrosc. Relat. Phenom.* **2015**, *204*, 208-−222.
68. Salzmann, I.; Heimel, G.; Oehzelt, M.; Winkler, S.; Koch, N. Molecular Electrical Doping of Organic Semiconductors: Fundamental Mechanisms and Emerging Dopant Design Rules. *Acc. Chem. Res.* **2016**, *49 (3)*, 370−378.
69. Ma, L.; Hu, P.; Jiang, H.; Kloc, C.; Sun, H.; Soci, C.; Voityuk, A.A.; Michel-Beyerle, M.E. and Gurzadyan, G.G. Single Photon Triggered Dianion Formation in TCNQ and F4TCNQ Crystals. *Scientific reports*. **2016**, *6*, 28510.
70. Liu, Y.; Onodera, K.; Takeda, N.; Ouali, A. and Unno, M. Synthesis and Characterization of Functionalizable Silsesquioxanes with Ladder-type Structures. *Organometallics*. **2019***, 38*(22), 4373-76.

Chapter 6. Unconventional Conjugation via Siloxane Bridges in Ladder Silsesquioxane Copolymers

Published: Guan, J., Sun, Z., Ansari, R., Liu, Y., Endo, A., Unno, M., Ouali, A., Mahbub, S., Furgal, J.C., Yodsin, N. and Jungsuttiwong, S. 2021. *Angewandte Chemie International Edition*, *60*(20), 11115-11119.

With contributions from the groups of Professors Masafumi Unno, Joseph Furgal, Siriporn Jungsuttiwong and John Kieffer.

Abstract

Multiple studies have explored using cage silsesquioxanes (SQs) as backbone elements in hybrid polymers motivated by their well-defined structures, physical and mechanical properties. As part of this general exploration, we reported unexpected photophysical properties of copolymers derived from divinyl double decker (DD) SQs, [vinyl(Me)Si($O_{0.5}$)$_2$][PhSi$O_{1.5}$]$_8$[($O_{0.5}$)$_2$Si(Me)vinyl] (vinylDDvinyl). These copolymers exhibit strong emission red-shifts from model compounds and implying unconventional conjugation, despite vinyl(Me)Si(O-)$_2$ siloxane bridges.

In an effort to identify minimum SQ structures that do/do not offer extended conjugation; we explored Heck catalyzed co-polymerization of vinyl-ladder(LL)-vinyl compounds, vinyl(Me/Ph)Si($O_{0.5}$)$_2$[PhSi$O_{1.5}$]$_4$($O_{0.5}$)$_2$Si(Me/Ph)vinyl, with Br-Ar-Br where Br-Ar-Br = 1,4-dibromobenzene, 4,4'-dibromo-1,1'-biphenyl, 4,4''-dibromo-*p*-terphenyl, 4,4'-dibromo-*trans*-stilbene, 2,7-dibromo-9,9-dimethyl-9H-fluorene, 2,5-dibromothiophene, 5,5'-dibromo-2,2'-bithiophene and 2,5-dibromo-thieno[3,2-*b*]thiophene. Most surprising, the resulting oligomers show *30-60 nm* emission red-shifts *beyond* those seen with vinylDDvinyl analogs *despite lacking a true cage*. Further evidence for unconventional conjugation includes apparent integer charge transfer (ICT) between LL-co-thiophene, bithiophene and thienothiophene with 10 mol% F_4TCNQ, suggesting potential as p-type doped organic/inorganic semiconductors. Brominating DD/LL-co-phenyl polymer vinyl groups eliminates emission red-shifts. Zn debromination thereafter restores vinyl groups and emission red-shifts but brominated phenyls remain providing potential access to families of "hairy" conjugated SQ polymers.

6.1 Introduction

There is growing impetus to explore silsesquioxanes (SQs) due to their ease of synthesis and purification, well-defined 3-D nanostructures, robust nature as well as high compatibility with multiple types of organics leading to large families of hybrid materials. The major story still centers on properties that can be typified as organic decorated silica moieties. In contrast, we find that cage SQs {$[RSiO_{1.5}]_{8,10,12}$ (R=R'phenyl, R'vinyl, R=conjugated moiety, R'=H, Me, MeO, NH_2, CN, etc)} offer photophysical properties not at all reflective of organic decorated silicas but commensurate with cage centered LUMOs.[1–5] We recently extended this concept of excited-state 3-D conjugation to sets of incomplete and modified cages including corner-missing T_8, [R'StilbeneSiO$_{1.5}$]$_7$[O$_{1.5}$SiMe/nPr], [R'StilbeneSiO$_{1.5}$]$_7$[O$_{0.5}$SiMe$_3$]$_3$,[6] and newly developed double decker (DD) [R'StilbeneSiO$_{1.5}$]$_8$[OSiMe$_2$]$_2$ and [R'StilbeneSiO$_{1.5}$]$_8$[O$_{0.5}$SiMe$_3$]$_4$.[7] Recent efforts on double decker SQs follow two parallel paths in their development exploring either molecular or macromolecular hybrid materials.[8] In the latter area, we recently synthesized a series of DD SQ based oligomers and polymers {vinyl(Me)Si(O$_{0.5}$)$_2$[PhSiO$_{1.5}$]$_8$(O$_{0.5}$)$_2$Si(Me)vinyl-Ar, vinylDDvinyl-Ar} that unexpectedly exhibit conjugation that appears to involve two vinyl(Me)Si(O-)$_2$ bridges evidenced by significant emission red-shifts from corresponding model compounds.[9] Schemes **6.1a,b** provide general synthetic routes and structures. In all systems, conjugation presents in the form of emission red-shifts of 50-120 nm from model compounds without cage components. Such novel combinations of structural, thermal, mechanical and photophysical properties, such as tunable broad-band UV-Vis fluorescence, may be important for applications as emissive layers in OLEDs,[10] multi-functional nano-drugs, in photothermal and photodynamic therapies for cancer, etc. [11–13]

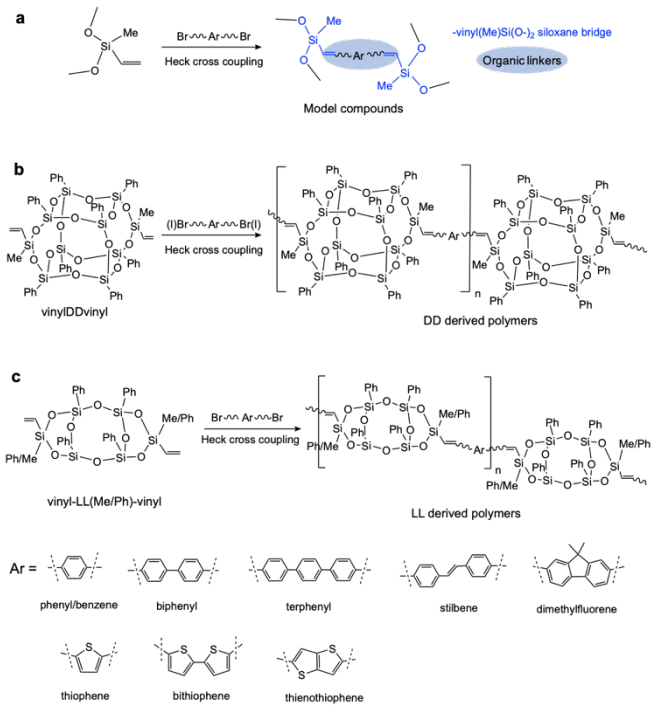

Scheme 6.1. Heck cross coupling of (a) model compounds, (b) vinylDDvinyl derived copolymers and (c) vinyl-LL-vinyl derived copolymers.

With the recent discovery of routes to ladder SQs (vinyl-LL-vinyl),[14] we can now explore vinyl-LL-vinyl equivalent systems of the type suggested in Scheme **6.1c**. The motivation is to ascertain the nature of LUMO formation in ladder SQs where the structure appears to be approximately one-half that of relatively complete double-deckers. Our initial presumption was that these compounds should represent the limiting case where not only is there no 3-D cage, but there are also two vinyl(Me/Ph)Si(O-)$_2$ bridges per cage in any oligomers/polymers we might synthesize. Contrary to our original thoughts, the resulting compounds actually offer emission *further red-shifted* than any analogous compounds previously studied,[1–7,9] seeming to imply conjugation and semiconducting behavior *where there should be none*. In the following sections, we begin by characterizing a set of ladder copolymers and thereafter assess their photophysical properties.

6.2 Experimental

The synthetic methods and characterization techniques are described in Chapter **2**.

6.3 Results and discussion

Two structurally similar ladder SQs [vinyl-(Me)LL(Me)-vinyl and vinyl-(Ph)LL(Ph)-vinyl] were explored, with only the end groups differing. Analytical characterization and photophysical behavior are essentially identical as expected, thus only data for vinyl-LL(Me)-vinyl co-polymers

are presented. Spectra for vinyl-LL(Ph)-vinyl derived copolymers are shown in Figures **D.9-D.14**. Both co-polymers were characterized by MALDI-TOF, GPC, FTIR, ^{1}H and ^{13}C NMR, and the starting ladder SQs were also characterized by ^{29}Si NMR as recorded in Tables **D.1-D.3** and Figures **D.1-D.8**. MALDI-TOF shows the expected m/z, consistent with GPC determined molar masses of the ladder SQs. The GPC retention time for vinyl-LL(Ph)-vinyl is ~0.3 min earlier than that for vinyl-LL(Me)-vinyl due to the slightly bulkier phenyl groups. Table **6.1** GPC data for the ladder copolymers indicates degrees of polymerization (DPs) of 3-18 units. MALDI-TOF analyses always show peaks every m/z for the co-monomer unit vinyl-LL-vinyl-Ar, suggesting no di-substitution of aromatic groups on any given vinyl and successful copolymerization.

The steady-state absorption and emission behavior of ladder polymers are shown in Table **6.1** and Figures **6.1** and **6.2**, compared with data for vinylDDvinyl derived polymers from our previous study.[9] All emission spectra were measured with excitation wavelength at corresponding absorption λ_{max}. The Table **6.1** data for vinyl(Me)DD(Me)vinyl and vinyl-LL(Me)-vinyl indicates that all exhibit absorption $\lambda_{max} \approx 265$ nm and emission $\lambda_{max} \approx 280$ nm, typical for phenyl rings. Vinyl-LL(Ph)-vinyl is slightly red-shifted with phenyls at two ends. Polymers were synthesized from both vinyl-LL-vinyl compounds. No essential spectral differences were observed as expected.

Table 6.1. GPC and steady-state photophysical data for vinylDDvinyl derived polymers[9] and vinyl-LL(Me)-vinyl derived polymers.

	DP[a]	Abs. λ_{max} (nm)	Em. λ_{max} (nm)[b]	Φ_F
Vinyl(Me)DD(Me)vinyl	1	264	281	
DD-co-phenyl	15	298	390, 412	0.08±0.001
DD-co-biphenyl	10	314	357, 373	0.66±0.05
DD-co-terphenyl	11	321	374, 392	0.87±0.04
DD-co-stilbene	7	357	412, 436	0.61±0.04
Co-dimethylfluorene	15	339, 353	424, 448	0.34±0.003
DD-co-thiophene	20	340	478, 505	0.09±0.001
DD-co-bithiophene	3	391	505, 538	0.17±0.02
Co-thienothiophene	4	358	496, 526	0.13±0.01
Vinyl-LL(Me/Ph)-vinyl	1	264	283	
LL-co-phenyl	8	298	392, 415	0.16±0.02
LL-co-biphenyl	6	312	412, 430	0.46±0.04
LL-co-terphenyl	18	321	418, 437	0.61±0.02
LL-co-stilbene	8	356	448, 472	0.35±0.03
Co-dimethylfluorene	7	337, 353	426, 451	0.68±0.02
LL-co-thiophene	7	343	540	0.07±0.01
LL-co-bithiophene	6	392	550	0.07±0.01
Co-thienothiophene	6	356, 371	530	0.09±0.01

[a] Degree of polymerization. [b] Excitation wavelength at Abs. λ_{max}

Divinylbenzene is the simplest organic linker tested. The steady-state data in Table **6.1** for LL-co-phenyl are essentially identical to those of DD-co-phenyl. The red shift of 70 nm in emission compared to 1,4-[$(MeO)_2$Sivinyl]$_2$benzene suggests formation of a LUMO even with a half cage and conjugation to co-phenyl in the excited state. Based on all our previous work, it appears that a LUMO does form and these results greatly extend the families of SQs that appear to offer extended conjugation. Even though the shifts are not significant in the absorption and emission λ_{max} of LL-co-phenyl from its DD analogue, there are significant changes in the shape of steady-state spectra as seen in Figure **6.1**. First, LL-co-phenyl with a DP of 8 displays distinct absorption shoulders around 355 nm compared to model compound and DD-co-phenyl with a DP of 15. Additionally, its emission is slightly red-shifted beyond DD-co-phenyl, along with the disappearance of the emission peak near 340 nm and a significant shoulder at ≈ 450 nm.

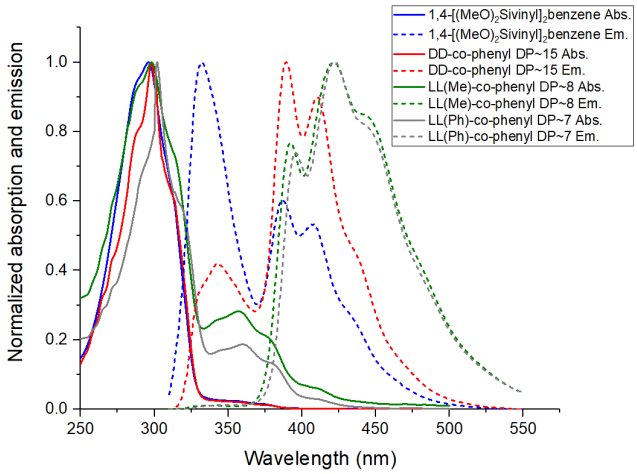

Figure 6.1. Normalized steady-state absorption and emission spectra of 1,4-[$(MeO)_2$Sivinyl]$_2$benzene, DD-co-phenyl and LL-co-phenyl in CH_2Cl_2.

Such changes in steady-state behavior are more apparent in LL-co-biphenyl, terphenyl, stilbene and thiophene as witnessed by 30~60 nm red-shifts beyond their DD analogues even with shorter chains, again suggesting LUMO formation even in ladder structures but also more efficient communication between the ladder SQ and the conjugated organic moieties in the excited state as compared to full and double-decker SQs. This finding is quite important in that it completely changes our assumptions about ladder SQs. To further probe such structure-property relationships, a shorter fraction of LL-co-thiophene was separated via TLC (silica, 1:1 DCM:hexane) and characterized by GPC and MALDI-TOF in Figure **D.15** and Table **6.2**.

Table 6.2. MALDI-TOF and GPC data for DD-co-thiophene, short LL-co-thiophene isolated by TLC and long LL-co-thiophene.

	GPC			MALDI-TOF	
	Mn	Mw	Đ [a]	Oligomers[b]	M/z
LL-co-thiophene DP~3	2540	3630	1.12	Dimer	1896[c]
LL-co-thiophene DP~7	5600	8000	1.42	Trimer	2797[c]
DD-co-thiophene DP~20	22540	43250	1.92	Decamer	13010[c]

[a] Polydispersity. [b] Largest oligomers identifiable. [c] As Ag^+ adduct.

The GPC of the starting vinyl-LL-vinyl, short LL-co-thiophene separated by TLC (DP~3) and long LL-co-thiophene (DP~7) are shown in Figure **D.15**. The GPC trace of the LL-co-thiophene with DP ~7 shows a broad peak around 27.5 min with a Đ of 1.43 for relatively long oligomers as well as a quite narrow peak at 33.2 min overlapping with vinyl-LL-vinyl with polydispersity (Đ) of 1.02, suggesting presence of unreacted starting material during copolymerization. The short LL-co-thiophene with DP~3 comes at 31.5 min with a small Đ of 1.12, dominated by dimers and trimers following removal of longer oligomers via TLC. The GPC and MALDI-TOF data are shown in Table **6.2**. The largest oligomers identifiable by MALDI-TOF with corresponding masses are presented. It is known that the peak intensities in MALDI corresponds to the ionization efficiencies of the species and are not necessarily representative of the quantity of each component. High M_w oligomers are not as readily ionizable as monomers thus even though the GPC shows even higher Mw oligomers, they are not necessarily "seen" in MALDI. Data for DD-co-thiophene with DP ~20 are also presented here. Since LL-co-thiophene is shorter than its DD analogue, it is safe to say that its red-shifted emission comes from more efficient electronic communication between LL SQs in the excited state rather than longer chains with extended conjugation lengths. extend the families of SQs that appear to offer extended conjugation.

Figure **6.2** presents the normalized steady-state emission spectra for 2,5-[$(MeO)_2$Sivinyl]$_2$thiophene, DD-co-thiophene, LL-co-thiophene with DPs of 3 and 7 respectively. The absorption λ_{max} is always around 340 nm and not shown here. The progressively red-shifted emission $\lambda_{max.}$ of short and long LL-co-thiophenes are 484 and 539 nm respectively, suggesting extended conjugation with further extensions in chain length and smaller HOMO-LUMO gaps. Short LL-co-thiophene, consisting mostly of dimers and trimers, still shows λ_{max} emission similar to long DD-co-thiophene, which is ~50 nm red-shifted from 2,5-[$(MeO)_2$Sivinyl]$_2$thiophene.

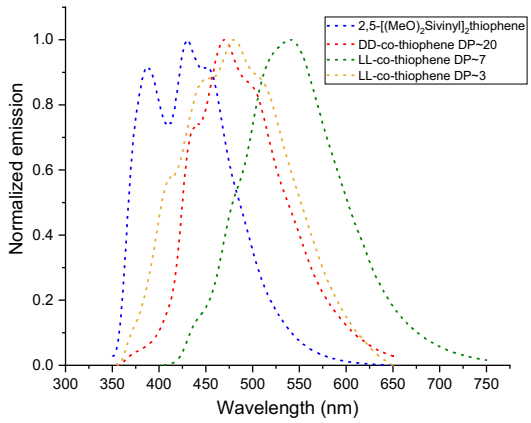

Figure 6.2. Normalized progressive emission spectra of 2,5-[$(MeO)_2$Sivinyl]$_2$thiophene, DD-co-thiophene, short (DP~3) and long (DP~7) LL-co-thiophene in CH_2Cl_2.

It has been reported that T_8 SQ cages exhibit electron-withdrawing capacities approximately equivalent to -CF_3.[15] One can extend this idea to DD SQs given similar structures and presumably LL systems. It then becomes possible to argue that DD-co-thiophene oligomers and even dimers and trimers of LL-co-thiophene should offer similar properties. This further confirms the efficient semiconducting behavior of such ladder SQs polymers. Similar study has also done on LL-co-biphenyl as an example from the phenyl system of LL copolymers and the GPC and steady-state emission spectra are shown in Figures **D.16, D.17**. The progressive red-shifts in the emission of LL-co-biphenyl as a function of DPs have also been observed.

Further evidence of unconventional conjugation includes the charge-transfer studies of thiophene systems of LL SQ copolymers. Integer charge transfer (ICT) is observed between electron-acceptor 2,3,5,6-tetrafluoro-7,7,8,8-tetracyanoquinodi-methane (F_4TCNQ) and DD-co-thiophene, bithiophene and thienothiophene as reported in our previous paper.[9] Similar ICT also occurred in 10 mol%F_4TCNQ doped LL-co-thiophene, bithiophene and thienothiophene using the mixed-solution method. The original orange-red color becomes dark green immediately on mixing.

The literature reports that poly(3-hexyl-thiophene-2,5-diyl) regioregular (P3HT) exhibits integer charge transfer interactions with F_4TCNQ and coincident nitrile-stretching mode shifts from a neutral value ν_0 = 2227 cm^{-1} to ν_1 = 2194 cm^{-1} on doping.[16,17] In marked contrast, however, quaterthiophene (4T) forms partial charge transfer with F_4TCNQ and thus shows only a small shift.[18] Shifts of characteristic cyano-vibrational bands from the neutral value to the anion value are observed in the FTIR for LL-co-bithiophene mixing with F_4TCNQ as shown in Figure **6.3** indicating integer charge transfer (ICT).

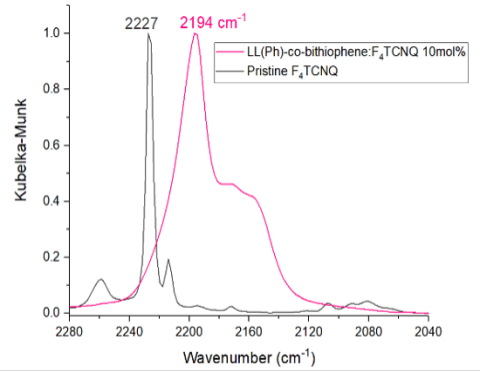

Figure 6.3. FTIR of νCN region for pristine F_4TCNQ and mixture of LL-co-bithiophene:F_4TCNQ 10 mol%.

The literature also reports that the electronic structure of F_4TCNQ anion includes doublet states because of the presence of an unpaired single electron.[19] The UV-Vis spectrum of $F_4TCNQ^{\bullet-}$ contains two main absorption peaks around 400 and 800 nm. $D_0 \rightarrow D_1$ transition corresponds to the absorption band around 600-900 nm with local maxima at 754 and 856 nm while $D_0 \rightarrow D_2$ transition gives absorption band at 410 nm. The absorption spectrum of LL(Ph)-co-bithiophene:F_4TCNQ in Figure **6.4** clearly shows spectral signatures from $F_4TCNQ^{\bullet-}$ at 600-900 nm and LL-co-bithiophene at 350-500 nm, strongly suggesting ICT, consistent with the FTIR data.

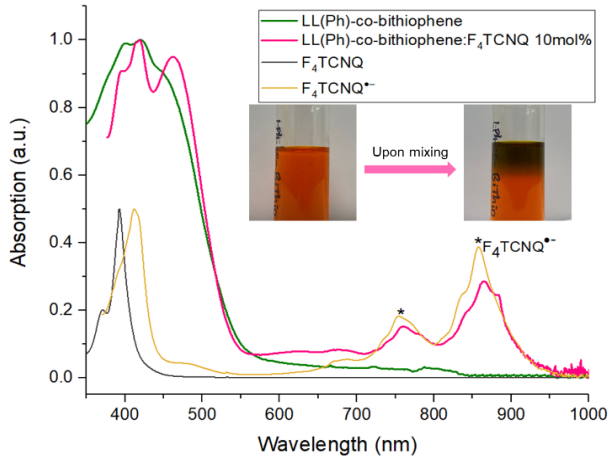

Figure 6.4. Absorption spectra of undoped LL-co-bithiophene and LL-co-bithiophene: F_4TCNQ 10 mol%, F_4TCNQ and $F_4TCNQ^{\bullet-}$ shown for reference.

Further evidence of unconventional conjugation comes from the breaking and restoring conjugation by brominating/de-brominating vinyls. Our original objective in brominating phenyl groups in DD/LL-co-phenyl polymers was to further functionalize the phenyl groups peripherally to

prepare 'hairy polymers' and explore possible 3-D conjugation. As expected, vinyl groups brominate first on as evidenced by Figures **D.16-D.19**. ^{13}C and ^{29}Si NMR coincident with elimination of conjugation and partial cage cleavage as tracked by GPC. As shown in Figure **6.5b**, brominated polymers display only characteristic phenyl absorption around 250 nm. The emission spectra are diminished and only show CH_2Cl_2 solvent background. The photophysical behavior of both DD/LL-co-phenyl reappear after zinc debromination,[20] with absorption λ_{max} around 300 nm and red-shifted emission λ_{max} around 400 nm with respect to the emission of 1,4-[$(MeO)_2$Sivinyl]$_2$benzene at 332 nm. This finding further proves the presence and reproducibility of the excited-state conjugation in the DD/LL SQ derived polymers via vinylSi(O-)$_2$ siloxane unit.

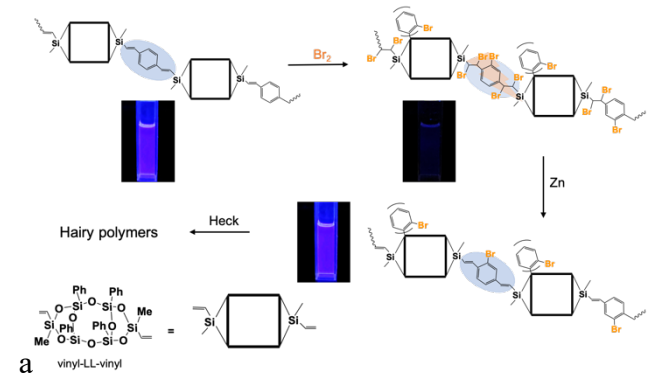

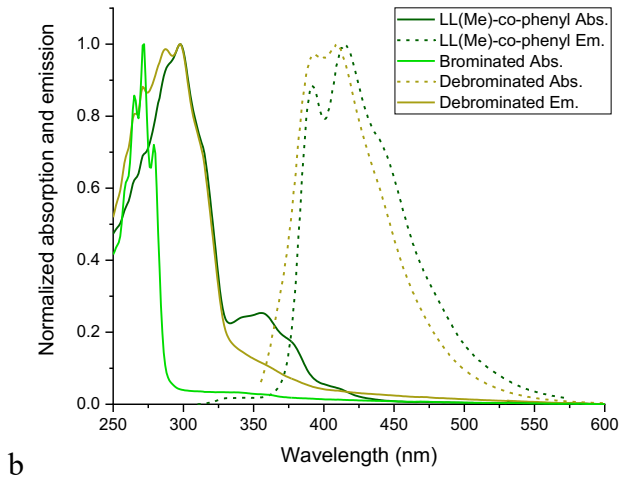

Figure 6.5. (a) Bromination and debromination of LL-co-phenyl. (b) Steady-state spectra in CH_2Cl_2.

Two modeling groups attempted to model the vinyl-LL-vinyl SQ structure. Professor Jungsuttiwong's group at Ubon Ratchathani University, Thailand, and Professor Kieffer's group at the University of Michigan, found both HOMOs and LUMOs reside on the peripheral phenyl groups

of vinyl-LL(Me/Ph)-vinyl, with an energy HOMO-LUMO gap of ~8.9 eV. The calculated absorption λ_{max} is always ~60 nm blue-shifted compared to the experimental data, as shown in Table **D.4**. In another effort from Professor Kieffer's group the peripheral phenyl groups are replaced by methyl for modeling purposes, LUMO+2 at 8.47 eV is from LL SQ core and extends out of the ladder frame, suggesting possible interaction between an SQ-centered LUMO and vinyl π*. Orbitals. When phenyls are retained, the LUMO+10 also resides in the center of LL SQ and extends out to vinyl π* with a lower energy level at 7.86 eV. These modeling results are presented in Figures **D.26-D.28**. At this time, modeling is still not as precise as we would like but these systems are quite unique as our results demonstrate.

6.4 Conclusions

In summary, a series of ladder (LL) SQ copolymers were synthesized via Heck catalytic cross-coupling of vinyl-LL-vinyl with various dibromo-aromatic compounds. Compared to model silane compounds and analogs of double-decker (DD) SQ copolymers, LL derived polymers display similar absorption peaks but with significant shoulders at longer wavelength. Furthermore, LL SQs linked with longer or more complex aromatic bridges, LL-co-biphenyl, terphenyl, stilbene and thiophene, show 30-60 nm emission red-shifts *beyond* those seen with the DD analogs and progressively red-shifted emissions with respect to longer chains were also observed. Integral charge transfer occurs in 10 mol% F_4TCNQ-doped LL-co-thiophene, bithiophene, thienothiophene, which also occur on mixing F_4TCNQ with DD analogous polymers. These results suggest not only a new perspective on the ease of formation of LUMOs in even LL SQs, but also more efficient communication of the LL SQ with conjugated organic moieties in the excited state as compared to full and double-decker SQs that potentially offer access to a wide variety of semiconducting polymers. In addition, brominating vinyl as well as phenyl groups in DD/LL derived copolymers and then debrominating vinyls not only restores through chain conjugation but also provides the potential to further peripherally functionalize these systems via a variety of catalytic cross-coupling reactions to explore 3-D conjugation in "hairy SQ polymers".

References

[1] Furgal, J. C.; Jung, J. H.; Goodson, T.; Laine, R. M. Analyzing Structure–Photophysical Property Relationships for Isolated T8 , T10 , and T12 Stilbenevinylsilsesquioxanes. J. Am. Chem. Soc. 2013, 135 (33), 12259–12269.

[2] Laine, R. M.; Sulaiman, S.; Brick, C.; Roll, M.; Tamaki, R.; Asuncion, M. Z.; Neurock, M.; Filhol, J.-S.; Lee, C.-Y.; Zhang, J.; Goodson, T.; Ronchi, M.; Pizzotti, M.; Rand, S. C.; Li, Y. Synthesis and Photophysical Properties of Stilbeneoctasilsesquioxanes. Emission

Behavior Coupled with Theoretical Modeling Studies Suggest a 3-D Excited State Involving the Silica Core. J. Am. Chem. Soc. 2010, 132 (11), 3708–3722.
[3] Asuncion, M. Z.; Laine, R. M. Fluoride Rearrangement Reactions of Polyphenyl- and Polyvinylsilsesquioxanes as a Facile Route to Mixed Functional Phenyl, Vinyl T10 and T12 Silsesquioxanes. J. Am. Chem. Soc. 2010, 132 (11), 3723–3736.
[4] Sulaiman, S.; Zhang, J.; Goodson, III, T.; Laine, R. M. Synthesis, Characterization and Photophysical Properties of Polyfunctional Phenylsilsesquioxanes: [O-RPhSiO1.5]8, [2,5-R2PhSiO1.5]8, and [R3PhSiO1.5]8. Compounds with the Highest Number of Functional Units/Unit Volume. J. Mater. Chem. 2011, 21 (30), 11177.
[5] Sulaiman, S.; Bhaskar, A.; Zhang, J.; Guda, R.; Goodson, T.; Laine, R. M. Molecules with Perfect Cubic Symmetry as Nanobuilding Blocks for 3-D Assemblies. Elaboration of Octavinylsilsesquioxane. Unusual Luminescence Shifts May Indicate Extended Conjugation Involving the Silsesquioxane Core. Chem. Mater. 2008, 20 (17), 5563–5573.
[6] Guan, J.; Tomobe, K.; Madu, I.; Goodson, T.; Makhal, K.; Trinh, M. T.; Rand, S. C.; Yodsin, N.; Jungsuttiwong, S.; Laine, R. M. Photophysical Properties of Partially Functionalized Phenylsilsesquioxane: [RSiO1.5]7[Me/NPrSiO1.5] and [RSiO1.5]7[O0.5 SiMe3]3 (R = 4-Me/4-CN-Stilbene). Cage-Centered Magnetic Fields Form under Intense Laser Light. Macromolecules 2019, 52 (11), 4008–4019.
[7] Guan, J.; Tomobe, K.; Madu, I.; Goodson, T.; Makhal, K.; Trinh, M. T.; Rand, S. C.; Yodsin, N.; Jungsuttiwong, S.; Laine, R. M. Photophysical Properties of Functionalized Double Decker Phenylsilsesquioxane Macromonomers: [PhSiO1.5]8[OSiMe2]2 and [PhSiO1.5]8[O0.5SiMe3]4. Cage-Centered Lowest Unoccupied Molecular Orbitals Form Even When Two Cage Edge Bridges Are Removed, Verified by Modeling and Ultrafast Magnetic Light Scattering Experiments. Macromolecules 2019, 52 (19), 7413–7422.
[8] Dudziec, B.; Marciniec, B. Double-Decker Silsesquioxanes: Current Chemistry and Applications. COC. 2017, 21(28), 2794-2813.
[9] Guan, J.; Arias, J. J. R.; Tomobe, K.; Ansari, R.; Marques, M. de F. V.; Rebane, A.; Mahbub, S.; Furgal, J. C.; Yodsin, N.; Jungsuttiwong, S.; Hashemi, D.; Kieffer, J.; Laine, R. M. Unconventional Conjugation via VinylMeSi(O−)2 Siloxane Bridges May Imbue Semiconducting Properties in [Vinyl(Me)SiO(PhSiO1.5)8 OSi(Me)Vinyl-Ar] Double-Decker Copolymers. ACS Appl. Polym. Mater. 2020, 2 (9), 3894–3907.
[10] Chan, K. L.; Sonar, P.; Sellinger, A. Cubic Silsesquioxanes for Use in Solution Processable Organic Light Emitting Diodes (OLED). J. Mater. Chem. 2009, 19 (48), 9103.
[11] Cai, Y.; Ni, D.; Cheng, W.; Ji, C.; Yaling Wang; Müllen, K.; Su, Z.; Liu, Y.; Chen, C.; Yin, M. Enzyme-Triggered Disassembly of Perylene Monoimide-based Nanoclusters for Activatable and Deep Photodynamic Therapy. Angew. Chem. Int. Ed. 2020, 59 (33), 14014–14018.
[12] Ji, C.; Gao, Q.; Dong, X.; Yin, W.; Gu, Z.; Gan, Z.; Zhao, Y.; Yin, M. A Size-Reducible Nanodrug with an Aggregation-Enhanced Photodynamic Effect for Deep Chemo-Photodynamic Therapy. Angew. Chem. Int. Ed. 2018, 57 (35), 11384–11388.
[13] Liu, C.; Zhang, S.; Li, J.; Wei, J.; Müllen, K.; Yin, M. A Water-Soluble, NIR-Absorbing Quaterrylenediimide Chromophore for Photoacoustic Imaging and Efficient Photothermal Cancer Therapy. Angew. Chem. Int. Ed. 2019, 58 (6), 1638–1642.
[14] Liu, Y.; Onodera, K.; Takeda, N.; Ouali, A.; Unno, M. Synthesis and Characterization of Functionalizable Silsesquioxanes with Ladder-Type Structures. Organometallics 2019, 38 (22), 4373–4376.

[15] Feher, F. J.; Budzichowski, T. A. Syntheses of Highly-Functionalized Polyhedral Oligosilsesquioxanes. Journal of Organometallic Chemistry 1989, 379 (1–2), 33–40.
[16] Méndez, H.; Heimel, G.; Winkler, S.; Frisch, J.; Opitz, A.; Sauer, K.; Wegner, B.; Oehzelt, M.; Röthel, C.; Duhm, S.; Többens, D.; Koch, N.; Salzmann, I. Charge-Transfer Crystallites as Molecular Electrical Dopants. Nat Commun 2015, 6 (1), 8560.
[17] Jacobs, I. E.; Moulé, A. J. Controlling Molecular Doping in Organic Semiconductors. Adv. Mater. 2017, 29 (42), 1703063.
[18] Salzmann, I.; Heimel, G.; Oehzelt, M.; Winkler, S.; Koch, N. Molecular Electrical Doping of Organic Semiconductors: Fundamental Mechanisms and Emerging Dopant Design Rules. Acc. Chem. Res. 2016, 49 (3), 370–378.
[19] Ma, L.; Hu, P.; Jiang, H.; Kloc, C.; Sun, H.; Soci, C.; Voityuk, A. A.; Michel-Beyerle, M. E.; Gurzadyan, G. G. Single Photon Triggered Dianion Formation in TCNQ and F4TCNQ Crystals. Sci Rep 2016, 6 (1), 28510.
[20] Brook, A. G.; Duff, J. M.; Reynolds, W. F. The Bromination, Debromination and Debromosilylation of Silylstyrenes and Other Vinylsilanes. Journal of Organometallic Chemistry 1976, 121 (3), 293–306.

Chapter 7. Double Decker Silsesquioxane Derived Alternating Terpolymers Give Excited-state Conjugation Averaging that of the Corresponding Co-polymers.

Manuscript in preparation, 2021.

Abstract

In this work we continue efforts to expand the family of silsesquioxane (SQ)-based oligomers and polymers that exhibit through-cage conjugation in the excited state and to map structure-property relationship for practical applications. We recently reported series of double decker (DD) and ladder (LL) SQ derived copolymers prepared via Heck cross-coupling that exhibit unconventional conjugation as evidenced by exceptional red-shifted emissions relative to model compounds.

When copolymerized with biphenyl, terphenyl and stilbene, the SQ polymers typically emit ca. 400 nm with quantum yields $\geqslant 0.6$. Copolymerization with thiophene, bithiophene and thienothiophene provides oligomers with emission $\approx$ 530 nm but with relatively low quantum yields.

Here we first report the successful synthesis of DD SQ derived terpolymers with alternating biphenyl and thiophene linkers characterization by ^{1}H, ^{13}C NMR, GPC, MALDI-TOF, TGA and FTIR with the goal of possible incorporation of long-wavelength emission and high quantum yields. Study of the UV−vis absorption and emission properties of these terpolymers indicates emission intermediate between those of the respective copolymers rather than emission from both units as would be expected from physical mixtures, again supporting electronic communication along the polymer chains and through the cages via disiloxane conjugated linkers. In addition, we have found two successful examples of terpolymers showing improved quantum yields from the DD-co-thiophene copolymer and red-shifted emission from the respective terphenyl/stilbene co-polymers.

7.1 Introduction

Studies of silsesquioxanes (SQs) compounds, oligomers and polymers have generated rapidly increasing attention arising from their well-defined nanostructures with high degrees of symmetry, rigidity and thermal stability coincident with the potential for appending multiple organic functional groups. These functional groups permit formulation of multiple hybrid materials.[1–7] The ability to manipulate properties at nanometer scales in 3-D offer unique properties that provide

considerable motivation to incorporate SQs into polymers via copolymerization, grafting or blending for proper-ties modifications e.g. by improving thermal stabilities, mechanical properties, oxidation resistance, surfacing hardening, porosity for low density applications and/or to trap pollutants, as well as re-duce flammability.[2,4,8–12]

Previously, we reported formation of cage-centered LUMOs that interact with appended 4-methyl/cyanostilbene groups that exhibit excited state conjugation resulting in strong emission red-shifts of ~70 nm vs the corresponding free stilbenes.[13–16] We also observed red-shifted emissions in the copolymers of Phenyl $T_{10/12}$ cages with divinyl benzene of 50 nm vs divinylbenzene[17] and an additional 20 nm with divinyl stilbene of vs divinylstilbene.[18] Most recently, we extended this type of copolymer to phenyl double decker (DD) SQs [vinylMeSi(O_2)($PhSiO_{1.5}$)$_8$$O_2$SiMevinyl] with multiple aromatic linkers all indicating red-shifted emissions of 50-80 nm from respective model compounds, implying through-chain conjugation involving both DD cages and organic linkers despite two vinylSi(O-)$_2$ siloxane units comprising an essential part of the bridges.[19]

Most surprising was the finding that eliminating the cage through use of ladder SQs but still with vinylSi(O-)$_2$ bridges using the same aromatic linked copolymers gave max emission red-shifts 30-60 nm beyond the DD analogues even with shorter chain lengths.[20] In both systems, bi-phenyl, terphenyl and stilbene linked SQ copolymers all exhibit high fluorescence quantum yields (Φ_F) up to ~80%, while thiophene, bithiophene and thieno-thiophene linked copolymers display long-wavelength emission around 530 nm and with Φ_F ~10%.

The easy syntheses and excited-state conjugation of sets of SQ-based polymers may offer potentially new hybrid organic-inorganic semiconducting materials in OLED and photovoltaic applications. For example, Jabbour's group explored the use of multifunctional SQ emitter based OLED components. Likewise, Sellinger's group reported Heck coupling of haloaromatics with octavinylSQ as a route to hybrid components for electroluminescent devices.[21–23] Thus one particular motivation of the current work targets mapping their structure-property relationships, especially exploring novel combinations of robust nature, long-wavelength emission and high Φ_F, of potential value in flat panel display applications.[3,24,25]

In this paper, we used Heck cross-coupling to access a variety of DD SQ derived alternating terpolymers as a means to expand our knowledge of this unusual form of conjugation while also exploring the potential to learn to control both emission wavelengths and Φ_F to probe the general nature of these unusual systems. The synthetic route is shown in Scheme **7.1**.

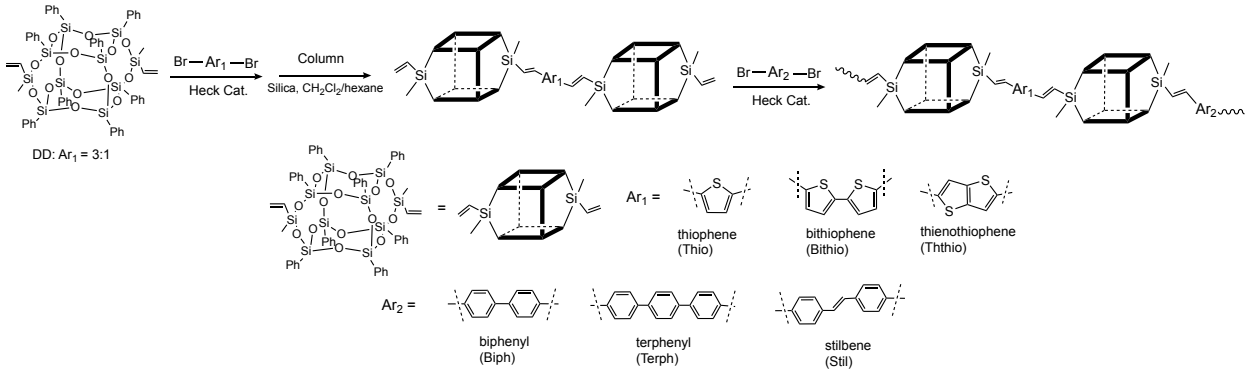

Scheme 7.1. Syntheses of DD derived alternating terpolymers.

7.2 Experimental

The synthetic methods and characterization techniques are described in Chapter **2**.

7.3 Results and discussion

Occam's razor suggests the simplest approach should be tried first. Thus, the direct co-polymerization of vinylDDvinyl with 2:1:1 molar ratio of dibromo-biphenyl and dibromo-thiophene was explored. However, divinylDD reacts with biphenyl much faster than with thiophene such that that no terpolymer forms. Instead, it appears that block co-polymers form with large segments of DD-co-biphenyl. One possible explanation is that the thiophene sulfur binds reversibly to Pd such that catalytic efficiency is decreased.[26–29] This is the likely reason both DD/LL SQs derived co-polymers with phenyl systems always results in much longer chains (DP~15) than thiophene sys-tems (DP~5).[19,20]

Thus, we turned to the more tedious approach to alternating terpolymers using step-by-step syntheses per Scheme **7.1**. We first coupled thiophene groups with DD SQs on both ends via Heck cross-coupling and with a 3:1 DD:thiophene molar ratio. The expected vinylDD-thiophene-DDvinyl was isolated via column chromatography (CH_2Cl_2: hexane 2:1 volume ratio). The reason for choosing thiophene systems in the first step is again that the polymerization of vinylDD-biphenyl-DDvinyl with thiophene will be even more difficult so to obtain longer terpolymers, vinylDD-thiophene-DDvinyl was synthesized first. All the products were characterized using standard methods as shown in Tables **7.1**, **E.1** and **E.2**.

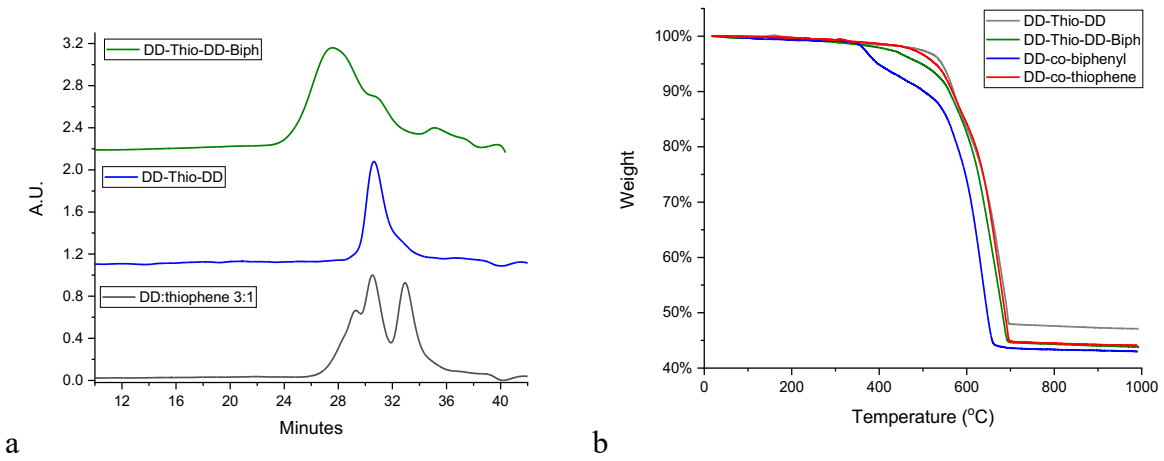

a b

Figure 7.1. (a) GPC of the product mixture of DD with thiophene (3:1 molar ratio), isolated DD-thiophene-DD via column chromatography and terpolymer of DD-thiophene-DD with biphenyl. (b) TGA of DD-thiophene-DD, terpolymer DD-thiophene-biphenyl, and copolymers of DD-co-biphenyl and DD-co-thiophene.

Figure **7.1a** and Table **7.1** give GPC data for these compounds. After Heck cross-coupling of divinyl-DD with a 3:1 molar ratio dibromo-Ar1, the product is a mixture of single-cage, two-cage and three-cage products as expected and evidenced by three narrow peaks (PDI ~1.04) at retention times of 32.9, 30.5 and 29.3 min respectively, due to the difference in hydrodynamic volumes resolved from intact SQ cores. The yield of the desired DD-Ar1-DD product peak is evident in the GPC trace and can be isolated via column chromatography.

MALDI in Figures **E.1- E.3** and TGA in Figure **7.1b** and Table **7.1** were used to characterize the end groups of isolated two-cage product, which indicates the end-capping of Ar1 with DD cages ac-cording to the expected m/z in MALDI and ceramic yields close to or the same as the theoretical value calculated from the chemical formula of DD-Ar1-DD. Note that the molecular weight suggested by GPC is always smaller than MALDI due to the sphere-like hydrodynamic volume of the DD cores.

The successful isolation of DD-Ar1-DD is also supported by ^{1}H and ^{13}C NMR in Figure **E.5** and Table **E.1**. The ^{1}H NMR of DD-thiophene-DD exhibits new signals for ethene groups bonded to thiophene at 6.9 and 6.4 ppm; distinct from peaks for unreacted vinyl groups at 6.20 and 6.05 ppm. The theoretical ratio of reacted to unreacted vinyl protons is 2:3, which matches the actual in-tegration ratio of 2.1 : 3.1. Additionally, there are two methyl peaks, likely indicating protons in two magnetically different environments originating from reacted and unreacted vinyls.

The ^{13}C NMR shows peaks for phenyl groups on the DD cage from 134 to 127 ppm. Reacted and unreacted vinyl groups also display distinct chemical shifts at 144.3, 139.1 ppm and 135.2, 134.5 ppm respectively. Thiophene carbon peaks appear at around 137 and 124 ppm.

Peaks are assigned by comparison with the NMR of starting di-vinyl DD. The isolated products are also characterized by FTIR as shown in Figure **E.7** and peak assignment in Table **E.2**, with the highest peak at 1132 cm^{-1} from the Si-O-Si framework. Peaks from νC=C and νC-H are also observed around 1400 and 3000 cm^{-1} respectively, characteristic of phenyl, vinyl and thiophene groups.

After Heck cross-coupling of DD-Ar1-DD with dibromo-Ar2, the alternating terpolymers DD-Ar1-Ar2 appear in the GPC with retention times of 25-28 min, with Đ of ~1.7 expected for step-growth type polymerization with average DPs of 4-8. The presence of oligomers is also confirmed by MALDI, which shows peaks every DD-Ar1-DD-Ar2 repeat unit.

In general, SQ monomers are readily ionizable; however, as the Mw of SQ-based oligomers in-creases, the ionization efficiency decreases resulting in smaller peaks. Thus the peak heights in MALDI cannot be considered as a quantitative measure of the amount of each species in the oligomeric mixture. From the TGA analyses, the $T_{d5\%}$ of the resulting terpolymers are all >400 ºC, indicating high thermal stabilities in air and the ceramic yields are close to the theorical value and in between of the corresponding copolymers DD-co Ar1/Ar2. ^{1}H NMR in Table **E.1** and Figure **E.6** suggests only trace amounts of end vinyl groups around 6.10 ppm and greater amounts of ethene bridges between DD cage and organic tethers Ar1 and Ar2 around 7.0 and 6.5 ppm, indicating successful polymerization. Finally, there are broad peaks in aromatic proton region around 7.8-7.1 ppm that are typical for these compounds and peaks in methyl proton region around 0.45 ppm. There are essentially no significant changes in FTIR as expected.

Table 7.1. MALDI-TOF, GPC and TGA data for terpolymers.

Compound	MALDI-TOF m/z[a]	GPC			TGA		
		M_n	M_w	Đ	Ceramic yield %	Theor yield %	$T_{d5\%/air}$ °C
DD-Thio-DD	2600	1690	1770	1.05	48	48	545
-Biph	2752[c]	7000	11900	1.70	44	45	500
-Terph	2823[c]	4500	7400	1.65	45	44	520
-Stil	2778[c]	4400	7400	1.68	44	45	410
DD-Bithio-DD	2574[b], 2682	1780	1890	1.06	46	47	500
DD-Thithio-DD	2655	1720	1790	1.04	46	47	530

[a] As Ag^+ adduct. [b] As H^+ adduct. [c] M/z of the repeating unit of terpolymers.

We previously reported the successful preparation of a series of DD copolymers/oligomers and the discovery of through-chain conjugation in the excited state even through the -$Si(O)_2$ siloxane units as evidenced by the exceptional red-shifted emission from the respective model compounds.[19] Figure **7.2a** compares the UV-vis absorption and emission of DD-thiophene-DD, short oligomers and long DD-co-thiophene synthesized using the ratio of DD:thiophene of 3:1 and 1:1 respectively. It is noteworthy that the emission maxima show progressive red-shifts from 390, to 465 to 505 nm as the function of chain length. In addition, even though the Abs. λ_{max} at 340 nm does not change, the absorption shoulder around 400 nm grows with extensions in chain length as well, which all indicate through-chain conjugation involving the SQ cages via siloxane units. Spectra of DD-bithiophene-DD and DD-thienothiophene-DD are displayed in Figures **E.11** and **E.12**, which also show simi-lar progressively red-shifted emissions with increasing chain lengths.

Figure **7.2b** provides absorption and emission data for the terpolymer DD-Thio-DD-Biph and the corresponding DD-co-biphenyl and DD-co-thiophene, as summarized in Table **7.2**. The absorp-tion spectrum of the alternating terpolymer shows a peak at 315 nm around the Abs. λ_{max} of DD-co-biphenyl and an increased shoulder around 400 nm, similar to DD-co-thiophene, which sug-gests successful Heck polymerization and no ground-state HOMO interaction. The Em. λ_{max} of the terpolymer is 430 nm, in between of DD-co-biphenyl (375 nm) and DD-co-thiophene (505 nm), which again points to the excited-state conjugation involving SQ cages and two different conjugated linkers and the opportunities to tune the emission of DD derived polymers. Compared to the starting DD-thiophene-DD, the Em. λ_{max} of terpolymer is red-shifted by 40 nm, indicating extended conjugation after biphenyl linking DD-thiophene-DD together to form a longer terpolymer chain.

When excited around the Abs. λ_{max} of DD-co-biphenyl (315 nm) and DD-co-thiophene (340 nm), the Em. λ_{max} remains 430 nm while the intensity is much higher using 345 nm as the excitation wave-length as shown in Figure **E.8**. As indicated in Table **7.2** and Figures **E.9 E10** and **E.13**, other terpolymers also show emission maxima between that of the two copolymers, all suggesting that the polymer LUMOs communicate between SQs through each type of conjugated unit.

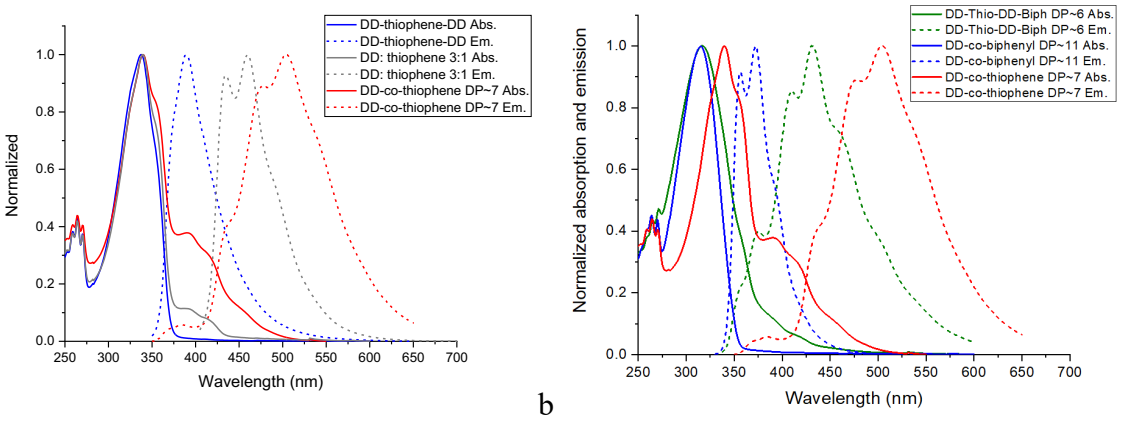

Figure 7.2. (a) Normalized absorption and emission of DD-thiophene-DD, mixture of DD:thiophene 3:1 and longer DD-co-thiophene (1:1). (b) Absorption and emission of terpolymer DD-Thio-DD-Biph and corresponding copolymers, DD-co-biphenyl and DD-co-thiophene.

Photoluminescence quantum yields were measured using a K-sphere integrating sphere in CH_2Cl_2 with the excitation wavelengths at Abs. λ_{max} of DD-co-Ar1 to explore the effect of incorporation of Ar2 into the system since DD-co-Ar2 displays a quite high Φ_F (90 %). Table **7.2** shows that the incorporation of biphenyl has little effect on the improvement of the Φ_f since the terpolymers display essentially the same Φ_F as those of the corresponding terpolymers.

Table 7.2. UV-vis, photoluminescent data and quantum yields for DD derived copolymers[19] and terpolymers.

Polymers	DP	Abs. λ_{max} (nm)	Em. λ_{max} (nm)	Φ_F
DD-co-thiophene	7	340	478, 505	0.09±0.001
DD-co-bithiophene	4	391	505, 538	0.17±0.02
DD-co-thienothiophene	5	358	496, 526	0.13±0.01
DD-co-biphenyl	11	314	357, 373	0.66±0.05
DD-co-terphenyl	11	321	374, 392	0.87±0.04
DD-co-stilbene	9	357	393, 412, 436	0.61±0.04
DD-Thio-DD-Biph	6	317	409, 432	0.07±0.004
DD-Thio-DD-Terph	4	324	415, 427	0.20±0.03
DD-Thio-DD-Stil	4	343,355	415, 446, 469	0.24±0.06
DD-Bithio-DD-Biph	6	312,378	437, 464, 495	0.14±0.004
DD-Bithio-DD-Terph	4	316,390	435, 460, 495	0.12±0.01
DD-Ththio-DD-Biph	5	316	411, 433 451	0.14±0.02

Terpolymers of DD-Thio-DD-Terph and DD-Thio-DD-Stil exhibit improved Φ_F from 0.09 to 0.20 and 0.24 respectively. Both DD-Thio-DD-Biph and DD-Thio-DD-Stil show red-shifted emission by ~35 nm from corresponding DD-co-biphenyl and DD-co-stilbene, which are two successful examples of combination of longer-wavelength emission and high quantum yields. While as for bithiophene and thienothiophene derived terpolymers, no significant increase was observed in their quantum yields, which is similar to those of DD-co-bithiophene and DD-co-thienothiophene

of ~0.15. More studies need to be done to explore the suitable combination of organic tethers so that they can display novel photophysical properties important for displaying devices. In addition, we recently have also prepared ladder (LL) silsesquioxane derived copolymers analogous to the DD copolymers, and among them LL-co-biphenyl, terphenyl and stilbene offer high quantum yields of 0.6 but further red-shifted emission beyond their DD analogues.[20] Studies of LL derived terpolymers can be more exciting since they exhibit superior photophysical properties while still maintain robust nature.

7.4 Conclusions

This report details the synthesis and characterization of sets of conjugated terpoly-mers/oligo-mers derived from double decker silsesquioxanes. Two different synthetic routes are explored: the direct polymerization of DD with 2:1:1 molar ratio of biphenyl and thiophene and polymerization step by step. Due to the different reaction rate between thiophene and biphenyl, polymerization step by step is a better method to yield alternating terpolymers. TGA indicates high thermal stabilities in air inherent from the DD SQ cages and photophysical studies of DD alternating terpolymers suggest that the absorption spectra display spectral characteristics from respective DD copolymers while the emission spectra are an average of both copolymers.

These results indicate no ground-state electronic communication along the chain but provide another strong evidence of unconventional conjugation in the excite-state involving two different organic tethers and all the way through DD cages even with siloxane units. Moreover, by incorporating terphenyl/stilbene to form terpolymers with DD and thiophene, the quantum yields are increased significantly with respect to the copolymer of DD and thiophene, pointing to new opportunities to tailor the photophysical properties that are important in applications such as displaying panels.

References

(1) Baney, R. H.; Itoh, M.; Sakakibara, A.; Suzuki, T. Silsesquioxanes. 22.

(2) Yoshida, K.; Hattori, T.; Ootake, N.; Tanaka, R.; Matsumoto, H. Silsesquioxane-Based Polymers: Synthesis of Phenylsilsesquioxanes with Double-Decker Structure and Their Polymers. In *Silicon Based Polymers*; Ganachaud, F., Boileau, S., Boury, B., Eds.; Springer Netherlands: Dordrecht, 2008; pp 205–211.

(3) Cordes, D. B.; Lickiss, P. D.; Rataboul, F. Recent Developments in the Chemistry of Cubic Polyhedral Oligosilsesquioxanes. *Chem. Rev.* 2010, *110* (4), 2081–2173.

(4) Li, G.; Wang, L.; Ni, H.; Jr, C. U. P. Polyhedral Oligomeric Silsesquioxane (POSS) Polymers and Copolymers: A Review. 32.

(5) Lee, D. W.; Kawakami, Y. Incompletely Condensed Silsesquioxanes: Formation and Reactivity. *Polym J* 2007, *39* (3), 230–238.
(6) Laine, R. M. Nanobuilding Blocks Based on the [OSiO1.5]x (X= 6, 8, 10) Octasilsesquioxanes. *J. Mater. Chem.* 2005, *15* (35–36), 3725.
(7) *Applications of Polyhedral Oligomeric Silsesquioxanes*; Hartmann-Thompson, C., Ed.; Advances in Silicon Science; Springer Netherlands: Dordrecht, 2011; Vol. 3.
(8) Dudziec, B.; Marciniec, B. Double-Decker Silsesquioxanes: Current Chemistry and Applications. *COC* 2018, *21* (28).
(9) Du, Y.; Unno, M.; Liu, H. Hybrid Nanoporous Materials Derived from Ladder- and Cage-Type Silsesquioxanes for Water Treatment. *ACS Appl. Nano Mater.* 2020, *3* (2), 1535–1541.
(10) Shen, R.; Liu, Y.; Yang, W.; Hou, Y.; Zhao, X.; Liu, H. Triphenylamine-Functionalized Silsesquioxane-Based Hybrid Porous Polymers: Tunable Porosity and Luminescence for Multianalyte Detection. *Chemistry – A European Journal* 2017, *23* (54), 13465–13473.
(11) Wang, D.; Feng, S.; Liu, H. Fluorescence-Tuned Polyhedral Oligomeric Silsesquioxane-Based Porous Polymers. *Chemistry – A European Journal* 2016, *22* (40), 14319–14327.
(12) Yang, X.; Liu, H. Ferrocene-Functionalized Silsesquioxane-Based Porous Polymer for Efficient Removal of Dyes and Heavy Metal Ions. *Chemistry – A European Journal* 2018, *24* (51), 13504–13511.
(13) Furgal, J. C.; Jung, J. H.; Goodson, T.; Laine, R. M. Analyzing Structure–Photophysical Property Relationships for Isolated T_8 , T_{10} , and T_{12} Stilbenevinylsilsesquioxanes. *J. Am. Chem. Soc.* 2013, *135* (33), 12259–12269.
(14) Laine, R. M.; Sulaiman, S.; Brick, C.; Roll, M.; Tamaki, R.; Asuncion, M. Z.; Neurock, M.; Filhol, J.-S.; Lee, C.-Y.; Zhang, J.; Goodson, T.; Ronchi, M.; Pizzotti, M.; Rand, S. C.; Li, Y. Synthesis and Photophysical Properties of Stilbeneoctasilsesquioxanes. Emission Behavior Coupled with Theoretical Modeling Studies Suggest a 3-D Excited State Involving the Silica Core. *J. Am. Chem. Soc.* 2010, *132* (11), 3708–3722.
(15) Guan, J.; Tomobe, K.; Madu, I.; Goodson, T.; Makhal, K.; Trinh, M. T.; Rand, S. C.; Yodsin, N.; Jungsuttiwong, S.; Laine, R. M. Photophysical Properties of Partially Functionalized Phenylsilsesquioxane: $[RSiO_{1.5}]_7[Me/NPrSiO_{1.5}]$ and $[RSiO_{1.5}]_7[O_{0.5}SiMe_3]_3$ (R = 4-Me/4-CN-Stilbene). Cage-Centered Magnetic Fields Form under Intense Laser Light. *Macromolecules* 2019, *52* (11), 4008–4019.
(16) Guan, J.; Tomobe, K.; Madu, I.; Goodson, T.; Makhal, K.; Trinh, M. T.; Rand, S. C.; Yodsin, N.; Jungsuttiwong, S.; Laine, R. M. Photophysical Properties of Functionalized Double Decker Phenylsilsesquioxane Macromonomers: $[PhSiO_{1.5}]_8[OSiMe_2]_2$ and $[PhSiO_{1.5}]_8[O_{0.5}SiMe_3]_4$. Cage-Centered Lowest Unoccupied Molecular Orbitals Form Even When Two Cage Edge Bridges Are Removed, Verified by Modeling and Ultrafast Magnetic Light Scattering Experiments. *Macromolecules* 2019, *52* (19), 7413–7422.
(17) Asuncion, M. Z.; Laine, R. M. Fluoride Rearrangement Reactions of Polyphenyl- and Polyvinylsilsesquioxanes as a Facile Route to Mixed Functional Phenyl, Vinyl T_{10} and T_{12} Silsesquioxanes. *J. Am. Chem. Soc.* 2010, *132* (11), 3723–3736.
(18) Furgal, J. C.; Jung, J. H.; Clark, S.; Goodson, T.; Laine, R. M. Beads on a Chain (BoC) Phenylsilsesquioxane (SQ) Polymers via F^- Catalyzed Rearrangements and ADMET or Reverse Heck Cross-Coupling Reactions: Through Chain, Extended Conjugation in 3-D with Potential for Dendronization. *Macromolecules* 2013, *46* (19), 7591–7604.
(19) Guan, J.; Arias, J. J. R.; Tomobe, K.; Ansari, R.; Marques, M. de F. V.; Rebane, A.; Mahbub, S.; Furgal, J. C.; Yodsin, N.; Jungsuttiwong, S.; Hashemi, D.; Kieffer, J.; Laine, R. M.

Unconventional Conjugation via VinylMeSi(O−) 2 Siloxane Bridges May Imbue Semiconducting Properties in [Vinyl(Me)SiO(PhSiO 1.5) 8 OSi(Me)Vinyl-Ar] Double-Decker Copolymers. *ACS Appl. Polym. Mater.* 2020, *2* (9), 3894–3907.

(20) Guan, J.; Sun, Z.; Ansari, R.; Liu, Y.; Endo, A.; Unno, M.; Ouali, A.; Mahbub, S.; Furgal, J. C.; Yodsin, N.; Jungsuttiwong, S.; Hashemi, D.; Kieffer, J.; Laine, R. M. Conjugated Copolymers That Shouldn't Be. *Angewandte Chemie International Edition* 2021, *60* (20), 11115–11119.

(21) Chan, K. L.; Sonar, P.; Sellinger, A. Cubic Silsesquioxanes for Use in Solution Processable Organic Light Emitting Diodes (OLED). *J. Mater. Chem.* 2009, *19* (48), 9103.

(22) Froehlich, J. D.; Young, R.; Nakamura, T.; Ohmori, Y.; Li, S.; Mochizuki, A.; Lauters, M.; Jabbour, G. E. Synthesis of Multi-Functional POSS Emitters for OLED Applications. *Chem. Mater.* 2007, *19* (20), 4991–4997.

(23) Sellinger, A.; TamakiPresent address: General Elec, R.; Laine, R. M.; Ueno, K.; Tanabe, H.; Williams, E.; Jabbour, G. E. Heck Coupling of Haloaromatics with Octavinylsilsesquioxane: Solution Processable Nanocomposites for Application in Electroluminescent Devices. *Chem. Commun.* 2005, No. 29, 3700.

(24) Burrows, P. E.; Gu, G.; Bulovic, V.; Shen, Z.; Forrest, S. R.; Thompson, M. E. Achieving Full-Color Organic Light-Emitting Devices for Lightweight, Flat-Panel Displays. *IEEE Trans. Electron Devices* 1997, *44* (8), 1188–1203. https://doi.org/10.1109/16.605453.

(25) Salzmann, I.; Heimel, G.; Oehzelt, M.; Winkler, S.; Koch, N. Molecular Electrical Doping of Organic Semiconductors: Fundamental Mechanisms and Emerging Dopant Design Rules. *Acc. Chem. Res.* 2016, *49* (3), 370–378.

(26) Ma, L.; Yuan, S.; Jiang, T.; Zhu, X.; Lu, C.; Li, X. Pd4S/SiO2: A Sulfur-Tolerant Palladium Catalyst for Catalytic Complete Oxidation of Methane. *Catalysts* 2019, *9* (5), 410.

(27) Monai, M.; Montini, T.; Melchionna, M.; Duchoň, T.; Kúš, P.; Chen, C.; Tsud, N.; Nasi, L.; Prince, K. C.; Veltruská, K.; Matolín, V.; Khader, M. M.; Gorte, R. J.; Fornasiero, P. The Effect of Sulfur Dioxide on the Activity of Hierarchical Pd-Based Catalysts in Methane Combustion. *Applied Catalysis B: Environmental* 2017, *202*, 72–83.

(28) Tiancun, X.; Lidun, A.; Weimin, Z.; Shishan, S.; Guoxin, X. Mechanism of Sulfur Poisoning on Supported Noble Metal Catalyst ? The Adsorption and Transformation of Sulfur on Palladium Catalysts with Different Supports. *Catal Lett* 1992, *12* (1–3), 287–296.

(29) Wilburn, M. S.; Epling, W. S. Sulfur Deactivation and Regeneration of Mono- and Bimetallic Pd-Pt Methane Oxidation Catalysts. *Applied Catalysis B: Environmental* 2017, *206*, 589–598.

Chapter 8. Future Work

8.1 Summaries

In this dissertation, we have demonstrated new routes to functionalize partially condensed polyhedral oligomeric silsesquioxanes and their derived organic-inorganic hybrid polymers and studied their properties especially photophysical behavior. Chapter **3** details work on the functionalization of trisilanol phenylsilsesquioxanes (T_7) via silylation followed by halogenation and Heck cross-coupling reactions, which produce corner-missing silsesquioxane cages with modified numbers of stilbene groups. These products exhibit excellent thermal properties with $T_{d5\%/air}$ above 400 ^{o}C and different photophysical properties depending on the number of functional groups.

With more than two stilbene groups per cage, these partial cages display electronic interactions between silsesquioxane cages and organic tethers in the excited state, similar to completely condensed silsesquioxanes in that a cage centered LUMO appears to form. While if there are only two stilbene groups, no interaction is observed, indicating a unique structure-property relationship. In Chapter **4**, we investigated another partially condensed tetrasilanol phenylsilsesquioxanes (DD) and the influence of the number of organic tethers per cage on the photophysical properties. In conclusion, similar results are observed, which points to new opportunities to tailor the properties of these silsesquioxanes by modifying their structures.

Chapter **5** describes our development of conjugated organic linked DD SQ copolymers. When copolymerized with thiophene, bithiophene and thienothiophene, these polymers with DD SQ in the main chains display large red-shifts in emission with respect to the model compounds that lack SQ cages, revealing electronic communication through the cage and even the two siloxane bridges per cage and along the polymer chains. In addition, those polymers with thiophene tethers easily form integer charge transfer complexes with electron-withdrawing F4TCNQ, providing further evidence of unconventional conjugation and possibilities in applications such as photonic devices.

In Chapter **6** we looked further into ladder silsesquioxane derived copolymers to explore the changes in photophysical properties as a result of changes in silsesquioxane polymer structures in. Copolymerization of ladder silsesquioxanes with phenyl linkers finds even further red-shifted

emissions compared to DD analog copolymers and still high photoluminescent quantum yields, revealing superior excited-state conjugation. Bromination of both DD and ladder silsesquioxane copolymers can occur not only on phenyl groups but also vinyl groups and thus break the conjugation. The vinyl groups can easily be restored via zinc debromination while the brominated phenyl groups can be the branching points for the formation of further functionalization to form 'hairy' polymers.

In expanding our work done in Chapters **5** and **6**, our group conducted preliminary studies preparing DD SQ derived terpolymers as shown in Chapter **7**, with the goal of possible combining visible light emission with high quantum efficiencies.

With these potentials in mind, it is of great significance to: (1) expand the number of architectures wherein cage centered LUMOs form; (2) develop a basic and detailed understanding of what factors control LUMO formation onset; and (3) assess the true character of the "semiconducting behavior" that appears to occur through vinylMeSi(O-)$_2$ siloxane links using multiple photonic and electrochemical probes, and via theoretical modeling. The following sections discuss our near-future research objectives on the syntheses and characterization of silsesquioxane derived materials to further expand the family of SQs that can offer novel photophysical properties and be potential candidates for components in photovoltaic and display devices.[1–3]

8.2 Hairy polymers

As discussed in Chapters **3** and **4**, stilbene-functionalized T_7 and DD cage emit around 440 nm while free stilbene emits around 360 nm.[4,5] Such red-shifts suggest 3-D electronic communication involving all stilbene chromophores and through the SQ cage and since we have also observed through-chain conjugation in the excited-state in DD and LL derived polymers in Chapter **5**, **6**, and **7**,[6,7] we can explore possible 3-dimentional conjugation by incorporation stilbene-functionalized cage with copolymers to form hairy polymers (Scheme **8.1**).

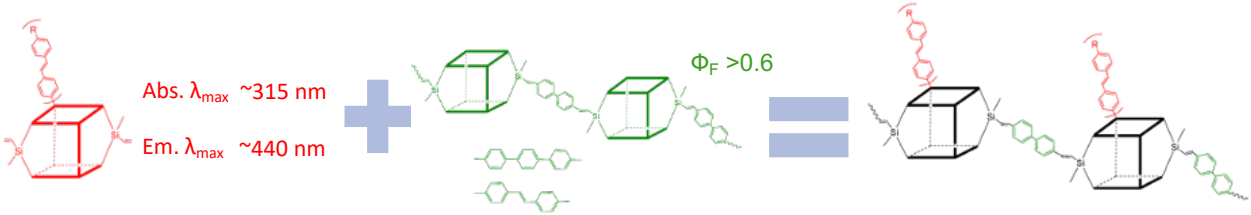

Scheme 8.1. Syntheses of hairy polymers.

Two different synthetic routes to silsesquioxane derived hairy polymers are presented in Schemes **8.2 a** and **b** (experimental in Appendix **F**). By brominating DD copolymers without catalyst at 45 °C, severe chain cleavage was observed within 2 h, as tracked by GPC, as shown in Figures **F.1** and **F.2**, likely due to the dissolved acidic byproduct HBr even with fast N_2 flow during the reaction.

One possible solution is to brominate at room temperature in the presence of an Fe catalyst. In addition, bromination also occurrs on cage-vinyls and co-aromatic groups as proved by comparison of FTIR of cyano-stilbene DD-co-biphenyl synthesized using both synthetic methods in Figure **8.1** and will be further discussed below. Successful restoring of brominated vinyl groups is evidenced by TGA as shown in Figure **F.6** and Table **F.1**, which displays a higher ceramic yield after the debromination (Br_5DD-co-biphenyl) compared to brominated DD-co-biphenyl (Br_9DD-co-biphenyl). In addition, the absorption and emission spectra of debrominated Br_5DD-co-biphenyl in Figure **F.7** are essentially the same as those of DD-co-biphenyl, indicating the successful recovery of through-chain conjugation by recovering the conjugated vinyl groups.

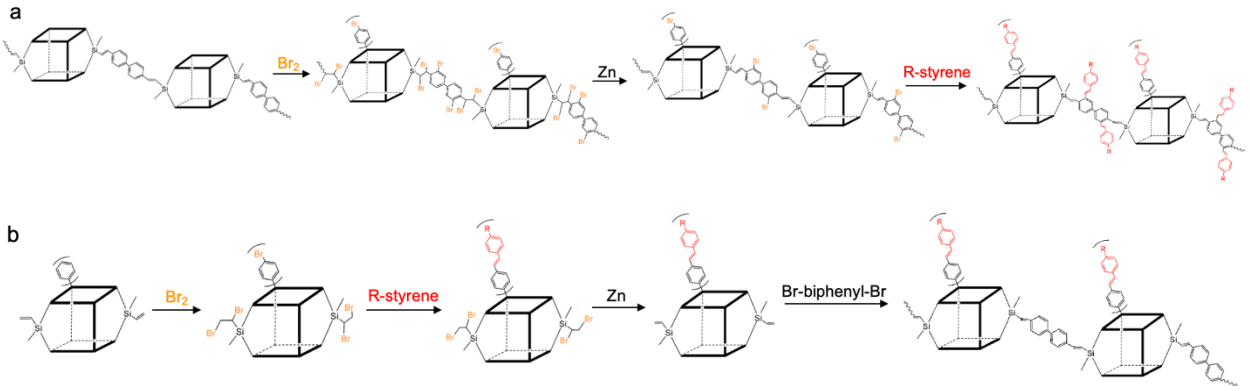

Scheme 8.2. (a) Syntheses by bromination of DD copolymers. (b) Syntheses by bromination of DD cage.

The characterization of products synthesized in Scheme **8.2b** are shown in Table **F.2** and Figures **F8-14**. Brominated vinylDDvinyl (Br_{12}DD) shows similar GPC to the starting vinylDDvinyl as expected for their similar hydrodynamic volumes (Figures **F.8**, **9**). GPC indicates slightly increased molecular size after the Heck cross-coupling with 4-cyanostyrene. The brominated vinyl groups survived Heck cross-coupling of brominated phenyls with 4-cyanostyrene as evidenced by the increased ceramic yield after debromination, which are also close to the theoretical values. The formation of polymers/oligomers is also confirmed by the broad peak in the GPC in Figure **F.12**.

Figure **F.14** compares the absorption and emission of CNStil$_8$Br$_4$DD, CNStil$_8$vinylDDvinyl and CNStil$_8$DDMe$_4$ and the three compounds essentially exhibit the same spectra, since the only structural difference comes from the pendant groups on the siloxane units (alkyl bromides vs vinyl vs methyl group), which would not influence the electronic interaction between the cyano-stilbene moieties and the DD cage.

Figure **8.1** compares the cyano-region in the FTIR of hairy polymers synthesized via two synthetic routes. By brominating DD cage and then polymerizing with dibromo-biphenyl, cyano-stilbene groups are only attached to the SQ cage corner and FTIR shows single $\nu C \equiv N$ peak at 2225 cm^{-1} while for a similar hairy polymers synthesized by brominating DD-co-biphenyl first, there is another small peak at 2160 cm^{-1}, reaving the bromination of co-biphenyl as well.

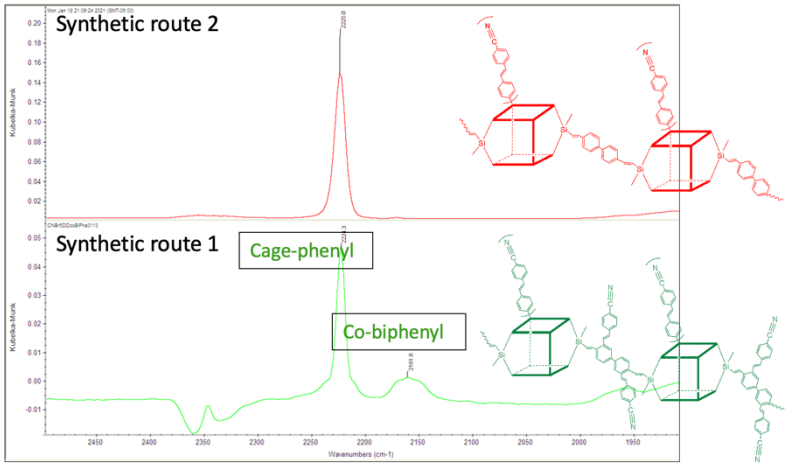

Figure 8.1. Cyano-region in the FTIR of cyano-stilbene DD-co-biphenyl.

Figure **8.2** compares with absorption and emission of cyano-stilbene DD-co-biphenyl synthesized by brominating DD cage (red) and brominating DD-co-biphenyl (green). Both hairy polymers display similar spectra to those of CNStil$_8$DD cage, while the quantum yields are both ~0.02, indicating the LUMOs are localized on the stilbene functionalized cages only and no interaction between cages via the biphenyl linkers is observed.

Hairy polymers prepared by brominating DD-co-biphenyl show an increased absorption shoulder around 375 nm and a slightly red-shifted emission, likely due to the conjugated stilbenes derived from brominated biphenyl. Considering the electron-withdrawing nature of SQ cages, red-shifted absorption and emission with high quantum yields may finally be achieved by exploring hairy polymers with electron-donating groups such as methoxy groups as well as different organic linkers.

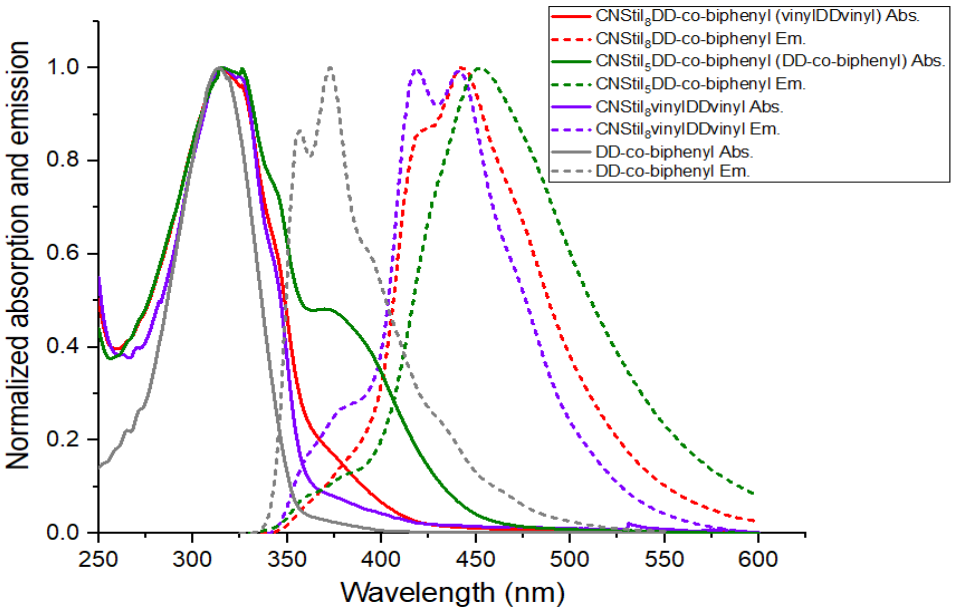

Figure 8.2. Normalized absorption and emission of cyano-stilbene hairy polymers synthesized by brominating DD-co-biphenyl (Scheme **8.2a**) and vinylDDvinyl (Scheme **8.2b**).

8.2 Bromination patterns in various SQ architectures

Cage architecture studies currently planned will expand the number of cage structures that may offer internal LUMOs and one simple way to do it is to study their bromination patterns. To this end, we have initiated collaborative efforts with the Gunma University team. Their work focuses on the synthesis of novel cage compounds as suggested by Figure **8.3**.[8,9]

These cages will allow us to test the limits to LUMO formation by further reducing the cage size (T_4 in Figure **8.3**) as well as introducing ever greater bridges between SQ rings ($T_8D_{2,4,6}$ in Figure **8.3**), and the chance to introduce alkyne groups and their influence on the LUMO formation. It is also possible that the expanded siloxane units will sterically block the interaction between the cage LUMOs and incoming Br_2, likely resulting reduced *ortho*-selectivity of the self-bromination without catalyst. After peroxide oxidation of the brominated SQs, the phenolic products are characterized in detail using GC-MS and ^{1}H, ^{13}C NMR.

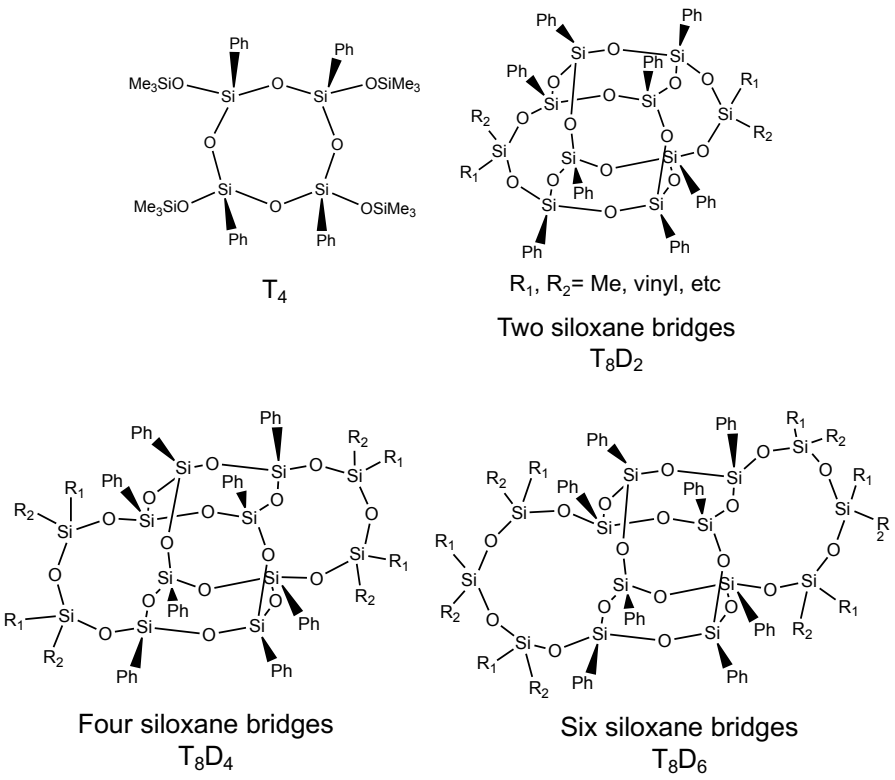

Figure 8.3. Novel SQ structures as probes for expanding structures wherein cage centered LUMOs form.

8.3 Donor-acceptor system

To further develop SQs as energy harvesting candidates, efforts should focus on making materials with higher absorption potential, ideal band gaps that will absorb photons at wavelengths in the range of 350-700 nm, and efficient charge transfer through exciton diffusion.[10] Incorporation of donor and acceptor units within a polymer backbone is one of the ways that researchers have used to improve energy harvesting polymers.[10] Through this method, the absorption spectrum can be broadened since each subunit could be introduced to absorb in different regions, which could also be achieved by the SQ derived terpolymers, even with block units.

Compounds and materials targeted would have to exhibit very efficient charge transfer due to stronger intrinsic dipoles, and also better interfacial interactions in multi-component systems. One could imagine that SQs could also be functionalized to offer donor-acceptor properties. For example, incorporating a donor (p-type) chromophore at one or more side/corners on the SQ cage, and an acceptors (n-type) chromophores on the remaining side/corners. This can be easily achieved by

functionalizing di-vinyl DD of donor and acceptor (Scheme **8.3**), leading to donor-acceptor system all the way through the SQ DD cages.

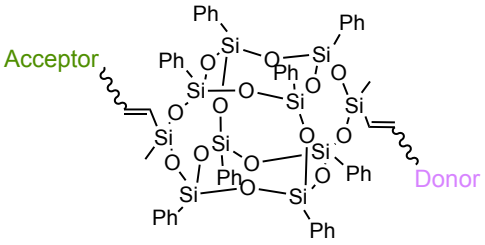

Scheme 8.3. Structure of donor-acceptor DD.

To study unsymmetrical push-pull functionalized DD compounds, our group first synthesized symmetrically functionalized derivatives as shown below for comparison purposes, including the styryl (generation 1, Scheme **8.4**), stilbenevinyl (generation 2, in Scheme **8.5**) derivatives. UV-vis absorption and emission data for all RStyrenes and corresponding mono-/di-/tri-functionalized RStyryl-DD SQs in dichloromethane (DCM) or acetonitrile (ACN) are presented in Table **8.1** in order of decreasing of electron-donating or increasing withdrawing characteristics.

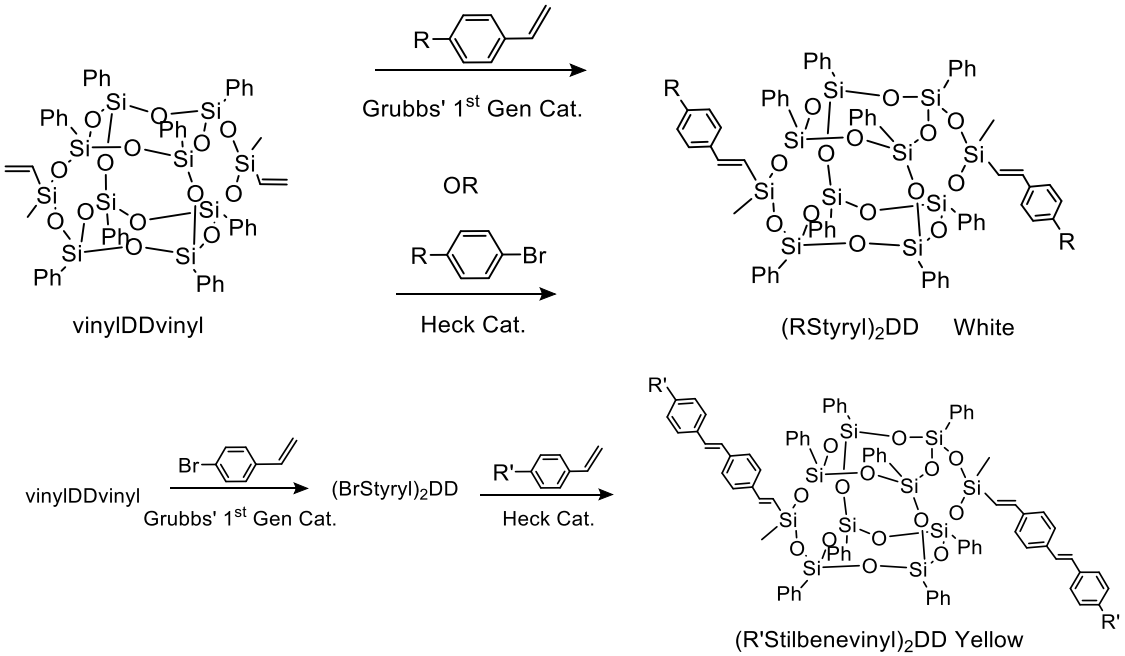

Scheme 8.4. Synthesis of di-styryl functionalized DD (Gen 1), and di-stilbenevinyl functionalized DD (Gen 2).

All DD SQs show slight red-shifts of 7-15 nm in absorption from respective untethered styrenes. The red-shifts increase as the functional groups on two sides of DD SQs become more electronic-donating. Most DD compounds exhibit mundane, red-shifted emissions except for

(BrStyryl)$_2$DD and (MeOStyryl)$_2$DD as marked in red. The reason these two di-functionalized styryl-DDs show red-shifted emissions is still unclear.

The emission λ_{max} of (BrStyryl)$_2$DD is 40 nm red-shifted from 4-BrStyrene, which is an indicator of electronic communication between organic moieties and DD SQ in the excited state. The emission λ_{max} of (MeOStyryl)$_2$DD is 50 nm red-shifted from 4-MeOStyrene as well as (MeOStyryl)DDvinyl, suggesting the minimal number of conjugated groups required to form a LUMO inside a DD SQ cage. However, the emission λ_{max} of octa-functionalized (MeOStyryl)$_8$T$_8$ in Table **8.1** is essentially same as that of 4-MeOStyrene. All these results support the fact that DD structured compounds show unexpected photonic characteristics.

Solvent studies indicate only 4-NH$_2$Styrene and the corresponding DD SQs show CT behavior as marked in green. The emission λ_{max} of 4-NH$_2$Styrene and (NH$_2$Styryl) DDvinyl are 7 nm red-shifted in polar ACN while the red-shift for (NH$_2$Styryl)$_2$DD is almost twice of that (Figure **8.4**).

Table 8.1. Steady-state spectra data of RStyrene and RStyryl-functionalized in DCM or ACN.

	Solvent	Abs. λ_{max} (nm)	Em. λ_{max} (nm)
(MeOStyryl)$_8$T$_8$[11]	DCM	275	326
4-NH$_2$Styrene	DCM	278	351
	ACN	280	358
4-MeOStyrene	DCM	261	324
	ACN	259	324
4-MeStyrene	DCM	254	311
Styrene	DCM	250	306
4-BrStyrene	DCM	258	313
	ACN	254	314
4-CNStyrene	DCM	266	312
	ACN	264	312
(NH$_2$Styryl)DDvinyl	DCM	292	364
	ACN	295	371
(NH$_2$Styryl)$_2$DD	DCM	292	363
	ACN	295	376
(MeOStyryl)DDvinyl	DCM	271	327
(MeOStyryl)$_2$DD	DCM	272	378
	ACN	271	374
(MeStyryl)$_2$DD	DCM	264	318
(Styryl)$_2$DD	DCM	259	309
(Styryl)$_3$DD	DCM	259	309
(BrStyryl)$_2$DD	DCM	266	354, 364
	ACN	264	343, 358
(CNStyryl)DDvinyl	DCM	271	318
(CNStyryl)$_2$DD	DCM	274	318
	ACN	271	317

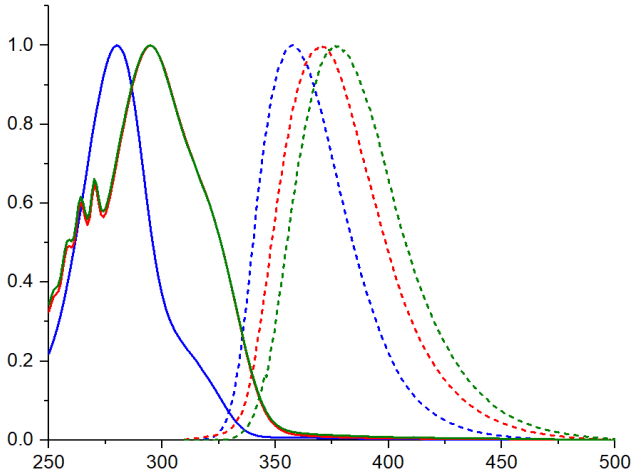

Figure 8.4. Absorption and emission of 4-NH_2Styrene (blue), (4-NH_2Styryl)DDvinyl (red) and (4-NH_2Styryl)$_2$DD.

Compared to the Gen 1 compound Styryl$_2$DD, Gen 2 (HStilV)$_2$DD exhibits a 0-0 transition as evidenced by 75 nm red-shifts in both absorption and emission, which can be ascribed solely to the extended conjugation length from styrene to stilbene-vinyl.[11] Indication of CT behavior is seen in all Stilbenevinyl-DD compounds except (HStilV)$_2$DD, as suggested by solvent studies. The emission λ_{max} are 25 and 15 nm red-shifted for (4-NH_2StilV)$_2$Me$_2$DD and (4-MeOStilV)$_2$Me$_2$DD respectively in ACN. It is notable that the degree of such red shifts is comparable to corresponding (4-MeO/NH_2StilV)$_8$T$_8$ despite having only two organic groups attached, likely suggesting that the conjugated stilbenes overlap better with the LUMO despite two siloxane linkages.

Table 8.2. Steady-state spectra data of Stilbene-compounds.

	Solvent	Abs. λ_{max} (nm)	Em. λ_{max} (nm)
4-VinylStilbene	DCM	329	374
	ACN	325	369
(4-NH_2StilV)$_8$T$_8$	DCM	358	482
	ACN	361	507
(4-MeOStilV)$_8$T$_8$	DCM	345	418
	ACN	343	431
(4-NH_2StilV)$_2$DD	DCM	357	484
	ACN	360	510
(4-MeOStilV)$_2$DD	DCM	346	433
	ACN	343	446
(HStilV)$_2$DD	DCM	335	385
	ACN	334	386
(4-CNStilV)$_2$Me$_2$DD	DCM	346	442
	ACN	343	460
(4-MeOStilV)MeDDMe(4-CNStilV)	DCM	346	430
	ACN	343	441

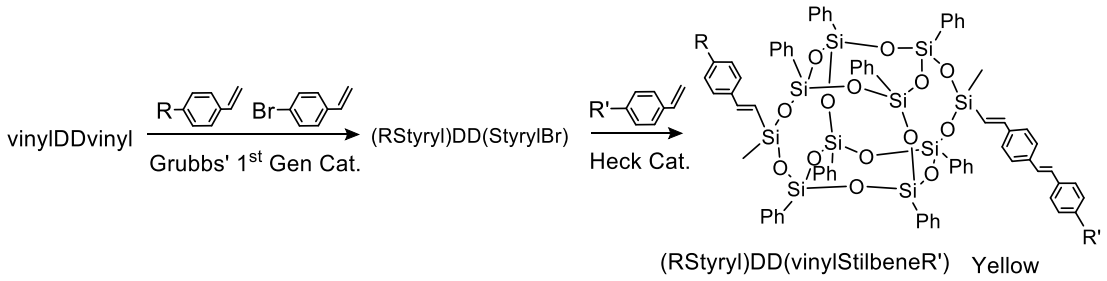

Scheme 8.5. Synthesis of symmetrical and unsymmetrical molecular DD compounds (Gen 1.5).

In addition to the above Gen1 and 2 compounds, we also synthesized Gen 1.5 (Scheme **8.5**) with styryl functionalization on one side and stilbenevinyl on the other. One example is shown in Figure **8.5**, which displays a broad absorption spectrum with two separate peaks and an emission that is the average of the corresponding Gen 1 and 2. Future work could explore donor-acceptor systems ranging from strongly electron withdrawing (e.g. CF_3) to electron donating (e.g. NH_2) to probe photo-physical properties as above.

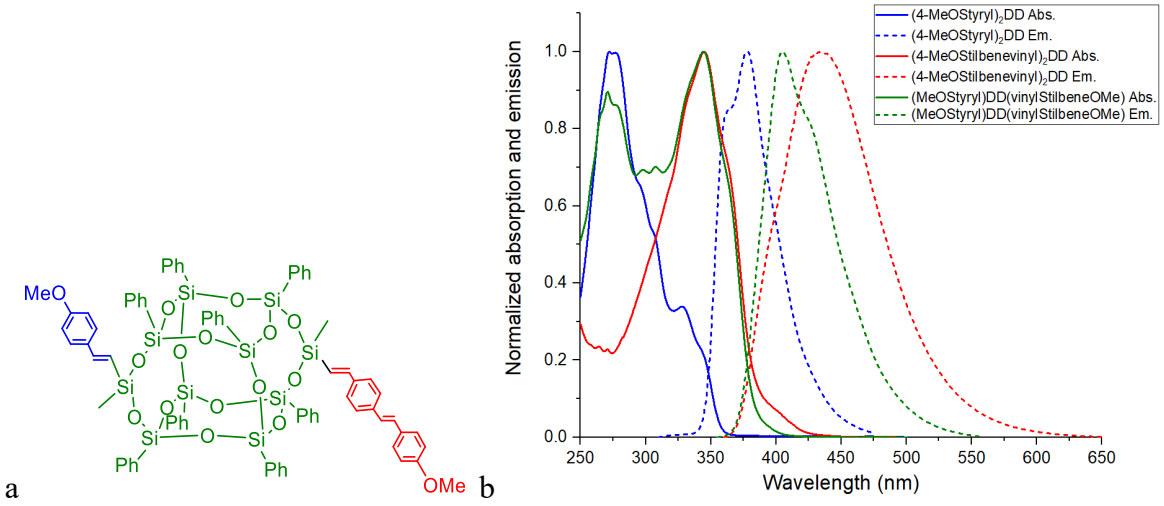

Figure 8.5. (a) Structure of unsymmetrical DD compounds; (b) Uv-Vis for set of model compounds with moieties of different degrees of conjugation.

References

(1) Chan, K. L.; Sonar, P.; Sellinger, A. Cubic Silsesquioxanes for Use in Solution Processable Organic Light Emitting Diodes (OLED). *J. Mater. Chem.* **2009**, *19* (48), 9103. https://doi.org/10.1039/b909234j.

(2) Froehlich, J. D.; Young, R.; Nakamura, T.; Ohmori, Y.; Li, S.; Mochizuki, A.; Lauters, M.; Jabbour, G. E. Synthesis of Multi-Functional POSS Emitters for OLED Applications. *Chem. Mater.* **2007**, *19* (20), 4991–4997. https://doi.org/10.1021/cm070726v.

(3) *Applications of Polyhedral Oligomeric Silsesquioxanes*; Hartmann-Thompson, C., Ed.; Advances in Silicon Science; Springer Netherlands: Dordrecht, 2011; Vol. 3. https://doi.org/10.1007/978-90-481-3787-9.

(4) Guan, J.; Tomobe, K.; Madu, I.; Goodson, T.; Makhal, K.; Trinh, M. T.; Rand, S. C.; Yodsin, N.; Jungsuttiwong, S.; Laine, R. M. Photophysical Properties of Functionalized Double Decker Phenylsilsesquioxane Macromonomers: [PhSiO $_{1.5}$] $_{8}$ [OSiMe $_{2}$] $_{2}$ and [PhSiO $_{1.5}$] $_{8}$ [O $_{0.5}$ SiMe $_{3}$] $_{4}$. Cage-Centered Lowest Unoccupied Molecular Orbitals Form Even When Two Cage Edge Bridges Are Removed, Verified by Modeling and Ultrafast Magnetic Light Scattering Experiments. *Macromolecules* **2019**, *52* (19), 7413–7422. https://doi.org/10.1021/acs.macromol.9b00700.

(5) Guan, J.; Tomobe, K.; Madu, I.; Goodson, T.; Makhal, K.; Trinh, M. T.; Rand, S. C.; Yodsin, N.; Jungsuttiwong, S.; Laine, R. M. Photophysical Properties of Partially Functionalized Phenylsilsesquioxane: [RSiO $_{1.5}$] $_{7}$ [Me/NPrSiO $_{1.5}$] and [RSiO $_{1.5}$] $_{7}$ [O $_{0.5}$ SiMe $_{3}$] $_{3}$ (R = 4-Me/4-CN-Stilbene). Cage-Centered Magnetic Fields Form under Intense Laser Light. *Macromolecules* **2019**, *52* (11), 4008–4019. https://doi.org/10.1021/acs.macromol.9b00699.

(6) Guan, J.; Arias, J. J. R.; Tomobe, K.; Ansari, R.; Marques, M. de F. V.; Rebane, A.; Mahbub, S.; Furgal, J. C.; Yodsin, N.; Jungsuttiwong, S.; Hashemi, D.; Kieffer, J.; Laine, R. M. Unconventional Conjugation via VinylMeSi(O−) $_{2}$ Siloxane Bridges May Imbue Semiconducting Properties in [Vinyl(Me)SiO(PhSiO $_{1.5}$) $_{8}$ OSi(Me)Vinyl-Ar] Double-Decker Copolymers. *ACS Appl. Polym. Mater.* **2020**, *2* (9), 3894–3907. https://doi.org/10.1021/acsapm.0c00591.

(7) Guan, J.; Sun, Z.; Ansari, R.; Liu, Y.; Endo, A.; Unno, M.; Ouali, A.; Mahbub, S.; Furgal, J. C.; Yodsin, N.; Jungsuttiwong, S.; Hashemi, D.; Kieffer, J.; Laine, R. M. Conjugated Copolymers That Shouldn't Be. *Angewandte Chemie International Edition* **2021**, *60* (20), 11115–11119. https://doi.org/10.1002/anie.202014932.

(8) Liu, Y.; Onodera, K.; Takeda, N.; Ouali, A.; Unno, M. Synthesis and Characterization of Functionalizable Silsesquioxanes with Ladder-Type Structures. *Organometallics* **2019**, *38* (22), 4373–4376. https://doi.org/10.1021/acs.organomet.9b00597.

(9) Liu, Y.; Takeda, N.; Ouali, A.; Unno, M. Synthesis, Characterization, and Functionalization of Tetrafunctional Double-Decker Siloxanes. *Inorg. Chem.* **2019**, *58* (7), 4093–4098. https://doi.org/10.1021/acs.inorgchem.9b00416.

(10) Kularatne, R. S.; Magurudeniya, H. D.; Sista, P.; Biewer, M. C.; Stefan, M. C. Donor–Acceptor Semiconducting Polymers for Organic Solar Cells. *Journal of Polymer Science Part A: Polymer Chemistry* **2013**, *51* (4), 743–768. https://doi.org/10.1002/pola.26425.

(11) Sulaiman, S.; Bhaskar, A.; Zhang, J.; Guda, R.; Goodson, T.; Laine, R. M. Molecules with Perfect Cubic Symmetry as Nanobuilding Blocks for 3-D Assemblies. Elaboration of Octavinylsilsesquioxane. Unusual Luminescence Shifts May Indicate Extended Conjugation Involving the Silsesquioxane Core. *Chem. Mater.* **2008**, *20* (17), 5563–5573. https://doi.org/10.1021/cm801017e.

Appendix A. Characterization of Partially Functionalized Phenylsilsesquioxane: $[RSiO_{1.5}]_7[Me/nPr\text{-}SiO_{1.5}]$ and $[RSiO_{1.5}]_7[O_{0.5}SiMe_3]_3$ (R = 4-Me/4-CN-Stilbene)

Table A.1. MALDI-TOF, GPC and ^{1}H-NMR data for Ph_7T_8R' and $Ph_7T_7(TMS)_3$.

	MALDI-TOF[a] (m/z)		GPC			^{1}H-NMR peaks (ppm)
	mass[b]	calcd	M_n	M_w	PDI	
Ph_7T_8Me	1079	1078	715	725	1.01	7.74 (m, 14H, Ph); 7.36 (m, 21H, Ph); 0.31 (s, 3H, Me)
Ph_7T_8Pr	1107	1106	757	770	1.02	7.73 (m, 14H, Ph); 7.36 (m, 21H, Ph); 1.53 (m, 2H, nPr); 0.98 (t, 3H, nPr); 0.85 (t, 2H, nPr)
$Ph_7T_7(TMS)_3$	1255	1254	766	779	1.02	7.43 (m, 7H, Ph); 7.31 (m, 14H, Ph); 7.12 (m, 14H, Ph); 0.25 (s, 27H, Me)

[a] As Ag^+ adduct. [b] As H^+ adduct.

Table A.2. ^{1}H-NMR peaks of *o*-$Br_xPh_7T_8R'$ and *p*-$I_xPh_7T_8R'$.

Compound	^{1}H-NMR peaks (ppm)
o-$Br_6Ph_7T_8Me$	7.73 (m, 7H, Ph); 7.54 (m, 7H, Ph); 7.37 (m, 7H, Ph); 7.26 (d, 7H, Ph); 0.42 (s, 3H, Me)
o-$Br_7Ph_7T_8Pr$	7.74 (m, 7H, Ph); 7.54 (m, 7H, Ph); 7.37 (m, 7H, Ph); 7.26 (d, 7H, Ph); 1.53 (m, 2H, nPr); 0.96 (t, 3H, nPr); 0.85 (t, 2H, nPr)
p-$I_7Ph_7T_8Me$	7.72 (d, 14H, Ph); 7.37 (d, 14H, Ph); 0.34 (s, 3H, Me)
p-$I_7Ph_7T_8Pr$	7.72 (d, 14H, Ph); 7.37 (d, 14H, Ph); 1.52 (m, 2H, nPr); 0.93 (t, 3H, nPr); 0.81 (t, 2H, nPr)

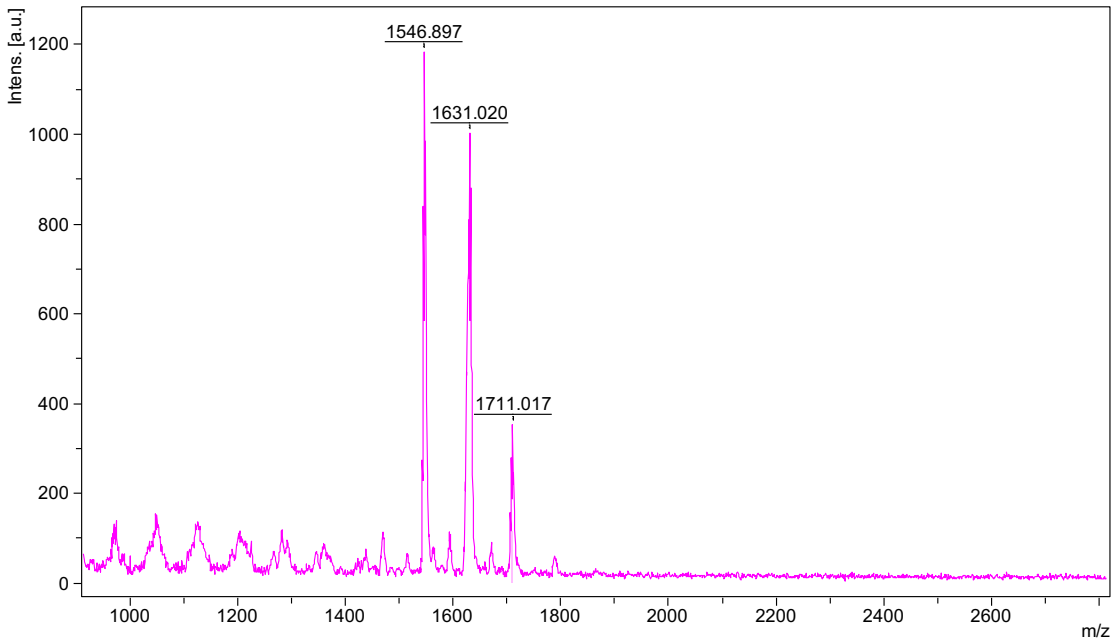

Figure A.1. MALDI-TOF of *o*-$Br_xPh_7T_8Me$.

Table A.3. MALDI-TOF ([a] As Ag^+ adduct), TGA and GPC data for *o*-$Br_xPh_7T_8R$', *o*-$RStil_xT_8R$', *p*-$I_xPh_7T_8R$', *p*-$RStil_xT_8R$', *o*-$Br_xPh_7T_7(TMS)_3$, *o*-$RStil_xT_7(TMS)_3$, *p*-$I_xPh_7T_7(TMS)_3$ and *p*-$RStil_xT_7(TMS)_3$.

	MALDI-TOF (m/z)	TGA (ceramic yield, %)			GPC		
	mass	actual	calcd	$T_{d5\%}$ (°C)	M_n	M_w	PDI
o-$Br_6Ph_7T_8Me$	1546[a]	30	32	436	531	540	1.02
o-$MeStil_6T_8Me$	1659	30	29	444	846	877	1.04
o-$CNStil_6T_8Me$	1843[a]	28	28	439	1286	1386	1.08
o-$Br_7Ph_7T_8Pr$	1540	31	31	435	546	556	1.02
o-$MeStil_7T_8Pr$	1812	28	27	414	1456	1550	1.03
o-$CNStil_6T_8Pr$	1871[a]	27	27	417	1322	1428	1.08
p-$I_7Ph_7T_8Me$	1962[a]	26	26	406	428	496	1.16
p-$MeStil_7T_8Me$	1894[a]	28	27	448	897	1196	1.33
p-$CNStil_7T_8Me$	1971[a]	26	26	443	1007	1151	1.14
p-$I_7Ph_7T_8Pr$	1990[a]	26	26	396	412	498	1.20
p-$MeStil_7T_8Pr$	1921[a]	27	27	454	765	848	1.11
p-$CNStil_7T_8Pr$	1999[a]	25	25	435	998	1231	1.23
o-$Br_7Ph_7T_7(TMS)_3$	1699				858	897	1.05
o-$MeStil_7T_7(TMS)_3$	2080[a]	30	31	415	1322	1434	1.08
o-$CNStil_7T_7(TMS)_3$	2137[a]	28	28	402	2193	2519	1.15
p-$I_2Ph_7T_7(TMS)_3$	1506[a]				931	965	1.04
p-$MeStil_2Ph_5T_7(TMS)_3$	1415[a]				1700	1987	1.17

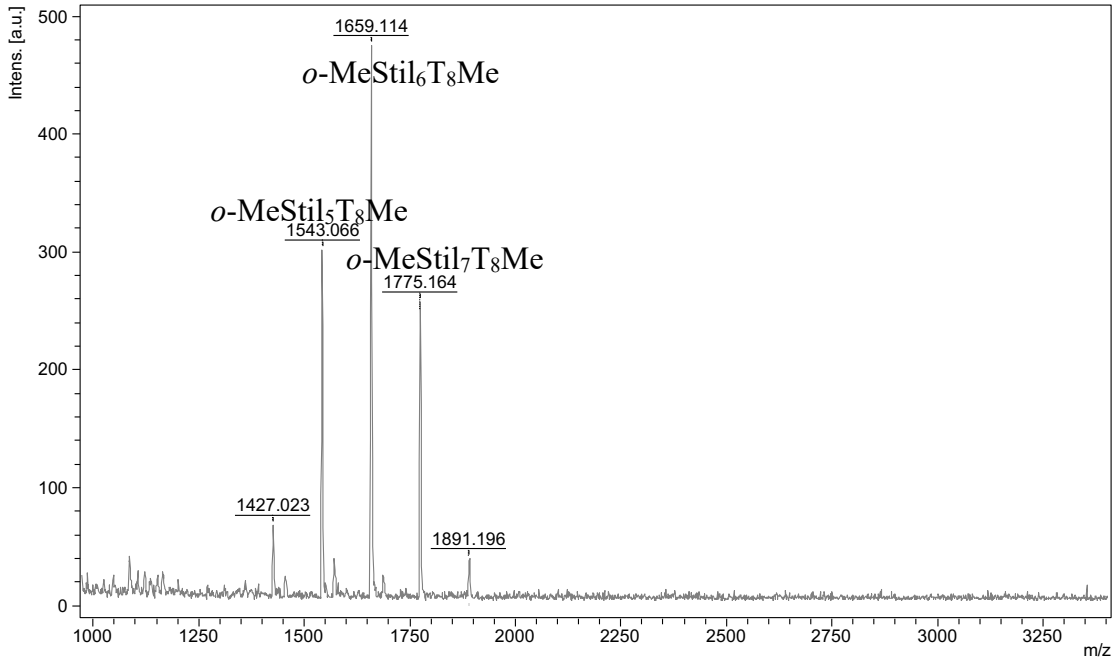

Figure A.2. MALDI-TOF of *o*-$MeStil_xT_8Me$.

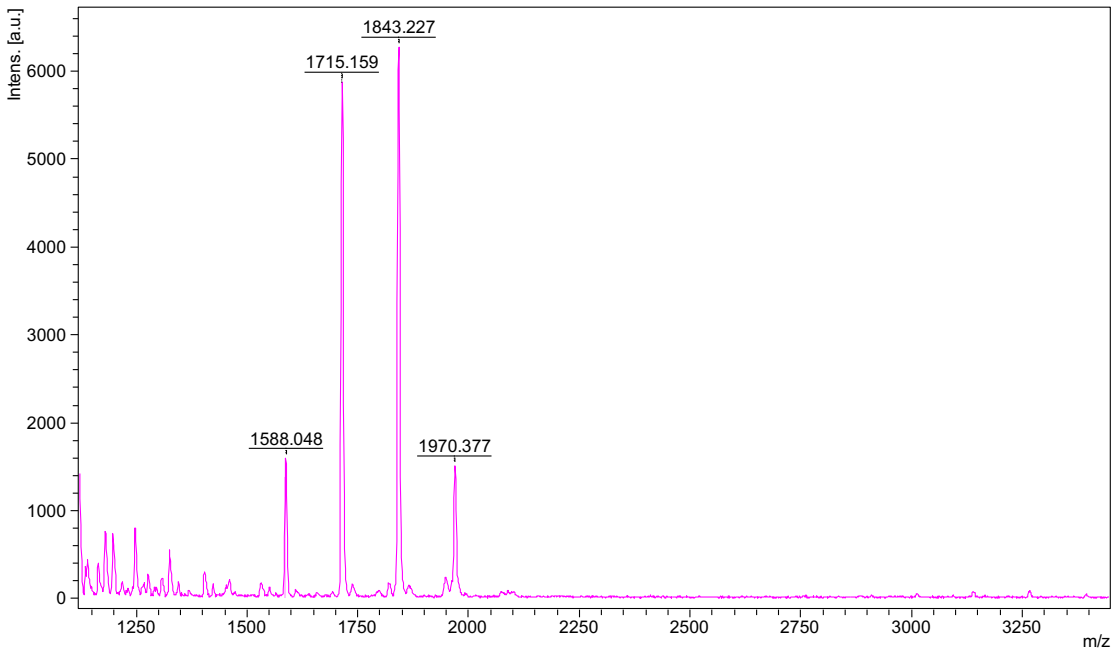

Figure A.3. MALDI-TOF of *o*-CNStil$_x$T$_8$Me.

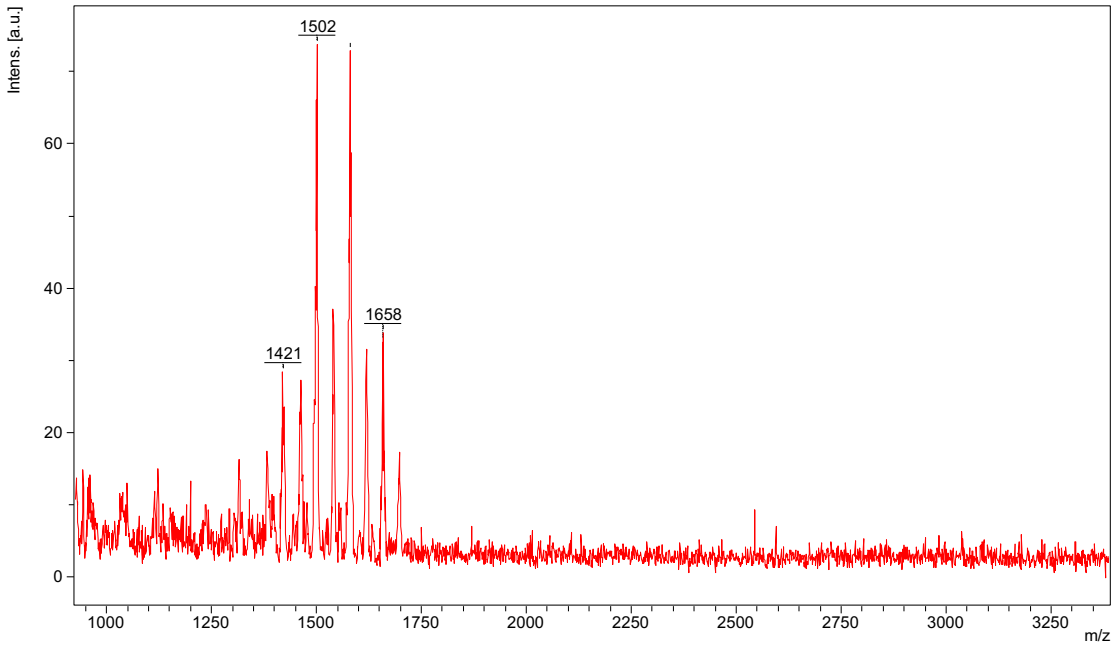

Figure A.4. MALDI-TOF of *o*-Br$_x$Ph$_7$T$_8$Pr.

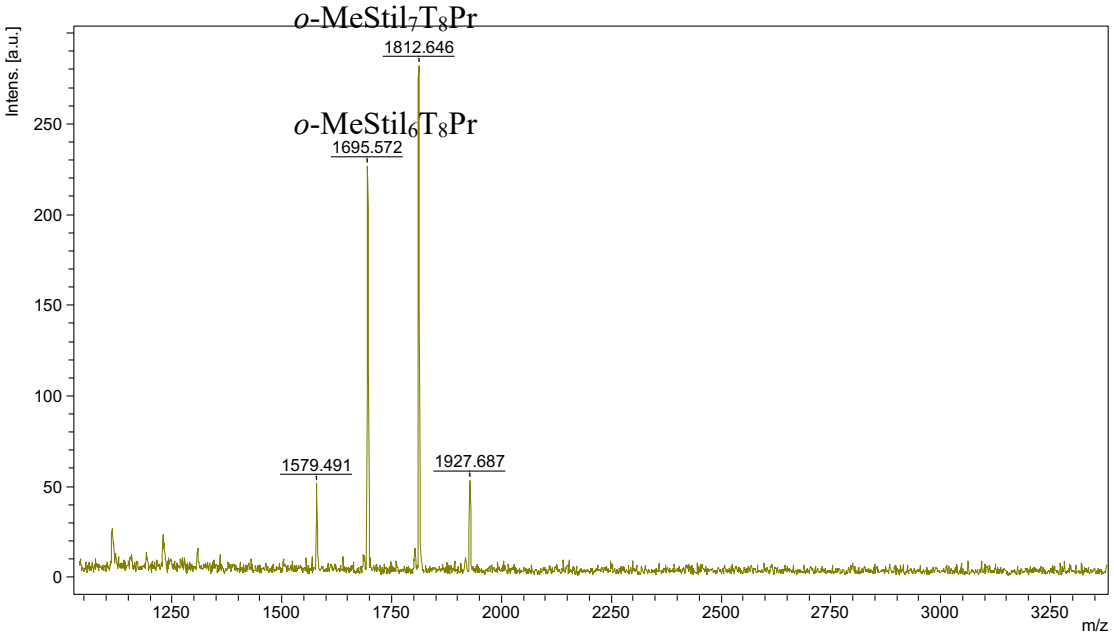

Figure A.5. MALDI-TOF of *o*-MeStil$_x$T$_8$Pr.

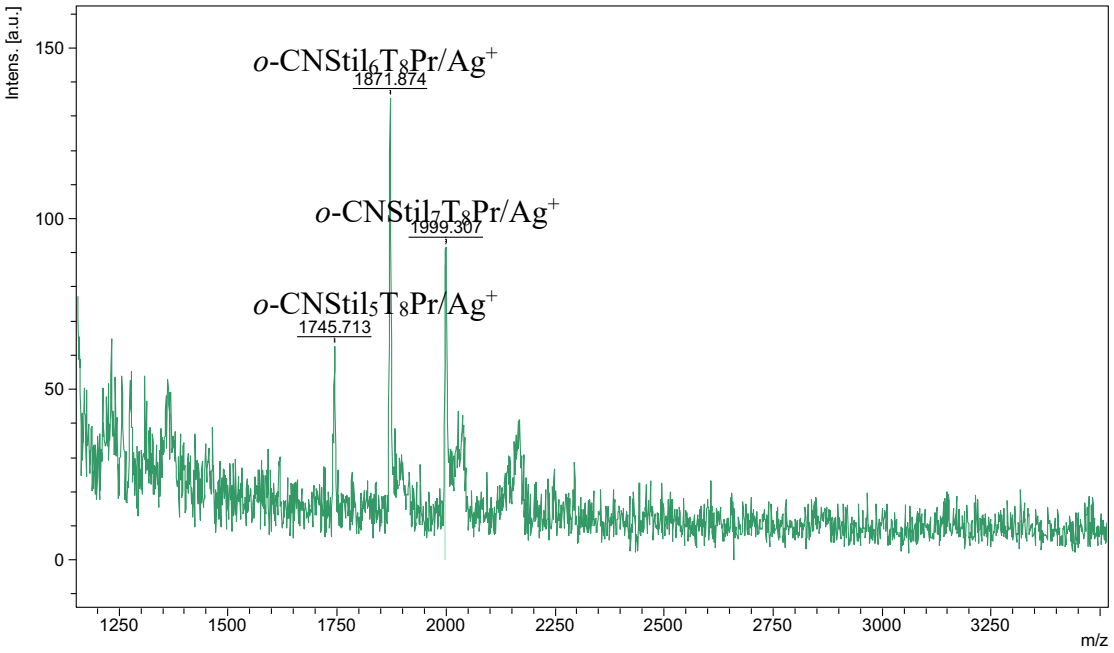

Figure A.6. MALDI-TOF of *o*-CNStil$_x$T$_8$Pr.

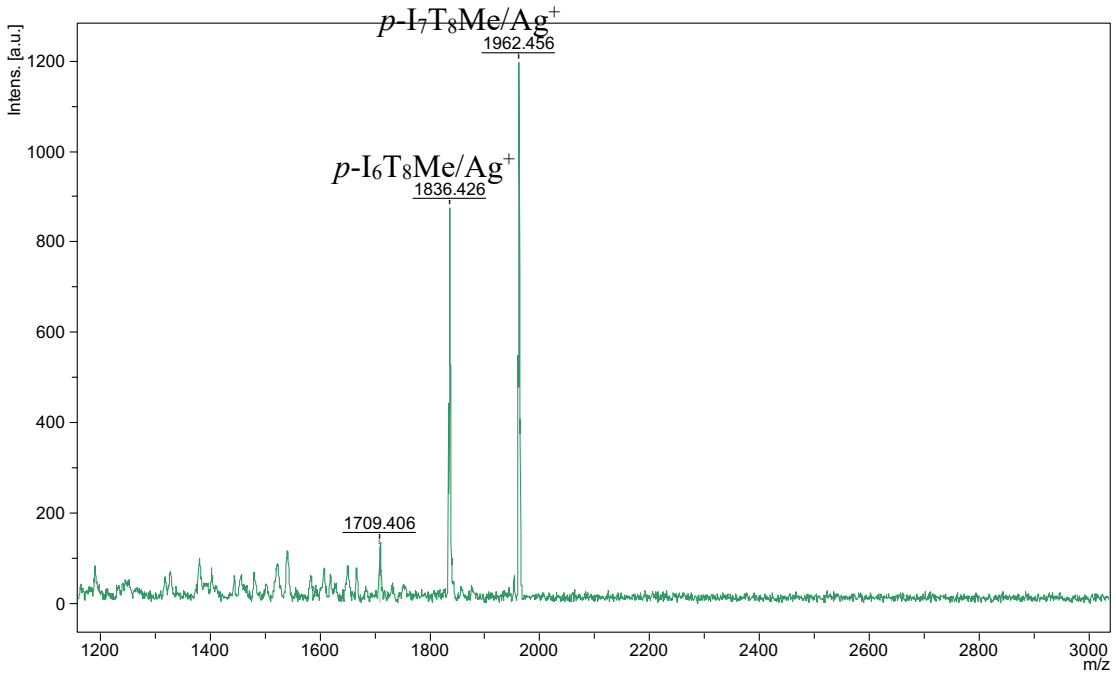

Figure A.7. MALDI-TOF of *p*-$I_xPh_7T_8Me$.

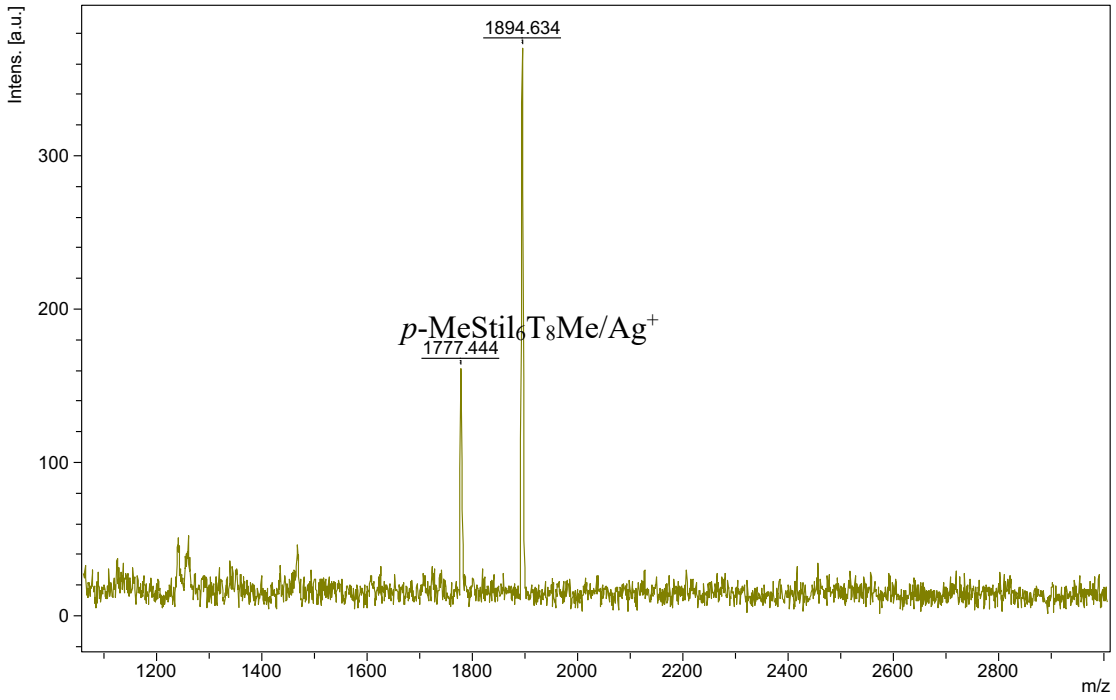

Figure A.8. MALDI-TOF of *p*-$MeStil_xT_8Me$.

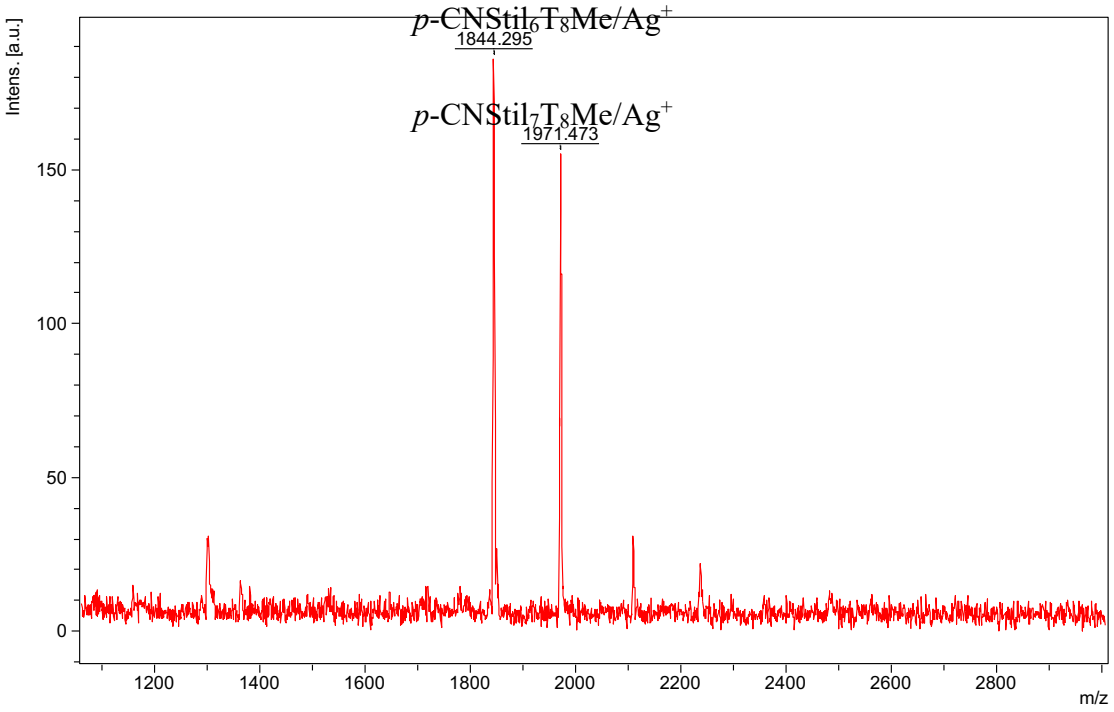

Figure A.9. MALDI-TOF of *p*-CNStil$_x$T$_8$Me.

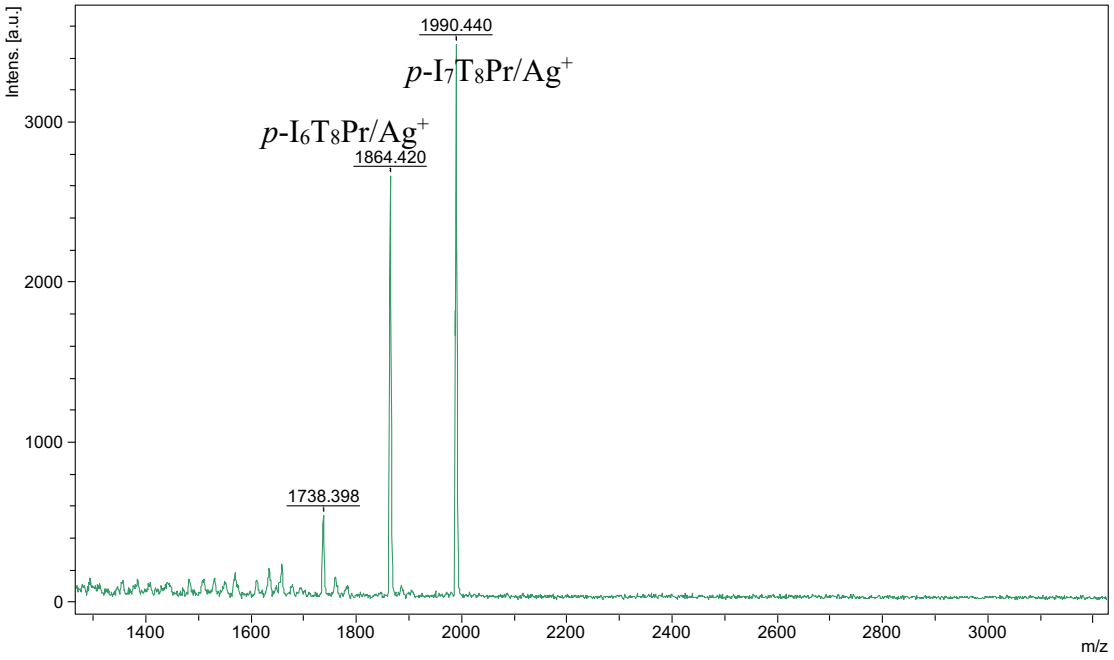

Figure A.10. MALDI-TOF of *p*-I$_x$ Ph$_7$T$_8$Pr.

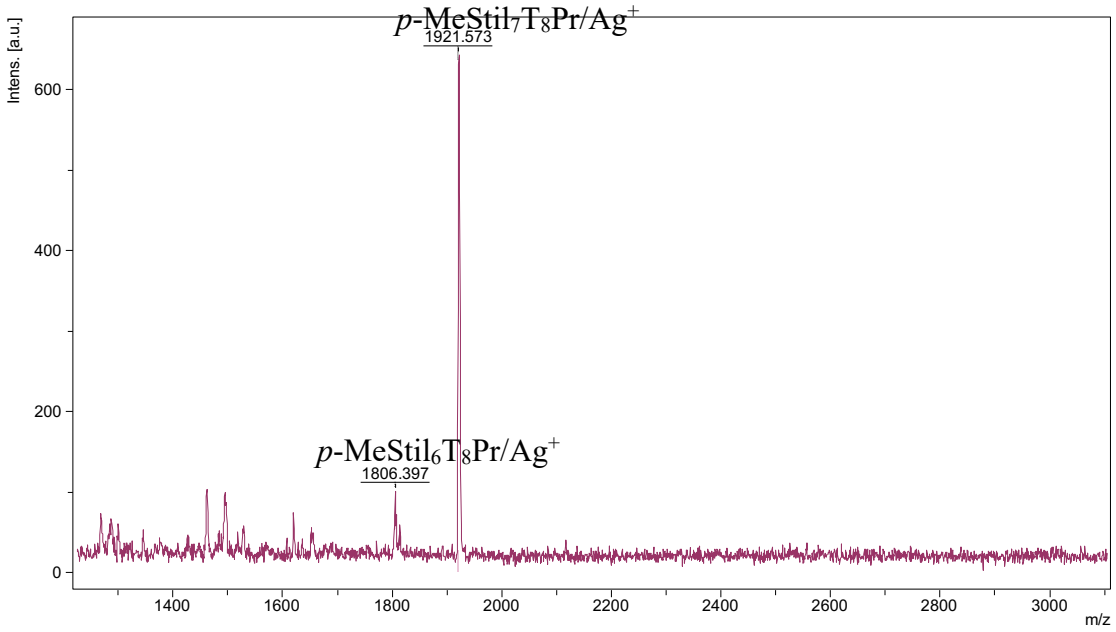

Figure A.11. MALDI-TOF of *p*-MeStil$_x$T$_8$Pr.

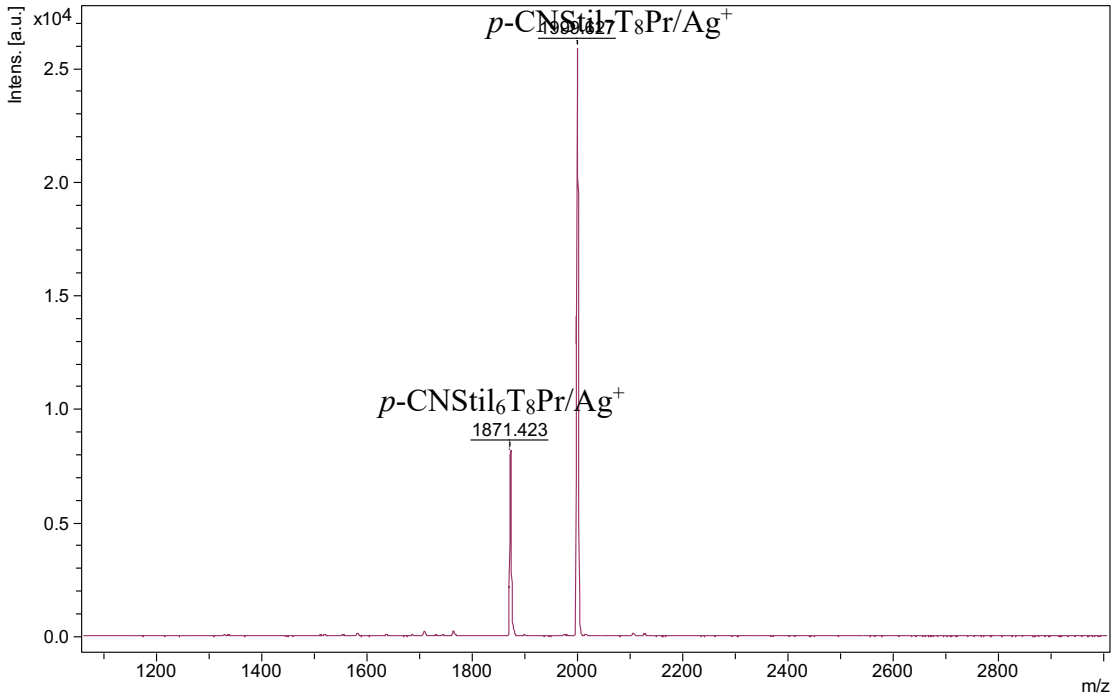

Figure A.12. MALDI-TOF of *p*-CNStil$_x$T$_8$Pr.

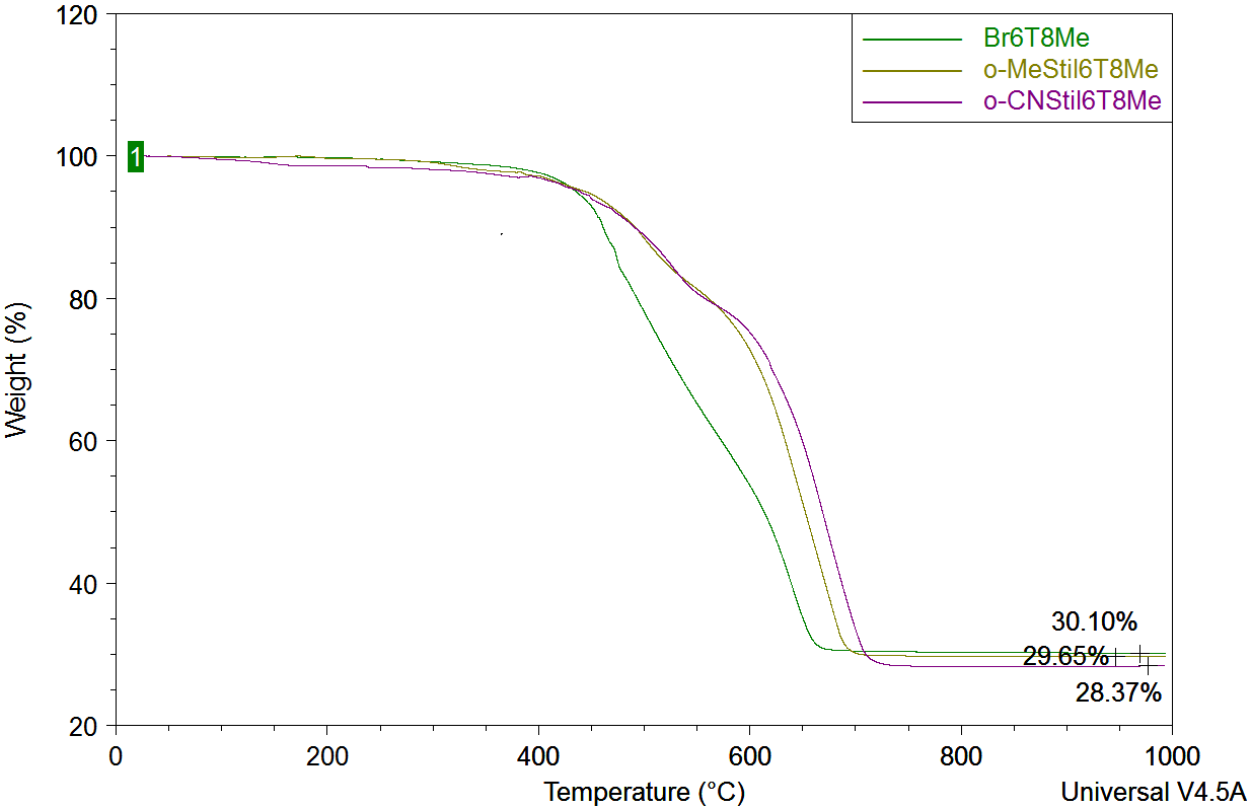

Figure A.13. TGA of $Br_6Ph_7T_8Me$ and o-$RStil_6T_8Me$.

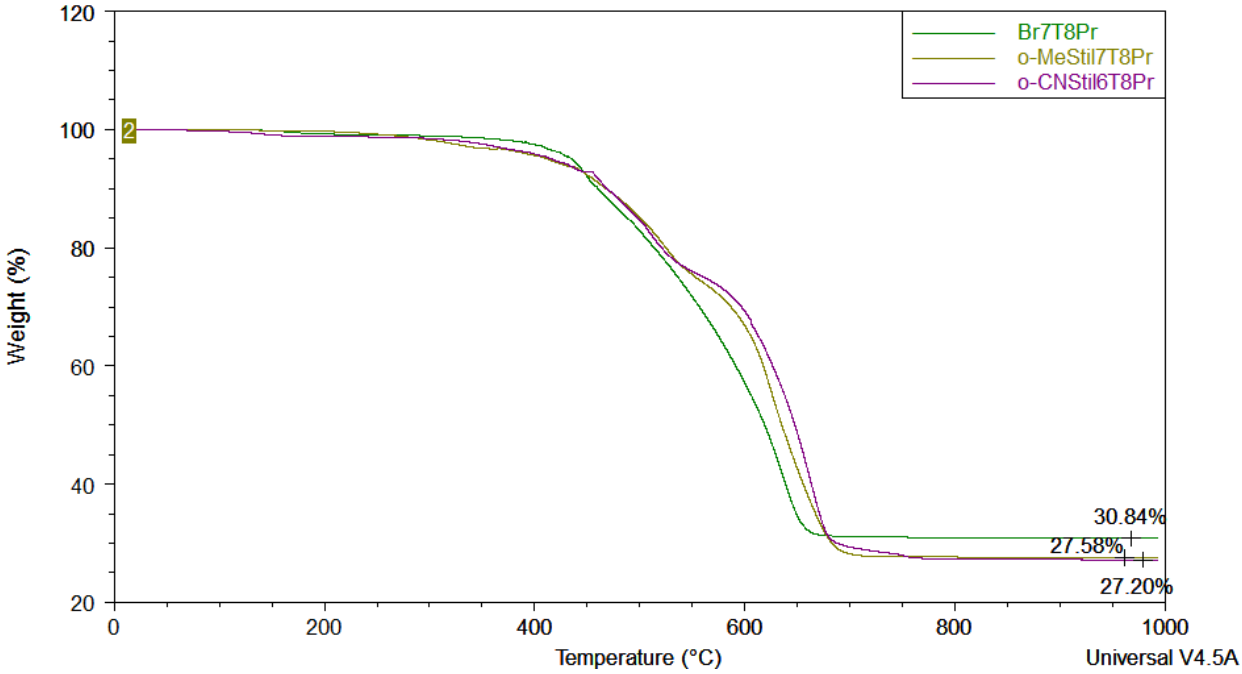

Figure A.14. TGA of $Br_7Ph_7T_8Pr$ and *o*-$RStil_xT_8Pr$.

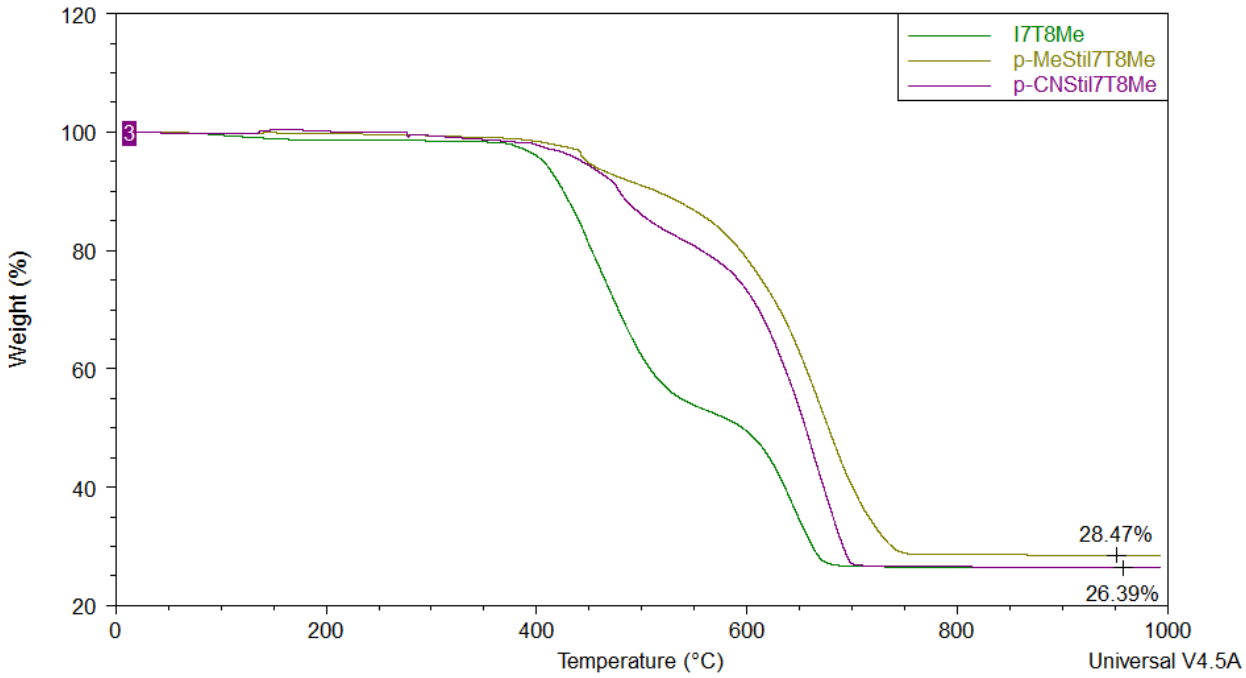

Figure A.15. TGA of $I_7Ph_7T_8Me$ and *p*-$RStil_7T_8Me$.

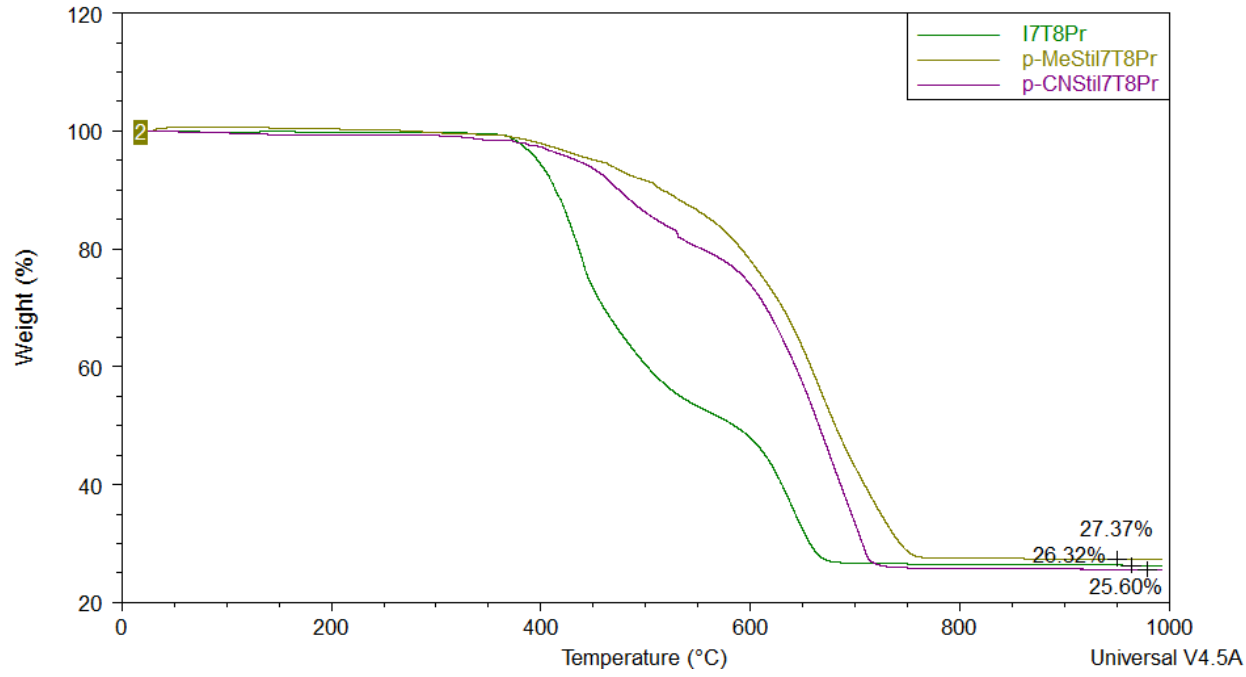

Figure A.16. TGA of $I_7Ph_7T_8Pr$ and *p*-$RStil_7T_8Pr$.

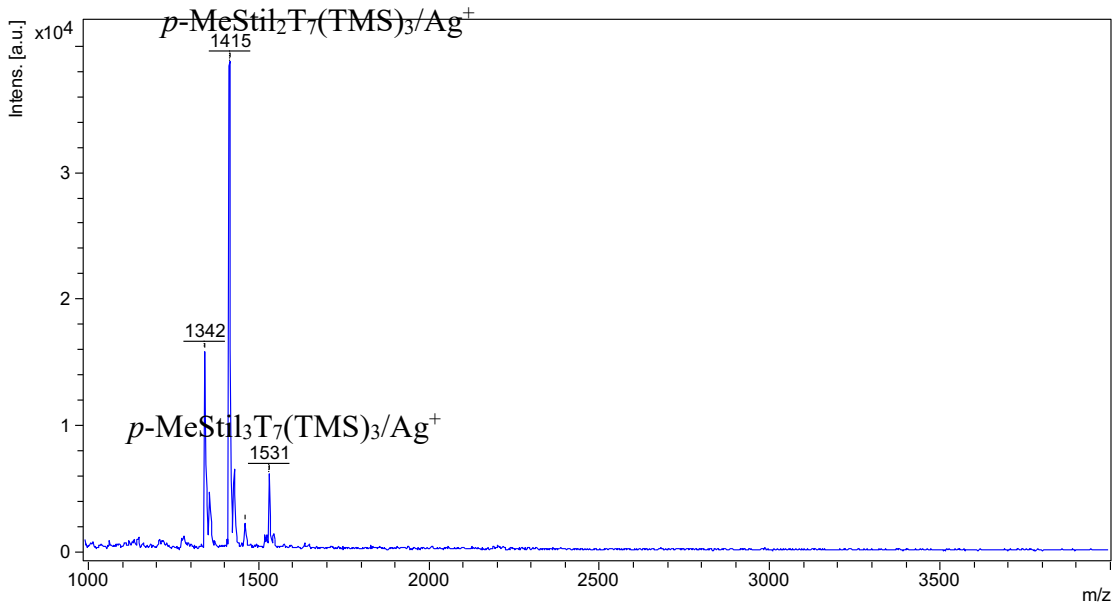

Figure A.17. MALDI of *p*-MeStil$_2$Ph$_5$T$_7$(TMS)$_3$.

Appendix B. Characterization of Partially Functionalized Double Decker Phenylsilsesquioxane Macromonomers: $[PhSiO_{1.5}]_8[O0.5SiMe_2]_2$ and $[PhSiO_{1.5}]_8[O_{0.5}SiMe_3]_4$

Table B.1. ^{1}H-NMR peaks for $DDMe_4$ and $DD(OTMS)_4$.

	^{1}H-NMR peaks (ppm)
$DDMe_4$	7.53 (t, 8H, Ph); 7.39 (m, 16H, Ph); 7.17 (d, 16H, Ph); 0.31 (s, 12H, Me)
$DD(OTMS)_4$	7.52 (m, 8H, Ph); 7.36 (m, 16H, Ph); 7.27 (m, 8H, Ph); 7.16 (t, 8H, Ph); 0.10 (s, 36H, Me)

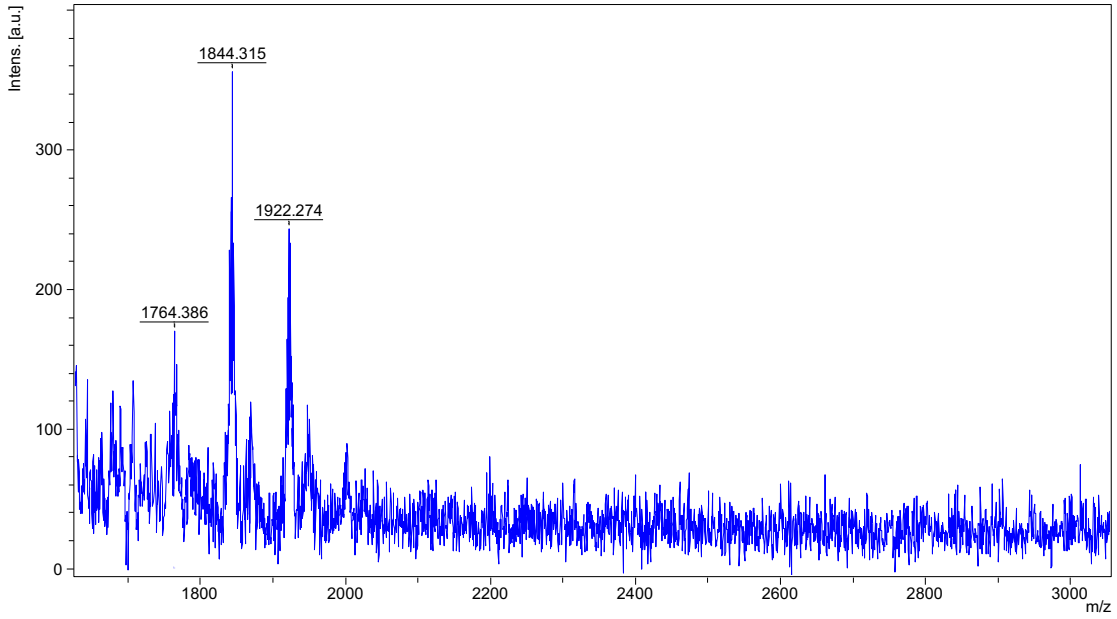

Figure B.1. MALDI-TOF of *o*-Br_7DDMe_4.

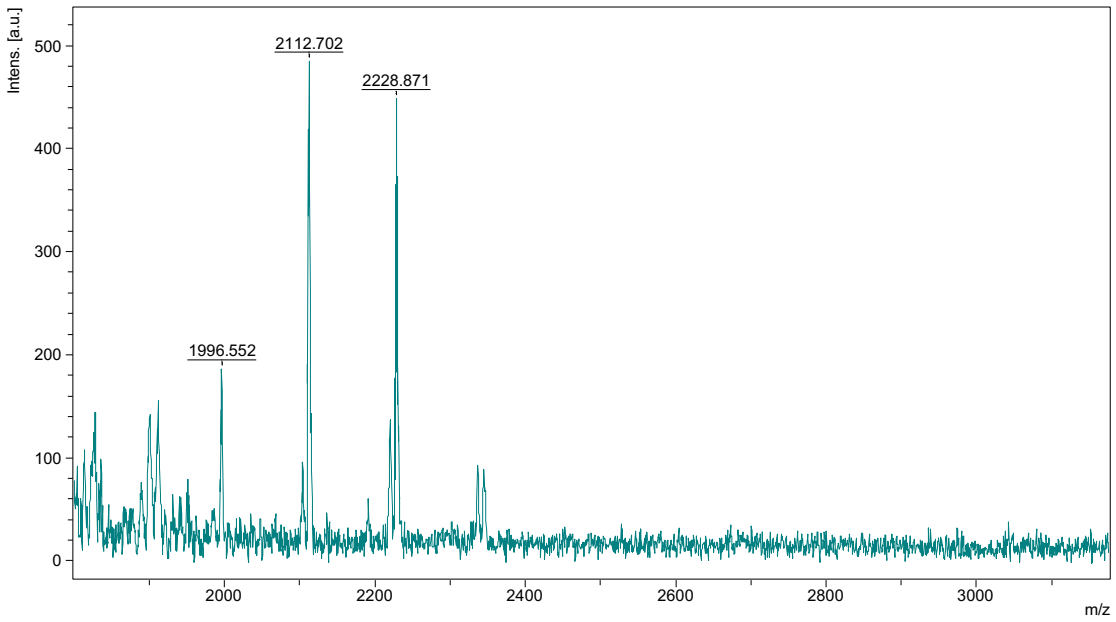

Figure B.2. MALDI-TOF of *o*-MeStil$_7$DDMe$_4$.

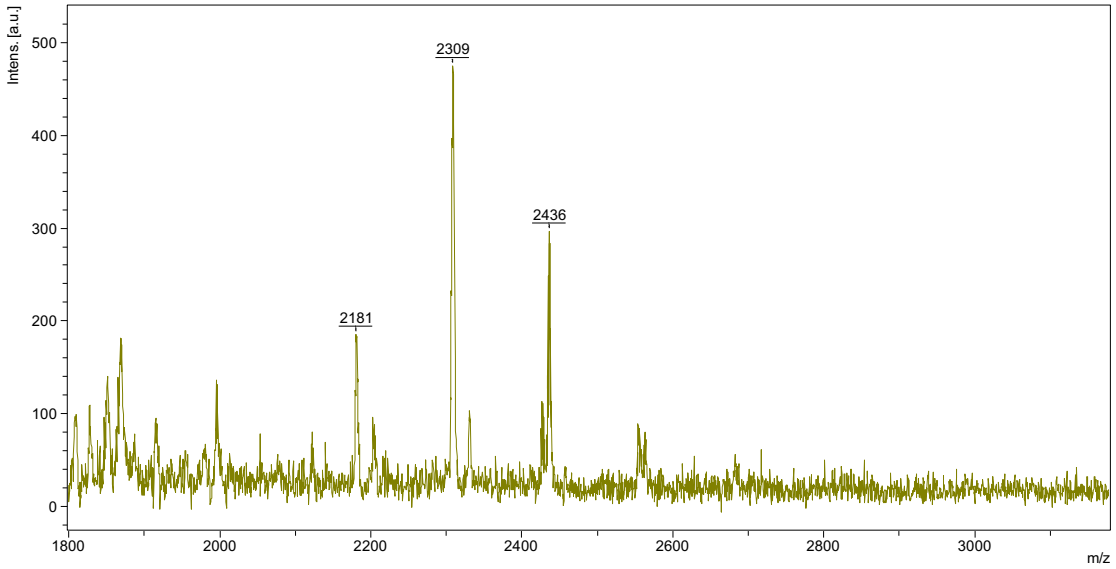

Figure B.3. MALDI-TOF of *o*-CNStil$_8$DDMe$_4$.

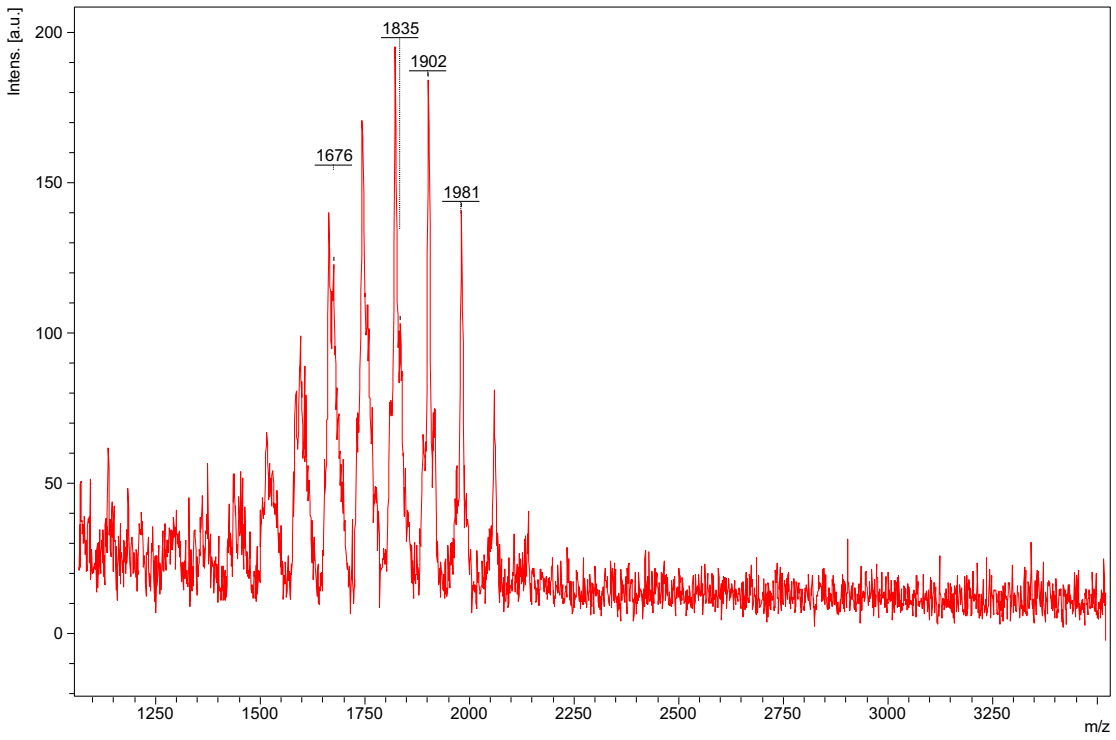

Figure B.4. MALDI-TOF of *o*-Br_7DD$(TMS)_4$.

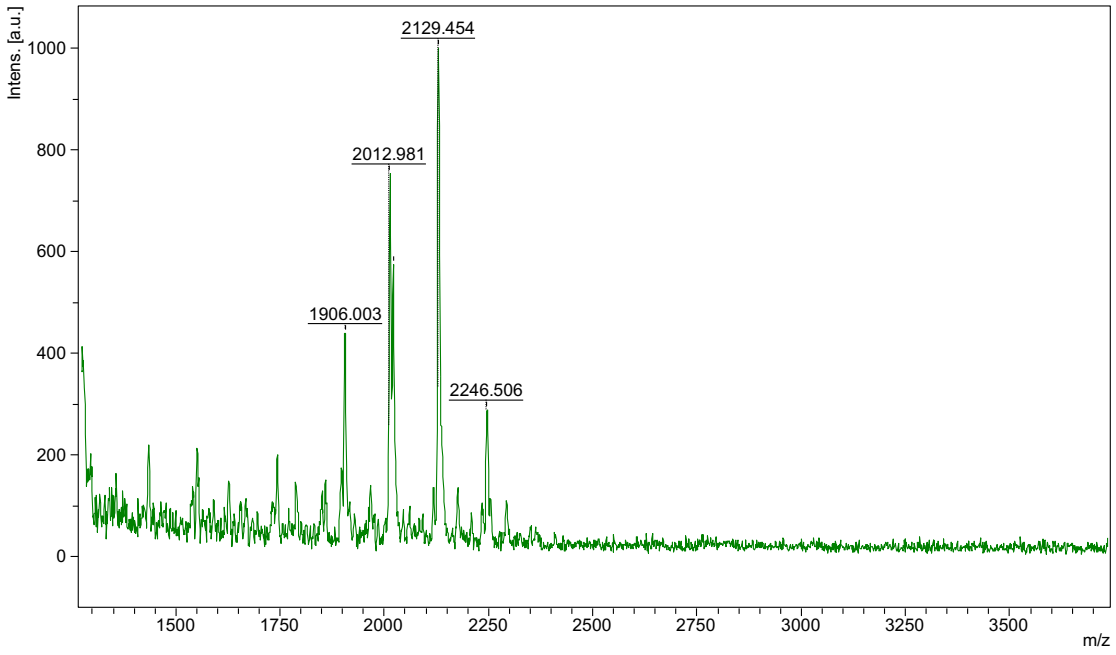

Figure B.5. MALDI-TOF of *o*-MeStil$_7$DD$(OTMS)_4$.

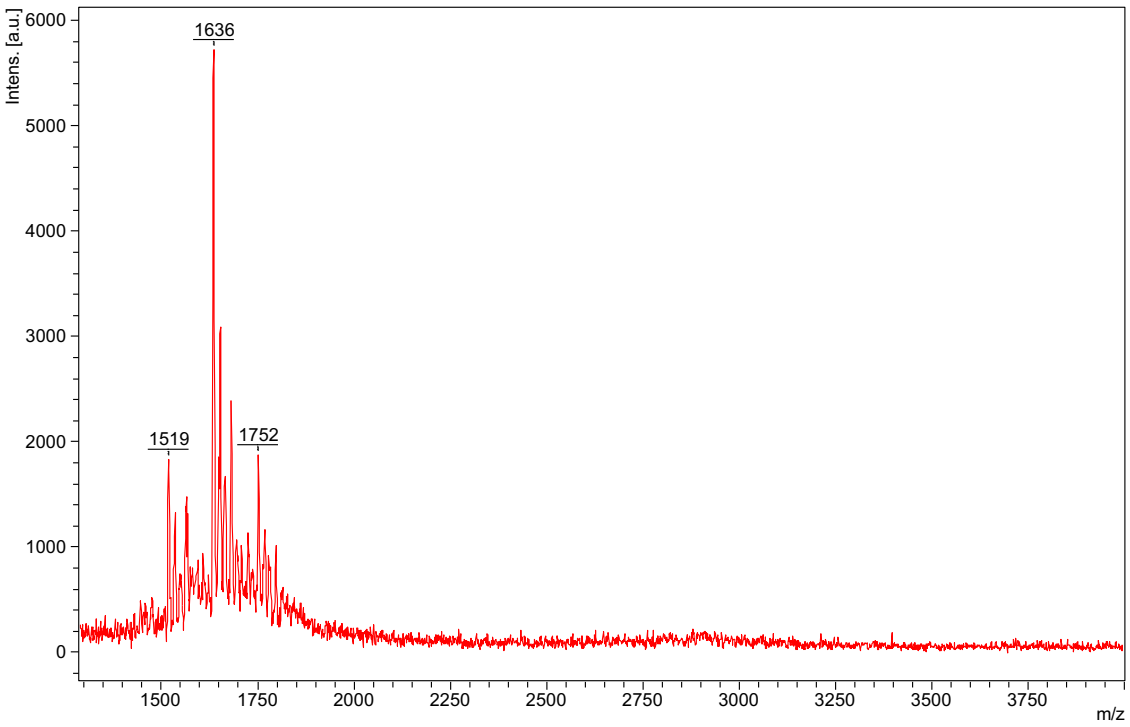

Figure B.6. MALDI-TOF of *p*-MeStil$_2$Ph$_6$DD(OTMS)$_4$.

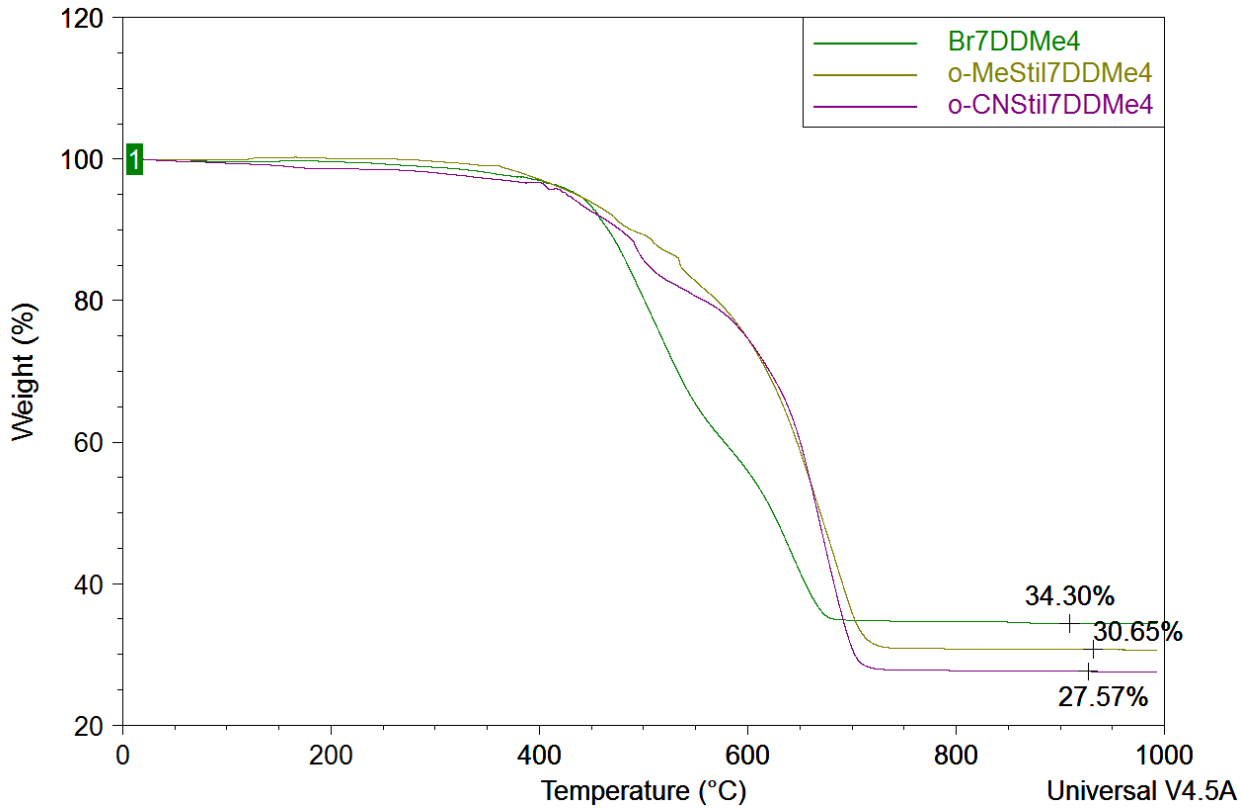

Figure B.7. TGA of *o*-Br$_7$DDMe$_4$ and *o*-RStil$_7$DDMe$_4$.

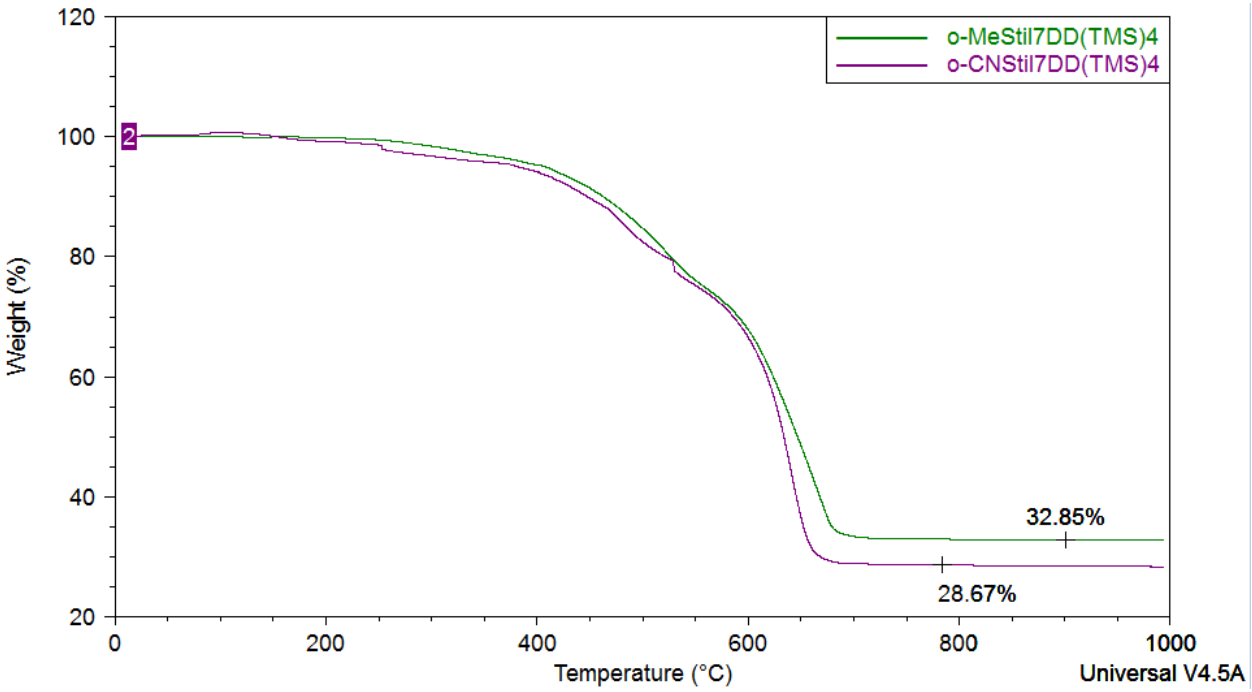

Figure B.8. TGA of *o*-RStil$_7$DD(OTMS)$_4$.

Appendix C. Unconventional Conjugation via Siloxane Bridges May Imbue Semiconducting Properties in Double Decker Copolymers

Table C.1. ^{1}H-NMR peaks of model silane compounds.

Compound	1H-NMR peaks (ppm)
1,4-[(MeO)2Sivinyl]2benzene	7.39 (d, 4H, Ph); 7.17 (d, 2H, vinyl); 6.31 (d, 2H, vinyl); 3.62 (s, 12H, MeO); 0.30 (s, 6H, Me)
4,4'-[(MeO)2Sivinyl]2biphenyl	7.64 (d, 4H, Ph); 7.41 (d, 4H, Ph); 7.09 (d, 2H, vinyl); 6.22 (d, 2H, vinyl); 3.60 (s, 12H, MeO); 0.27 (s, 6H, Me)
4,4''-[(MeO)2Sivinyl]2terphenyl	7.69 (d, 4H, Ph); 7.63 (d, 4H, Ph); 7.57 (d, 4H, Ph); 7.16 (d, 2H, vinyl); 6.33 (d, 2H, vinyl); 3.60 (s, 12H, MeO); 0.30 (s, 6H, Me)
4,4'-[(MeO)2Sivinyl]2stilbene	7.52 (d, 4H, Ph); 7.44 (d, 4H, Ph); 7.20 (m, 4H, vinyl); 6.33 (d, 2H, vinyl); 3.62 (s, 12H, MeO); 0.33 (s, 6H, Me)
2,5-[(MeO)2Sivinyl]2thiophene	7.22 (d, 2H, thiophene); 7.21 (d, 2H, vinyl); 6.40 (d, 2H, vinyl); 3.70 (s, 12H, MeO); 0.30 (s, 6H, Me)
5,5'-[(MeO)2Sivinyl]2bithiophene	7.61 (m, 2H, thiophene); 7.22 (m, 2H, thiophene); 7.11 (d, 2H, vinyl); 6.23 (d, 2H, vinyl); 3.61 (s, 12H, MeO); 0.29 (s, 6H, Me)
2,5-[(MeO)2Sivinyl]2thienothiophene	7.49 (s, 2H, thiophene); 7.21 (d, 2H, vinyl); 6.41 (d, 2H, vinyl); 3.70 (s, 12H, MeO); 0.30 (s, 6H, Me)
2,7-[(MeO)2Sivinyl]2dimethylfluorene	7.98 (m, 2H, fluorene); 7.74 (m, 2H, fluorene); 7.52 (m, 2H, fluorene); 7.23 (d, 2H, vinyl); 6.30 (d, 2H, vinyl); 3.63 (s, 12H, MeO); 1.78 (s, 6H, Me); 0.32 (s, 6H, Me)
4,7-[(MeO)2Sivinyl]2BTH	7.68 (m, 2H, BTH); 7.26 (d, 2H, vinyl); 7.08 (d, 2H, vinyl); 3.62 (s, 12H, MeO); 0.34 (s, 6H, Me)
3,6-[(MeO)2Sivinyl]2carbazole	11.7 (s, 1H, carbazole); 8.41 (s, 2H, carbazole); 7.59 (m, 4H, carbazole); 7.40 (m, 2H, vinyl); 6.38 (d, 2H, vinyl); 3.63 (s, 12H, MeO); 0.32 (s, 6H, Me)

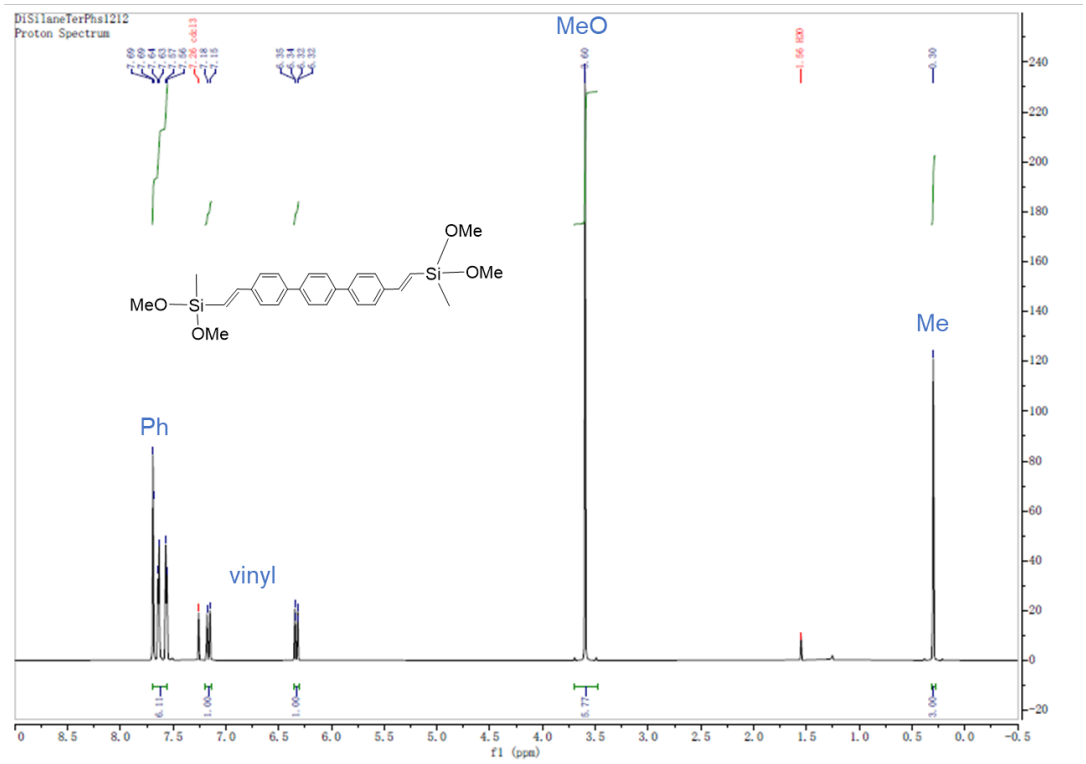

Figure C.1. ^{1}H NMR of 4,4''-[$(MeO)_2$Sivinyl]$_2$terphenyl.

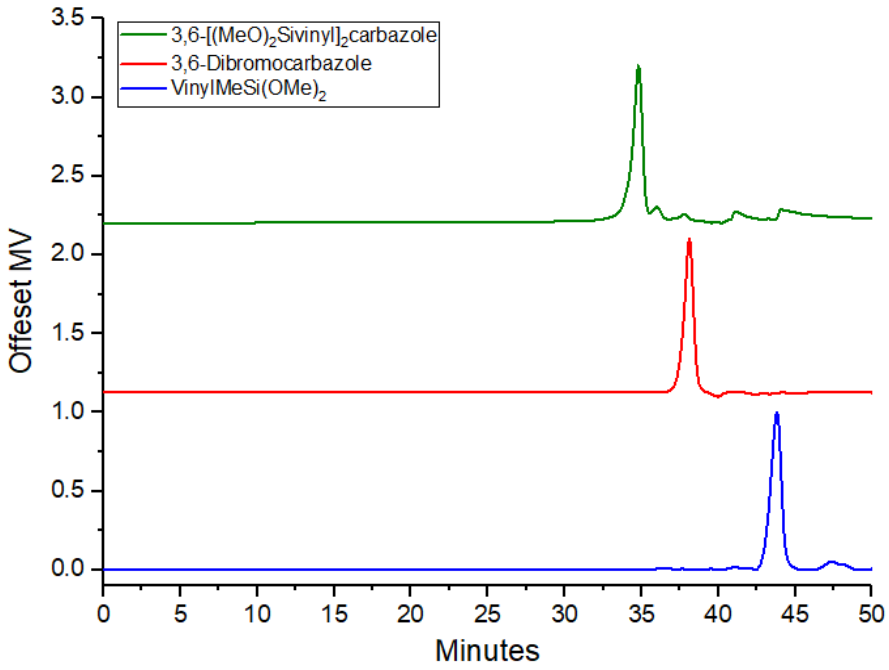

Figure C.2. GPC of 3,6-[$(MeO)_2$Sivinyl]$_2$carbazole, 3,6-dibromocarbazole and vinyl-MeSi$(OMe)_2$.

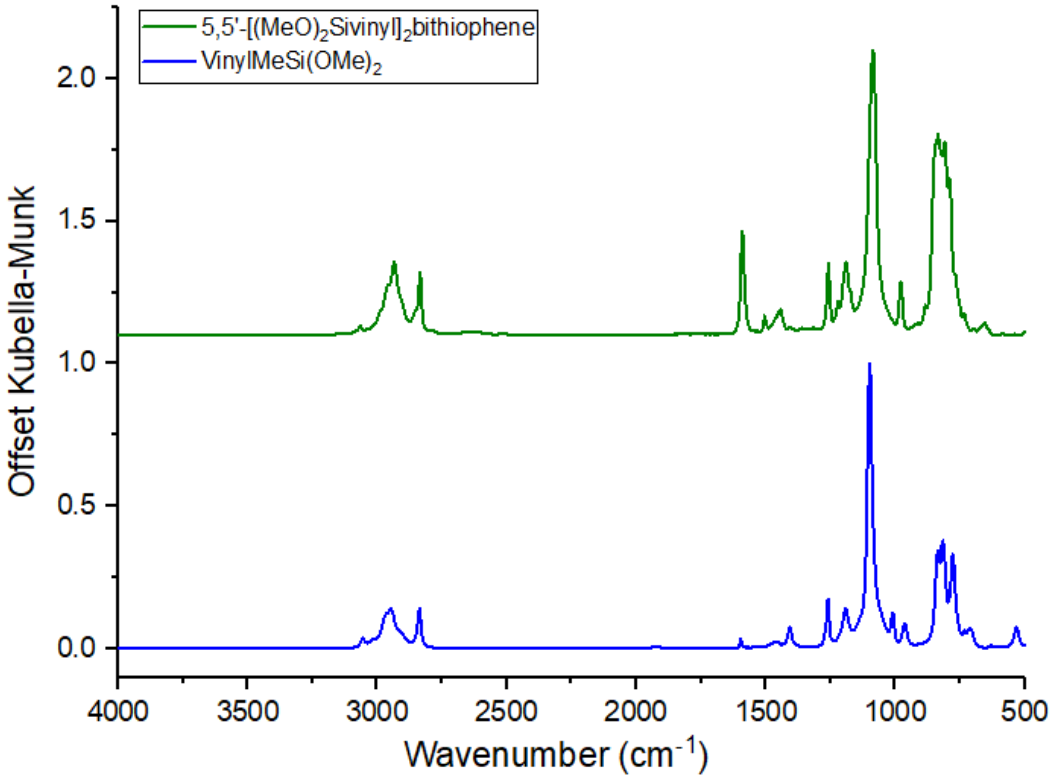

Figure C.3. FTIR of 5,5'-[(MeO)$_2$Sivinyl]$_2$bithiophene and vinylMeSi(OMe)$_2$.

Table C.1. Representative FTIR data of selected compounds.

Compound	v	Wavenumber (cm^{-1})	Intensity
VinylMeSi(OMe)$_2$		778	Weak, sharp
		816	Medium, sharp
		836	Weak, sharp
	Si-O-Si	1087	Strong, sharp
	C=C	1260	Weak, sharp
	C=C	1407	Weak, sharp
	C=C	1596	Weak, sharp
	C-H	2837	Weak, sharp
	C-H	2950	Weak, broad
1,4-[(MeO)$_2$Sivinyl]$_2$ben-zene		789	Weak, sharp
		835	Medium, sharp
		991	Weak, sharp
	Si-O-Si	1087	Strong, sharp
	Si-O-Si	1133	Medium, sharp
	C=C	1410	Weak, sharp
	C=C	1452	Weak, sharp
	C=C	1508	Weak, sharp
	C=C	1600	Weak, sharp
	C-H	2836	Weak, broad
	C-H	2937	Weak, broad
VinylDDvinyl		698	Weak, sharp
		731	Weak, sharp

		811	Weak, sharp
	Si-O-Si	1029	Weak, sharp
	Si-O-Si	1132	Strong, sharp
	C=C	1261	Weak, sharp
	C=C	1430	Weak, sharp
	C=C	1594	Weak, sharp
	C-H	2875	Weak, broad
	C-H	2923	Weak, broad
	C-H	3072	Weak, broad
DD-co-phenyl		697	Weak, sharp
		729	Weak, sharp
		814	Weak, sharp
	Si-O-Si	1029	Weak, sharp
	Si-O-Si	1132	Strong, sharp
	C=C	1262	Weak, sharp
	C=C	1430	Weak, sharp
	C=C	1594	Weak, sharp
	C-H	2875	Weak, broad
	C-H	2923	Weak, broad
	C-H	3072	Weak, broad
$(Styryl)_2DD$		698	Weak, sharp
		734	Weak, sharp
		820	Weak, sharp
	Si-O-Si	1029	Weak, sharp
	Si-O-Si	1132	Strong, sharp
	C=C	1262	Weak, sharp
	C=C	1430	Weak, sharp
	C=C	1594	Weak, sharp
	C-H	2875	Weak, broad
	C-H	2923	Weak, broad
	C-H	3072	Weak, broad

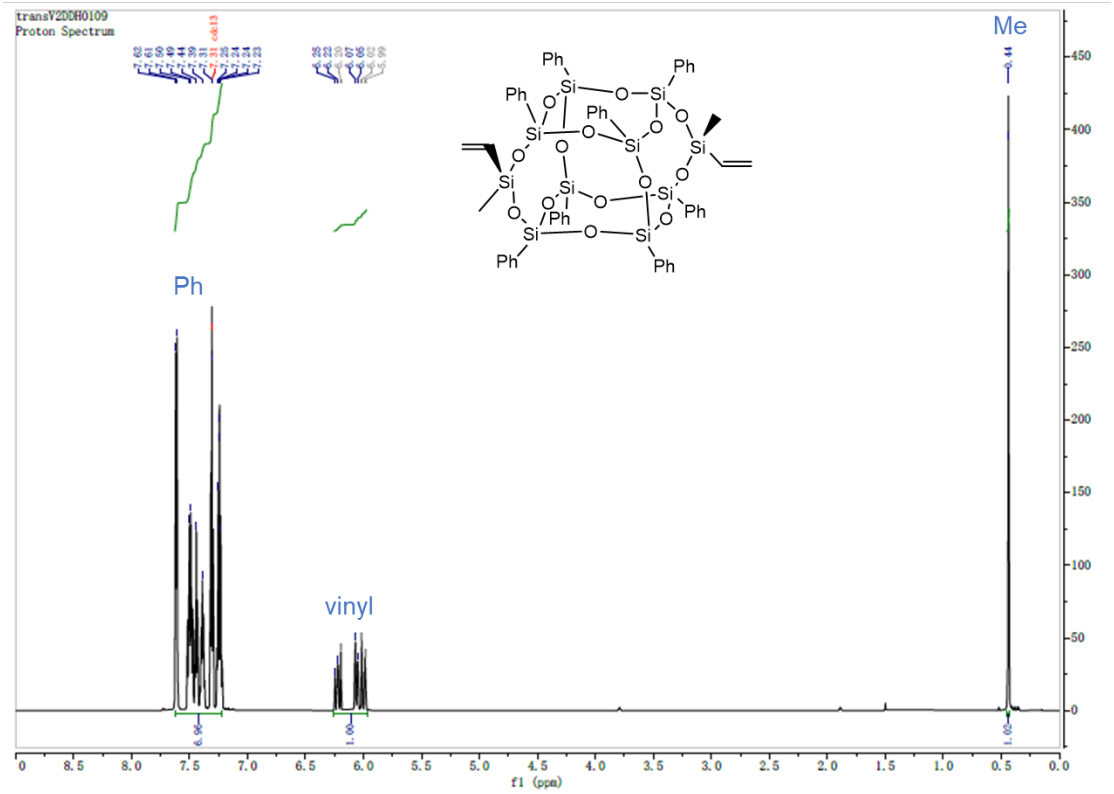

Figure C.4. ^{1}H NMR of pure *trans*-vinylDDvinyl.

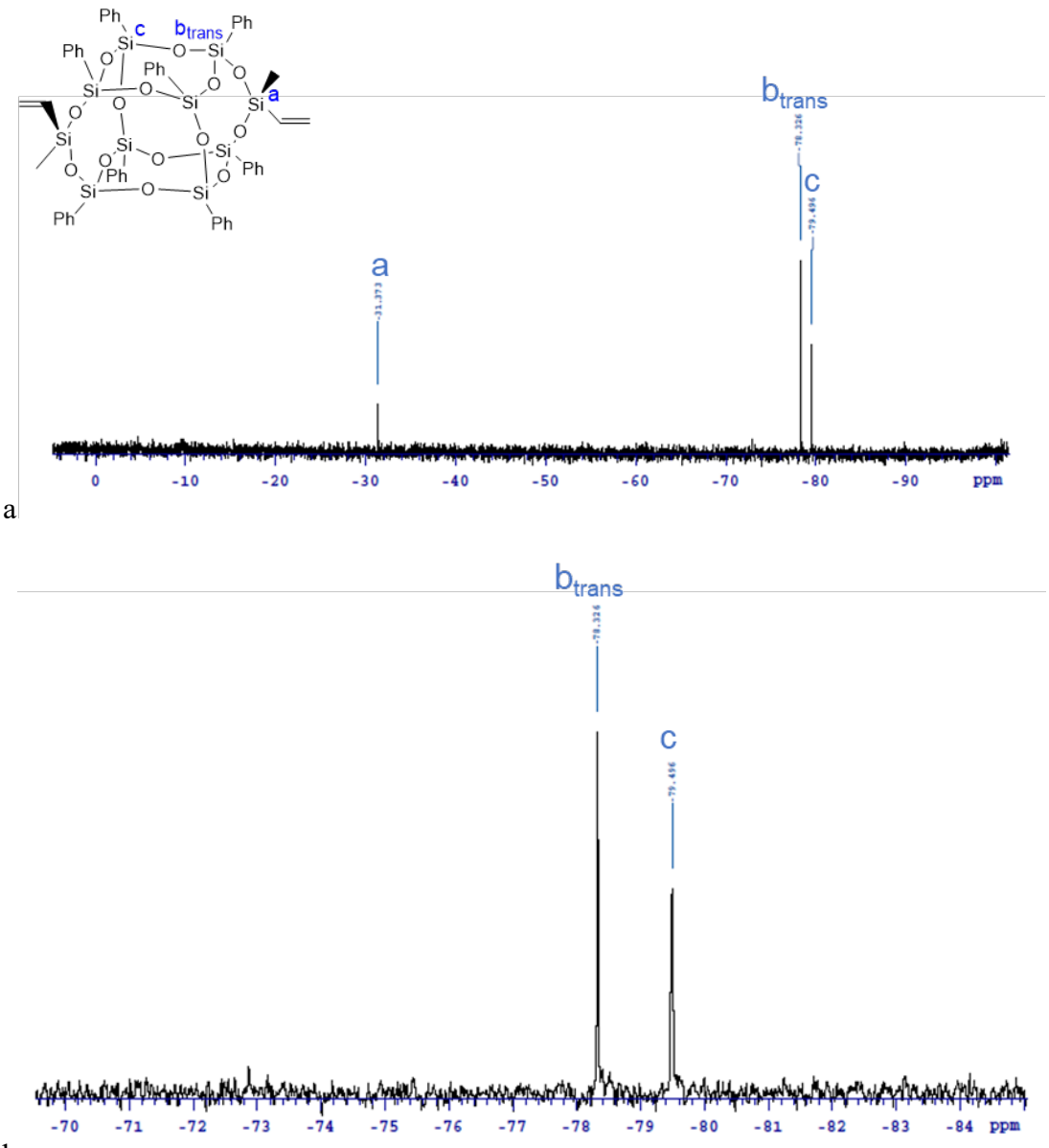

Figure C.5. (a) ^{29}Si NMR of pure *trans*-vinylDDvinyl; (b) zoom-in.

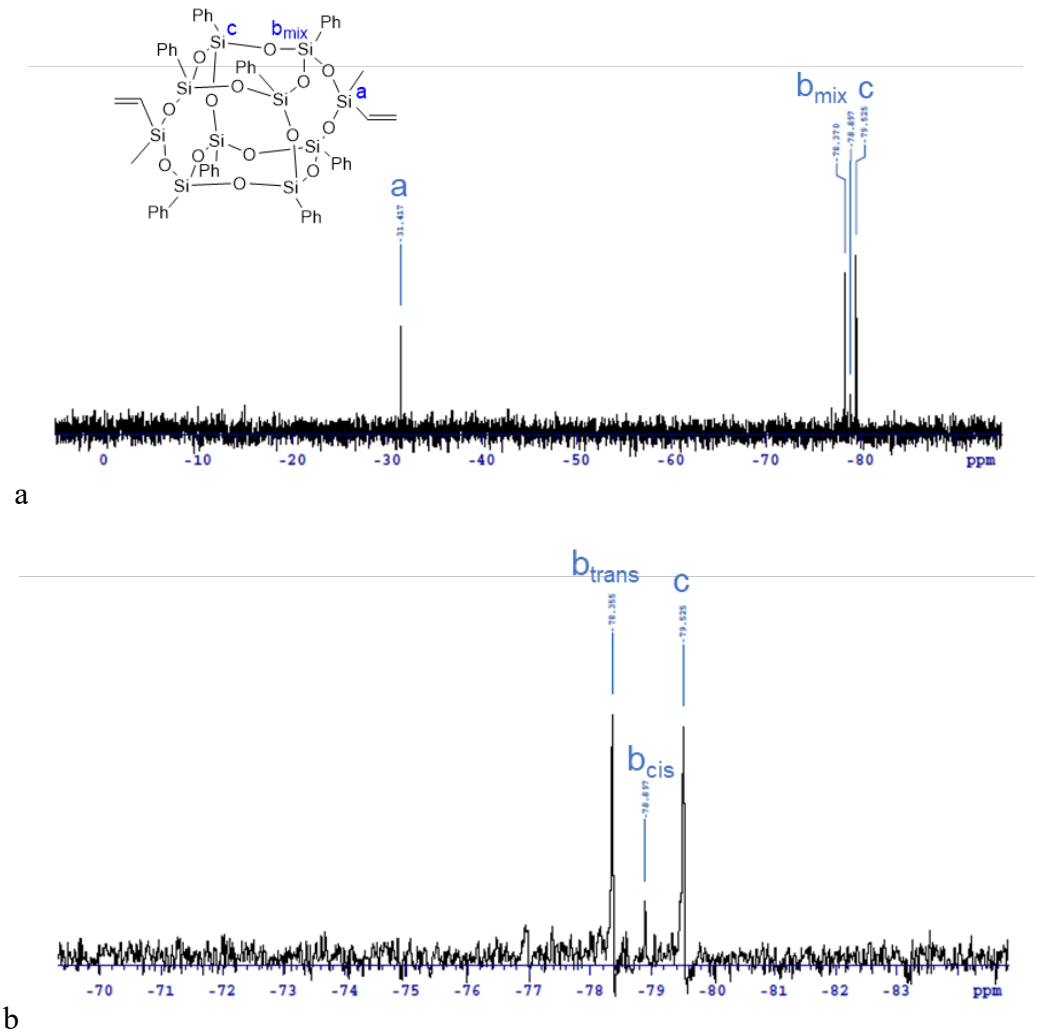

Figure C.6. (a) ^{29}Si NMR of mixed cis-, *trans*-vinylDDvinyl; (b) zoom-in.

Table C.3. MALDI-TOF, GPC and TGA data for vinylDDvinyl and derived polymers.

Compound	MALDI-TOF m/z		GPC			TGA		
	Monomer	Theor	M_n	M_w	Đ	Ceramic yield %	Theor yield %	$T_{d5\%}$ °C (air)
VinylDDvinyl	1315[a]	1314[a]	1010	1080	1.07	49.3	49.7	540
-phenyl	1280	1280	19550	49410	2.53	46.3	46.9	460
-biphenyl	1355	1356	11690	24480	2.09	43.2	44.1	400
-terphenyl	1430	1432	15780	34770	2.20	41.7	41.8	410
-stilbene	1380	1382	9210	25390	2.76	42.8	43.3	400
-thiophene	1290	1286	22540	43250	1.92	46.5	46.7	540
-bithiophene	1370	1368	3580	7200	2.01	42.2	43.8	520
-thienothio-phene	1340	1342	4480	10040	2.24	42.7	44.4	500
dimethylfluo-rene	1400	1396	20790	46100	2.22	41.4	43.0	510
-BTH	1335	1338	8390	17380	2.07	44.0	44.8	540
-carbazole	1370	1369	13680	33850	2.47	42.8	43.8	540

[a] As Ag^+ adduct.

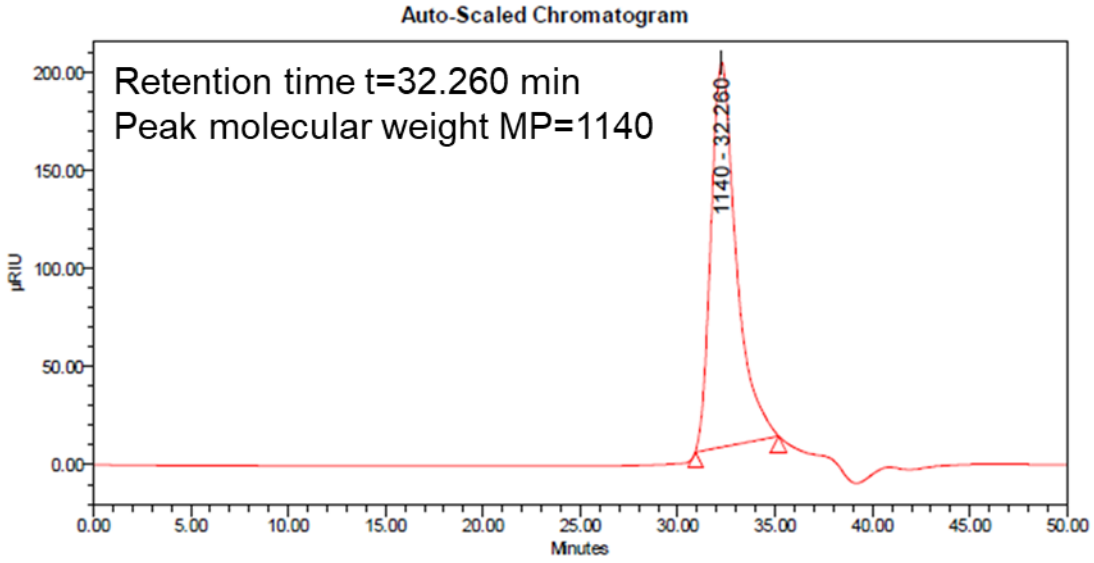

Figure C.7. GPC of vinylDDvinyl.

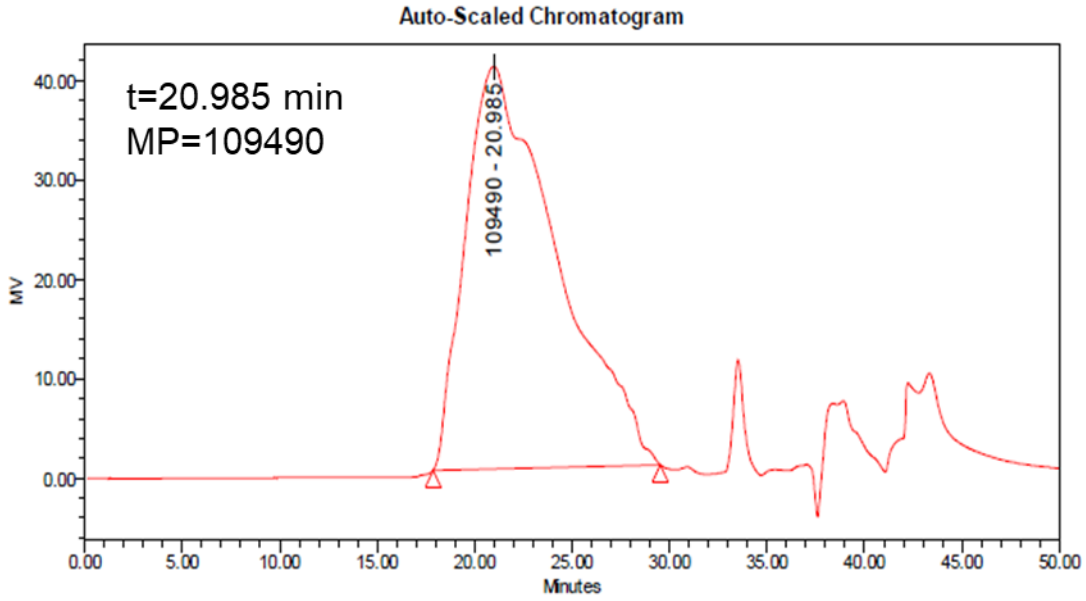

Figure C.8. GPC of DD-co-benzene.

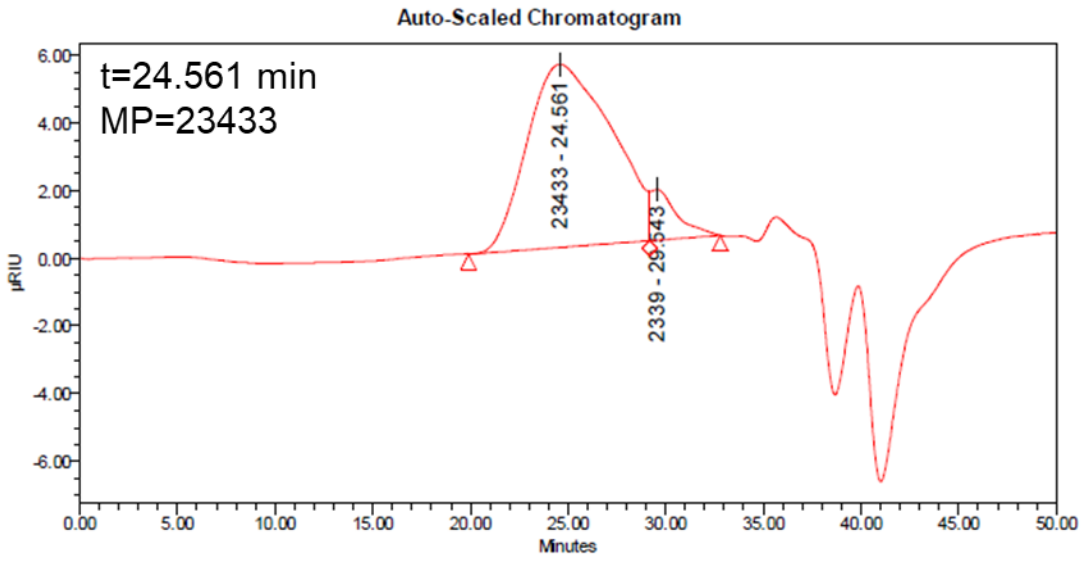

Figure C.9. GPC of DD-co-biphenyl.

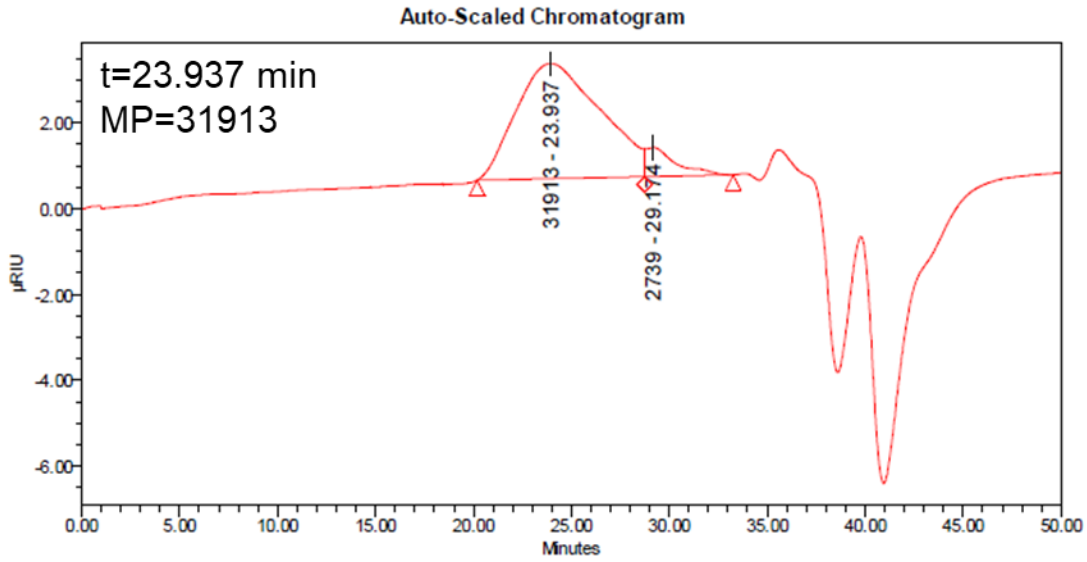

Figure C.10. GPC of DD-co-terphenyl.

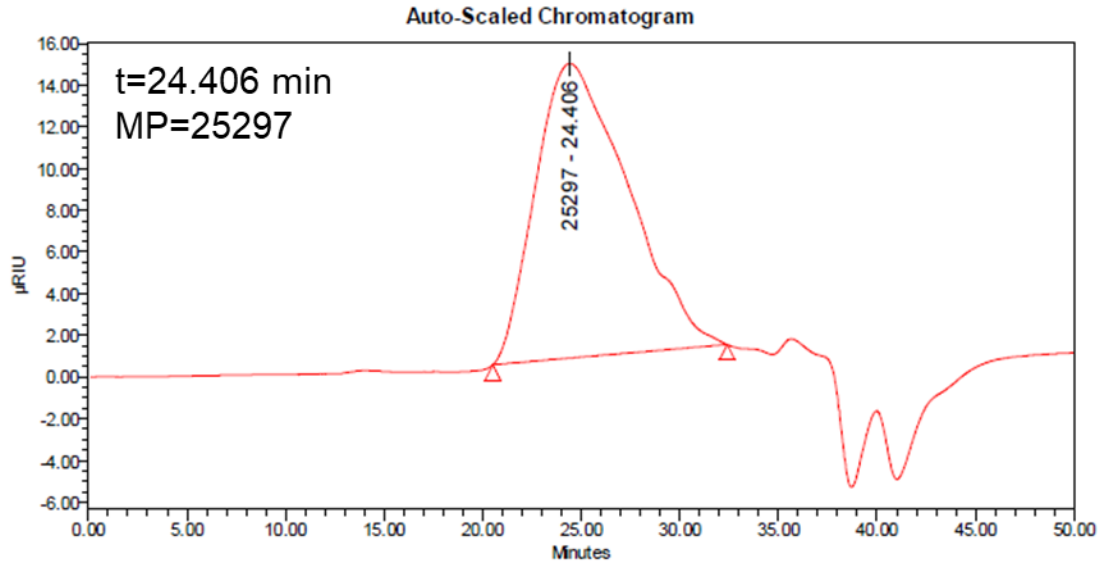

Figure C.11. GPC of DD-co-stilbene.

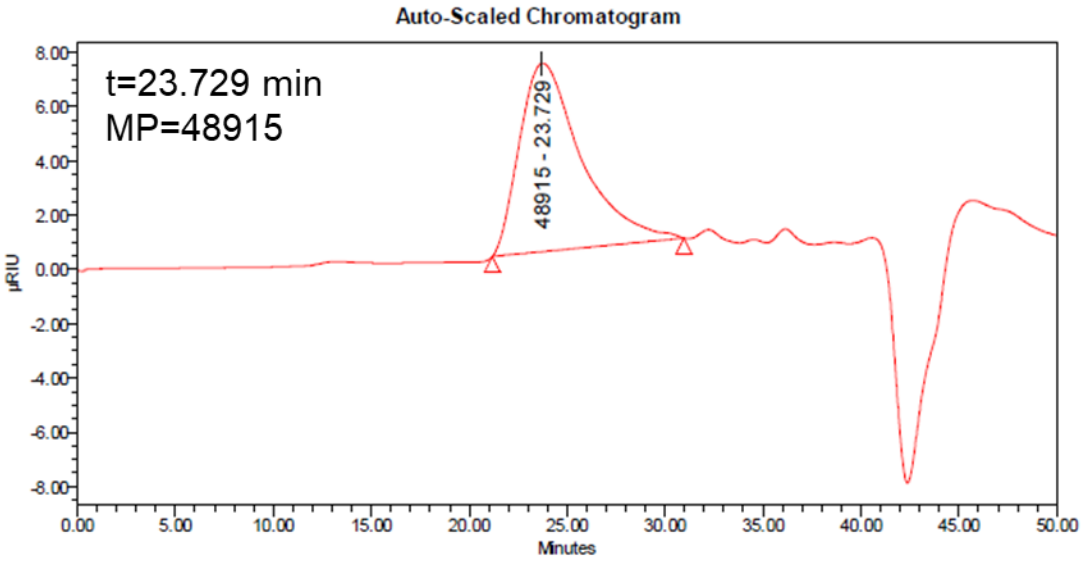

Figure C.12. GPC of DD-co-thiophene.

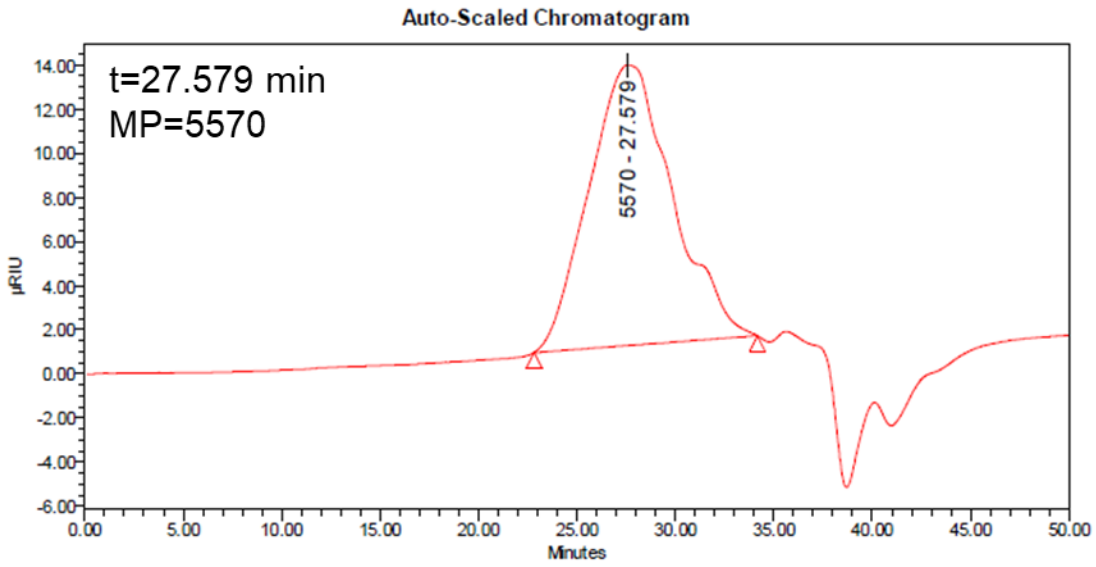

Figure C.13. GPC of DD-co-bithiophene.

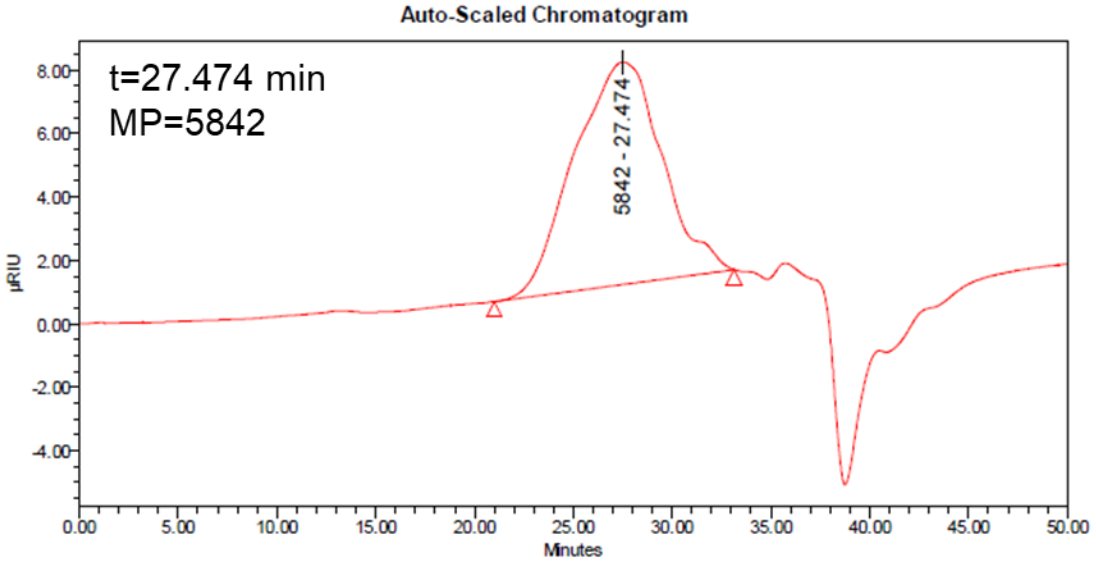

Figure C.14. GPC of DD-co-thienothiophene.

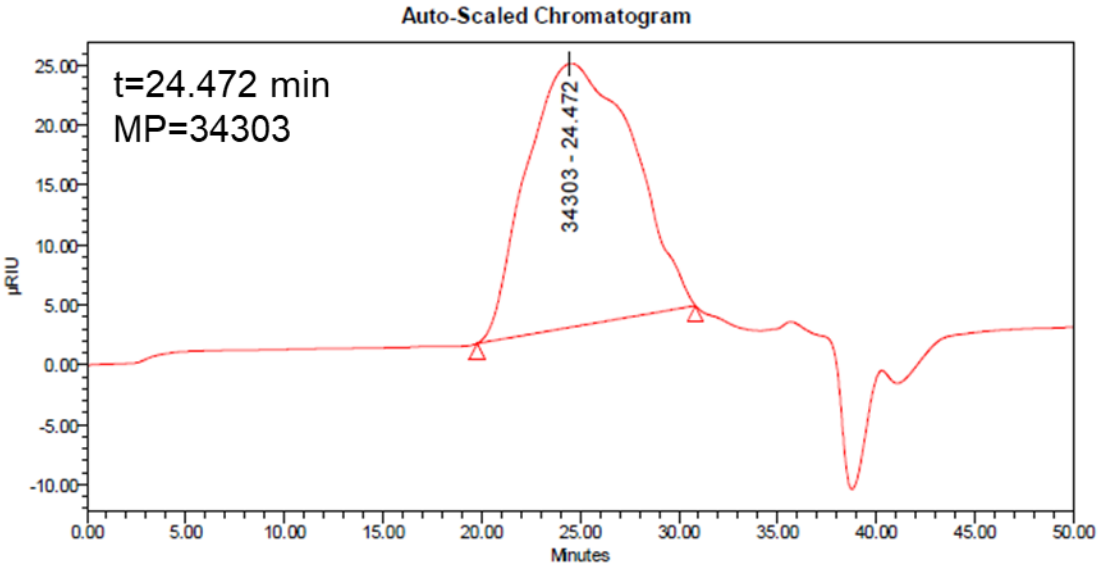

Figure C.15. GPC of DD-co-dimethylfluorene.

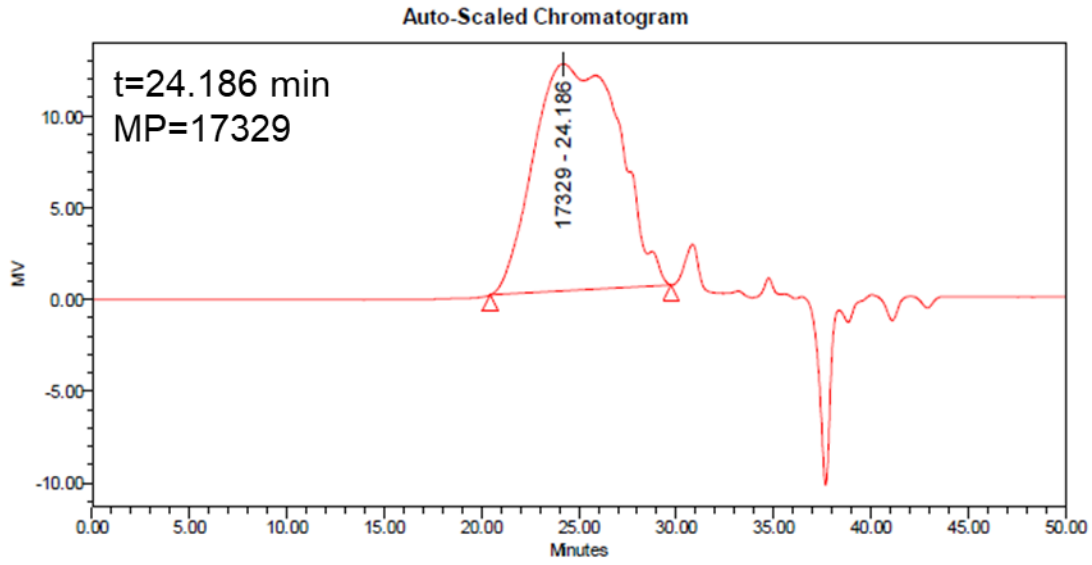

Figure C.16. GPC of DD-co-BTH.

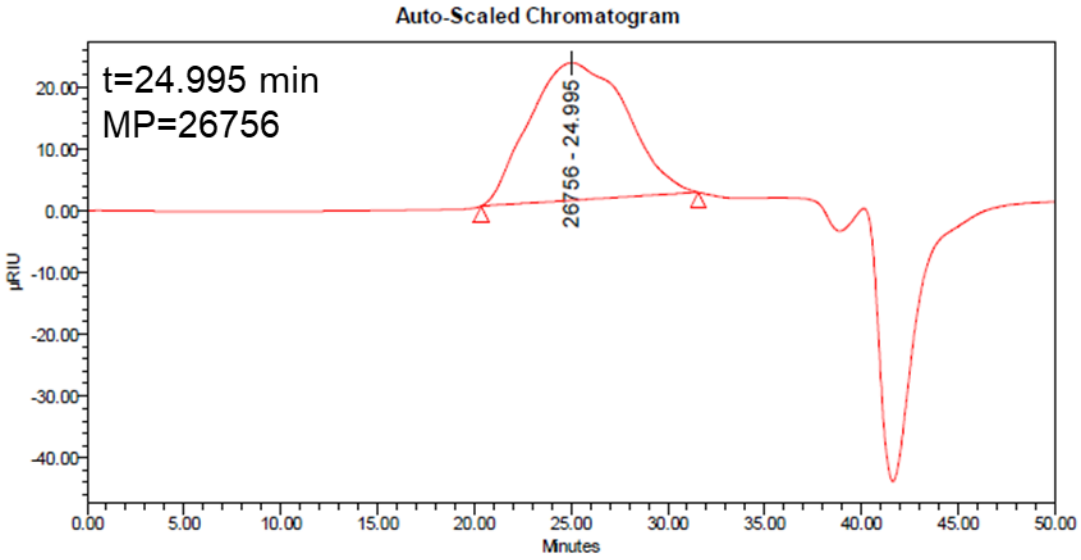

Figure C.17. GPC of DD-co-carbazole.

Table C.4. MALDI-TOF, GPC and TGA data for vinylDDvinyl derived model cage compounds.

	MALDI-TOF m/z		GPC			TGA (air)		
	Actual	Theor	M_n	M_w	Đ	Ceramic yield %	Theor yield %	$T_{d5\%}$ °C
$(Styryl)_2DD$	1467[a]	1466[a]	1121	1129	1.01	42.9	44.2	431
$(Styryl)_3DD$	1543[a]	1542[a]	1126	1149	1.02	41.8	41.8	435
$(Thiophenevinyl)_2DD$	1480[a]	1478[a]	1149	1161	1.01	43.2	43.8	445
$(Dimethylfluorenevinyl)_2DD$	1697[a]	1698[a]	1545	1663	1.07	36.2	37.7	358
$(Dimethylfluorenevinyl)_4DD$	1977[b]	1976[b]	1715	1828	1.07	30.3	30.3	400

[a] As Ag^+ adduct. [b] As H^+ adduct.

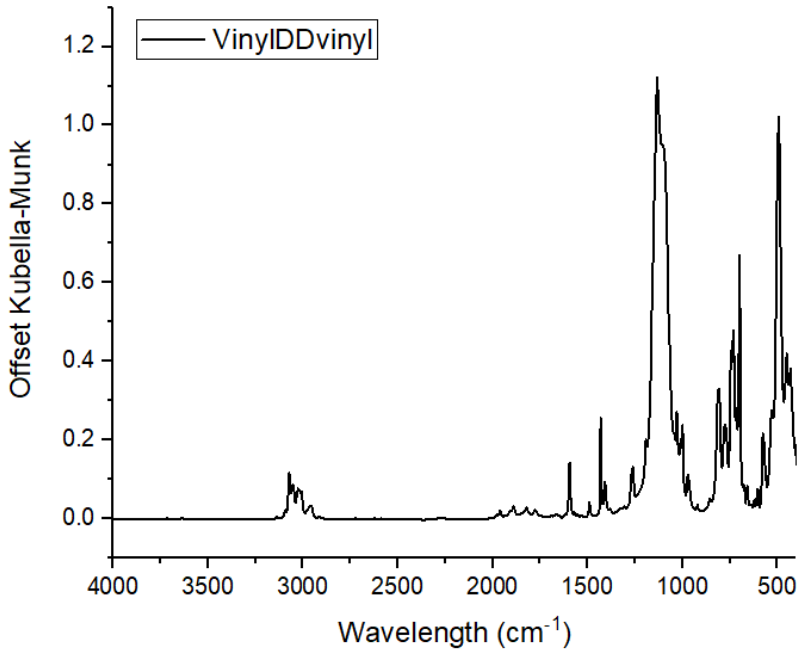

Figure C.18. FTIR of vinylDDvinyl.

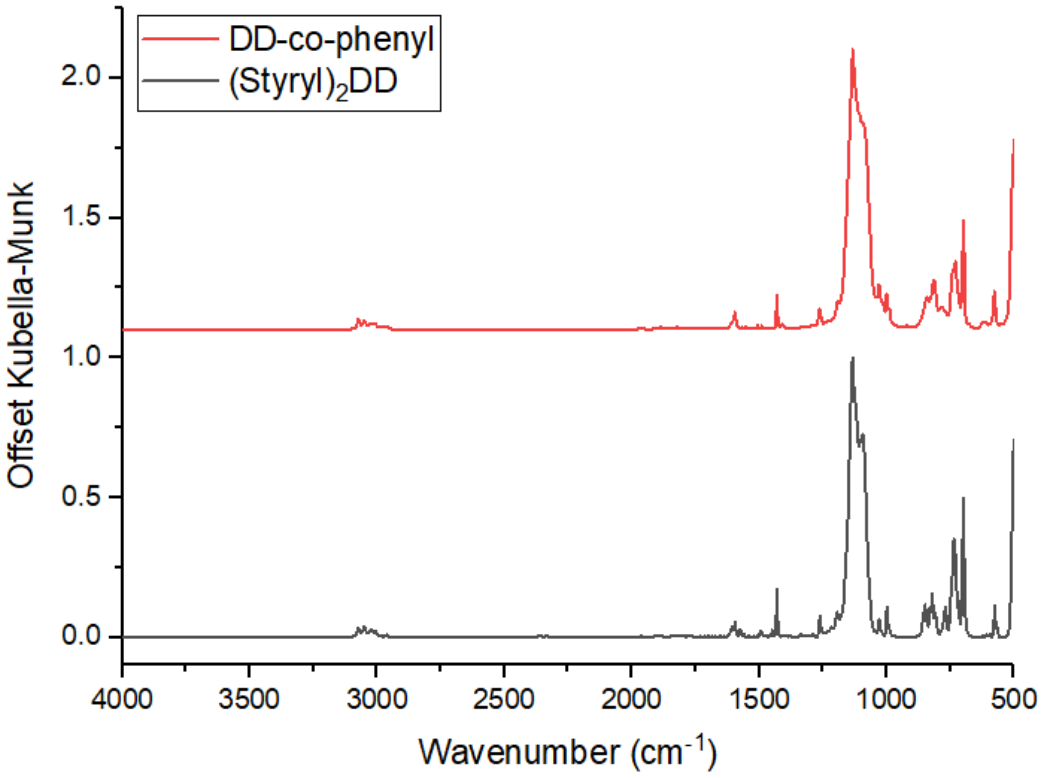

Figure C.19. FTIR of DD-co-phenyl and $(Styryl)_2DD$.

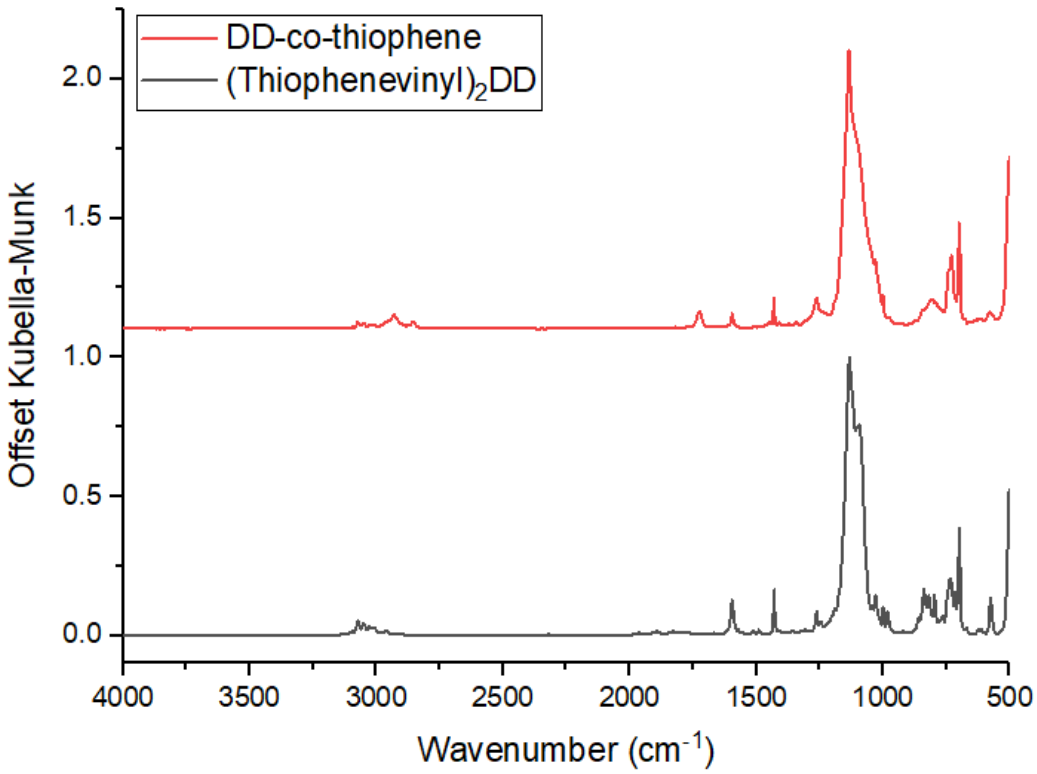

Figure C.20. FTIR of DD-co-thiophene and (Thiophenevinyl)$_2$DD.

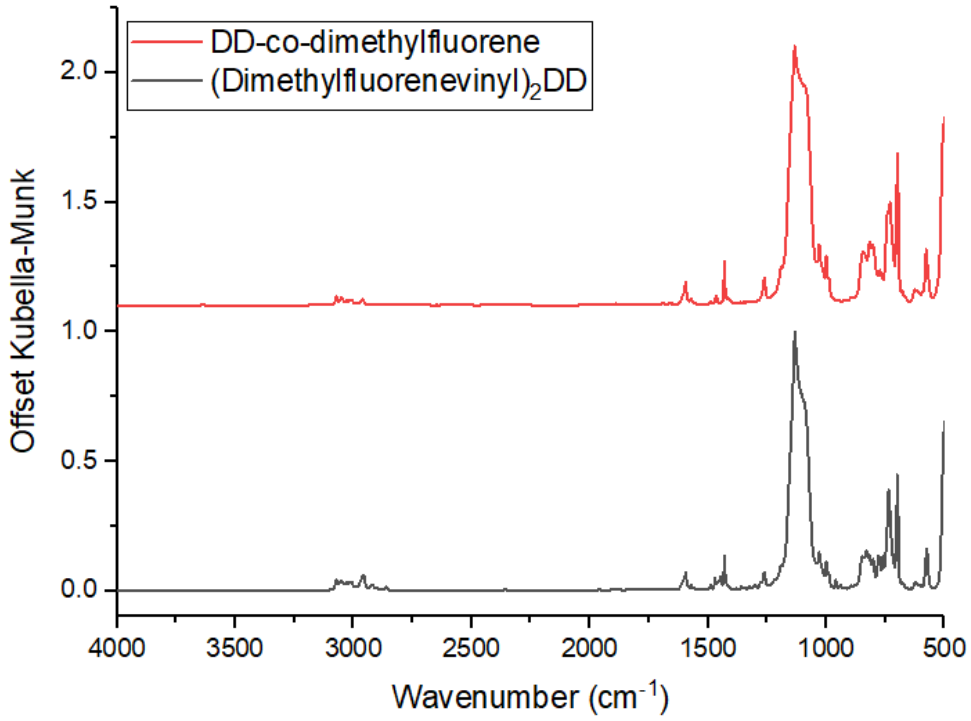

Figure C.21. FTIR of DD-co-dimethylfluorene and (Dimethylfluorenevinyl)$_2$DD.

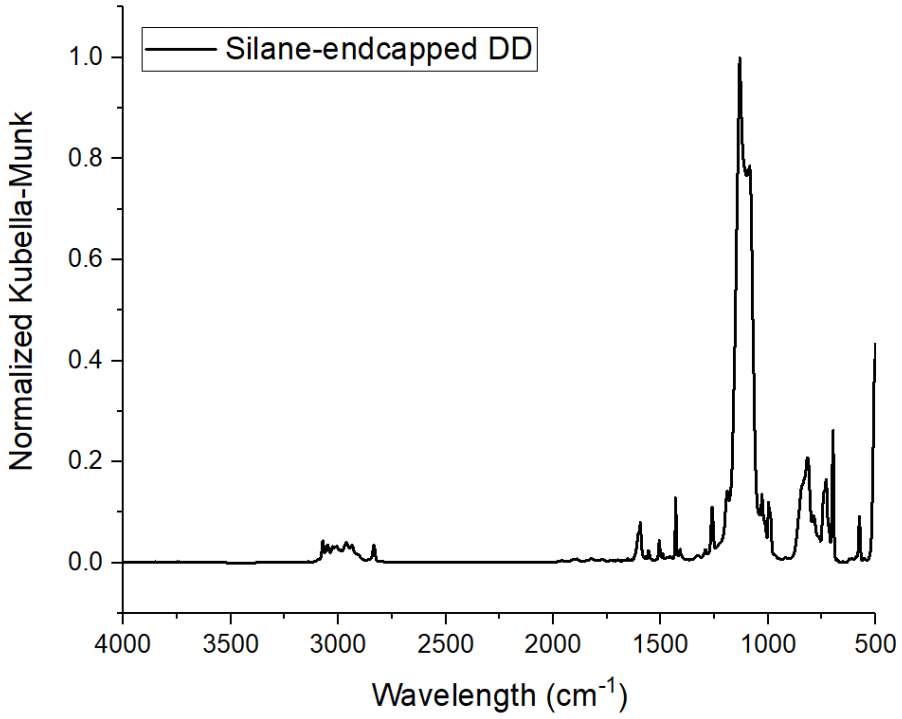

Figure C.22. FTIR of Silane-end-capped DD.

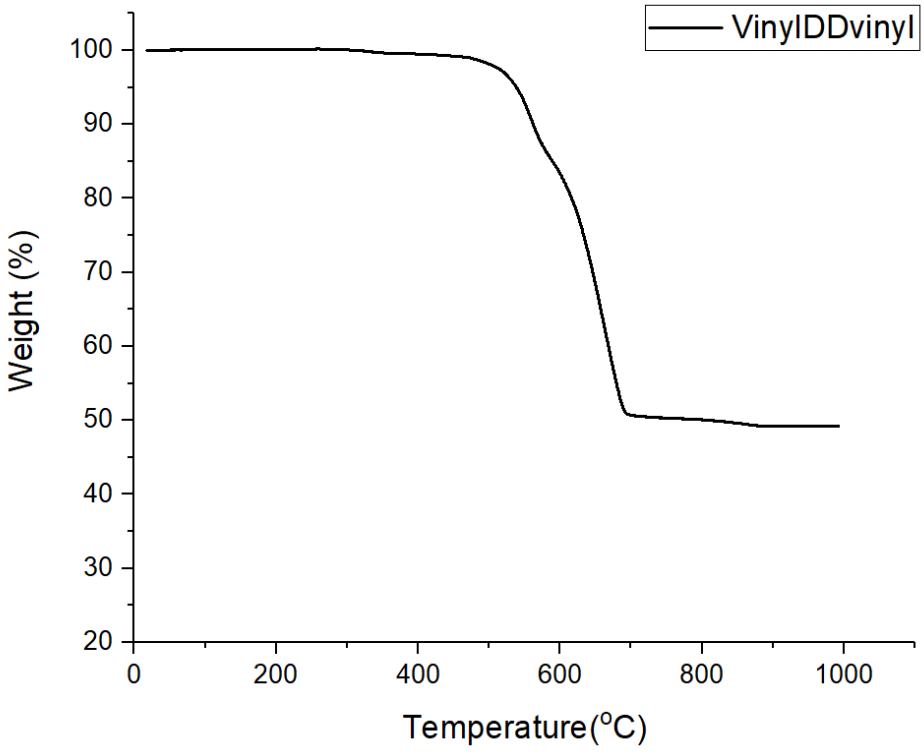

Figure C.23. TGA of vinylDDvinyl.

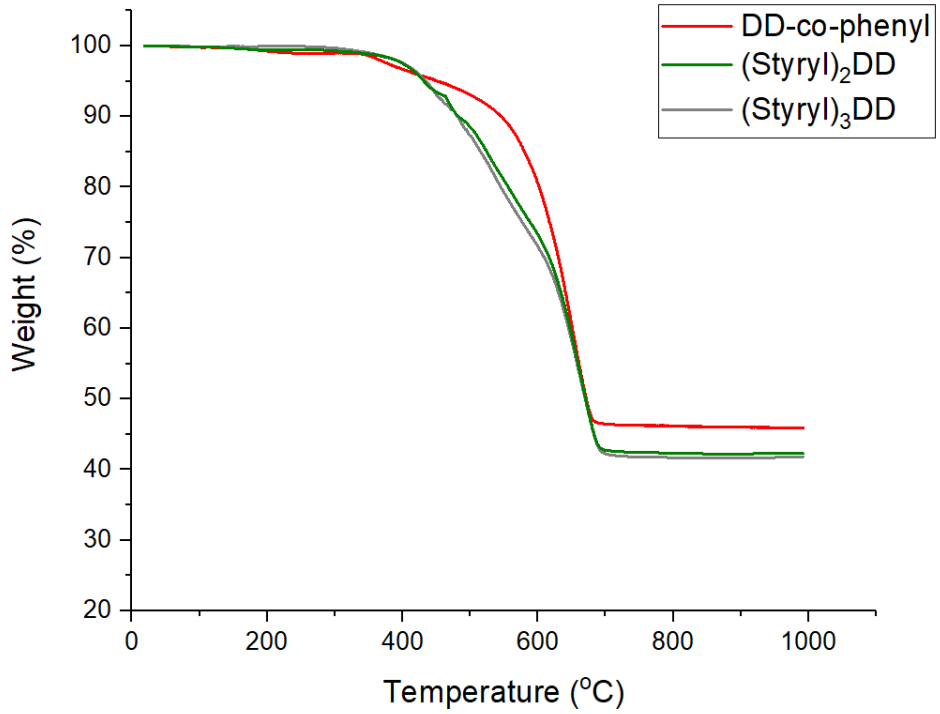

Figure C.24. TGA of DD-co-phenyl, $(Styryl)_2DD$ and $(Styryl)_3DD$.

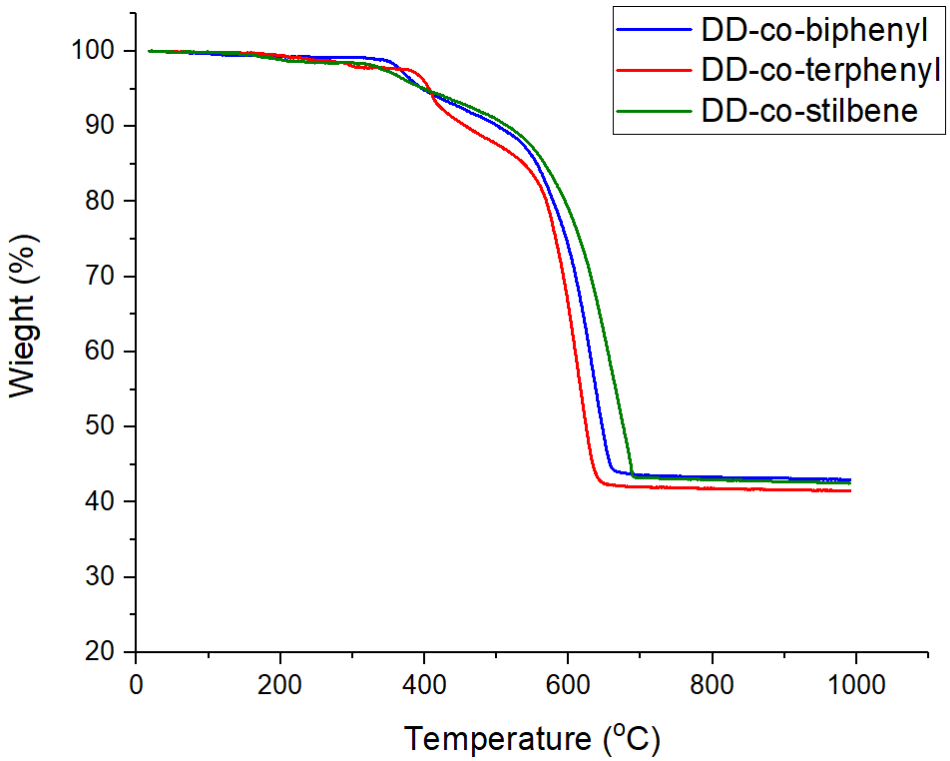

Figure C.25. TGA of DD-co-biphenyl, DD-co-terphenyl and DD-co-stilbene.

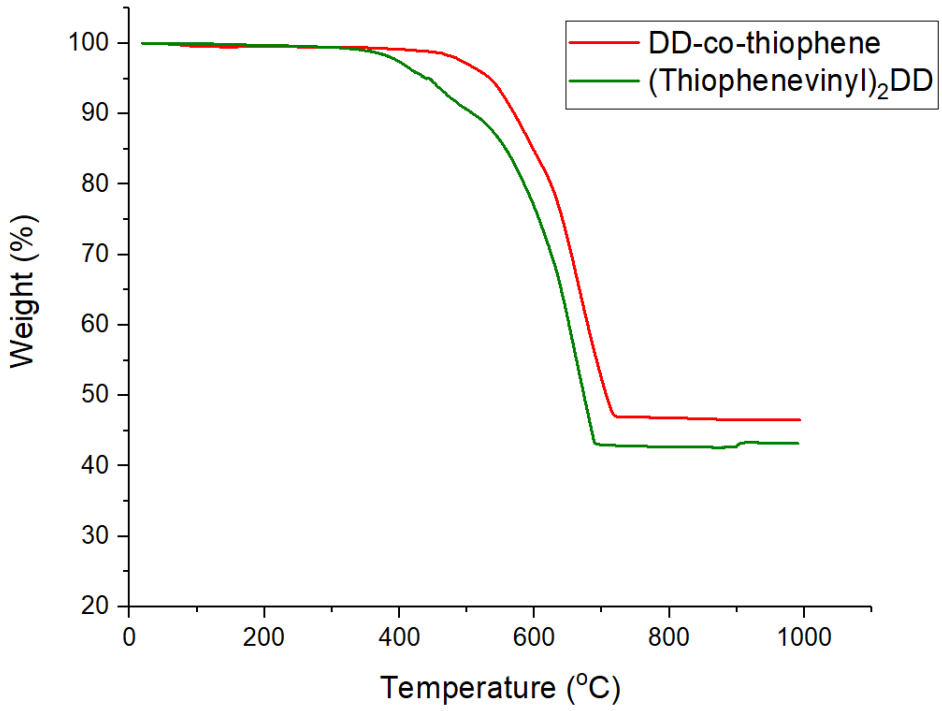

Figure C.26. TGA of DD-co-thiophene and (Thiophenevinyl)$_2$DD.

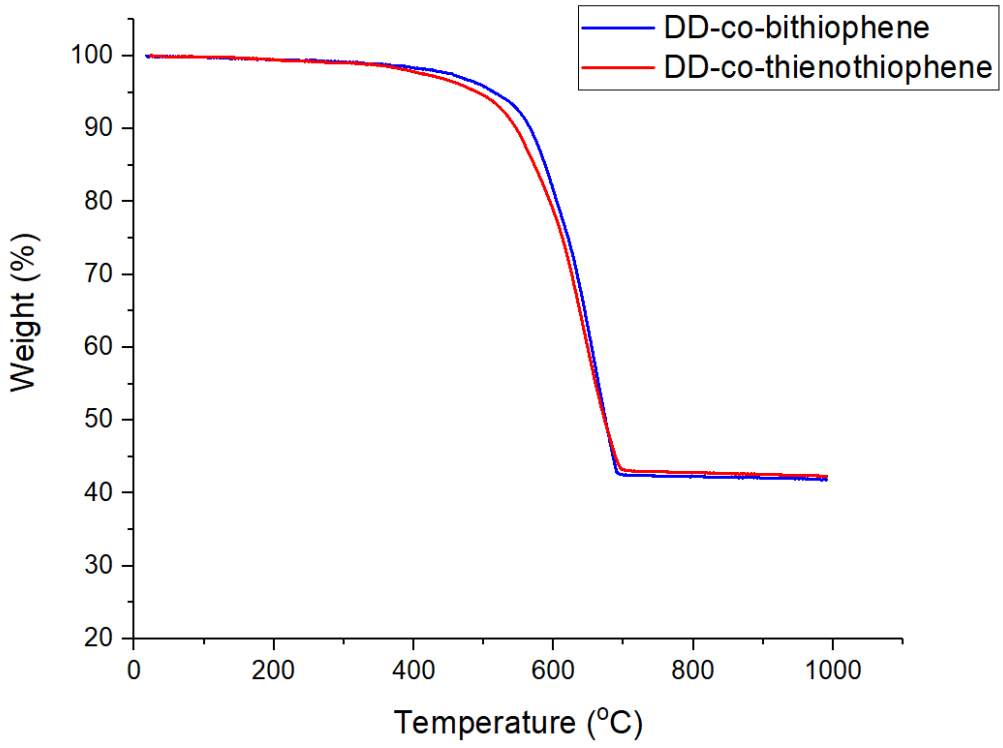

Figure C.27. TGA of DD-co-bithiophene and DD-co-thienothiophene.

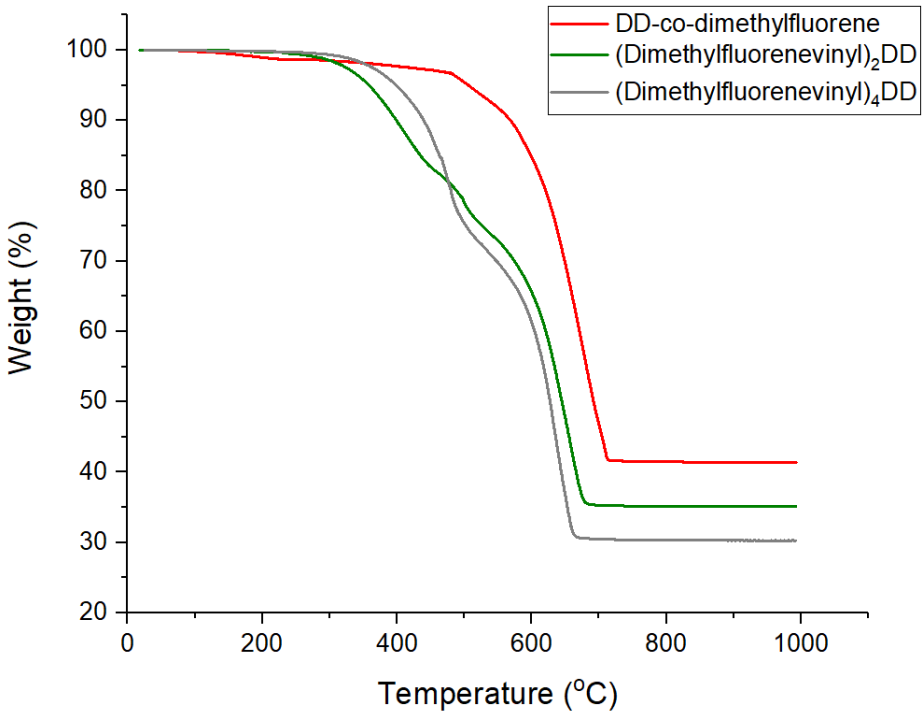

Figure C.28. TGA of DD-co-dimethylfluorene, (Dimethylfluorene)$_2$DD and (Dimethylfluorene)$_4$DD.

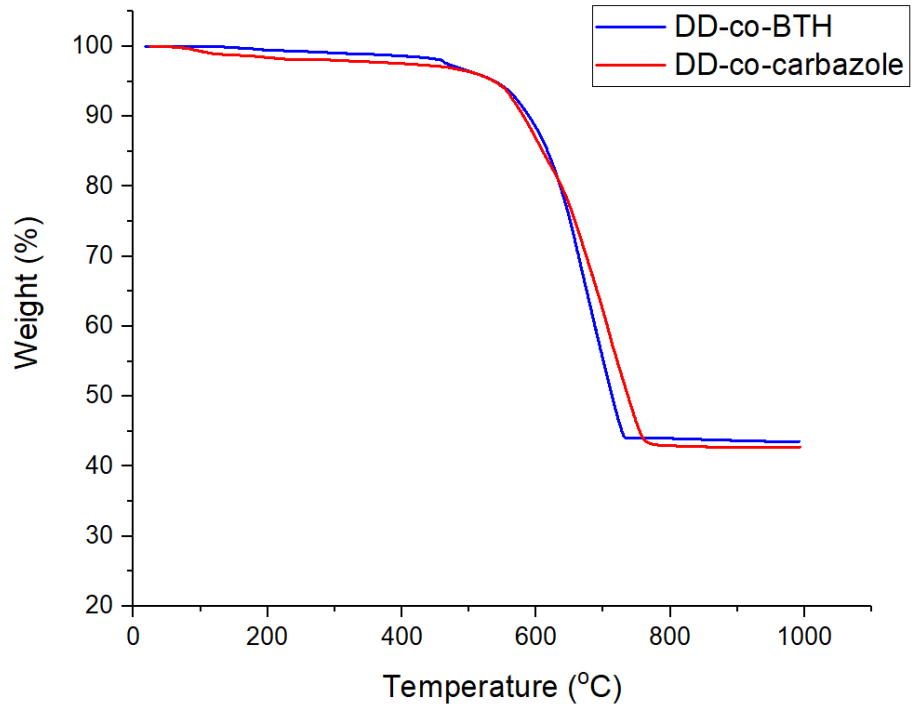

Figure C.29. TGA of DD-co-BTH and DD-co-carbazole.

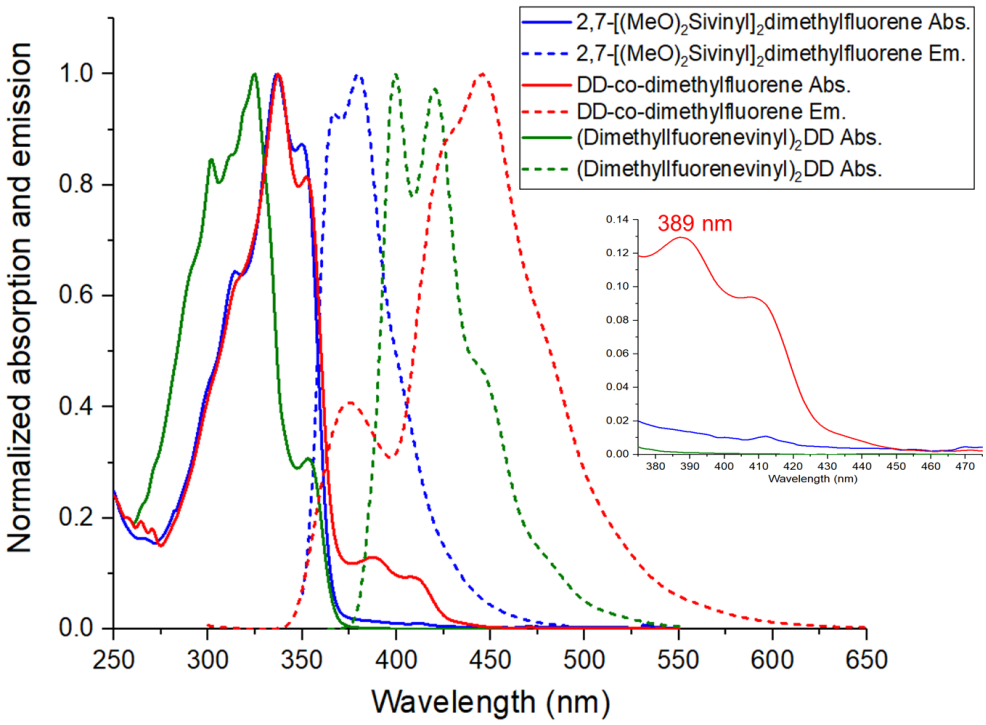

Figure C.30. Normalized steady-state spectra of 2,7-[(MeO)$_2$Sivinyl]$_2$dimethylfluorene, DD-co-dimethylfluorene and (Dimethylfluorene)$_2$DD inserted with amplification of absorption shoulders around 389 nm.

Table C.5. Two photon absorption (2PA) cross section values of polymers DD-co-phenyl, -thiophene, -dimethylfluorene, -BTH and -carbazole and model cage compound (Styryl)$_2$DD at discrete excitation wavelength.

	2PA-δ (GM)			
λTPA (nm)	550	600	650	700
DD-co-phenyl		2.0	1.1	0.6
DD-co-thiophene		31	24	12
DD-co-dimethylfluorene		50	49	20
DD-co-BTH	13	4.4	3.4	0.38
DD-co-carbazole		10.2	2.5	2.4
(Styryl)2DD	4.6	0.64	0.54	0.62

Modeling studies. Previous modeling studies of SQ cage compounds focused on the addition of simple substituents to the T$_{8,10,12}$ cage including H, OH, and F. The first studies with H substitution found cage-centered LUMOs.[1] In modeling studies in previous papers,[2,3] we introduced methyl groups to completely/incompletely-condensed cages including corner-missing and double-decker compounds, again finding cage-centered LUMOs, which correlate well with experimental data. However, multiple previous attempts to model stilbene-functionalized cages were unsuccessful,[2,3] finding stilbene-localized HOMOs and LUMOs, which is inconsistent with experimental

absorption and emission results for both single and two photon experiments done in two separate laboratories. These studies were also inconsistent with magnetic field generation studies which also show formation of cage centered magnetic fields. Modeling studies done on vinylDDvinyl and its derived copolymers by Professor Jungsuttiwong's group at Ubon Ratchathani University, Thailand are shown in Figure C.31. Modeling indicates that cage centered LUMOs occur inside the cage with methyl substituents on cage corners for both cis and trans configurations. With phenyl substituents, LUMOs reside on phenyl groups, which is consistent with published modeling results. The trans structure is more stable than the cis according to their HOMO, LUMO levels, which may explain why in the synthesis of vinylDDvinyl themajority product is always trans.

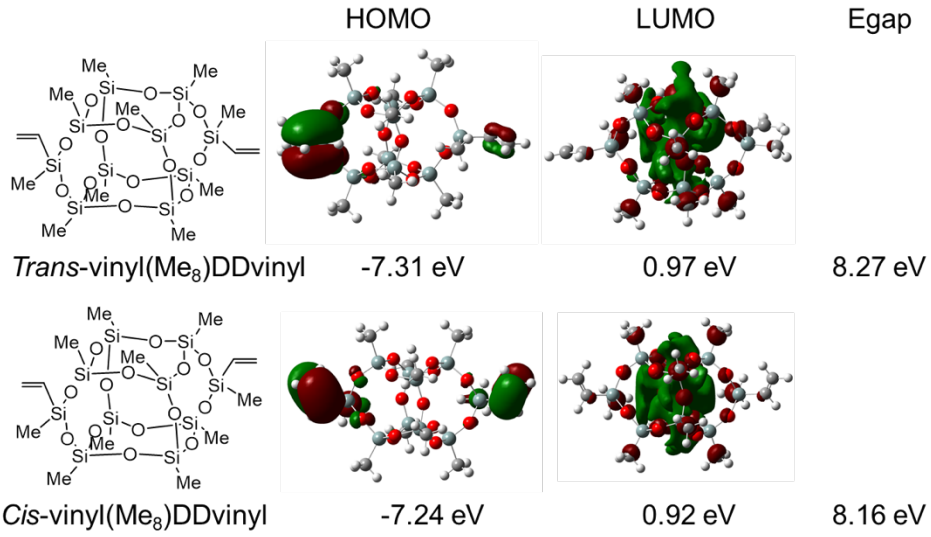

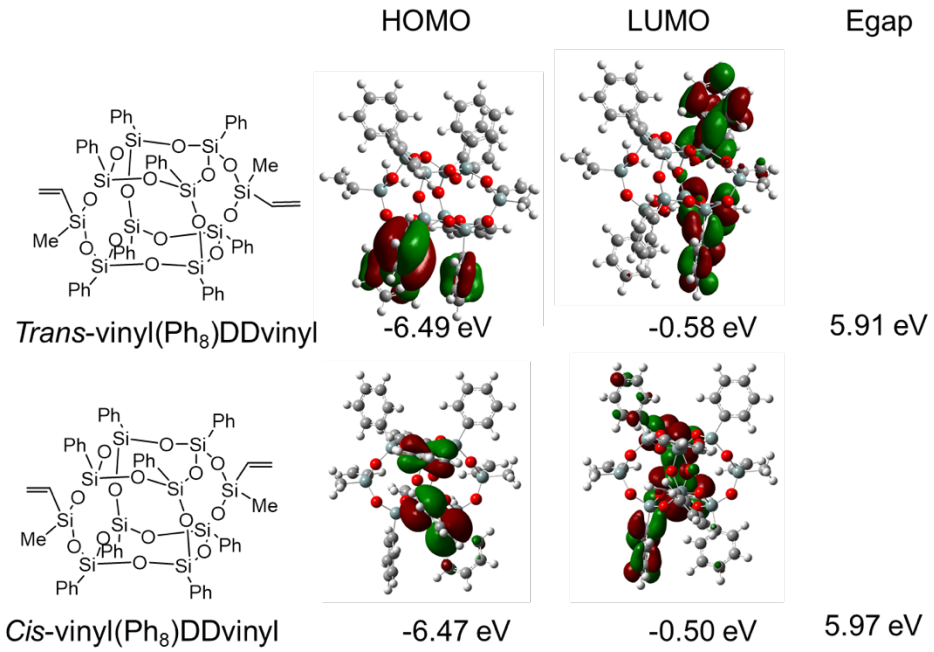

Figure C.31. HOMO and LUMO modeling of vinylDDvinyl.

However, the introduction of co-monomer units as shown in Figure **C.32** below, again places the LUMO on the organic co-monomer.

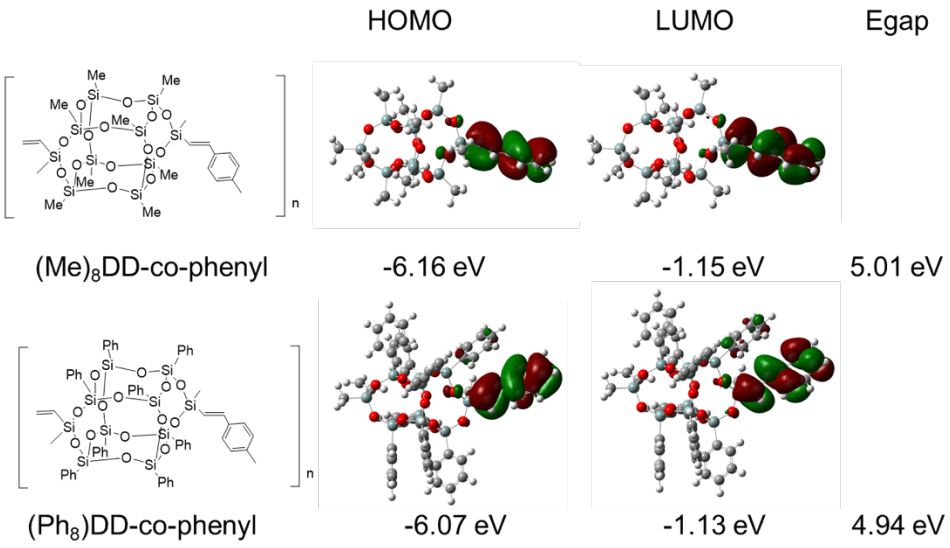

	HOMO	LUMO	Egap
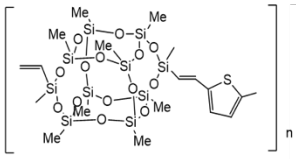	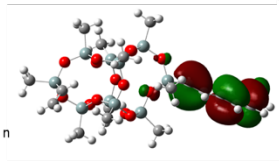	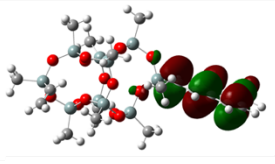	
$(Me)_8$DD-co-thiophene	-5.71 eV	-1.27 eV	4.44 eV
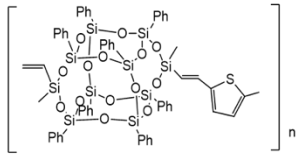	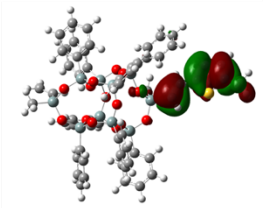	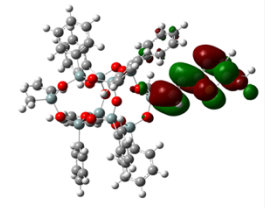	
(Ph_8)DD-co-thiophene	-5.62 eV	-1.23 eV	4.39 eV

	HOMO	LUMO	Egap
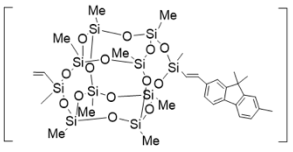	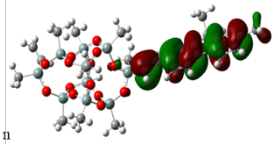	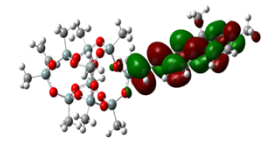	
$(Me)_8$DD-co-dimethylfluorene	-5.49 eV	-1.35 eV	4.14 eV
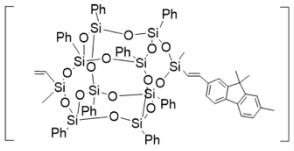	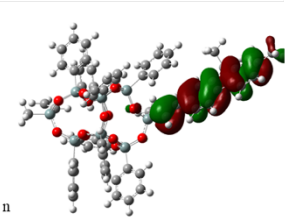	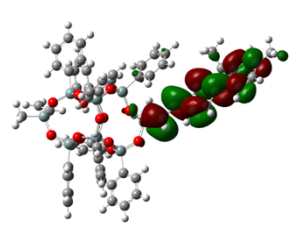	
(Ph_8)DD-co-dimethylfluorene	-5.47 eV	-1.35 eV	4.12 eV

	HOMO	LUMO	Egap
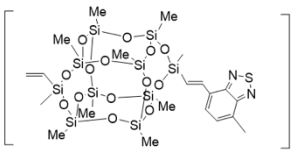	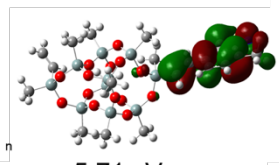	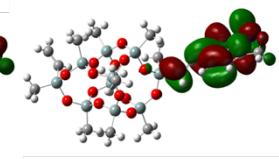	
$(Me)_8$DD-co-BTH	-5.71 eV	-2.01 eV	3.70 eV
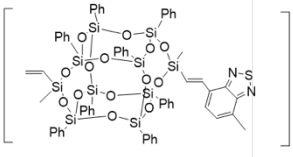	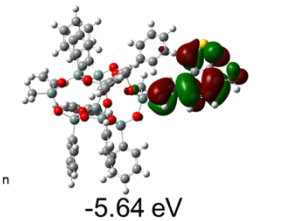	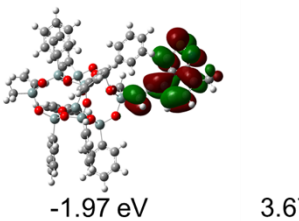	
(Ph_8)DD-co-BTH	-5.64 eV	-1.97 eV	3.67 eV

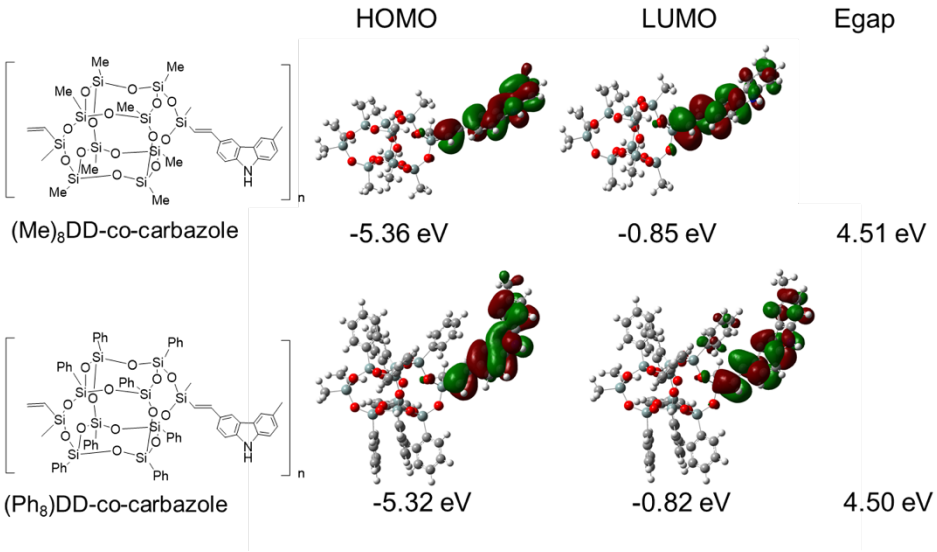

Figure C.32. HOMO and LUMO modeling of *trans*-vinylDDvinyl derived polymers DD-co-phenyl, -thiophene, -dimethylfluorene, -BTH and carbazole.

Modeling indicates LUMOs of *trans*-vinylDDvinyl derived copolymers sit on the organic linkers only, without involving SQ cages. Calculated absorption spectra and date are presented below in Figure **C.33** and Table **C.6**, and experimental data are shown for comparison. There is some similarity in the shape of experimental and calculated absorption spectra; as might be expected given the comments made above, but the calculated absorption λ_{max} is always blue-shifted from experimental by 35–68 nm.

One might choose to argue that current modeling methods are unable to successfully address the interaction of cage centered LUMOs with conjugated moieties. Hence efforts to model the unique structures developed with the DD polymers wherein cage centered LUMOs must interact with co-monomer LUMOs through vinylMeSi(O-)$_2$ bridges (assuming our arguments are valid) must search for new modeling approaches.

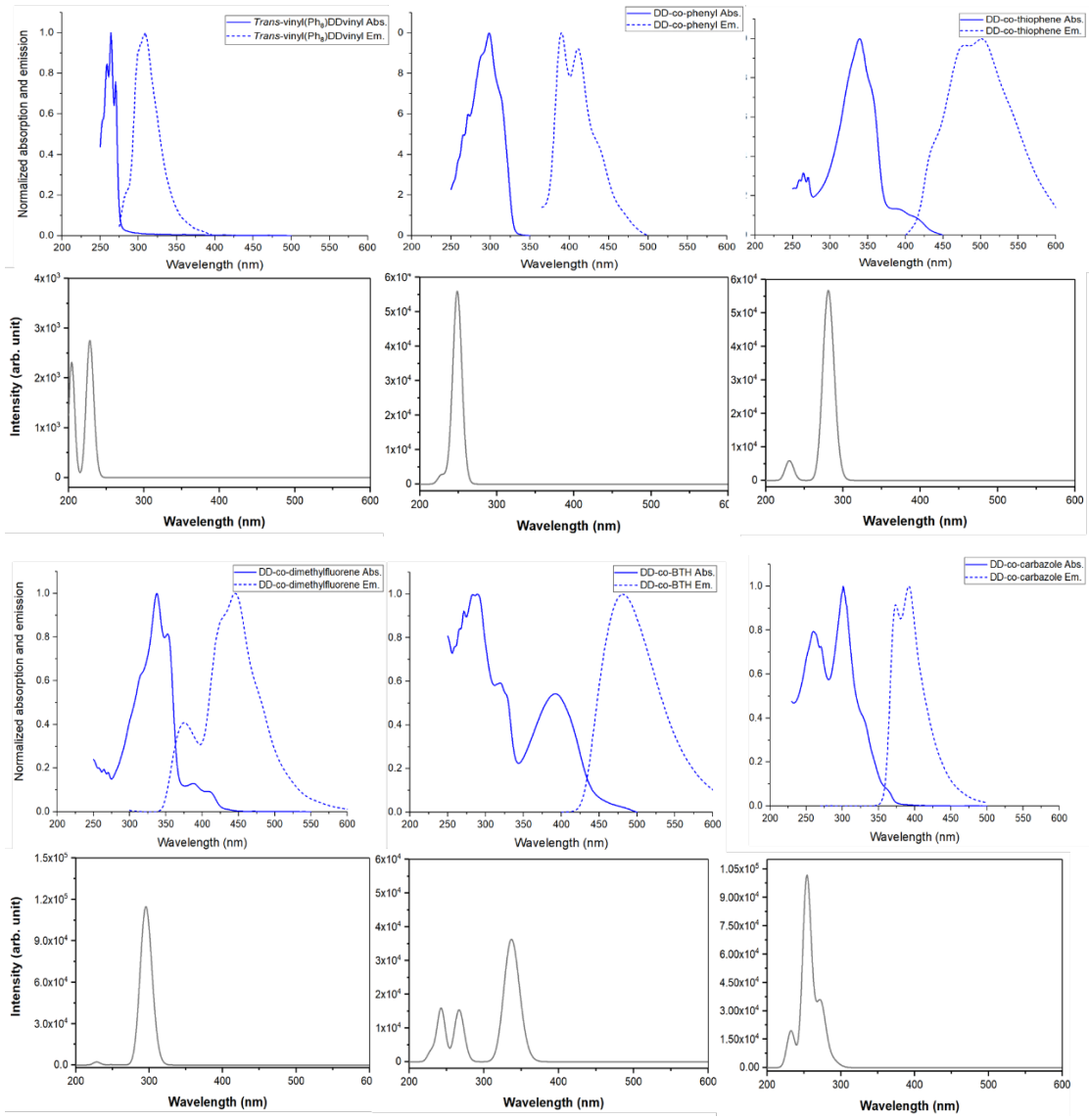

Figure C.33. Experimental absorption and emission spectra (blue) and modeling absorption spectra (grey) for *trans*-vinylDDvinyl and its derived polymers DD-co-phenyl, -thiophene, -dimethylfluorene, -BTH and -carbazole calculated at TD-CAM-B3LYP/6-31G(d) level of theory.

Table C.6. Experimental and modeling data for *trans*- vinylDDvinyl and its derived polymers DD-co-phenyl, -thiophene, -dimethylfluorene, -BTH and -carbazole.

	Experimental Abs. λ_{max} (nm)	Modeling Abs. λ_{max} (nm)	Transition	HOMO (eV)	LUMO (eV)	Egap (eV)
Trans-vinylDDvinyl	264	228	H-10 to L+9	-8.32	1.16	9.48
-phenyl	298	249	HOMO to LUMO	-7.43	0.11	7.54
-thiophene	340	281	HOMO to LUMO	-6.94	-0.03	6.91

-dimethyl-fluorene	339, 353	295	HOMO to LUMO	-6.72	-0.19	6.53
-BTH	392	337	HOMO to LUMO	-6.93	-0.87	6.06
-carbazole	301	254	H-1 to L+1	-7.03	0.44	7.47

Modeling studies were also explored on vinylDDvinyl with corner phenyls substituted by methyls by Professor Kieffer and Dr. Hashemi's group at University of Michigan. In these modeling studies, LUMO+4 and LUMO+5 are from SQ core and cage centered as shown in Figure **C.34** Furthermore, the energy difference is only ~0.6 eV between LUMO in cage and vinyl π*, which makes interaction between cage LUMO and vinyl π* possible. Modeling of a similar structure where two $Si(O-)_2$ units are inserted into the each opposing edge is also investigated in Figure **C.35**. With all methyl substituents, the structure again exhibits cage centered LUMO and LUMO+1.

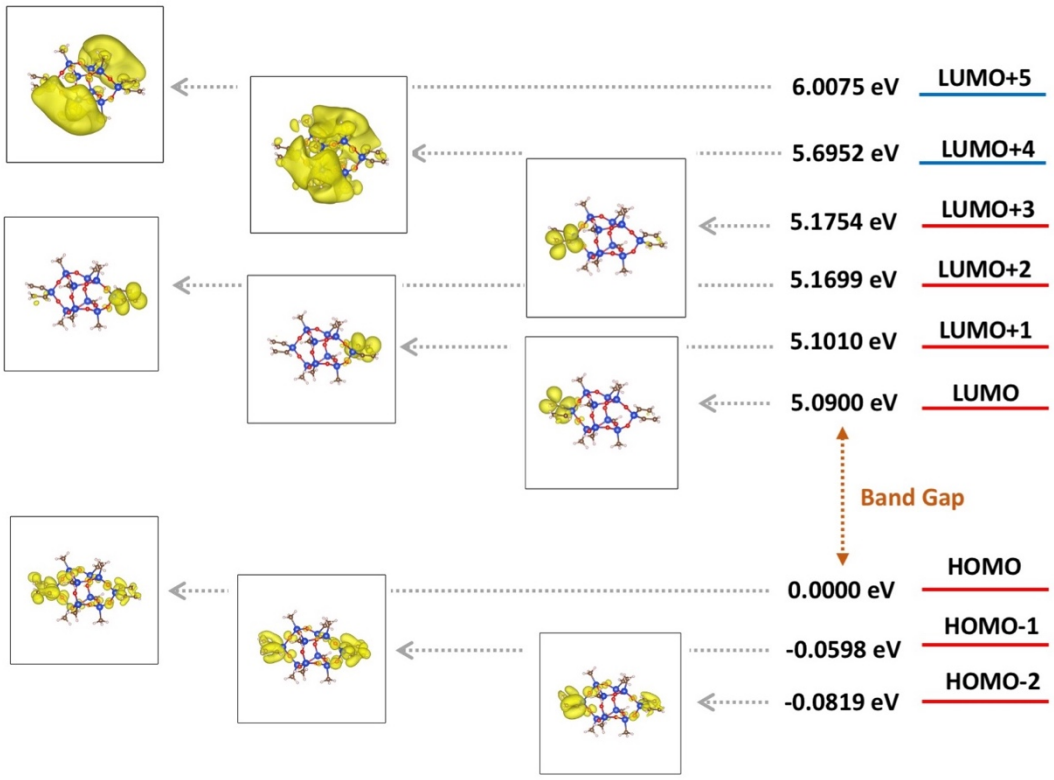

Figure C.34. Energy diagram of the molecular orbitals of vinylDDvinyl showing cage centered LUMO+4 and LUMO+5, calculated using PBE potentials as implemented in VASP.

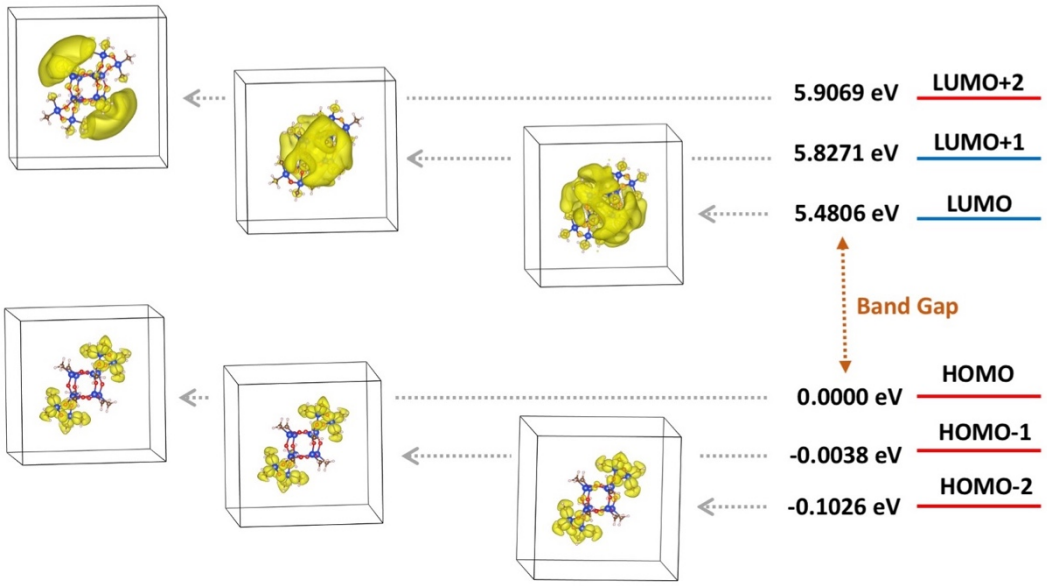

Figure C.35. Energy diagram of the molecular orbitals of methyl substituted DD with two $Si(O-)_2$ unites per opposing edge showing cage centered LUMO and LUMO+1, calculated using PBE potentials as implemented in VASP.

Cyclic voltammetry. We have previously demonstrated that cyclic voltammetry (CV) can be used to measure HOMO LUMO energies in $(RvinylT)_{10/12}$ cages with conjugated moieties.[4] Cyclic voltammograms were run on a CHI 600C electrochemical analyzer using a three-electrode setup. A glassy carbon working electrode was used in conjunction with a platinum wire counter electrode and a silver/silver nitrate reference electrode. All scans were taken in 0.1 M NBu_4PF_6 in acetonitrile at 0.1 V/s. Ferrocene was used for calibration. Samples were dropcast onto the working electrode from THF for each scan polarity because reversible redox behavior was not observed. The LUMO-HOMO levels were inferred from the onset of reduction/oxidation (the intercept of the slope and baseline) for each sample.[4] In these previous studies, we learned to manipulate HOMO LUMO energies by designing $(RvinylT)_{10/12}$ cages with different strongly electron donating/accepting moieties (R). The results of this study again support the existence of cage centered LUMOs and 3-D conjugation; otherwise, one would not anticipate the found energy levels based on those of the individual moieties. In the current studies, we were unable to identify (easily accessible) redox behavior either in solution using the same setup above or in the solid state for the thiophene

copolymers which we believe would be most likely to be easily accessible as they show the greatest red-shifts.

References

(1) Bahrami, M.; Hashemi, H.; Ma, X.; Kieffer, J.; Laine, R. M. Why Do the $[PhSiO_{1.5}]_{8,10,12}$ Cages Self-Brominate Primarily in the Ortho Position? Modeling Reveals a Strong Cage Influence on the Mechanism. *Phys. Chem. Chem. Phys.* **2014**, *16* (47), 25760–25764. https://doi.org/10.1039/C4CP03997A.

(2) Guan, J.; Tomobe, K.; Madu, I.; Goodson, T.; Makhal, K.; Trinh, M. T.; Rand, S. C.; Yodsin, N.; Jungsuttiwong, S.; Laine, R. M. Photophysical Properties of Partially Functionalized Phenylsilsesquioxane: $[RSiO_{1.5}]_7[Me/NPrSiO_{1.5}]$ and $[RSiO_{1.5}]_7[O_{0.5}SiMe_3]_3$ (R = 4-Me/4-CN-Stilbene). Cage-Centered Magnetic Fields Form under Intense Laser Light. *Macromolecules* **2019**, *52* (11), 4008–4019. https://doi.org/10.1021/acs.macromol.9b00699.

(3) Guan, J.; Tomobe, K.; Madu, I.; Goodson, T.; Makhal, K.; Trinh, M. T.; Rand, S. C.; Yodsin, N.; Jungsuttiwong, S.; Laine, R. M. Photophysical Properties of Functionalized Double Decker Phenylsilsesquioxane Macromonomers: $[PhSiO_{1.5}]_8[OSiMe_2]_2$ and $[PhSiO_{1.5}]_8[O_{0.5}SiMe_3]_4$. Cage-Centered Lowest Unoccupied Molecular Orbitals Form Even When Two Cage Edge Bridges Are Removed, Verified by Modeling and Ultrafast Magnetic Light Scattering Experiments. *Macromolecules* **2019**, *52* (19), 7413–7422. https://doi.org/10.1021/acs.macromol.9b00700.

(4) Hwan Jung, J.; Furgal, J. C.; Goodson, T.; Mizumo, T.; Schwartz, M.; Chou, K.; Vonet, J.-F.; Laine, R. M. 3-D Molecular Mixtures of Catalytically Functionalized $[VinylSiO_{1.5}]_{10}$ /$[VinylSiO_{1.5}]_{12}$. Photophysical Characterization of Second Generation Derivatives. *Chem. Mater.* **2012**, *24* (10), 1883–1895. https://doi.org/10.1021/cm300587s.

Appendix D. Unconventional Conjugation Siloxane Bridges in Ladder Silsesquioxane Copolymers

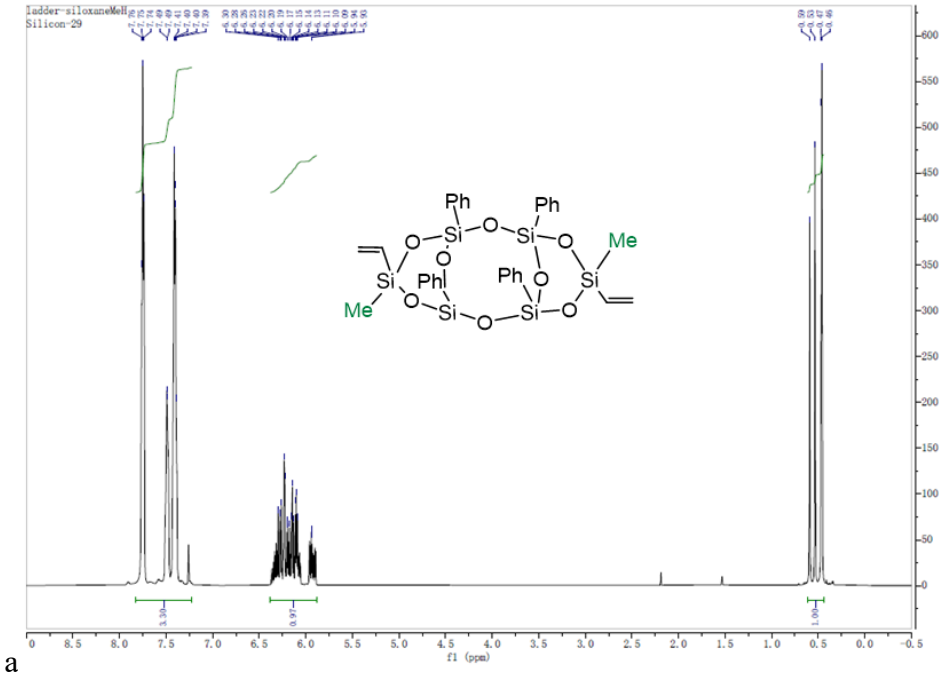

a

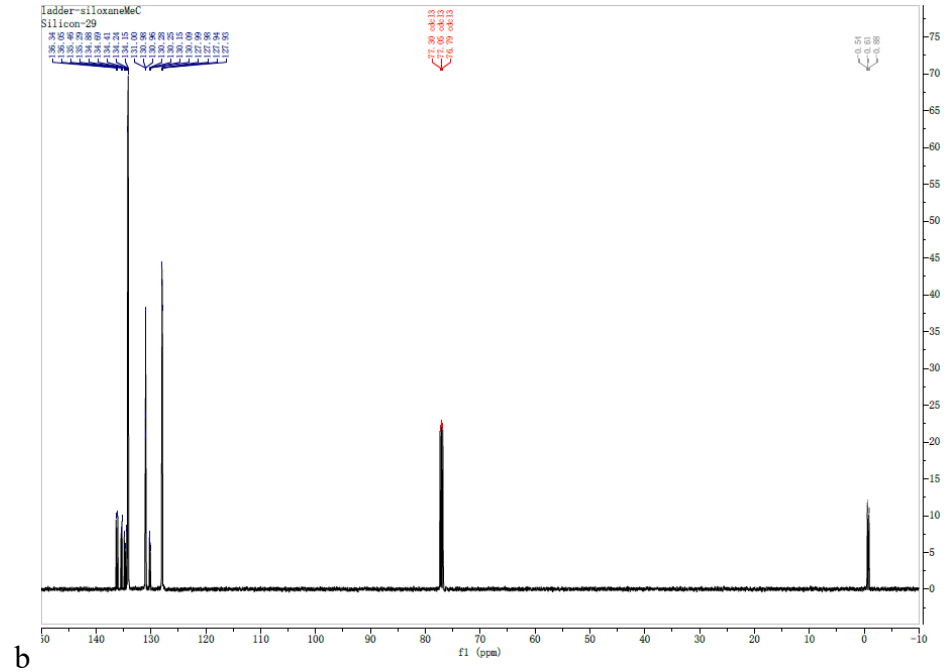

b

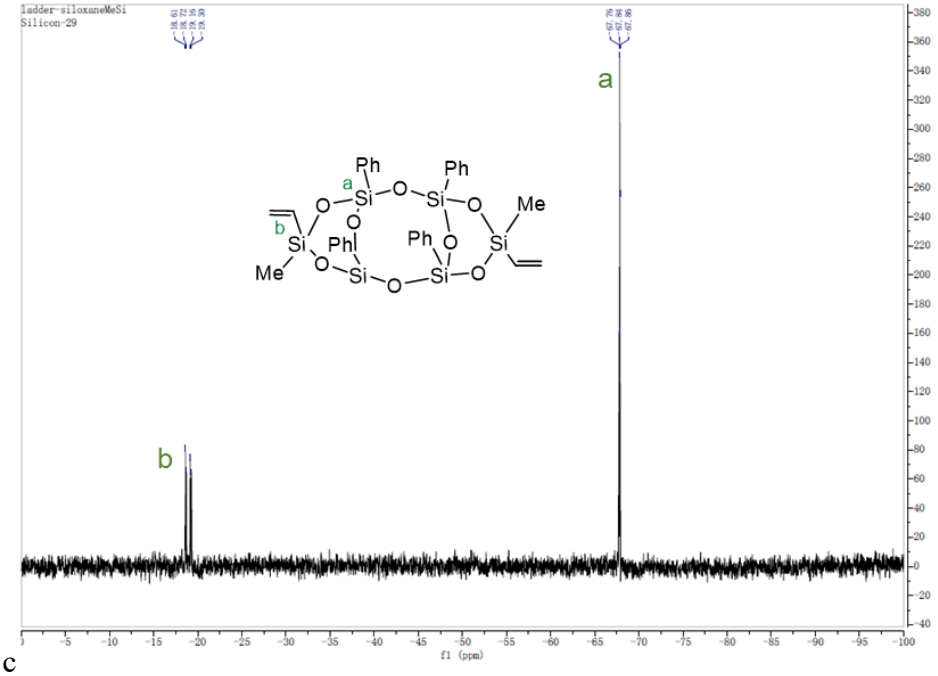

c

Figure D.1. (a) ^{1}H NMR, (b) ^{13}C NMR, (c) ^{29}Si NMR of vinyl-LL(Me)-vinyl.

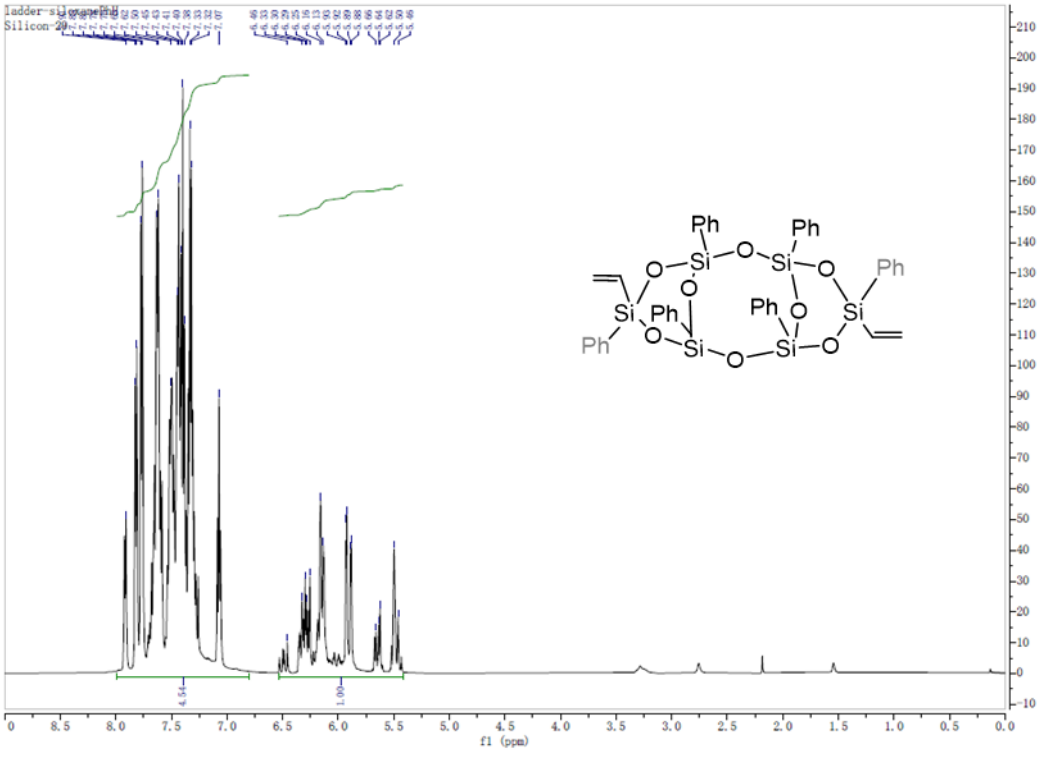

a

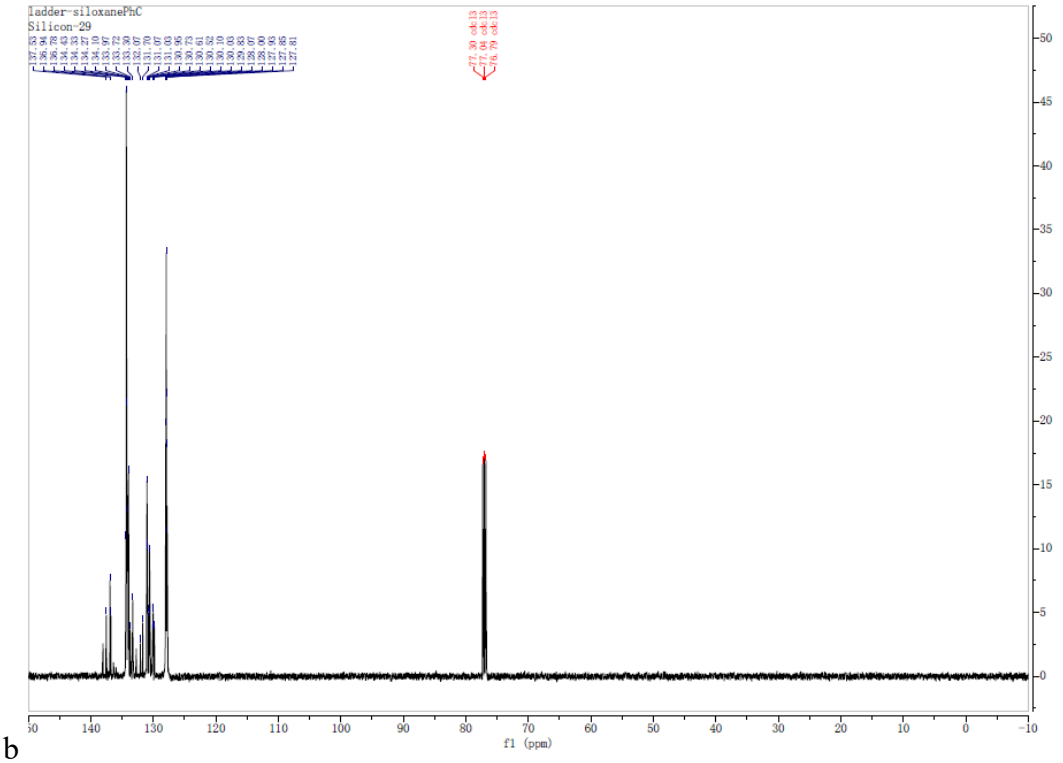

b

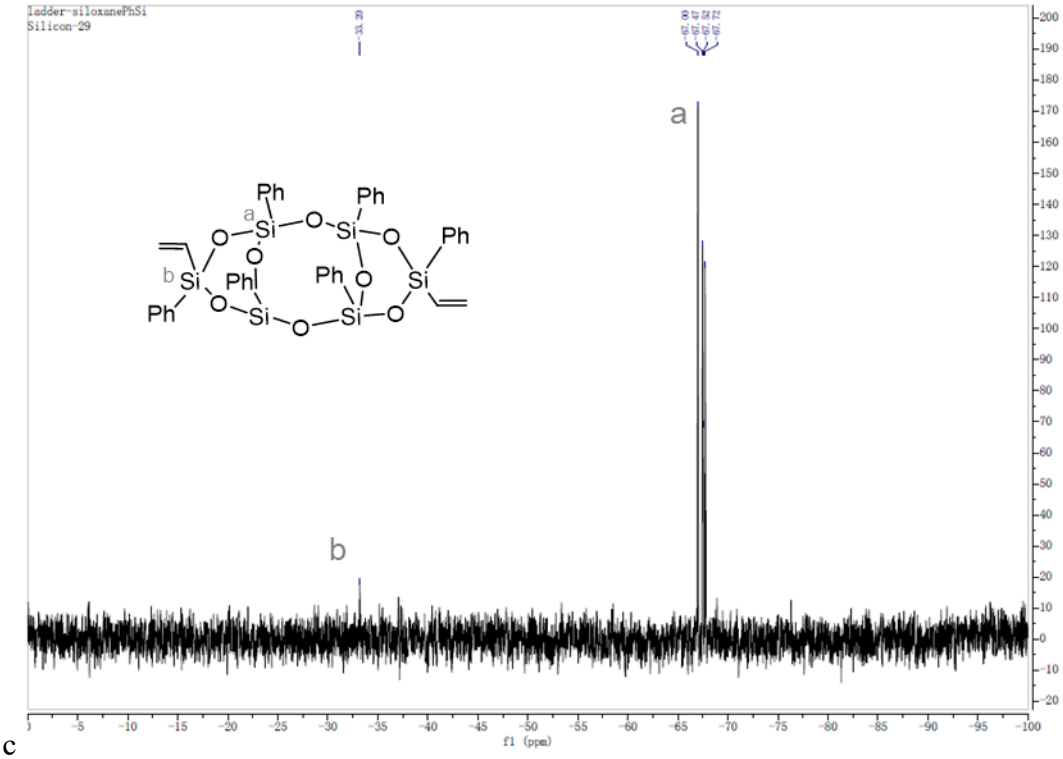

c

Figure D.2. (a) ^{1}H NMR, (b) ^{13}C NMR, (c) ^{29}Si NMR of vinyl-LL(Ph)-vinyl.

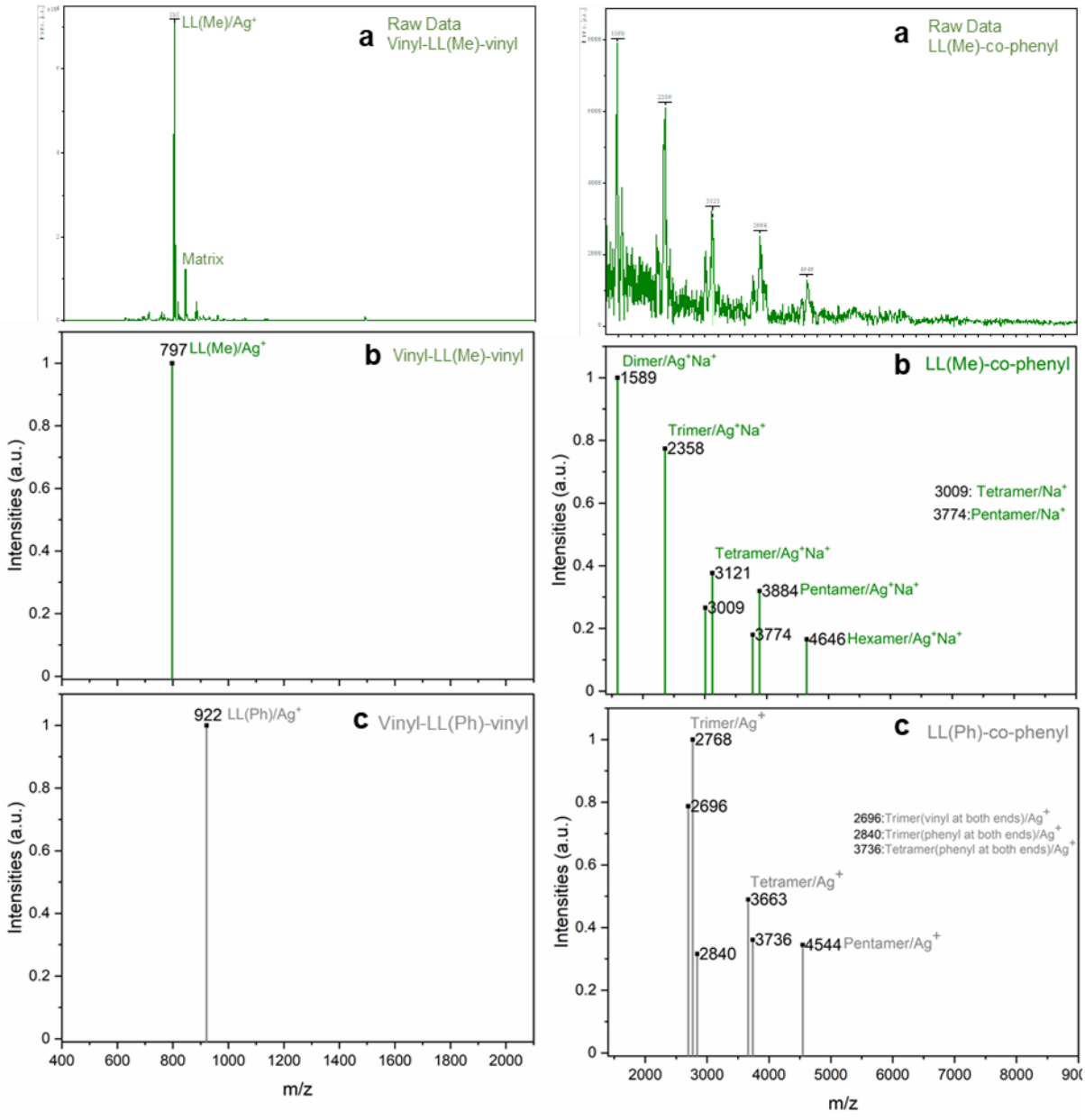

Figure D.3. Left: (a) Raw MALDI-TOF of vinyl-LL(Me)-vinyl, (b) Modified MALDI-TOF of vinyl-LL(Me)-vinyl, (c) Modified MALDI-TOF of vinyl-LL(Ph)-vinyl. Right: (a) Raw MALDI-TOF of LL(Me)-co-phenyl, (b) Modified MALDI-TOF of LL(Me)-co-phenyl, (c) Modified MALDI-TOF of LL(Ph)-co-phenyl.

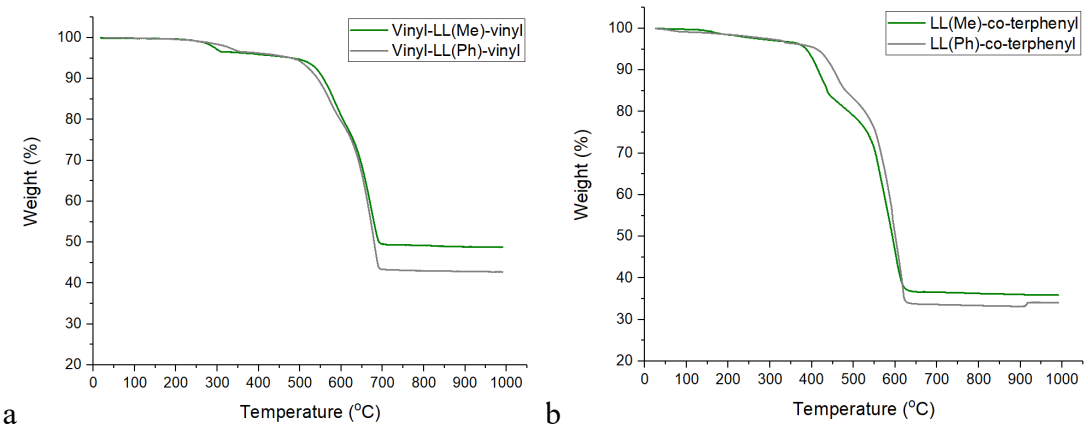

Figure D.4. (a) TGA of vinyl-LL(Me)-vinyl and vinyl-LL(Ph)-vinyl, (b) TGA of LL(Me)-co-terphenyl and LL(Ph)-co-phenyl.

Table D.1. MALDI-TOF, GPC and TGA data for vinyl-LL-vinyl and derived polymers.

Compound	MALDI-TOF m/z		GPC			TGA		
	Mer	Theor	M_n	M_w	Đ[b]	Ceramic yield %	Theor yield %	$T_{d5\%}$ °C (air)
Vinyl-LL(Me)-vinyl	797[a]	797[a]	490	530	1.08	49	51	490
Co-phenyl	764	765	5420	15190	2.80	46	46	430
Co-biphenyl	839	841	11700	44000	3.78	42	42	410
Co-terphenyl	921	917	15850	46580	2.95	37	39	390
Co-stilbene	870	867	6280	19620	3.12	40	41	340
Co-dimethylfluorene	881	881	5810	15780	2.72	39	40	400
Co-thiophene	772	771	3170	6190	1.95	46	46	450
Co-bithiophene	853	853	5540	11330	2.05	40	42	440
Co-thienothiophene	831	827	7400	17100	2.31	41	43	390
Vinyl-LL(Ph)-vinyl	922[a]	921[a]	540	620	1.15	43	43	490
Co-phenyl	891	889	5690	15000	2.63	40	40	430
Co-biphenyl	963	965	8180	28050	3.43	35	37	380
Co-terphenyl	1041	1041	8390	22070	2.63	34	34	420
Co-stilbene	988	991	6620	15990	2.42	35	36	390
Co-dimethylfluorene	1006	1005	5950	17770	2.99	34	35	400
Co-thiophene	895	895	4360	8060	1.85	38	40	400
Co-bithiophene	979	977	4330	6710	1.55	36	36	460
Co-thienothiophene	952	951	7470	19410	2.60	35	37	440

[a] As Ag^+ adduct. [b] Polydispersity.

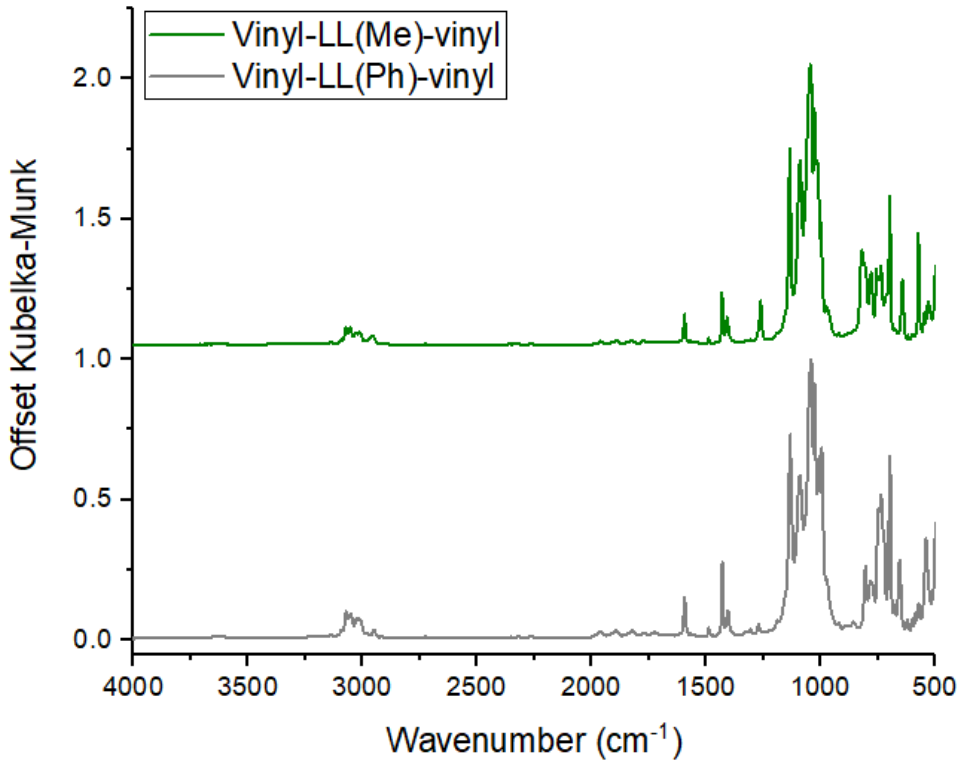

Figure D.5. FTIR of vinyl-LL(Me)-vinyl and vinyl-LL(Ph)-vinyl.

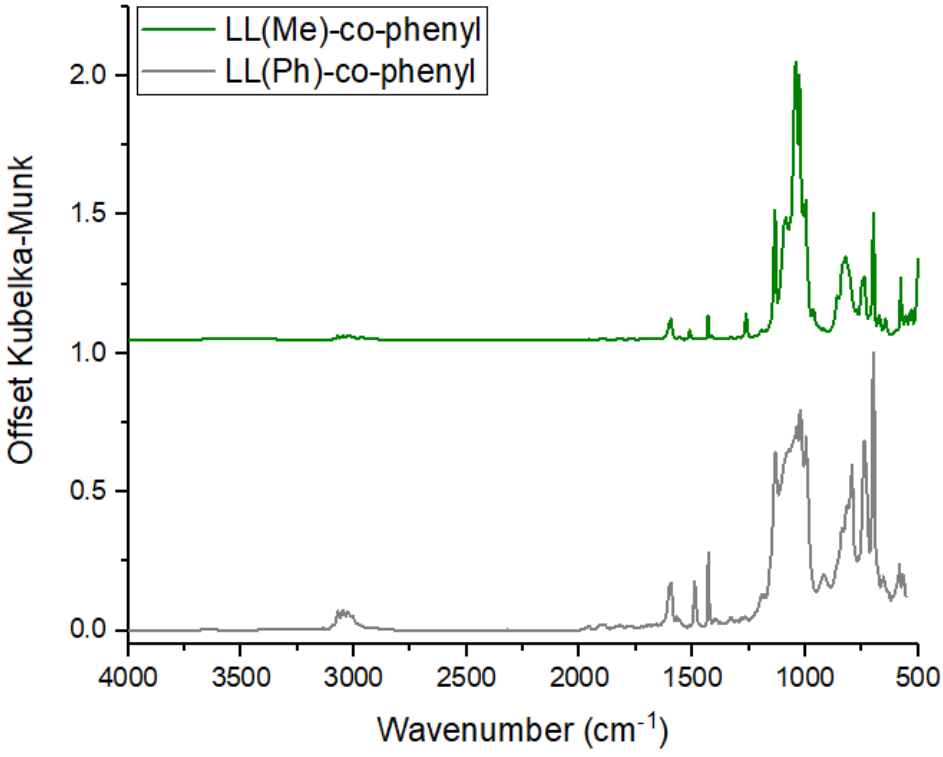

Figure D.6. FTIR of LL(Me)-co-phenyl and LL(Ph)-co-phenyl.

Table D.2. Representative FTIR data of selected compounds.

Compound	v	Wavenumber (cm^{-1})	Intensity
Vinyl-LL(Me)-vinyl	Si-O-Si	998	Medium, sharp
	Si-O-Si	1027	Strong, sharp
	Si-O-Si	1044	Strong, sharp
	Si-O-Si	1090	Strong, sharp
	Si-O-Si	1134	Strong, sharp
	C=C	1262	Medium, sharp
	C=C	1408	Weak, sharp
	C=C	1431	Medium, sharp
	C=C	1595	Medium, sharp
	C-H	2950	Weak, broad
	C-H	3073	Weak, broad
LL(Me)-co-phenyl	Si-O-Si	998	Medium, sharp
	Si-O-Si	1026	Strong, sharp
	Si-O-Si	1041	Strong, sharp
	Si-O-Si	1086	Medium, sharp
	Si-O-Si	1135	Medium, sharp
	C=C	1262	Medium, sharp
	C=C	1430	Medium, sharp
	C=C	1595	Medium, sharp
	C-H	3070	Weak, broad
Vinyl-LL(Ph)-vinyl	Si-O-Si	996	Medium, sharp
	Si-O-Si	1026	Strong, sharp
	Si-O-Si	1042	Strong, sharp
	Si-O-Si	1091	Medium, sharp
	Si-O-Si	1134	Strong, sharp
	C=C	1405	Weak, sharp
	C=C	1430	Medium, sharp
	C=C	1594	Medium, sharp
	C-H	2925	Weak, broad
	C-H	3072	Weak, broad
LL(Ph)-co-phenyl	Si-O-Si	996	Strong, sharp
	Si-O-Si	1022	Strong, sharp
	Si-O-Si	1037	Strong, broad
	Si-O-Si	1133	Strong, sharp
	C=C	1429	Medium, sharp
	C=C	1490	Medium, sharp
	C=C	1594	Medium, sharp
	C-H	2925	Weak, broad
	C-H	3049	Weak, broad

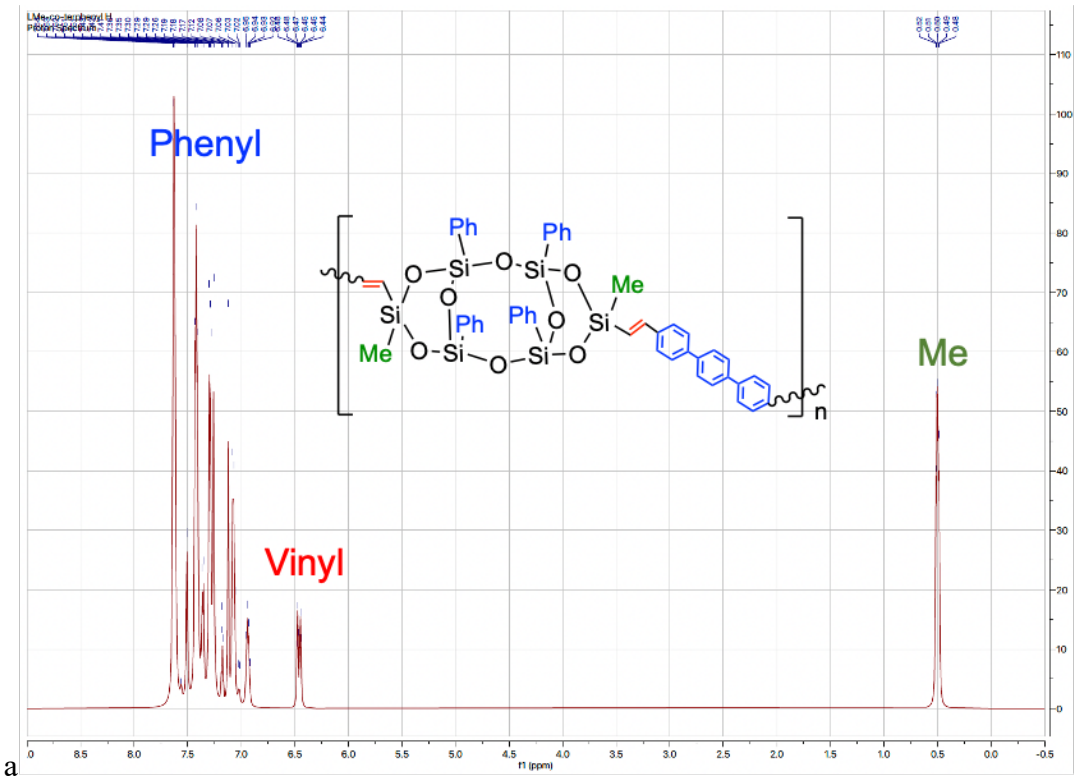

a

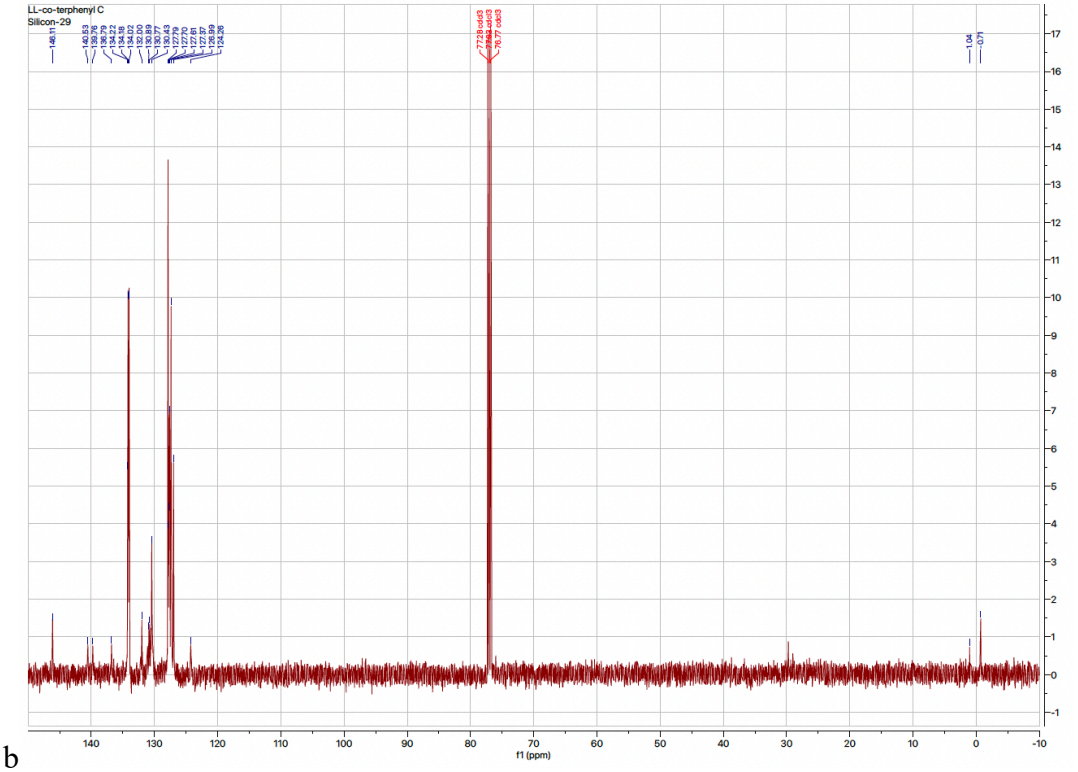

b

Figure D.7. (a) ^{1}H NMR, (b) ^{13}C NMR of LL(Me)-co-terphenyl.

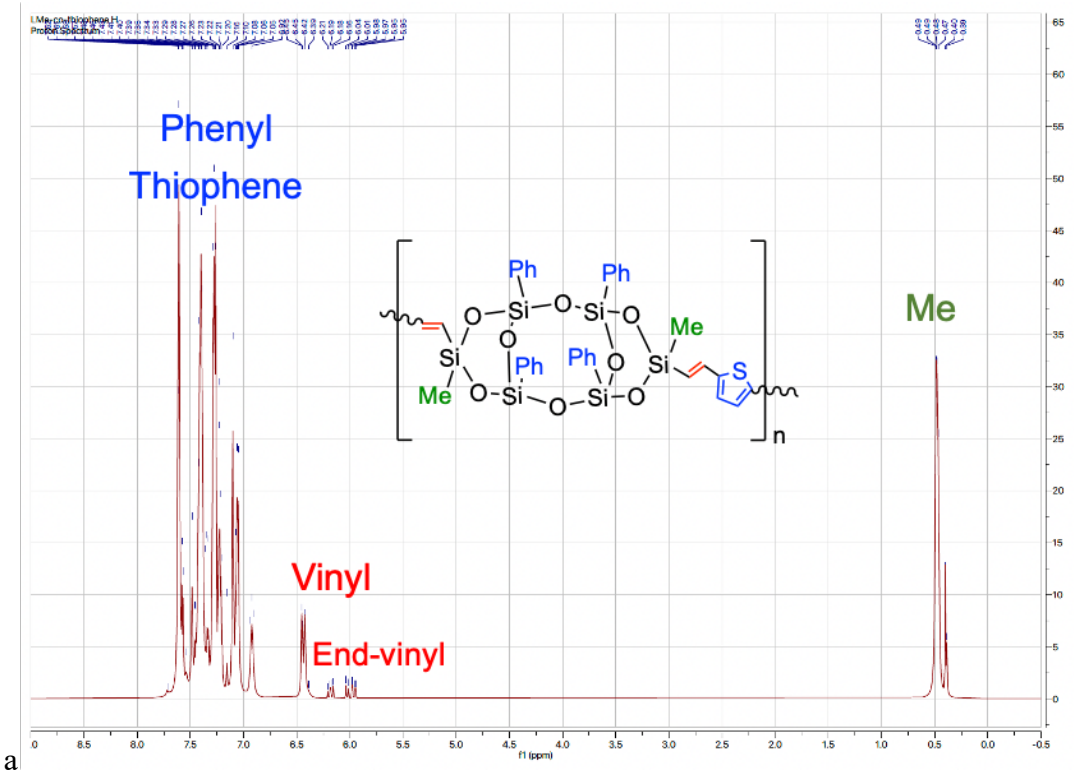

a

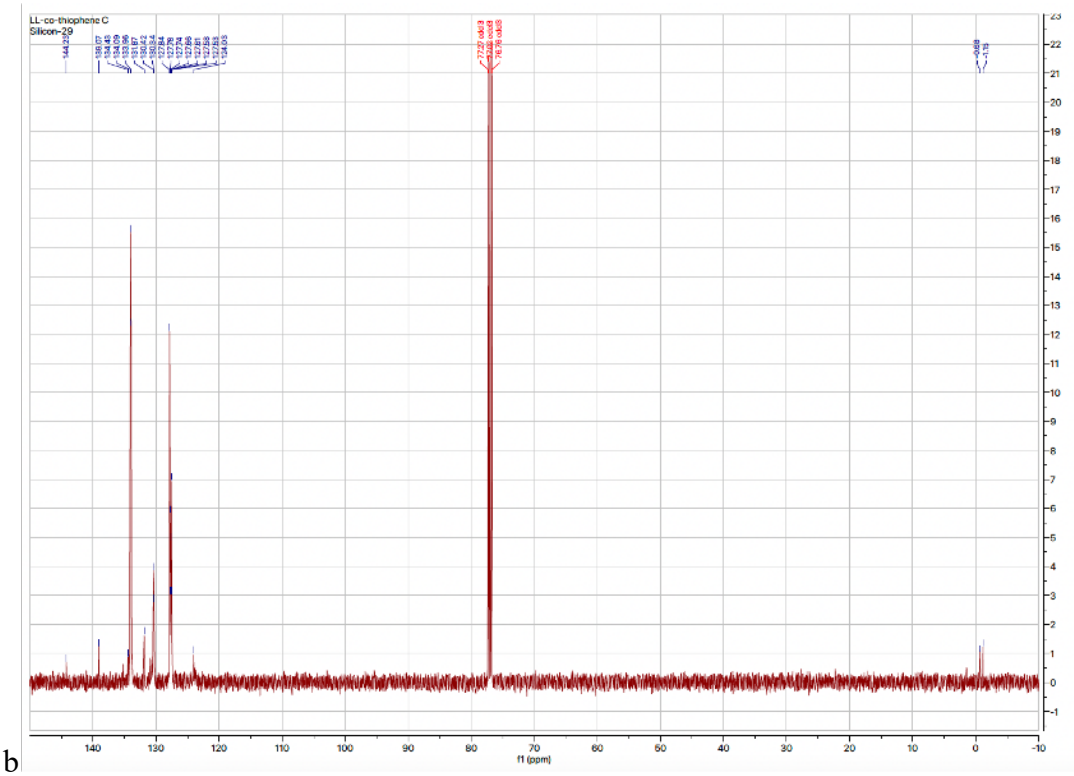

b

Figure D.8. (a) ^{1}H NMR, (b) ^{13}C NMR of LL(Me)-co-thiophene.

Table D.3. ^{1}H and ^{13}NMR data of vinyl-LL(Me)-vinyl derived polymers.

Compound	^{1}H NMR peaks (ppm)	^{13}C NMR peaks (ppm)
LL-co-phenyl	7.7-7.2 (m, 20H, cage-Ph); 7.2-7.0 (m, 4H, co-Ph); 6.9 (d, 2H, vinyl); 6.5 (d, 2H, vinyl); 0.5 (m, 6H, Me)	146.1; 137.8; 134.0; 132.0; 131.1; 127.7; 127.0; 124.2; -0.6
LL-co-biphenyl	7.6-7.2 (m, 20H, Ph); 7.2-7.0 (m, 8H, Ph); 6.9 (d, 2H, vinyl); 6.5 (d, 2H, vinyl); 0.4 (m, 6H, Me)	146.1; 140.6; 136.7; 134.2; 132.0; 130.8 127.8; 126.9; 124.3; -0.7
LL-co-ter-phenyl	7.7-7.3 (m, 20H, Ph); 7.3-7.0 (m, 12H, Ph); 7.0 (d, 2H, vinyl); 6.5 (d, 2H, vinyl); 0.5 (m, 6H, Me)	146.1; 140.5; 139.8; 136.8; 134.2; 132.0; 130.7; 127.9; 127.0; 124.3; -0.7
LL-co-stilbene	7.8-7.0 (m, 28H, Ph); 6.9 (m, 3H, vinyl); 6.4 (m, 3H, vinyl); 0.5 (t, 6H, Me)	146.2; 137.7; 137.5; 136.1 134.0; 132.0; 131.1; 127.9; 127.0; 124.3; -0.6
LL-co-dimethylfluorene	8.0-7.2 (m, 26H); 7.0 (d, 2H, vinyl); 6.5 (d, 2H, vinyl); 1.8 (s, 6H, Me); 0.4 (m, 6H, Me)	147.8; 146.2; 141.0; 137.7; 134.0; 131.9; 130.8; 129.6; 127.6; 126.7; 123.2; 121.6; 45.5; 30.9; -0.6;
LL-co-thiophene	7.6-7.1 (m, 22H); 6.9 (d, 2H, vinyl); 6.4 (d, 2H, vinyl); 6.2 (t, 2H, vinyl); 6.0 (q, 1H, vinyl); 0.5 (m, 6H, Me)	144.2; 139.1; 134.4; 134.0; 131.9; 130.4; 127.8; 127.5; 124.0; -0.7
LL-co-bithiophene	7.7-7.2 (m, 24H); 6.9 (d, 2H, vinyl); 6.5 (d, 2H, vinyl); 6.2 (t, 2H, vinyl); 5.9 (q, 1H, vinyl); 0.5 (m, 6H, Me)	144.2; 139.1; 138.1; 134.1; 134.0; 132.5; 131.8; 130.4; 127.7; 127.5; 124.0; -0.7
LL-co-thienothiophene	7.6-7.2 (m, 22H); 6.9 (d, 2H, vinyl); 6.5 (d, 2H, vinyl); 6.2 (t, 2H, vinyl); 5.9 (m, 1H, vinyl); 0.5 (m, 6H, Me)	144.1; 139.1; 134.4; 133.9; 131.8; 130.3; 129.3; 127.7; 127.5; 124.0; -0.6

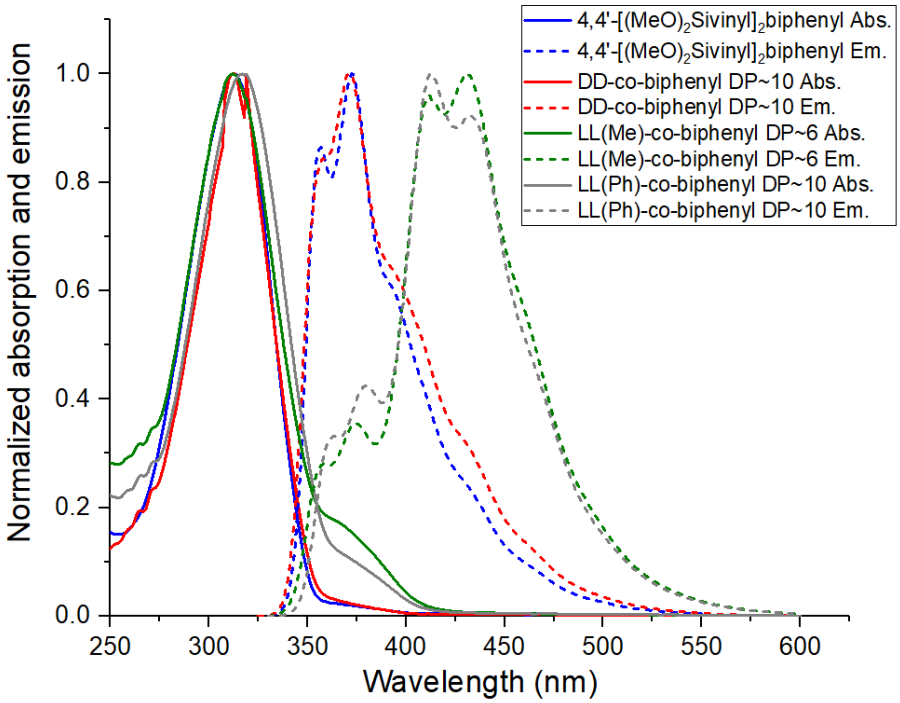

Figure D.9. Normalized steady-state spectra of 4,4'-[(MeO)$_2$Sivinyl]$_2$biphenyl, DD-co-biphenyl and LL(Me/Ph)-co-biphenyl in CH_2Cl_2.

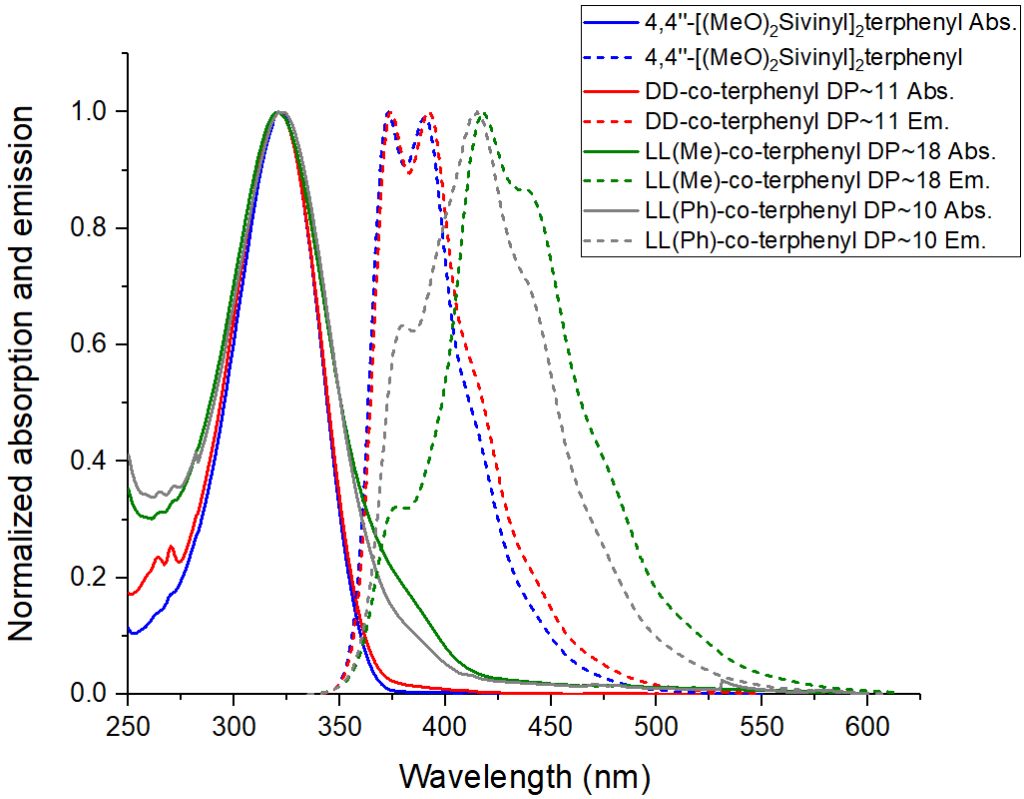

Figure D.10. Normalized steady-state spectra of 4,4''-[$(MeO)_2$Sivinyl]$_2$terphenyl, DD-co-terphenyl and LL(Me/Ph)-co-terphenyl in CH_2Cl_2.

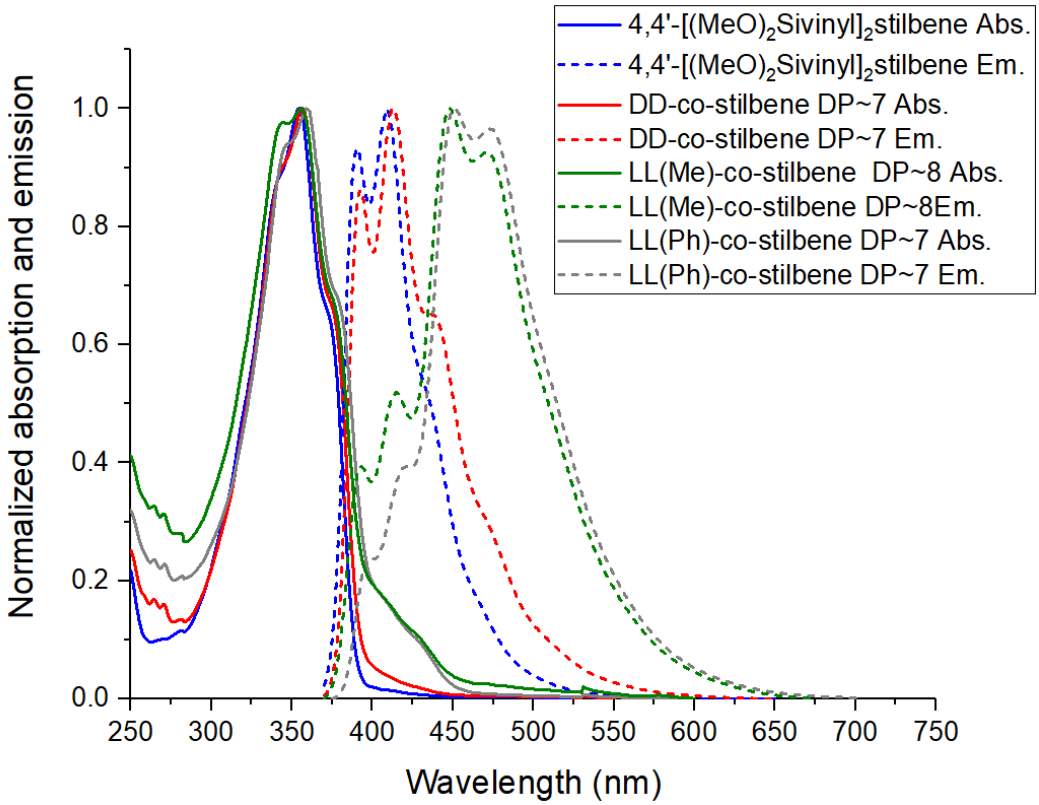

Figure D.11. Normalized steady-state spectra of 4,4'-[$(MeO)_2$Sivinyl]$_2$stilbene, DD-co-stilbene and LL(Me/Ph)-co-stilbene in CH_2Cl_2.

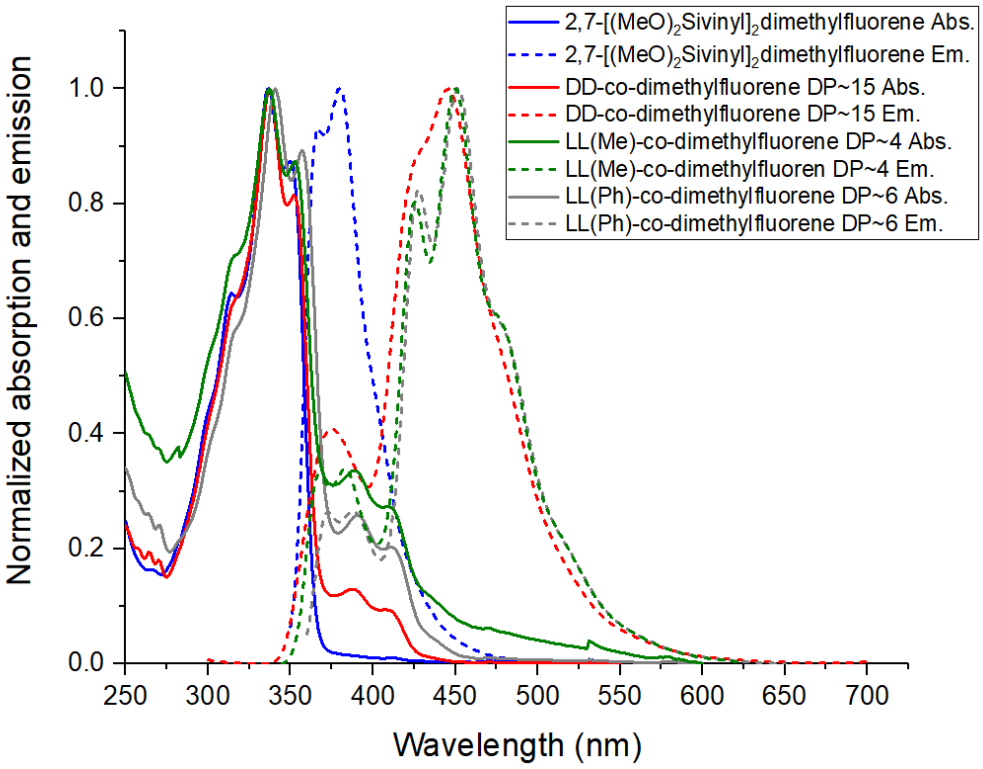

Figure D.12. Normalized steady-state spectra of 2,7-[$(MeO)_2$Sivinyl]$_2$dimethylfluorene, DD-co-dimethylfluorene and LL(Me/Ph)-co-dimethylfluorene in CH_2Cl_2.

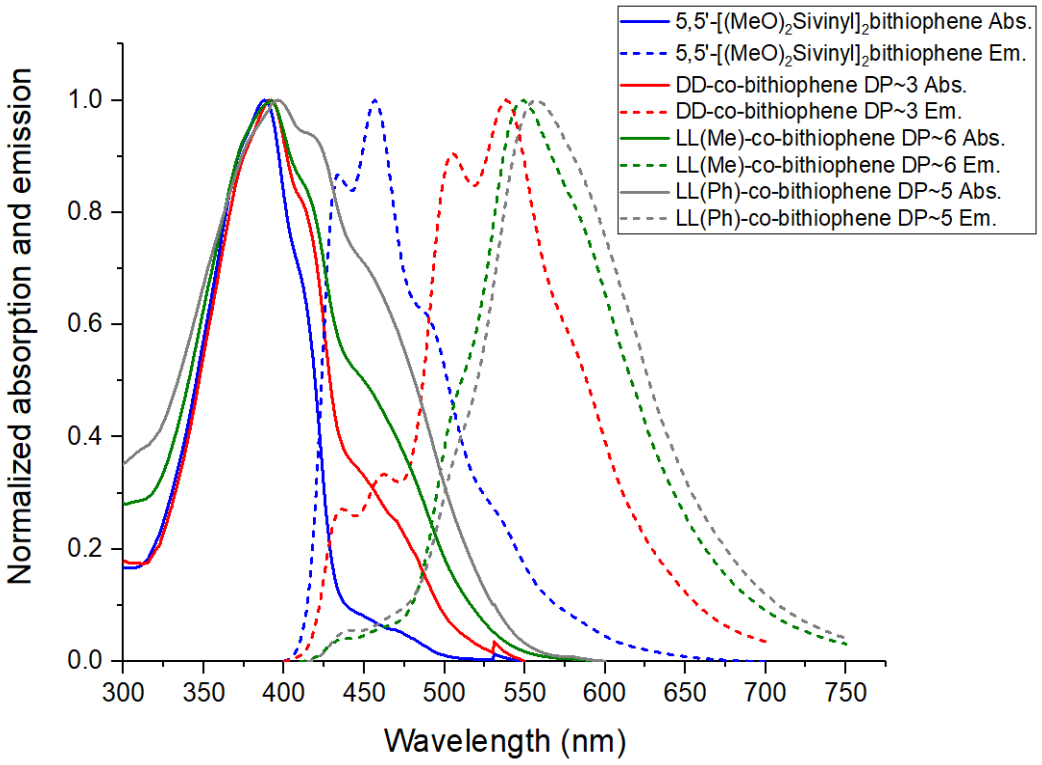

Figure D.13. Normalized steady-state spectra of 5,5'-[$(MeO)_2$Sivinyl]$_2$bithiophene, DD-co-bithiophene and LL(Me/Ph)-co-bithiophene in CH_2Cl_2.

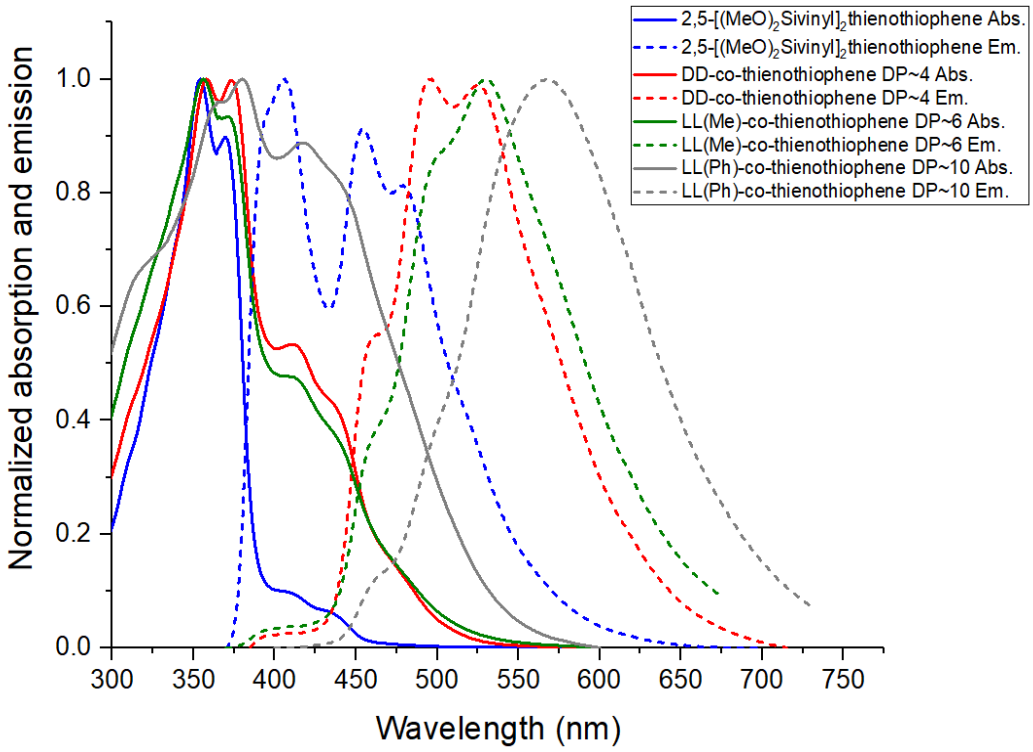

Figure D.14. Normalized steady-state spectra of 2,5-[$(MeO)_2$Sivinyl]$_2$thienothiophene, DD-co-thienothiophene and LL(Me/Ph)-co-thienothiophene in CH_2Cl_2.

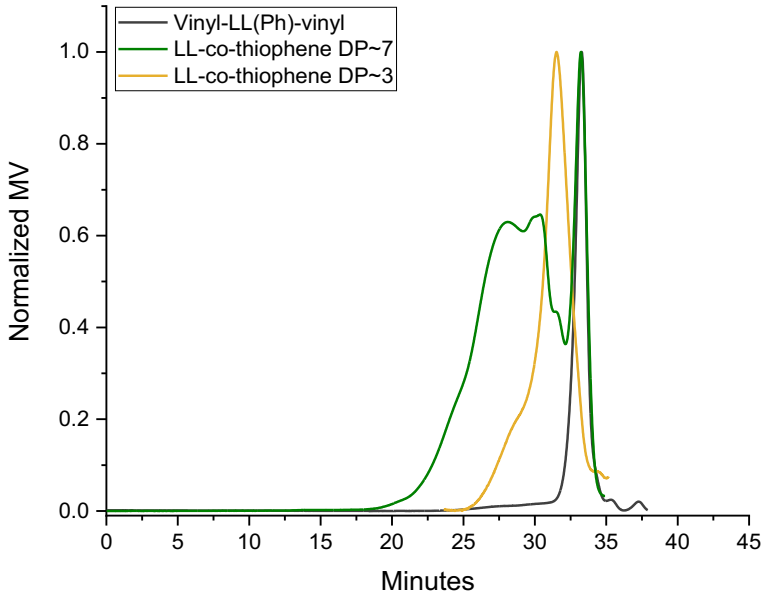

Figure D.15. GPC of vinyl-LL-vinyl, short oligomers of LL-co-thiophene separate from TLC and long oligomers of LL-co-thiophene.

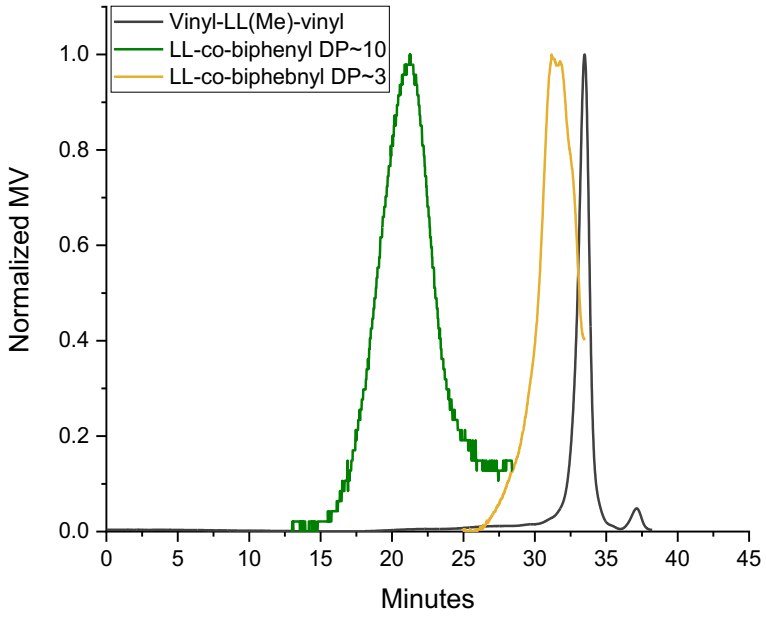

Figure D.16. GPC of vinyl-LL-vinyl, short oligomers of LL-co-biphenyl separate from TLC and long oligomers of LL-co-biphenyl.

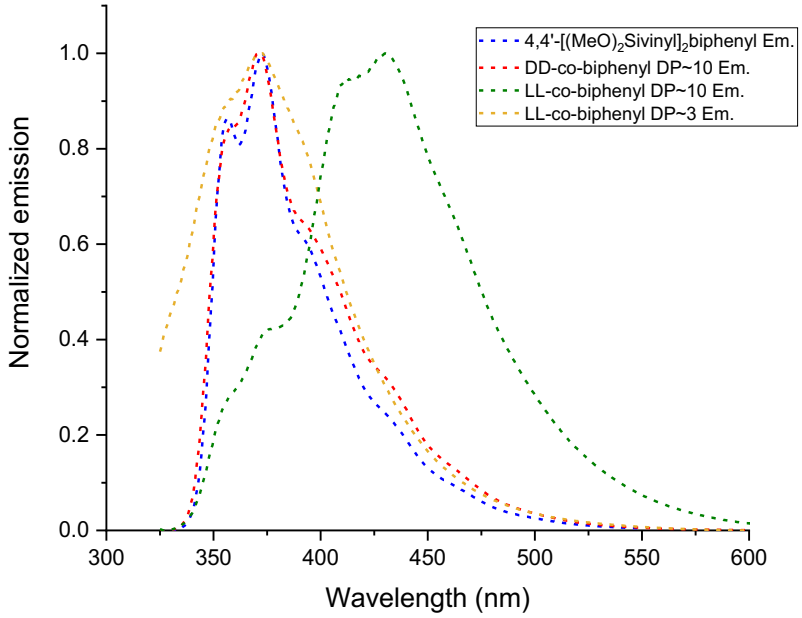

Figure D.17. Normalized progressive emission spectra of 4,4'-[$(MeO)_2$Sivinyl]$_2$biphenyl, DD-co-biphenyl, short (DP~3) and long (DP~8) LL-co-biphenyl in CH_2Cl_2.

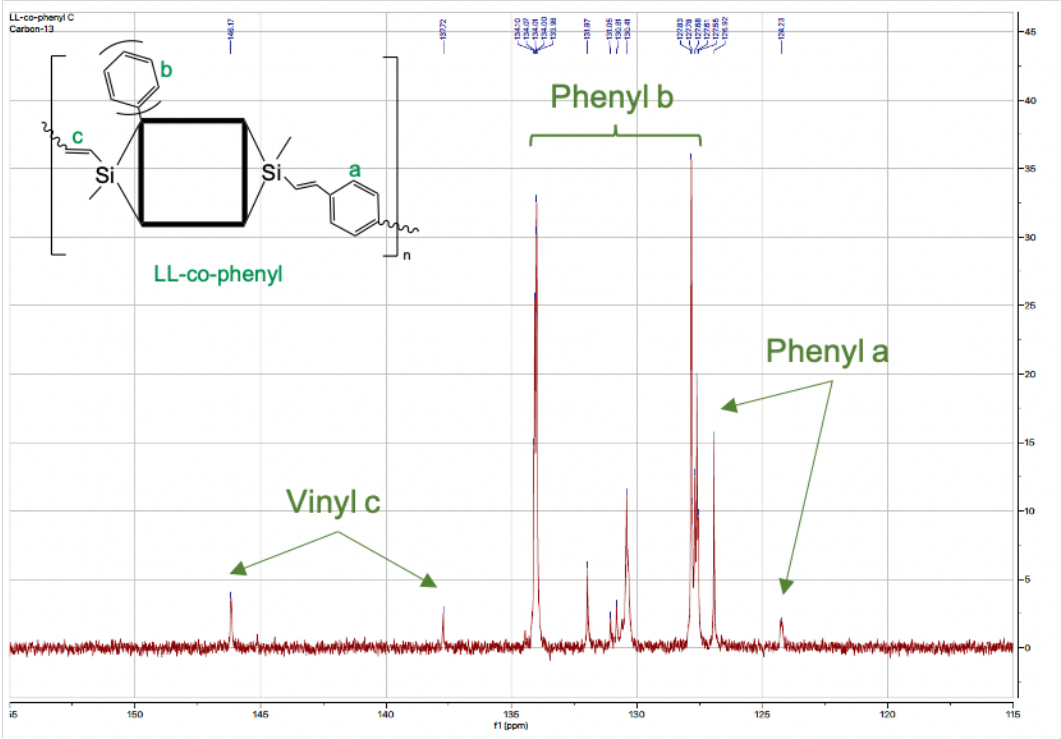

Figure D.18. ^{13}C NMR of LL-co-phenyl (zoom-in).

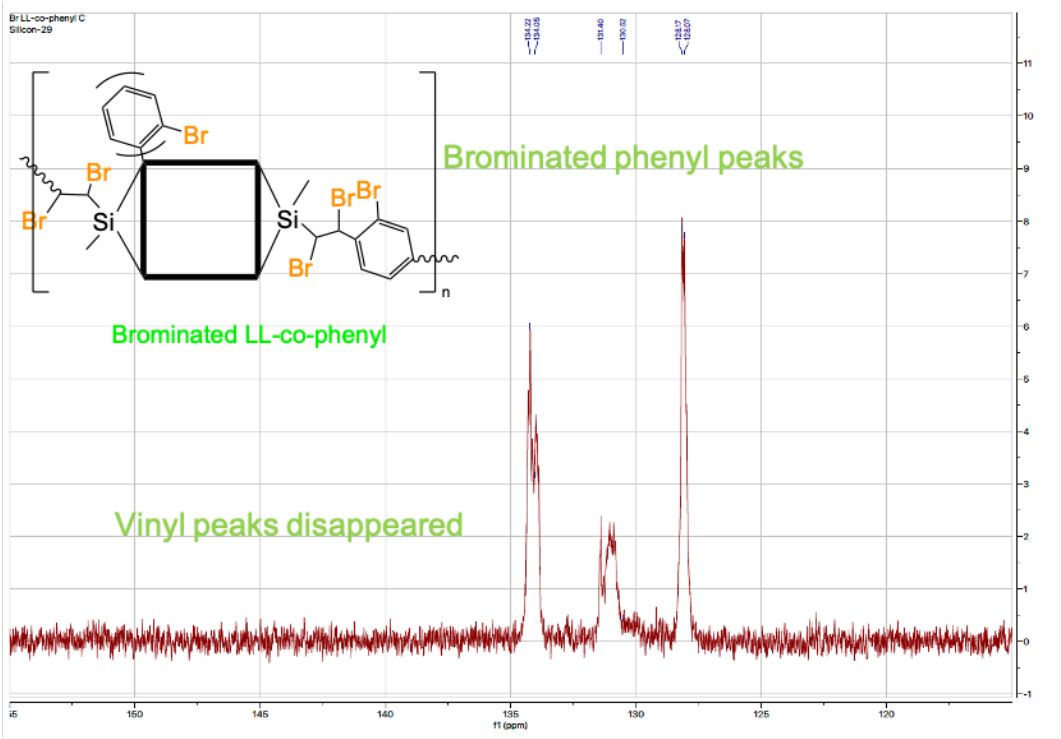

Figure D.19. ^{13}C NMR of brominated LL-co-phenyl (zoom-in).

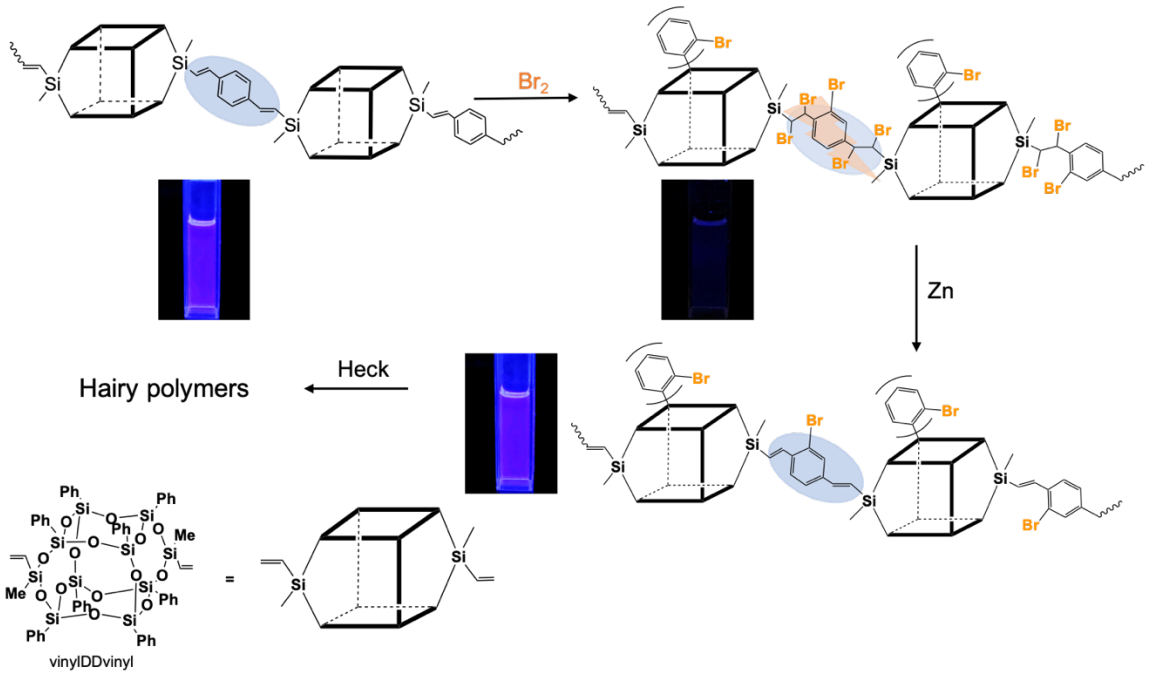

Figure D.20. Bromination and debromination of DD-co-phenyl.

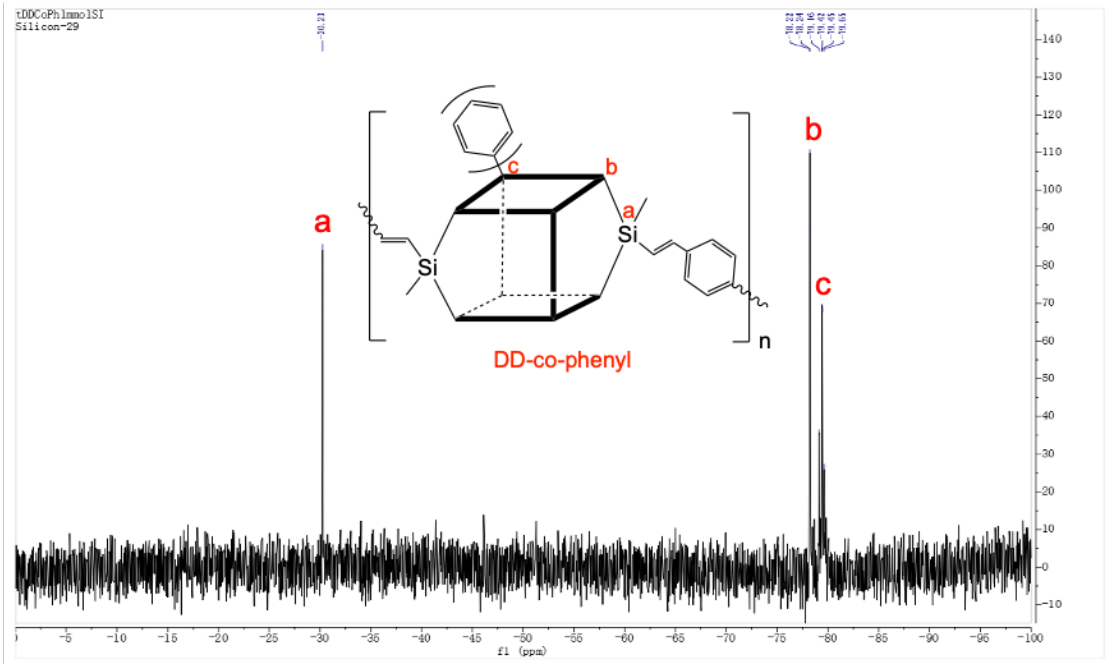

Figure D.21. ^{29}Si NMR of DD-co-phenyl.

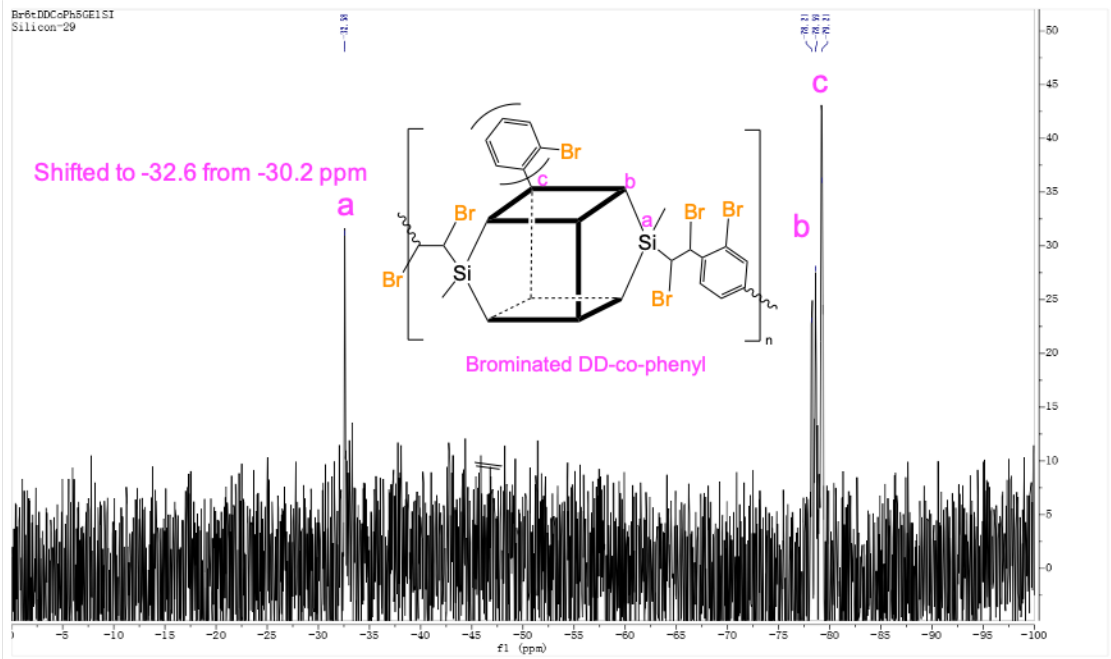

Figure D.22. ^{29}Si NMR of brominated DD-co-phenyl.

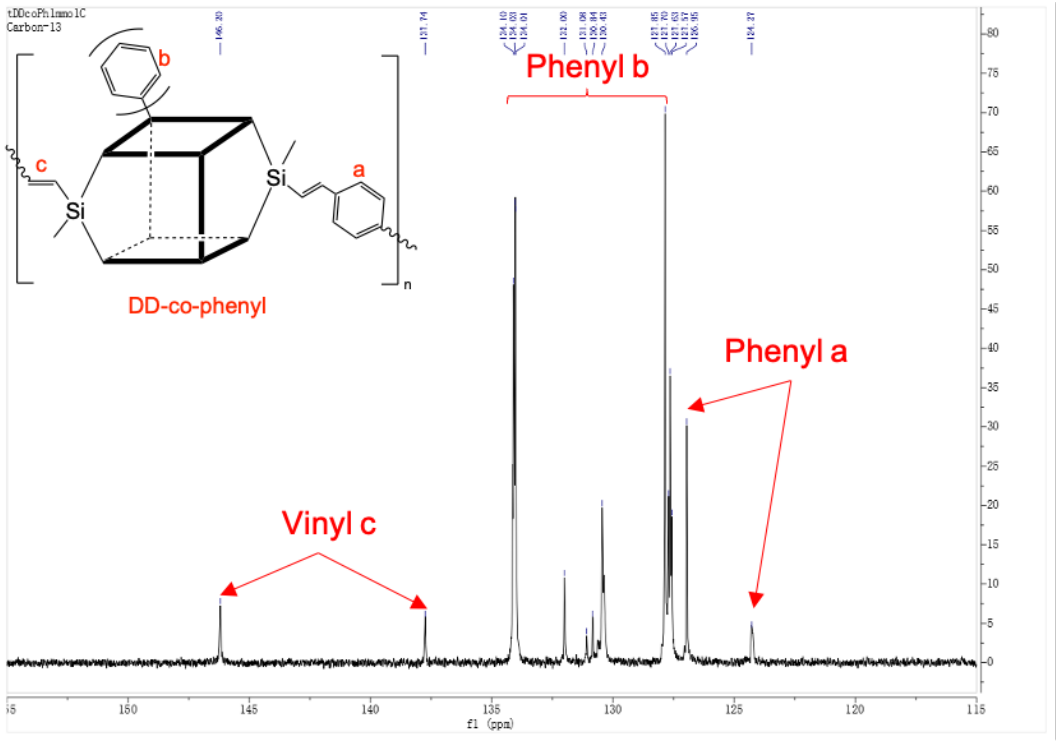

Figure D.23. ^{13}C NMR of DD-co-phenyl (zoom-in).

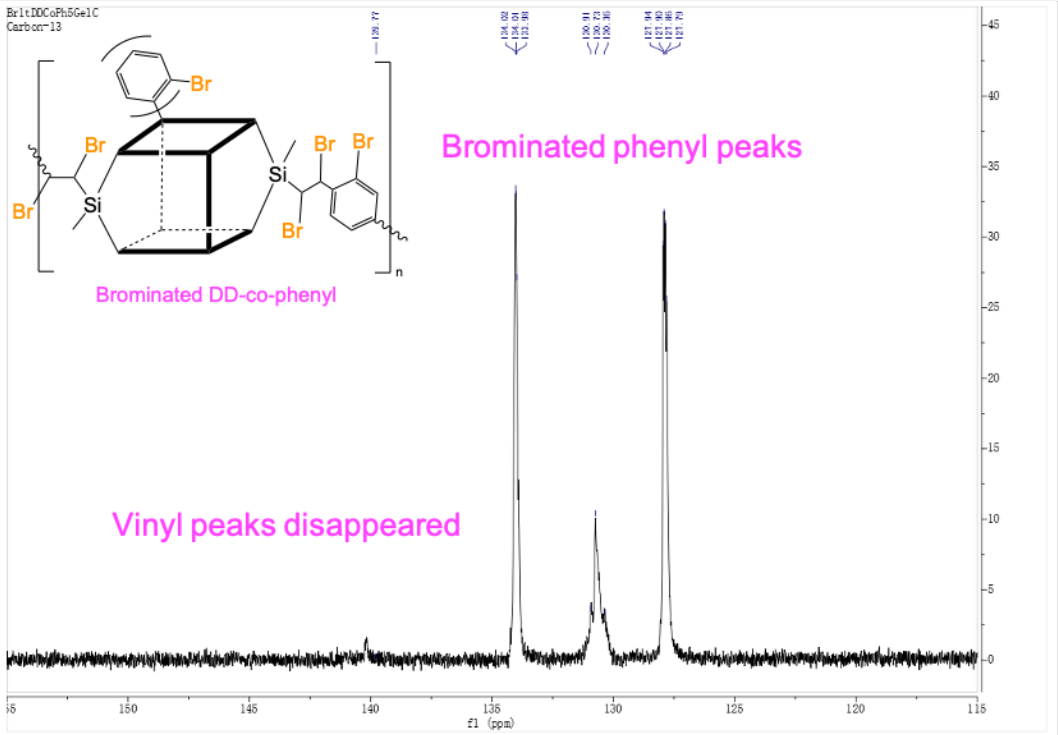

Figure D.24. ^{13}C NMR of brominated DD-co-phenyl (zoom-in).

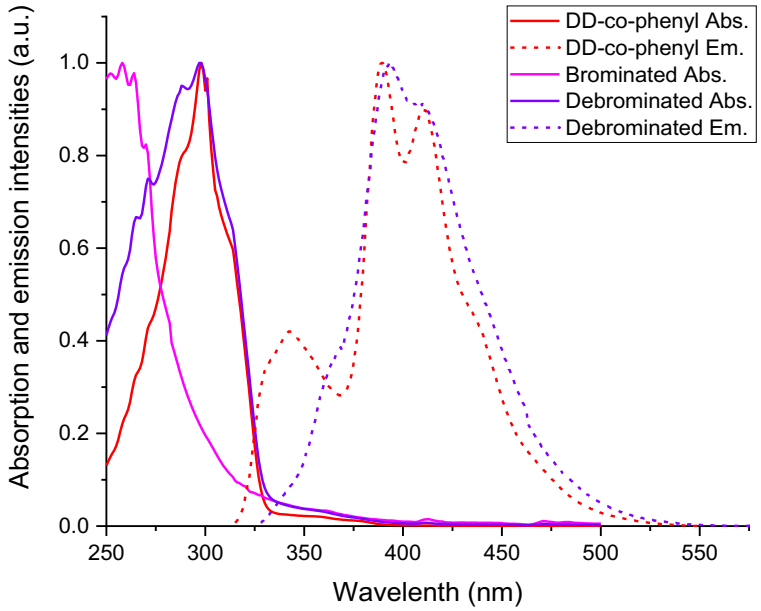

Figure D.25. Steady-state spectra of DD-co-phenyl, brominated and debrominated DD-co-phenyl in CH_2Cl_2.

Modeling of vinyl-LL(Me)-vinyl and vinyl-LL(Ph)-vinyl done by Professor Jungsuttiwong's group at Ubon Ratchathani University, Thailand are shown in Table **D.4**. Modeling suggests LUMOs reside on phenyl groups and the calculated absorption λ_{max} is always blue-shifted from experimental by ~60 nm. One might choose to argue that current modeling methods are unable to successfully address the interaction of LL SQ centered LUMOs with conjugated moieties. Hence efforts to model the unique structures developed with the LL polymers wherein centered LUMOs must interact with co-monomer LUMOs through vinylMeSi(O-)$_2$ bridges (assuming our arguments are valid) must search for new modeling approaches.

Table D.4. Experimental and modeling data for vinyl-LL(Me/Ph)-vinyl.

	Experimental Abs. λmax (nm)	Modeling Abs. λmax (nm)	Transition	HOMO (eV)	LUMO (eV)	Egap (eV)
Vinyl-LL(Me)-vinyl	264	203	HOMO to L+1 (40%)	-8.07	0.81	8.88
Vinyl-LL(Ph)-viny	265	201	H+9 to L+2 (26%)	-8.28	0.72	8.99
		203	H+6 to LUMO (18%)	-8.32	0.80	9.13

Modeling indicates studies done on vinyl-LL(Me)-vinyl by Professor Kieffer and Dr. Hashemi's group at University of Michigan are shown in Figure A 4.26-4.28. In these modeling studies, both cis and trans isomers have about the same energy, which may explain why it is always a mixture of cis and trans. The energy of cis isomer is ~0.025 eV slightly lower than trans. Additionally, there are two different conformation, chair and boat conformation as shown in Figure A 4.26, similar to cyclohexane. The chair conformation is more stable with the energy difference of ~0.13 eV. What's more important is that LUMO+2 at 8.47 eV is from LL SQ core and extends out of the ladder structure in Figure **D.27**, which makes interaction between SQ-centered LUMO and vinyl π^* possible. Phenyl groups are replaced by methyl for modeling. When phenyl unreplaced, LUMO+10 is from LL SQ core with energy level at 7.86 eV as shown in Figure **D.28**, which has a lower energy level than LUMO+2 of methyl-replaced model.

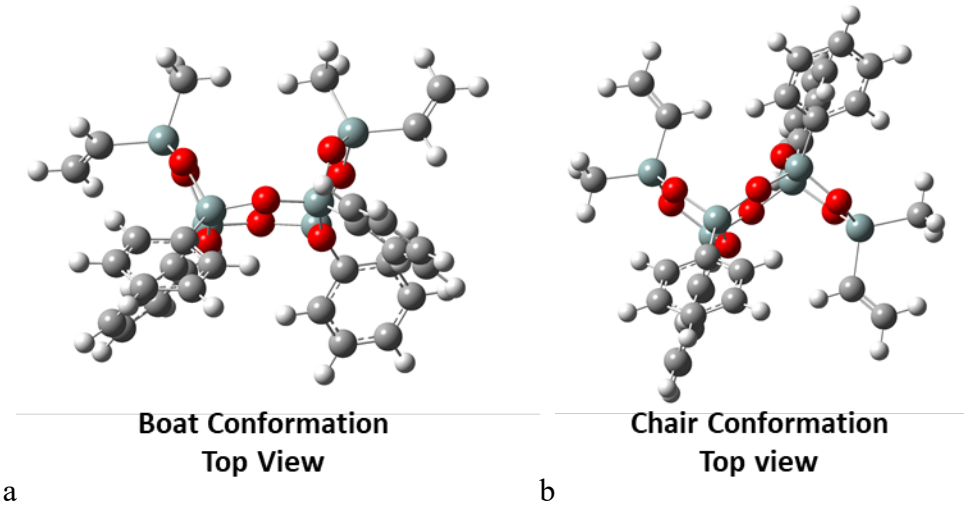

a b

Figure D.26. (a) boat conformation of *trans*-vinyl-LL(Me)-vinyl, (b) chair conformation, calculated at B3LYP/6-31G(d,p) level.

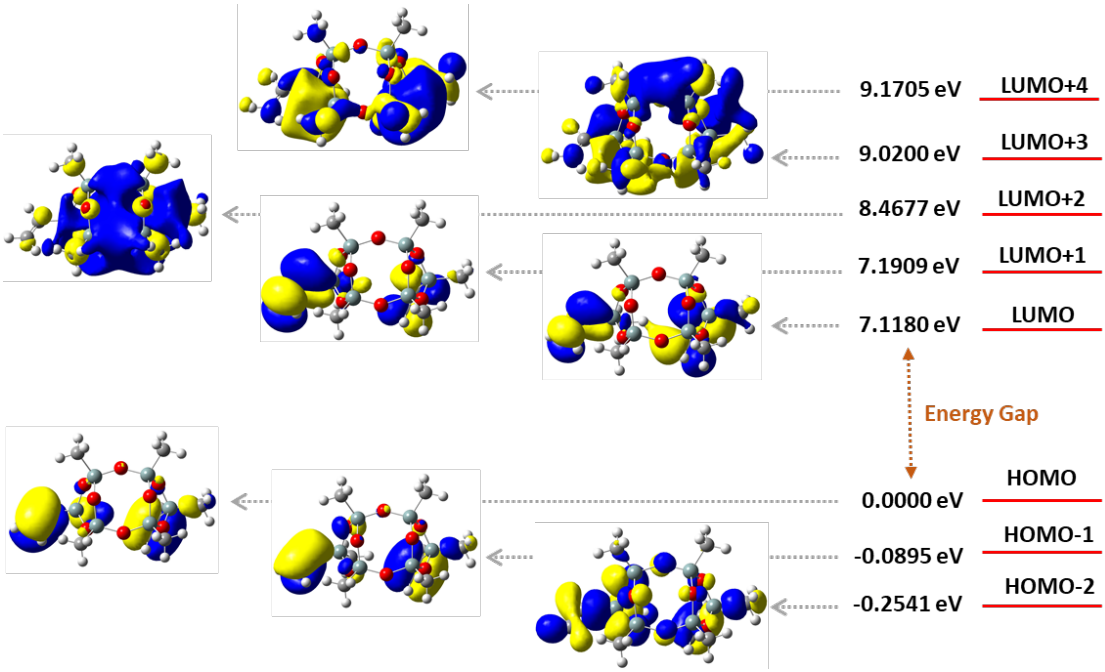

Figure D.27. Energy diagram of the molecular orbitals of methyl substituted vinyl-LL(Me)-vinyl.

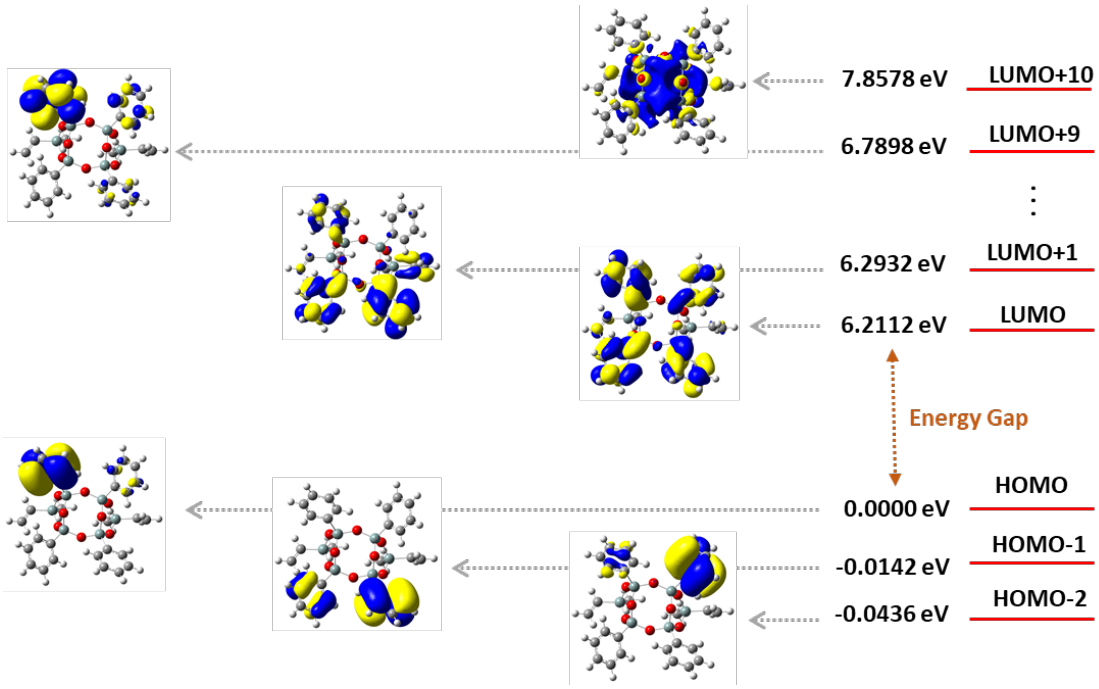

Figure D.28. Energy diagram of the molecular orbitals of vinyl-LL(Me)-vinyl.

Appendix E. Double Decker Derived Alternating Terpolymers Give Excited-state Conjugation Averaging that of the Corresponding Co-polymers.

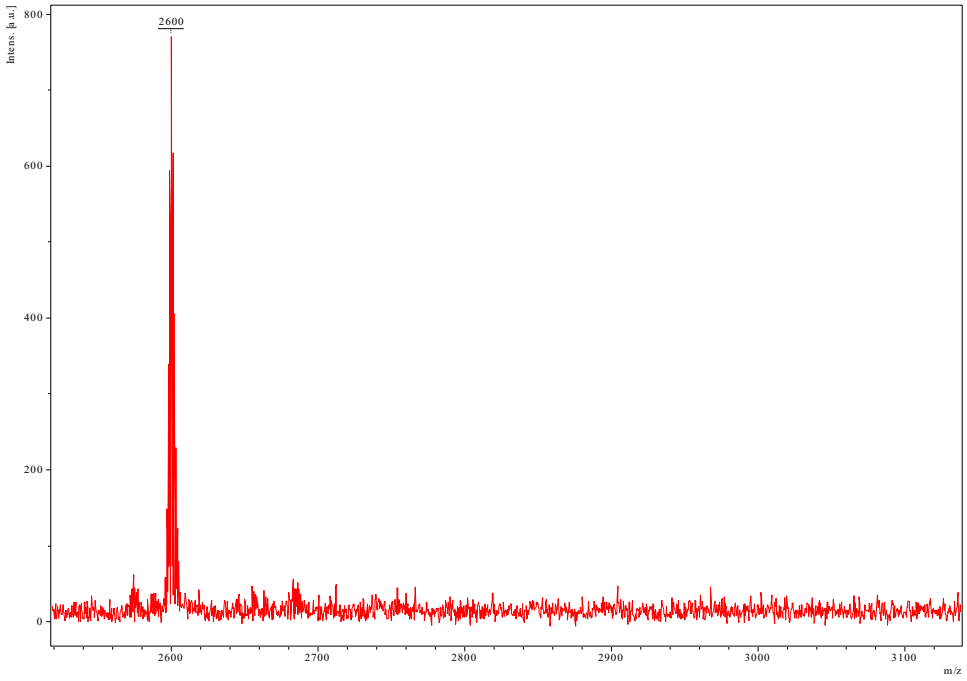

Figure E.1. MALDI of DD-thiophene-DD/Ag^{+}.

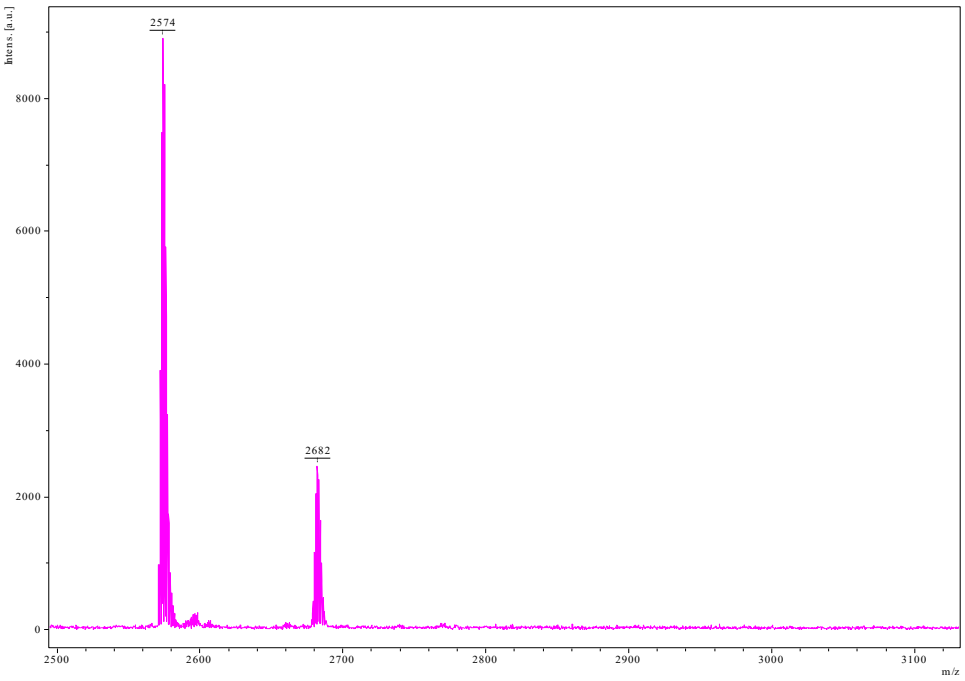

Figure E.2. MALDI of DD-bithiophene-DD/H^+ (2574 m/z) and DD-bithiophene-DD/Ag^+(2682 m/z).

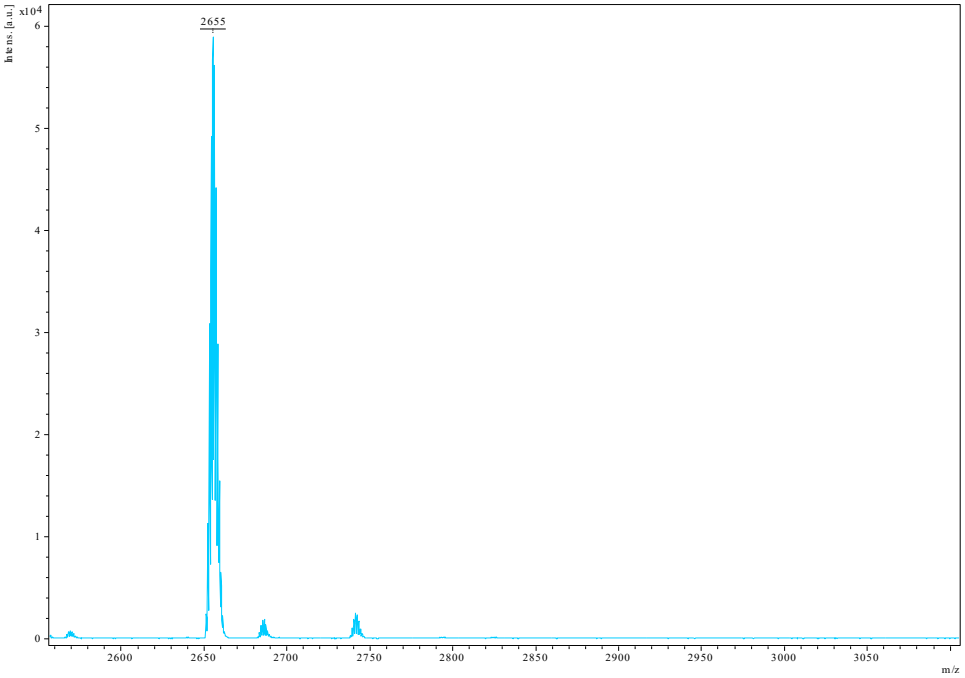

Figure E.3. MALDI of DD-thienothiophene-DD/Ag^+.

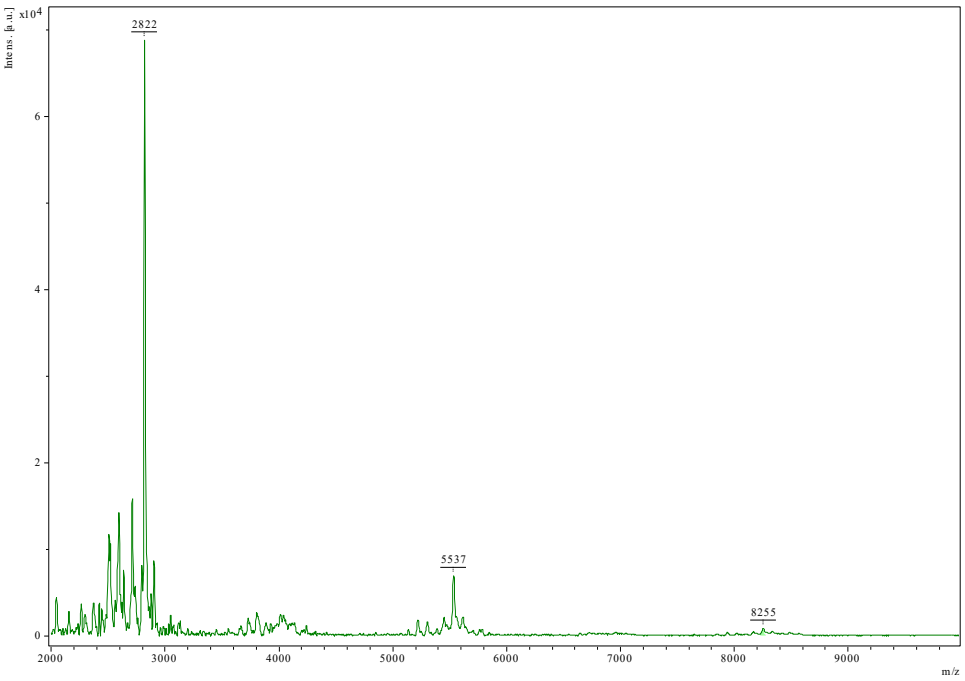

Figure E.4. MALDI of terpolymer DD-thiophene-terphenyl/Ag^{+}.

Table E.1. ^{1}H and ^{13}C NMR peaks.

Compound	^{1}H NMR peaks (ppm)	^{13}C NMR peaks (ppm)
DD-thiophene-DD	7.80 (d, 2H, -C4H2S-); 7.77-7.06 (m, 80H, -C6H5); 6.94 (d, 2H, -CH=CH-); 6.45 (d, 2H, -CH=CH-); 6.20-6.14 (m, 2H, -CH=CH2); 6.05-5.99 (m, 4H,-CH=CH2); 0.42 (s, 6H, -CH3); 0.37 (s, 6H, -CH3)	144.3, 139.1,137.4, 135.2, 134.5, 134.2, 134.1, 134.0, 132.0, 131.9, 131.1, 131.0, 130.7, 130.6, 130.4, 130.3, 127.9, 127.8, 127.7, 127.6, 124.1, -0.66, -1.13.
DD-bithiophene-DD	7.77 (d, 2H, -C8H4S2-); 7.73 (d, 2H,-C8H4S2-); 7.64-7.06 (m, 80H, -C6H5); 6.89 (d, 2H, -CH=CH-); 6.53 (d, 2H, -CH=CH-); 6.20-6.12 (m, 2H, -CH=CH2); 6.06-5.96 (m, 4H,-CH=CH2); 0.43 (s, 6H, -CH3); 0.38 (s, 6H, -CH3)	144.2, 138.8, 137.4, 135.2, 134.4, 134.1, 134.0, 131.9, 130.4, 127.8, 127.8, 127.6, 127.5, 124.5, 124.2, 123.8, -0.70, -1.17.
DD-thienothiophene-DD	7.81 (d, 2H, -C6H2S2-); 7.77-7.07 (m, 80H, -C6H5); 6.98 (d, 2H, -CH=CH-); 6.46 (d, 2H, -CH=CH-); 6.22-6.14 (m, 2H, -CH=CH2); 6.06-5.96 (m, 4H,-CH=CH2); 0.46 (s, 6H, -CH3); 0.42 (s, 6H, -CH3)	146.9, 139.7, 138.8, 135.2, 134.5, 134.2, 134.1, 134.0, 132.0, 131.9, 131.1, 131.0, 130.8, 130.5, 130.4, 130.3, 127.9, 127.8, 127.7, 127.6, 123.7, 112.0, -0.53, -1.13.
DD-Thio-DD-Biph	7.77-7.07 (m, 90H, -C6H5, -C4H2S-); 7.00-6.95 (m, 4H, -CH=CH-); 6.53-6.49 (m, 4H, -CH=CH-); 6.13-6.11 (m, -CH=CH2); 0.49 (s, 6H, -CH3); 0.44 (s, 6H, -CH3)	146.1, 140.6, 136.8, 134.2, 134.1, 134.0, 132.0, 131.9, 130.8, 130.4, 127.9, 127.8, 127.7, 127.6, 127.3, 126.9, 124.1, 1.05, -0.72.
DD-Thio-DD-Terph	7.90-7.04 (m, -C6H5, -C4H2S-); 6.99-6.90 (m, 4H, -CH=CH-); 6.53-	146.1, 140.5, 139.7, 139.0, 136.8, 134.5, 134.2, 134.1,

	6.46 (m, 2H, -CH=CH-); 0.47 (s, 6H, -CH3); 0.41 (s, 6H, -CH3)	134.0, 134.0, 131.9, 130.6, 130.4, 127.9, 127.8, 127.7, 127.6, 127.4, 127.0, 124.1, 1.05, -0.71.
DD-Thio-DD-Stil	7.72-7.04 (m, -C6H5, -C4H2S-); 6.94-6.90 (m, 4H, -CH=CH-); 6.46-6.42 (d, 4H, -CH=CH-); 6.10-6.07, (d, -CH=CH2); 0.45 (s, 6H, -CH3)	146.0, 140.5, 139.7, 139.0, 134.0, 130.4, 127.8, 127.6, 1.01.
DD-Ththio-DD-Biph	7.74-7.04 (m, -C6H5, -C6H2S2-); 7.00-6.95 (m, 4H, -CH=CH-); 6.50-6.45 (m, 4H, -CH=CH-); 6.14-6.02 (m, -CH=CH2); 0.45 (s, 6H, -CH3)	146.9, 139.7, 138.8, 134.1, 134.0, 131.9, 130.4, 127.8, 127.7, 127.6, 127.3, 126.9, 1.03, -0.74.

Table E.2. Representative FTIR data of selected compounds.

Compound	v	Wavenumber (cm^{-1})	Intensity
DD-thiophene-DD		495	Medium, sharp
		698	Medium, sharp
		730	Weak, sharp
	Si-O-Si	1029	Weak, sharp
	Si-O-Si	1132	Strong, broad
	C=C	1262	Weak, sharp
	C=C	1430	Medium, sharp
	C=C	1594	Medium, sharp
	C-H	2837	Weak, sharp
	C-H	2950	Weak, broad
DD-Thio-DD-Biph		495	Medium, sharp
		697	Medium, sharp
		729	Weak, sharp
	Si-O-Si	1209	Weak, sharp
	Si-O-Si	1132	Strong, broad
	C=C	1262	Weak, sharp
	C=C	1430	Medium, sharp
	C=C	1594	Medium, sharp
	C-H	2836	Weak, sharp
	C-H	2937	Weak, broad

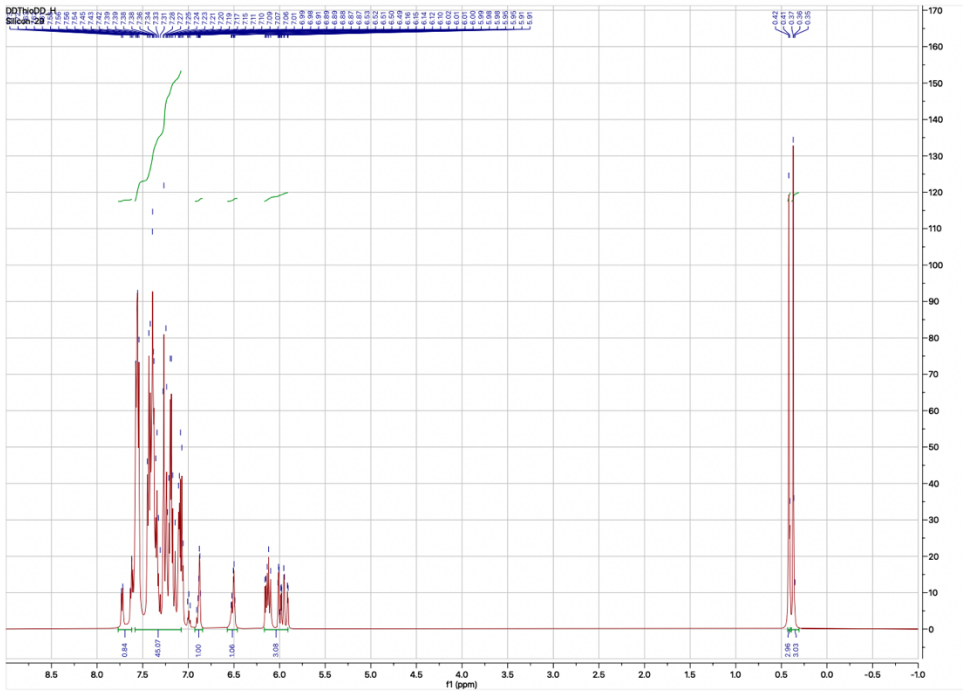

a

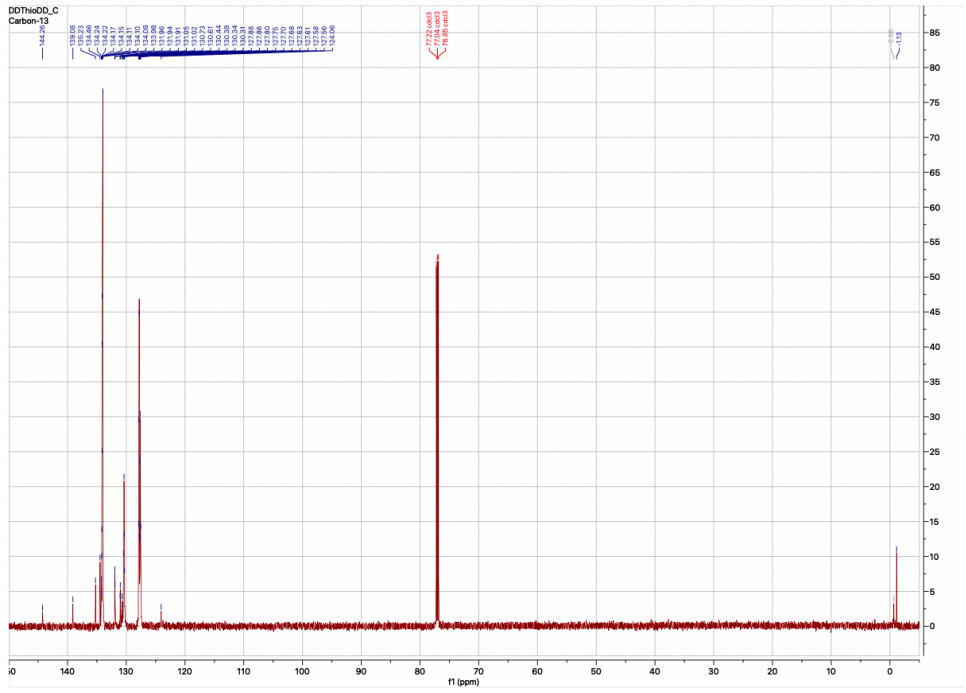

b

Figure E.5. (a)^{1}H NMR of DD-thiophene-DD. (b) ^{13}C NMR in $CDCl_3$.

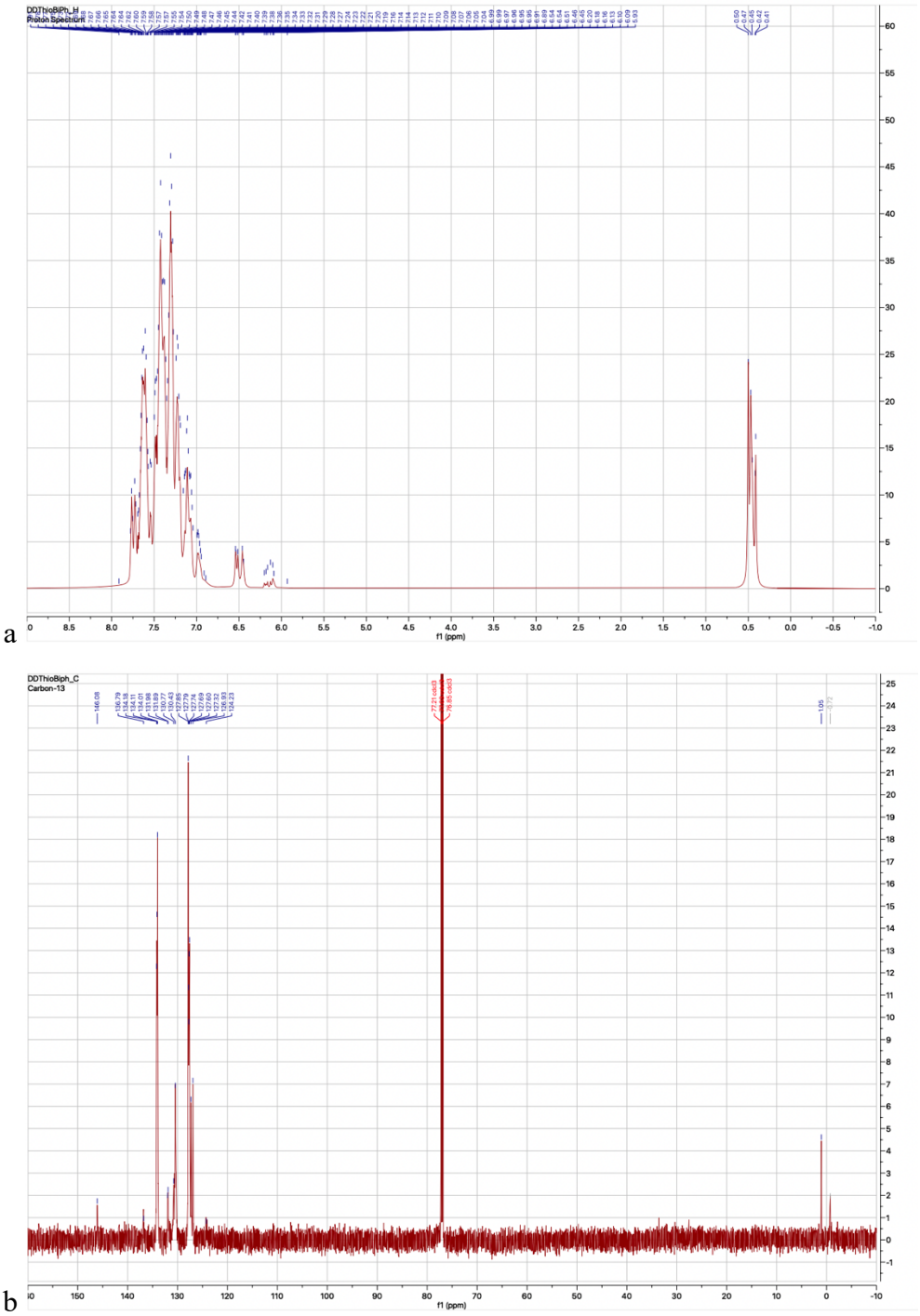

Figure E.6. (a) ^{1}H NMR of DD-Thio-DD-Biph. (b) ^{13}C NMR in $CDCl_3$.

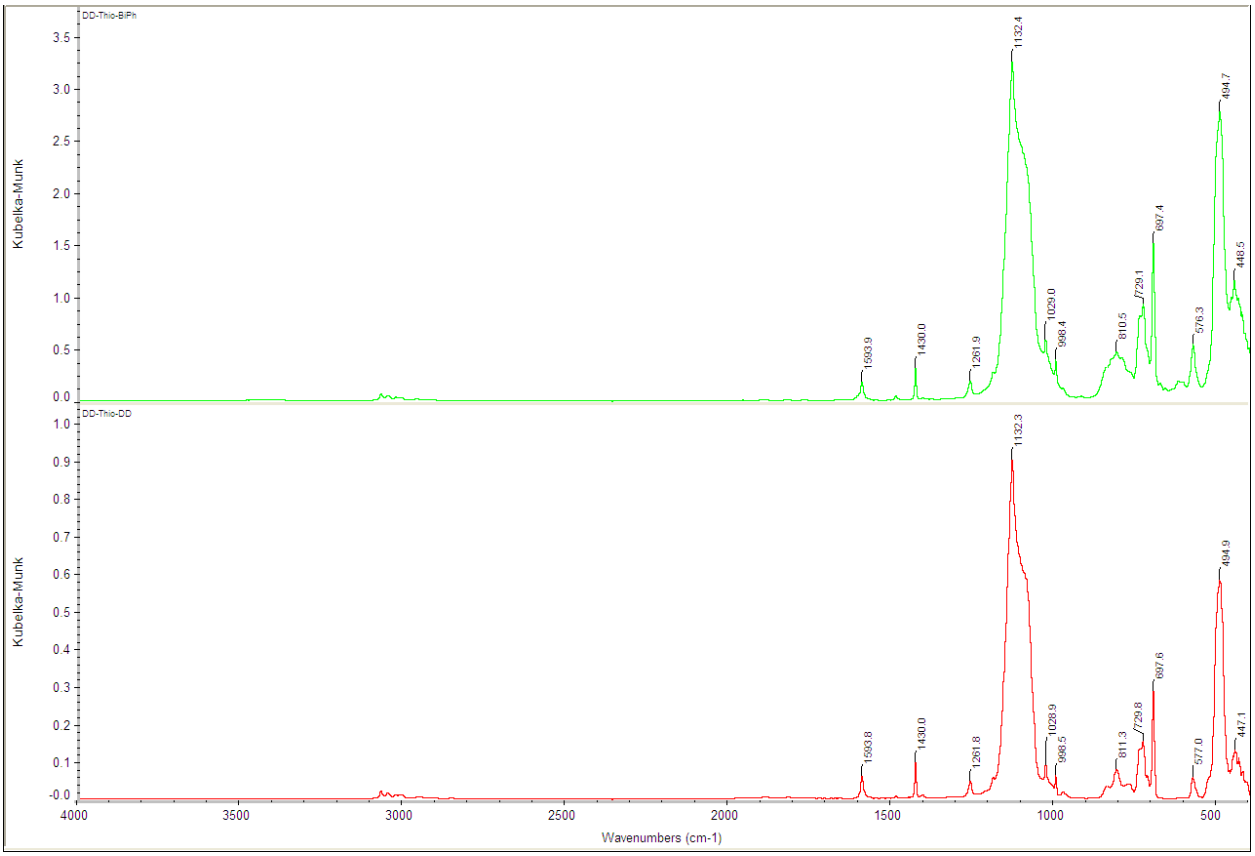

Figure E.7. FTIR of DD-thiophene-DD/H^+ (red) and terpolymer DD-Thio-DD-Biph (green).

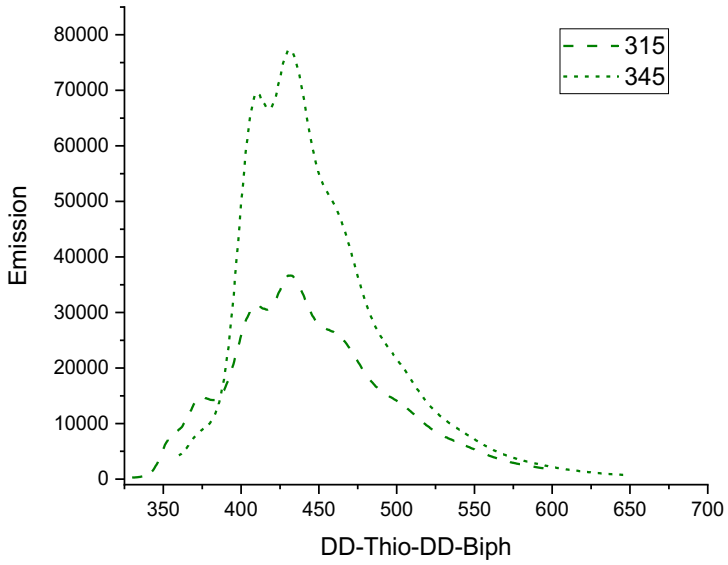

Figure E.8. Emission of terpolymer DD-Thio-DD-Biph exited at 315 nm (Abs. $\lambda_{max.}$ of DD-co-biphenyl) and 345 nm (Abs. $\lambda_{max.}$ of DD-co-thiophene).

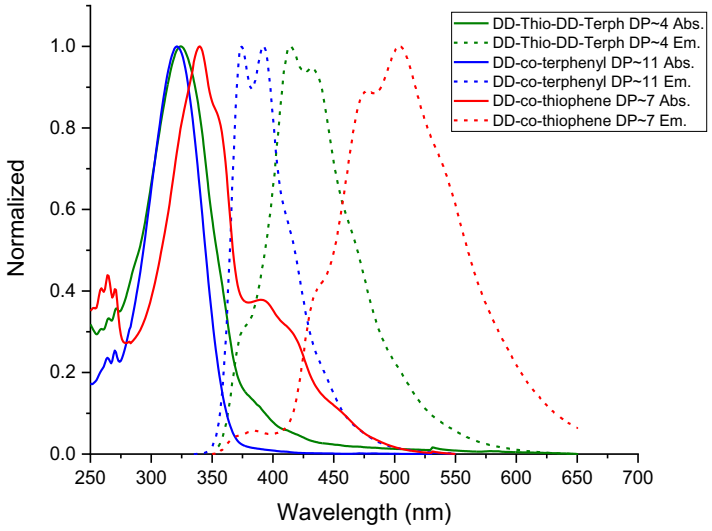

a

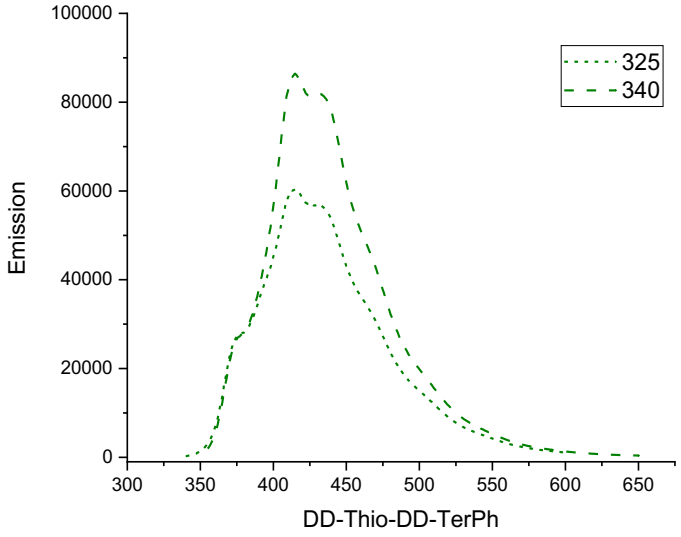

b

Figure E.9. (a) Normalized absorption and emission of terpolymer DD-Thio-DD-Terph. (b) Emission excited at 325 and 340 nm.

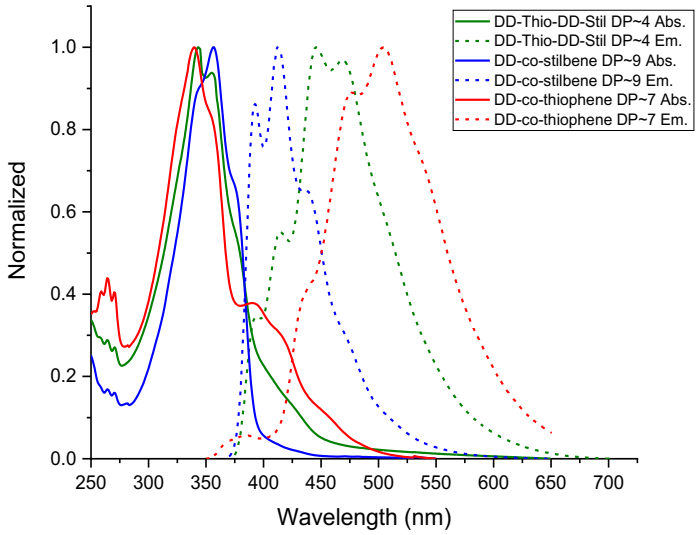

a

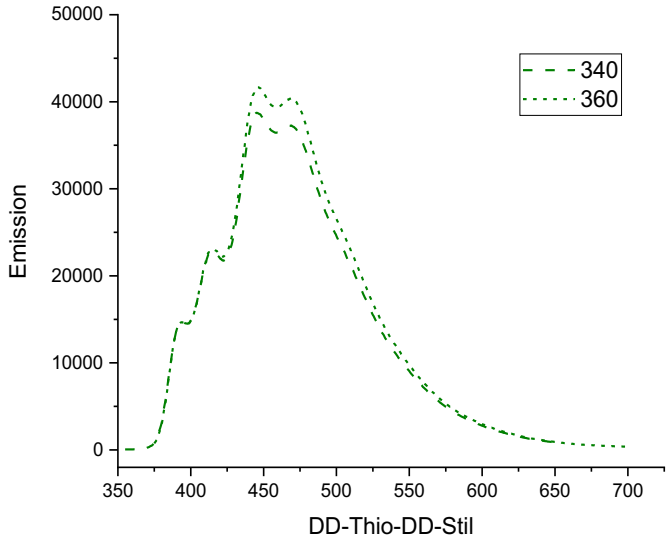

b

Figure E.10. (a) Normalized absorption and emission of terpolymer DD-Thio-DD-Stil. (b) Emission excited at 340 and 360 nm.

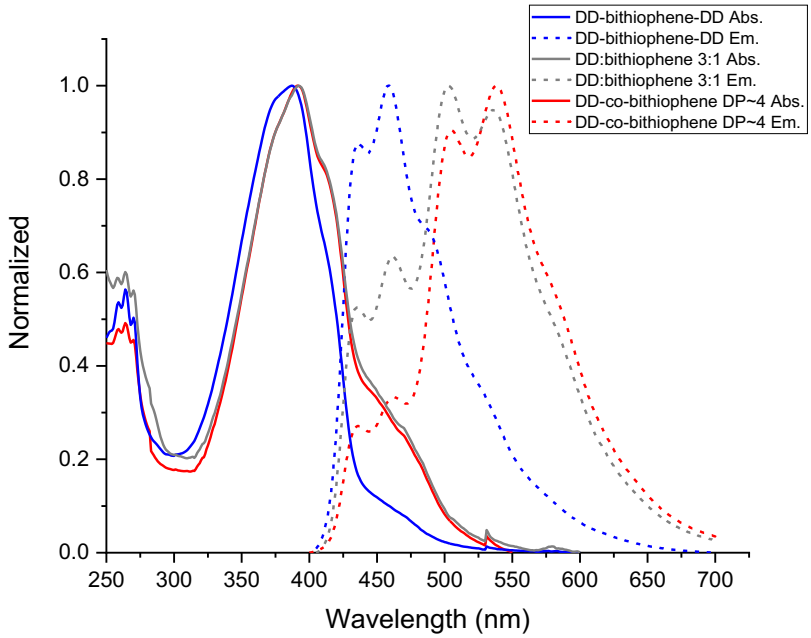

Figure E.11. Normalized absorption and emission of DD-bithiophene-DD, mixture of DD:bithiophene 3:1 and longer DD-co-bithiophene.

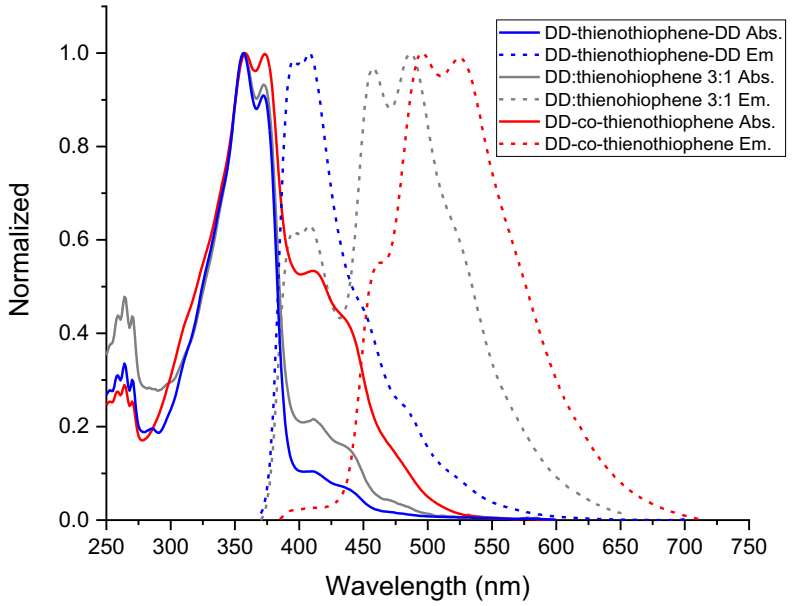

Figure E.12. Normalized absorption and emission of DD-thienothiophene-DD, mixture of DD:thienothiophene 3:1 and longer DD-co-thienothiophene (DP~5).

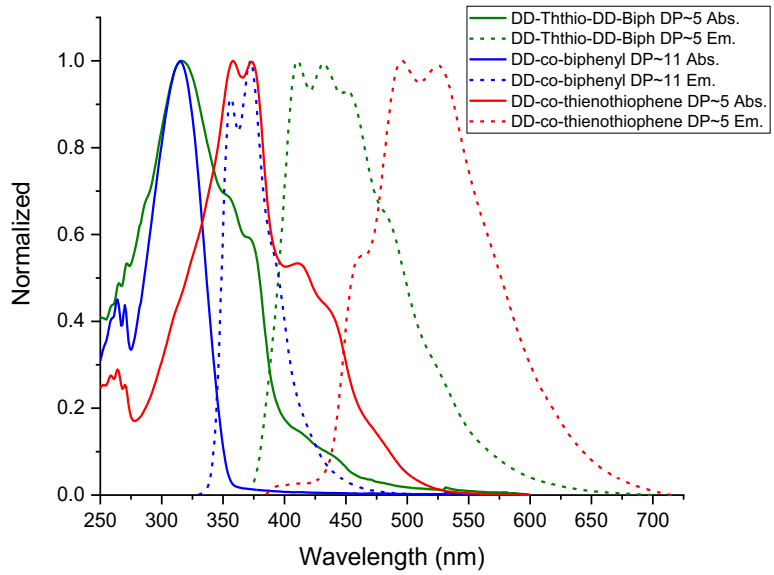

a

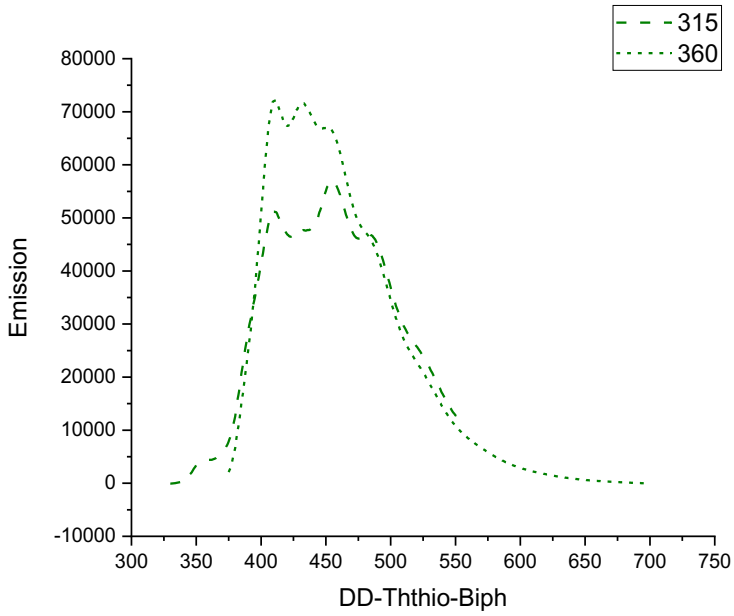

b

Figure E.13. (a) Normalized absorption and emission of terpolymer DD-Ththio-DD-Biph. (b) Emission excited at 315 and 360 nm.

Appendix F. Double Decker Silsesquioxane Derived Hairy Polymers

Table F.1. GPC and TGA data for DD-co-biphenyl and derived products as in Scheme **8.2a**.

Compound	GPC			TGA		
	M_n	M_w	Đ	Ceramic yield %	Theor yield %	$Td_{5\%}$ °C (air)
DD-co-biphenyl	11500	22600	1.97	43.1	43.9	400
Br_9DD-co-biphenyl (brominated)	3300	4700	1.42	28.8	28.8	215
Br_5DD-co-biphenyl (debrominated)	3000	5100	1.71	34.9	34.0	255
$CNStil_5$DD-co-biphenyl (Heck cross-coupled)	3600	5800	1.62	32.6	30.0	275

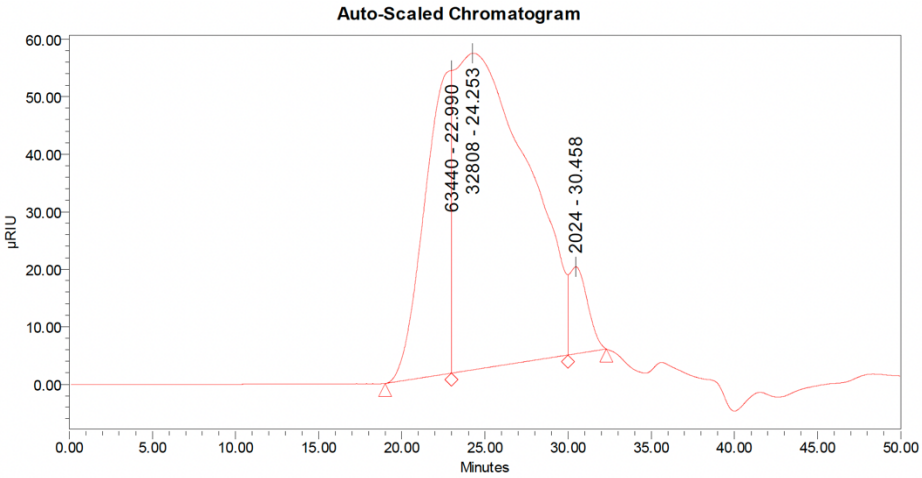

Figure F.1. GPC of the starting DD-co-biphenyl.

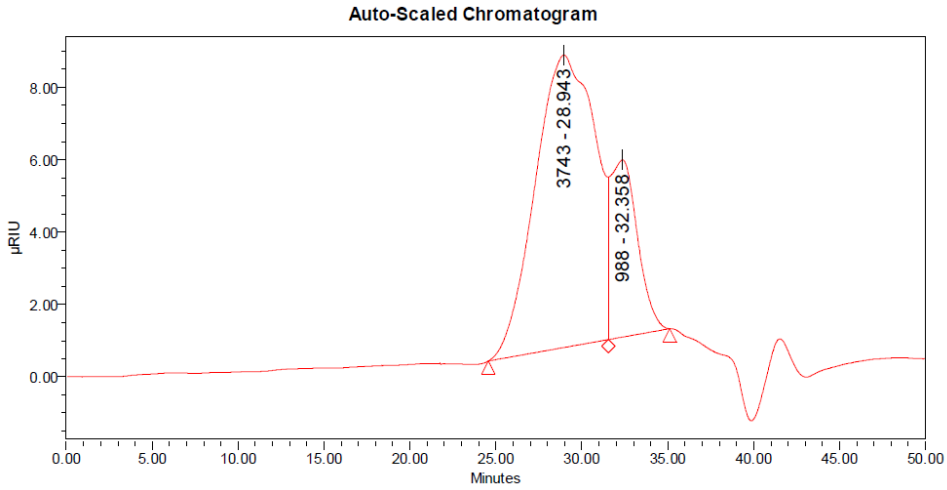

Figure F.2. GPC of the self-bromination of DD-co-biphenyl after 2 h.

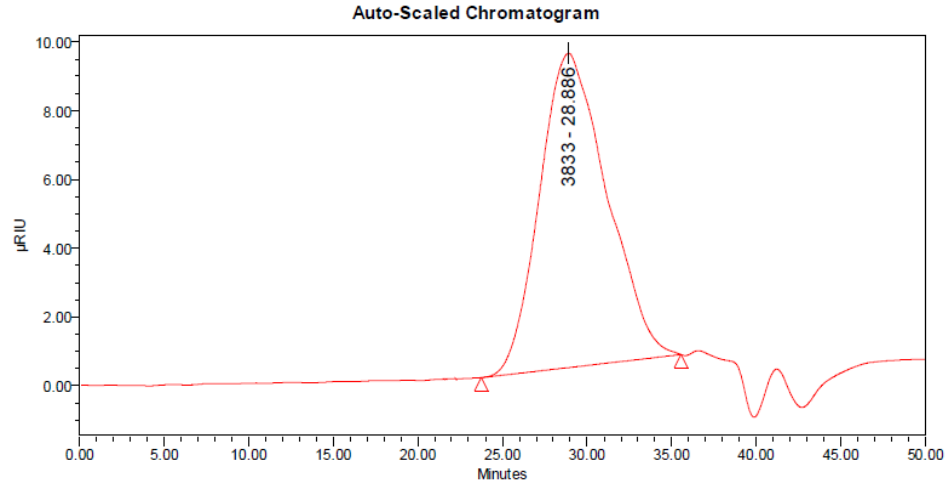

Figure F.3. GPC of the brominated DD-co-biphenyl (Br_9DD-co-biphenyl).

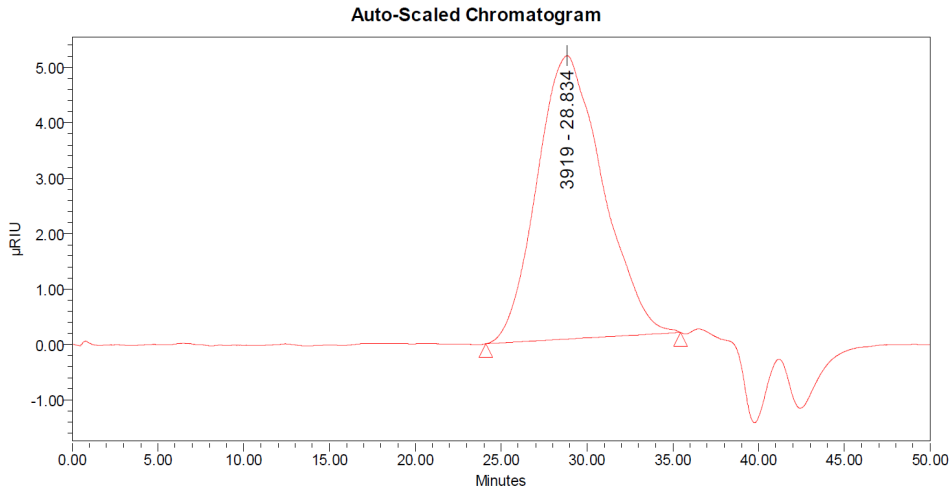

Figure F.4. GPC of the zinc debrominated DD-co-biphenyl (Br_5DD-co-biphenyl).

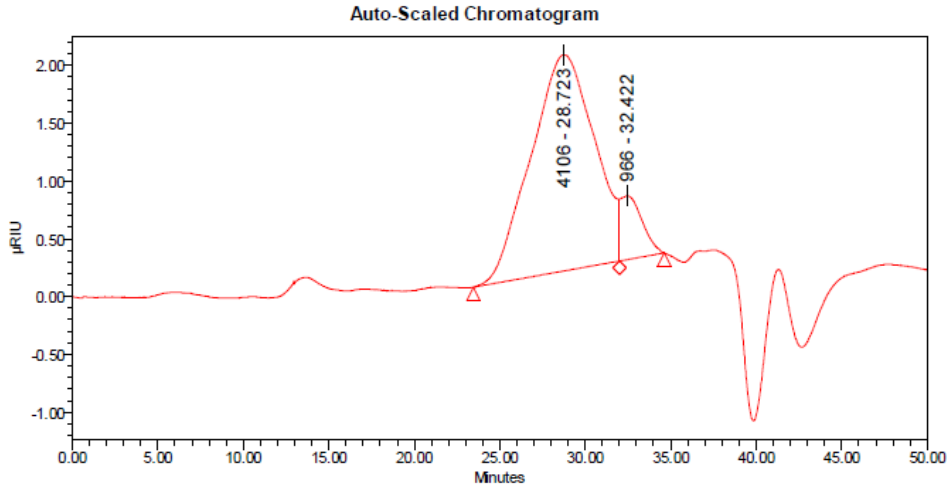

Figure F.5. GPC of CNStil$_5$DD-co-biphenyl.

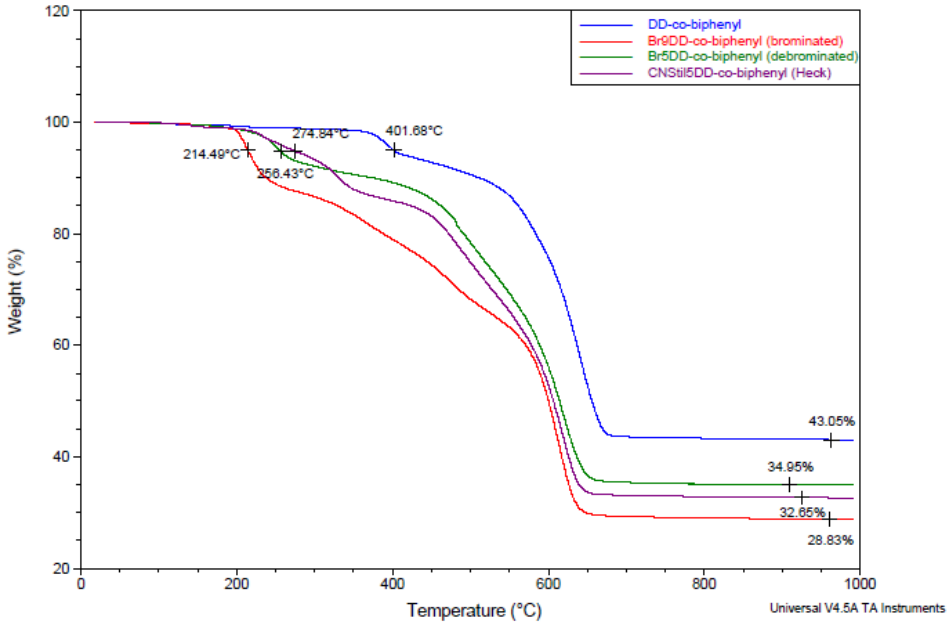

Figure F.6. TGA of the starting DD-co-biphenyl, Br$_9$DD-co-biphenyl, Br$_5$DD-co-biphenyl and CNStil$_5$DD-co-biphenyl.

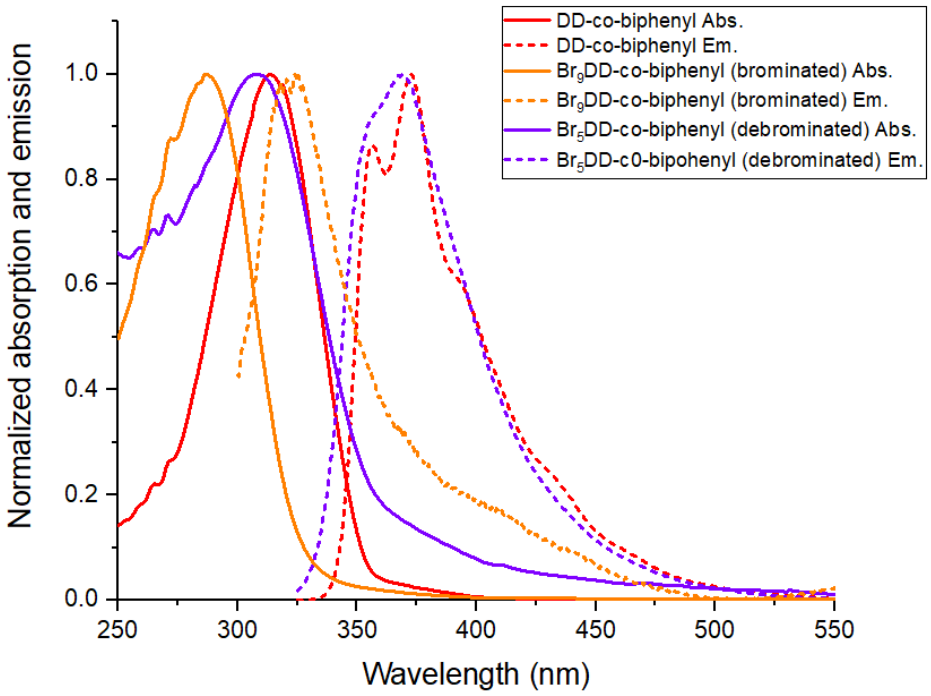

Figure F.7. Normalized steady-state spectra of the starting DD-co-biphenyl, Br_9DD-co-biphenyl, Br_5DD-co-biphenyl and CNStil$_5$DD-co-biphenyl.

Table F.1. GPC and TGA data for brominated vinylDDvinyl and derived products as in Scheme **8.2b**.

Compound	GPC			TGA		
	M_n	M_w	Đ	Ceramic yield %	Theor yield %	$Td_{5\%}$ °C (air)
Br_{12}DD (brominated)	760	820	1.08	27.1	27.7	305
CNStil$_8$Br$_4$DD (Heck cross-coupled)	1300	1500	1.15	24.1	23.4	310
CNStil$_8$vinylDDvinyl (Debrominated)	1300	1580	1.22	26.8	26.7	325
CNStil$_8$DD-co-biphenyl (Heck polymerization)	7800	22300	2.89	25.2	24.9	300

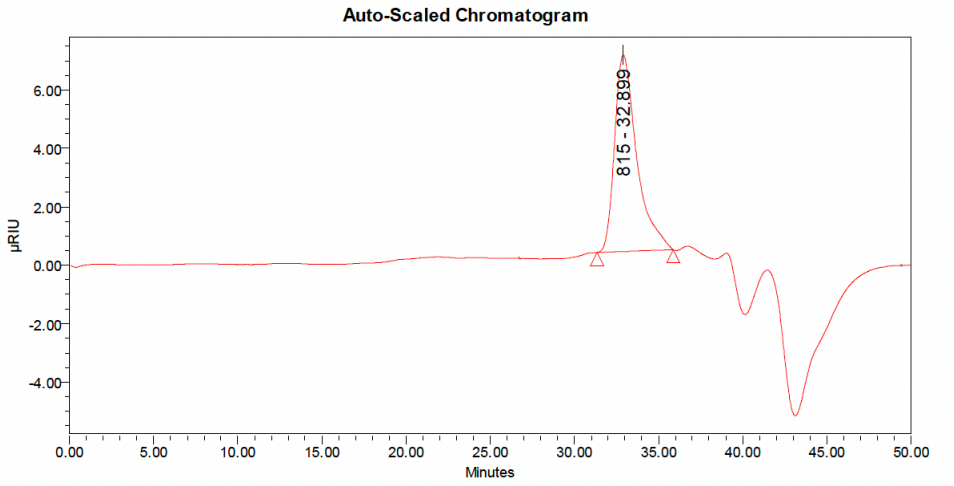

Figure F.8. GPC of the starting vinylDDvinyl

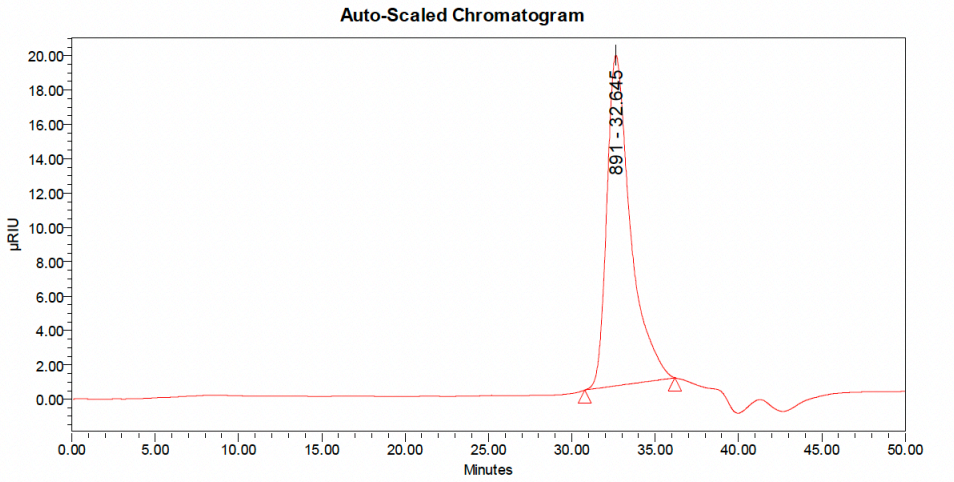

Figure F.9. GPC of the brominated DD ($Br_{12}DD$).

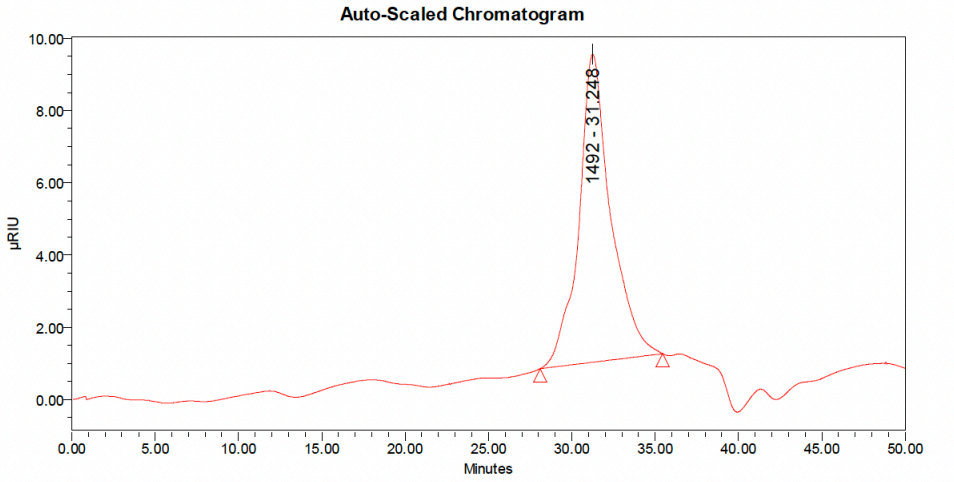

Figure F.10. GPC of the Heck cross-coupled DD ($CNStil_8Br_4DD$).

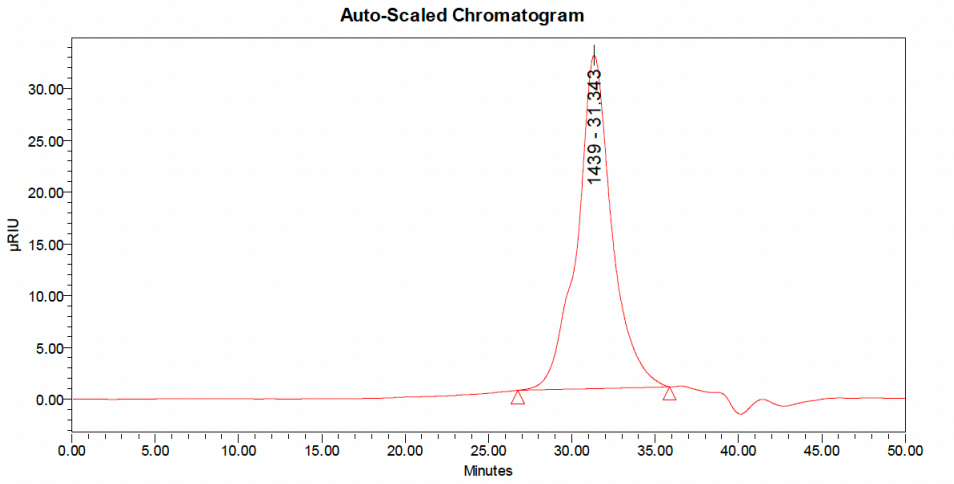

Figure F.11. GPC of the debrominated DD (CNStil$_8$vinylDDvinyl).

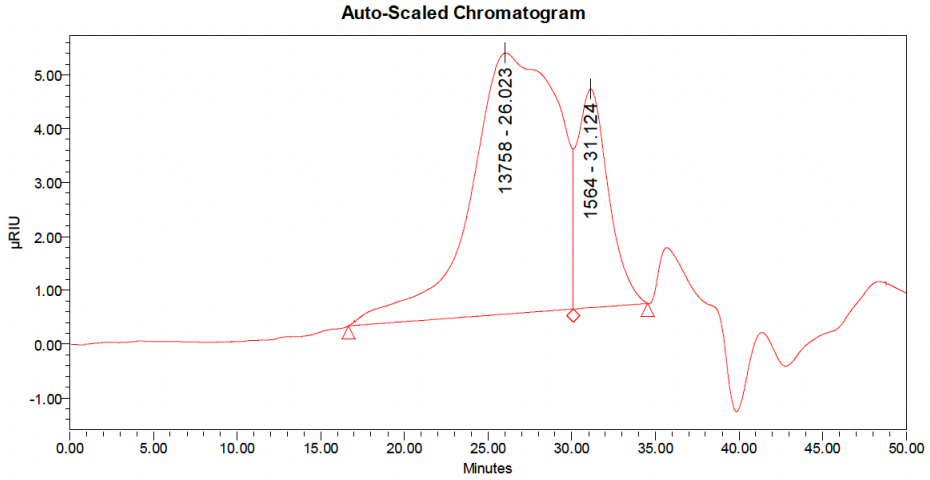

Figure F.12. GPC of CNStil$_8$DD-co-biphenyl (Heck polymerization).

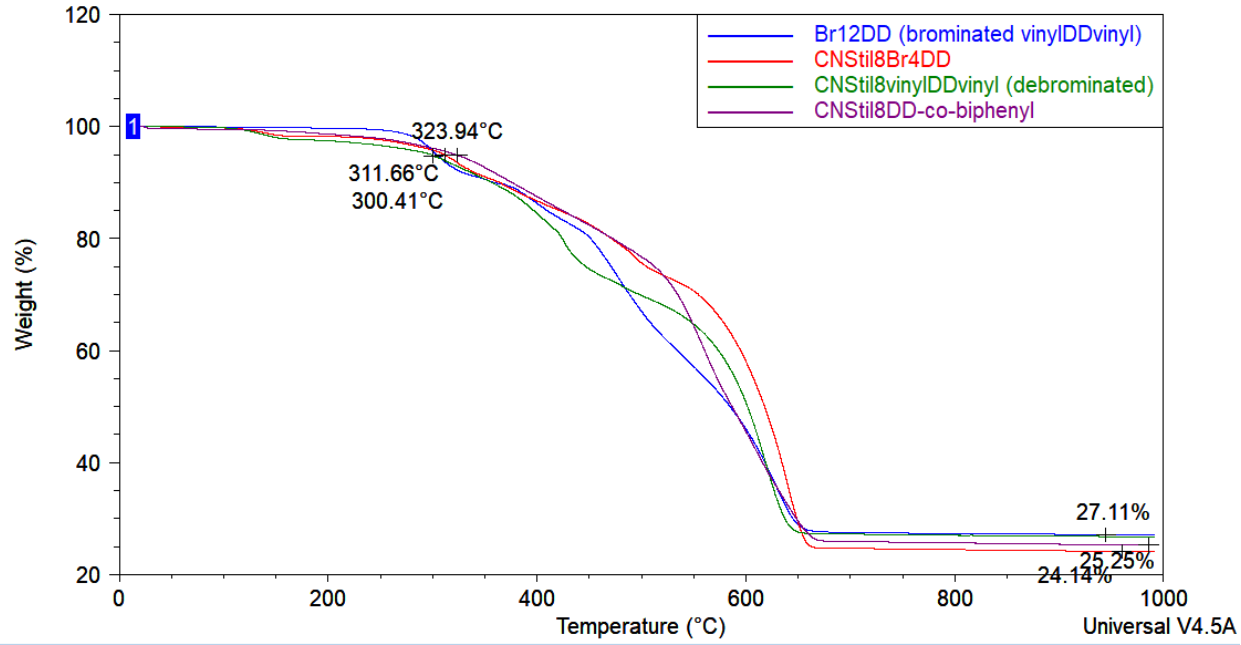

Figure F.13. TGA of $Br_{12}DD$ (brominated vinylDDvinyl), $CNStil_8Br_4DD$, $CNStil_8$vinylDDvinyl and $CNStil_8DD$-co-biphenyl.

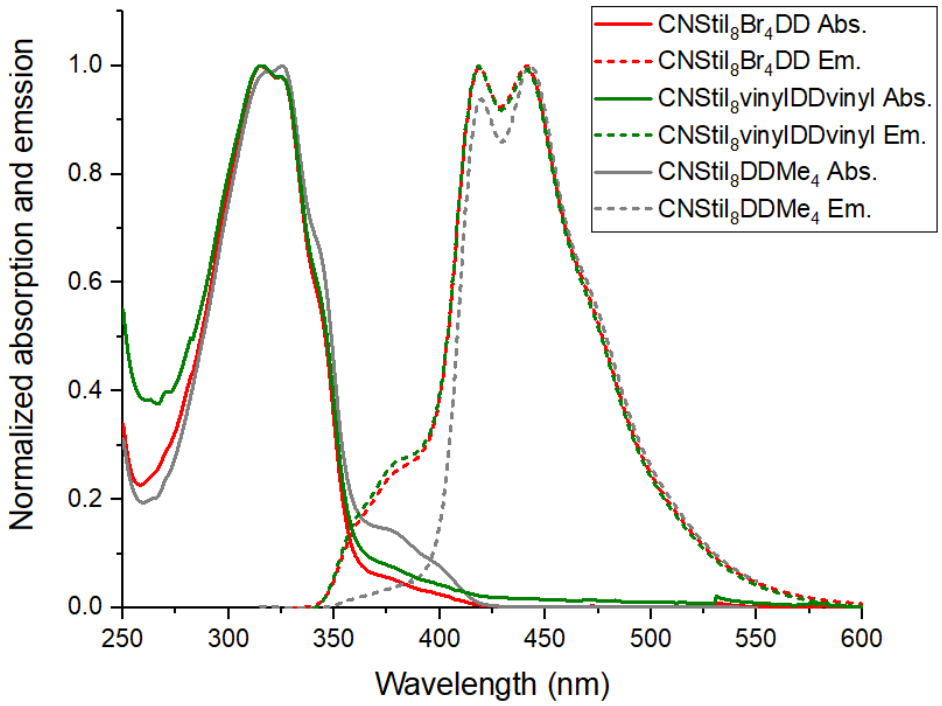

Figure F.14. Normalized steady-state spectra of $CNStil_8Br_4DD$, $CNStil_8$vinylDDvinyl and $CNStil_8DDMe_4$ in CH_2Cl_2.

Experimental of Scheme **8.2a**

Zn debromination of Br_9DD-co-biphenyl. To a dry 100 ml Schlenk flask under N_2 were added 1.13 g (0.55 mmol) Br_9DD-co-biphenyl, 20 ml diethyl either and 5 ml THF, followed by 3 drops of glacial acetic acid and 100 mg (1.5 mmol) Zn dust. The mixture was stirred vigorously over the weekend and tracked by steady-state spectroscopy. Another 30 mg (0.5 mmol) Zn dust was added after 2 d. After the grey Zn dust turned white, the reaction mixture was quenched by filtration. The resulting filtrate was then concentrated and precipitated into 100 ml cold, well-stirred methanol to give 0.6 g yellowish product and then MeOH filtrate was also concentrated to give more product.

Heck cross-coupling of Br_5DD-co-biphenylwith 4-cyanostyrene. To a dry 50 ml Schlenk flask under N_2 were added 0.66 g (0.38 mmol) debrominated Br_5DD-co-biphenyl, 38.7 mg (0.08 mmol) $Pd[P(t\text{-}Bu)_3]_2$ and 34.6 mg (0.04 mmol) $Pd_2(dba)_3$, followed by 30 ml distilled THF, 1.01 g (5 mmol) NCy_2Me and 0.40 g (3 mmol) 4-cyanostyrene. The mixture was stirred magnetically under N_2 at 70 °C and tracked by steady-state spectroscopy. Another 9.7 mg (0.02 mmol) $Pd[P(t\text{-}Bu)_3]_2$, 8.7 mg (0.01 mmol) $Pd_2(dba)_3$ and 0.20 g (1.5 mmol) 4-cyanostyrene was added after 2 d. The reaction was quenched after 7 d by filtration. The resulting filtrate was then concentrated and precipitated into 100 ml cold, well-stirred methanol to give 0.4 g yellow product.

Experimental of Scheme **8.2b**

Bromination of vinylDDvinyl. To a dry 100 ml Schlenk flask under N_2 were added 6.03 g (5.0 mmol) vinylDDvinyl and 30 ml of CH_2Cl_2. After completely dissolving, 3.61 ml (70.0 mmol) Br_2 was added dropwise and an additional 5 ml of CH_2Cl_2 was added. A condenser was then attached and a vent to a bubbler containing aqueous base was added. The solution was stirred magnetically under reflux at 40 °C for 1 d and tracked by MALDI. At this point, 20 g $Na_2S_2O_5$ and 10 g Na_2CO_3 were dissolved in 40 ml water and then added to the solution with vigorous stirring, until the Br_2 color disappeared. The mixture was then transferred to a separatory funnel and the organic layer was extracted and washed sequentially with 30 ml brine. Thereafter, the organic layer was dried over $MgSO_4$. Then celite were added and stirred for 10 min. The mixture was filtered to give a clear, colorless liquid. Most solvent was removed by rotary evaporation and the resulting solid was redissolved in a minimal amount of THF and slowly poured into cold, well-stirred 150 ml methanol to fully precipitate 7.5 g (yield: 70%) white product, which was further purified by redissolving in a minimal amount of warm THF and reprecipitating into 150 ml methanol.

Heck cross-coupling of Br_{12}DD with 4-cyanostyrene. To a dry 100 ml Schlenk flask under N_2 were added 2.154 g (1.0 mmol) above Br_{12}DD, 38.7 mg (0.08 mmol) $Pd[P(t\text{-}Bu)_3]_2$ and 34.6 mg (0.04 mmol) $Pd_2(dba)_3$, followed by 30 ml distilled THF, 5.05 g (25 mmol) NCy_2Me and 3.33 g (25 mmol) 4-cyanostyrene. The mixture was stirred magnetically under N_2 at 70 °C and tracked by GPC. The reaction was quenched after 4 d by filtering through 1 cm celite, which was washed with 5 ml THF. The solution was then concentrated and precipitated into 150 ml cold, well-stirred methanol to give 1.0 g yellowish product. The cyano-stilbene derived product has some solubility in methanol and thus the MeOH filtrate was also concentrated to give more product.

Zn debromination of $CNStil_8Br_4$DD and its characterization. To a dry 50 ml Schlenk flask under N_2 were added 0.98 g (0.39 mmol) $CNStil_8Br_4$DD, 20 ml diethyl either and 5 ml THF, followed by 3 drops of glacial acetic acid and 80 mg (1.20 mmol) Zn dust. The mixture was stirred vigorously and another 20 mg (0.3 mmol) Zn and 2 drops of acid were added after 1 d. The reaction was quenched after another 2 d by filtration. The resulting filtrate was then concentrated to give 0.6 g yellow product.

Heck polymerization of $CNStil_8$vinylDDvinyl with 4,4'-dibromo-1,1'-biphenyl.To a dry 50 ml Schlenk flask under N_2 were added 0.48 g (0.22 mmol) above $CNStil_8$vinylDDvinyl, 19.4 mg (0.04 mmol) $Pd[P(t\text{-}Bu)_3]_2$, followed by 25 ml distilled THF, 0.20 g (1.0 mmol) NCy_2Me and 70 mg (0.22 mmol) 4,4'-dibromo-1,1'-biphenyl. The mixture was stirred magnetically under N_2 at 70 °C overnight before another 19.4 mg (0.04 mmol) $Pd[P(t\text{-}Bu)_3]_2$ and 34.6 mg (0.04 mmol) $Pd_2(dba)_3$ were added. The reaction was tracked by GPC and steady-state spectroscopy. The reaction was quenched after 6 d by filtration. The resulting filtrate was then concentrated and precipitated into 100 ml cold, well-stirred methanol to give 0.31 g yellow product.